Imperial College London

Department of Earth Science and Engineering

Life Cycle Modelling of Carbon Dioxide Capture and Geological Storage in Energy Production

by

Zhenggang Nie

A Thesis submitted for in fulfilment of requirements for the degree of Doctor of Philosophy of Imperial College London

February 2009

Affirmation

"I hereby declare that this submission is my own work and that, to the best of my knowledge and belief, it contains no material previously published or written by another person or material which to a substantial extent has been accepted for the award of any other degree or diploma of the university or other institute or higher learning, except where due acknowledgement is made in the text"

Zhenggang Nie

Abstract

Carbon dioxide (CO_2) capture and geological storage (CCS) is recognised as one of the main options in the portfolio of greenhouse gas (GHG) mitigation technologies being developed worldwide. The CO_2 capture and storage technologies require significant amounts of energy during their implementation and also change the environmental profile of power generation. The holistic perspective offered by Life Cycle Assessment (LCA) enables decision makers to quantify the trade-offs inherent in any change to the power production systems and helps to ensure that a reduction in GHG emissions does not result in significant increases in other environmental impacts. Early LCA studies of power generation with CCS report a wide range of results, as they focus on specific CO_2 capture cases only. Furthermore, previous work and commercial LCA software have a rigid approach to system boundaries and do not recognise the importance of the level of detail that should be included in the Life Cycle Inventory (LCI) data.

This research developed a complete LCA framework for the "cradle-to-grave" assessment of alternative CCS technologies in carbon-containing fuel power generation. A comprehensive and quantitative Life Cycle Inventory (LCI) database, which models inputs/outputs of processes at high level of detail, accounts for technical and geographic differences, generates LCI data in a consistent and transparent manner was developed and arranged and flexible structure.

The developed LCI models were successfully applied to power plants with alternative post-combustion chemical absorption capture and oxy-fuel combustion capture. The results demonstrate that most environmental impacts come from power generation with CCS and the upstream process of coal production at a life-cycle perspective. LCA results are sensitive to the type of coal used and the CO_2 capture options chosen. Moreover, the models developed successfully trace the fate of elements (including trace metals) of concern throughout the power generation, CO_2 capture, transport and injection chain. Monte Carlo simulation method combined with the LCI models was applied to quantify the uncertainty of emissions of concern.

A novel analytical framework for the LCA of CO_2 storage was also developed and applied to a saline aquifer storage field case. The potential CO_2 leakage rates were quantified and the operational and geological parameters that determine the ratio of CO_2 leakage total volume of CO_2 injected were identified.

“The fear of the Lord is the beginning of knowledge.”

Proverbs 1:7

Acknowledgements

I would especially like to thank my supervisors Professor Sevket Durucan and Dr. Anna Korre for their dedication and continuous support and supervision throughout this Thesis. Many of the achievements of the present research would not have been possible without their guidance, encouragement, and original ideas. Their comments and suggestions were always precise and led to significant improvements of my work. Their help and support with many practical aspects regarding my living in London, my bursary and the Hilary Bauerman Trust funding are also very much appreciated. I also would like to thank Dr. Anna Korre for teaching me the GaBi LCA software.

Thanks also extended to the Vattenfall Research and Development AB for exchanging data for oxy-fuel combustion processes and organising a short visit to their offices. Their experiences of building the world first oxy-fuel combustion pilot power generation plant helped me to get the insight into the oxy-fuel combustion processes.

I feel fortunate to meet a group of intelligent people, my previous and current colleagues in the research group, who have accompanied me through the past four years. In the sequence of appearance, they are: Dr. Ji-Quan Shi, Dr. Claire Imrie, Dr. Gabriela Munoz-Melendez, Dr. Ruben Martinez-Rubio, Dr. Mustafa Ahsan, Dr. Munyindei Masialeti, Paula Ramirez-Munoz, Fei Xia, Maria Lathouri, Annuwat Wattanawan, Sharidah Mohd Amin, Shafiuddin Amer Syed, Rajesh Govindan, James Smith, Giacomo Bacci, Meng Wang and Dr. Calgar Sinayuc. Many thanks for their interesting discussions on all sorts of topics. Best wishes for the future to you all.

Finally, last, but definitely not least, thanks to my parents, my brother Zhengqiang and my best friend Xiaoqi for all their support, encouragement and understanding throughout.

Table of Contents

List of Figures

List of Tables

List of Abbreviations

ADP:	Abiotic Resources Depletion Potential
AFT:	Adiabatic Flame Temperature
Ag:	Silver
AMP:	2-amino-2-methyl-1-propanol
AP:	Acidification Potential
As:	Arsenic
ASFH:	Air Separation Filter House
ASU:	Air Separation Unit
ATR:	Autothermal Reforming
Ba:	Barium
BAT:	Best Available Techniques
Be:	Beryllium
BF:	Biased Firing
BHIP:	Bottombole Injection Pressure
BOOS:	Burners-Out-of-Service
BP:	British Petroleum
CBA:	Costs Benefit Analysis
CCL:	Compacted Clay Liner
CCS:	Carbon Dioxide Capture and Storage
CCWs:	Combustion Solid Wastes
Cd:	Cadmium
CDM:	Clean Development Mechanism
CDM:	Clean Development Mechanism
CDM:	Clean Development Mechanism
CFCs:	Chlorofluorocarbons
CH_3Br:	Methyl Bromide
CH_4:	Methane
Cl:	Chlorines
CML:	Centre of Environmental Science
Co:	Cobalt
CO_2:	Carbon Dioxide
CO2CRC:	Cooperative Research Centre for Greenhouse Gas Technologies
COE:	Costs of Electricity
Cr:	Chromium
Cu:	Copper
Daf:	Dry ash-free basis
DCB:	Dichlorobenzene
DCC:	Direct Contact Cooler
DEA:	Diethanolamine

DGA:	Diglycolamine
DIPA:	Diisorpropanolamine
DMC:	Direct Material Consumption
DMI	Direct Material Input
DTI:	Department of Trade and Industry
EA:	Environmental Auditing
EA:	Energy Analysis
EC:	EC: European Commission
ECBM:	Enhanced Coalbed Methane
ECBM:	Enhanced Coalbed Methane
EF:	Ecological Footprint
EGR:	Enhanced Gas Recovery
EIA:	Environmental Impact Assessment
EIA:	Environmental Impact Assessment
ELS:	Eco-Label Scheme
ELS:	Eco-Label Scheme
EMAS:	Eco-Management and Audit Scheme
EMAS:	Eco Management and Audit Scheme
EMS:	Environmental Management System
EOR:	Enhanced Oil Recovery
EOR:	Enhanced oil Recovery
EP:	Eutrophication Potential
EP:	Ecotoxicity Potential
EPA:	Environmental Protection Agency
EPA:	Environmental Protection Agency
EPD:	Environmental Product Declarations
EPD:	Environmental Product Declarations
EPER:	European Pollutant Emissions Register
ESP:	Electrostatic Precipitators
EU:	European Union
EUP:	Energy Using Products Directive
EUP:	Energy Using Products Directive
FAETP:	Freshwater Aquatic Ecotocicity Potential
FD:	Force Draft
FeS_2:	Pyritic Sulphur
FGD:	Flue Gas Desulphurisation
FGRR:	Flue Gas Recycle Ratio
GaBi	GaBi LCA software
GCL:	Geosynthetic Clay Liner
GE:	General Equilibrium
GHGs:	Greenhouse Gases

GTL:	Gas to Liquid
GWP:	Global Warming Potential
H:	Hydrogen
HCFCs:	Hydrochlorofluorocarbons
HCL:	Hydrochloric Acid
HEED:	Hydroxyethyl ethylenediamine
HEI:	Hydroxyethyl imidazolidone
HF:	Hydroflouric Acid
Hg:	Mercury
HHV:	Higher heating value
HSS:	Heat Stable Salts
HTP:	Human toxicity Potential
HTS:	High Temperature Shift
IEA:	International Energy Agency
IGCC:	Integrated Gasification Combine Cycles
IOA:	Inpute-Output Analysis
IPCC:	Intergovernmental Panel on Climate Change
IPP:	Integrated Product Policy
IPP:	Integrated Product Policy
ISO:	International Organisation for Standardisation
JI:	Joint Implementation
JT:	Joint Implementation
JT:	Joint Implementation
KS1:	A kind of hindered amine developed by Japanese company Mitsubishi
K^+/PZ	Promoted potassium carbonate
LCA:	Life Cycle Assessment
LCC:	Life-Cycle Costing
LCI:	Life Cycle Inventory
LCIA:	Life Cycle Impact Assessment
LCIA:	Life Cycle Impact Assessment
LCM:	Life-Cycle Management
LEA:	Low Excess Air
LHV:	lower heating value
LNB:	Low NOx Burners
LP:	Low pressure
LSFO:	Limestone with Forced Oxidation
MAC:	Main Air Compressor
MAETP:	Marine Aquatic Ecotoxicity Potential
MCS:	Monte Carlo Simulation
MD:	Measured Depth
MDEA:	N-methyldiethanolamine

MEA:	Monoethanolamine
MEL:	Magnesium-Enhanced Lime
MFA:	Material Flow Analysis
MFA:	Material Flow Accounting
MIPS:	Material Intensity Per Unit Service
Mn:	Manganese
MTS:	Medium Temperature Shift
MW:	Megawatt
N:	Nitrogen
NGCC:	Natural gas combined cycle power plant
NH_3:	Ammonia
Ni:	Nickel
NMHC:	Non-methane hydrocarbon
NMVOC:	Non-Methane Volatile Organic Compounds
NO:	Nitrogen Oxide
NO_2:	Nitrogen Dioxide
NO_2:	Nitrogen Dioxide
NOx:	Nitrogen Oxides
O:	Oxygen
ODP:	Ozone Depletion Potential
OECD:	Organisation for Economic Co-operation and Development
OFA:	Overfire Air
OOIP:	Original Oil in Place
PAS:	pressure swing operation
Pb:	Lead
PCDDs:	Polychlorinated Diebenzofurans
PCDFs:	Polychlorinated Dibenzodioxins
PCF:	PCF: pulverised coal fired power plant
PCFs:	Perfluorochemicals
PDF:	Probability Distribution Functions
PHX:	Primary Heat Exchanger
PM:	Particulate Matter
POCC:	Partial Oxidation (nature gas) Combined Cycle
POCP:	Photochemical Oxidant Creation Potential
POX:	Partial Oxidation
PPM	Part Per Million
S:	Sulfur
Sb:	Antimony
SCGT:	Semi-Closed Gas Turbine Cycle
SCNR:	Selective Non-catalyst Reduction
SCR:	Selective Catalyst NOx Reduction

Se:	Selenium
SEA:	Strategic Environmental Assessment
SEEA:	System of Economic and Environmental Accounting
SEEA:	System of Economic and Environmental Accounts
SETAC:	Society of Environmental Toxicology and Chemistry
SETAC:	Environmental Toxicology and Chemistry
SFA:	Substance Flow Analysis
SFs:	Sulfur hexafluoride
SMR:	Steam Methane Reforming
SOx:	Sulfur Oxides
SV	Space Velocity
TAR:	3rd Assessment Report
TDS:	Total dissolved solids
TEA:	Triethaolamine
TETP:	Terrestrial Ecotoxicity Potential
Ti:	Thallium
TMR:	Total Material Requirement
TR:	Transformer-Rectifier
TSA:	Temperature-Swing Adsorption
TVD:	True Vertical Depth
UCT:	Upper column Turbine
UNFCCC:	United Nations Framework Convention on Climate Change
USCPF:	Ultra-supercritical pulverised coal fired power plant
V:	Vanadium
WMUs:	Waste Management Units
Zn:	Zinc

Chapter 1 Introduction and Objectives

1.1 Introduction

The world relies heavily on carbon-containing fuels and virtually all the energy produced from carbon-containing fuels is generated by directly burning fuels in air. Approximately 86% of global energy utilised and about 75% of current anthropogenic CO_2 emissions originate from fossil fuels. The total emissions from fossil fuel use and flaring of natural gas were 24 $GtCO_2$ per year (6.6 GtC) in 2001(IPCC, 2005), which is considered to be the dominating contributor to the global warming. Primary energy will continue to be dominated by carbon-containing fuels in the 21st century. In order to stabilise the atmospheric CO_2 concentration at 450 to 750 ppmv, the level that prevents dangerous anthropogenic interference with the climate system, cumulative emissions of hundreds of gigatonnes of CO_2 would need to be prevented during this century (IPCC, 2001).

Carbon dioxide capture and storage (CCS) is a process consisting of separation of CO_2 from industrial and energy-related sources, transport to a storage location, and long-term isolation from the atmosphere (Figure 2.1). Due to its compatibility with the current energy infrastructures and the potential to reduce CO_2 emissions significantly, CO_2 capture and geological storage is recognised as one of the main options in the portfolio of greenhouse gas (GHG) mitigation technologies being developed worldwide.

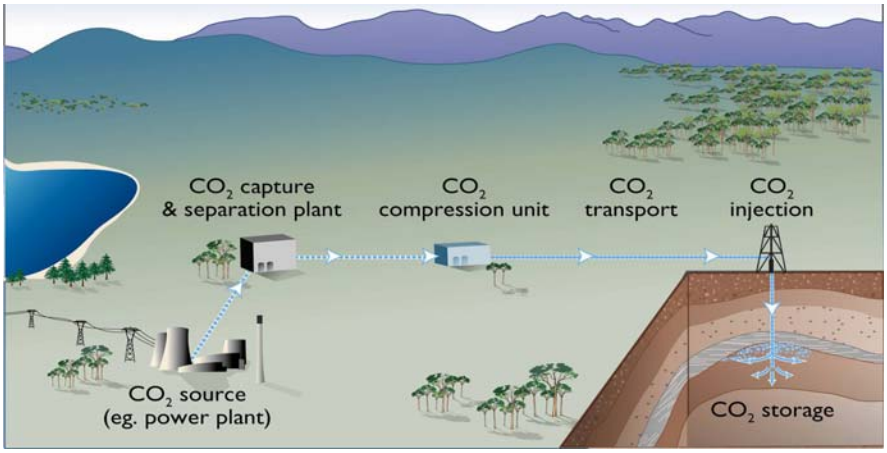

Figure 1.1: An example of carbon dioxide capture and storage (CCS) system (After CO2CRC, 2005).

The large deployment of CCS is likely to occur around 2030 and it is estimated that this can achieve a 25% cut in global emissions by 2050 (IEA, 2004; IPCC, 2005). Since power production is responsible for over 30% of global CO_2 emissions, capturing from electricity plants offers the best initial potential for capturing and storing the CO_2 generated from carbon-containing fuel use. IEA predicts that CO_2 capture in the electricity sector will represent around 65% of total CO_2 capture in 2050 (IEA, 2004). Major energy players worldwide, such as BP, Shell and Vattenfall, have already made a commitment to initiate projects of power generation with CCS, with the expectation that, in the medium term, power generated from plants with CCS will be cheaper, more convenient and more flexible than alternative energies. Moreover, CCS allows the use of coal resources while reducing CO_2 emissions dramatically, and the use of coal instead of oil or gas may also have important benefits such as security of supply and lower the volatility of global oil and gas prices.

However, CO_2 capture and storage systems require significant amounts of energy during their implementation. For example, the increase in fuel consumption per kWh for plants that capture 90% CO_2 by using best current technology ranges from 24–40% for new supercritical pulverized coal plants, 11–22% for Natural Gas Combined Cycle (NGCC) plants, and 14–25% for coal-fired Integrated Gasification Combined Cycle (IGCC) systems compared to similar plants without CCS facilities (IPCC, 2005). Furthermore, the increased consumption of fuels and chemicals, such as monoethanolamine (MEA) and limestone used for CO_2 capture and flue gas desulphurisation, results in an increase in both on-site and upstream GHG emissions and other environmental impacts per kWh generated relative to plants without CO_2 capture.

The known and currently developed CCS technologies offer a number of alternatives, which involve different energy consumption and subsequent environmental impacts. Therefore, it is imperative to conduct a comprehensive environmental assessment on alternative CCS options in power generation, which is capable of tracking GHG releases throughout all stages of power generation life cycle and provide accurate information for decision makers to ensure that a CCS option selected does not result in upstream or downstream changes that will increase the overall release of GHGs. It is also important to ensure that CCS processes used do not aggravate other environmental concerns, such as solid and hazardous waste generation and the release of toxic substances which impact upon human health and ecological systems. This requires a holistic and system-wide environmental assessment rather than focusing on emissions of greenhouse gases only.

Life cycle assessment (LCA) meets this criteria as it not only tracks energy and non-energy related GHG releases but also tracks various other environmental releases (e.g. solid wastes, toxic substances and common air pollutants) as well as the consumption of other resources (e.g. water, minerals and land use). This holistic perspective offered by LCA helps decision makers to quantify the trade-offs inherent in any change to the power production systems and helps to ensure that a reduction in GHG emissions does not result in increases in other environmental impacts. The other strength of LCA is that the International Organization for Standardization (ISO) has developed the ISO 14040 series of LCA standards, which provide guidance on setting appropriate system boundaries, reliable data collection, evaluating environmental impacts, interpreting results, and reporting in a transparent manner. This offers an excellent starting point for the development of measurement protocols for GHGs and other environmental impacts (Brady, 2000). Finally, under the Kyoto Protocol, three flexible mechanisms (Emissions Trading, Joint Implementation (JI) and the Clean Development Mechanism (CDM)) were developed to help emitters in developed countries to meet their GHG emission targets. As a credible and internationally accepted tool, LCA offers the means to include CCS projects into the CDM framework and help the participants of flexible mechanisms to assess their proposed projects and verify their emission reductions from a life-cycle perspective.

Previous LCA studies (Akai *et al*., 1997; Flaschi *et al*., 2000; Doctor *et al*., 2001; CISS, 2003; Lombardi *et al*, 2003; Corti and Lombardi, 2004; Odeh and Cockerill, 2008; Jitsopa *et al*., 2006) have investigated power generation plants with alternative CO_2

capture systems and concluded that CO_2 capture can reduce CO_2 emissions by around 80% throughout the life-cycle of power generation. However, rather than investigating full life-cycle emissions and environmental impacts of the CCS system, majority of these studies analysed life-cycle Greenhouse Gas (GHG) emissions or energy efficiencies only, and they all neglected CO_2 storage processes. Pehnt and Henkel (2008) investigated the full chain of power generation with CCS but focused on air emissions only, not considering the emissions to water and soil in full. CO_2 leakage is briefly discussed in the study but storage processes are not fully investigated. Another recent LCA study carried out by Knoorneef *et al*. (2008) investigated post-combustion CO_2 capture, transport and injection with full Life Cycle Impact categories, yet the study is case specific and does not capture the technical and geographical differences in power generation with CCS. This study does not investigate fully the storage processes either. Moreover, previous studies and commercial LCA software (e.g. TEAM, GaBi 4, Ecoinvent, SimaPro 7, ETH-ESU 96, and U.S. LCI Database) have a very rigid approach to system boundaries and do not recognise the importance of the level of detail that should be included in the Life Cycle Inventory (LCI) data. So far, the LCI data considered for power generation have all been at plant level (or gate-to-gate data) rather than being at the level of unit processes inside the plants. The gate-to-gate data used in previous studies imply that the electricity generation systems have been largely simplified to a single black-box with constants and linear coefficients used as inputs and outputs, covering a broad range of technological and geographical differences, in which the actual variability of process technological parameters and operating conditions are thus implicitly neglected. Consequently, these simplifications limit the possibility of tracing emissions back to individual unit processes and restrict one's ability to represent technical and geographical differences in the environmental assessment of power generation systems.

Furthermore, unlike conventional LCA studies covering manmade systems only, the LCA of CO_2 storage processes involve natural systems – the CO_2 storage formations. After CO_2 is injected into a storage formation, some fraction of it remains as a free phase, some dissolves into the in situ formation fluids (oil or water), some is immobilised by capillary forces and some is converted to minerals. The distribution of these phases will change spatially and temporally. In some cases, the injected CO_2 may leak from the storage formations through fractures, permeable zones, and abandoned wells that intersect the CO_2 storage formation. Currently, there is no LCA analytical

framework for the CO_2 storage processes.

Therefore, it is essential to develop a complete and dynamic LCA model dedicated to CCS, which can characterise the environmental profiles of alternative CCS technologies at a high level of detail and allow for technical and spatial differences. The main objectives the research described in this thesis were:

i) to develop a complete LCA framework for the "cradle-to-grave" assessment of alternative CCS technologies in carbon-containing fuel power generation; and
ii) to develop a comprehensive and quantitative Life Cycle Inventory (LCI) database, which models inputs/outputs of processes at high level of detail (at component unit process level), allows for technical and geographic differences, aims at generating reliable and precise LCI data in a consistent and transparent manner and with a clearly arranged and flexible structure for long term strategic energy system planning and decision-making; and
iii) to compare alternative CCS technologies in power generation and to identify opportunities which can reduce environmental impacts and improve energy efficiencies in a life-cycle perspective.

Given that there are a number of fossil fuel sources, capture technologies, and storage options for power generation with CCS; priority was given to the development of an LCA model which represented at least one technological option at every stage of the process in order to ensure that the functionality of the model is demonstrated.

1.2 Thesis Structure

This thesis is presented in 12 Chapters. Chapters 2 and 3 present the background and literature review of CCS technologies and the LCA applications on power generation with CCS. Chapter 4 develops a methodological framework for the application of LCA on power generation with CCS. Chapters 5, 6, 7, 8, and 9 develop life cycle inventory (LCI) models for the processes throughout the power generation and CCS Chain. Chapters 10 and 11 present the LCIA results obtained using the LCI models developed.

Chapter 2 introduces the general concept of alternative CO_2 capture technologies and the three routes of integrating CO_2 capture technologies into fossil fuel power generation systems. Alternative CO_2 geological storage methods and their storage mechanisms are also reviewed in this Chapter.

By means of literature review, Chapter 3 introduces the concept and methodological framework of LCA and previous LCA applications on power generation with CCS. The limitations of previous LCA applications are also discussed in this Chapter.

After having reviewed the alternative CCS technologies in Chapter 2 and previous LCA applications in Chapter 3, Chapter 4 develops a complete and dynamic framework for the application of LCA on power generation with alternative CCS options, which can characterise the environmental profiles of these CCS technologies at high level of detail (component unit process level) and account for the technical and spatial differences, as well as quantifying the uncertainty of LCA results. The LCA for CO_2 geological storage systems is also analysed in this Chapter.

Using the life cycle inventory (LCI) modelling methodology developed in Chapter 4, , Chapter 5 presents the life cycle inventory (LCI) models for component processes in conventional power generation plants, including the LCI models of coal combustion, particulate matters control, NO_x emission control, SO_x emission control, and solid waste disposal.

Having developed LCI models for basic processes in conventional power plants, Chapter 6 presents the LCI models for specific processes in oxy-fuel combustion CO_2 capture power plants, including the LCI models of the air separation unit, oxy-fuel combustion process, and CO_2 conditioning.

Chapter 7 presents the LCI models for specific processes in post-combustion CO_2 capture power plants, including the LCI models of chemical absorption CO_2 capture and CO_2 conditioning units.

Chapter 8 presents the LCI models for the processes connecting CO_2 capture and CO_2 storage, including the LCI models of CO_2 pipeline transportation and CO_2 injection.

Utilising the LCI models developed in Chapters 5, 6, 7 and 8, Chapters 9 and 10 present the LCA results of power plants with post-combustion capture and oxy-fuel combustion capture with transport and injection respectively. The results of direct emissions, resource consumption, and the materials used by power plants with post-combustion and oxy-fuel combustion systems are generated in Chapters 9 and 10 respectively. The Life cycle impact analysis, sensitivity analysis and uncertainty analysis are also conducted in these Chapters to identify the opportunities to reduce the environmental impacts in a life-cycle perspective.

Due to the complexity of CO_2 storage process and the uncertainties associated with the potential CO_2 leakages, the saline aquifer CO_2 storage system is analysed separately. Chapter 11 presents the LCI model of the CO_2 saline aquifer storage system, which captures the spatial and geological differences of CO_2 saline aquifer storage and potential leakage. A case study with sensitivity analysis is also conducted in this Chapter to demonstrate the strength of the model developed and to identify the most important parameters for CO_2 storage process or CO_2 leakage.

Finally, Chapter 12 presents the main conclusions and accomplishments of the research and makes recommendations for further research.

Chapter 2 Carbon Capture and Storage

2.1 Introduction

The world's climate has always varied naturally, but compelling evidence from around the world, including increases in global average air and ocean temperatures, widespread melting of snow and ice and rising global average sea level, indicate that "warming of the climate system is unequivocal", and most of the observed rise in global average temperatures since 1950 is "very likely" (>90% likelihood) due to the observed increase in anthropogenic carbon dioxide and other greenhouse gases (GHGs) (e.g. methane and nitrous oxide) concentrations in the atmosphere (IPCC, 2007a). GHGs affect the climate system by altering the outgoing infrared (thermal) radiation reflected by the Earth's surface and the increase of GHG concentrations in the Earth's lower atmosphere can lead to a warming of the climate system. The global atmospheric concentrations of CO_2, CH_4, and N_2O increased from pre-industrial values of about 280ppm, 715ppb and 270ppb to 379ppm, 1774ppb and 319ppb in 2005 respectively (Figure 2.1), and the total CO_2 equivalent concentration of these gases currently being estimated to be around 455 ppm CO_2-eq (range: 433–477 ppm CO_2-eq) (Forster *et al.*, 2007). The world faces a temperature rise in the range of 4-6°C by 2100 if greenhouse gas emissions continue to increase at their current pace and the climate change is liable to disrupt natural patterns of climate and consequently increases the frequency and/or intensity of natural disasters, such as heat waves, cold days, heavy precipitations, and incidence of extreme high sea level (IPCC, 2007b; IEA, 2008).

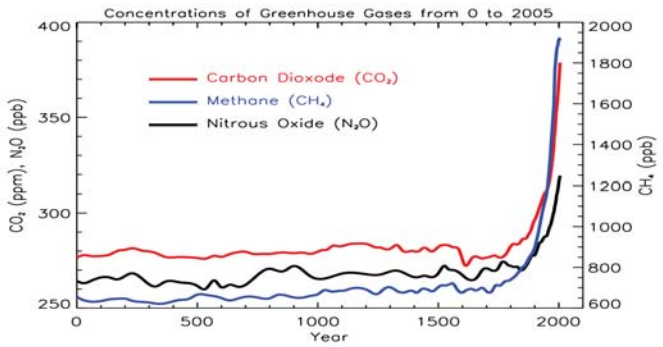

Figure 2.1: Atmospheric concentrations of important long-lived greenhouse gases over the last 2,000 years. Increases since about 1750 are attributed to human activities in the industrial era. Concentration units are parts per million (ppm) or parts per billion (ppb), indicating the number of molecules of the greenhouse gas per million or billion air molecules, respectively, in an atmospheric sample (After Forster *et al.*, 2007).

2.1.1 Global Anthropogenic Greenhouse Gas Emissions and Energy Consumption

Global anthropogenic GHG emissions arise from emissions of CO_2 (76.7%), CH_4 (14.3%), N_2O (7.9%) and F-gases (HFCs, PFCs and SF_6) (1.1%), Figure 2.2 (Oliver *et al.*, 2006; IPCC, 2007b). The anthropogenic CO_2 emissions are due primarily to fossil fuel use, with deforestation providing another significant but smaller contribution; the CH_4 emissions due to human activities predominantly come from agriculture and fossil fuel use; and anthropogenic N_2O emissions are primarily due to agriculture, Figure 2.2 (Oliver *et al.*, 2006; IPCC, 2007b). It is worthy of note that energy-related CO_2 emissions (or CO_2 emissions from fossil fuel use) alone account for 56.6% of total anthropogenic GHG emissions (in CO_2 equivalent), and energy supply (electricity and heat generation) represents the single largest source of GHG emissions, about 26% of total anthropogenic GHG emissions in 2004, Figure 2.2. GHG emissions from energy supply, industry, transport, and residential sector are predominantly energy-related CO_2 emissions.

On the other hand, global consumption of primary energy and the energy-related emissions of CO_2 continue an upward trend from 1980 to the early years of the 21st century, and fossil fuels are the dominant form of primary energy utilised in the world (80.5% in 2004), Figure 2.3 (IEA, 2005; Sims *et al.*, 2007; IEA, 2008). World primary energy demand will continuously increase, and fossil fuels will still be the dominant form of energy utilised in the world if no new climate change policies are imposed worldwide (IPCC, 2005; IPCC, 2007b; IEA, 2008). IEA predicts that fossil fuels will

account for 83% of world primary energy consumption in 2030 and world primary energy demand will expand by 45% between 2006 and 2030, with an average rate of increase of 1.6% per year, with coal accounting for more than a third of the overall rise, and energy-related CO_2 emissions solely will reach 41 Gt in 2030 (26.1 Gt in 2004), without the introduction of effective policies by governments, Figure 2.3 (IEA, 2008).

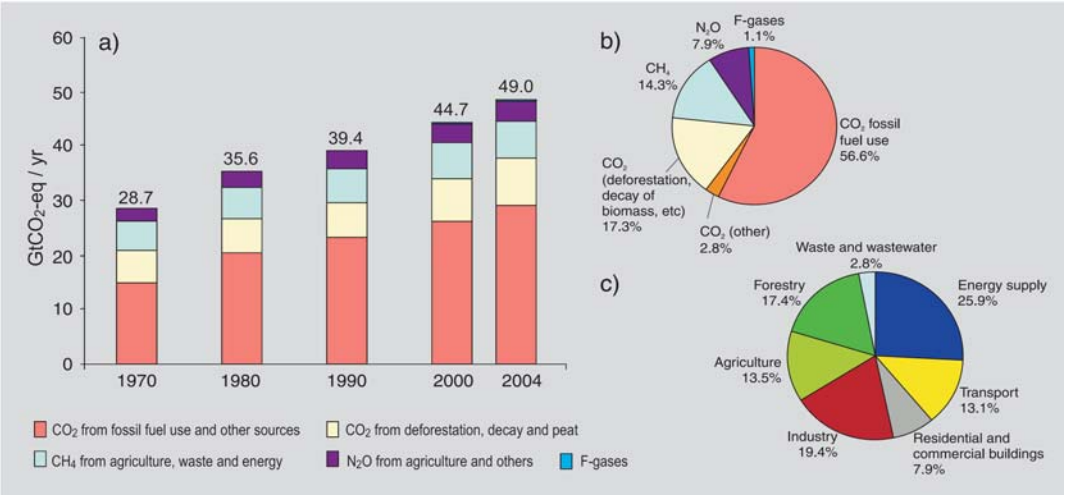

Figure 2.2: (a) Global annual emissions of anthropogenic GHGs from 1970 to 2004; (b) Share of different anthropogenic GHGs in total emissions in 2004 in terms of CO_2-eq.; (c) Share of different sectors in total anthropogenic GHG emissions in 2004 in terms of CO_2-eq (After IPCC, 2007b).

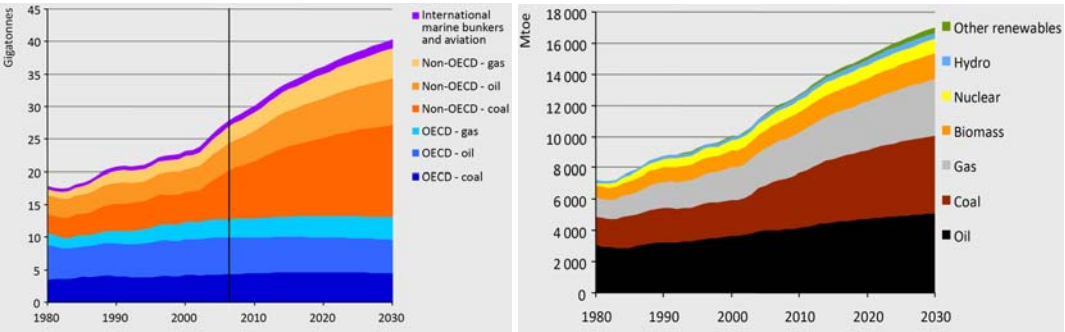

a) b)

Figure 2.3: a) Projected world primary energy demand; b) Energy-related CO_2 emissions predicted (After IEA, 2008)

2.1.2 Options for the Reduction of Greenhouse Gas Emissions

Article 2 of United Nations Framework Convention on Climate Change (UNFCCC) sets its objective as the 'stabilisation of greenhouse gas concentrations in the atmosphere at a level that would prevent dangerous anthropogenic interference with the climate system' (UN, 1992). In order to meet this objective, hundreds and thousands Gt of GHGs are required to be reduced over the course of the century (IPCC, 2005).

A wide variety of technological options have the potential to reduce net GHG emissions and/or GHG atmospheric concentrations, and there may be further options developed in the future. These options mainly include: to improve energy efficiency, to switch to less carbon-intensive fossil fuels, renewables (hydro power, wind, solar, bio-energy, geothermal energy), nuclear, CO_2 capture and storage (CCS in power generation, CCS in industry, CCS in fuel transformation), or to sequester CO_2 through the enhancement of natural or biological sinks (IPCC, 2005).

2.1.3 The Role of Carbon Dioxide Capture and Storage

It is commonly accepted that no single technology can provide all of the mitigation potential in any sector, and a large portfolio of technological options either currently available or expected to be commercialised in coming decades will be used to meet both energy demand and GHG emission mitigation targets over the course of the century (IPCC, 2005; Sims *et al.*, 2007; IEA, 2008). Carbon dioxide capture and storage (CCS) is a process consisting of separation of CO_2 from industrial and energy-related sources, transport to a storage location, and long-term isolation from the atmosphere (Figure 2.4). The estimates of the role CCS to mitigate GHG emissions vary, because the contribution of different GHG mitigation technologies varies over time and region and depends on the availability of these technologies, relative costs, environmental policies and the GHG emission mitigation targets (Sims *et al.*, 2007).

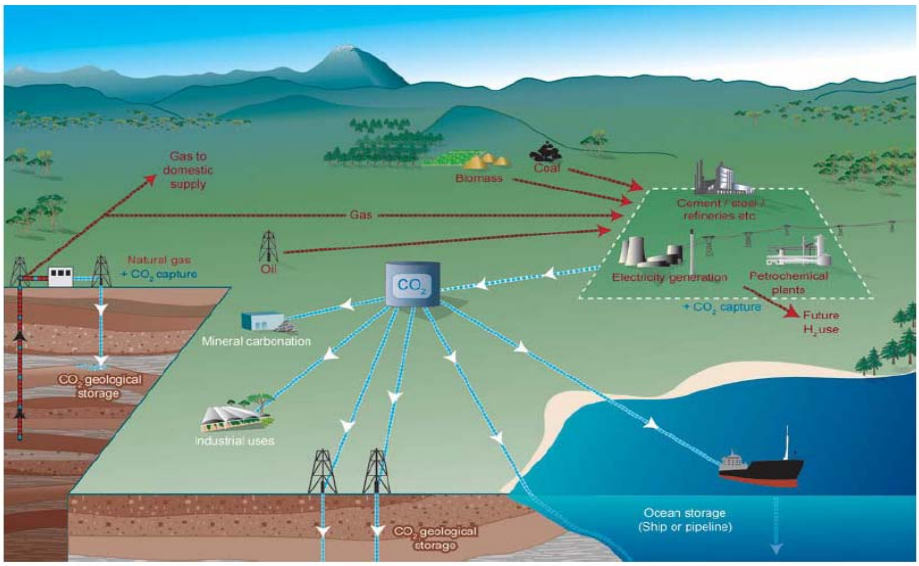

Figure 2.4: Possible carbon dioxide capture and storage systems illustrating the sources for which CCS might be relevant, as well as CO_2 transport and storage options (After CO2CRC, 2005).

Based on IPCC 3rd Assessment Report (TAR) mitigation scenarios, the average share of CCS in total emissions reductions (2000–2100) ranges from 15% for scenarios aiming at the stabilisation of CO_2 concentrations at 750 ppmv to 54% for 450 ppmv scenarios, and the average cumulative CO_2 storage (2000–2100) across the scenarios ranges from 380 Gt CO_2 in the 750 ppmv stabilisation scenarios to 2,160 $GtCO_2$ in the 450 ppmv scenarios (IPCC, 2001; IPCC, 2005).

2.1.4 Large Stationary Carbon Dioxide Sources

The feasibility of a particular CO_2 source for capture and storage is determined by its volume, concentration, partial pressure and distance to the storage formations. It is preferred to apply CO_2 capture to large point sources, and the CO_2 would then be compressed and transported to the appropriate geological formation (IPCC, 2005).

Table 2.1 lists the profile of worldwide large stationary CO_2 sources, where CO_2 is emitted as large emission volumes (>0.1 Mt CO_2 yr^{-1}) that make them amenable to the addition of CO_2 capture technology (IPCC, 2005). The table illustrates that more than 50% of energy-related CO_2 emissions come from large stationary CO_2 sources and CO_2 emissions from power generation account for 78% of CO_2 emissions from large stationary CO_2 sources.

Table 2.1: Profile by process or industrial activity of worldwide large stationary CO_2 sources with emissions of more than 0.1 $MtCO_2$ per year (Adapted from IPCC, 2005).

Process	Number of sources	Emissions ($MtCO_2$/yr)	Average emissions per source ($MtCO_2$/yr)
Fossil fuels			
Power (coal, gas, oil and others)	4,942	10,539	2.13
coal	2,025	7,984	3.94
gas	1,728	1,511	0.87
oil	1,345	980	0.73
others	81	64	0.79
Cement production	1,175	932	0.79
Refineries	638	798	1.25
Iron and steel industry	269	646	2.40
Petrochemical industry	470	379	0.81
Oil and gas processing	N/A	50	
Other sources	90	33	0.37
Biomass			
Bioethanol and bioenergy	303	91	0.30
Total	7,887	13,466	
Energy-related CO_2 emission in that year	-	22,639	

The majority of these emission sources has concentrations of CO_2 typically lower than 15% and has CO_2 partial pressure in the range of 0.01-0.06 MPa, Table 2.2 (IPCC, 2005). This implies that energy used for the capture of CO_2 from various sources is similar. The lower concentrations of CO_2 in flue gases also rule out the possibility of storing all flue gases instead of storing CO_2 solely, because it requires more storage capacity and large amount of energy for flue gas compression, transportation and injection. Carbon dioxide concentration in the flue gas from cement kilns or blast furnaces in steel mills are usually higher than that in power generation processes (IEA GHG, 1999).

Table 2.2 Properties of candidate gas streams that can be inputted to a capture process (After IPCC, 2005).

Source	CO_2 concentration % vol (dry)	Pressure of gas stream MPa[1]	CO_2 partial pressure MPa
CO_2 from fuel combustion			
Power station flue gas:			
Natural-gas-fired boilers	7–10	0.1	0.007–0.010
Gas turbines	3–4	0.1	0.003–0.004
Oil-fired boilers	11–13	0.1	0.011–0.013
Coal-fired boilers	12–14	0.1	0.012–0.014
IGCC[2]: after combustion	12–14	0.1	0.012–0.014
Oil refinery and petrochemical plant fired heaters	8	0.1	0.008
CO_2 from chemical transformations + fuel combustion			
Blast furnace gas:			
Before combustion[3]	20	0.2–0.3	0.040–0.060
After combustion	27	0.1	0.027
Cement kiln off-gas	14–33	0.1	0.014–0.033
CO_2 from chemical transformations before combustion			
IGCC: synthesis gas after gasification	8–20	2–7	0.16–1.4

1. 0.1 MPa = 1 bar.
2. IGCC: Integrated gasification combined cycle.
3. Blast furnace gas also contains significant amounts of carbon monoxide that could be converted to CO_2 using the so-called shift reaction.

The geographical distribution of large CO_2 emission sources (> 0.1 MtCO2 yr^{-1}) falls in four clusters by region: North America (the Midwest and the Eastern Seeboard of the USA), North West Europe, South East Asia (eastern coast) and Southern Asia (the Indian sub-continent), Figure 2.5. Mapping the geographical distribution of the large emission sources with geological storage opportunities, previous studies demonstrate that there is a good match between sources and opportunities, and a substantial proportion of the emission sources are either on top of, or within 300 km from, a site with potential for geological storage (Bradshaw and Dance, 2004; IPCC, 2005).

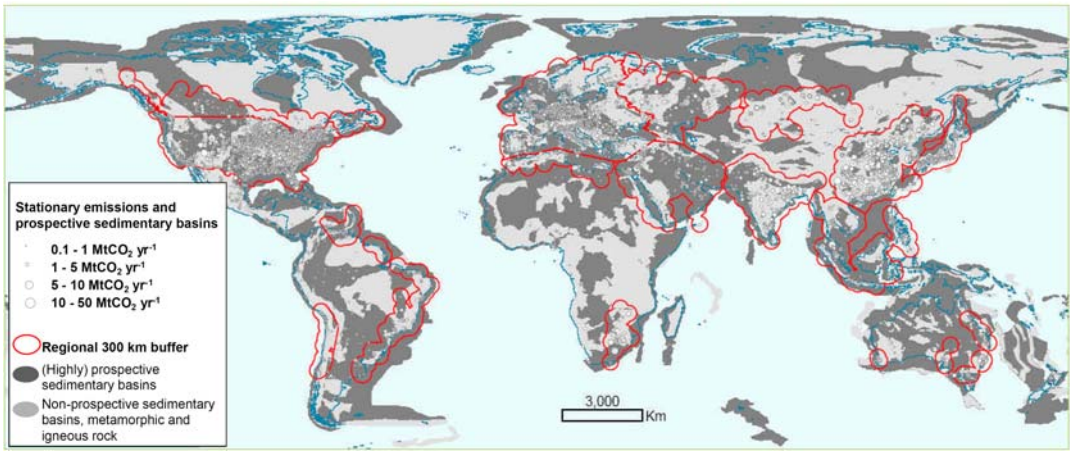

Figure 2.5: Regional emission clusters with a 300 km buffer relative to world geological storage prospectively (After IPCC, 2005).

2.2 Carbon Dioxide Capture

The purpose of CO_2 capture is to produce a concentrated CO_2 stream that can be readily transported and stored. A wide variety of methods have been developed for the capture of CO_2 from gas streams. These methods and their principles can be described as follows:

- Chemical absorption, using reversible chemical reaction of absorption liquids (solvents) with CO_2 to separate gases. Solvents can be regenerated by heating up the CO_2-rich loading solvent (Figure 2.6a);
- Physical absorption, using the different solubility of gaseous components in absorption liquids (solvents) to separate gases, and solvents can be regenerated by lowering the pressure (Figure 2.6a);
- Adsorption, using the different solubility of gaseous components in a solid (sorbent) to separate gases. Sorbent regeneration is achieved by lowering the pressure (pressure swing adsorption) or increasing the temperature (temperature swing adsorption) (Figure 2.6a);
- Membrane separation, using selective barriers to separate gases (Figure 2.6b);
- Cryogenic distillation, utilising the difference in points of condensation of separate gases (Figure 2.6c).

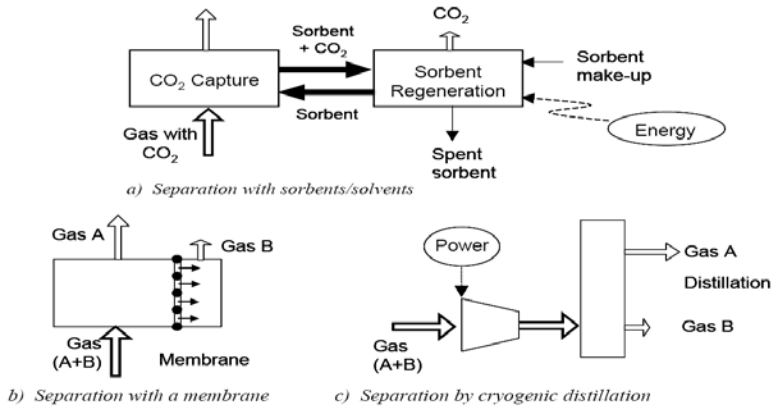

Figure 2.6: General schemes of the main separation processes relevant to CO_2 capture (After IPCC, 2005).

The characteristics of alternative CO_2 capture methods are summarised in Table 2.3. Capture of CO_2 from power generation process generally means that at some point in the process CO_2 needs to be separated from the flue gases. Three alternative approaches can integrate CO_2 capture technologies with power generation systems: post-combustion, pre-combustion and oxy-fuel combustion capture (Figure 2.7).

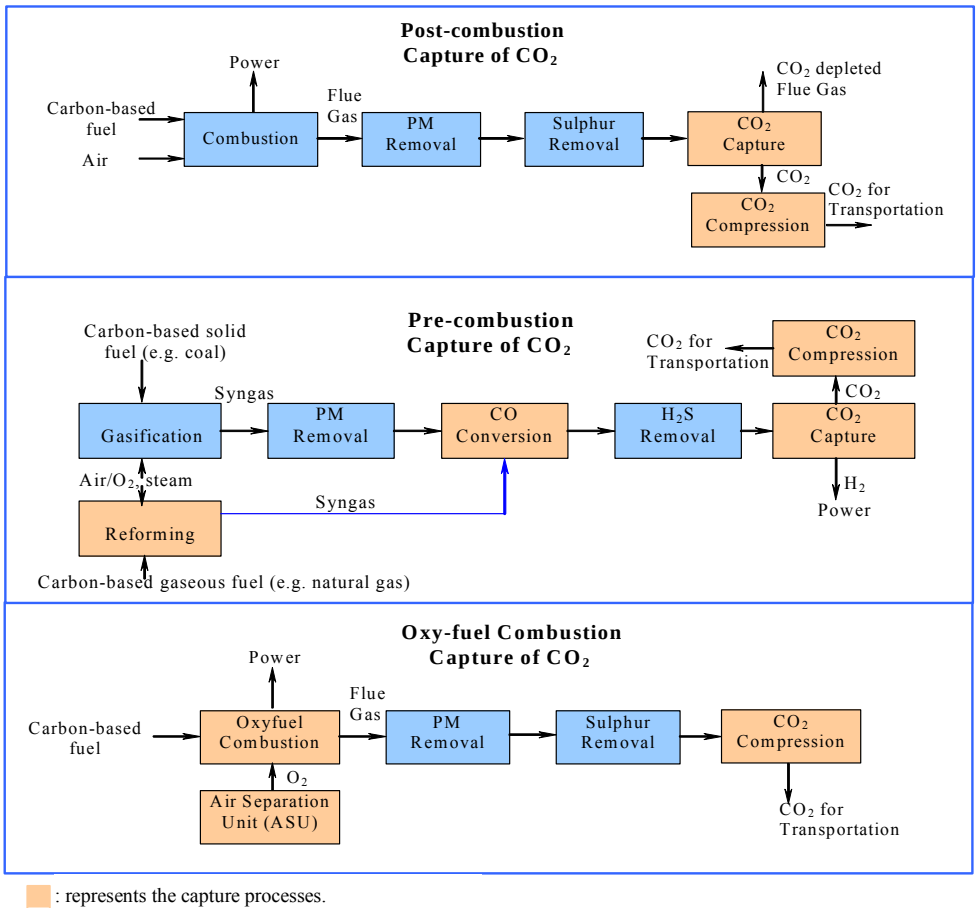

Figure 2.7: CO_2 capture approaches in power generation.

Table 2.3: Summary of CO_2 capture methods (Modified from Sass *et al*, 2005 and IPCC, 2005).

Capture Methods		Description	Example Separation Material	Comments
Absorption	Chemical absorption	Process involves capturing CO_2 using a reversible reaction between CO_2 and an aqueous solution of an amine or an alkaline salt. The amine or alkaline salt is regenerated (by pressure reduction and heating) and recirculated.	Monoethanolamine (Klusman 2003c),Diethanolamine (DEA), diglycolamine (DGA), methyldiethanolamine (MDEA), sterically hindered amines; Potassium carbonate with additives such as boric acid or glycine to increase the solution capacity for CO_2.	Used at the commercial scale to remove low concentrations of acid gases (e.g. CO_2) from natural gas or breathing air. Solution tends to saturate with high CO_2 loading, so the process is more efficient for lower CO_2 concentrations. CO_2 capacity of salt solution (even with additives) is lower than that of amine solutions
	Physical absorption	CO_2 captured using physical dissolution in an absorption fluid. The fluid is regenerated (by pressure reduction and moderate heating) and recirculated.	Propylene carbonate, N-methyl-2-pyrrolidone (or Purisol), methanol (or Rectisol), dimethyl ether of polyethylene glycol (or Selexol), methyl-isopropyl ether of polyethylene glycol.	Used at the commercial scale to remove high concentrations of acid gases (e.g. CO_2) from natural gas. More efficient for high CO_2 partial pressure (i.e. concentration and/or pressure). Does not typically remove acid gases as completely as chemical or hybrid absorption.
	Hybrid absorption	CO_2 captured using a combination of chemical absorption and physical dissolution. The fluid is regenerated (by pressure reduction and moderate heating) and recirculated.	Sulfolane (tetrahydrothiopene 1,1-dioxide) (physical solvent) and diisopropanolamine (DIPA) or MDEA (chemical solvent), sterically hindered amines, MDEA plus proprietary solvents.	Used at the commercial scale to remove intermediate concentrations of acid gases (e.g. CO_2) from natural gas.
Adsorption		Process involves using the intermolecular forces between gases and the surfaces of solid sorbent materials to capture CO_2. The sorbent is loaded at high pressure and regenerated by pressure reduction and, in some cases, heating.	Molecular sieves, activated alumina, zeolites, activated carbon.	Used at the commercial scale to remove CO_2 and other impurities from H_2. Some hydrogen gas cleanup processes also produce high purity CO_2.
Membrane	Gas separation membrane	Process involves pressurising the flue gas and separating CO_2 from other gases by preferential permeation through a membrane. CO_2 is collected near atmospheric pressure as a permeate.	Semipermeable membranes made of polymeric (e.g. polyphenylene oxide, cellulose acetate, polysulfone, or polyamide), metallic (e.g. Pd/Ag), ceramic (e.g. Alumina, Silica) materials.	Used at the commercial scale to recover CO_2 used for enhanced oil recovery (EOR) (i.e. high CO_2 concentration). Requires two or more separation stages to reach a CO_2 removal of 90% and purity of 99%. Each stage requires compression, and the process typically is used for gas with high CO_2 content (e.g. pulverized coal/O_2 plants). Membranes are very sensitive to particulate fouling.
	Gas absorption membrane	The process involves using a semipermeable membrane as a barrier between the flue gas and an absorption fluid. Preferential removal of CO_2 from the gas stream occurs because the fluid (e.g. MEA) selectively absorbs CO_2	Microporous membranes made of Teflon®, polyphenyleneoxide, or polydimethylsiloxane	Innovative process. The membrane allows a high surface area for transfer between the gas liquid phases without requiring two streams to mix. As a result gas separation unit is more compact than the tall towers needed for chemical or physical absorption Membranes are very sensitive to particulate fouling.
Cryogenic separation		Flue gas is cooled and compressed to condense CO_2 which can then be captured and purified by distillation	Not applicable	Used at the commercial scale to recover CO_2 used for EOR (i.e. high CO_2 concentration). Gas fed to the cryogenic separation unit must be dehydrated to prevent formation of solids (e.g. ice and CO_2 clathrates). Due to energy needed to reach cryogenic conditions, cryogenic separation typically is used for gas with high CO_2 content (e.g. pulverized coal/O_2 plants).

Post-combustion systems separate CO_2 from the flue gases produced by combustion of a primary fuel (coal, natural gas, oil or biomass) in air. The fraction of CO_2 present in the flue gas streams is typically 3–15% by volume, and other main constituent in flue gas is nitrogen. Due to the low concentration and low pressure of CO_2 in flue gas, chemical absorption carbon capture methods are more applicable to post-combustion systems. Main systems of reference for post-combustion capture are the current installed capacity of 2,261 GWe of oil, coal and natural gas power plants and, in particular, 155 GWe of supercritical pulverized coal fired plants and 339 GWe of natural gas combined cycle (NGCC) plants, both representing the types of high efficiency power plant technology where CO_2 capture can be best applied (IPCC, 2005).

In pre-combustion capture systems, carbon-based fuels are reacted with oxygen or air and/or steam in a gasifier (for solid fuels) or reformer (for gaseous fuels) to give a 'synthesis gas (syngas)' mainly composed of carbon monoxide (CO) and hydrogen (H_2). The syngas passes through a CO Conversion Unit, where the carbon monoxide is reacted with steam in a catalytic reactor, called a shift reactor, to give CO_2 and more hydrogen. The high concentrations of CO_2 produced by the shift reactor (typically 15 to 60% by volume on a dry basis) and the high pressures often encountered in these applications are more favourable for CO_2 separation. Therefore, physical absorption or membranes can be used for CO_2 capture in pre-combustion systems. The power plant systems of reference for pre-combustion are oil and coal-based, integrated gasification combine cycles (IGCC), which are around 0.1% of total installed capacity worldwide but they are considered to be strategically important in an increasingly carbon-constrained world, because of their capacity to deliver a suitable mix of electricity, hydrogen and lower carbon-containing fuels at a large scale and at high thermal efficiencies.

Oxy-fuel combustion systems use pure oxygen for combustion instead of air, resulting in a flue gas with high CO_2 concentrations (greater than 80% by volume), which may be directly delivered to storage site after the water vapour is removed by cooling and compressing the gas stream. Oxy-fuel combustion requires the upstream separation of oxygen from air, with a purity of 95–99% oxygen assumed in most current designs. Oxygen is usually separated from air by cryogenic distillation. The power plant system of reference for oxy-fuel combustion capture systems are the same as those noted in post-combustion capture systems. Oxy-fuel combustion systems are still in demonstration phase. The Vattenfall pilot plant at Schwarze Pumpe in Germany, the

world's first oxy-fuel combustion pilot plant, with a capacity of 30 MWh and a CO_2 capture rate of 90%, commenced operations in September 2008 and aims to verify the interaction between all components, the achievable level of CO_2 capture, and the ability to scale up the plant (Vattenfall, 2008).

The choice of specific capture method for a power generation system is determined largely by the power plant conditions. The schemes of the possible technology options for capture of CO_2 in power generation are represented in Figure 2.8.

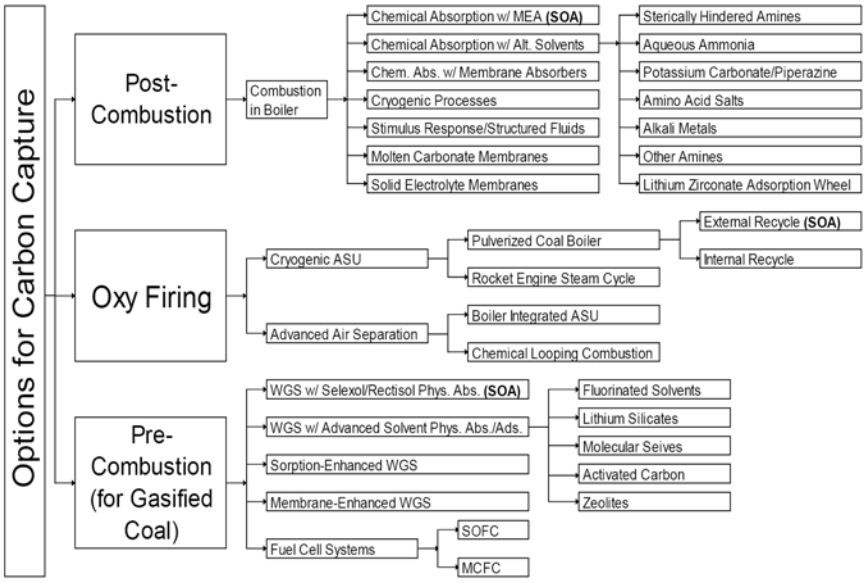

SOA = state of the art; WGS = water gas shift reaction

Figure 2.8: Schematic representation of technology options and pathways for CO_2 capture (After Esber, 2006).

To date, CO_2 chemical or physical absorption are well-developed technologies that have been applied to numerous commercial processes, including gas treatment and ammonia production, but, when capturing CO_2 from power plants, the improvement of solvent performance is obviously needed to reduce plant sizes and the energy required for sorbent regeneration (IPCC, 2005). Other CO_2 capture methods may have been applied in niche applications, but significant advancements are required in these technologies before implementation in power plants can be considered. For instance, with membranes, high purity streams are difficult to achieve, particularly on the large scale CO_2 capture; Adsorption has been tested, but a low capacity and poor CO_2 selectivity limit the potential for application to CO_2 capture; Cryogenic separation of CO_2 would produce a high pressure, liquid CO_2 stream, but the costs of refrigeration are often prohibitive.

2.3 Carbon Dioxide Geological Storage

Sedimentary basins are the mostly likely location for storing CO_2, because typical sedimentary basins consist of alternating layers of coarse sandstone, which have high porosity and permeability, allowing the CO_2 to be injected into it and serving as storage reservoir, and fine-textured sediments (clay, shale, or evaporates), which have very low permeability, acting as seals to prevent CO_2 migrating back to the surface (Benson, 2005; IPCC, 2005). Naturally occurring CO_2 reservoirs existing worldwide have proved that the CO_2 can remain underground for millions of years or longer (IPCC, 2005). In addition, many oil and gas reservoirs also contain large quantities of CO_2 confirming that oil and gas reservoirs can store CO_2 over geologic time scales (Benson, 2005). Four principle types of geologic formations are considered to have significant potential for storing large amounts of CO_2 (Benson, 2005):

- active and depleted oil reservoirs;
- active and depleted gas reservoirs;
- saline formations; and
- deep coal seams and coalbed methane formations.

2.3.1 Carbon Dioxide Storage Mechanisms

Carbon dioxide can remain underground by a combination of physical or chemical trapping mechanisms, including: structural and stratigraphic trapping, residual CO_2 trapping, solubility trapping, mineral trapping, and adsorption trapping. These five trapping mechanisms are described in the following sections.

Structural and Stratigraphic Trapping

Structural and stratigraphic trapping refers to trapping CO_2 below low-permeability seals (caprocks), such as very-low-permeability shale or salt beds, which is the principal means to store CO_2 in geological formations. Structural traps comprise folded or fractured rocks. Faults can act as permeability barriers in some circumstances and as CO_2 leakage pathways in other circumstances (Salvi *et al.*, 2000). Stratigraphic traps are formed by changes in rock type caused by variation in the setting where the rocks were deposited (IPCC, 2005). Structural and stratigraphic trapping requires that the formation pressure must not exceed the allowable overpressure to avoid fracturing the caprock or re-activating faults (Streit *et al.*, 2005).

Residual Trapping (or Capillary Trapping)

Carbon dioxide can be trapped as a residual, non-wetting phase in the pore spaces of the rock, which is referred to as residual trapping. When CO_2 is injected into a saline formation, it displaces the saline formation water and then migrates upwards driven by buoyancy forces, because it is less dense than the formation water. As free phase CO_2 migrates upward, the gas saturation of zones from which free gas CO_2 is migrating out decrease. It is that decrease in saturation that can act to trap CO_2 by capillary snap-off (Ide *et al*., 2006). This means that once the saturation of CO_2 drops below the residual "gas" saturation, it is no longer mobile and consequently will remain trapped (Benson, 2005). The importance of this trapping mechanism is expected to contribute significantly to the security of geologic storage (Benson, 2005; Ide *et al*., 2006).

Solubility Trapping

Solubility trapping refers to the dissolution of CO_2 in the formation water or the reactions between CO_2 and the water to form carbonic acid and other aqueous carbonate species (Nelson *et al.*, 2005). Solubility trapping also occurs during CO_2 flooding EOR, where the injected CO_2 dissolves in the crude oil contained in the reservoir (Nelson *et al.*, 2005). The pore space where the immobile, nonrecoverable fraction of the crude oil remains is the geologic formation for the CO_2 storage (Shaw and Bachu, 2002).

Mineral Trapping

In mineral trapping, dissolved CO_2 undergoes chemical reactions with the sodium and potassium basic silicate, or calcium, magnesium, and iron carbonate, or silicate minerals in the reservoir formation to form bicarbonate ions, and continued reaction of the bicarbonate ions with calcium, magnesium, and iron from silicate minerals such as clays, micas, chlorites, and feldspars present in the rock matrix to finally form carbonate minerals (IPCC, 2005). Sandstone aquifers rich in glauconite, illite, anorthite, chlorite, or smectite minerals and low in carbonates are the most favourable geologic sinks for mineral trapping of CO_2 (Nelson *et al.*, 2005). Mineral trapping results in the most stable, permanent form of geologic CO_2 storage, but it is slow (thousands to millions of years) (White *et al.*, 2003; IPCC, 2005).

Adsorption Trapping

In physical adsorption, CO_2 molecules are immobilised at near liquid like densities on micropore wall surfaces of coal organic matter, kerogen, or minerals (Nelson *et al.*,

2005). The hydrostatic pressure in the formation controls the gas adsorption process (IPCC, 2005). Coal seams and shales are types of geological formations for physical adsorption trapping (White *et al*., 2003).

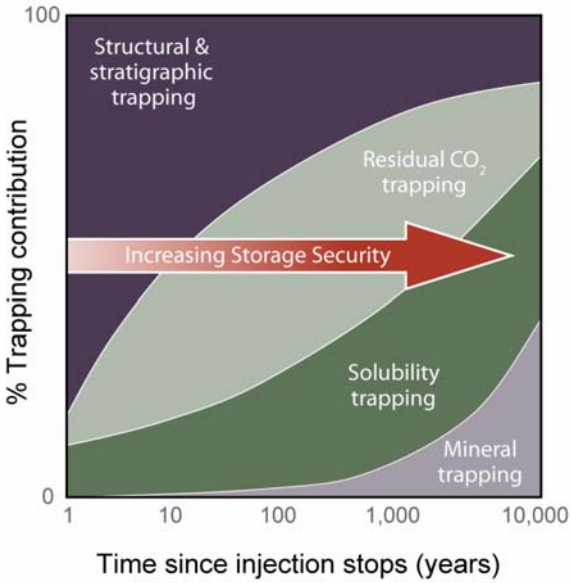

Figure 2.9: Storage mechanisms and changes over time (After IPCC, 2005)

Carbon dioxide storage depends on the combination of these mechanisms. Over time, the contribution of each of these mechanisms to provide secure long-term storage will change as illustrated in Figure 2.9. Initially, physical trapping will be the dominant mechanism for retaining CO_2 in the storage formation. As CO_2 migrates away from the injection well it will displace some fraction of the in situ fluids and simultaneously dissolve in the pore fluids. After CO_2 injection ceased, a fraction of CO_2 will be immobilised by residual trapping, as the CO_2 plume migrates up driven by buoyancy. Over a long time, a further fraction of CO_2 is dissolved in pore fluids by the convection flows (described in detail in the CO_2 saline aquifer storage LCI modelling section). Mineral tapping is expected to be slow but, over long time scales (over thousands to millions of years) may trap a significant fraction of the CO_2, the extent of which will depend on the mineralogy of the formation.

2.3.2 Alternative Carbon Dioxide Geological Storage Operations

Figure 2.10 demonstrates that geological storage of CO_2 can be operated in a variety of geological settings in sedimentary basins.

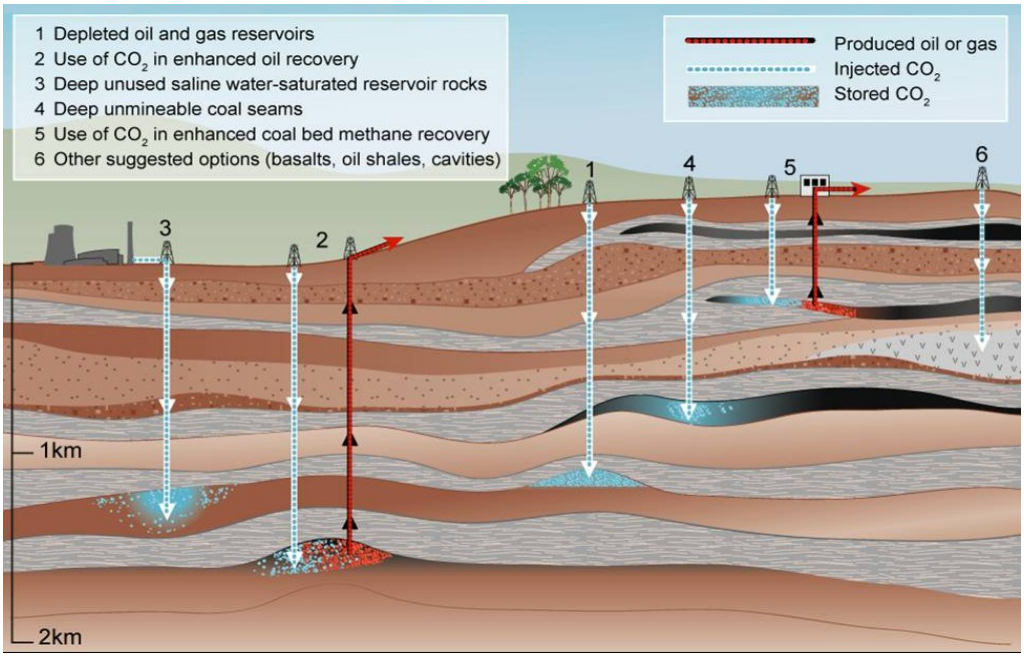

Figure 2.10: An overview of geological storage options (After CO2CRC, 2005).

Carbon Dioxide Enhanced Oil Recovery

Carbon dioxide enhanced oil recovery (CO_2-EOR) technology achieves incremental oil recovery by CO_2 flooding through miscible or immiscible displacement. Miscible displacement involves the injected CO_2 dissolving in the oil and lower its viscosity to improve the flow rate of the oil. In the case of the immiscible displacement, the CO_2 remains physically distinct from the oil and it expands and thereby pushes additional oil to production wells, after CO_2 is injected into the reservoir. Miscible or immiscible displacements are strongly dependant on the reservoir temperature, pressure and crude oil composition (IPCC, 2005). Miscible displacement leads to an incremental recovery of about 7 to 15 percent of the original oil in place (OOIP) and immiscible displacement yields an incremental recovery of up to 10% of OOIP (Heddle *et al*., 2003). In CO_2-EOR applications, more than 50% of the injected CO_2 returns with the produced oil and is usually separated and re-injected into the reservoir (Bondor, 1992), and the remainder is trapped in the oil reservoir by various mechanisms, such as irreducible gas saturation, dissolution and capillary trapping (IPCC, 2005). CO_2-EOR has been applied in many existing projects for more than 50 years and may be further implemented because of the incremental oil recovery (IPCC, 2005). For instance, Weyburn CO_2-enhanced oil recovery (CO_2-EOR) project located in the Williston Basin (Canada) is expected to inject 23 $MtCO_2$ and extend the life of the oil field by 25 years (Law, 2005). Since CO_2 injection began in late 2000, the EOR project has performed largely as predicted and all

produced CO_2 is captured and recompressed for reinjection into the production zone (IPCC, 2005).

Carbon Dioxide Enhanced Coalbed Methane

In the case of CO_2 enhanced coalbed methane (CO_2-ECBM), the CO_2 is injected in the coal seam and it displaces methane in the coal matrix, consequently enhancing coalbed methane recovery, because CO_2 has a greater affinity to coal than methane (Shi and Durucan, 2005). Coal contains fractures (cleats) and between cleats, solid coal has a very large number of micropores into which gas molecules from the cleats can diffuse and be tightly adsorbed. Coal can physically adsorb many gases such as CO_2 and methane and, if saturated, coalbed methane reservoirs can absorb five times the methane by volume than a conventional natural gas reservoir of comparable size (Shi and Durucan, 2005). Carbon dioxide enhanced coalbed methane recovery is potentially attractive because it can store the injected CO_2 and enhance methane production from the coal seam at the same time, however, this option is not well developed, and a better understanding of the injection and storage processes in coals is needed (IPCC, 2005).

Saline Aquifer Storage

In the case of saline aquifer storage, CO_2 is injected to the deep saline aquifers. Saline formations are deep sedimentary rocks saturated with formation waters or brines containing high concentrations of dissolved salts, which make the formation water unsuitable for agriculture or human consumption (IPCC, 2005). To make full use of the storage capacity, the injected CO_2 should be stored in its dense or supercritical phase, i.e., above the critical pressure of 7.4 MPa and critical temperature of 31^{o}C, which requires that the depth of the saline formation is more than 800 m (Heddle *et al*., 2003). Since the CO_2 at supercritical phase is still less dense than formation water, it will naturally migrate to the top of the formation, therefore, a low permeability caprock is needed to prevent CO_2 from moving upwards. Over the time, the CO_2 injected in the saline aquifer is trapped by a combination of trapping mechanisms including: structural or stratigraphic trapping, solubility trapping, capillary trapping and mineral trapping. Deep saline formations are believed to have the largest capacity for CO_2 storage and are more widespread than other options (IPCC, 2005). Sleipner project in North Sea demonstrated the first successful industrial scale CO_2 storage in saline aquifers.

Depleted Oil or Gas Reservoirs

Oil and gas reservoirs can be used for CO_2 storage after their oil or gas reserves are depleted. Injected CO_2 is immobilised in the supercritical phase by structural or stratigraphic trapping. In the depleted oil or gas reservoirs, the injected CO_2 will generally occupy the pore space previously occupied by oil and/or natural gas. However, not all the previously (hydrocarbon-saturated) pore space will be available for CO_2 because some residual water may be trapped in the pore space due to capillary forces, viscous fingering, and gravity effects (Stevens *et al.*, 2001). CO_2 storage in depleted oil and natural gas reservoirs is promising in some areas, because reservoir structures are well known and infrastructure is already in place.

Other geologic formations such as marine and arctic hydrates, mined cavities in salt domes and oil shale can provide niche opportunities but are likely to be developed only after the principle storage formations are utilised (Benson, 2005).

The global capacity of CO_2 storage in deep underground is promising. According to the IPCC report (IPCC, 2005), depleted oil and gas reservoirs are estimated to have a storage capacity of 675–900 Gt CO_2; deep saline formations are likely to have a storage capacity of 10,000 Gt CO_2; the capacity of unminable coal formations is uncertain, with estimates ranging from as little as 3 Gt CO_2 up to 200 Gt CO_2. It is likely that potential storage capacity will exist in the areas where CO_2 is generated from large stationary sources, because most of world's population is concentrated in the regions underlain by sedimentary basins (Gunter *et al.*, 2004).

2.3.3 Carbon Dioxide Leakage and Potential Leakage Pathways

The injected CO_2 that exists as a separate phase (supercritical, liquid, or gas) serving as leakage source in the CO_2 geological storage formations may escape from the formations driven primarily by the buoyancy (as CO_2 is less dense than formation water) through the following pathways:

- Any new or abandoned wells intersecting the storage formations and surrounding zone;
- Any geological faults intersecting the storage formation(s) and surrounding zone;
- Permeable zones existing in the caprock and consisting of permeable silt and sand lenses or subseismic fault-fracture networks;

- The "spill point" of the storage site;
- Seismic movement (Earthquake) induced fractures.

Figure 2.11 demonstrates the potential CO_2 leakage pathways considered for saline aquifer formations.

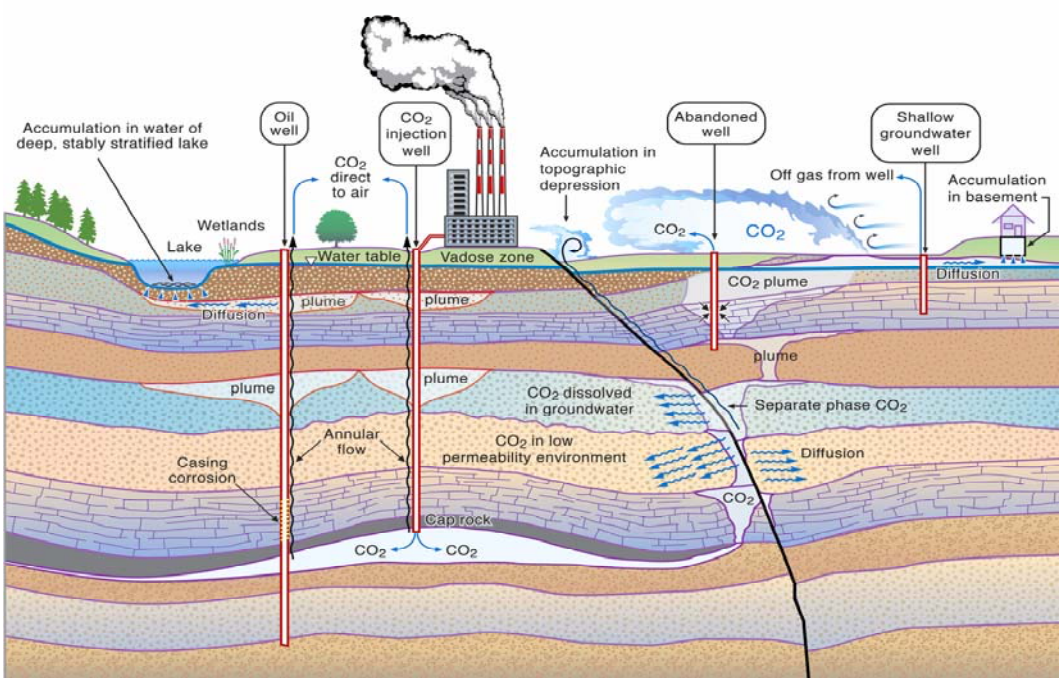

Figure 2.11: Potential CO_2 leakage pathways in saline aquifer CO_2 storage formations (After Zhang *et al.*, 2006).

In fact, worldwide accepted CO_2 storage performance standards with respect to leakage rate have not been established. IPCC Special Report on CCS considers that 1% leakage over 1,000 years (0.001% annually) is likely for well selected and managed storage sites (IPCC, 2005). CO2CRC (2005) concluded the retention rate of 99% over 1,000 years as a good performance standard. Hepple and Benson (2004) concluded that 0.01% leakage from storage formations per year would be effective as a greenhouse gas mitigation method.

2.3.4 Potential Environmental Impacts of Carbon Dioxide Leakage

Potential environmental impacts of CO_2 leakage include global warming, human health and safety, adverse effect on ecosystems, groundwater contamination, metals mobilisation, and soil gas replacement (see Figure 2.12).

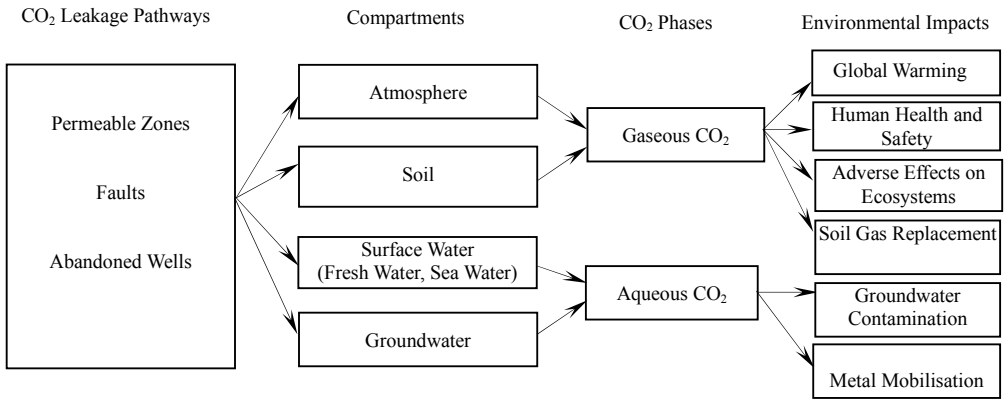

Figure 2.12: Potential environmental impacts of CO_2 storage and leakage

Global Warming

When CO_2 is leaked to the atmosphere, it causes global warming impacts. This is the primary environmental impact of CO_2. A general warming effect felt on Earth's surface, produced by GHGs, e.g. CO_2 is defined by the increase of the average temperature on Earth (IPCC, 2007b). GHGs allow incoming solar radiation to pass through the Earth's atmosphere, but trap heat by preventing some of the infrared radiation from the Earth's surface from escaping to outer space. This process occurs naturally and has kept the Earth's temperature about 33^{o}C warmer than it would otherwise be (IPCC, 2007b). However, the greenhouse effect is becoming stronger as a result of human activities, which is causing the warming observed over the past century (IPCC, 2007b).

Human Health and Safety and Adverse Effects on Ecosystems

Hazards to human health and safety arise exclusively from elevated CO_2 concentrations in ambient air, which results in oxygen defficiency. At concentrations between 2-5%, CO_2 has an effect on respiratory physiology, and at concentrations between 7–10%, it can cause unconsciousness after minutes to hours, and at concentrations between 10–15%, CO_2 can cause unconsciousness within minutes, with death taking place shortly thereafter with continued exposure. Upon breathing 30% CO_2 and above unconsciousness occurs in under a minute and perhaps after several breaths; death takes place after several minutes (Benson, 2005; IPCC, 2005). Animals can tolerate higher concentrations of CO_2 without adverse effects. Tests on soil invertebrates, for instance, showed first physiological responses at 2-3% concentrations of CO_2 with death occurring at concentrations as low as 15 % and as high as 60% (Benson *et al.*, 2002).

Groundwater Contamination and Metal Mobilisation

Dissolved CO_2 can adversely impact groundwater in two ways. First, if CO_2 migrates from a storage reservoir into shallow groundwater, the dissolution of CO_2 will acidify the groundwater, potentially affecting shallow groundwater used for potable water and industrial and agricultural needs (Singleton, 2007). Secondly, dissolved CO_2 forms carbonic acid, reducing the pH of the solution and potentially causing the dissolution of sulphate, chloride, and additional metals that previously were bound within the formation rock; and possibly giving the water an odd odour, colour, or taste (IPCC, 2005). In the worst case, contamination might reach dangerous levels, and groundwater may not be used for drinking or irrigation. In addition, the acidic groundwater adversely affects the root structures of plants and vegetation and may result in widespread death of the vegetation (Singleton, 2007).

Soil Gas Replacement

When CO_2 releases into vegetated areas, the soil gas is replaced by CO_2. This may cause noticeable die-off of vegetation. In the areas where CO_2 makes up about 20–95% of the soil gas, whereas normal soil gas usually contains about 0.2–4% CO_2, significant impacts to vegetation have occurred (IPCC, 2005). At concentrations above 5% CO_2 may be dangerous for vegetation, and as concentration approaches 20%, CO_2 becomes phytotoxic, as CO_2 can cause death of plants through 'root anoxia' (IPCC, 2005).

2.3.5 Environmental Impacts of Impurities Presented in Injected Carbon Dioxide

Impurities such as SOx, NOx, H_2S and other trace elements, such as As, B, Ba, Be, Cd, Co, Cr, Cu, Ge, Hg, Mn, Mo, Ni, Pb, Sb, Se, Sn, Sr, U, V and Zn, may be injected along with CO_2 into CO_2 geological storage formations, because these impurities are incorporated in CO_2 when captured from power plants. This may cause additional environmental impacts (Bryant and Lake, 2005; Knauss *et al.*, 2005; Apps, 2006).

Under normal circumstances, since power plants are equipped with SOx and NOx control processes, only small amounts of SOx, NOx constituents are likely be co-injected with CO_2 in the storage formation, and their impact in corroding the injection zone host rocks and modifying ground water composition would be minor (Apps, 2006).

Many hazardous trace elements in coal are volatilised during combustion processes and these volatilised species either nucleate as solid or liquid particles, or are adsorbed on the fly ash. Therefore, trace elements co-injected with CO_2 would be at low concentrations, which is comparable to or less than the confining shale beds of the injected aquifer and their average concentrations could be less than the native concentrations of these elements in the host rock (Apps, 2006). It is suggested that the trace elements would be present at negligible concentrations, and have no impact on the chemistry of the injected geological formations (Apps, 2006).

When SOx and NOx are deliberately injected with CO_2 into geological formations, Preliminary modelling studies conducted by Xu *et al*. (2005a) to investigate the fate of SOx and NOx co-injected with CO_2 in deep saline aquifers concluded that the major chemical changes in the injection zone is expected in the case of the injection of SO_2 and the injection of NOx species is expected to be less consequential, but nitrogen chemistry, particularly in association with injected SO_2, is not well-understood and requires further investigation (Xu *et al*., 2005a, b).

2.3.6 Current Commercial Scale Projects with Carbon Capture and Storage

To date, there are four commercial-scale CCS projects in operation: the Sleipner project in Norway where CO_2 is captured from natural gas and stored in a deep saline aquifer since 1996; the Weyburn project in US/Canada where CO_2 is captured from coal gasification based polygeneration system and is used to enhance oil recovery and ultimate storage since 2000; the In Salah project in Algeria where CO_2 is captured from natural gas and stored in the aquifer zone of one of the shallow gas producing reservoirs since 2004; and the Snøhvit project which started in 2007 in the Barrents Sea where natural gas produced offshore is transported to a liquefied natural gas (LNG) plant onshore through a 143 kilometres multiphase pipeline, while the CO_2 extracted from the natural gas is re-injected into a saline aquifer zone. However, there are no existing projects with fully integrated power generation with CCS at large scale which would characterise their future deployment. The worldwide ongoing and planned CO_2 capture and storage projects are listed in Appendix A, Tables A1 and A2.

2.4 Conclusions

Power generation with CCS plays an important role in the portfolio of GHG mitigation options. CO_2 capture involves complex processes and all CO_2 capture methods require additional energy and material inputs for operation as well as releasing environmental emissions. As a consequence, CCS may increase the environmental impacts due to onsite CO_2 capture processes or due to the upstream processes such as coal mining or solvent production such as monoethanolamine (MEA). Therefore, it is necessary to compare the life cycle environmental impacts of power generation with CO_2 capture and power generation without CO_2 capture in a holistic perspective by considering the processes involved in power generation, CO_2 capture, transport and storage, as well as the upstream processes concerned.

Geological CO_2 storage involves complex natural systems, which may contain potential CO_2 leakage pathways. If CO_2 would leak from the storage formations through these pathways, it would result in environmental impacts such as groundwater contamination, metal mobilisation, soil gas replacement, adverse impacts on ecosystems as well as human health and safety issues. Moreover, the time frame of a CO_2 storage system lasts thousands of years. These require an innovative framework to analyse the environmental impacts of natural systems, as conventional environmental impact assessment methods all deal with manmade systems or processes and only cover a time frame of several decades.

There are a number of alternative CO_2 capture and storage options. This implies that there is no simple or common model that could represent all the environmental impacts of various CO_2 capture or storage options. Therefore, all CCS technologies available have to be considered and modelled in a modular fashion to take advantage of the common aspects in each GHG mitigation option selected.

Chapter 3 Life Cycle Assessment and its Applications in CO_2 Capture and Storage

3.1 Introduction

One of great challenges faced by current world economies is "to integrate environmental sustainability with economic growth and welfare by decoupling environmental degradation from economic growth" (EC, 2008). New environmental policies have been introduced by many nations, aiming to transform the environmental challenges to economic opportunities. The focus of environmental policies has shifted away from regulating direct emissions to single environmental media (e.g. water, soil or air) in the 1970s/80s; to attention on the distribution, consumption and disposal of products in 1990s; and, finally, to all ecological aspects of a product (or a service) along its whole life-cycle from raw material extraction to final disposal since 2000 (Neumann, 2007). Many examples of life-cycle thinking are found in EU environmental policies such as the Eco-Management and Audit Scheme (EMAS), the Eco-Label Scheme (ELS), the Eco-design of Energy Using Products Directive (EUP), and numerous other regulations (EC, 2008). Currently, product-related analysis of life-cycle environmental impacts is voluntary. However, indirect requirements such as a tightening of the waste avoidance act or direct enforcement by the expected future tightening environmental policies encourages producers to carry out life cycle analysis studies.

Life Cycle Assessment (LCA) is a powerful tool for evaluating environmental performance in the family of life-cycle thinking methods. With more than 30 years

development since the LCA concept was introduced in 1969, the methodology of LCA is widely accepted and well established (Contadini, 2002). There are numerous applications of LCA at social and industrial level around the world. For instance, Netherlands uses LCA as the basis of regulatory and permitting systems (ACLCA, 2004). In European Union (EU), Integrated Product Policy (IPP) is implemented through the use of LCA methods (EC, 2008). Vattenfall, EDF, Shell and other leading energy companies use LCA to assess the environmental impact of operations or new projects aiming to improve their environmental performance (Vattenfall, 2007; Le Bocq, 2008; Five winds international, 2005).

As already discussed in Chapter 2, CO_2 capture and storage systems require significant amounts of energy for their operation, and the CCS technologies available offer a number of alternatives, which require variable energy consumption and subsequently produce different environmental impacts. In order to ensure that a given CCS option, besides reducing CO_2 emissions, does not result in a significant increase in other environmental impacts, and in order to identify opportunities for improved designs that minimise the environmental impacts along the CCS chain, the well established LCA method provides the necessary methodological framework. In addition, the use of LCA is very much in line with the life-cycle thinking of current environmental policies and expected future regulations.

This chapter firstly introduces LCA and the LCA methodological framework, discusses the application of LCA at social and company levels including the limitations of the method and current trends of LCA development. Then, the reasons for conducting LCA on CCS systems are explained in detail. Finally, this chapter analyses the previous studies of LCA on power generation and LCA on power generation with CCS and identifies the limitations of these studies.

3.2 Life Cycle Assessment

3.2.1 Definition

The roots of LCA go back to the late 1960s and early 1970s. The detailed history of LCA was described by several authors (Hunt *et al*, 1996; Oberbacher *et al*, 1996; Boustead, 1996; Gabatuler, 1997). The first guidelines for LCA, termed as "Code of Practice", were published in 1993, developed by the Society of Environmental

Toxicology and Chemistry (SETAC). The "Code of Practice" promoted LCA both as a generally accepted term, and as a robust method to assess the environmental performance of products (Jensen et al., 1997). Today the "Code of Practice" has been replaced by a set of standards developed by the International Organization for Standardization in the period 1997 to 2006 (ISO 14040-44).

As defined in ISO 14040 (1997), Life Cycle Assessment (LCA) is a "compilation and evaluation of the inputs and outputs and the potential environmental impacts of a product system throughout its life cycle". In principle, LCA assesses the environmental impacts associated with the whole life cycle of a product system, from raw material extraction, through production, processing, use of the product during the fulfilment of its function, to waste processing of the discarded product (Carlson and Pålsson, 2001). LCA is actually a systems method that facilitates the identification, evaluation and comparison of the environmental impacts of a product system or competing product systems through all stages of their life cycle, as indicated by the occurrences of multi-disciplinarity, the presence of complex systems and handling of a systems model, and the existence of case studies and their iterative nature (Tillman, 2000).

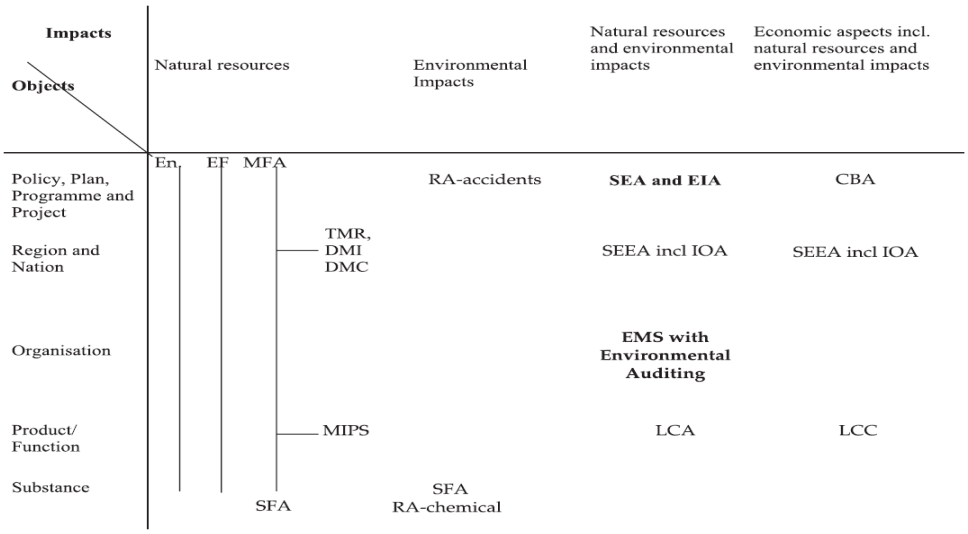

Figure 3.1: The tools are shown in relation to their focus, i.e. the object to which the impacts are related and to which aspects are included in the study. (After Finnveden and Moberg, 2005)

Where: CBA: Costs Benefit Analysis; DMC: Direct Material Consumption; DMI: Direct Material Input; EF: Ecological Footprint; EIA: Environmental Impact Assessment; EMAS: Eco Management and Audit Scheme; EMS: Environmental Management System; En: Energy Analysis; EU: European Union; GE: General Equilibrium; IOA: Inpute-Output Analysis; LCA: Life-Cycle Assessment; LCC: Life-Cycle Costing; LCM: Life-Cycle Management; MFA: Material Flow Accounting; MIPS: Material Intensity Per Unit Service; SEA: Strategic Environmental Assessment; SEEA: System of Economic and Environmental Accounts; SFA: Substance Flow Analysis; TMR: Total Material Requirement.

A large number of tools for assessing environmental impacts are available, such as Environmental Impact Assessment (EIA), System of Economic and Environmental Accounting (SEEA), Environmental Auditing, and Material Flow Analysis (MFA).

Figure 3.1 demonstrates that only LCA addresses both the life-cycle environmental impacts and the product systems (or service systems), while other tools focus on regional environmental impacts, or site specific environmental impacts, or policy or economic aspects (Finnvedden and Moberg, 2005).

3.2.2 The Methodological Framework of Life Cycle Assessment

In order to deal with the complexity of LCA, ISO published four international standards on the topic of LCA, which established a fixed protocol and methodological framework for performing an LCA study, including Goal and Scope, Inventory Analysis, Impact Assessment and Interpretation (Figure 3.2).

Goal and Scope definition states the aim of an intended LCA study, the system boundary, the functional unit, the competing systems considered, and the breadth and depth of (or level of detail) the LCA study in relation to this aim. The functional unit is the quantified performance of a product system for use as a reference unit in an LCA study (ISO 14040,1997).

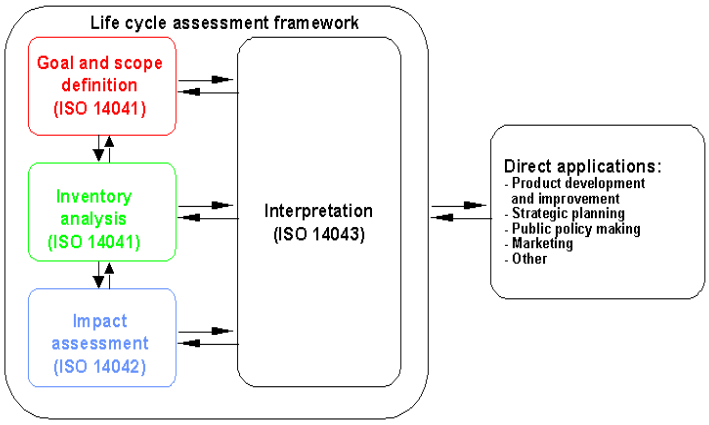

Figure 3.2: Methodological framework of LCA: phases of an LCA (After: ISO 14040, 1997)

The life cycle inventory (LCI) is aimed at quantifying the input/output relationship and prepare an inventory of input/output data for all processes involved in the life cycle of the system(s) under study. The input/output flows to be quantified for a unit process include economic and environmental flows (Figure 3.3). The input/output data are normally generated by following four methods: monitoring data measurement, emission factor estimations, mass balance and engineering calculations. For every unit process, LCI generates a unit process table (matrix), illustrated in Equation [3.1], in which

variables represent the changes of economic flows or environmental interventions, relating to functional unit. The total process along the life-cycle of a product, relating to functional unit, can be represented as a set of column vectors Equation [3.2]. Conventional LCI models are based on three basic simplifications: the first one is the linearisation of process characteristics, which means that unit processes are treated as 'black boxes', with constant and linear input/output coefficients and the actual variability of process parameters and operating conditions are thus implicitly disregarded; the second related simplification is to neglect the actual objectives of process operators, i.e. plant owners, managers and investors, and as a consequence, changes in exogenous circumstances do not lead to endogenous changes in process parameters; thirdly, "the inter-connectedness of processes is also modelled very mechanically and statically, in a steady-state model, ignoring all market mechanisms, as well as all other social, cultural, and political relations"(Guinée *et al.*, 2001). These basic simplifications are obvious limitations, and overcoming them is a worthy endeavour.

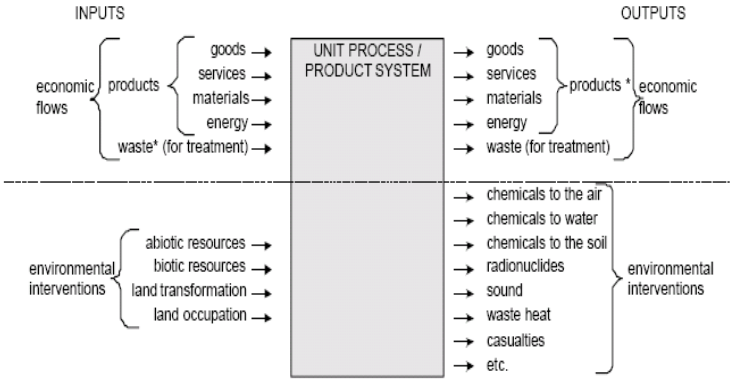

Figure 3.3: Environmental interventions and economic flows (After Guinée *et al.*, 2001).

$$P_i = \begin{Bmatrix} ecf\ (1) \\ ecf\ (2) \\ \vdots \\ ecf\ (N_{ec}) \\ evf\ (1) \\ evf\ (2) \\ \vdots \\ evf\ (N_{ev}) \end{Bmatrix}$$ Equation [3.1]

$$P = \begin{bmatrix} P_1 & P_2 \cdots P_{np} \end{bmatrix}$$ Equation [3.2]

Where:
Unit process, i, is represented as a column vector, P_i;
First N_{ec} rows – economic flows; Next N_{ev} rows– environmental flows;
Total process can be represented as a set of column vectors, P, with (N_{ec}+ N_{ev}) rows and np columns.

The Life Cycle Impact Assessment (LCIA) is aimed at understanding and evaluating the magnitude and significance of the potential environmental impacts of a product system"

(ISO, 1997E). In this phase, impact categories (e.g. global warming, acidification, and human toxicity), category indicators[1], and characterisation factors[2] are defined, and LCI results are assigned to categories and then converted into category indicators via characterisation factors (Figure 3.4).

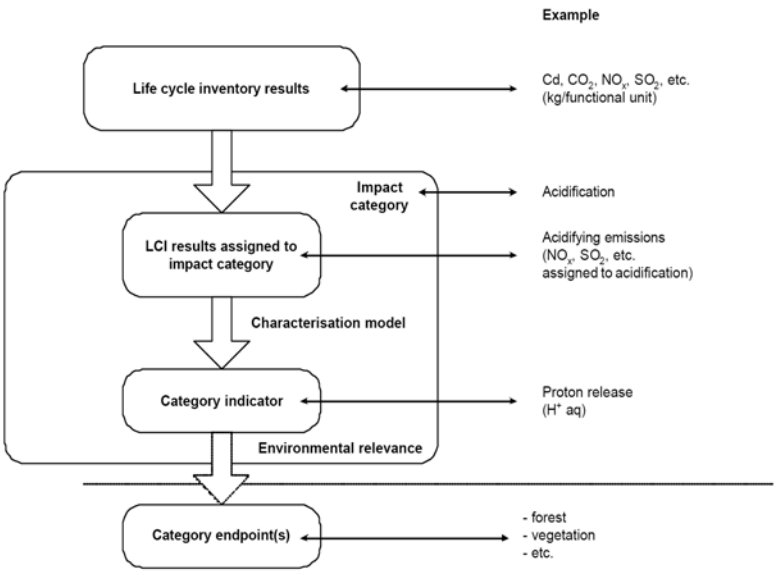

Figure 3.4: The conceptual framework of Life Cycle Impact Assessment (After: Guinée *et al*., 2001).

Interpretation is defined as "a systematic procedure to identify, qualify, check, and evaluate information from the results of the LCI and/or LCIA of a product system, and present them in order to meet the requirements of the application as described in the goal and scope of the study. Furthermore, Life Cycle Interpretation includes communication to give credibility to the results of other LCA phases (namely the LCI and LCIA) in a form that is both comprehensible and useful to the decision maker (ISO, 2000)."

3.2.3 Applications of Life Cycle Assessment

Life Cycle Assessment can be applied for the identification of improvement possibilities, decision-making, choice of environmental performance indicators, and market claims (ISO, 1997). In many practices, LCA is also used in conjunction with other

[1] Category indicator (or potential indicators) is a measure of the state of a particular impact category (e.g. global warming is measured by kg of CO_2 equivalent).

[2] Characterisation factors can convert environmental flows into environmental impacts. There are two characterisation approaches: midpoint method (e.g. Guinée *et al*., 2001) and endpoint method (e.g. Eco-indicator 99). Midpoint approach stops quantitative modelling at any point before the end of cause-effect chain (including fate, exposure, effect and damage) and uses midpoint indicators (such as global warming potential, acidification and so on) to reflect the relative environmental importance of an emission or extraction. Endpoint approach models the cause-effect chain up to the final environmental damages, the damages to human health, ecosystems and resources.

environmental tools (such as life-cycle management and life-cycle costing) for policy making, environmental marketing and industrial decision-making.

Life Cycle Assessment has been used to assist public policy making in many nations. For instance, Swedish Environmental Protection Agency (EPA) extended producer responsibility of packaging and included beverage cans and bottles, to increase the level of recycling, based on the results of LCA studies that the recycling of packaging is good for the environment and saves energy and other resources (Vagt, 2008). In the Netherlands, LCA is used as the basis of regulatory and permitting systems, and as LCA is focused on performance rather than compliance, regulatory oversight has been greatly reduced (ACLCA, 2004). The European Union (EU) has several policies (e.g. the Integrated Product Policy (IPP)) implemented through the use of LCA, for example (EC, 2008):

- Type I Eco-labels indicate the environmental performance of the product or service, based on multiple criteria over the entire life;
- Type III Environmental Product Declarations (EPD) are a communication format for quantified LCA information using predetermined parameters based on independently verified rules for the product category.

With the goal of producing greener, more environmentally friendly products, companies use LCA to (EC, 2008):

- Compare different design options during product development;
- Identify the most important environmental problems (hot spots) in the life-cycle of their own product and of competitors' products (benchmarking);
- Document improvements in the environmental performance of products;
- Select amongst suppliers in a green supply chain management;
- Communicate the environmental performance of products or services, through the use of environmental labels and product declarations.

Many energy companies around the world conducted LCA studies to improve their production processes or to convince the public that their energy products are greener. For instance, Vattenfall uses LCA as one method to assess the environmental impact of its operations, and LCAs have led to improved environmental performance in many areas, including reduced use of water in operations, and reduced risk of oil leaching to soil and water (Vattenfall, 2007). Dong Energy uses LCA for improving processes,

explaining relation between impacts and steps of the life cycle. EDF carried out LCA on the different electricity production ways (Le Bocq, 2008); Shell, Sasol Chevron and ConocoPhillips conducted LCA studies on Gas to Liquid (GTL) processes to estimate life-cycle GTL environmental impacts (Five winds international, 2005).

3.2.4 Limitations of Life Cycle Assessment

The uncertainty of LCA results (including both LCI data and environmental impact results) is an acknowledged problem, because LCA modelling involves complex systems and is constrained by lack of data, theoretical expertise and the capacity to handle complexity, which cause data uncertainty, model uncertainty and uncertainty due to choices in LCA modelling (Guinée *et al*., 2001; Reap, *et al.*, 2008). The trend of LCA research dealing with uncertainty is towards a broadening and deepening LCA:

- Broadening may involve including economic and social aspects, or covering new environmental aspects (Zamagni *et al*., 2008);
- Deepening may mean including more fate and exposure mechanisms in impact assessment; developing more temporal and spatial related environmental impact assessment models; developing LCI models that can capture the basic physical or empirical relations for processes in product systems, are capable of producing ranges for LCI data, and allow designers to incorporate more parameters into design problems (Reap, *et al.*, 2008).

3.2.5 Why Life Cycle Assessment is Relevant for CO_2 Capture and Storage

CO_2 capture and storage systems require additional energy for their operation, and the known and currently developed capture and storage options offer a number of alternatives, which involve different energy consumption and subsequent environmental impacts. In order to provide a representative and accurate evaluation of the alternative CCS options, it is necessary to conduct a comprehensive environmental assessment, which is capable of tracking GHG releases throughout all of the stages in the power generation life-cycle to ensure that the CCS option undertaken does not result in upstream or downstream changes that will increase the overall release of GHGs and do not significantly aggravate other environmental concerns such as resource depletion,

solid and hazardous waste generation, and the release of toxic substances which impact human health and ecological systems.

Life Cycle Assessment meets these criteria for the following reasons:

• Life cycle assessment (LCA) tracks energy and non-energy related GHG releases and typically also tracks various other environmental releases (e.g. solid wastes, toxic substances and air pollutants) and the consumption of resources (e.g. minerals). This holistic perspective helps decision makers to ensure that a reduction in GHG emissions by CCS would not result in dramatic increases in other environmental impacts.

• LCA can be used to compare the environmental impact potential for different CCS concepts in the search for greener alternatives, when planning CCS projects.

• LCA can quantify the environmental trade-offs of any process option along the CCS chain and help companies to minimise environmental impacts of the CCS life cycle by designing most eco-friendly component processes or setting appropriate operational parameters.

• LCA can identify which substances have significant environmental impact potentials in the CCS life cycle and help companies to design environmental control processes to minimise the impacts of the release of these substances.

• LCA can help to identify the stage in the CCS life cycle where the environmental impact potential is most significant, i.e. whether it is during raw material extraction, in the material manufacturing, the power generation, the CO_2 capture, the transport process, or during the CO_2 storage stage. At company level this can be important knowledge in the search for eco-friendly suppliers and at society level it can be used to adjust the environmental policies and regulation.

• LCA can provide stakeholders with information about the 'green' credentials of the energy products in the market and provide the necessary evidence consumers may use to choose which products to buy.

• The other strength of LCA is that the International Organization for Standardization (ISO) has developed the ISO 14040 series of LCA standards, which provide guidance on setting appropriate system boundaries, reliable data collection, evaluating environmental impacts, interpreting results, and reporting in a transparent manner. This

offers an excellent starting point for the development of measurement protocols for GHGs and other environmental impacts (Brady, 2000).

• In addition, under the Kyoto Protocol, three flexible mechanisms (Emissions Trading, Joint Implementation (JI) and the Clean Development Mechanism (CDM)) were developed to help emitters in developed countries to meet their GHG emission targets, and these flexible mechanisms are already a reality, as the Kyoto Protocol entered into force on 16 February, 2005. LCA provides a credible and internationally accepted means for the participants of these flexible mechanisms to evaluate the proposed projects or reduction options, to verify whether emission reduction is real, and advance the Kyoto Protocol from policy to implementation level.

3.3 Previous Life Cycle Assessment Applications in Power Generation and Power Generation with CO_2 Capture and Storage

3.3.1 Previous Life Cycle Assessment Applications in Power Generation

The roots of LCA applications in power production systems go back to net energy analysis studies which were popular in the 1970s. Since the 1990s, numerous studies have adopted the LCA methodology to assess alternative power generation systems. Recent LCA studies on power generation systems and the results of life-cycle GHG emissions are provided in Table 3.1 and Table 3.2. Their results, compiled in Figure 3.5, show a fairly wide range of emission values. This is because previous studies focus on specific power plants that have different configurations, fire a variety of fuels, employ alternative emission control devices and waste treatment methods, and are located in different areas in the world.

It is worth noting here that the variability of life-cycle GHG emissions from different studies may be the lowest when compared to other life-cycle emissions. This is because CO_2 emissions depend on the efficiency of the equipment and the carbon content of the fuel in the main, whereas other life-cycle emissions (such as SO_2, NOx, CO, and trace elements) are more dependent on technological options employed and location. The wide variability of emissions implies that standalone LCA case studies of power generation can not sufficiently represent the universe of power generation.

Table 3.1: Life cycle GHG emissions of coal fired power plant

Source	GHG Emissions (gCO2eq/kWh)	Notes	Reference
IEA Clean Coal Centre, 2005,"Coal full life cycle analysis"	762-1310		
	932		CISS,2001a
	766	IGCC	CISS,2001a
	1042	average coal	Spath et al, 1999
	960	newer coal plant	Spath et al, 1999
	757	advanced coal plant	Spath et al, 1999
	842	SCSC	CISS,2001d
	716	USCSC	CISS,2001d
	895	USCSC	Uchiyama, 1996
	762	Switzerland, future PC	
	771	Switzerland, future PFBC	Dones et al, 1999
	803	Australian, PFBC	CISS,2001b
	1010	UK, PFBC	
	823	UK, IGCC	WEC, 2004
	988	present, PC plant	Hondo, 2000
	1071	present, PC plant	Hirschberg, 2003
	765	future PC	Hirschberg, 2003
	1340	present, lignite	Hirschberg, 2003
	755	future, lignite	Hirschberg, 2003
	969-1310	present, PC plant	Spdaro et al, 2000
	756	future PC	Spdaro et al, 2000
	958-1343	present, lignite	Spdaro et al, 2000
	863	future, lignite	Spdaro et al, 2000
Dones *et al*, 2004, "Greenhouse gas emissions from energy systems: comparison and overview"	949-1280	European	
	850-1300	World	Surry, 1997
	949-1280	UCET countries	Swiss study, 2003
	980	Japan	Japanese study, 2003
	1040	US	US study, 2000
	970-1680	Shandong,China	China study, 2003
World Energy Council, 2004, “Comparison of Energy system using life cycle assessment”	932	Bayswater	
	803	Australia, PFBC	
	766	Australia, IGCC	
	500	Australia, H2,SOFC	
	860	Meri-Pori, FGD, SCR	
	1085	France, FGD	
	898	Germany,FGD	
	980	Amsterdam, FGD	
	834	Pego, FGD	
	1026	Spain, FGD	
	960	UK,FGD	
	972	UK,FGD+SCR	
	1075	UK, AFBC	
	1010	UK, PFBC	
	823	UK, IGCC	
	959	USA, low-Nox	
	757	USA,CuO	
	847	USA	
UIC Nuclear Issues Briefing Paper, 2005, Energy analysis of power systems	975	Japan	
	980	Sweden	
	894	Finland	
Nuclear Energy Institute, 2006, Life-cycle Emissions Analysis	790-1182		
Meier, 2002, Life-cycle assessment of electricity generation system and application for climate change policy analysis	1041	US	
IER, 1997, ExternE National Implementation Germany, ExternE-Externalities of Energy	815	Germany	

Table 3.2: Life cycle GHG Emissions of natural gas combined cycle (NGCC) power plant

Source	GHG Emissions (gCO_2eq/kWh)	Notes	Reference
IEA Clean Coal Centre, 2005,"Coal full life cycle analysis"	390-690		
	392	Switzerland, future plant	Dones *et al*, 1999
	524	NGCC+LNG	CONCAWE,2004; DTI, 2004; Ricketts, 2005
	605	NGCC	Hirschberg, 2003
	389	NGCC	Hirschberg, 2003
	440-690	NGCC	Spdaro *et al*, 2000
	389	NGCC	Spdaro *et al*, 2000
	420	UCET countries	Swiss study, 2003
	510	Japan, NGCC+LNG	Japenese study, 2003
	500	US	US study, 2000
World Energy Council, 2004, "Comparison of Energy system using life cycle assessment"	439	Australia	
	433	France	
	398	Germany	
	448	Italy	
	421	Eemshaven	
	440	Tapada do Outeiro	
	407	Spain, low-NOx	
	440	Sweden	
	411	UK, low-Nox	
	499	USA, SCR	
	469	Cass County	
UIC Nuclear Issues Briefing Paper, 2005, Energy analysis of power systems	519	Japan	
	450	Sweden	
	472	Finland	
Nuclear Energy Institute, 2006, Life-cycle Emissions Analysis	389-511		
Meier, 2002, Life-cycle assessment of electricity generation system and application for climate change policy analysis	662	US	
IER, 1997, ExternE National Implementation Germany, ExternE-Externalities of Energy	362	Germany	

Moreover, previous research and the mainstream LCA software and LCA databases (e.g. TEAM, GaBi 4, Ecoinvent, SimaPro 7, ETH-ESU 96, and U.S. LCI Database) pay much more attention to the system boundaries rather than prioritise the detail level and accuracy of the LCI data as well as the technical and geographical differences inherent in LCI data. All LCI data for power generation are at plant level (or gate to gate data) rather than at the level of component unit processes inside plants.

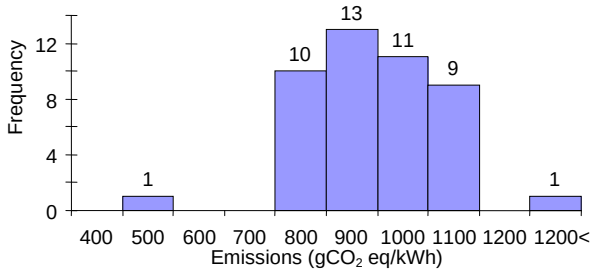

a. Life-cycle GHG emissions from coal-fired power plants

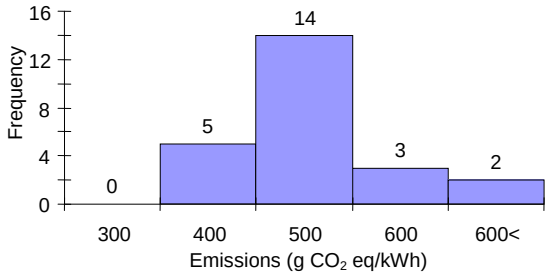

b. Life-cycle GHG emissions from NGCC power plants

Figure 3.5: The variability of life-cycle GHG emissions calculated from previous studies.

Figure 3.6 illustrates a typical definition of system boundaries for electricity generation systems in which the LCI data used are at power plant level. This confirms that the electricity generation systems have been largely simplified to a single black-box with constant and linear coefficients representing relationships between inputs and outputs, and consequently the simplification limits the possibility of tracing emissions back to individual unit processes and allowing for technical and geographical differences.

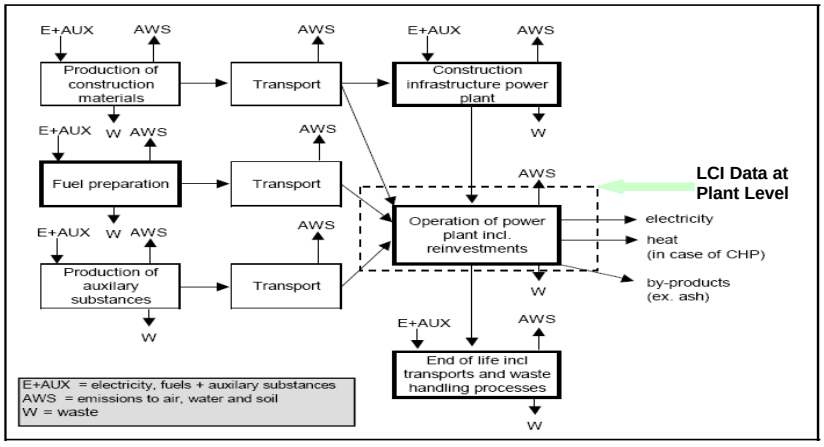

Figure 3.6: An illustration of life cycle boundaries of power generation systems used previously (After Setterwall C. *et al.*, 2004).

Modelling the environmental burdens of electricity generation systems is far from a simple or straightforward task. Indeed, the electricity generation system is among the most complex of all the industries addressed in the context of LCA, and existing LCI data sets generally fail to capture the effects of these complexities. Curran, *et al.* (2005) listed the following complexities that introduce difficulties when modelling power generation systems: a) the wide variation among generation stations in emissions and inputs per unit energy generated across and even within fuel types; b) the rapid ongoing evolution and regional variety of the electricity system and the regulatory environment in which it operates; c) the rapid and ongoing evolution of electricity generation technologies and uncertainties about future market penetration of new technologies.

3.3.2 Previous LCA Studies on Power Generation with CCS

There are a number of LCA studies of power generation with CCS in literature, which provide preliminary environmental characteristics of power generation with CCS in the context of LCA. A few recent examples of these LCA studies are listed in Table 3.3. The majority of these studies focus on Life Cycle GHG emissions, air emissions, or overall energy efficiency (Odeh and Cockerill, 2008; Suebsiri *et al.*, 2006; Corti and Lombardi, 2004; Lombardi, 2003; Muramatsu *et al.*, 2002; and Akai *et al.*, 1997). Some studies include most categories of LCI data but cover power generation and CO_2 capture only and do not address the CO_2 transportation and storage processes (Schreiber *et al.*, 2007; IEA GHG, 2006, Flaschi *et al.*, 2000; Doctor *et al.*, 2001; and CISS, 2003). Pehnt and Henkel, (2009) investigated the full chain of power generation with CCS but focused on atmospheric emissions, while emissions to water and soil are not fully considered. CO_2 leakage is discussed in this study but storage processes are not fully investigated. The other most recent LCA study (Knoorneef *et al.*, 2008) investigated the CO_2 post-combustion capture, transport and injection including the complete LCI category set, however, storage processes are not investigated. In addition, the study is case specific and cannot capture the technical and geographical difference of power generation with CCS.

Table 3.3: Published LCA studies on carbon capture and storage

Study	Power Generation	CO_2 Capture	CO_2 Capture Method	CO_2 Transport	CO_2 Storage Option	LCI Category
Pehnt M. and Henkel J., 2009	PCF	Post-combustion	Amine solution absorption (MEA)	Pipeline	Depleted gas field (CO_2 leakage discussed, storage not investigated)	Full LCI category, LCI focused on atmospheric emissions, emissions to water and soil are not fully considered.
		Oxy-fuel-combustion	Separation of oxygen from air			
	IGCC	Pre-combustion	Physical solvent absorption (Selexol process)			
Knoorneef J., et al., 2008	PCF USCPF	Post-combustion	Amine solution absorption (MEA)	Pipeline	Not investigated (only CO_2 injection is considered)	Full LCI category, case specific. LCI data estimated from emission factors or literature.
Odeh N. A. and Cockerill T. T., 2008	USCPF	Post-combustion	Amine solution absorption (MEA)	Pipeline	Not investigated	GHG emissions
	NGCC					
	IGCC	Pre-combustion	Physical solvent absorption (Selexol process: Glycol)			
Schreiber A. et al., 2007	PCF	Post-combustion	Amine solution absorption (MEA)	Pipeline	Not investigated	Full LCI category (LCI data at plant level and from the LCA software Ecoinvent, GaBi 4.2)
	IGCC	Pre-combustion	Amine solution absorption (MEA)	Pipeline		
IEA GHG, 2006	PCF	Post-combustion	Amine solution absorption (MEA)	Not investigated	Not investigated	Full LCI category (LCI data at plant level and from the LCA software Ecoinvent)
	NGCC					
	IGCC	Pre-combustion	Amine solution absorption (MDEA)			
	POCC					
Suebsiri, J. et al., 2006	Not disclosed	Not disclosed	Not disclosed	Pipeline	EOR (storage not investigated)	GHG emissions
Khoo H. H. 2006 a	Coal-fired plant	Post-combustion	Chemical absorption	Not investigated	Mineral sequestration alternatives	Full LCI category (all LCI data at plant level and from literature)
			Membrane separation			
		Oxyfuel combustion	Cryogenics			
		Pre-combustion	Pressure Swing Adsorption			
Khoo H. H. 2006 b	Coal-fired plant	Post-combustion	Chemical absorption	Pipeline, Ship	Ocean, EOR, ECBM, and saline aquifer (storage is not investigated)	Full LCI category (all LCI data at plant level and from literature)
			Membrane separation			
		Oxyfuel combustion	Separation of oxygen from air (Cryogenics)			
		Pre-combustion	Pressure Swing Adsorption			
Spath P. and Mann, M., 2004	Coal-fired plant Biomass-fired plant Biomass/coal co-fired NGCC	Post-combustion	Amine solution absorption (MEA)	Pipeline	Not investigated	GHG emissions and energy efficiency
	Biomass-IGCC	Pre-combustion	Amine solution absorption (MEA)			
Corti and Lombardi, 2004	Biomass-IGCC	Pre-combustion	Amine solution absorption (mix of DEA and MDEA)	Not investigated	Not investigated	GHG emissions
CISS, 2003	O_2 Blown-IGCC	Pre-combustion	Not disclosed	Not investigated	Not investigated	GHG, NOx, SOx, PM, water consumption, solid waste
Lombardi, 2003	IGCC	Pre-combustion	Amine solution absorption (mix of DEA and MDEA)	Not investigated	Not investigated	GHG emissions
	SCGT/CC	Pre-combustion	Amine solution absorption (mix of DEA and MDEA)			
	E-MATIANT	Oxy-fuel combustion	N/A			
Muramatsu E. and Iijima M., 2002	PCF	Post-combustion	Amine solution absorption (MEA; KS-1)	Pipeline	EOR (only CO_2 injection considered)	GHG emissions
Doctor R. D. et al., 2001	IGCC+H_2 production	Pre-combustion	Physical solvent absorption (Selexol process: Glycol)	Not investigated	Not investigated	Full LCI category (including all inputs/outputs)
Fiaschi D. et al., 2000	L-MATIANT	Oxy-fuel combustion	N/A	Not investigated	Not investigated	GHG, NOx, SOx, PM, Solid wastes
Akai M. et al., 1997	O_2 Blown-IGCC	Pre-combustion	Physical solvent absorption (Selexol process: Glycol)	Pipeline, Ship	Ocean, geological storage (storage processes are not fully investigated)	GHG, NOx and SOx emissions
	Molten carbonate fuel cell (MCFC)	Pre-combustion	Amine solution absorption			
	LNG combined-cycle	Post-combustion	Amine solution absorption			

PCF: pulverised coal fired power plant; USCPF: Ultra-supercritical pulverised coal fired power plant; IGCC: Integrated gasification combined cycle power plant; NGCC: Natural gas combined cycle power plant; POCC: Partial oxidation (nature gas) combined cycle power plant; SCGT: Semi-closed gas turbine cycle. E-MATIANT or L-MATIANT: a type of innovative methane fuelled cycle where, due to combustion in pure oxygen, CO_2 is the cycle working fluid and not emission at stack.

Due to the fact that there are no current commercial power plants with CO_2 capture in full operation, the LCI data used in previous studies are based on hypothetical power plants and relate to specific cases. The majority of previous studies collect LCI data from the literature. Few studies (Corti and Lombardi, 2004; Lombardi, 2003; Flaschi *et al.*, 2000; Doctor *et al.*, 2001) employ power plant design software to generate LCI data. Power plant design software can generate accurate mass balance spreadsheets related to specific cases, but such software, focused on the power plant design, are not designed to conduct detailed analysis of environmental-concerned mass flows such as, N_2O, trace elements, etc. It is worthy to note that all LCI data in the previous studies are at power plant level. LCI models at plant level, however, restrict the flexibility of the model to allow for the technical and geographical differences in power generation with CCS systems, which can be configured with alternative CO_2 capture routes, a variety of CO_2 capture technologies, and located in different geographical areas that determine the emission control options, waste treatment methods, as well as the type of fuels used. In addition, plant level analysis also limits the capacity of the model to quantify the trade-offs inherent in any change to the power production systems.

Four previous studies investigated CO_2 transportation and alternative CO_2 geological storage options (e.g. CO_2-ECBM, CO_2-EOR, and CO_2-EGR) (Suebsiri *et al.*, 2006, Khoo *et al.*, 2006a, Khoo *et al.*, 2006b, Aycaguer, 2001). Nevertheless, these studies do not fully analyse the CO_2 storage processes and do not consider some important components in the context of LCA, including: above ground processes; well(s); CO_2 storage geological formation(s); and the geological zones surrounding the CO_2 storage formation(s). The potential amount of CO_2 leakage and temporal profile of CO_2 leakage from the CO_2 storage geological formation(s), the potential environmental impacts on zones exposed to CO_2 leakage pathway are not fully discussed in previous LCA studies either.

In addition, the disposal of solid wastes (e.g. bottom ash, fly ash) from power plants is not fully investigated in previous studies. In fact, the amounts of most trace metals in solid wastes are at least 20-100 times higher than the amounts emitted directly from the stack (Finnveden, 1995). The potential leakage of trace metals from landfills to underground water both during the landfill surveyable time period (around 100 years) and beyond the surveyable time period cannot be neglected (Hellweg et al., 2005; Finnveden, 1995). The trace metal potential emissions to underground water from coal combustion waste landfills will depend on the type of coal used, hydrological and

geological characteristics of landfill sites during the life-cycle and should indeed be included in the LCA boundary.

With respect to the conclusions of previous studies, one study (Doctor et al., 2001), which compares two types of IGCC plants (a base-case IGCC system without CO_2 removal and a multi-product system producing electricity and hydrogen (H_2) with CO_2 capture) concludes that the plant with CO_2 capture has larger environmental impact than the plant without CO_2 capture in almost all impact categories. This is due to the higher auxiliary power requirement connected to CO_2 capture and CO_2 compression, but the removal of CO_2 and deeper reduction of acid gas emissions makes the co-product system better in the Global Climate Change (GCC), toxicity, and eutrophication categories. Flaschi *et al*., (2000) demonstrates that the L-Matiant cycle (a type of novel CO_2 reduction power plant) and conventional NGCC have equal life-cycle environmental impacts in almost all categories except for the GHG impacts. Lombardi (2003) concludes that three solutions for carbon reduction in power plants (IGCC+DeCO_2, SCGT/CC+DeCO_2, E-MATIANT+DeCO_2) have almost similar results in all environmental impact categories. IEA GHG report (2006) concludes that power plants with CO_2 capture can significantly mitigate life-cycle global warming impacts, but the environmental impact is increased for all other environmental impact categories, except for the USPCF plant with post-combustion CO_2 capture that results in fewer impacts in the categories of acidification and photochemical oxidation. Schreiber, et al., (2007) demonstrate that a power plant with MEA post-combustion CO_2 capture can achieve 80% life-cycle GWP reduction, but all other impact category indicators (e.g. human toxicity, acidification, etc.) are higher than conventional power plants, and that the up- and downstream processes contribute significantly to the LCA results.

The previous LCA studies of power generation with CCS do not fully investigate the CO_2 storage and solid waste disposal processes. If these processes are included, a different picture may be proven because CO_2 storage processes also produce environmental impacts. In addition, some CO_2 storage options (CO_2-ECBM, CO_2-EOR) recover unconventional natural resources, and hence can offset the additional energy consumption of capture processes and the corresponding environmental credits should be allocated to these storage options. Moreover, the conclusions of previous studies focusing on special cases cannot capture the technical and geographical difference of power generation with alternative CCS. Therefore, their results cannot be directly applied to other projects of power generation with CCS.

3.4 Conclusions

Life cycle Assessment is a well established methodology of environmental assessment for products (or systems) in a life-cycle view. However, the uncertainty of LCA results is a widely acknowledged limitation of the method. The uncertainty of LCA results primarily results from the uncertainty of LCI data or LCI models and the uncertainty of environmental impact models used. One of aims of this research is to reduce the uncertainty of LCI results by developing LCI models with high level of detail that can characterise the physical and chemical principles or empirical relations of the processes investigated and reduce the LCI model uncertainty.

Previous LCA applications in power generation with CO_2 capture are generally case specific and their results may not be applicable to power generation with CO_2 capture systems with different technical and geographical specifications. This study aims to quantify the technical and geographical variability of power generation with CCS systems, by developing LCI models that can characterise the physical and chemical principles or empirical relations of the processes along the CCS chain and incorporate technical and geographical parameters into LCI models at the necessary level. In addition, previous LCA applications did not develop analytical frameworks and LCI models for alternative CO_2 storage options in the context of LCA. The LCA analytical framework and LCI model for saline aquifer CO_2 storage were developed and are presented in Chapters 4 and Chapter 11.

Chapter 4 Research Methodology

4.1 Introduction

Power generation with CCS systems involves not only complex manmade systems but also complex natural systems. This requires the LCA system boundaries to include all the components/compartments of the natural system (CO_2 storage systems) that may have potential environmental impacts. CO_2 storage systems have a lifespan of more than thousands of years. Therefore, an appropriate LCA timescale should be set to represent both the nature of the CO_2 storage system and the purpose of CO_2 storage (GHGs mitigation). In order to provide a high level of detail that could characterise the physical and chemical principles of the processes involved in the CCS chain the LCI models developed should identify and break-down the alternative power generation, CO_2 capture and storage options into their component unit processes so that the technical and geographical parameters of concern can also be incorporated. This chapter presents the methodological framework proposed for an LCA model for fossil fuel power generation with CCS

4.2 Guiding Principles in the Development of the Methodology

The main objective of the research presented in this thesis was to develop a comprehensive LCI database for the analysis of power generation with alternative CO_2 capture and storage options in a consistent and transparent manner. The underlying

principle applied in developing this methodology can be summarised as:

i) Transparency: to show precisely how life cycle impacts are calculated, the uncertainty associated with the results and the extent to which the inputs/outputs of any unit process have been fully quantified.
ii) Comprehensiveness: to identify all of the inputs/outputs that may give rise to significant environmental impacts.
iii) Consistency of methodology: models and assumptions to allow valid comparisons to be made between different CCS options.

In order to comply with these principles, much of the effort in this research was devoted to identifying and characterising the emissions arising from power generation with different CCS options. The main variables considered as having an important role in determining the magnitude of emissions and the environmental impacts were:

- The power generation and CCS technologies used;
- The geographic location of the power generation plant and CO_2 storage site;
- The type and composition of the fuel used;
- The pollution abatement and waste treatment options available.

4.3 The System Boundaries and the Level of Detail Considered

4.3.1 System Boundaries

The system boundaries of LCA in power generation with CCS, which is presented in Figure 4.1, covers power generation, alternative CO_2 capture options, CO_2 conditioning processes, CO_2 transportation, CO_2 storage options, and upstream processes such as extraction and production of fossil fuels, raw material and consumables production, transportation of fossil fuel and consumables, and the construction of power plant, CO_2 capture facilities and CO_2 pipeline. This research focuses on modelling in detail the processes of power generation, alternative CO_2 capture options, CO_2 transportation, and CO_2 storage. In the case of the upstream processes, the system boundaries include the construction of power plant, CO_2 capture facilities and CO_2 pipeline. The LCI data for the upstream processes are either based on materials from the literature or are calculated using the GaBi LCA software v.4. This research does not consider the decommissioning of the power plant and other infrastructures (disassembly of power plant and relevant facilities and recycling or disposal of the resulting materials) because their contribution

is considered very minor. This is in agreement with earlier work reporting that decommissioning processes have minor impacts on the overall LCA results (Spath and Mann, 2004; Lombardi, 2003). Alternative technologies of power generation with CCS systems are demonstrated in Figure 4.2. Due to limited time and limited availability of resources, this research only investigated the systems relating to pulverized coal-fired power generation with post-combustion capture, oxy-fuel combustion capture, pipeline transport, injection and saline aquifer CO_2 storage (highlighted in blue background in Figure 4.2).

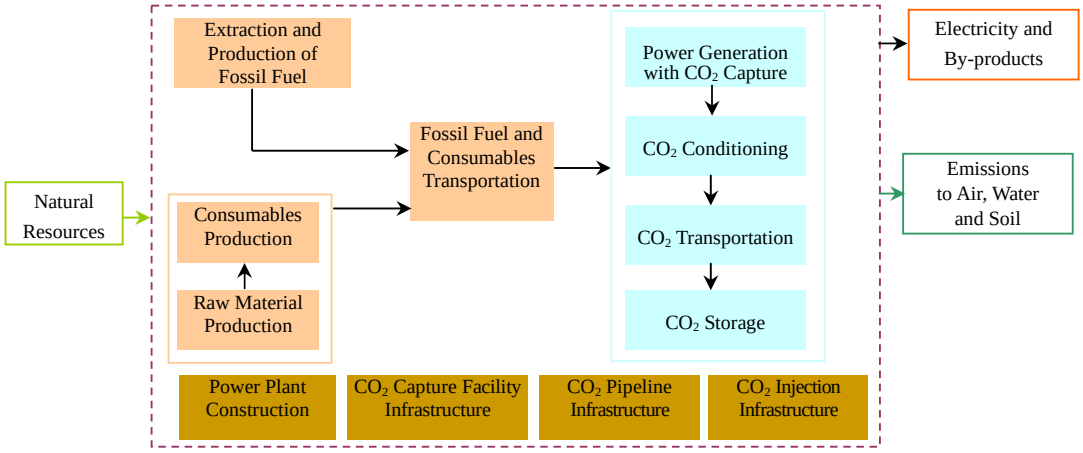

Figure 4.1: System boundaries of LCA on power generation with CCS.

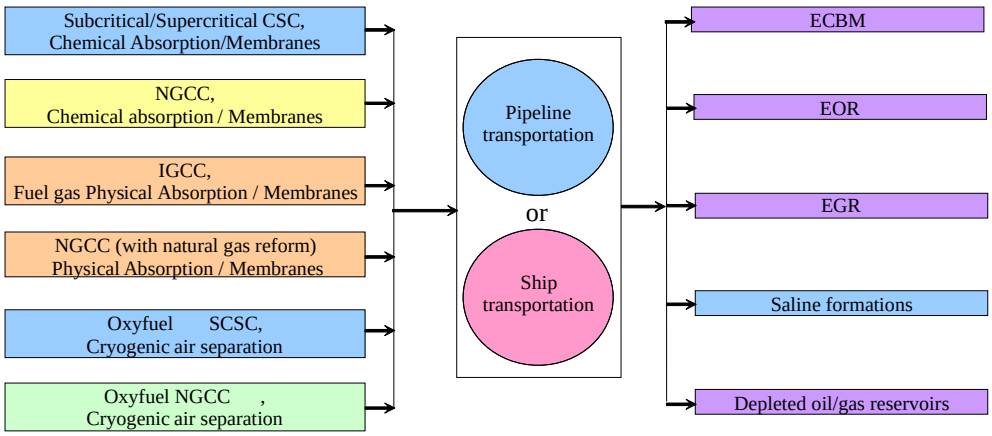

Figure 4.2: Alternative technologies of power generation with CCS systems.

The LCA system boundaries for CO_2 geological storage

When CO_2 is injected into a geological storage formation, some fraction of it remains as a free phase, some dissolves into the in situ formation fluids (oil or water), some is

immobilised by capillary forces and some is converted to minerals. As a result of this complex, spatially and temporally, varying distribution of CO_2 phases, modelling the situ CO_2 life-cycle in inventory will be difficult. On the other hand, the potential CO_2 leakage from storage formations for every geological formation differs in its geological attributes (including the storage formation, the surrounding zones, and manmade structures, such as the abandoned wells). Therefore, the system boundaries of the CO_2 geological storage need to be defined in the context of LCA. The following components are considered to be important in defining the LCA system boundaries, Figure 4.3:

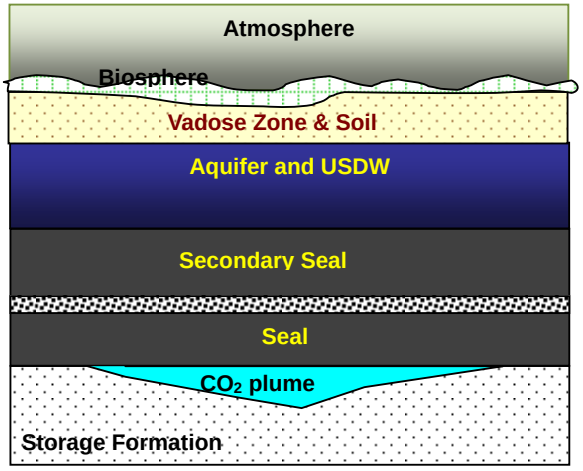

Figure 4.3: The LCA system boundaries for CO_2 geological storage (Modified from Hovorka, 2007).

- Facilities above ground (facilities associated with CO_2 injection, CO_2 enhanced hydrocarbon recovery, etc.).
- Well(s), including exploration wells, production wells for CO_2 enhanced hydrocarbon recovery, and abandoned wells intersecting the CO_2 storage formation;
- Geological storage formation(s). The boundaries of the geological storage formations should define the vertical and lateral extent of the primary formation(s) and the maximum spatial extent of potential CO_2 migration, and take into account the total planned amount of CO_2 to be stored (IEA GHG, 2007);
- Zones surrounding the storage formation(s), including the biosphere, the surface or near-surface environment and the geosphere, which includes a number of geological and hydrogeological units above and below the storage formation(s) (IEA GHG, 2007). If any CO_2 seeps or migrates away from the proposed primary CO_2 storage formation(s), the zones surrounding the storage formation will be

acting as receptors. Potential receptors for any seeped CO_2 include (IEA GHG, 2007):

- Overlying primary aquifers/reservoirs;
- Potable groundwater resources;
- Soil gas;
- Terrestrial and freshwater flora and [micro] fauna;
- Benthic sediments;
- Benthic waters;
- Marine flora and [micro] fauna;
- Atmosphere

This research considered only the potential leakages of CO_2 in to the atmosphere and the other environmental impacts that may be caused by CO_2 leakages are not considered, mainly because such impacts were not fully understood at the time of this project (IPCC, 2005).

4.3.2 Environmental Flows Quantified

The pollutants that are emitted to the atmosphere, soil or water from a CCS system originate from material or fuel inputs to the system, primarily coal and limestone. This research aimed at tracking down all the elements/substances of environmental concern from their point of entry to their partition and final emission in to all environmental compartments (atmosphere, soil or water) in a CCS system. As shown in Figures 4.4 and 4.5, the fate of following elements is of particular concern:

- C, which forms CO_2, CO and the unburnt carbon during the combustion processes. The energy consumption of the unit processes which generate CO_2, CO_2 capture and storage are calculated as well;
- S, N, Cl, and F, which form SOx, NOx, N_2O, HCl and HF during the combustion processes. The processes that generate SOx, NOx, HCl and HF, as well as the emissions involved in the pollution abatement systems used are also considered;
- Trace elements such as As, Cd, Cr, Cu, Hg, Ni, Pb, Zn, Sb, Be, B, F, Mn, Se, V, Co, Ba, Ag and Tl, and their partitioning and final emission to atmosphere, water or soil are also calculated.

There is no worldwide agreement on the trace elements of environmental concern produced as coal combustion products. The trace elements reported in a number of

national and international regulations, including the European Pollutant Emissions Register (EPER), UK pollution inventory, US pollution inventory and US toxic release inventory, which are listed in Table 4.1 were considered in this research.

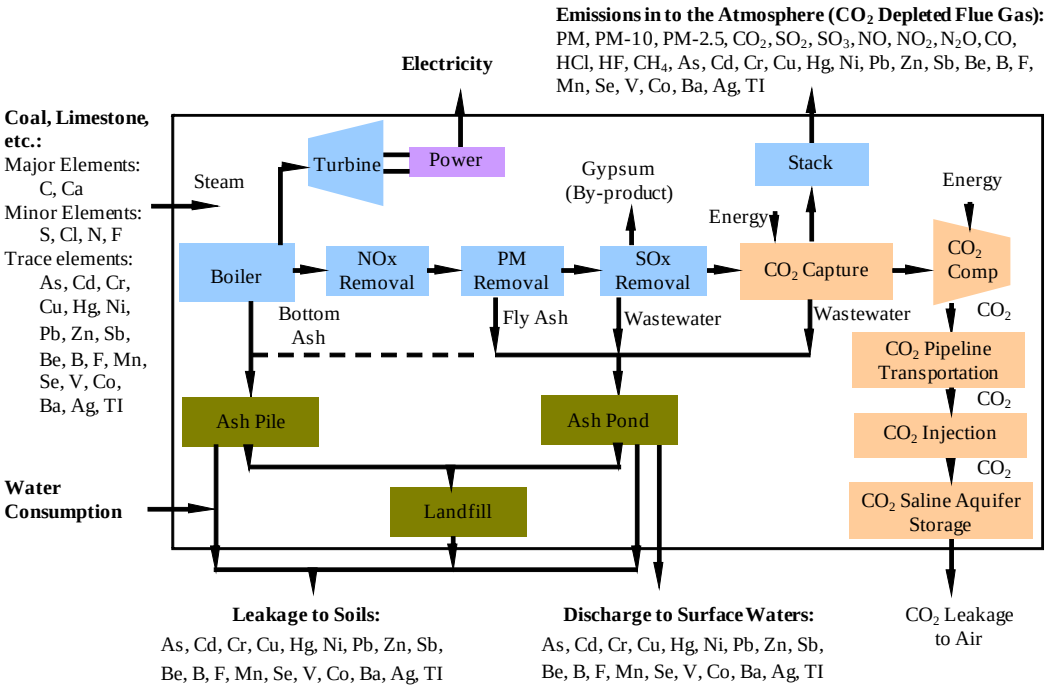

Figure 4.4: The level of detail involved in the LCA of post-combustion CCS system.

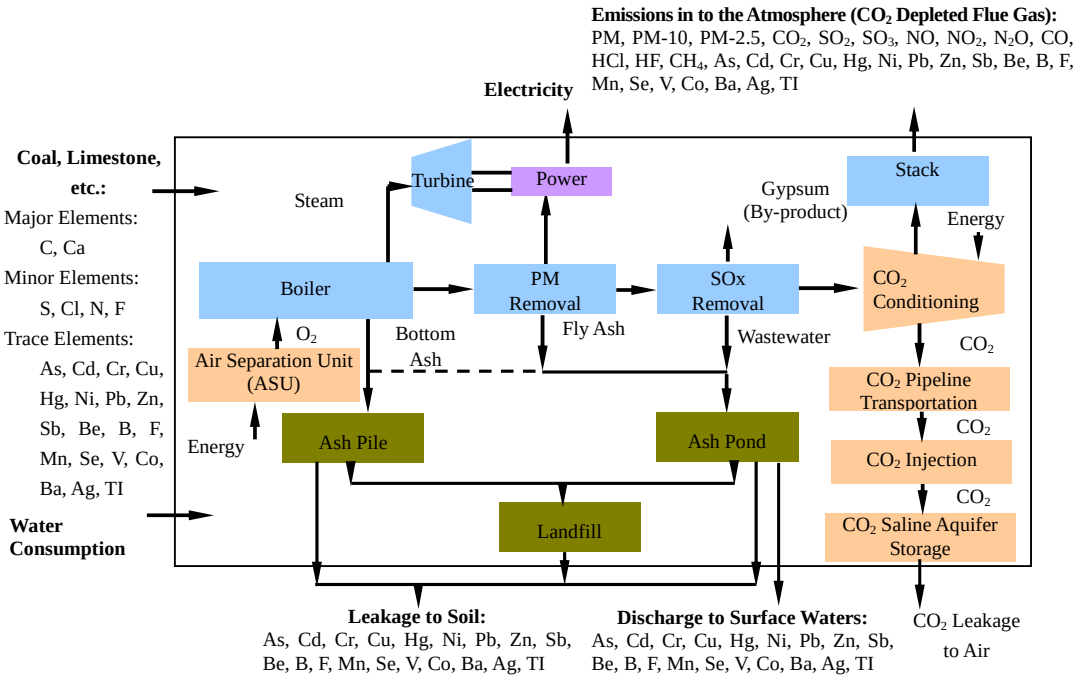

Figure 4.5: The level of detail involved in the LCA of oxy-fuel-combustion CCS system.

Table 4.1: Trace elements of regulatory interest (After DTI, 2004).

Element	Symbol	European Pollutant Emissions Register	UK Pollution Inventory	US Clean Air Act Amendments -1990	US Toxic Release Inventory
No. on list		8	15	11	17
Arsenic	As	X	X	X	X
Cadmium	Cd	X	X	X	X
Chromium	Cr	X	X	X	X
Copper	Cu	X	X		X
Mercury	Hg	X	X	X	X
Nickel	Ni	X	X	X	X
Lead	Pb	X	X	X	X
Zinc	Zn	X	X		X
Antimony	Sb		X	X	X
Beryllium	Be		X	X	X
Boron	B		X		
Fluorine	F		X		
Manganese	Mn		X	X	X
Selenium	Se		X	X	X
Vanadium	V		X		X
Cobalt	Co			X	X
Barium	Ba				X
Silver	Ag				X
Thallium	Tl				X

4.3.3 Temporal Domain

The lifetime for the LCA of power generation is about 30 to 50 years, which is the expected lifespan of power plants. However, when the CO_2 geological storage is included in the LCA system boundaries, two other characteristics of the system are needed to be considered: one is the fate of CO_2 in the storage formation; the other one is the potential leakage of CO_2 from the storage formation. This requires LCI modelling of CO_2 storage to cover thousands of years. Unified CO_2 storage performance standards have not been established worldwide. IPCC Special Report on CCS and CO2CRC consider the time framework of 1,000 years for the assessment of CO_2 storage performance (IPCC, 2005). In addition, the primary objective of CO_2 geological storage is to postpone the current emissions of CO_2 into atmosphere for 1,000 years. Therefore, the time framework of LCA in CCS was defined as 1,000 years in this research.

It is debatable to set a unified time frame for CO_2 storage in terms of LCA, because the CO_2 storage processes and the potential CO_2 leakage would very much depend on the geological condition setting. The choice of a 1,000-year time frame means that CO_2 leakage after this period is not considered. The choice of a 1,000-year time frame is

based on the assumption that in 1,000 years the technologies for power generation would not result in significant GHG emissions and GHG control technologies will be fully developed resulting in significantly reduced global emissions of GHGs. Consequently, global warming will not be an issue of concern in 1,000 years. In addition, the potential for CO_2 leakage from storage formations is expected to have exponential sharp decline over time after the end of CO_2 injection period.

4.3.4 The Functional Unit

The functional unit defined in this research is 1 MWh electricity generated with CO_2 capture and 1,000 years of CO_2 geological storage.

There are several time horizons involved in the LCA of power generation with CCS. For instance, the electricity generated is with the unit of Kilowatt hour (KWh). The operational life of power plant is 30-50 years. The CO_2 storage processes cover thousands of years. In order to allocate the CO_2 leakage to the electricity generated, this research allocates the accumulated CO_2 leakage over 1,000 years per MWh electricity generated, on the basis of the total electricity generated during the operational life of the power plant (e.g. 50 years).

4.4 Life Cycle Inventory Modelling

4.4.1 Modularisation of the System

A power generation system with CCS has a set of inter-related components and relationships between them. In this research, power generation with CCS systems is broken down, or modularised, into simple manageable subsystems connected by flows of intermediate products or emissions. This actually is the systems analysis method, which is the study of the composition and functioning of component systems. The purpose of modularisation is to make complex systems more easily understood and more precisely modelled. Figure 4.6 presents the modularisation principle introduced in modelling the alternative CCS systems and the unit processes considered.

Through modularisation, the LCI models quantify the flows of materials, natural resources, energy, intermediate products or emissions in a more detailed fashion, or in component unit process level, which allows for the representation of technical, spatial and temporal differences to a greater extent by modifying the parameters of component

unit processes as necessary. This not only addresses the limitations of conventional LCA studies which use linear input/output coefficients for the LCI models (described in Chapter 2), but also resolves the second limitation of the conventional LCI models by accommodating the specific operational needs of the industry users. Moreover, known and currently developed CCS technologies offer a number of capture alternatives, as well as the alternative emission reduction technologies available to power plants. Through modularisation, the LCI database can attain a clear and flexible structure. This enables the LCA practitioners to select the component unit processes considered as necessary, so that different technological options can be considered without the need of redesigning the LCI model or lose information (Durucan *et al.*, 2006).

Although most components of power generation with CCS systems are commercially available in one form or another, currently there is no existing project which configures all of these components in to a fully integrated power generation system with CCS which would characterise their future deployment (IPCC, 2005). ISO 14041 (1998E) focuses on LCA of existing plants and does not offer LCA methodologies for novel systems that are not commercially operated. Therefore, the modularisation method developed in this research provides an approach to conduct LCA by configuring virtual systems of power generation with CCS, based on the best available techniques and component unit processes of the system.

4.4.2 Classification and Quantification of Input/Output Flows

Depending on the level of detail required, unit processes can be represented by using two different types of models; the so called black box models or the white box models. In a black box model, only the inputs and outputs are known and the details of how the processes transform inputs to outputs are not specified. The transformation is modelled by a parameter or parameters defining the relationship of outputs to inputs, e.g. majority of conventional LCI models. On the other hand, in a white box model, all elements of the physical processes transforming inputs to outputs are known and specified. There are very few systems that can be modelled with white box models, therefore most models, being based on a mixture of physically based and empirical approaches, fall in between white and black to form various shades of grey boxes (Wainwright and Mulligan, 2004). A mixture of physically based and empirical approaches, or the grey box modelling methodology, is used for the LCI models developed in this research.

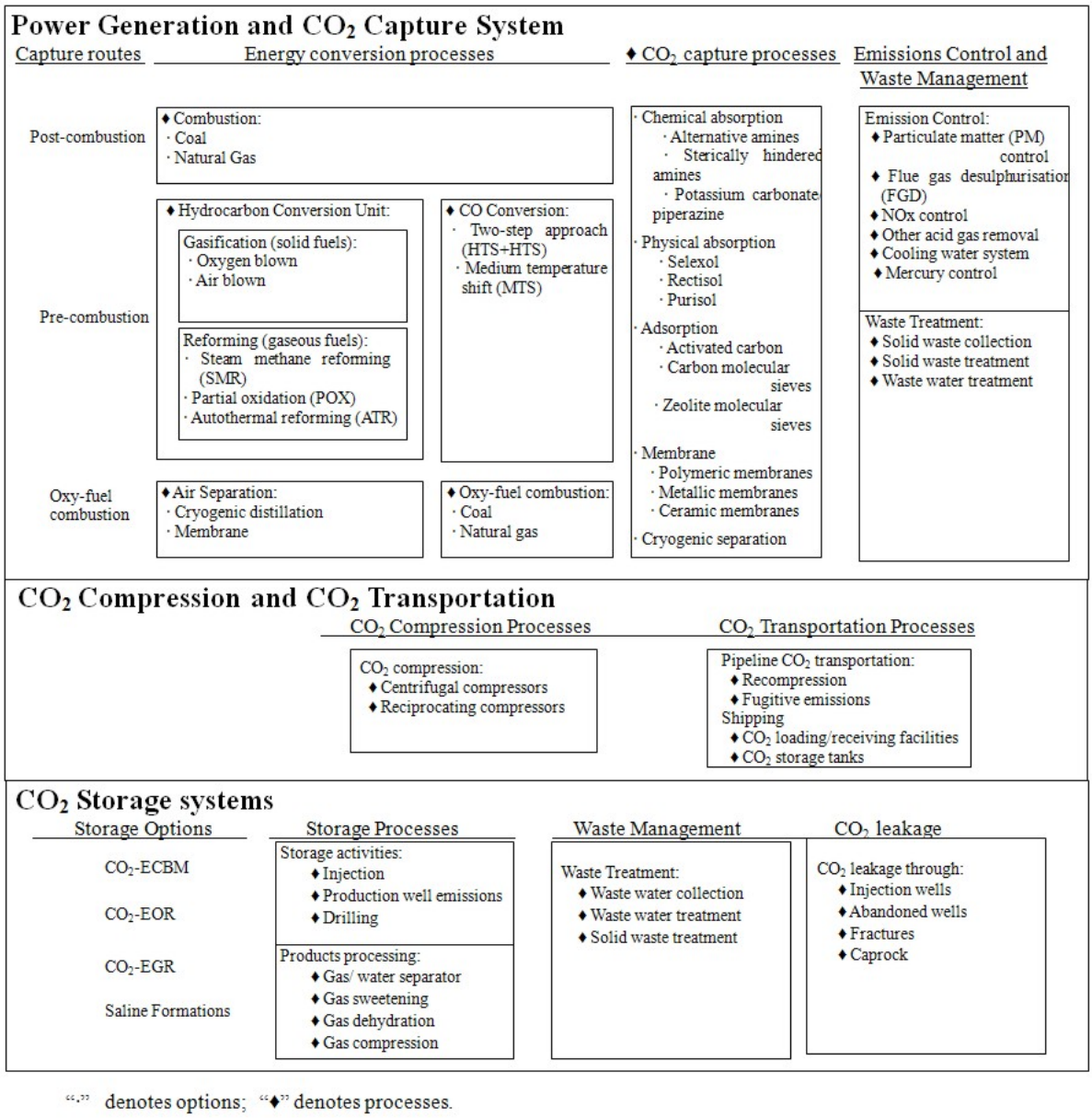

Figure 4.6: Illustration of the unit processes considered for the LCA model.

In order to facilitate the grey box modelling approach, the input and output flows of a unit process can be further divided in to the following categories according to the expected variability and uncertainty:

i) Raw material flows, energy flows, intermediate product flows or product flows generally have the smallest uncertainties in the LCI data. For the quantification of these data, process engineering models (or the white box method) are used, which utilise physical or chemical principles in modelling the transformation of input/output flows and quantify the technical and geographical differences;

ii) Emissions that occur mainly as a result of the substances present in input flows (e.g. carbon in fossil fuels) are emitted in known and fixed proportions to the amount of input flows. For this type of emissions, the uncertainty is of the same order as it is for the input flows in which they occur, i.e. below 20% (Weidema *et al*., 2003). For the quantification of these data, process engineering models are used;

iii) Emissions that are generated during a unit process which vary significantly depending on the physical conditions prevail during production, e.g. the amount of CO and NOx generated during combustion of fossil fuels, may depend on temperature, the amount of oxygen present etc. These emissions may vary by a factor of 5-10 (Weidema *et al*., 2003). In this case, the emissions will usually be highly dependent on the specific production process, which generally leads to significant uncertainty. For the quantification of these data, emission factors predefined for specific production processes are used;

iv) Emissions that vary significantly due to variability of the composition of fossil fuels or the geological conditions in the CO_2 storage sites, e.g. cadmium, mercury and other trace metals in coal combustion; chloride and sulphate in ash pond water discharge. In extreme cases, these emissions may vary by a factor of 1,000 or more. Assumptions or average values are used for modelling this kind of LCI data.

4.4.3 Identification of Significant Environmental Burdens

Rather than taking only the GHG emissions or energy efficiencies into account, as was the case in previous studies, this research identified and targeted the following broad categories of 'environmental burdens' :

i) Gaseous and particulate air pollutants;
ii) Solid emissions;
iii) Liquid emissions.

During the identification of burdens no distinction was made between those which may have likely and serious environmental impacts or not. Rather, the objective was to make sure that all potential impacts are listed in order to provide the basis for the analysis of different CO_2 capture and storage routes to be conducted in a consistent and transparent manner. This also provided a firm basis for the revision and update of the analysis as

more information on the environmental impacts of different burdens becomes available in the future (IER, 1997). Furthermore, ecosystem acidification, global warming and depletion of the ozone layer are currently recognised as some of the most important environmental concerns facing the world; therefore, it is believed that a comprehensive set of environmental burdens should be included in the LCI model developed.

4.4.4 Accounting for Technological Differences in CCS Applications

One of the distinguishing features of this research is the inclusion of technology dependence. This research deals closely with each CCS technology option and, for each type of emission, LCI models are developed for alternative emission reduction technologies. The application of LCA on CCS in energy production is aimed at long term strategic energy systems planning, which involves best available and novel energy technologies. Moreover, the concept of Best Available Technology (BAT), coupled with more stringent emission limits and environmental quality standards, have been the guiding principle behind the regulation of new power projects in developed countries, which promotes the application of new plant designs and new technologies of emissions control. Therefore, this research is more concerned with best available technologies or novel technologies that are being pushed to commercialisation, rather than focusing on older technologies which are gradually being decommissioned.

4.4.5 Accounting for Geographical Differences in CCS Applications

In this research, the LCI models developed recognise the importance of the geographical location of a plant and account for this at unit process level by modifying the inputs, or the model parameters, or by replacing component unit processes. The reason for carrying out the analysis at this level of detail is that the plant location is important in determining the magnitude of emissions. There are several factors involved in this, the most important of which are:

i) The installation of emission control systems (such as ESP, FGD, SCR or carbon capture systems) has usually been piecemeal, following the introduction of legislation that necessitate the use of these systems in order to control one kind of emission to achieve compliance. Variations in plant designs and emissions control technologies used determine the magnitude of emissions. For instance, most power plants in EU, Japan and US are equipped with SO_2 and NOx control

systems and the emissions of SO_2 and NOx are much lower than that in China and India, where the legislation is not as tight;

ii) CO_2 storage performance may vary considerably due to various geological conditions and complexity of the CO_2 storage sites. For instance, Korre *et al.*, (2007) illustrates that the variability and uncertainty of the reservoir parameters have a significant impact on the CO_2 geological storage performance predictions;

iii) In many parts of the world the choice of fossil fuel used in power generation is limited to local resources and transport distance. This results in geographical differences in emissions, as the quality and the composition of fossil fuels vary significantly across different areas;

4.4.6 Quantification of the Uncertainties Involved in Environmental Emissions

As already discussed above, the uncertainty involved in environmental emissions from power generation with CCS systems are caused by a number of factors: these include the variability of the S, N or trace metal contents of coals used; the complexity of environmental emissions generated during combustion, such as NOx emissions which depend on a number of physical and chemical conditions; variability of the efficiencies of emission control units; and the variability of geographical factors, such as the temperature and precipitation over a landfill site where power generation waste products may be stored.

One of the advantages of modelling LCIs at process level is that the factors or parameters that determine the environmental emissions can be indentified and quantified independently and easily. In order to quantify the uncertainty involved in environmental emissions, the Monte Carlo simulation approach was used to generate the probability distribution function (pdf) for each environmental emission. Monte Carlo simulation (MCS) is a stochastic method that randomly samples values from the probability distribution functions (pdf's) of variables in a model to compute the likely outcomes. A substantial number of iterations are run to cover different possible scenarios, and the results are used to form a pdf of probable outcomes. Statistical outputs, such as mean, median, standard deviation, and different levels of confidence (e.g. 95th percentile) can be generated from the results. The methodological framework of the Monte Carlo simulations used for LCA uncertainty analysis in this research is

presented in Figure 4.7. For each unit process, a pdf is assigned to each substance (or material) used as the input, process parameter or emission factor. Unit processes are then connected together to configure the system to be researched. Finally, Monte Carlo simulation is carried out to compute the probable outcomes including emissions, consumption of energy or resources, products and by-products.

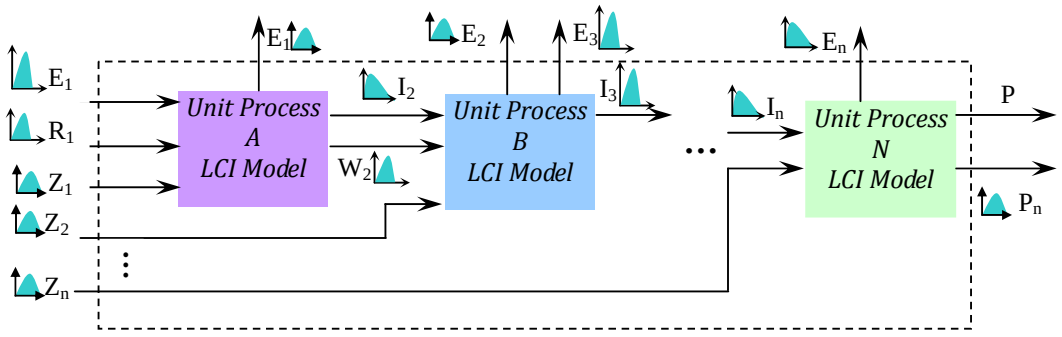

Figure 4.7: The methodological framework of the Monte Carlo simulation technique used in LCA uncertainty analysis

4.5 Life Cycle Impact Analysis

The selection of impact categories, category indicators, and characterisation methods depends on the LCA goal and scope. In order to provide a comprehensive profile of environmental impacts for emissions from power generation with CCS, this research employed the CML 2001 baseline impact categories, category indicators, and characterisation methods (midpoint approach) as standard method for LCIA. The CML 2001 baseline impacts categories are described in Table 4.2.

Some products, resources, or emissions may contribute to two or more exclusive categories in a parallel or sequential manner, and the emission should be divided or allocated to the relevant categories to avoid double accounting. It is also possible that the product or result of the effect in one impact category may be the starting point for another effect in another impact category. To deal with such complexities, this research uses the following guiding principles:

i) for environmental impact analysis on a specific location, the local environmental characteristics and the allocation of emissions among different applicable impact categories for these emissions, which contribute to two or more categories of impacts, are identified and closely analysed, so that the geographical differences can be fully characterised at LCIA level;

ii) for a general environmental impact analysis, not related to a specific location, two types of analysis are used: firstly, average allocation of emissions among different applicable impact categories are used, so that all potential environmental impacts can be identified; secondly, only the primary emission impacts are accounted for and the full value of a particular emission is assigned to each applicable category to determine the worst-case impact.

Table 4.2: Impact categories and characterisation factors (Compiled after Guinée *et al*, 2001 and US EPA, 2006).

Impact Category	Scale	Relevant LCI Data (i.e., classification)	Common Characterisation Factor	Description of Characterisation Factor
Global Warming	Global	Carbon Dioxide (CO_2) Nitrogen Dioxide (N_2O) Methane (CH_4) Chlorofluorocarbons (CFCs) Hydrochlorofluorocarbons (HCFCs) Methyl Bromide (CH_3Br)	Global Warming Potential	Converts LCI data to carbon dioxide (CO_2) equivalents. Note: global warming potentials can be 50, 100, or 500 year potentials.
Stratospheric Ozone Depletion	Global	Chlorofluorocarbons (CFCs) Hydrochlorofluorocarbons (HCFCs) Halons Methyl Bromide (CH_3Br)	Ozone Depleting Potential	Converts LCI data to trichlorofluoromethane (CFC-11) equivalents.
Acidification	Regional Local	Sulphur Oxides (SOx) Nitrogen Oxides (NOx) Hydrochloric Acid (HCL) Hydroflouric Acid (HF) Ammonia (NH_3)	Acidification Potential	Converts LCI data to hydrogen (H^+) ion equivalents.
Eutrophication	Local	Nitrogen Oxide (NO) Nitrogen Dioxide (NO_2) Nitrates Ammonia (NH_3)	Eutrophication Potential	Converts LCI data to phosphate (PO_4) equivalents.
Photo-oxidant formation	Local	Non-methane hydrocarbon (NMHC)	Photochemical Oxidant Creation Potential	Converts LCI data to ethane (C_2H_6) equivalents.
Ecotoxicity	Local	Toxic chemicals, including As, Cd, Cr, Cu, Hg, Ni, Pb, Zn, Sb, Be, B, F, Mn, Se, V, Co, Ba, Ag, Tl, with a reported lethal concentration to rodents or to fish	LC_{50}	Converts LC_{50} data to equivalents.
Human toxicity	Global Regional Local	As, Cd, Cr, Cu, Hg, Ni, Pb, Zn, Sb, Be, B, F, Mn, Se, V, Co, Ba, Ag, Tl, release to air, water, and soil.	LC_{50}	Converts LC_{50} data to equivalents.
Depletion of abiotic resources	Global Regional Local	Quantity of minerals used Quantity of fossil fuels used	Resource Depletion Potential	Converts LCI data to a ratio of quantity of resource used versus quantity of resource left in reserve.
Land Use	Global Regional Local	Quantity disposed of in a landfill	Solid Waste	Converts mass of solid waste into volume using an estimated density.

It is worth noting that CO_2 leakage can cause several types of environmental impacts as described Section 2.3.4, however, only the global warming impact can be recognised by the conventional LCA systems, e.g. “Life cycle assessment: An operational guide to the ISO standards”. The other potential environmental impacts of CO_2 leakage analysed in Section 2.3.4 are not considered as environmental impacts in the conventional LCA context. Therefore, in this research, only the global warming impacts were accounted for, due mainly to lack of widely recognised and accepted standards for the assessment of other impacts, more research is needed to further the understanding of these impacts. At this stage, this research focuses on quantifying the quantity of CO_2 leakage to different compartments in the environment. This could serve as a basis for further analysis of other aspects of environmental impacts of CO_2 leakage. In addition, because the environmental impact of impurities co-injected with CO_2 is not fully understood at the moment, while one researcher (Apps, 2006) suggests that the impurities that may be co-injected with CO_2 have a negligible environmental impact on the geological storage formations, this research does not consider the environmental impacts of the impurities co-injected with CO_2.

4.6 Conclusions

System boundaries of LCA on power generation with CCS are set, including power generation, CO_2 capture, CO_2 transportation, CO_2 storage and the upstream processes (e.g. extraction and production fossil fuels, production of consumables, and transportation of fossil fuels and consumables). The focus of this research was power generation with CCS systems rather than the upstream processes. The system boundaries were designed to incorporate the CO_2 storage systems, by covering geological storage formation(s), zones surrounding the storage formation(s), wells intersecting the storage formation(s) and the surrounding zones, and the CO_2 injection facilities on the surface. The lifetime of a project in the context of LCA was set as 1,000 years. The functional unit of power generation with CCS was set as 1MW electricity generated with CO_2 capture and 1,000-years of CO_2 storage respectively.

A methodological framework for LCI modelling was developed to allow for the technical, spatial and temporal differences that may be experienced for different plants, by breaking down the power generation with CCS systems into manageable component processes, which can be modelled based on the physical or chemical principles concerned or by using empirical relationships for component unit processes. This not

only addresses the limitations of conventional LCA studies which use linear input/output coefficients for the LCI models, but also resolves the second limitation of the conventional LCI models by accommodating the specific operational needs of the industry users which are often ignored. The methodological framework developed utilises the Monte Carlo simulation method to quantify the uncertainty involved in the LCI results. ISO 14041 (1998E) focuses on LCA study of existing plants and does not offer options for novel systems that are not commercially operated at the moment. The methodological framework developed in this research also provides the means to conduct LCA for novel systems by configuring virtual systems at component unit process level.

The level of detail included in the LCI models developed is at individual substance level. The substances of concern are traced from their entry into the power generation, through the changes that take place in component process units along the power generation system within the CCS chain, ultimately to their final release to the environmental compartments (e.g. air, water and soil).

Chapter 5 Life Cycle Inventory Modelling of Conventional Coal Combustion and Emission Control Processes

5.1 Introduction

This chapter presents the life cycle inventory (LCI) model developed for conventional power generation plants (without CCS). A conventional coal combustion power generation system is shown in Figure 5.1. The LCI model developed for conventional power plants include LCI models for the conventional coal combustion process, electrostatic precipitator particulate matter control process, SOx control process, NOx control process, and solid waste disposal. These LCI models can also be used for power plants with CCS, because these processes are also used in power generation systems with post-combustion CCS. For this reason, the specific process parameters that are relevant for conventional plants and plants fitted with post-combustion capture will also be discussed in this chapter. The LCI modelling results for conventional systems are used as reference power plants for comparison with power plants with CCS.

Unlike previous LCA applications on conventional power plants, which are all at plant level, the LCI model developed in this research was designed at component process level so that technical and geographical differences can be considered. Moreover, the solid waste disposal and the leakage of heavy metals from solid waste disposal units,

which are not considered in previous LCA applications are included. LCI models for alternative solid waste management options including waste piles, surface impoundments, and landfills were developed for a 1,000-year period, which is the lifespan of CCS systems in the context of LCA.

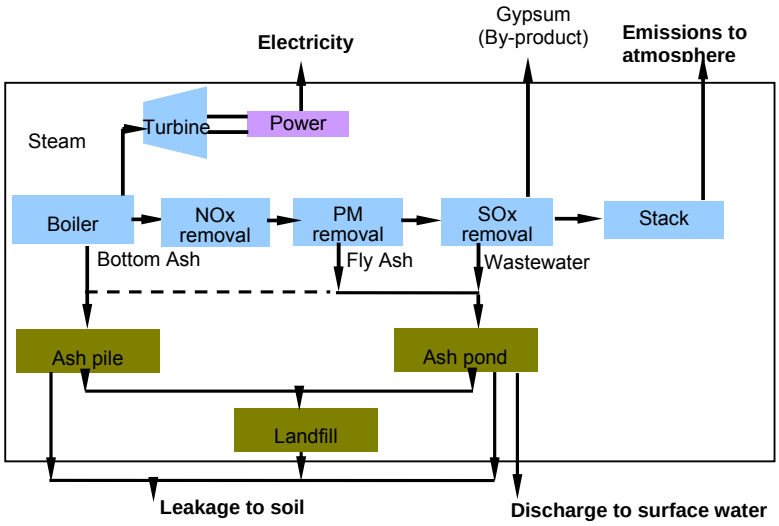

Figure 5.1: A conventional coal combustion power generation system

5.2 Coal Combustion Life Cycle Inventory Model Development

5.2.1 Principles of Coal Combustion Boiler Function

Boilers utilise the heat generated by fossil fuel combustion to produce hot water, steam, or both. The combustion process is defined as the rapid oxidation of substances (fossil fuels) with the evolution of heat. Figure 5.2 presents a simplified schematic of a coal-fired electric utility boiler with steam turbines. The coal is ignited and burned in the section of the boiler called the "furnace chamber." Force induced (ID) fans blow ambient air into the furnace chamber which provides the oxygen required for combustion. When coal burns, it is converted into CO_2 and water, which are referred to as the primary combustion products. Combustion products from boiler operation can also include partially oxidized hydrocarbons, CO, SO_2, SO_3, NOx, acids such as hydrochloric acid, organohalides such as dioxins and furans (USEPA, 2001). These hot combustion products are vented from the furnace in a gas stream called flue gas. The non-combustible portion of a fuel (including mineral matter) remains as a solid residue or ash. The coarser, heavier portion remains within the combustion chamber and is called "bottom ash." The finer portion, referred to as "fly ash," exits the furnace with the flue gas. Unburned or partially burned solid carbon particles are

also entrained in the flue gas. The composition of flue gas is strongly influenced by the fuel characteristics, the boiler type, and the operating conditions of the boiler.

The walls of the furnace chamber are lined with vertical tubes containing water, and heat generated from the combustion boils the water in the tubes to produce high-temperature, high-pressure steam. This steam flows to a steam turbine, where the thermal energy in the steam is converted to mechanical energy to drive a shaft that spins a generator, which produces electricity. After the steam exits the turbine, it is condensed and the water is pumped back to the boiler. It is worthy to note that, in order to improve the overall energy conversion efficiency, modern coal-fired electric utility boilers contain a series of heat recovery sections (including "superheater", "reheater", "economiser" and "air heater"[1]), which are located downstream of the furnace chamber and are used to extract additional heat from the flue gas. Therefore, when modelling combustion processes, it is necessary to consider the overall plant energy conversion efficiency, which is determined by the plant configuration and ambient temperature.

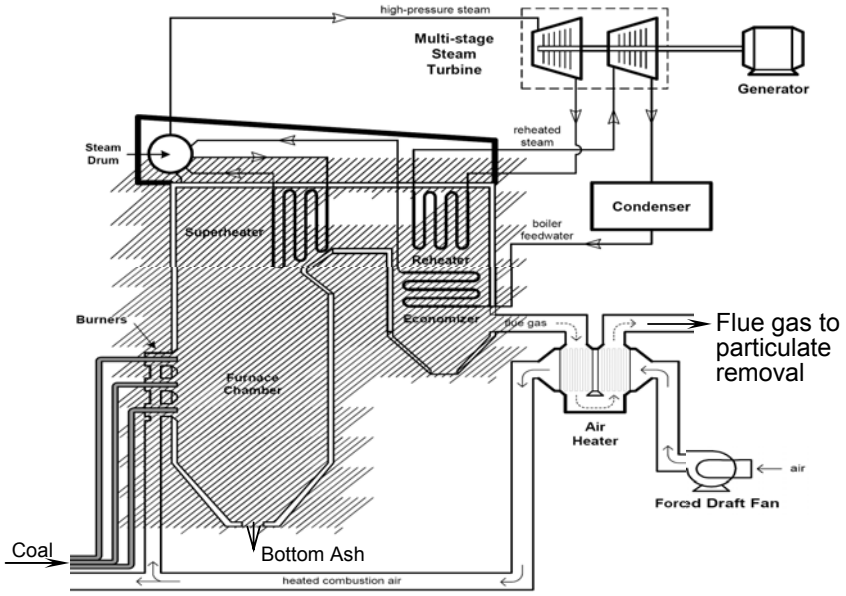

Figure 5.2: A simplified schematic of a coal-fired electric utility boiler with steam turbines (Modified from US EPA, 2002).

[1] The"Superheater" is used to increase the steam temperature. The "Reheater" reheats the steam exhausted from the first stage of the turbine. This steam is then returned for another pass thorough a second stage of the turbine. The reheater is followed by an "Economiser" which preheats feed water to the boiler tubes in the furnace. The "Air heater" preheats ambient air used for combustion of the coal.

Boiler types are classified by the heat transfer method (watertube, firetube, or cast iron), the arrangement of the heat transfer surfaces (horizontal or vertical, straight or bent tube), and the firing configuration (suspension, stoker, or fluidized bed) (USEPA, 1998). Watertube boilers with suspension firing of pulverised coal (including pulverised coal (PC) and cyclone boilers) are primarily used in power generation. Pulverised coal boilers can be further classified as either dry or wet bottom, depending on the ash removal technique. Dry-bottom boilers may either be tangential- or nontangential-fired units. Some examples of nontangential-fired pulverised coal boilers are wall-fired, cell-fired, vertical, and arch. Dry-bottom boilers fire coal with high ash fusion temperatures, whereas wet-bottom furnaces fire coal with low ash fusion temperatures. Wet-bottom furnace designs have higher nitrogen oxides (NOx) emission rates and are no longer being built, though many remain in operation (USEPA 2001). The distribution of coal-fired boiler types for power generation in the U.S. is summarised in Figure 5.3, as an example.

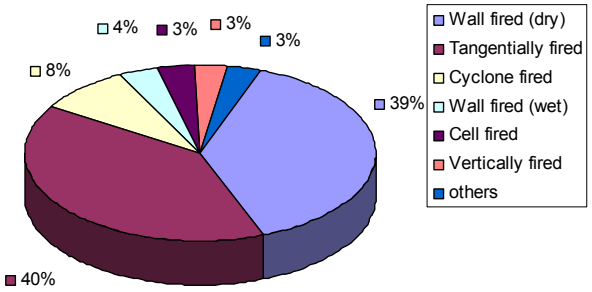

Figure 5.3: Summary of U.S. coal fired boilers (After Hitachi Zosen Engineering Ltd., 2002)

5.2.2 Coal Combustion Life Cycle Inventory Model Development

In this research, the coal combustion LCI model developed quantifies mass flows (coal, CO_2, N_2, O_2, H_2O) based on stoichiometric reactions, estimates emissions (CO, SO_2, SO_3, NOx, acids, PM and trace metals) based on USEPA AP-42 emission factors (USEPA, 1998), and computes energy consumption and heat (steam) output by engineering calculations. In order to characterise technological and geographical differences of coal combustion process, the LCI model allows for the coal characteristics, six types of boiler, the power plant configuration and the plant location to be considered. The scheme of the LCI model developed is shown in Figure 5.4.

5.2.2.1 Mass Flow Rate of Coal

The mass flow rate of coal (M_{coal}) is calculated as:

$$M_{coal}=\text{Designed power output (kwh)} /(\text{LHV}\times \eta_{plant}) \quad [5.1]$$

Where: LHV is the lower heating value of coal;

η_{plant} is the plant gross efficiency (LHV basis).

In Equation [5.1], the designed power output, LHV and η_{plant} are the variables representing the plant configuration, coal characteristics and plant operation conditions.

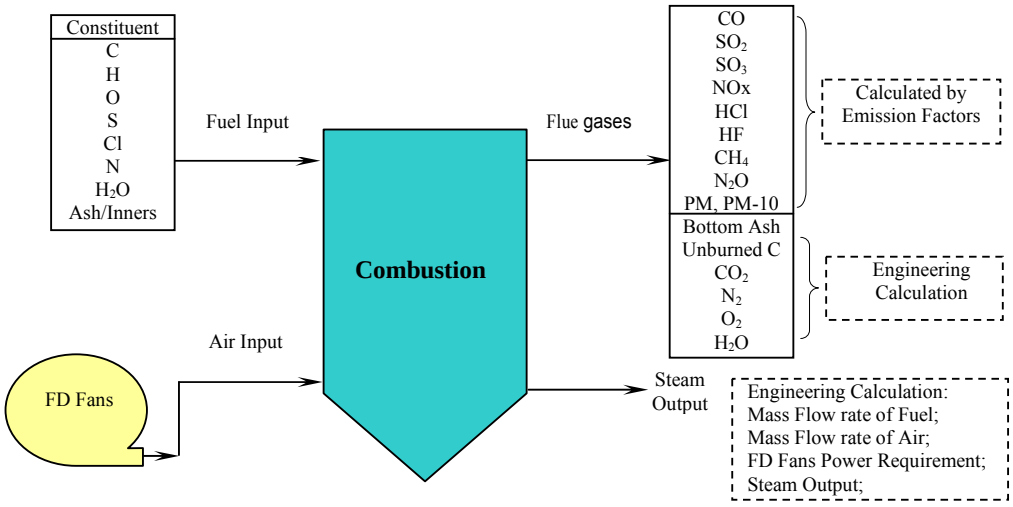

Figure 5.4: The scheme of coal combustion process LCI model developed

Designed Power Output

Power output from conventional boilers in coal-fired power plants reached unit sizes of over 1,000 MW in the 1970s. Average value of coal-fired plant size in OECD countries is 750 MW, however, as large plants can take many years to reach full utilisation, the average unit sizes of OECD power plants have been dropping since the mid 1970s (IEA, 1999). In this research, it is assumed the default plant size is 500 MW.

Plant Gross Efficiency (η_{plant})

Plant gross efficiency (η_{plant}) is the efficiency of converting heating value of fuel to electricity determined by the efficiency of the combustor (typically 90%), the thermal efficiency of the reversible cycle (typically 50%), the isentropic efficiency of the turbine (typically 94%), the mechanical efficiency of the turbine (typically 99%), and the electrical generator efficiency (typically 99%), excluding the efficiency loss caused by onsite auxiliary power consumption. The thermal efficiency of the reversible cycle, which depends on plant configuration, is the crucial factor in determining η_{plant}. Conventional power plants with subcritical steam conditions are characterised by gross efficiencies of some 40% (IEA, 2004); advanced plants with supercritical steam can

attain gross efficiencies of 45-50% and ultra-supercritical plants may achieve gross efficiencies of 55-60% (IEA, 2003). In this research, it is assumed that the gross efficiencies of subcritical, supercritical or ultra-supercritical plant are 40%, 45% and 55% respectively. In order to reflect geographical difference of gross efficiencies, regional average gross efficiencies are used for subcritical plants in various regions across the world as shown in Table 5.1 (due to the data availability, only average regional efficiencies for hard coal-fired power plant are presented in this table).

Table 5.1: Average regional efficiencies for coal-fired power plants (After IEA, 2004)

Regions	Hard coal-fired (%)
Africa	35
Australia/New Zealand	38
China	35
Central and South America	35
Eastern Europe	27
India	28
Japan	38
Middle East	40
Mexico	-
Other Asia	33
South Korea	36
USA/Canada	36
Western Europe	39

Note: Based on gross efficiency (LHV basis)

Boiler Operating Conditions

The boiler operating conditions used in this research mainly include availability rate and capacity utilisation rate of plant, which also influence the plant efficiency. Modern power plants, both subcritical and supercritical, are capable of achieving very high availability, typically ranging from 88 to 92%, and the majority of the lost availability is attributed to planned outages for about 4 weeks in a year (IEA, 1995). It is assumed that availability of power plants is 90%.

The average capacity utilisation rate of OECD power plants is only about 50% and these rates are higher in developing countries, because surplus generation capacity under the rapid growth in energy demand in these countries is unlikely (IEA, 1999). On the other hand, carbon capture only makes sense in new power plants because of their high thermal efficiency (IEA, 2004) and new coal-fired power plants are normally intended for base load operation. Based on this analysis, it is assumed that plants with CCS are for base load[2] operation and the utilisation rate is 75% and 80% for industrialised countries and developing countries respectively. As the efficiencies of

[2] According to their plant utilisation rate, power plants can be classified in to three categories: based-load power plants (utilisation rate > 68%, such as large coal fired and nuclear plants), intermediate-load power plants (utilisation rate between 28% and 68%, such as older less efficient plants), and peaking power plants (utilisation < 28%, such as gas turbine and diesel engine power plants) (IEA, 1995).

coal-combustion based plants do not fall off significantly at part load (IEA, 1995), it is assumed that there is no efficiency loss for power plants at part load.

The Composition and Heating Value of Coal

The principal chemical constituents of coal are carbon, hydrogen, oxygen, nitrogen, and sulphur. Coal also contains incombustible mineral matter and trace amounts of metallic elements, oxides, and rare gases. The composition of coal is an important factor which determines the composition and amount of combustion products. Coal composition is always reported by ultimate analysis, which is the determination by prescribed methods of the ash, carbon, hydrogen, nitrogen, sulphur, oxygen content and its heating value. Table 5.2 gives the composition, HHV, and LHV of typical coal types. Based on ultimate analysis, coals are classified by rank from lignite, subbituminous coal, bituminous coal to anthracite. Typically, coal rank increases as the amount of fixed carbon increases and the amount of volatile matter and moisture decreases. Lignite, subbituminous, and bituminous coal are mostly used for power generation.

Table 5.2: Average composition, heating value of coal (After Khartchenko, 1997)

Fuel type	Ash (%)	Water(%)	Ultimate analysis (daf**) by mass (%)					HHV MJ/kg	LHV MJ/kg
			C	H	S	O	N		
Lignite	2-8	50-60	65-75	5-8	0.5-4	15-26	0.5-2	10-13	8-10.5
Hard coal*	3-12	0-10	80-90	4-9	0.7-1.4	4-12	0.6-2	29-35	27-34
Anthracite	2-6	0-5	90-94	3-4	0.7-1	0.5-4	1-1.5	33.5-35	32.5-34

* Hard coal mainly refers to steam coal and coking coal; ** daf: dry, ash-free basis.

In many parts of the world, the choice of coal is limited to that produced locally. This results in geographical differences in emissions from power generation. For instance, in China coal fired power plants nearly completely depend on indigenous coals with average 1.3% sulphur content. On the other hand, power plants in Germany still fire on lignite. In order to represent the characteristics of the coal at a regional level, the model developed considers the composition and heating value of coal when calculating the mass flow of coal, air requirements and environmental emissions.

5.2.2.2 Heat Output of a Boiler

The heat output of boiler (H) is:

$$H = M_{coal} \times LHV \times \eta_{boiler} \qquad [5.2]$$

Where: η_{boiler} is the boiler efficiency (η_{boiler} = Total heat added to the working fluid/ Total fuel input energy), which ranges 75% to 95%, typically around 90% (Black and Veatch, 1996; Tyler, 1986).

5.2.2.3 Mass Flow of Air

The mass flow of oxygen (M_{oxygen}) needed for coal combustion is calculated by [5.3], based on stoichiometric reactions[3].

$$M_{oxygen} = \left(\frac{C(1-u)}{12} + \frac{H}{4} - \frac{O}{32} + \frac{S}{38}\right) \times M_{coal} \times 32 \quad [5.3]$$

Where H, O, S and C are the decimal weights of these elements in coal and u is the rate of unburned carbon, typically 1% (US EPA, 1998).

Then, the mass flow of nitrogen ($M_{nitrogen}$):

$$M_{nitrogen} = 3.78 \times M_{oxygen} \quad [5.4]$$

The dry air needed for combustion is:

$$\text{Dry combustion air} = (1+\theta) \times (M_{nitrogen} + M_{oxygen}) \quad [5.5]$$

Where θ represents the extra air for combustion. The excess air ratio θ depends on the coal rank, the furnace design, and the burner type and load. Typically, the excess air level for subbituminous coal and lignite is 20% operating excess air, and for bituminous coal is 25% operating excess air (Black and Veatch, 1996).

The combustion air utilised in the boiler also contains moisture in the form of water vapour, which is a function of temperature and relative humidity of air. In this research, a typical moisture content of 0.013 kg H_2O/kg dry air (air at 60% relative humidity and 27 ^oC) is used, and the wet combustion air is calculated using the following equation:

$$\text{Wet combustion air} = (1+\text{moisture content}) \times \text{Dry combustion air} \quad [5.6]$$

5.2.2.4 Combustion Products

CO_2, H_2O, O_2, N_2 and Unburned Carbon

The intermediate product flows of CO_2, H_2O, O_2 and N_2 after combustion are calculated using the following equations based on stoichiometric reactions:

$$M_{CO_2} = M_{coal} \times C \times (1-u) \times (44/12) \quad [5.7]$$

$$M_{H_2O} = M_{coal} \times H \times 18/2 + \text{Moisture} \quad [5.8]$$

---

[3] The main stoichiometric reactions of coal combustion are:

$$C + O_2 \rightarrow CO_2$$
$$2H_2 + O_2 \rightarrow 2H_2O$$
$$S + O_2 \rightarrow SO_2$$

$$M_{outO_2}=\theta\times M_{oxygen} \quad [5.9]$$

$$M_{nitrogen}=3.78\times(1+\theta)\times M_{oxygen}+M_{coal}\times N \quad [5.10]$$

$$\text{Unburned carbon} = M_{coal} \times u \quad [5.12]$$

Where u is the rate of unburned carbon, typically 1%.

Other Gaseous Combustion Products

Other products (SOx, NOx, etc) of combustion largely depend on the type of boiler. In this research, the following six types of boilers are considered as follows:

- PC Wall-fired dry bottom boiler
- PC Wall-fired wet bottom boiler
- PC, Cell burner fired dry bottom boiler
- PC Tangential-fired dry bottom boiler
- PC Tangential-fired wet bottom boiler
- Cyclone boiler

The emission factors relating to these types of boilers for bituminous coal, subbituminous coal and lignite are provided in Tables B1, B2 and B3in the Appendix, as summarised from US EPA (1998).

5.2.2.5 Particulate Matter Emissions

The majority of inorganic matter present in coals occurs in the form of minerals of various types and grain sizes. During crushing, grinding and milling processes, prior to coal combustion, inorganic matter may be liberated from the organic matrix. Thus, mineral matter in pulverised coal particles presents different mineral–organic associations and is classified into organically associated mineral matter and discrete mineral grains, referred to as included mineral and excluded mineral. During coal combustion, ash particles are formed from the inorganic matter present in coal. The information on mineral–organic association is extremely important for coal utilisation processes. For example, during coal combustion, different mineral matter may experience different temperature-time histories resulting in different physical–chemical transformations, thus generating ash particles of different sizes and chemistry, which influence flyash-related utilisation and related environmental issues. The majority of ash particles are formed from four formation mechanisms, shown in Figure 5.5 (Buhre et al. 2006):

- Included mineral coalescence;
- Char fragmentation;
- Excluded mineral fragmentation, and
- Vaporization and subsequent condensation of inorganic matter.

The mechanisms of ash formation are affected by the combustion conditions and the coal characteristics.

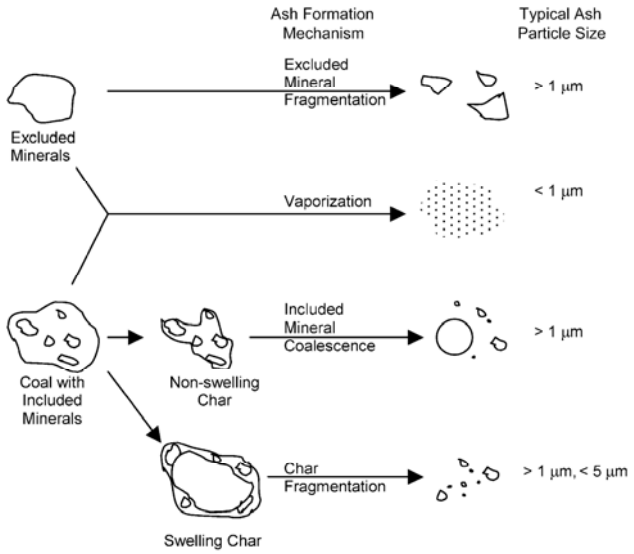

Figure 5.5: Schematic of ash formation mechanisms during pulverised coal combustion (After Buhre *et al.* 2006)

The size distributions of the coal combustion ash particles can be classified in four modes, one in the submicron region (less than 1μm and greater than 100nm in diameter), one in the ultrafine region (less than 100nm, down to the size of individual molecules, in aerodynamic diameter) and the other two around 10 and 100μm, respectively. The size fraction of legislative interest is the size less than 10μm, because these fine particles can cause inverse impact on human respiration systems. In this research, the notation PM_{10} is used to describe particles of 10μm or less and $PM_{2.5}$ represents particles less than 2.5μm in aerodynamic diameter.

The submicron and ultrafine mode was expected to form under the vaporization and condensation mechanism, while the 10 and 100μm modes were believed to form through bulk fragmentation and coalescence (Sheng *et al.*, 2007).

The PM emission factors relating to various types of boilers for bituminous coal, subbituminous coal and lignite are provided in Tables B1, B2 and B3 in the Appendix, as summarised from US EPA (1998).

5.2.2.6 Emissions of Trace Metals in Flue Gases

Because coal is a natural substance comprising both the organic coal matter and inorganic material from the earth's surface, practically every element from the Periodic Table is present to varying levels (DTI, 2004). The term "trace element" in this research refers to chemical elements present in a natural material at concentrations < 0.1 %wt, besides the minor elements (0.1-1 %wt) and the major elements (> 1%wt). The elements of environmental concern in this research are defined in Table 4.1 in Chapter 4.

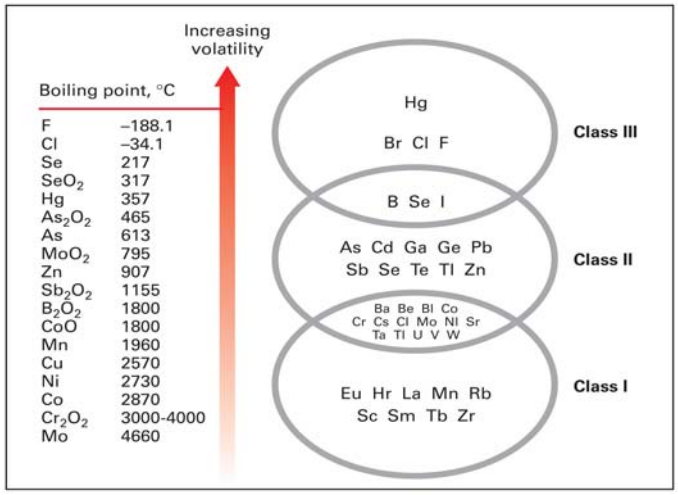

Figure 5.6: Trace element groupings (After DTI, 2004; Zevenhoven and Kilpinen, 2004)

Coal combustion in utility boilers takes place at operating temperatures of over 1400°C. While coal injected as fine power is heated in the boiler, volatile matter is released and mineral matter is exposed to rapid heating and high temperatures, which may result in thermal decomposition, fusion, disintegration and agglomeration (DTI, 2004). Any trace elements in the mineral matter may be released and dispersed among the fly ash, bottom ash and combustion flue gases. Generally, trace element partitioning behaviours during coal combustion are classified into three groups (see Figure 5.6) (Zevenhoven and Kilpinen, 2004; DTI, 2004; AP 42, 1996; Lee and Lesley, 1992):

- Class I: elements do not volatilise during combustion or gasification and are distributed more or less equally in bottom ash and fly ash;

- Calss II: elements are vaporised but are found mainly in the fly ash after condensation on particulates and nucleation mechanisms as a result of decreasing temperature in e.g. the flue gas duct. A significant part of these fine particles are in the sub-micron size class where dust control systems are less effective;
- Class III: elements which volatilise most readily. They are found in the vapour phase even at flue gas exit temperatures of just over 100°C and are depleted in all solid phases, typically Hg, Br, I.

Trace metals are a sub-class of the trace elements. Trace metals may form a threat to the environment or to human health (e.g. Hg, Cd, Pb, As, Cr), they may cause corrosion problems (e.g. Zn, Pb), lead to fouling of turbine blades (mainly Ca), or pollute or poison catalysts (mainly As) or sorbents downstream (Zevenhoven and Kilpinen, 2004). The majority of trace elements of concern in Table 4.1 are trace metals, except Boron (B) and Fluorine (F). The majority of these trace metals falls in Class II, except Hg and Se which are fall in Class III and Mn in Class I.

Table 5.3: Emission factor for trace metals from uncontrolled coal combustion and typical concentration of trace metal in coal (Compiled after US EPA, 1998 and Lee and Lesley, 1992)

Pollutants	Group	Emission factor (lb/10^{12} Btu)	Typical concentration of trace metal in coal (ppm)
Antimony (Sb)	II	$0.92 \times (C/A \times PM)^{0.63}$	1
Arsenic (As)	II	$3.1 \times (C/A \times PM)^{0.85}$	10
Beryllium (Be)	II	$1.2 \times (C/A \times PM)^{1.1}$	1.3
Cadmium (Ca)	II	$3.3 \times (C/A \times PM)^{0.5}$	0.52
Chromium (Cr)	II	$3.7 \times (C/A \times PM)^{0.58}$	18.6
Cobalt (Co)	II	$1.7 \times (C/A \times PM)^{0.69}$	6.4
Lead (Pb)	II	$3.4 \times (C/A \times PM)^{0.80}$	8.1
Manganese (Mn)	I	$3.8 \times (C/A \times PM)^{0.60}$	22.4
Nickel (Ni)	II	$4.4 \times (C/A \times PM)^{0.48}$	16.1

Emission factor: The equations were developed from emissions data from bituminous coal combustion, subbituminous coal combustion, and from lignite combustion. The equations may be used to generate factors for both controlled and uncontrolled boilers. The emission factor equations are applicable to all typical firing configurations for electric generation (utility), industrial, and commercial/industrial boilers firing bituminous coal, subbituminous coal, and lignite.
C: concentration of trace metal in coal, parts per million by weight (ppmwt);
A: the weight fraction of ash in the coal;
PM: particulate emissions. Site-specific emission factor for total particulate matter, lb/106 Btu.

The quantity of any given metal emitted, in general, depends on the physical and chemical properties of the metal, the concentration of the metal in the coal, and the combustion conditions (USEPA, 1998). In this research, the USEPA trace element emission factors for coal air combustion, shown in Table 5.3, are used for the calculation of trace metal emissions. The trace metals of concern (Table 4.1) including Se, Zn, Co, V, Ba, TI, Ag and Hg are covered by the USEPA emission factors. For the Group I trace metals Cu, V, Ba, TI and Ag, this research assumes that they are equally distributed between bottom ash and fly ash. For trace metals Se and Zn, which are

classed in Group II, it is assumed that 80% is apportioned in the fly ash stream and rest in bottom ash.

Mercury in the flue gas can be found in three forms classified as gaseous mercury existing as either oxidised mercury (Hg^{2+}) or elemental mercury (Hg^0) and particle-bound mercury (Hg_{part}). This is because the Hg existing in coal completely vaporises and converts into gaseous Hg^0 in the combustion zone of a boiler system, and as gaseous Hg^0 entrails with the flue gas in the boiler it can undergo gas-phase oxidation to form gaseous Hg^{2+} (USEPA, 2002). The regression equations 5.13, 5.14 and 5.15 from literature are used to calculate the mercury speciation leaving the furnace (Laudal *et al.*, 2000:

Elemental Mercury (Hg^0)

$\%Hg^0$ (percent of Hg in coal) = 39.0 + 0.00211 Ca – 0.0391 Cl [5.13]

P = 0.99 P = 0.99

$R^2 = 0.95$

Oxidized Mercury (Hg^{2+})

% Hg^{2+} (percent of Hg in coal) = 109 – 0.00471 Ca – 0.00205 S + 0.0190 Cl [5.14]

P = 0.99 P = 0.99 P = 0.88

$R^2 = 0.94$

Particulate Mercury (Hg_{part})

% Hg_p (percent of Hg in coal) = 1-$\%Hg^0$ - $\%Hg^{2+}$ [5.15]

Where, $\%Hg^0$, $\%Hg^{2+}$, and $\%Hg_p$ represent the proportion of mercury speciation in form: Hg^0, Hg^{2+} and Hg_p respectively; Hg, S, Cl, and Ca represent concentrations in parts per million on a moisture-free basis. P represents the probability that the x coefficient is significantly different from zero. R^2 is the coefficient of determination.

5.2.2.7 Solid Waste Emissions

Solid waste emissions include the bottom ash. The mass flow of bottom ash is calculated using Equation [5.16]:

$$\text{Bottom ash} = M_{coal} \times \text{Ash in coal (\%)} - \text{Fly Ash (PM)} \quad [5.16]$$

5.2.2.8 Auxiliary Power Requirements

Auxiliary power requirements in combustion process is caused by force draft (FD) fans, which provide a high enough pressure capacity for combustion air to overcome the pressure drop between the air intake of the fan and the boiler. The auxiliary power requirement by force draft fans can be calculated using the following engineering calculation (Black and Veatch, 1996):

$$\text{Power (kW)} = 2.67\times10^{-6}Q\times\Delta P/\eta_{fan} \qquad [5.17]$$

where:

Q is the fan volume (m^3/hr) (density of air used is 1.29kg/m^3);

ΔP is the total change of pressure in kPa, which is typically 5.086 kPa; and

η_{fan} is the energy conversion efficiency of fans, typically 75%.

5.3 Life Cycle Inventory Modelling of the Particulate Matter Control Process

5.3.1 Particulate Matter Control Technologies

As already discussed in the previous section, during combustion or gasification the inorganic mineral impurities in fuels are converted into solid, liquid and gaseous compounds, which finally leave the system as bottom ash, fly ash or vapour. Fly ash typically contains regulated elements such as arsenic, barium, boron, cadmium, chromium, lead, mercury, selenium, etc. The direct release of these elements to the air will generate significant impacts to human health, wildlife and the ecosystem. Particulate matters (PM) process units are used to control the fly ash emissions. As illustrated by Figure 5.7, PM control devices can be classified in two types: processes where an external force is applied to the particle and processes where the gas stream is forced through a barrier that cannot be passed by the dispersed particles, in the form of holes smaller than the particles, or a droplet cloud (Zevenhoven and Kilpinen, 2004).

This research focuses on the development of the cold side (dry) Electrostatic Precipitator (ESP) LCI model, since cold side ESP can be applied to a variety of coal combustion sources and a wide range of plant sizes as well as achieve high PM removal efficiency.

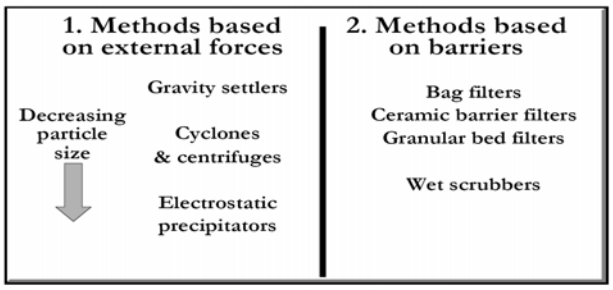

Figure 5.7: General classification of PM control devices (After Zevenhoven and Kilpinen, 2004)

5.3.2 Life Cycle Inventory Modelling of the Electrostatic Precipitator

The cold side (dry) electrostatic precipitator (ESP) is located after the air preheater and operates in a temperature range of 130-180°C (IEA, 2004). ESPs comprise a series of parallel plates with rows of electrodes in between them and carry a high voltage of opposite polarity. As the particle laden flue gas enters the unit, the particles are charged by the electrodes and are attracted to the plates (Berkenpas, *et al.*, 1999). The operating parameters that influence ESP performance include fly ash mass loading, particle size distribution, fly ash electrical resistivity, and precipitator voltage and current (USEPA, 1998a). The ESP design factors that determine ESP collection efficiency are collection plate area, gas flow velocity, and cleaning cycle (IEA, 2004). PM removal efficiencies of ESPs are greater than 99 percent for fine (less than 0.1 micrometer) and coarse particles (greater than 10 micrometers) (USEPA, 2002). The PM removal design efficiencies of EPSs range from 99% to 99.99% (Buonicore *et al*., 1992). The typical removal efficiency of 99.7% is used in this research.

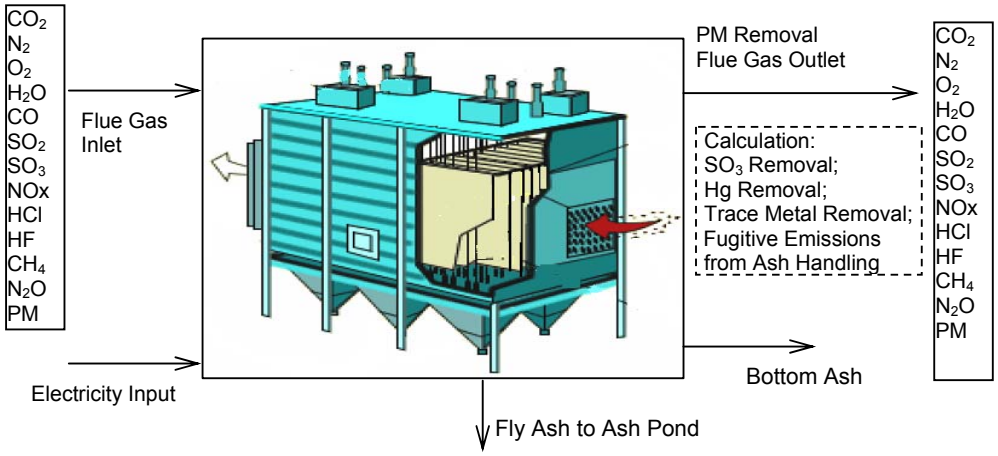

Figure 5.8: The scheme of the ESP LCI modelling

The scheme of the ESP LCI modelling is demonstrated in Figure 5.8. The LCI model developed calculates the electricity consumption of ESP, PM removal, trace metal removal, SO_3 removal, and fugitive emissions removal from fly ash handling as explained in the following paragraphs.

5.3.2.1 Power Required for the Electrostatic Precipitator Operation

The power required to operate system fans, transformer-rectifier (TR) sets, and cleaning equipment needs to be calculated. Assuming fan-motor efficiency of 0.65 and a specific gravity of 1.0 at standard temperature and pressure , the fan power for primary gas movement is calculated from the following equation (Buonicore and Davis, 1992):

$$F_{power} = 1.54Q \times \Delta p \qquad [5.18]$$

where

F_{power} is fan power requirement, kWh;

Q is system flow rate, (m^3/s);

Δp is system pressure drop in water. ESP pressure drop is typically between 0.022 and 0.095 kPa (Buonicore and Davis, 1992).

The energy for TR sets and motor-driven cleaning equipment is sum of the energy consumption for operating both items. Manufactures' average data indicate that the following relationship can be used:

$$H_{Power}=2.09\times10^{-2}\ A \qquad [5.19]$$

where:

H_{Power} is annual ESP operating power, KWh;

A is ESP plate area, m^2, A= SCA*V, V is volumetric flue gas flow rate, m^3/s. Typically, the SCA value of 78.75 s/m is for power plants.

5.3.2.2 Mercury Removal Efficiency in the Electrostatic Precipitator

The ESP unit can remove up to 60% of mercury in flue gas, which is mostly oxidised mercury (Hg^{2+}) and small amount elemental mercury (Hg^0) (Nalbandian, 2004; US DOE, 2001). The capture of mercury in ESP is temperature sensitive, with the capture efficiency being higher at lower temperature (Lissianski, 2004). For bituminous coal fired units, mercury removal efficiency in EPS units is calculated using the following regression equation derived from Figure 5.9:

$$Hg_{ESP\ reduction} = 171.83\exp(-0.0012T_{ESP}) \qquad (R^2 = 0.8849) \qquad [5.20]$$

Where, $Hg_{ESP\ reduction}$ is the mercury removal efficiency (%); T_{ESP} is the ESP operation temperature (°C).

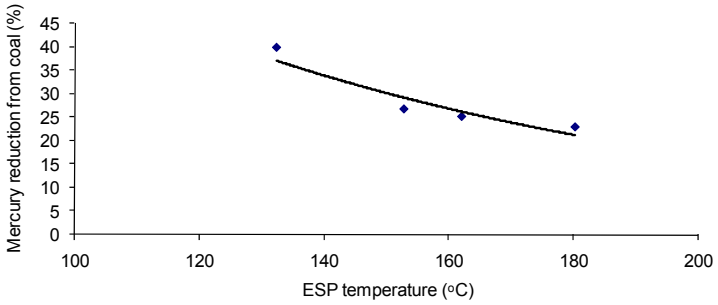

Figure 5.9: Temperature effect on mercury removal for bituminous coal (After Lissianski, 2004)

Electrostatic Precipitators (ESPs) are found to achieve poor mercury removal on lignite fired and subbituminous coal fired units, because they are operated at relatively high temperatures (Sjostrom *et al.*, 2001). A summary of average mercury removal in ESPs for lignite and subbituminous coals, is given in Table 5.4.

Table 5.4: Summary of average mercury removal in ESPs (Sjostrom *et al.*, 2001)

Coal type	$Hg_{ESP\ removal}$ (%)
Subbituminous	9
Lignite	2

5.3.2.3 Sulphur Trioxide (SO_3) Removal Efficiency in the Electrostatic Precipitator

ESPs provide extended residence time (10-15 seconds) for the flue gas at relatively low temperatures, allowing contact between sulphuric acid and fly ash particles. Therefore, ESPs can remove SO_3 from the flue gas by retaining sulphuric acid particles on the collecting plates (IEA 2004). The ESPs' SO_3 removal efficiency for different types of coal are provided in Table 5.5:

Table 5.5: Cold-side ESP SO_3 removal efficiency (After EPRI, 2007)

Equipment Type	Coal Type	SO_3 removal efficiency (%)
Cold-side ESP	Low Sulphur Bituminus	51
	High Sulphur Bituminus (>2.5%)	23
	Subbituminous	27

5.3.2.4 Trace Metal Removal Efficiency in the Electrostatic Precipitator

ESPs have demonstrated high removal efficiencies for trace metals that condense on or form fine particulate. These metals include arsenic, barium, beryllium, cadmium, cobalt,

chromium, manganese, nickel, lead, antimony, and selenium (Amrhein *et al.*, 1999). The removal of trace metals is strongly related to the overall particulate collection efficiency. However, due to many of the trace compounds being enriched in the smaller fly ash particles, some species are less efficiently removed than the fly ash in ESP. The metals which exhibit the highest variability in removal efficiency are arsenic and selenium (Amrhein *et al.*, 1999). For a typical particulate matter (PM) removal efficiency of 99.7%, the trace metal removal efficiencies are provided in Table 5.6.

Table 5.6: Average trace element removal efficiency in ESP (After Amrhein *et al.*, 1999)

Trace Element	Removal efficiency (%)
Arsenic	81.0
Barium	96.9
Beryllium	93.7
Cadmium	94.1
Chromium	96.4
Cobalt	99.0
Lead	98.5
Manganese	98.3
Nickel	97.5
Selenium	50.9

For the trace elements that are not in Table 5.6 including antimony, zinc, copper, thallium, vanadium, and silver it is assumed that the removal efficiency of ESP is 98%, as they are all Group II trace elements and may have similar removal efficiency with other Group II trace metals such as cobalt and lead.

5.2.2.5 Fugitive Emissions from Ash Unloading Activities

Emissions from unloading activities are estimated use the following equation (USEPA, 1998):

$$E = k0.0016\left(\frac{U}{2.2}\right)^{1.3}\left(\frac{M}{2}\right)^{-1.4} \quad kg/t \qquad [5.21]$$

k=0.74 for particles less than 30 micrometres aerodynamic diameter

k= 0.35 for particles less than 10 micrometres aerodynamic diameter

U= mean wind speed in m/s

M= material moisture content (%)

It is assumed that the emission control factor for unloading activities is 75% since water sprays are applied. Wind speed and ash moisture are assumed to be 4.2m/s (15km/h) and 1% respectively.

5.4 Life Cycle Modelling of Sulphur Dioxide Control Processes

5.4.1 Sulphur Dioxide Control Technologies

All coals contain sulphur. Some of this sulphur, known as inorganic sulphur, is in the form of pyritic sulphur (FeS_2), and sulphates (Na_2SO_4, $CaSO_4$, $FeSO_4$) (Zevenhoven and Kilpinen, 2004). The rest of the sulphur is organic sulphur, which is intimately associated with the coal matrix. Typical values for the sulphur content of coals range from 0.2 to 4% (DTI, 2002). During the combustion of the coal, most of the sulphur is converted to SO_2, with a small amount being further oxidized to sulphur trioxide (SO_3). Because, in the absence of a catalyst, the formation of SO_3 is slow, over 98% of the combusted sulphur is in the form of SO_2 (DTI, 2002). Burning typical medium- and high-sulphur coals produces SO_2 emissions that exceed the allowable limits (USDOE, 1999).

The emission of SOx to the atmosphere has been associated with the following health and environmental impacts (USEPA, 1998b):

- Acid rain − SOx can form acidic compounds ("acid rain") through reactions with water and oxidants in the atmosphere. The low pH associated with the acid rain can be harmful to plant and aquatic life.
- High levels of SO_2 can cause human respiratory illness.

The SO_2 emission standards for large combustion plants in EU are provided in Table 5.7.

Table 5.7: SO_2 emission standards for large coal combustion plant in EU (After Zevenhoven and Kilpinen, 2004)

Fuel	New /Existing	Plant size (MW)	Emission standard (mg/m^3STP, dry)
Coal	Existing	50-100	2,000 at 6% O_2
		100-500	2,000- 4(P-100) at 6% O_2
		>500	400 at 6% O_2
	New	50-100	850 at 6% O_2
		100-300	200 at 6% O_2
		>300	200 at 6% O_2

*P = plant size in MW

In principle, the sulphur in the coal can be removed before use; however, in practice, it is uneconomic to remove more than a small percentage of the sulphur and the most efficient means of SO_2 emissions control is to remove the SO_2 from the flue gases before they are released to the atmosphere (DTI, 2002). Flue Gas Desulphurisation (FGD) processes can be categorised as wet, dry and semi-dry systems. Some of the major FGD processes are classified as shown below (DTI, 2002):

• Wet processes:
  - limestone gypsum
  - sea-water washing
  - ammonia scrubbing
  - Wellman-Lord.
• Semi-dry processes:
  - circulating fluidised bed
  - spray dry
  - duct spray dry.
• Dry processes
  - furnace sorbent injection
  - sodium bicarbonate injection.

In wet FGD systems, SO_2 is removed from the flue gas by reaction with a calcium-based sorbent in an aqueous solution or slurry. Wet FGD systems normally achieve a relatively high degree of SO_2 removal (>90%), with a high level of sorbent utilisation (USDOE, 1999). Dry and semi-dry FGD systems involve injecting a solid sorbent (dry), usually limestone, or a sorbent slurry (semi-dry), usually lime, into the furnace or flue gas duct (USDOE, 1999). Compared with wet FGD systems, SO_2 removal efficiency and sorbent utilisation are usually lower.

Because power plants with CCS are new and/or large plants that would require higher SO_2 removal rate by regulation, this research assumes that the power plants with CCS are equipped with wet FGD systems. Almost all commercial wet FGD processes remove the SO_2 from flue gas by reaction with limestone (calcium carbonate, $CaCO_3$), or quicklime (calcium oxide, CaO) (DTI, 2002). Both limestone-based (limestone with forced oxidation, LSFO) and lime-based (magnesium-enhanced lime, MEL, with forced oxidation) FGD technologies are investigated in this research.

5.4.2 The Development of Wet Flue Gas Desulphurisation Life Cycle Inventory Model

In wet FGD processes, flue gas from the ESP flows to the SO_2 absorber, where SO_2 intimately contacts with calcium-based sorbent slurry and reacts with the slurry, forming calcium sulphite. Following contact with the slurry, the scrubbed flue gas passes through mist eliminators, which remove entrained slurry droplets, and then flows out of the FGD system. The sulphate generated in the absorber is subsequently oxidised

in a reaction tank to form calcium sulphate, which crystallises as gypsum ($CaSO_4 \cdot 2H_2O$). The dewatering system is employed to concentrate the gypsum crystals to an ultimate solids content of 85% to 90%, which is conveyed to an on-site waste disposal landfill or is utilised for wallboard or cement manufacture (USDOE, 1999). The major chemical reactions occurring in wet FGD systems (including LSFO and MEL) are described in Table 5.8.

Table 5.8: Process chemistry of LSFO and MEL systems (After Sargent & Lundy, 2003; USDOE, 1999)

Limestone with forced oxidation (LSFO)	Magnesium-enhanced lime (MEL) with forced oxidation*
Desulphurisation reaction: $SO_2+CaCO_3 + ½ H_2O \rightarrow CaSO_3 \cdot ½H_2O+CO_2$	Desulphurisation reaction: $SO_2 + Ca(OH)_2 \rightarrow CaSO_3 \cdot ½ H_2O + ½ H_2O$ $4SO_2+3Mg(OH)_2 \rightarrow 2MgSO_3+Mg(HSO_3)_2+2H_2O$
Oxidation and Crystallization: $CaSO_3 \cdot ½H_2O+½O_2+1.5H_2O \rightarrow CaSO_4 \cdot 2H_2O$	Oxidation and Crystallisation: $CaSO_3 \cdot ½H_2O+½O_2 +3/2\ H_2O \rightarrow CaSO_4\ 2H_2O$ $MgSO_3 + ½O_2 \rightarrow MgSO_4$ $Mg(HSO_3)_2 + O_2 \rightarrow MgSO_4 + H_2SO_4$

* In the MEL system, lime used in the process is composed of 83 to 91 % weight calcium oxide (CaO) and 2 to 8 % weight magnesium oxide (MgO), which greatly increases SO_2 capture and allows reduction in power consumption and equipment costs.

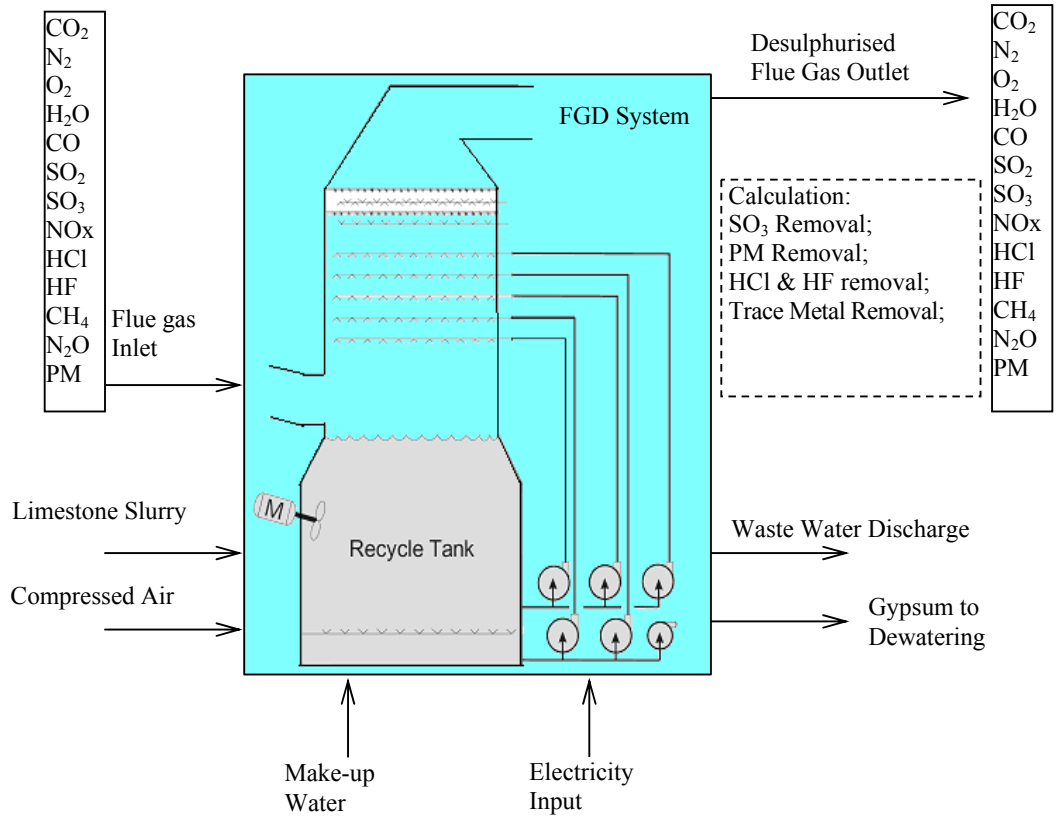

Figure 5.10: The scheme of the FGD LCI model

The scheme of the FGD LCI model is demonstrated in Figure 5.10. The LCI model estimates the limestone consumption, gypsum output, water make-up, and electricity

input as well as calculate the SO_2 removal, SO_3 removal, PM removal, HCl and HF removal, and trace metal removal while flue gas passing through the FGD system.

5.4.2.1 Sulphur Dioxide (SO_2) Removal Efficiency

LSFO systems and MEL systems are known to achieve SO_2 removal efficiencies as high as 98% and 99% respectively in power plants firing a variety of high- and low-sulphur fuels (Sargent & Lundy, 2003). Liquid-to-gas (L/G) ratio is a key variable for LSFO or MEL systems to achieve high SO_2 removal efficiency since it increases both the available liquid phase alkalinity and the interfacial mass transfer area (Bhat *et al.*, 1993; Berkenpas *et al.*, 1999). In this research, the empirical regression equations used to calculate SO_2 removal efficiency (η_{SO_2}) in relation to the L/G ratio for the LSFO system and MEL systems are shown in equations 5.22 and 5.23 respectively (Berkenpas *et al.*, 1999):

$$\eta_{\text{LSFO-SO}_2} = 1 - \exp\{-(0.725 + 0.0175 \times L/G)\} \quad [5.22]$$

$$\eta_{\text{MEL-SO}_2} = 1 - \exp\{-(0.2 + 0.07 \times L/G)\} \quad [5.23]$$

5.4.2.2 Sulphur Trioxide (SO_3) Removal Efficiency

As the flue gas is rapidly cooled by the sprays of liquid in the LSFO or MEL system, the SO_3 undergoes a shock condensation process that produces very fine sulphuric acid aerosol particles (H_2SO_4 mist with 0.4 micron size) (Adams and Senior, 2006). These aerosol particles are, for the most part, too small to be effectively captured in the FGD system and are emitted into the air as a sulphuric acid mist (Moser, 2007). The SO_3 removal efficiency is generally in the 30% to 40% range (Adams and Senior, 2006). Effective removal of the very small sulphuric acid aerosol particles normally requires a significantly higher pressure drop than that at which FGD systems are designed to operate (Paschke, 2006). It is difficult to differentiate between SO_3 and H_2SO_4 in the flue gas after wet FGD process; in fact, the two quantities often are used interchangeably (Adams and Senior, 2006). In this research, the SO_3 removal efficiency is calculated using the regression equation 5.24 derived from the simulation results (Figure 5.11) provided in the literature (Paschke, 2006):

$$\eta_{SO_3} = 35.23\text{Ln}(\Delta p) + 7.47 \ (R^2 = 0.9931) \quad [5.24]$$

Where, η_{SO_3} is the SO_3 removal efficiency as a function of the flue gas pressure drop Δp across the FGD system. R^2 is the coefficient of determination. The typical wet FGD system pressure drop values are provided in Table 5.9.

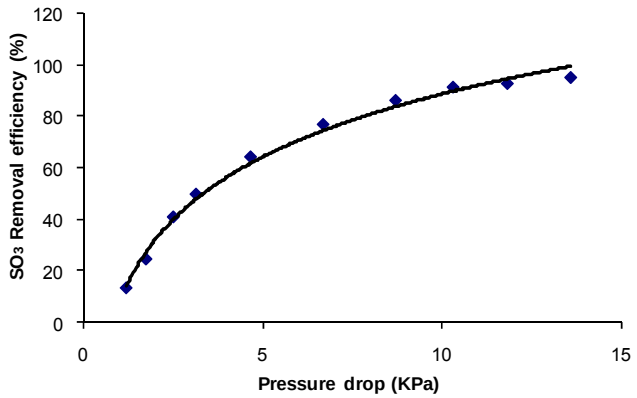

Figure 5.11: SO_3 removal efficiency and pressure drop (After Paschke, 2006)

Table 5.9: Typical FGD system pressure drop (After Sargent and Lundy, 2003)

	LSFO High-sulphur	LSFO Low-sulphur	MEL High-sulphur	MEL Low-sulphur
Pressure drop (KPa)*	0.89	0.77	0.69	0.66

*w.c. is pressure loss in inches of water column

5.4.2.3 Hydrogen Chloride and Hydrogen Fluoride Removal Efficiency

For power plants firing low chlorine coal (~ 0.01 %-wt Cl or less) the emissions of HCl and HF are usually not a problem when considering emission standards or process operation (Zevenhoven and Kilpinen, 2004). When a flue gas desulphurisation unit (FGD) is present for SO_2 emissions control, this can also remove HCl and HF. The liquid to gas ratio and the rate of recycling and removal of products also influence the HCl and HF scrubbing efficiency (Constance, 2007). Measurements for pulverised coal combustion units with FGD from literature show that 87~ 95% of the flue gas chlorine (mainly HCl) and 35%~ 70% of the fluorine (as HF) are removed (Zevenhoven and Kilpinen, 2004; ICAC, 2006; Constance, 2007). Based on these analyses, this research sets the default values for the HCl and HF removal efficiency at 90% and 70% respectively.

5.4.2.4 Particulate Matter (PM) Removal Efficiency

The wet FGD systems also provide significant removal of particulate matter. The removal of the PM in wet FGD systems depends on the pressure drop across the FGD and with smaller particles requiring more pressure drop. Wet FGD systems are not very efficient at scrubbing particles of a size less than 0.5 micron in diameter (Paschke, 2006). In this research, the PM removal efficiency is calculated using the equation 5.25 derived from empirical results (Figure 5.10) provided by Paschke (2006):

$$\eta_{FGD\ PM} = 38.51(\Delta p)^{0.4947} \qquad (R^2 = 0.9938) \qquad [5.25]$$

Where, $\eta_{FGD\ PM}$ is the PM removal efficiency as a function of the flue gas pressure drop Δp across FGD system. R^2 is the coefficient of determination. The typical wet FGD system pressure drop values are provided in Table 5.9.

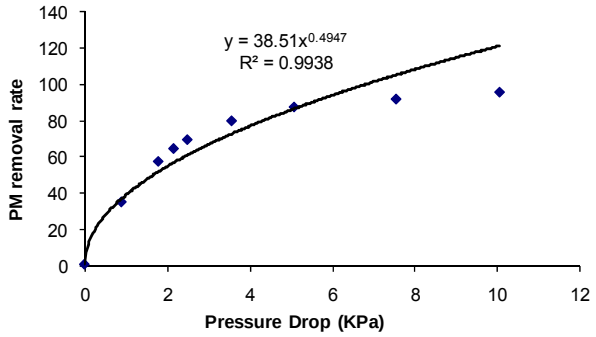

Figure 5.12: PM removal efficiency and pressure drop (After Paschke, 2006)

From Table 5.12, which provides the typical size distribution of particulate matters in flue gas, it can be seen that after a typical 70% PM removal rate in the wet FGD process the particulate matter remaining in the flue gas is equal or smaller than 1 microns in size.

Table 5.10: The typical size distribution of particulate matter in flue gas (After Paschke, 2006)

Size (microns)	Percentage (wt%)
<0.1	0.1
<0.3	4
< 1	35
<1.5	54
<3.0	75
>20	6

5.4.2.5 Flue Gases Trace Metal Removal Efficiency

Since trace elements in flue gas, such as As, Be, Cd, Cr, Pb, and Mn, are associated with the particulate phase, the removal of particulates effectively removes the trace elements. The removal efficiencies of the trace elements across wet FGD system are provided in Table 5.11. Trace metals including Thallium (Tl), Barium (Ba), Cobalt (Co) and Silver (Ag) are not included in Table 5.11, it is assumed that the removal efficiencies of these trace metals are 90%, because they are Group I metals that are associated with particulate phase.

Table 5.11: FGD retention of trace elements (After DTI, 2004)

Element	FGD retention factor (solid)	FGD retention factor (vapour)
Arsenic (As)	0.91	–
Selenium (Se)	0.58	0.82
Lead (Pb)	0.9	0.37
Antimony (Sb)	0.9	–
Boron (B)	1	0.8
Nickel (Ni)	0.86	–
Chromium (Cr)	0.88	–
Copper (Cu)	0.69	–
Manganese (Mn)	0.93	–
Vanadium (V)	0.92	–
Zinc (Zn)	0.84	–
Beryllium (Be)	0.95	–
Cadmium (Cd)	0.8	0.52
Mercury (Hg)	1	0.76

5.4.2.6 Calculation of the Mass Requirement of Calcium-based Sorbent

The mass requirement of calcium-based sorbent is calculated based on the chemical reactions described in Table 5.8.

• LSFO system

The limestone requirement by LSFO system is calculated using the following equation 5.26:

$$M_{\text{limestone}} = \sum_i \left(\eta_i \times \phi_i \times gas_i \times r_i\right) \times MW_{CaCO_3} / R_{purity} \qquad [5.26]$$

where,

$M_{\text{limestone}}$ is the mass of limestone required (kg/hr);

η_i is the removal efficiency of gas *i*;

ϕ_i is the stoichiometric ratio of reaction involving gas *i*;

gas_i are moles of inlet gas *i* (mole/hr);

gas_i (SO_2, SO_3, HCl);

r_i are moles of reagent required per mole of species with $r_i \in (1, 1, ½)$;

$MWCaCO_3$ is the molecular weight reagent of $CaCO_3$;

R_{purity} is the reagent purity (weight fraction of $CaCO_3$).

• MEL system

The lime requirement by LSFO system is calculated by following equation 5.27:

$$M_{\text{lime}} = \sum_i \left(\eta_i \times \phi_i \times gas_i \times r_i\right) \times MW_{CaO} / R_{purity} + \sum_i (\eta_i \times gas_i \times q_i) \times MW_{MgO} / R_{purity} \qquad [5.27]$$

where,

$M_{\text{lime}}$is the mass of lime required (kg/hr);

η_i is the removal efficiency of gas i;

ϕ_i is th e stoichiometric ratio of reaction involving gas *i*;

gas_i are the moles of inlet gas *i* (mole/hr);

$gas_i \in (SO_2, SO_3, HCl)$;

r_i are the moles of CaO required per mole of species with $r_i \in (1, 1, ½)$;

q_i are the moles of MgO required per mole of species with $q_i \in (3/4, 3/4, ½)$;

MW_{CaO} is the molecular weight of reagent CaO;

MW_{MgO} is the molecular weight of reagent MgO;

R_{purity} is the reagent purity (weight fraction of CaO and MgO).

5.4.2.7 Solid Waste Generation

The amount of solid waste produced depends on the amount of reactive species scrubbed from the flue gas ($M_{disposal}$ kg/hr), the total amount of inert material in the slurry (M_{inerts}, kg/hr) and the amount of unused reagent in the slurry ($M_{unused\ reagent}$, kg/hr). The mass of the solid waste generated is calculated based on the chemical reactions described in Table 5.8.

• LSFO system

$$M_{waste} = \sum_i (\eta_i \times \phi_i \times gas_i \times r_i) \times MW_i / R_{purity} \quad [5.28]$$

$$M_{inerts} = M_{reag} \times \sum_i (1 - R_{purity}) \quad [5.29]$$

$$M_{unused\ limestone} = \sum_i (\eta_i \times \phi_i \times gas_i \times r_i \times (\phi_i - 1)) \times MW_{CaCO_3} \quad [5.30]$$

where,

M_{waste} is the mass of wastes generated (kg/hr);

η_i is the removal efficiency of gas i;

ϕ_i is the stochiometric ratio of reaction involving gas i;

gas_i are the moles of inlet gas i (mole/hr) with $gas_i \in (SO_2, SO_3, HCl)$;

r_i are the moles of solid waste generated per mole of species with $r_i \in (1, 1, 1/2)$;

$M_i \in (MW_{CaSO_4 \cdot 2H_2O}, MW_{CaSO_4 \cdot 2H_2O}, MW_{CaCl_2})$

• MEL system

$$M_{waste} = (\sum_i (\eta_i \times \phi_i \times gas_i \times r_i) \times MW_i \times R_{CaO} + \sum_i (\eta_i \times gas_i \times q_i) \times NW_i \times R_{MgO}) / R_{Purity} \quad [5.31]$$

$$M_{inerts} = M_{reag} \times \sum_i (1 - R_{purity}) \quad [5.32]$$

$$M_{unused\ reag} = \sum_i (\eta_i \times gas_i \times r_i \times (\phi_i - 1)) \times MW_{CaCO_3} \quad [5.33]$$

where,

M_{waste} is the mass of wastes generated (kg/hr);

η_i is the removal efficiency of gas *i*;

ϕ_i is the stochiometric ratio of reaction involving gas *i*;

gas_i are moles of inlet gas *i* (mole/hr) with $gas_i \in (SO_2, SO_3, HCl)$;

r_i are moles of waste generated per mole of species with $r_i \in (1, 1, ½)$;

q_i are moles of waste generated per mole of species with $q_i \in (3/4, 1, ½)$;

MW_i and NW_i are the molecular weights of waste generated with

$MW_i \in (MW_{CaSO_4 \cdot 2H_2O}, MW_{CaSO_4 \cdot 2H_2O}, MW_{CaCl_2})$ and $NW_i \in (MW_{MgSO_4}, MW_{MgSO_4}, MW_{MgCl_2})$

5.4.2.8 Constituents of Concern in Wet Flue Gas Desulphurisation Solid Waste and Liquid Wastes

Figure 5.13 demonstrates the FGD by-product handling system, in which the bleed stream from the reaction tanks for the LSFO process or from the oxidation tank for the MEL process is pumped to a set of hydrocyclones for primary dewatering and then is fed to belt filters for secondary dewatering. The dewatered gypsum discharged from the belt filters is transported offsite for use as by-product or disposed off at a landfill site as solid waste. A small blowdown of waste water from hydroclones and belt filters, required to remove chloride, is treated in a special water treatment system or discharged directly to an ash pond.

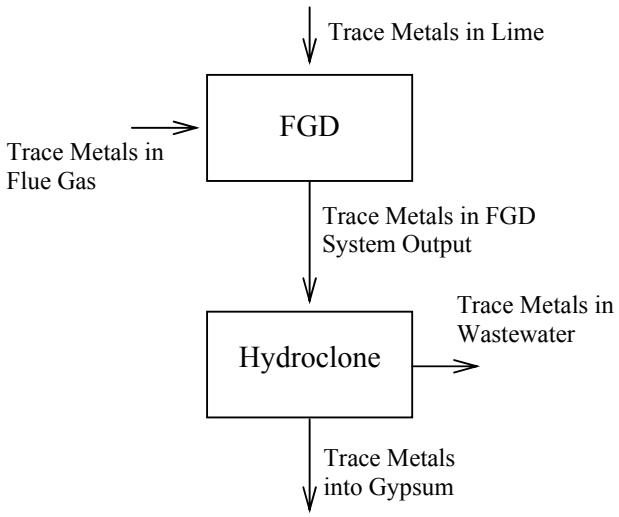

Figure 5.13: The FGD by-product handling system

The constituents of concern in the waste solid (or by-product) from wet FGD systems are trace metals. The constituents of concern in waste water from wet FGD systems are as follows:

- Trace metals including selenium, arsenic, mercury, aluminum, antimony, beryllium, and thallium may be present and cause potential environmental impacts.

- FGD wastes contain high fluoride, chloride, and sulfate levels (ppm range) and even percent concentrations of total dissolved solids (TDS), which may comprise anions of fluoride, chloride and sulphate. All of these anions can be present at or above regulatory limits. For instance, if power plants reuse ash pond water, chloride in FGD wastewater discharged to ash pond will typically cause the pond water chloride concentration to increase above levels recommended for most common steels (Chu, 2006).

5.4.2.9 Partitioning of Trace Metals between Wet Flue Gas Desulphurisation Solid Wastes and Liquid Wastes

Figure 5.13 also shows that, in the wet FGD systems, trace metals from flue gas and from limestone (or lime) will combine together and ultimately leave FGD system in two ways: in by-product gypsum and in waste water (see Figure 5.13). Some trace metals captured by the FGD were found to be associated primarily with the particulate phase. These metals end up in the gypsum and only a small percentage of these metals are present in the FGD wastewater. Other metals such as selenium are more present in soluble form and partition into the wastewater (Chu, 2006). The portioning factors in Table 5.12 are used in this research to determine the mass of a trace metal that is associated with wet FGD waste water. For the trace metals that are not included in Table 5.12, this research assumes that 50% of these metals are assigned to gypsum.

Table 5.12: Trace element portioning factors (After Chu, 2006)

Trace metals	Percentage in FGD waste water (%)
Iron	1
Aluminium	2
Mercury	2
Copper	15
Arsenic	20
Chromium	22
Barium	12
Antimony	86
Cadmium	90.5
Selenium	73
Boron	99.5

5.4.2.10 The Flue Gas Desuphurisation Power Consumption

The power consumption of a wet FGD system can range from 1%-2% of the total conventional power plant electric output (Westra and Boston, 1996). The booster ID fan power required to overcome the draft loss across the absorber and the power requirement for slurry recirculation pumps are the primary power consumptions and can be calculated by following equations (Berkenpas *et al.*, 1999):

$$P_{ID} = 1.70 \times 10^{-5} \times F_{gas} \times \Delta p / \eta_{fan} \quad [5.34]$$

where,

P_{ID} is the electricity consumption of the ID fans (kW);

F_{gas} is the flue gas flow rate (m^3/s);

Δp is the total pressure drop (kPa);

η_{fan} is the fan efficiency (fraction);

$$P_{pumps} = 9.51 \times 10^{5} \times k_t \times Q + c \quad [5.35]$$

where,

P_{pumps} is the electricity consumption of the slurry recirculation pumps (kw);

Q is the flow rate of the slurry (m^3/s =LG×Fgas×60);

K_t and c are the regression coefficients. The value of these regression coefficients are provided in Table 5.13.

Table 5.13: Regression Coefficients for P_{pumps} (After Berkenpas *et al.*, 1999)

Technology	LSFO	MEL
kt	3.62E-05	3.25E-05
c	-	0.21
R^2	0.99	0.99

5.4.2.11 Water Consumption

Water from the scrubbing slurry is lost due to evaporation in the scrubber and the bleed stream from the scrubber. The water consumption for LSFO and MEL are 6.18E-6 and 6.81E-5 (m^3/s) per megawatt (MW) electricity generated respectively (Berkenpas *et al.*, 1999).

5.5 Life Cycle Modelling of Nitrogen Oxides Control Process

5.5.1 Nitrogen Oxides Formation

There are a number of oxides of nitrogen, including nitric oxide(NO), nitrogen dioxide (NO_2), nitrous oxide (N_2O), nitrogen trioxide (N_2O_3), and nitrogen pentoxide (N_2O_5), that are referred to collectively as NOx. The two oxides of nitrogen that are of primary concern to air pollution are NO and NO_2. The formation of NOx during coal combustion is due to three mechanisms (Schnelle and Brown, 2001): (1) by oxidising nitrogen in the combustion air (or thermal NOx), (2) by oxidising nitrogen in the fuel (or fuel NOx), and (3) involving the reaction between nitrogen in combustion air and radicals such as O and OH in hydrocarbon fuel (prompt NOx). The two oxides of nitrogen that are of primary concern to air pollution are nitric oxide (NO) and nitrogen dioxide (NO_2). NOx in flue gas consists of 90-95% NO and 5% to 10% NO_2 (Schnelle, *et al.*, 2001). Generally, for coal-fired combustion, less than 25% of the NOx produced is thermal NOx, 50-70% of the NOx produced is fuel NOx, and prompt NOx is less than 5% of total NOx emissions (Nordin and Merriam, 1997; Schnelle and Brown, 2001).

5.5.2 Environmental Impacts of Nitrogen Oxides emissions

The emission of NOx to the atmosphere has been associated with the following health and environmental impacts (USEPA 1998b; Lani, *et al*., 2005):

- Acid Rain − NOx can form acidic compounds ("acid rain") through reactions with water and oxidants in the atmosphere. Studies have shown that the low pH associated with the acid rain can be harmful to plant and aquatic life.

- Ground-level Ozone − NOx can react with volatile organic compounds in the presence of heat and sunlight to form ground-level ozone. Ozone can trigger respiratory problems in sensitive individuals such as children, the elderly, and those suffering from asthma.

- Fine Particulate Matter − NOx can react with ammonia, moisture, and other compounds in the atmosphere to form secondary fine particulate matter that may adversely impact human cardio-pulmonary functions.

- Visibility Impairment − Nitrogen dioxide gas and secondary fine particulate matter nitrates can block the transmission of light leading to reduced visibility known as regional haze.

- Water Quality Deterioration − The deposition of nitrogen compounds in and around bodies of water has been linked to "eutrophication" – an over-enrichment of nutrients that can deplete the oxygen content of lakes and rivers and result in a reduction of fish and shellfish populations.

- Nitrogen Dioxide (NO_2) − Human exposure to excessive concentrations of NO_2 can lead to respiratory problems.

The NOx emission standards for large combustion plants in EU are provided in Table 5.14.

Table 5.14: NOx emission standards for large combustion plant in EU (After Zevenhoven and Kilpinen, 2004)

Fuel	New/Existing	Plant size (MW)	Emission standard (mg/m^3STP dry)
Coal	Existing	50-500	600 at 6% O_2
		>500	500 at 6% O_2
		>500	200 at 6% O_2
	New	50-100	400 at 6% O_2
		100-300	200 at 6% O_2
		>300	200 at 6% O_2

5.5.3 Alternative Nitrogen Oxides Control Techniques Coal Fired Boilers

Two categories of available NOx emission control techniques are (1) combustion controls, and (2) flue gas treatment (or post-combustion controls). The principle underlying combustion controls is the reduction of combustion temperature and/or oxygen levels of fuel combustion by staging the air and/or the fuel supply, and consequently reducing the thermal NOx and fuel NOx formation during combustion. In post-combustion control, the NOx is captured by chemical reactions after fuel combustion. The alternative technologies of NOx control and their efficiencies are summarised in Table 5.16.

It is expected that the technology of choice would be towards selective catalyst reduction (SCR) for the larger, higher baseline NOx power generation units and towards combustion control for smaller units or units with lower baseline NOx emissions. Therefore, this research focuses on the SCR LCI modelling with the assumption that the

future power plants with CCS will be large generation units. For other NOx control options, the emission control factors presented in Table 5.15 are used.

Table 5.15: NOx emission control options and NOx removal efficiency (%) (After USEPA, 1998a)

Combustion controls	
Operational modifications: burners-out-of-service (BOOS); low excess air (LEA), biased firing (BF), combination of these	10 – 20%
Overfire Air (OFA)	20 – 30%
Low NOx Burners (LNB)	35 – 55%
LNB with OFA	40 – 60%
Reburn	50 – 60%
Post-Combustion controls	
Selective non-catalyst reduction (SNCR)	30 – 60%
Selective catalyst reduction (SCR)	75 – 85%
LNB with SNCR	50 – 80%
LNB with OFA and SCR	85 – 95%

5.5.4 The Development of the Life Cycle Inventory Model of Nitrogen Oxides Control – Selective Catalyst Reduction Technology

The SCR technology uses ammonia (NH_3) to reduce NOx to nitrogen and water and a catalyst bed can be used with ammonia as a reducing agent to promote the reduction reaction and to lower the effective temperature. The most commonly used catalysts are a vanadium/titanium formulation (V_2O_5 stabilized in a TiO_2 base) and zeolite materials. The chemistry of the SCR process and the side reactions are as follows (Schnelle and Brown, 2001; USDOE and SCS, 1997):

Chemistry of the SCR process:

$$4NO + 4NH_3 + O_2 \rightarrow 4N_2 + 6H_2O$$
$$2NO_2 + 4NH_3 + O_2 \rightarrow 3N_2 + 6H_2O$$

Side reactions:

$$SO_2 + 1/2O_2 \rightarrow SO_3$$
$$2NH_3 + SO_3 + H_2O \rightarrow (NH_4)_2SO_4$$
$$NH_3 + SO_3 + H_2O \rightarrow NH_4HSO_4$$

The reaction between NO and NH_3 is dominant, because the NO concentration in the flue gas from combustion systems usually is high (90-95%), other reactions are not particularly significant to the overall NOx reduction or to the reagent requirement. Besides these actions, a small fraction of the SO_2, produced in the boiler by oxidation of sulphur in the coal, is oxidized to sulphur trioxide (SO_3) over the SCR catalyst.

The SCR operation includes ammonia storage and an injection system, as well as a catalytic reaction bed and a reaction vessel with steam-operated sootblowers to remove

dust. The Scheme of LCI model of SCR is described in Figure 5.14. The SCR design parameters that are required as inputs are listed in Table 5.16. The LCI model developed calculates the NOx removal rate, the rate of SO_2 oxidised to SO_3, the mercury oxidisation rate, the ammonia consumption, the catalyst consumption, the electricity input, the steam required for ammonia injection, the catalyst sootblowing steam requirement, and the ammonia release.

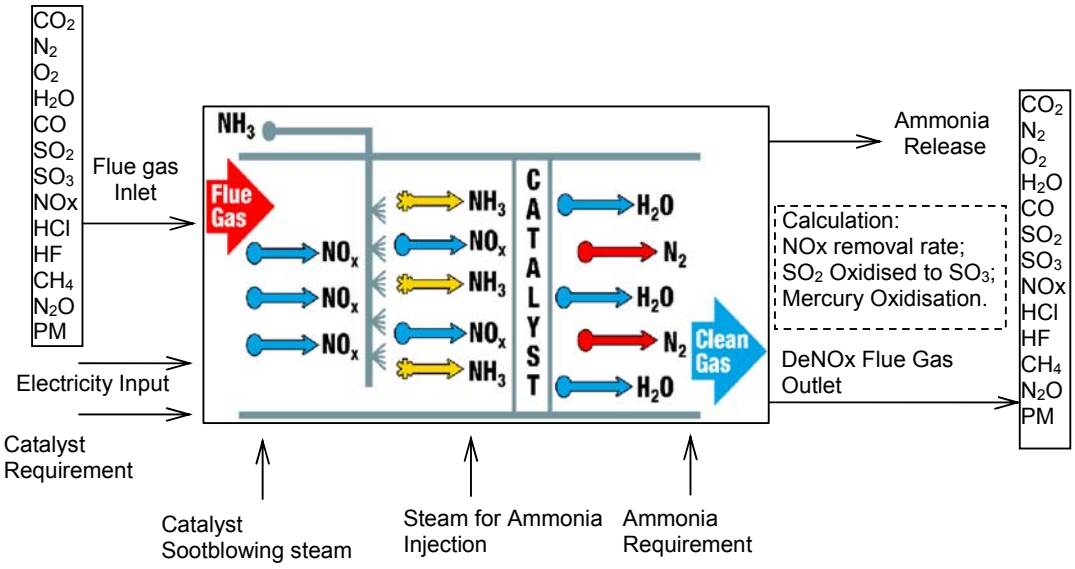

Figure 5.14: The scheme of the SCR LCI modelling

Table 5.16: SCR design parameters

Parameters	Default value	Unit
Size	500	MW
Fuel	Coal	-
Configuration	High Dust	-
Gas temperature	649	F
NH_3/NOx	0.8	-
Space Velocity (SV)	4,000	-
Pressure Drop	2.8	WG
Catalyst Life	3	years

5.5.4.1 The Calculation of Nitrogen Oxides Removal Efficiency

There are a number of factors that affect the NOx removal efficiency, including NH_3-to-NO mole ratio, reaction temperature, catalyst loading, oxygen concentration and space velocity (Oh, 2004). The NH_3-to-NO mole ratio and the reaction temperature are the most influential factors and the NO removal rate increases with increasing NH_3-to-NO mole ratio or reaction temperature (Lee, 2002). In this research, the NO removal efficiency is calculated, accounting for NH_3-to-NO ratio and reaction temperature, by the equations 5.36 to 5.40, which are based on the empirical results presented in Figure

5.15 that describe the influence of NH_3-to-NO ratio of inlet on the conversion of NO at various reaction temperatures on a typical V_2O_5-$MoO_3WO_3/TiO_2/Al_2O_3$/cordierite honeycomb catalysts with space velocity of 6,000 h^{-1} and oxygen ratio of 5% (Liuqing et al., 2003).

T= 573K,	$\eta_{SCR\ NO} = 47.56 \exp(0.1504\ r_{NH_3/NO})$	($R^2 = 0.9787$)	[5.36]
T= 773K,	$\eta_{SCR\ NO} = 13.53Ln(r_{NH_3/NO})+77.03$	($R^2 = 0.9941$)	[5.37]
T= 623K,	$\eta_{SCR\ NO} = 7.45Ln(r_{NH_3/NO})+78.58$	($R^2 = 0.9734$)	[5.38]
T= 673K,	$\eta_{SCR\ NO} = 9.74Ln(r_{NH_3/NO})+90.56$	($R^2 = 0.9978$)	[5.39]
T=723K,	$\eta_{SCR\ NO} = 10.39Ln(r_{NH_3/NO})+93$	($R^2 = 0.9619$)	[5.40]

Where, T is the temperature; $\eta_{SCR\ NO}$ is the conversion of NO (%);$r_{NH_3/NO}$ is the NH_3/NO ratio of inlet. R^2 is the coefficient of determination.

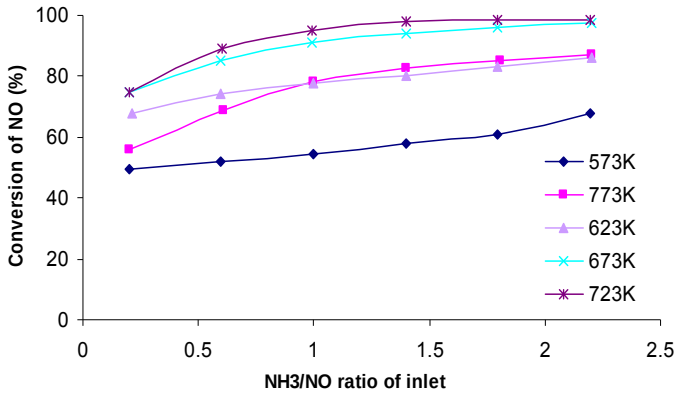

Figure 5.15: The effects of NH_3/NO ratio of inlet on the conversion of NO at various temperatures (After Liuqing *et al.*, 2003)

5.5.4.2 The Mass Flow Requirement of Ammonia

The SCR processes require NH_3 as input, given the NH_3/NOx ratio, the molar flow rate of NH_3 can be calculated by equation 5.41:

$$M_{NH_3}in = r_{NH_3/NO} \times M_{NOxin} \qquad [5.41]$$

where, M_{NH_3}in (kg/hr) is the mass flow rate of NH_3; $r_{NH_3/NO}$is the NH_3/NO ratio and M_{NOxin} (kg/hr) is the mass flow rate of NO in the flue gas inlet.

5.5.4.3 The Calculation of Ammonia Slip Rate

An insufficient amount of ammonia can result in unacceptably high NOx emission rates, while excess ammonia can lead to the ammonia "slip", that is when portion of the injected NH_3 passes through the SCR unreacted. The NH_3 slip rate increases with the

increase of the NH_3/NO ratio and NH_3 slip generally remains constant at about 2 ppm at low levels of NH_3/NOx ratio (less than 0.6), increasing significantly above a ratio of about 0.9 (see Figure 5.16) (Lee, 2002; USDOE and SCS, 1997).

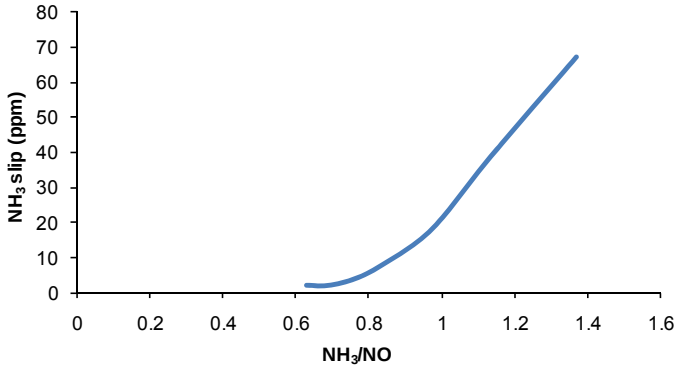

Figure 5.16: The influence of NH_3/NOx ratio on NH_3 slip rate (After USDOE and SCS, 1997)

Given NOx removal rate and the NH_3/NO ratio, the NH_3 slip rate (NH_{3out}/NH_{3in}) can be calculated using equation 5.42 assuming stoichiometric chemical reactions in the SCR reactor (1 mole of NH_3 per mole NO reduced and 2 mole of NH_3 per mole of NO_2 reduced):

$$NH_{3out}/NH_{3in} = r_{NH_3/NO} - \eta_{SCR\ NO}\ (r_{NO/NOx} + 2\ r_{NO_2/NOx}) \qquad [5.42]$$

where $r_{NO/NOx}$ and $r_{NO_2/NOx}$ are the ratios of NO/NOx and NO_2/NOx respectively.

The mass of NH_3 slip is given by:

$$M_{NH3slip} = M_{NH3in} \times (NH_{3in}/NH_{3out}) \qquad [5.43]$$

5.5.4.4 The Calculation of the Conversion of Sulphur Dioxide to Sulphur Trioxide

A portion of the SO_2 in the flue gas entering the SCR reactor is oxidized to SO_3 as the side reaction in the SCR system. Previous studies show that the increase of SCR reactor operating temperature increases SO_2 to SO_3 conversion and the increase of SO_2 inlet concentration, NH_3 inlet concentration, and NH_3/NO ratio decrease the conversion (Erickson and Jambhekar, 2002). The SCR reactor operating temperature has a strong influence on the conversion ratio among the factors affecting the conversion of SO_2 to SO_3 (Erickson and Jambhekar, 2002; Nielsen and Topsøe, 2003). The equation 5.44 originating from empirical data (Figure 5.17) is used to calculate the rate of the SO_2 conversion to SO_3 at various SCR reactor operating temperatures.

$$\eta_{SCR\ SO_2} = 0.0008 \exp(0.002\ T) \qquad (R^2 = 0.9995) \qquad [5.44]$$

Where, T is the temperature (^oC. $\eta_{SCR\ SO_2}$ is the SO_2 to SO_3 conversion ratio. R^2 is the coefficient of determination.

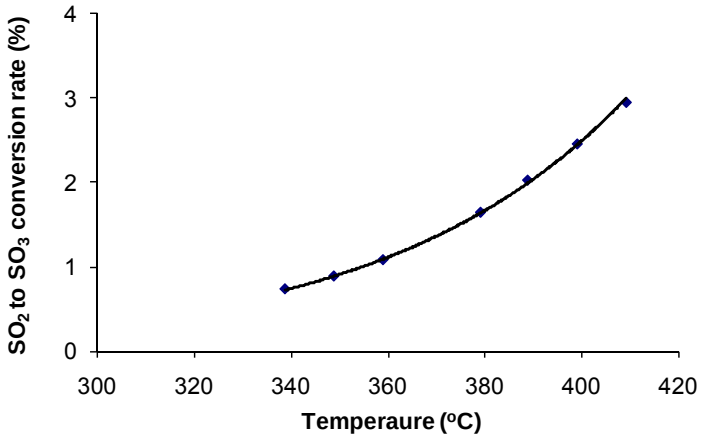

Figure 5.17: The effect of the temperature on SO_2 to SO_3 conversion ratio (After Erickson and Jambhekar, 2002)

5.5.4.5 Sulphur Trioxide and Ammonia Reduction by Reaction between Sulphur Trioxide and Ammonia Slip (at Pre-heater)

Ammonia slip can react with SO_3 or sulfuric acid to form ammonium sulfate $[(NH_4)_2SO_4]$ and/or ammonium bisulfate (NH_4HSO_4). The reactions were described as side reactions at the beginning of this section. The reactions occur in the air preheater and result in a solid product that may deposit or accumulate on the surface of the fly ash (EPRI, 2007). Any SO_3 or H_2SO_4 that participates in these reactions is no longer chemically present as sulphuric acid. Therefore, the reactions remove from the flue gas some of the SO_3 and reduce the amount of NH_3 and SO_3 released.

An SCR-equipped unit firing bituminous coals with low-to-medium sulphur content will always produce an excess of sulphuric acid over ammonia slip. Accordingly, ammonium bisulphate is the primary by-product anticipated (EPRI, 2007). For subbituminous, and lignite coals, any sulphuric acid produced is typically adsorbed by the ash and it is likely that residual ammonia will exceed sulphuric acid content on a mole basis and ammonium sulphate is the likely product (EPRI, 2007).

With the purpose of calculating sulphuric acid emissions, it can be assumed that all sulfuric acid forms ammonium bisulphate before any further reaction to the ammonium sulfate form occurs, and if additional ammonia is available, the ammonium bisulphate can react with another ammonia molecule to form ammonium sulphate (EPRI, 2007).

Based on the stoichiometry of the reactions, given the NH_3 (NH_3 slip) to SO_3 mole ratio R ($R= M_{NH_3slip}/M_{SO_3}$), the emissions of SO_3 and NH_3 at the preheater (after SCR) are calculated using the following method:

If R>2, then $$E_{SO_3} = 0 \text{ and } E_{NH_3} = M_{NH3slip} - 2 \times M_{SO_3} \quad [5.45]$$

If R<1, then $$E_{SO_3} = M_{SO_3} - M_{NH3slip} \text{ and } E_{NH_3} = 0 \quad [5.46]$$

If 1≤R≤2, then $$E_{SO_3} = 0 \text{ and } E_{NH_3} = 0 \quad [5.47]$$

Where, M_{NH_3slip} denotes the moles of NH_3 slip (moles); M_{SO_3} denotes the moles of SO_3 outlet from SCR (moles); E_{NH_3} and E_{NH_3} are the moles of SO_3 emission and NH_3 emission outlet from the preheater respectively (moles).

5.5.4.6 Oxidation of the Elemental Mercury

At the hot-side SCR inlet, mercury is present in three forms: as particle-bound mercury (Hg_{part}) and gaseous mercury existing as either oxidised mercury (Hg^{2+}) or elemental mercury (Hg^0). In the SCR process, a portion of elemental mercury in the flue gas is oxidised from Hg^0 to Hg^{2+}. The oxidized mercury is water-soluble and has a tendency to associate with particulate matter, allowing it to be controlled downstream of the SCR, along with ash and SO_2, in existing air pollution control devices such as ESPs and wet-flue gas desulfurization (wet-FGD) scrubbers (Cao *et al.*, 2005).

The chlorine content of coal and the SCR reactor temperature have the greatest impacts on elemental mercury (Hg^0) oxidation in SCR systems (Senior, 2004). The equations 5.48, 5.49 and 5.50 are used to calculate the rate of the elemental mercury oxidisation, accounting for the chlorine content of coal and the SCR reactor temperature. The equations are derived from simulation results found in literature (see Figure 5.18), which show a good agreement between the predicted and measured mercury speciation for the data points corresponding to temperatures in the range of 320°C to 371°C (625°F to 700°F).

T=371°C $$\eta_{SCR\ Hg} = 0.9963\exp(-0.0019\ C_{Cl}) \quad (R^2 = 0.9922) \quad [5.48]$$

T=350°C $$\eta_{SCR\ Hg} = 0.7768\exp(-0.0029\ C_{Cl}) \quad (R^2 = 0.9517) \quad [5.49]$$

T=320°C $$\eta_{SCR\ Hg} = 0.3739\exp(-0.0041\ C_{Cl}) \quad (R^2 = 0.8321) \quad [5.50]$$

where, T is the SCR operating temperature. $\eta_{SCR\ Hg}$ is the percentage of the elemental mercury remaining at SCR outlet. C_{Cl} is the chlorine content of the coal. R^2 is the coefficient of determination.

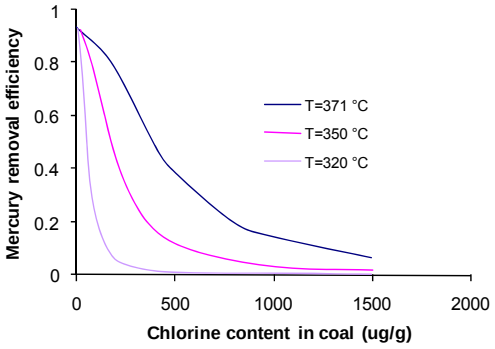

Figure 5.18: Effects of chlorine contents and temperature on mercury removal efficiency (After Constance, 2004)

5.5.4.7 Energy Consumption by Ammonia Compression

The ammonia injection requires the NH_3 to be compressed. The energy consumption associated with ammonia compression is calculated assuming a 690 KPa differential compression with an 85 percent compression efficiency (Berkenpas, 1999):

$$E_{compression} = 4.46 \times 10^{-3} \times MNH_3in \qquad [5.51]$$

where, $E_{compression}$ is the energy consumption by ammonia compression (kW). MNH_3in is the mass flow rate of ammonia (kg/s).

5.5.4.8 Steam Required for Ammonia Injection and Catalyst Sootblowing

In the ammonia injection system, the ammonia is normally vaporised by mixing it with steam prior to injection into the flue gas. For safety reasons, ammonia dilution to 5 percent by volume may be required, leading to a requirement for a steam-to-ammonia ratio of 19 (Berkenpas, 1999). Then, the steam requirement for ammonia injection is given by:

$$M_{steam,NH_3} = 19 \times M_{NH_3},in \qquad [5.52]$$

Catalyst sootblowing is required to remove ash that may mask or plug the catalyst. The study by Bauer and Spendle (1984) has shown that the catalyst sootblowing steam requirement is 101.17 kg/s for a total of approximately one hour per day, or an average of 4.21 kg/s for typical SCR systems with catalyst volumes ranging from 283.2 to 849.5 m^3. In this research, the steam (Msteam,blowing) required for catalyst sootblowing is set to 4.21 kg/s.

5.4.4.9 Energy Consumption Equivalence of the Steam Required for Ammonia Injection and Catalyst Sootblowing

Assuming that the steam is extracted from an LP turbine, the electricity equivalence of the LP steam can be calculated using the method described in section 5.6.2.1.

5.5.4.10 Energy Consumption by Force Draft Fans

The auxiliary power requirement by force draft (FD) fans can be calculated using the following engineering calculation method:

$$P_{FD} = 2.72\times10^{-5}Q\times\Delta P/\eta_{fan} \quad [5.53]$$

where, P_{FD} (kW) is the energy used by FD fans. Q is the volume of flue gas (m^3/hr). ΔP is the total change of pressure (kPa), which is typically 0.996 to 1.49 kPa. (Drbal *et al.*, 1996). η_{fan} is the energy conversion efficiency of fans, typically 85%.

5.5.4.11 Catalyst Consumption

Previous study by Lietti, *et al*. (2000) concluded that, for a typical SCR design, 0.022 kg catalyst is required at the flue gas flow rate 1m^3/hr. Assuming the average catalyst life is approximately 20,000 hours (Berkenpas, 1999; Foerter and Jozewicz, 2001), the catalyst consumption by SCR in lifespan can be estimated by:

$$R_{catalyst}=0.022\times F/20{,}000\times(t/2{,}000) \quad [5.54]$$

where, $R_{catalyst}$ is the catalyst consumption (kg). F is flow gas flow rate (m^3/hr). t is the life of the power plant (hr).

5.6 Life Cycle Inventory Modelling of Solid Waste Disposal

5.6.1 Introduction of Solid Waste Disposal

Over time, the airborne emissions from power plants have been reduced considerably, mainly in response to tight environmental restrictions on the air emissions. However, as a result many substances of concern, such as heavy metals, have been transferred to the solid waste produced. In fact, in power plants, between 95 and 99% or more of the trace elements in coal (such as Cu, Zn, Mn, Pb, Cr, Cd, Co, Ni, As, Se, B, Mo, Hg, etc.) are transferred to coal combustion solid wastes (CCWs). Thus the amounts of these trace elements in solid waste management units (WMUs) (including landfills, surface impoundments and waste piles) are at least 20-100 times higher than the amounts

emitted directly to atmosphere through flue gas emissions (Hellweg, 2000). These trace elements may cause the potential release of toxic constituents to soil and groundwater.

Ash disposal in solid waste management units (WMUs) can influence adjacent aquatic ecosystems directly, through surface runoff, and indirectly, through leaching and transport of heavy metals from the WMUs into groundwater. Changes in the concentration of heavy metals in groundwater is a major environmental concern, because heavy metals have high persistence and significant toxic effects. The risk of future trace element releases from landfills is often underestimated because current emission levels and concentrations in the environment are generally below regulatory levels (Muraka *et al.*, 1993). Landfills accumulate large amounts of heavy metals and therefore contribute greatly to this potential risk.

Traditional LCA studies of power generation focus on environmental releases from the power plants and neglect future emissions of solid waste management units. This is mainly due to the time framework of conventional LCAs usually set at the power plant lifespan (20-50 years). However, for the reasons explained above, it is necessary to predict the future emissions from solid waste management units.

This research includes the WMUs into the LCA boundary and the LCI model developed covers three types of WMUs: landfills, surface impoundments and waste piles. Surface impoundments and waste piles are modelled as a temporary waste management unit with a prescribed operational life. At the end of the unit's operational life, the model assumes that the wastes in surface impoundments and waste piles are transferred to landfills and there is no further release of waste constituents to the ground water. The LCI model for landfills covers a 1000-year time period. Emission predictions for WMU are made based on short-term measurement data or leaching test results from the literature.

5.6.2 The Development of Life Cycle Model for Landfills

Landfills are facilities in which waste is placed for disposal on land. Figure 5.19 shows a simple illustration of a landfill. Landfills are usually natural depressions or excavations that are gradually filled with waste. At the time for the landfill closure, a cover is placed on the filled wastes in order to secure the waste stored and prevent infiltration. CCWs managed in landfills may be transported dry from the point of

generation, or they may be placed after dredging from a surface impoundment or a waste pile. Some residual liquids may be placed along with the dredged solids, or liquids may be added during the construction of the landfill for dust control purposes (USEPA, 1999). The leachate from landfills may have a negative impact to the groundwater in the surrounding region.

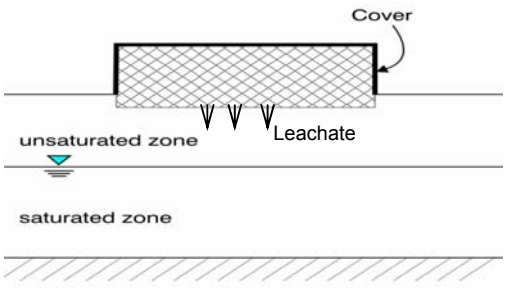

Figure 5.19: A simple illustration of a landfill.

The scheme of the LCI modelling for landfills is illustrated in Figure 5.20. The landfill is modelled as a rectangular cuboid unit with length, width, and depth. The input is the precipitation (rainwater) and output is the leachate. Within the cover system, rainwater can be stored, drained laterally, or be returned to the atmosphere via evapotranspiration. The hydraulic characteristics and functions of the layers within the cover system are summarised in Table 5.17. The cover is designed to minimise the percolation of water by maximising runoff, lateral drainage and evapotranspiration. In the LCI modelling, the layers within the cover system are modelled separately in order to accurately calculate the percolation of the water and represent the temporal and geographical differences of landfills.

Table 5.17: Hydraulic Characteristics of layers within cover (After Koerner and Daniel, 1997)

Type of layer	Hydraulic Characteristics
Cover soil	The cover soil is defined as the soil from the ground surface down to the top of the drainage layer. Water that enters the cover soil flows downward by gravitational forces. In cover soil, storage of water by capillary forces and removal of water by evapotranspiration limit the percolation of the water through the cover.
Lateral Drainage Layer	This layer promotes lateral drainage to collection system. Hydraulic conductivity is typically $>10^{-4}$m/s and the underlying layer is normally a liner.
Geomembrane liner	Geomembranes can be of any type. They are assumed to permit leakage via vapour diffusion, manufacturing flaws (pinholes), and installation defects.
Barrier soil liner	Barrier soil liner are low-permeability soils, normally a compacted clay liner (CCL) or geosynthetic clay liner (GCL). The barrier soil layer normally has a hydraulic conductivity less than 10^{-8} to 10^{-9} m/s.

∗The geomembrane placed on a barrier soil liner (either CCL or GCL) is called composite liner.

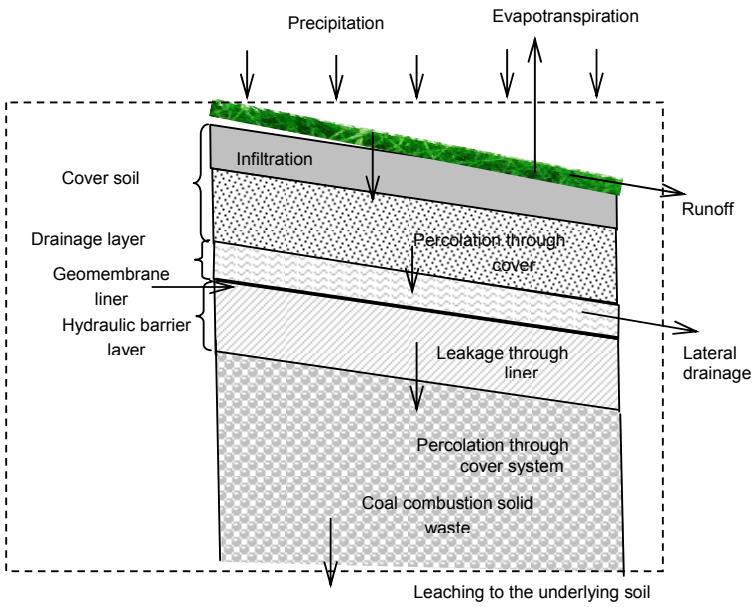

Figure 5.20: The scheme of LCI model of landfills after closure

5.6.2.1 Calculation of the Water Percolation through Cover Soil by Water Balance Analysis

Based on the mass conservation, the water balance method is used to quantify the percolation of water through the cover soil. The water balance method means that the quantity of water that percolates through cover soil equal that the precipitation minus the surface runoff, minus evapotranspiration and minus the change in amount of water stored within the cover soil, as following equation:

$$I = P - ET - R - \Delta S \qquad [5.55]$$

where,

I is the average water percolation rate (mm/s);

P is the average precipitation rate (mm/s);

ET is the rate of water loss through evapotranspiration (mm/s);

R the average surface runoff rate (mm/s);

ΔS is the cover soil moisture change rate (mm/s).

The table of water balance analysis shown in Table 5.18 is used to compute the monthly water percolation rate over the landfill area based on Equation 5.55. The calculation methods used to complete the Table for a given landfil are modified from literature (Koerner and Daniel, 1997) and provided in Appendix C.

Table 5.18: Table used for water balance analysis for the landfill (After Koerner and Daniel, 1997)

Row	Parameter	January	February	March	...	December
A	Avg. Monthly Temp (°C)					
B	Monthly Heat Index					
C	Unadjusted Daily Potential Evapotranspiration (UPET), mm					
D	Possible Monthly Duration of Sunlight (N)					
E	Potential Evapotranspiration (PET)					
F	Precipitation (P), mm					
G	Runoff Coefficient (C),m					
H	Runoff (R),m					
I	Infiltration (IN), mm					
J	IN - PET, mm					
K	Accumulated Water Loss (WL), mm					
L	Water Stored (WS), mm					
M	Change in Water Storage (CWS), mm					
N	Actual Evapotranspiration (AET), mm					
O	Percolation (PERC),mm					
P	Check (CK), mm					
Q	Percolation rate (FLUX),m/s					

5.6.2.2 Calculation of the Average Hydraulic Head in the Drainage Layer

The water that percolates through the cover will be drained by a drainage layer and impeded from further downward movement by one or more hydraulic barriers such as a composite liner or a compacted clay liner CCL. The water collected by the drainage layer normally has no adverse environmental impacts and is discharged to the surface water. However, a small portion of water will migrate downward caused by gravity. The amount of it depends on the average head of the water in the drainage layer and property of the underlying layer such as composite liner or CCL.

The average head of liquid in the drainage layer (h_{avg}) can be computed and used as the hydraulic head of liquid on underlying layer. Based on Darcy's law, the average head of liquid in the drainage layer (h_{avg}) is calculated by the following equations (Koerner and Daniel, 1997):

$$q=k_d(\triangle H_d/L_d)A= k_d\ (\triangle H_d/L_d)\ (h_{avg})\ W$$

or

$$h_{avg} = q\ /\ W[k_d\ (\triangle H_d/L_d)] \qquad [5.56]$$

where q is the rate of flow that percolates the cover (m^3/sec), k_d is the hydraulic conductivity (m/s) of the material comprising the drainage layer (default value 0.01m/s), $\triangle H_d$ is the head loss (length) over distance L along the path of flow, and A is the cross-sectional area of flow, which equals to the average height of liquid in the drainage layer (h_{avg}) times the width of the layer (W).

5.6.2.3 Calculation of the Water Infiltration through a Composite Liner

A composite liner consists of a geomembrane liner placed on a clay liner (either a CCL or a GCL). The leakage pathways of a composite liner are illustrated in Figure 5.21. The water can pass through the defects of the geomembrane and then infiltrate the underlying GCL or CCL. The infiltration rate is determined by a number of factors including area of defects, thickness of the GCL or CCL, and the hydraulic head on the geomembrane liner. This research employs the equations published by Touze-Foltz1 and Giroud (2003) to calculate the leakage rate of a composite liner (see Table 5.19).

Table 5.19: Leakage rates through composite liners (After Touze-Foltz1 and Giroud, 2003)

Defect	Contact conditions	Empirical equation for flow rate	
Circular defect	Excellent	$Q = 0.096 h_w^{0.9} a^{0.1} k_s^{0.74} [1 + 0.1(h_w / H_s)^{0.95}]$	[5.57]
	Good	$Q = 0.21 h_w^{0.9} a^{0.1} k_s^{0.74} [1 + 0.1(h_w / H_s)^{0.95}]$	[5.58]
	Poor	$Q = 1.15 h_w^{0.9} a^{0.1} k_s^{0.74} [1 + 0.1(h_w / H_s)^{0.95}]$	[5.59]
Defect of infinite length	Excellent	$Q_L = 0.42 h_w^{0.45} b^{0.004} k_s^{0.87} [1 + 0.52(h_w / H_s)^{0.59}]$	[5.60]
	Good	$Q_L = 0.65 h_w^{0.45} b^{0.004} k_s^{0.87} [1 + 0.52(h_w / H_s)^{0.59}]$	[5.61]
	Poor	$Q_L = 1.64 h_w^{0.45} b^{0.004} k_s^{0.87} [1 + 0.52(h_w / H_s)^{0.59}]$	[5.62]
Damaged wrinkle	Excellent	$Q_L = 0.63 h_w^{0.45} b^{0.1} k_s^{0.87} [1 + 0.28(h_w / H_s)^{0.82}]$	[5.63]
	Good	$Q_L = 0.89 h_w^{0.45} b^{0.1} k_s^{0.87} [1 + 0.28(h_w / H_s)^{0.82}]$	[5.64]
	Poor	$Q_L = 1.98 h_w^{0.45} b^{0.1} k_s^{0.87} [1 + 0.28(h_w / H_s)^{0.82}]$	[5.65]

Notes:

1) The following symbols are used in this table: Q=flow rate; Q_L=flow rate per unit length; h_w=hydraulic head on top of geomembrane; a=circular defect area; b=width of defect of infinite length or damaged wrinkle; k_s=soil layer hydraulic conductivity; and H_s=soil layer thickness. These equations must be used with the following units: Q (m^3/s), Q_L (m^2/ s), h_w (m), a (m^2), b (m), ks (m/s), and Hs (m).
2) Three types of defect are considered: (i) circular defects located in a flat area of the geomembrane (i.e. an area where the geomembrane has no wrinkles), which correspond to geomembrane puncture; (ii) defects of infinite length, located in a flat area of the geomembrane, which correspond to long cuts or tears and defective seams; and (iii) defects of any shape located on wrinkles in the geomembrane resulting in what is called 'damaged wrinkles'. Defects of infinite length and damaged wrinkles are grouped under the generic term 'two-dimensional defect'.
3) Contact conditions are defined as: (i) poor contact conditions corresponding to a geomembrane that has been installed with a certain number of wrinkles, and/or has been placed on a low-permeability soil layer that has not been well compacted and does not have a smooth surface. (ii) good contact conditions correspond to a geomembrane installed with as few wrinkles as possible, on top of a low-permeability soil layer that has been adequately compacted and has a smooth surface. Furthermore, it is assumed that there is sufficient compressive stress to maintain the geomembrane in contact with the low-permeability soil layer. (iii) excellent contact conditions correspond to a geomembrane installed with no wrinkles on top of a soil component of a composite liner that consists of a bentonite geocomposite installed on top of, and in close contact with, a low-permeability soil layer that has been adequately compacted and has a very smooth surface. Furthermore, it is assumed that there is sufficient compressive stress to maintain the geomembrane in contact with the bentonite geocomposite.

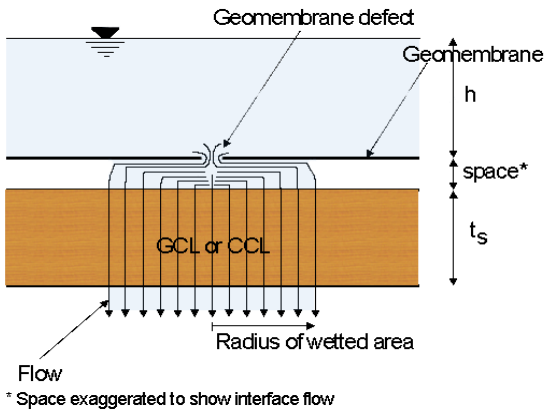

Figure 5.21: Leakage pathways of a composite liner (After AGS, 2001)

The equations in Table 5.19 require that hydraulic heads range between 0.03 and 3 m. According to most landfill regulations, the leachate head above the geomembrane component of the composite liner must not exceed 0.3 m (HELP, 1992; Koerner and Daniel, 1997). This research assumes that the landfills are well designed and the maximum designed hydraulic head in drainage layer is less or equal to 0.3m. Therefore the equations above can be used.

Size of Defects

Circular defect sizes often used in landfill design calculations typically range between 1 cm^2 (i.e. a radius of 5.64 mm) and 3.1×10^{-2} cm^2 (i.e. a radius of 1 mm) (Giroud and Bonaparte, 1989).

The widths of defects of infinite length range between 2×10^{-3} and 2×10^{-2} m, which is approximately consistent with the diameters of circular defects considered in the research by Touze-Foltz1 and Giroud (2003).

Touze-Foltz et al. (1999) conclude that the wrinkle width controls the flow rate rather than the defect size in a wrinkle. A theoretical analysis of wrinkles by Giroud and Morel (1992) shows that, for high-density polyethylene (HDPE) geomembranes, the height of wrinkles is typically of the order of 0.1 m and the width/height ratio is typically of the order of 1 to 3: hence a wrinkle width of the order of 0.1–0.3 m.

The Density of Installation Defects

The density of installation defects is a function of the quality of installation, testing, materials, surface preparation, and equipment. The estimation of installation defect densities as a function of the quality of installation is given in Table 5.20.

Table 5.20: Defect density in geomembrane (after HELP, 1994)

Installation Quality	Defect Density (number per acre)	Frequency (percent)
Excellent	Up to 1	10
Good	1 to 4	40
Fair	4 to 10	40
Poor	10 to 20*	10

* Higher defect densities have been reported for older landfills with poor installation operations and materials; however, these high densities are not characteristic of modern practice.

Typical for liner performance evaluation one defect per acre (4,000 m^2) is considered with a defect area of 0.1 cm^2 (equivalent to defect radius of 1.75 mm), for a conservative design a defect area of 1 cm^2 (equivalent defect radius of 5.64 mm) can be considered (Giroud *et al.*, 1994).

The lifespan of the geomembrane

Rowe (1998) concluded that the service life of the geomembrane at 25^0C was about 150 years.

5.6.2.4 Calculation of the Water Infiltration through Clay Barriers

If clay barriers are under the drainage layer rather than the composite liner, the water may flow through clay barriers. Clay barriers can be compacted clay liners (CCLs), geosynthetic clay liners (GCLs), or both. Water flow through both types of clay liners can be computed by Darcy's formula:

$$q=k[(H+D)/D]A \qquad [5.67]$$

where D is the thickness of the clay liner and H is the depth of water head on the liner. k is the effective hydraulic conductivity of the clay liner, which is normally less than 10^{-8} to 10^{-9} m/s (Koerner and Daniel, 1997). This equation assumes that suction existing at the clay liner/subsoil interface is negligible (HELP, 1992), which means that the pressure head on the base of the clay liner is zero. As the depth of pounded liquid (H) approaches zero, the term (H+D)/D, which is the hydraulic gradient, approaches unity (1) and gravity drainage of the soil at constant water content normally occurs under unit hydraulic gradient (HELP, 1992; Koerner and Daniel, 1997).

Both CCLs and GCLs are installed in an unsaturated condition. A rigorous, time-dependent analysis of leakage through an initially unsaturated GCL would involve consideration of flow through an unsaturated porous medium. However, the CCL or

GCL is usually assumed to be fully saturated because CCLs and GCLs hydrate quickly (within a few weeks) as soon as there is enough water (Koerner and Daniel, 1997).

5.6.2.5 Calculation of Water Infiltration through Solid Waste

The water that infiltrates the composite layer (or clay liner) will enter into the solid waste. In this research, it is assumed that all the water that infiltrates through the composite layer (or clay barriers) will pass through the solid waste and then leach into the soil underlying the solid waste.

5.6.2.6 Leachate Constituents of Concern

When water is passing through the solid waste, some constituents of the waste will be extracted as leachate and transported to the underlying soil. The constituents that are present in the coal combustion waste leachate may have potential environmental impacts on the groundwater. To identify the leachate constituents of concern, USEPA (1998) investigated five categories of constituents: heavy metals, other inorganics, conventional organics, polychlorinated dibenzofurans and polychlorinated dibenzodioxins (PCDDs and PCDFs), and radionuclides, and concluded that the heavy metals are indeed constituents of concern. To further identify the heavy metals of concern, USEPA (1998) conducted a screening analysis by comparing leachate concentrations from coal combustion solid waste with the toxicity thresholds used to protect human health and concluded that metals that are present in coal combustion waste leachate at concentrations greater than the corresponding health based benchmarks (developed by EPA) were: arsenic, barium, cadmium, chromium, lead, mercury, nickel, selenium, and zinc. In this research the heavy metals that USEPA used in screening analysis are considered as the constituents of concern, and additionally include: antimony, copper, silver, vanadium, and zinc.

5.6.2.7 Concentration of Leachate Constituents of Concern

The leaching of trace metals from landfills of coal combustion solid waste depends upon the balance at the solid-liquid interface and the pH of the liquid phase as well as the characteristics of the contact between waste and leaching water, which influences chemical processes. These processes are the basis of mass transfer in the waste leachate system, such as dissolution, chemical precipitation, redox and sorption reactions (Andreottolia and Cannas, 1992). The concentration of leachate constituents will gradually diminish with time, as the amount of constituent that remains in the landfill is depleted, and the leachate concentration is waste- and constituent-specific with no

default value or distribution for this parameter (USEPA, 2003a; Rowe, 1998; Wigh, 1979). A more realistic modelling analysis in the case of a closed landfill with no continued waste addition to the unit, can be conducted by assuming that linear equilibrium partitioning between the solid and liquid phase of the waste leads to an exponential decrease in the leachate concentration over time as a result of depletion of the source and the leachate concentration as a function of time (t) is given by (USEPA, 2003a):

$$C_L(t) = C_L^0 \exp\left\{\left(\frac{-I \times K_w}{D_{LF} \times F_h \times \rho_{hw}}\right)t\right\} \quad [5.68]$$

$$C_L^0 = \frac{C_w}{K_w} \quad [5.69]$$

where,

C_L is the leachate concentration (mg/L), which represents the concentration of the leachate constituents emanating from the base of the waste management unit;

t is the time since leaching began at landfill closure (y);

C_L^0 is the initial leachate concentration at the time of landfill closure (mg/L);

I is the average infiltration rate (m/y);

D_{LF} is the landfill depth (m);

F_h is the waste fraction, defined as the volume fraction of the waste in the landfill (F_h) that is occupied by the waste of concern when the landfill is closed, ranging from very small value to 1.0;

ρ_{hw} is the waste density (g/cm^3);

C_w is the waste concentration (mg/Kg), represents the total mass fraction of a constituent in the waste which may eventually leach out. In this research, the total waste concentration is used as C_w. This approach is protective because the ~~meatured~~ total waste concentration should always be at least as high as the potentially "leachable" waste concentration, which is more difficult to quantify (USEPA, 2003a);

K_w is the waste-concentration-to-leachate-concentration ratio, or C_w/C_L.

If the annual infiltration rate over the area is constant, then the accumulated emission of a constituent at year T is given by:

$$E(t) = \frac{C_L^0 \times D_{LF} \times F_h \times \rho_{kw}}{K_w} \cdot [1 - \exp\left\{\left(\frac{-I \times K_w}{D_{LF} \times F_h \times \rho_{hw}}\right)T\right\}] \quad [5.70]$$

Equations 5.68 and 5.70 require knowledge of the the waste-concentration-to-leachate-concentration ratio, C_w/C_L. The pore water (i.e. interstitial water from borings) waste-concentration-to-leachate-concentration ratios of various constituents for coal combustion wastes in landfills and surface impoundments are given in Table 5.21.

Table 5.21: Pore water waste-concentration-to-leachate-concentration ratios for coal combustion wastes in landfills and surface impoundments (After USEPA, 1998)

Trace metals	Waste-concentration-to-leachate-concentration ratios (C_w/C_L)
Antimony*	10,000
Arsenic	1,200
Beryllium*	10,000
Cadmium*	10,000
Chromium	58,000
Cobalt*	10,000
Lead	7,500
Manganese*	10,000
Nickel	17,000
Selenium	42
Zinc	3,000
Copper	13,000
Thallium	10,000
Vanadium	480
Barium	14,000
Silver*	10,000
Mercury*	10,000

* indicates that a default C_w/C_L value of 10,000 was used in all landfill scenarios where chemical specific values could not be calculated or not available.

5.6.3 The Development of Life Cycle Inventory Model for Surface Impoundments

Surface impoundments are natural depressions, excavated ponds, or basins that typically contain a mixture of liquids and solids (see Figure 5.22). CCWs managed in surface impoundments typically are sluiced with water from the power plants to the impoundment. The solid CCWs gradually settle out of this slurry, accumulating at the bottom of the impoundment as loose and consolidated sediment layers. This process also results in a standing layer of relatively clear water at the surface. The distance between the surface of the head and the top edge of the impoundment indicates the remaining capacity of the impoundment. The value of this distance in an impoundment may fluctuate as wastes are added, rainfall accumulates, and liquids are removed for discharge to surface water or recirculated to sluicing operations (USEPA, 2003a). The impoundment also may be periodically dewatered and the solids are removed for disposal in a landfill.

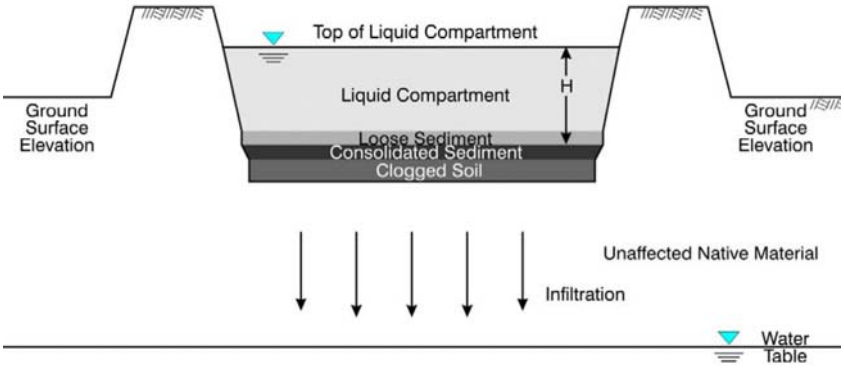

Figure 5.22: The scheme of LCI model developed for surface impoundments (After USEPA 2003a).

The purpose of the LCI model is to estimate the amount of leachate and quantify the leachate constituents emanating from the base of the surface impoundment to the underlying soil. The scheme of the LCI model of surface impoundment is illustrated in Figure 5.22. In the LCI model, the surface impoundment is modelled as a temporary waste management unit with a prescribed operational life, same as the power plant operational life. At the end of its operational life, the model assumes that the solid waste is transferred to a landfill for disposal and that there is no further release of waste constituents to the ground water from the surface impoundment. The surface impoundment is modelled as a unit with a square foot print, with a constant ponding depth, H, during its operational life. The model also assumes that a constant consolidated layer of sediment accumulates at the bottom during the operational life. The LCI model accounts for three options of the configuration of the surface impoundment: unlined, single liner, and composite liner.

5.6.3.1 Unlined Surface Impoundment

It is assumed that the pressure head on the base of the clay liner is zero, which means that suction at the clay liner/subsoil interface is negligible (HELP, 1992). The effective hydraulic conductivity of the combined layer (including consolidated sediment and clogged soil) is given by (HELP, 1992):

$$K = \frac{D_{fc} + D_{c\log}}{\frac{D_{fc}}{K_{fc}} + \frac{D_{c\log}}{K_{c\log}}} \qquad [5.71]$$

where:

K is the effective hydraulic conductivity (m/s);

D_{fc} is the thickness of consolidated sediment layer (m);

D_{clog} is thickness of clogged soil layer (m), typically 0.5m;

K_{fc} is the saturated hydraulic conductivity of the consolidated sediment (m/s);

K_{clog} is the saturated hydraulic conductivity of clogged soil (m/s).

The rate of infiltration is then given by:

$$I = \frac{D_{fc} + D_{c\log}}{\frac{D_{fc}}{K_{fc}} + \frac{D_{c\log}}{K_{c\log}}} \cdot \frac{H_p + D_{fc} + D_{c\log}}{D_{fc} + D_{c\log}} = \frac{H_p + D_{fc} + D_{c\log}}{\frac{D_{fc}}{K_{fc}} + \frac{D_{c\log}}{K_{c\log}}} \quad [5.72]$$

I is the average infiltration rate (m/s);

H_p is the ponding depth of waste water in the surface impoundment unit (m).

The sediment layer at the base of the impoundment normally has a thickness of 20 cm and has a permeability with a relatively narrow range of variation between 1.26×10^{-7} and 1.77×10^{-7} cm/s (USEPA, 2003a). Based on literature (USEPA, 2003a), it is assumed that the depth of clogging underneath the impoundment is 0.5 m as default value, and that the saturated hydraulic conductivity of the clogged layer is 10% of that of the original soil underlying the impoundment.

5.6.3.2 Single-lined Surface Impoundments

For single-lined surface impoundments, a CCL or a GCL layer is placed at the bottom of the surface impoundment. In the case of single-lined surface impoundments, there is no clogged layer due to the filter effect of the liner (USEPA, 2003a). The infiltration rate is calculated in the same manner as described in the above section for unlined units, given by:

$$I = \frac{H_p + D_{fc} + D_{liner}}{\frac{D_{fc}}{K_{fc}} + \frac{D_{liner}}{K_{liner}}} \quad [5.73]$$

where:

I is the infiltration rate (m/s);

H_p is the ponding depth of waste water in the surface impoundment unit (m);

D_{fc} is the thickness of consolidated sediment layer (m);

D_{liner} is the thickness of liner (m);

K_{fc} is the saturated hydraulic conductivity of the consolidated sediment (m/s);

K_{liner} is the saturated hydraulic conductivity of liner (m/s), which is typically 1×10^{-7} cm/s (USEPA, 2003a).

5.6.3.3 Surface Impoundments with Composite Liner

For the surface impoundment scenario, the research derives a model for leakage through circular defects (pin holes) in a composite liner using the following equation developed by Bonaparte et al. (1989):

$$Q = 0.21a^{0.1}h^{0.9}K_s^{0.74}\rho S \qquad [5.74]$$

where:

Q is the steady-state rate of leakage through holes in the composite liner (m^3/s);

a is the area of holes in the geomembrane (m^2);

h is the head of liquid on top of geomembrane (m);

K_s is the hydraulic conductivity of the low-permeability soil underlying the geomembrane (m/s);

ρ is the leak density (holes/m^2);

S is the footprint of the surface impoundment (m^2).

This equation is applicable to cases where there is good contact between the geomembrane and the underlying compacted clay liner. This research assume that typical hydraulic conductivity of the compacted clay liner underlying the geomembrane is 1×10^{-7} cm/s, based on literature (USEPA, 2003a).

The sizes of the circular defects and the density of the circular defects are as same as described in section 5.6.2.3.

5.6.3.4 Concentrations of Constituents in Leachate

The constant concentration of constituents in leachate is most appropriate for surface impoundment modelling, because surface impoundments operate for a prescribed period of time, followed by clean closure, because during the active life of the unit, continual addition of "fresh" waste will serve to keep the leachate concentration at a more or less constant value (USEPA, 1998).

The constituents of concern in the leachate are as same as the landfill case, including: antimony, arsenic, barium, cadmium, chromium, copper, lead, mercury, nickel, selenium, silver, vanadium, and zinc. The pore water waste-concentration-to-leahate-concentration ratios of various constituents for coal combustion wastes in surface

impoundments shown in Table 5.20 are used for the estimation of content concentration of constituents in leachate using equation 5.69.

5.6.4 Life Cycle Inventory Model for Waste Piles

Waste piles are conceptually similar to landfills, but differ in a number of key aspects. Landfills are fitted with a cover while waste piles are normally uncovered landfills. Landfills represent a long-term waste management scenario, while waste piles represent a more temporary waste management scenario. Typically at the end of the active life of a waste pile, the waste material is either removed for land filling, or the waste pile is covered and left in place (USEPA, 2003). If at the end of its operational life a waste pile is covered and left in place, it then becomes equivalent to a landfill, which can be modelled using the LCI models developed in section 5.9.2.

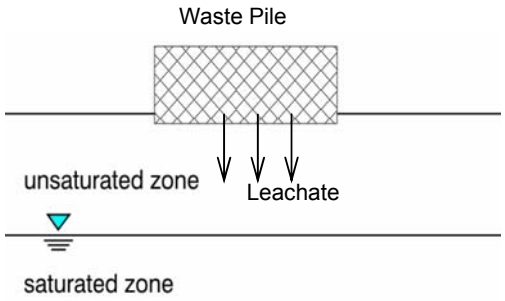

Figure 5.23: The scheme of the LCI model for waste piles

The scheme of the LCI model for waste pile is shown in Figure 5.23. The waste pile is modelled as a one-layer landfill with the continual addition of "fresh" solid waste material comprising the layer. It is assumed that the waste is a rectangular cuboid unit with its length, width and depth and the addition of the "fresh" solid waste is evenly distributed on the waste pile. After the waste is removed for landfill at the end of its operational life, there is no longer a source of potential contamination. The input data required for the LCI model include the area of the waste pile, monthly average addition of the "fresh" waste to the pile; the monthly precipitation rate, and the operational life the waste pile. The outputs of the model are the leakage rate at the base of the waste pile and the leachate composition, that is the concentration of constituents in the leachate.

5.6.4.1 Thickness of the "Fresh" Waste Layer

During the operational life, continual addition of "fresh" solid waste material is added on the waste pile and becomes a layer on the pile. The thickness of the cover comprising by the monthly addition of "fresh" solid waste is given by following equation:

$$T_{waste} = \frac{m}{\rho \cdot s} \quad [5.135]$$

where:

T_{waste} is the thickness of layer (m);

M is the mass of the monthly addition of "fresh" solid waste (kg);

ρ is the density of the addition of "fresh" solid waste (kg/m^3), typically 1360 kg/m^3 (USEPA, 2003);

S is the area of the footprint of the waste pile (m^2), 4170m^2 is set as the default value in this research based on the USEPA (2003) database of waste pile.

5.6.4.2 Rate of Water Infiltration through the "Fresh" Waste Layer

The layer comprising by the monthly addition of "fresh" solid waste is analogous to the cover soil of the landfill and can be analysed by the water balance method:

$$I_{layer} = P - E - R - AW \quad [5.76]$$

where:

I_{layer} is the average infiltration rate (mm/s), which is defined as the rate at which water percolates through the layer;

P is the average precipitation (mm/s);

E is the average water loss through evaporation in the layer (mm/s);

R is the runoff (mm/s);

AW is the average moisture change of the layer (mm/s)

Since the waste pile surface normally holds no vegetation, the waste pile LCI model does not account for transpiration. The evaporation will continue until the layer reaches a permanent wilting point (the point at which the moisture content of the soil prevents the soil from supplying water at a sufficient rate essentially due to intermolecular surface tension) (Bagchi, 2004). Both Stroonsnjider (1987) and Gallardo *et al.* (1996) found a good relationship between cumulative bare soil evaporation and cumulative reference evapotranspiration. Because of the unsaturated state of the solid waste, the average evaporation from the waste pile surface will be lower (Bagchi, 2004). Based on

the above analysis, this research assumes that the rate of evaporation of the waste pile is set as 50 percent of the evaportranspiration calculated in the landfill model. With this modification, the landfill LCI model developed in section 5.6.2.1 can be used as waste pile LCI model. Three categories of waste (see Table 5.22) are used in the LCI model to give a range of the infiltration rate.

Table 5.22: Moisture retention parameters for the modelled waste pile materials (After USEPA, 2003)

Waste Type	Total Porosity (vol/vol)	Field Capacity (vol/vol)	Wilting Point (vol/vol)	Hydraulic Conductivity (cm/sec)
Low Permeability	0.541	0.187	0.047	0.00005
Moderate Permeability	0.578	0.076	0.025	0.0041
High Permeability	0.375	0.055	0.02	0.041

5.6.4.3 Rate of Water Infiltration through the Waste Pile

The model used to calculate the water infiltration through the "fresh" layer, I_{layer}, is based on monthly data. Due to fact that the monthly temperature and monthly precipitation may differ significantly throughout the year, in some months water can not infiltrate through the "fresh" waste layer. This creates conditions for unsaturated waste layers, which will absorb water when infiltration occurs in later time. In an annual time framework, there may no water infiltration. The annual water balance analysis is conducted in this research to analyse if there is water infiltration at annual level. Annual water balance analysis is given by:

$$I_a = P_a - E_a - (FC - W) \times T_a \qquad [5.77]$$

where,

I_a is the average water infiltration per year (mm/year);

P_a is the average precipitation per year (mm/year);

E_a is the average evaporation per year (mm/year);

FC is the field capacity (vol/vol);

W is the initial water content of the "fresh" waste (vol/vol);

T_a is the thickness of the "fresh" waste layer accumulated during one year (mm/year).

If I_a is positive, the rate of water infiltration through the waste pile equal to I_a. If I_a is negative or zero, the rate of water infiltration through the waste pile is zero.

Additionally, the modelling assumes that there is no leachate collection system and no increase in hydraulic conductivity (that is, the infiltration rate is constant) over the modelling period.

5.6.4.4 Concentrations of Constituents of Concern in the Leachate

The waste pile LCI model assumes a constant leachate concentration applied uniformly over the area of the waste pile unit for a period of time equal to the unit's operating life. Due to continual addition of "fresh" waste, this practise will serve to keep the leachate concentration at a more or less constant value (USEPA, 1998). The pore water waste-concentration-to-leachate-concentration ratios of various constituents for coal combustion wastes in landfills in Table 5.20 are used for the estimation of content concentration of constituents in leachate using equation 5.69.

5.7 Conclusions

This chapter has presented the procedure of LCI models developed for coal combustion processes, particulate control processes, NOx control processes, SOx control processes, and solid waste disposal.

The type of boiler, coal characteristics (e.g. carbon or trace metal content in coal), and boiler efficiency represent the technological and geographical differences and are important aspects determining the emissions of coal combustion process. The coal combustion LCI model developed allows for different coal characteristics, six types of boiler, and different options of power plant configuration or plant location, in order to characterise technological and geographical differences of the coal combustion process.

The Electrostatic Precipitator (ESP) LCI model is developed as a representative for PM control process. ESP not only removes PM but also affects emissions of SO_3, mercury vapor and other trace metals. The ESP LCI model developed estimates the mercury vapour removal, removal of other trace metals of concern, and SO_3 removal by ESP based on empirical relations.

Two typical NOx control processes, the LSFO and MEL have been included in the LCI model developed. Liquid-to-gas (L/G) ratio is a key variable for LSFO or MEL systems to achieve high SO_2 removal efficiency. FGD processes also remove other acid gases present in flue gases (including SO_3, HCl, and HF), particulate matter, and trace metals. The LCI model calculates the SO_2 removal, SO_3 removal, PM removal, HCl and HF

removal, and trace metal removal rates based on empirical relations, and computes limestone consumption, gypsum output, water make-up, and electricity input based on engineering calculations. The LCI model also uses partitioning factors to calculate the partition of trace metals between wet FGD solid wastes and liquid wastes, which are neglected by previous studies.

The NOx removal rate of SCR NOx control process is determined by NH_3-to-NOx ratio, reaction temperature, and type of catalyst. SCR can also oxidise SO_2 (to SO_3) and elemental Hg^0 (to oxidised Hg^{2+}). The LCI model developed can calculate the NOx removal rate, the rate of SO_2 oxidised to SO_3, the mercury oxidisation rate, and catalyst consumption based on empirical relations. LCI model computes ammonia consumption, electricity input, steam required for ammonia injection, catalyst sootblowing steam requirement, and ammonia release by engineering calculations.

The leakage of 17 trace metals of concern from solid waste disposal units (including landfills, surface impoundments and waste piles) to underlying soil is modelled using basic physical principles or empirical relations of the leakage processes. The LCI model of landfills can cover 1,000-year period. Different configurations of solid waste disposal units (especially those that relate to the liner used) have significant influence on the leachate reaching underlying soils. Weather conditions (e.g. precipitation and temperature), which represent geographic differences, have considerable impact on potential for leachate generation. The waste-concentration-to-leachate-concentration ratio of trace metals is the key parameter that determines the concentration of trace metals in the leachate from solid waste disposal units. The concentration of trace metals in leachate from landfills diminishes gradually with time. The concentration of trace metals in leachate from surface impoundments or waste piles are constant.

Chapter 6 Life Cycle Inventory Modelling of Oxy-fuel Combustion Processes

6.1 Introduction

The oxy-fuel combustion approach combusts the fuel using almost pure oxygen (90 to 99%) at near stoichiometric conditions and generates flue gas consisting mainly of CO_2 (> 90-98 % on a dry basis), water vapour, O_2 and minor amounts of noble gases and, depending on the fuel composition, SOx and NOx. The oxygen is generated by an air separation unit (ASU). After the removal of particulate matters in flue gas, a proportion of the flue gas (typically 70%) is recycled to the combustion process to control the combustion temperature. The rest of flue gas passes through a heat exchange unit, where water in the flue gas is condensed and energy in flue gas is extracted to the power cycle. The flue gas then enters into the SOx control unit to remove more than 95% of the SOx. The desulphurised flue gas is sent to the distillation unit, where water in the flue gas is condensed and the small amounts of impurities such as SOx, NOx, O_2, noble gases and particulates are removed to meet transport and storage requirements, after which the CO_2 is compressed and ready for transport and storage. The general scheme of an oxy-fuel combustion plant is presented in Figure 6.1.

Oxy-fuel combustion has been considered to be one of the most promising options of the technologies for CO_2 capture from coal-fired power plants, due to the advantage of adapting advanced steam technology, reducing boiler size, improving combustion efficiency, reduction of NOx and SOx emissions and simplified flue gas processing (Suriyawong *et al.,* 2006). This technology, however, also causes engineering

challenges in the areas of combustion and heat transfer, boiler design, boiler materials, energy-efficient oxygen production and flue gas processing (Jordal, 2004).

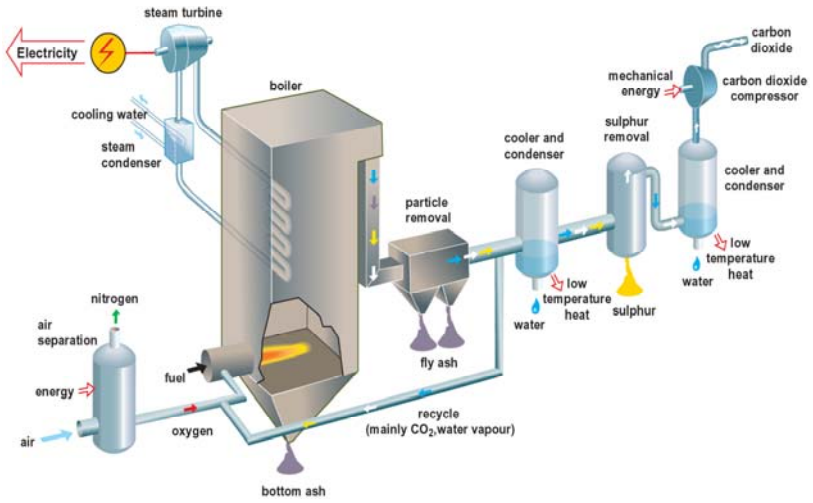

Figure 6.1: The scheme of oxy-fuel combustion plant (Strömberg, 2006).

At present, large scale oxy-fuel combustion plants have not become a reality, however, a number of pilot or demonstration projects are under construction. A list of current oxy-fuel combustion power generation projects is presented in Table 6.1. A summary of previous studies of technical-economic assessment for oxy-fuel combustion power plants is provided in Table 6.2. It can be seen that the CO_2 reduction rates range from 79-100%, the costs of electricity (COE) increases by 20-55% compared with conventional power plants and the plant efficiencies decrease to 65-85% of that of conventional power plants.

Table 6.1: Oxy-fuel combustion power generation projects in the world.

Project Name	Location	Feedstock	Size MWh	CO_2 Fate	Plant commissioning
Vattenfall Oxy-fuel	Germany	Lignite	30 (pilot plant); 300 (demon plant); 1,000 (commercial)	Pilot scale no storage	pilot plant 2008; demo plant 2015; commercial 2020
Callide-A Oxy Fuel	Australia	Hard coal	30	Depleted gas reservoir	2009
Victoria	Australia	Lignite	350	Undecided	2014
Jupiter Oxygen	Tx, USA	Hard coal	45 (demonstration)	Undecided	2011
RWE npower	Tilbury, UK	Hard coal	800 (retrofit)	Undecided	2016
SEQ and ONS Energy,	Drachten Holland	Hard coal	55	EOR	2011
SaskPower Clean Coal	Canada	Lignite	300	Saline aquifer and/or EOR	Undecided
Total Lacq	France	Oil	35	Depleted gas reservoir	2008
ZENG Worsham-Steed	USA	Gas	70	EOR	Undecided
ZENG Risavika	Norway	Gas	50-70	Undecided	Undecided

Table 6.2: Summary of technical-economic studies of coal power plant (Adapted from Nsakala, 2007 and Tan, *et al*, 2005)

Author(s)	Description	Economic Analysis Results	Plant Efficiency (%)	Efficiency Relative to Base Case	Relative CO_2 Reduction
Strömberg (2006)	Lignite/bituminous fired baseline plants and oxy-fuel power plants using lignite/bituminous with ASU and FGD and CO_2 conditioning.	Costs of electricity (COE), COE relative to baseline plant, and CO_2 avoidance costs respectively: Lignite plant 44€/MW, 1.42, 18€/ton CO_2; Bituminous plant 45€/MW, 1.45, 20€/ton CO_2	Lignite plant: 41%; Bituminous plant: 37%	Lignite plant: 83.7%; Bituminous plant: 82%	---
Andersson and Johnsson (2006)	865 MW lignite-fired baseline plant and two oxy-fuel power plants with ASU and CO_2 capture conditioning with electricity supplied by original plant; net power after retrofit is 677 and 865 MW.	Costs of electricity increase 42.1%relative to baseline plant. CO_2 avoidance costs are 26 \$/ton CO_2.	33.4%	78.4%	99.5%
Yamada (2006)	Assessment of oxy-fuel combustion technology applied to a 1,000 MW pulverized coal-fired power plant in Japan	---	30%	75%	95%
Varagani *et al*. (2004)	500 MW baseline power plant; net power after retrofit 405 – 409 MW	Power cost 33% higher than baseline; CO_2 capture cost is US$19 – 21 per ton	29.9% – 31.4%	80.8% – 84.8%	99%
Kakaras *et al.* (2004)	280 MW baseline power plant; net output after retrofit 184 MW	---	23.8%	64.9%	79%
Singh *et al*. (2003)	400 MW power plant fired with sub-bituminous coal; power for ASU and CO_2 capture supplied by auxiliary NGCC plant.	Retrofit cost is US$76.4 million, resulting in a 20% increase in power cost. CO_2 capture cost is US$35 per ton	---	---	---
Simbeck (2001)	300 MW power plant fired with sub-bituminous coal; power for ASU and CO_2 capture supplied by auxiliary NGCC plant.	Total cost relative to baseline plant is 2.98; CO_2 capture cost is US$28 per ton.	29.2%	80.7%	87.2%
Nsakala *et al.* (2001)	433 MW baseline plant with power for ASU and CO_2 capture supplied by original plant; net power after retrofit is 280 MW.	CO_2 capture cost of US$42 per ton	24.1%	65.7%	82.3%
Okawa *et al.* (1997)	1,000 MW power plant with power from ASU and CO_2 capture supplied by original plant	Retrofit cost is 3.8 billion yen per year	29.1%	73.5%	--
McPhail *et al.* (1997)	660 MW power plant retrofitted with different heat integration configurations: net output reduced to 446 – 513 MW	Optimal cost of power is 55% higher than in base case; capital cost increases by 50%	28.5% – 32.7%	69.2% – 79.4%	95 – 100%

This chapter demonstrates the procedure for LCI modelling of oxy-fuel combustion process, air separation processes, and CO_2 conditioning for oxy-fuel combustion.

6.2 Life Cycle Inventory Modelling of the Air Separation Process

6.2.1 Basic Principles

There are currently three methods of separating oxygen from air: cryogenic distillation, adsorption in pressure swing or vacuum swing absorber, and diffusion in a membrane unit.

The three separation methods have many common characteristics. They are all physical processes (no chemical reaction involved), and compressors and/or blowers are used to drive the separation. The comparison of these technologies is provided in Table 6.3. This research considered only the cryogenic distillation process, since this is most widely used for oxygen production in large scale.

Table 6.3: Air separation technology comparison table (After Smith and Klosek, 2001).

Process	Status	By-product capability	Purity limit (vol%)	Start-up time
Adsorption	Semi-mature	Poor	95	Minutes
Chemical	Developing	Poor	99+	Hours
Cryogenic	Mature	Excellent	99+	Hours
Membrane	Semi-mature	Poor	~40	Minutes
ITM	developing	poor	99+	Hours

Typical steps of cryogenic distillation process are illustrated in Figure 6.2. Here the process begins with the intake of large volumes of air from the atmosphere. Ambient air is drawn through an air separation filter house (ASFH) for the removal of dust and large airborne particles prior to entering the three stage main air compressor (MAC). In the MAC the filtered air is compressed to approximately 550 kPa (65 psig) and then flows through the two-stage direct contact after-cooler (DCA) (ALSTOM, 2003b). The after-cooled air is then passed through the pre-purification system, where a two-bed temperature-swing adsorption (TSA) process or a two-bed pressure-swing adsorption (PSA) process is used to remove water, carbon dioxide, and most of the hydrocarbons from the air stream. The after-cooler air then enters into the cryogenic equipment package, including the primary heat exchanger (PHX), refrigeration system (generator, upper column turbine (UCT)) and the distillation column. In the cryogenic equipment package, air is cooled to about -185°C (-300°F) and then, based on different boiling points, separated into its elemental components in the form of liquid oxygen, argon and nitrogen (ALSTOM, 2003b).

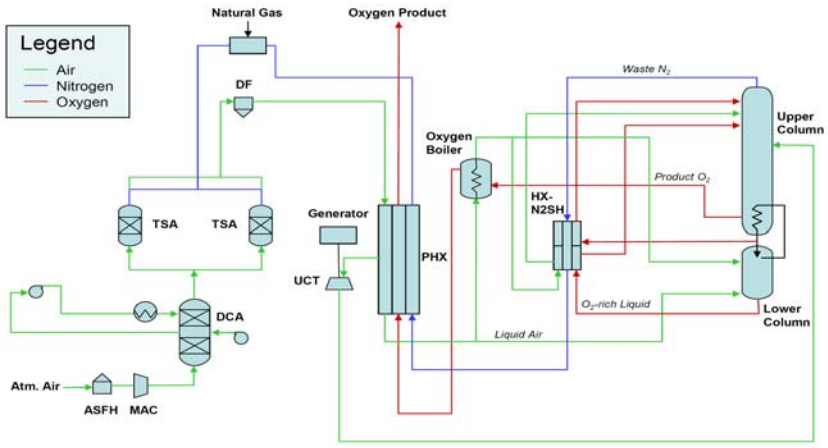

Figure 6.2: Typical steps of a cryogenic distillation process (After: ALSTOM, 2003b).

6.2.2 The Development of a Life Cycle Inventory Model for the Air Separation Unit

The ASU LCI model quantifies the removal rates of impurities in the pre-purification process, energy consumption of ASU, absorbent consumption by the TSA, cooling water requirement by DAC, emissions from refrigeration, and specification of oxygen product. The schematic of the ASU LCI model developed is shown in Figure 6.3.

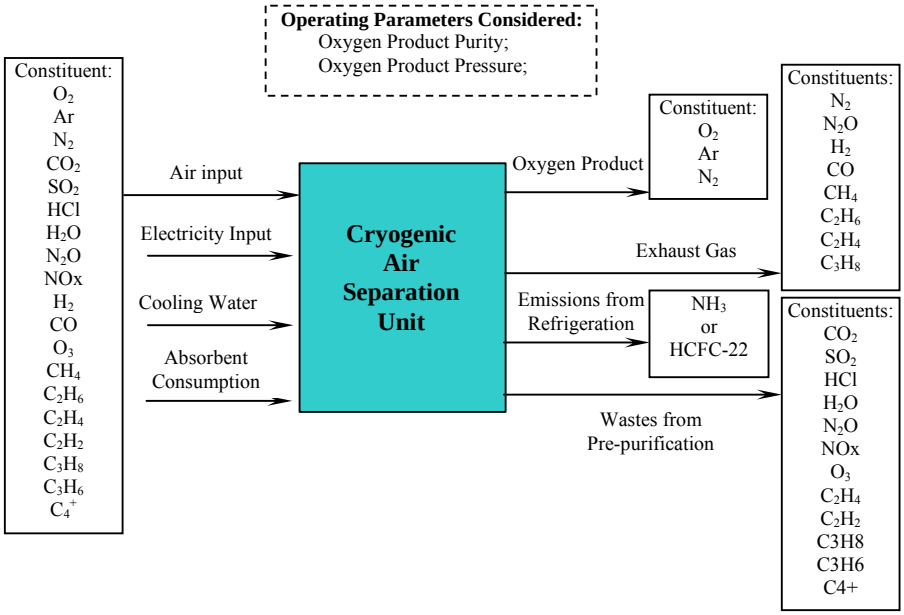

Figure 6.3: The schematic of the ASU LCI model developed.

6.2.2.1 The Removal Rate of Impurities in the Pre-purification Unit

Ambient air primarily contains Nitrogen, Oxygen, Argon, and Carbon Dioxide. It may have up to about 5% (by volume) water content and may contain a number of other gases (usually in trace amounts) as shown in Table 6.4. The CO_2, H_2O, NO_X and hydrocarbon traces must be removed before the air stream enters the heat exchanger and the distillation column. The pre-purification unit (PPU) normally uses a two-bed temperature-swing adsorption (TSA) process that allows continuous operation. One bed purifies the feed air while the other bed is being regenerated with first hot then cool waste nitrogen. A natural gas regeneration heater is normally used to provide regeneration energy. Up-to-date purification technology is adsorption, using beds of alumina, or molecular sieve to remove water, carbon dioxide, and most of the hydrocarbons from the air stream. The typical removal rate of impurities in PPU is provided in Table 6.4.

Table 6.4: Typical removal rate of impurities in the PPU (After Schmidt *et al*., 2004)

Species	Typical design basis for air concentration (ppm)	Typical % removal in PPU
N_2	780,800	0
O_2	209,500	0
Ar	9,300	0
CO_2	400	>99%
SO_2	0.1	100%
HCl	0.05	100%
H_2O	10,000	100%
N_2O	0.3	30-70%
NOx ($NO+NO_2$)	0.05	100%
H_2	10	0%
CO	20	0%
O_3	0.2	100%
CH_4	10	0%
C_2H_6	0.1	0%
C_2H_4	0.3	50%
C_2H_2	1.0	100%
C_3H_8	0.05	67%
C_3H_6	0.2	100%
C_4^+	1.0	100%

The regeneration of adsorbent will release the adsorbed water, carbon dioxide, and hydrocarbons from adsorption bed. The emissions of these gases can be calculated by the following Equation 6.1:

$$E_i = m_{air} \times C_i \times R_i \qquad [6.1]$$

E_i is the emission of i^{th} gas from pre-purification process (kg/hr);

m_{air} is the mass flow rate of air intake by ASU (kg/hr);

C_i is the i^{th} gas concentration in air;

R_i is the removal rate of i^{th} gas by pre-purification process.

Adsorbent Consumption by Temperature-swing Adsorption Process and Natural Gas Consumption by Adsorbent Regeneration

The adsorbent consumption by TSA, energy consumption by adsorbent regeneration, and energy consumption related emissions caused by natural gas combustion are calculated by the same method described in Section 7.2.3.3, 7.2.3.4 and 7.2.3.5.

Cooling Water Requirement

The cooling water used by direct contact after-cooler can be calculated by the same method described in Section 7.3.2.2. In this case, the outlet pressure of compressed air is 550 kPa (65 psig).

6.2.2.2 Electricity Requirement of the ASU

The power required to operate an ASU unit can be divided into three, including: air compression, refrigeration, and auxiliary and control system. Figure 6.4 illustrates the power required by an ASU is strongly affected by the oxygen purity of the product stream (McKetta, 1990).

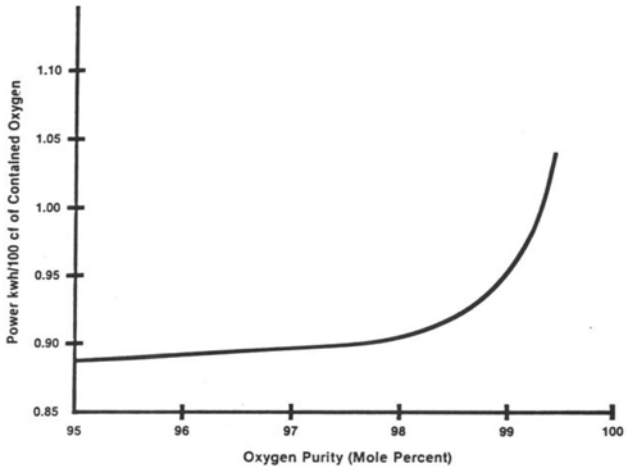

Figure 6.4: The effect of oxygen purity on ASU power consumption.

In this research, the electricity requirement for the ASU is calculated by following equations (Rubin, 2007):

$$E_{ASU} = 0.00172\eta_{ox} + 0.1498 \qquad \eta_{ox} < 97.5 \qquad [6.2]$$

$$E_{ASU} = \frac{0.0260}{(100 - \eta_{ox})^{1.316}} + 0.31 \qquad \eta_{ox} > 97.5 \qquad [6.3]$$

where,

E_{ASU} is the ASU energy requirement (kW/m^3 oxygen produced);

η_{ox} is the oxygen purity.

In Equations 6.2 and 6.3, the oxygen product exits at 115 kPa (16.7 psi). If higher pressure is required, the oxygen product is needed to feed through oxygen compressors. The energy consumption for the compressors is given below in Equation 6.4 (Göttlicher, 2004):

$$E_c = mRTLn\left(\frac{P_o}{P_i}\right)\times\frac{1}{\eta_{comp}} \qquad \textbf{[}6.4\textbf{]}$$

where,

E_c is the energy consumption (kJ);

R is the gas constant, 0.2598 for Oxygen;

m is the mass flow rate of oxygen (kg/s);

T is the temperature (^oC);

P_i is the inlet oxygen pressure (Pa);

P_o is the outlet oxygen pressure (Pa);

η_{comp} is the efficiency of the compressor with a typical value of 0.75;

6.2.2.3 Emissions from Refrigeration

The air separation unit requires refrigeration equipment to cool the incoming air. In principle, the refrigeration cycle used in the ASU is similar to those used in industrial refrigeration. F-gas (HFCs and PFCs) and chlorinated solvents are used as cooling liquids and as solvents. They are volatile compounds and without proper control part of them may disappear as emissions to the atmosphere. Halocarbons can cause potential environment impacts, such as destroying the ozone layer. At present, NH_3 and HCFC-22 are dominant refrigerants used in industrial refrigeration and, NH_3 and CO_2 are increasingly used. In industrial refrigeration, the annual refrigerant emission rate is 17% of banked system refrigeration charge (Neksa, 2004). The typical F-gas charge size for industrial refrigeration ranges from 4,000 to 6,000 kg. This research assumed that the F-gas charge size for refrigerant for the ASU is 6,000kg and the annual refrigerant emission rate is 17%.

6.2.2.4 Distillation and Oxygen Products

Ambient air contains 0.93% argon by volume. Argon has a boiling point of -186 ^{o}C (-303°F), which is much closer to the boiling point of oxygen than nitrogen, and the argon in air will preferentially stay with the oxygen through the main distillation column. If high purity oxygen is required, more distillation stages are used to separate argon from oxygen. An earlier study (Andersson and Johnsson, 2006) reports that 95% oxygen purity is the optimum rate. This implies that the removal of argon is not required, because with the naturally-occurring ratio of argon in air (0.93%), oxygen production will have about 4.4% of argon (by volume) or 5.5% by weight. This research assumes that the oxygen product contains 95% oxygen, 4.4% argon and 0.6% nitrogen by volume.

6.2.2.5 Other Chemical Requirements

There are no major on-going chemical requirements, as follows:

- Cooling water is supplied by water treatment plant, thus major treatment chemicals are part of this plant.
- With a small closed loop cooling system, some minor treatment chemicals are required.
- Minor consumable items such as analyzer zero span and fuel gas cylinders, lube oil top-up are required.
- Pre-purifier adsorbent is typically not replaced.

Since the chemicals requirement of the ASU unit is minimum, the chemicals consumed are not included in the ASU LCI model developed in this research.

6.3 Life Cycle Inventory Modelling of Oxy-fuel Combustion Process

The schematic of a flue gas recycled coal oxy-fuel combustion process LCI model is presented in Figure 6.5. The oxy-fuel combustion LCI model quantifies mass flows such as coal, CO_2, O_2, N_2 and H_2O using stoichiometric reactions; calculates SOx, NOx CO, N_2O and unburned carbon emissions using data from the literature; estimates emissions of PM_{10} and trace metals using modified USEPA AP-42 emission factors; generates emissions of HCl, HF, CH_4 and PM from USEPA AP-42 emission factors; and finally computes energy consumption and heat (steam) output by engineering calculations.

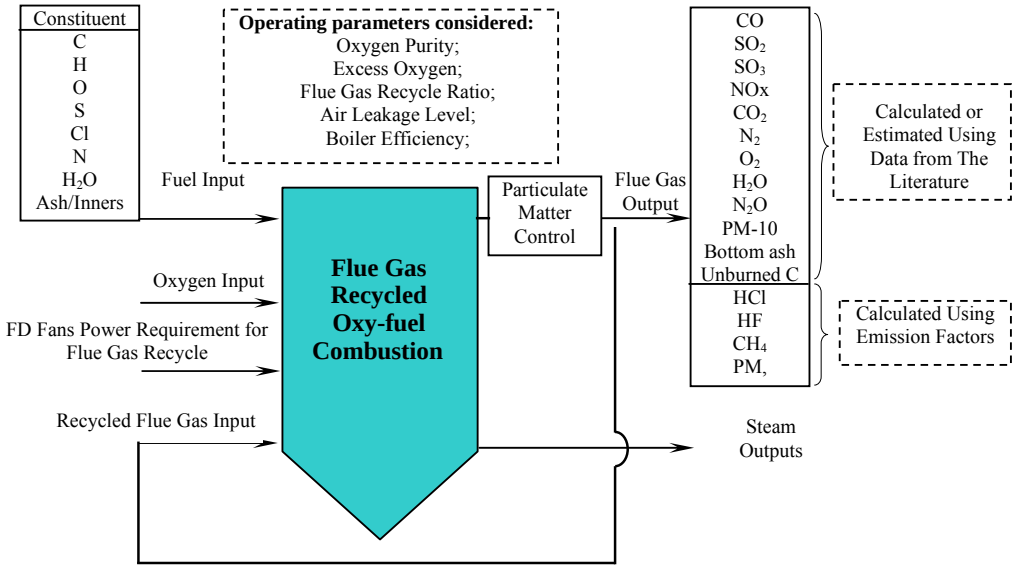

Figure 6.5: The schematic of flue gas recycled oxy-fuel combustion process LCI model.

6.3.1 Operating Parameters

Oxygen Purity

An oxygen purity of 95% is reported as an optimum level in many studies, since the energy penalty of ASU increases sharply with higher oxygen purity and 95% level gives an exchange rate (oxygen to oxygen) of nearly 1.0 without nitrogen in the product gas, but with nearly 5% argon content (Andersson and Johnsson, 2006). In this research, 95% has been used as a default value in oxygen combustion process modelling, and argon is the main impurity in the oxygen product, with some traces of nitrogen.

Excess Oxygen

In order to complete the combustion of the fuel and to avoid the formation of CO, excess oxygen is needed. In conventional coal combustion, the excess air rate is 15-20%, which is equivalent to 3-4% excess oxygen. The excess oxygen ratio falls into the range 1.5-5% in majority of the previous studies. A default value of 3% is used in this research.

Flue Gas Recycle Ratio

To attain an adiabatic flame temperature (AFT) that is similar to that for coal combustion in air, a fraction of total flue gas generated in oxy-fuel combustion is recycled back into the boiler to control the combustion temperature and to make up for

the volume of missing N_2 to ensure there is enough gas to carry the heat through the boiler (Buhre *et al.,* 2005). The flue gas recycle ratio (FGRR) values are in the range of 60-85% and a typical FGRR rate is 70% because oxy-fuel combustion with 70% flue gas recycle can have a similar AFT with that of coal combustion in air (Wall, 2007). A default value of 70% was selected for FGRR in this research.

Air Leakage Level

Ideally, the oxy-fuel system uses only pure oxygen for combustion. However, in practice, it may be impossible to seal the boiler and flue gas ductwork completely to avoid air ingress, which causes air leakage into the boiler. Air leakage values in the range of 1-5% have been assumed by various studies (Rao *et al.,* 2007). In this research, it is assumed that oxy-fuel systems are better sealed and the default value for air leakage is taken as 2% of the theoretical (stoichiometric) oxygen.

Boiler Efficiency

For O_2/CO_2 recycle combustion boiler, there is no bulk nitrogen in the flue gas, which means that the heat losses with the flue gas from the boiler can be significantly reduced and boiler efficiencies are improved (Jordal, 2004). Based on previous studies, this research assumes that the boiler efficiency improves from about 90% (in air combustion) to about 94% in the case of an oxy-fuel combustion system.

6.3.2 Mass Flow Rate of Coal

The mass flow rate of coal (M_{coal}) is calculated as:

$$M_{coal}=\text{Designed power output} /(LHV\times \eta_{plant}) \quad [6.5]$$

where

LHV is the low heating value of coal, and

η_{plant} is the plant gross efficiency (LHV basis).

Designed power output, LHV and η_{plant} are variables representing the plant configuration, coal characteristics and plant operating conditions.

6.3.3 The Heat Output of a Boiler

The heat output of a boiler (H) is:

$$H= M_{coal}\times LHV\times \eta_{boiler} \quad [6.6]$$

where:

η_{boiler} is the boiler efficiency (η_{boiler} = total heat added to the working fluid/total fuel input energy), which is assumed to be around 94%.

6.3.4 Mass Flow of Oxygen

The mass flow of oxygen (M_{oxygen}) needed for coal combustion is calculated using stoichiometric reactions.

$$M_{oxygen} = (\frac{C(1-u)}{12} + \frac{H}{4} - \frac{O}{32} + \frac{S}{38}) \times M_{coal} \times 32 \times (1+\theta) \quad [6.7]$$

where

H, O, S and C are the decimal weights of these elements in coal. u and θ are the rate of unburned carbon and rate of excess oxygen respectively. For oxy-fuel combustion u is 0.386% (Liu *et al.*, 2005).

6.3.5 Products of Combustion

6.3.5.1 Carbon Dioxide, Water, Oxygen and Unburned Carbon

Post combustion outputs of CO_2, H_2O, O_2 and N_2 are calculated using the following equations:

$$M_{CO2} = M_{coal} \times C \times (1-u) \times (44/12) \quad [6.8]$$

$$M_{H2O} = M_{coal} \times H \times 18/2 + Moisture \quad [6.9]$$

$$M_{outO2} = (\theta+\beta) \times M_{oxygen} \quad [6.10]$$

$$\text{Unburned carbon} = M_{coal} \times u \quad [6.11]$$

where

u is the rate of unburned carbon with a default value of 0.386%,

θ is ratio of excess oxygen with default value 3%,

β is air leakage ratio with default value of 2%.

6.3.5.2 Sulphur Oxides Emissions

Sulphur oxides (SOx) emissions depend on sulphur content in coal and the conversion of sulphur into SO_2 is independent of the oxygen concentration (Liu *et al.*, 2006; Croiset

and Thambimuthu, 2001). However, the type of environment (air, or oxy-fuel recycle) has some impact on the conversion and can decrease the SO_2 emissions (up to 40%) compared to that in air combustion, due to increased sulphur retention on ash deposits and on the cool surface of the flue gas cooler during flue gas recycle (Tan, 2006). The conversion rate of coal sulphur to SO_2 for air combustion and oxy-fuel combustion ranges from 71-100% and 37-100% respectively (see Table 6.5).

Table 6.5: Summary of SO_2 emission results (Adapted from Nsakala, 2007 and Tan*, et al*., 2005).

Author(s)	Conversion (%)		Experimental Conditions
	Air Combustion	Oxy-fuel combustion	
Yamada (2007)	70-80	45-50	Experimental results using 3 different bituminous coals with 0.24 – 0.88% sulphur.
Andersson (2007)	510 (mg/MJ)	199 (mg/MJ)	Use lignite to evaluate the combustion fundamentals of lignite fired flames in air and various O_2/CO_2 environments.
Woycenko *et al*. 1994	96	60 – 75	Experimental results using Göttelborn coal with 1.02% sulphur.
Kiga *et al*. (1997)	70 – 78	37 – 41	Experimental results using 3 different bituminous coals with 0.38 – 0.96% sulphur.
Hu *et al*. (2000)	6 – 12*	5 – 12*	20 – 100% O_2 mixed with N_2 or CO_2 at temperature of 1123 – 1573 K and equivalence ratios 0.4 – 1.4.
Croiset and Thambimuthu, (2001)	91	56 – 66	Experimental results using US eastern bituminous coal with 0.96% sulphur; 28 – 42% oxygen in O_2/RFG mixture using oxygen feed of 90 – 100% purity.
Zheng and Furimsky (2003)	91 – 100	90 – 100	Computations based on chemical equilibrium.

* In mg SO_2 (as S) per g coal

In conventional pulverized coal fired systems the conversion of SO_2 to SO_3 usually ranges from 1 to 5% depending on the sulphur content of the coal, the air/fuel mixing patterns and the excess O_2 conditions in the furnace. For oxy-fuel combustions, Tan *et al.* (2006) has shown that SO_2 to SO_3 conversion level is consistently around 5% for bituminous coals, but less than 2% for sub-bituminous coals. Tan *et al.* (2006) also revealed that less than 2% of the input sulphur from the bituminous coals appeared in the ash deposits given the low alkali and alkaline earth content of the bituminous coal ash. On the other hand, for low sulphur content sub-bituminous coals, nearly 14% of the input sulphur is retained in the ash deposits.

It is worth noting that flue gas recycled without removal of SO_2 would lead to a significant accumulation of SO_2 and consequently, increased SO_3 in the recycled stream, with serious implications for the corrosion of the boiler systems.

Based on the analysis above, this research assumed that, for oxy-fuel combustion, the conversion factor of coal sulphur to SO_2 is 0.6, and the conversion rates of SO_2 to SO_3 are 5% and 2% for bituminous coals and sub-bituminous coals respectively. The rest of

sulphur in coal turns to fly ash and bottom ash in equal proportions. The emissions of SO_2, SO_3, S in bottom ash and S in flue gas can be calculated by the following equations:

$$M_{SO2}=0.6\times M_{coal}\times S\times (64/32) \quad [6.12]$$

$$M_{SO3}=\alpha\times M_{coal}\times S\times (80/32) \quad [6.13]$$

$$M_{S\ to\ bottom\ ash}= 0.5\times(1-0.6-\alpha)\times M_{coal}\times S\times (64/32) \quad [6.14]$$

$$M_{S\ to\ fly\ ash}=0.5\times(1-0.6-\alpha)\times M_{coal}\times S\times (64/32) \quad [6.15]$$

Where S represents the decimal weight of sulphur in coal, α represents the conversion ratio of SO_2 to SO_3, α is 5% when bituminous coals are used and 2% when sub-bituminous coals are used respectively.

6.3.5.3 Nitrogen Oxides Emissions

During oxy-fuel combustion the amount of NOx emissions can be reduced considerably through several mechanisms: decrease of thermal NOx due to the very low concentration of N_2 from air in the combustor; the reduction of recycled NOx as it is reburnt in the volatile matter release region of the flame; the reaction between recycled NOx and char. Recycled NOx is the dominant mechanism for the reduction in NOx emissions (Okazaki *et al.*, 1997). A summary of NOx emissions reported in previous studies is listed in Table 6.6.

Based on the results provided in Table 6.6 and the analysis above, it is assumed that the conversion ratio of coal-nitrogen to NOx for the typical oxy-fuel combustion (30% O_2/70% CO_2) is 15%, which is 50% of the conversion ratio of coal-nitrogen to NOx in the case of air combustion. The proportion of NO to NO_2 is assumed as 95:5, which is NO to NO_2 rate used in coal air combustion process. The remaining coal-nitrogen converts to N_2 during combustion. Therefore, the NOx emissions are calculated from the following equations:

$$M_{NO} = 15\%\times 95\%\times (30/14)\times M_{coal}\times N \quad [6.16]$$

$$M_{NO2} = 15\%\times 5\%\times (46/14)\times M_{coal}\times N \quad [6.17]$$

where, N is the decimal weight of nitrogen in coal.

Table 6.6: Summary of NOx emissions reported in the literature (After Nsakala, 2007 and Tan *et al*., 2005)

Author(s)	Emission (mg/MJ)	Conversion Ratio	Conclusion
Yamada (2007)	Air:220-410 RFG (27%O_2): 80-120	Air: 20-22 RFG (27%O_2): 9-10	NOx emissions under oxygen firing are 60-70% lower than during air firing of the bituminous coal
Andersson (2007)	Air: 233 RFG (25% O_2): 56 RFG (25% O_2): 65	----	SOx emission rates [mg/MJ] significantly lower than that of air combustion, less than 30% of air combustion
Nsakala *et al*. (2007)	Air: 43-52 g/GJ RFG (30% O_2): 6-12 g/GJ	---	NOx emissions under oxygen firing were consistently more than 60% lower than during air firing of the bituminous coal
Liu (2005)	---	Air: 27.6% RFG (30% O_2): 22.6% RFG (30% O_2 with oxidant staging): 7.5%	Compared with coal combustion in air, oxy-fuel combustion produces less nitric oxides. Air/oxidant staging is a very effective method in reducing NOx emissions for both coal combustion in air and oxy-fuel combustion.
Croiset and Thambimuthu (2001)	Air: 340 RFG (28% O_2): 100 RFG (42% O_2): 210	Air: 35%[1] RFG (28% O_2): 10% RFG(42% O_2): 22%	High NOx concentration inside the furnace but lower NOx emissions in flue gas than baseline case
Chui *et a*l. (2003)	Air: 110 RFG: 140 – 150	Air: 14% RFG: 18 –19%	NOx production strongly dependent on swirl number. RFG mode can produce the same or even higher amount of NOx within the combustor than in baseline case. The observed reduction of NOx in exhaust gas is due primarily to the fraction of NOx removed with the recycle stream.
Kiga *et a*l. (1997)	Air: 75 – 370 RFG: <53	Air: 7 – 35% RFG: <5%	The conversion ratio of fuel nitrogen into NOx is much higher in baseline case than with oxy-coal FRG combustion.
Nozsaki *et a*l. (1997)	---	---	The recycled NOx is rapidly reduced to HCN or NH3 in the combustion zone and NOx formation for O_2/CO_2 combustion is lower than for air combustion.
Kimura *et al.* (1995)	Air: 340 RFG: <90	Air: 30 – 33% RFG: <8%	NOx conversion ratio in O_2/CO_2 combustion is very much lower than that in normal air combustion because of the higher reduction in the combustion zone.
Hu *et al*. (2000)	---	Air: 28%2 Oxy-coal: 14%	NOx emission is strongly dependent on the O_2 concentration. Peak value of NOx emission in air combustion is double the value in O_2+CO_2 combustion.
Woycenko *et al*. (1994)	Air: 320 RFG: 50 – 150	Air: 30%3 RFG: 5 – 14%	NOx formation is much lower in oxy-coal with RFG combustion than in baseline case.
Zheng and Furimsky (2003)	---	Air: RFG: up to 2%	NOx formation in O_2/CO_2 atmosphere predicted to be reduced by a factor of at least 15 relative to air combustion based on chemical equilibrium calculations.
Liu and Okazaki (2003)	---	Air: 30% ARFG: 4 – 8%	Very high flue gas recycle ratios are possible through heat recirculation. Stable flames at 15% O_2 allows reduction in fuel-N conversion by a factor of 7.
Chatel-Pelage *et al*. (2003)	Air: 120 – 190 RFG: 35 – 90	---	1.5 MAW Pilot-scale demonstration of potential for drastic NOx reduction.

1 Conversion made using coal HHV.
2 Both values are at 1,273K temperature and at the stoichiometric point. The oxy-coal value is with 80% CO_2 in inlet gas.
3 Conversion made using coal LCV

It should be noted that the above discussions on the reduction of NOx emission refer to the emission amount, e.g. mass per unit energy produced from coal or mass per kg of coal fed. The emission concentration of NO_2 (in ppm) may be higher compared to air combustion due to the recycle of NO_2 in the recycled flue gas and the smaller amount of flue gas produced in oxy-fuel combustion.

6.3.5.4 Carbon Monoxide Emissions

Carbon monoxide emissions depend strongly on fuel type and on furnace temperature. Generally, increasing the oxygen concentration decreases the CO emission (Chui, 2003). Liu (2005) concluded that oxy-fuel combustion with $30\%O_2/70\%CO_2$ mixture emits less CO, around 68% of coal combustion in air and, for oxy-fuel combustion with $21\%O_2/79\%CO_2$ mixture, the CO emission is around 4 times higher than that for coal combustion in air.

Based on the literature analysed above, the CO emission factor for oxy-fuel combustion is calculated from:

$$\text{CO emission factor for oxy-fuel combustion} = \gamma \times \text{CO emission factor of air combustion} \quad [6.18]$$

where:
γ represents the corrected coefficient. γ is 68% when coal combustion is with$30\%O_2/70\%CO_2$ and γ is 4 when coal combustion with $21\%O_2/70\%CO_2$. The USEPA AP-42 CO emission factor is employed as CO emission factor for coal combustion in air.

It is worth noting that some researchers have reported conflicting results, for instance, Nsakala *et al*. (2007) conclude that CO emissions during oxygen firing with $30\%O_2/70\%CO_2$ were 25 to 45% higher than that of air firing of the bituminous coals, because high CO_2 partial pressure (i.e., the reaction $CO + O_2 \rightarrow CO_2$) is suppressed. These conflicting results confirm that CO emissions are combustion conditions dependent.

6.3.5.5 Nitrous Oxide Emissions

Emissions of N_2O are strongly dependent on temperature. Pulverized coal furnaces usually generate less than 4 g/GJ (10 ppmv) N_2O (Nsakala *et al*., 2007). Nitrous oxide (N_2O) is a greenhouse gas, which is currently not regulated. Although N_2O is released

in much smaller quantities than CO_2, it is a more potent greenhouse gas, because N_2O has roughly 300 times the global warming potential (GWP) of an equal mass of CO_2. Previous studies have investigated N_2O emissions in oxy-fuel combustion and conclude that oxy-fuel combustion has lower N_2O emissions, about 2-30% of that emitted by air combustion (Nsakala *et al*., 2007). In order to calculate the N_2O emission in the LCI model, this research assumed that N_2O emission is 15% of that in the case of air combustion.

6.3.5.6 Unburned Carbon in Ash

Oxy-fuel combustion has higher carbon burnout efficiency than coal combustion in air. Previous research carried out by Liu (2005) concluded that, in oxy-fuel combustion, carbon in ash decreases to 38.6% of that for coal combustion in air. Yamada (2007) concluded that the carbon in ash in oxy-fuel combustion is 30-40% lower than that in air combustion. For coal combustion in air, unburned carbon is typically 1%, therefore, this research assumes that for oxy-fuel combustion the unburned carbon is 0.4%.

6.3.5.7 Particulate Matter Emissions

During oxy-fuel combustion, the oxygen concentration in the gas passing through the burner is changed (typically around 30% by volume). This changes coal particle combustion temperature and consequently affects the associated vaporization of metals and minerals in coal particles. Thus, this may affect the formation of ash.

Previous research has shown that the change in combustion conditions (i.e., replacing N_2 with CO_2) does not alter particle formation mechanisms, but rather the rates at which they take place (Sheng *et al*., 2007b). The results of previous studies also indicate that at the same temperature and oxygen concentration the ashes generated from O_2/CO_2 combustion and O_2/N_2 combustion show no significant difference in the size distribution, see Figure 6.6 (Sheng *et al*., 2007b; Wall *et al*., 2006).

However, the oxy-fuel combustion can affect the formation of submicron ash (Sheng, *et al*., 2007; Suriyawong, 2006; Krishnamoorthy and Veranth, 2003). Results from these previous studies indicate that mean particle size and total particle volume of submicron ash increase as the O_2/CO_2 mixing ratio increases during combustion and the total submicron particle volume increases drastically when the mixing ratio of O_2/CO_2 is greater than 2:3. The total volume of submicron ash generated during combustion in 20% O_2/80% CO_2 or 40% O_2/60% CO_2 is 68% or 205% of that of air combustion

(Suriyawong, 2006). The results are attributed to the change in the temperature in the vicinity of the burning particle, because the change in the particle combustion temperature changes the associated vaporization of elements (metals and minerals inherent in coal particles) and the formation of sub micrometer-sized ash (Wall, 2007; Suriyawong, 2006).

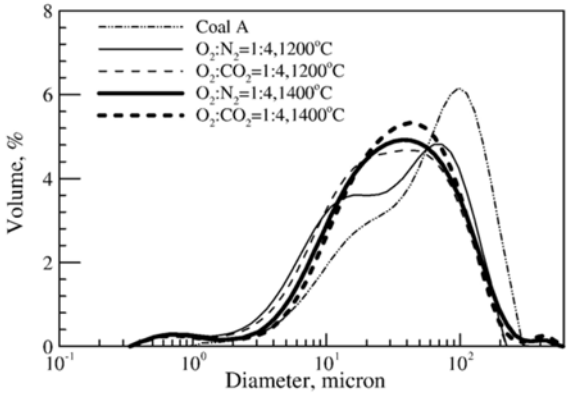

Figure 6.6: Volumetric particle size distribution of the residue ashes (After Sheng *et al*., 2007b)

Since a typical oxy-fuel combustion with 30%O_2/70CO_2 mixture has a similar adiabatic flame temperature (AFT) to that of air combustion, US EPA PM emission factors for air combustion are used for the calculation of PM emissions and PM_{10} emissions for typical oxy-fuel combustion in this research. For oxy-fuel combustion with 20% O_2/80CO_2 or 40% O_2/60CO_2 mixtures, corrected emission factors are used for PM_{10} emissions, as follows:

Corrected PM_{10} emission factor = γ x air combustion PM_{10} emission factor

where: γ represents the corrected coefficient. If O_2/CO_2 mixture is 20%/80%, γ is taken as 68%; if O_2/CO_2 mixture is 40%/60%, γ is taken as 205% (Suriyawong, 2006).

6.3.5.8 Trace Metals in Flue Gas

Since trace metals are enriched in submicron fly ash, the effect of oxy-fuel combustion on submicron fly ash formation may affect the trace metal emissions. However, few researchers have investigated the emission of trace metals during oxy-fuel combustion. Zheng and Furimsky (2003) concluded that the combustion medium had little effect on the amount and type of the Hg-, Cd-, As-, and Se-containing emissions in the vapour phase.

In this research, USEPA suggested trace element emission factors for coal air combustion as presented in Table 5.3 are used for the calculation of trace metal emissions from a typical oxy-fuel combustion with O_2 concentration at 30%, which has the similar adiabatic flame temperature as in coal air combustion. For oxy-fuel combustion with 20% and 40% O_2 concentration, corrected emission factors are used, as follows:

$$\text{Corrected trace element emission factor} = \gamma \times \text{air combustion trace element emission factor} \quad [6.19]$$

where: γ represents the corrected coefficient; if O_2/CO_2 is 20%, γ is 68%; if FGRR is 40%, then γ is 205% (Suriyawong, 2006),

6.3.5.9 Other emissions

It is not clear if emission characteristics of HCl, HF, CH_4 and TOC in oxy-fuel combustion differ significantly from air combustion. This research assumes that these emissions do not change significantly and the USEPA AP 42 emission factors are used to calculate these emissions.

6.3.6 Flue Gas Recirculation Fan Power Requirement

Flue gas recirculation (FGR) fan is used to provide the pressure head for the recycled flue gas stream going back to the boiler. The FGR fan pressure head, along with the recycled flue gas flow rate, determine the energy used by the FGR fan. The typical value for this pressure head is 96.53 kPa (Rubin *et al.*, 2007). Power requirement can be calculated using the same equation suggested in the air combustion Section 5.2.2.7.

6.3.7 Flue Gas Cooling Water Requirement

The cooling water requirement, determined by the flue gas flow rate and the desired temperature difference, is calculated by the following equation (Rubin *et al.*, 2007):

$$M_{cooling} = 7.94 \times 10^{-4} \times V_{fg} \times \Delta T \quad [6.20]$$

where $M_{cooling}$ is the cooling water requirement (m^3/min);V_{fg} is the flue gas flow rate (actual m^3/ min) at 37.78 ^oC and ΔT is the desired temperature difference (^oC), typical value of which is 6.67 ^oC after the flue gas passes through the air preheat unit (APH).

6.4 Life Cycle Inventory Modelling of Carbon Dioxide Conditioning for Oxy-fuel Combustion

6.4.1 Introduction of Carbon Dioxide Conditioning

After CO_2 is captured, the CO_2-rich gas enters into the CO_2 conditioning unit, where it is cleaned, dehydrated and compressed before entering the transport system. The design of CO_2 conditioning unit is influenced by several factors (Anheden *et al*., 2005):

- Fuel type (natural gas, low-sulphur coal, high-sulphur coal, etc.), CO_2 capture methods and flue gas treatment influences the composition of the CO_2-rich stream. For instance, CO_2 product from oxyfuel combustion systems may contain impurities of O_2, SO_2, and NO. CO_2 product from pre-combustion systems may contain impurities of H_2, CO and H_2S.

- Specification of the final CO_2 stream. This depends on several factors such as final use (pure storage/EOR/ECBM/EGR), transport conditions and material, safety requirements (which may depend on population density and vary from one country to another). For instance, if the CO_2 product is used for EOR, it requires stringent specification of the O_2, SO_2, H_2S content in the CO_2 product stream. Pipeline transportation requires low H_2O content if SO_2 and/or O_2 present. Furthermore, pipeline networks may be affected by the interaction of impurities from different CO_2 sources (e.g. O_2, SO_2, and NO from oxyfuel combustion systems; H_2 CO, and H_2S from pre-combustion systems). In the case of CO_2 for saline aquifer storage, the impact of impurities on the injection well integrity and geological storage formation is also an issue of concern. Typical specifications of CO_2 products are listed in Table 6.7.

Table 6.7: Final CO_2 product stream specification (pipleline transportation) (After Xu *et al*., 2007, Panesar *et al*., 2007)

CO_2 product stream	*Sub-bituminous coal fuel*	*Bituminous coal fuel*		*Lignite fuel*
	EOR	Coalbed Methane	Saline Aquifer	EOR
CO_2	≥95%	≥95%	≥90%	≥95%
N_2	≤4%	≤4%	≤4%	≤4%
Hydrocarbons	≤5%	≤5%	≤5%	≤5%
H_2O	50 ppm	50 ppm	500 ppm	50 ppm
O_2	≤100 ppm	≤100 ppm	≤100 ppm	≤100 ppm
CO	≤0.1%	≤0.1%	≤0.1%	≤0.1%
H_2S	≤50 ppm	≤50 ppm	≤1.5%	≤50 ppm
Glycol	0.174 $m^3/10^6$ m^3	0.174 $m^3/10^6$ m^3	0.174 $m^3/10^6$ m^3	0.174 $m^3/10^6$ m^3
Temperature	≤50°C	≤50°C	≤50°C	≤50°C
Pressure	13.8MPa	13.8MPa	13.8MPa	13.8MPa

- Transport type (pipeline at 13.8 MPa and ambient temperature and vessel at 2 MPa with a temperature of -20°C) influences the choice of process (liquefaction/ compression).

Heggum *et al*. (2005) demonstrated that the captured CO_2 may contain up to 5% CH_4, 5% N_2, 0.5% water, 100 ppm H_2S and an unknown amount of amines. Generally, the CO_2-rich gas captured from different fossil fuel conversion and alternative capture routes can be divided into three categories (Aspelund and Jordal, 2007):

i) CO_2-rich gases containing only CO_2 and water (possibly traces of amines and minor fraction of inert gases from the fuel). These types of CO_2-rich gases are produced from CO_2 capture processes including pre- and post-combustion using amines. The small fraction of nitrogen comes from the fuel;
ii) CO_2-rich gases containing CO_2, water and non-combustible volatiles. This is the typical result of an oxy-fuel combustion capture with a cryogenic air separation unit (ASU) for the separation of oxygen from air;
iii) CO_2-rich gases containing CO_2, water, and both inert and combustible volatiles. These type of CO_2-rich gases are produced from pre-combustion CO_2 capture with H_2 or CO_2 separating membrane or sorption enhanced reactors.

The CO_2 conditioning units for post-combustion or oxy-fuel combustion capture are different in many aspects. This research distinguishes the CO_2 conditioning unit for the oxy-fuel combustion capture from the CO_2 conditioning unit for post-combustion capture and models these two units separately.

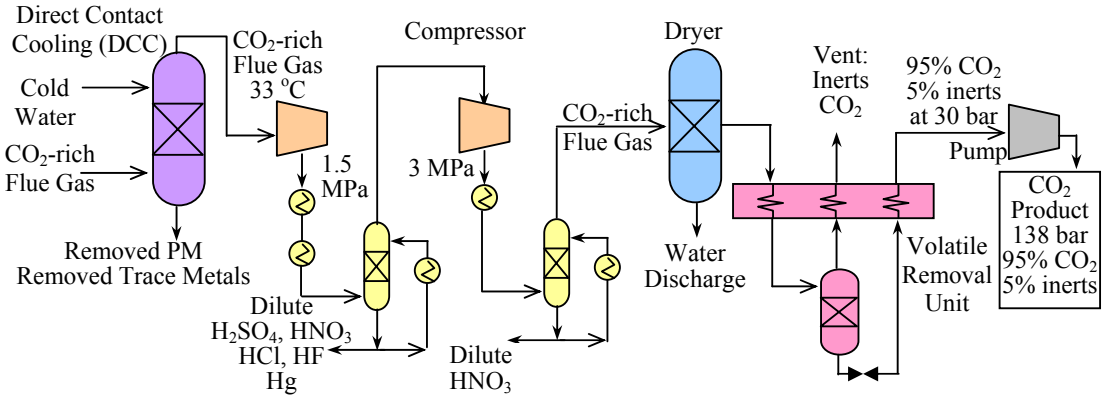

Figure 6.7: The schematic of a CO_2 conditioning unit for oxy-fuel combustion capture.

A schematic of a CO_2 conditioning unit for oxy-fuel combustion capture is illustrated in Figure 6.7. After the CO_2-rich flue gases leave the heat recovery system of the oxy-fuel power plant at approximately 65-75°C, the CO_2-rich flue gas is passed through a direct contact cooler (DCC) to remove the moisture by condensation. The flue gas leaves the top of the DCC column at approximately 33°C and the liquid water stream and ash are removed from the bottom of the DCC at approximately 43°C (Aspelunda and Jordal, 2007). After passing through the DCC unit the CO_2-rich flue gas is compressed to 3 MPa in a two-stage compressor, where SOx and NOx removal columns are installed with compressor cooling water system. If there is efficient holdup in the SOx and NOx removal column, the SOx, NOx and mercury may be totally removed depending on the amount of SOx and NOx in the flue gas (White, 2008). The flue gas is then delivered to a temperature swing dual-bed adsorption dryer, where CO_2 is dried to required level. The dried CO_2-rich flue gas is fed to the "Volatile Removal System" (the cold box) and is cooled to -55^{o}C. The cooled feed stream is partially liquefied and distilled to remove impurities such as Ar, N_2 and O_2 in order to meet the CO_2 product specification. The CO_2 product is then compressed to the required pressure (typically 13.8 MPa) for pipeline transmission. The removed impurities are vented to the atmosphere.

6.4.2 The Life Cycle Inventory Model of Carbon Dioxide Conditioning Unit for Oxy-fuel Combustion Capture

The LCI model of the CO_2 conditioning unit for oxy-fuel combustion quantifies the energy input for the compressor, heat input for the drier, adsorbent consumption of the drier, and cooling water consumption using engineering calculations. The model also calculates the removal rate of SOx, NOx, HCl, HF, PM, trace metals, the purity of the CO_2 product and the components of vented gas. A schematic of the LCI model is shown in Figure 6.8.

6.4.2.1 The Sulphur Oxides, Nitrogen Oxides and Mercury Removal Rate

Due to the presence of water and oxygen in the CO_2-rich flue gas from oxy-fuel combustion, the $SO_2$and NO_2 can be removed in the SOx and NOx removal column during the CO_2 compression process, where SO_2 is converted to Sulphuric Acid and NO_2 is converted to Nitric Acid (Xu *et al*., 2007; White, 2008). The reactions involved are described as follows (White, 2008):

$NO + ½\ O_2 = NO_2$	Slow
$2\ NO_2 = N_2O_4$	Fast

$2\ NO_2 + H_2O = HNO_2 + HNO_3$	Slow
$3\ HNO_2 = HNO_3 + 2NO + H_2O$	Fast
$NO_2 + SO_2 = NO + SO_3$	Fast
$SO_3 + H_2O = H_2SO_4$	Fast

NO acts as a catalyst (NO is oxidised to NO_2 and then NO_2 oxidises SO_2 to SO_3) and no Nitric Acid is formed until all the SO_2 is converted (White, 2008). With well designed pressure, reactor and residence times, full SOx removal can be achieved and NOx removal can reach 90-99% (White, 2008; Anheden, 2008). Hg in flue gas can be removed by reacting with the nitric acid formed from the reactions above. The products of these reactions can be removed together with discharged water. In this research, it was assumed that removal rates of SOx, NOx and Hg are 100%, 95% and 100% respectively during CO_2 compression process.

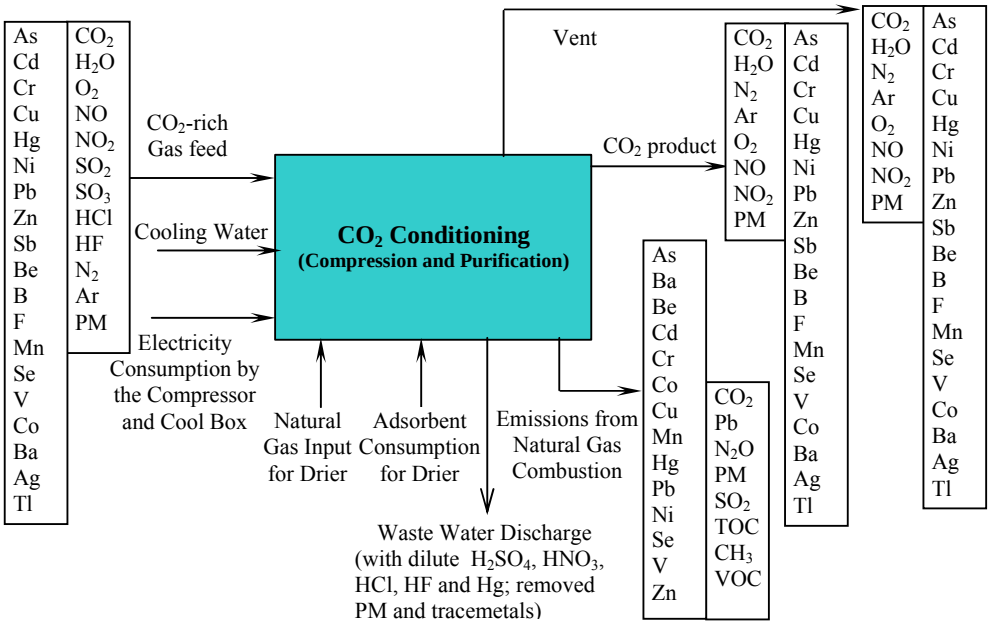

Figure 6.8: A schematic of the LCI model for the CO_2 conditioning unit in oxy-fuel combustion capture.

6.4.2.2 The Hydrogen Chloride and Hydrogen Fluoride Removal Rate in the Liquid-vapour Separator Drum

The components with high solubility in water (such as HCl, HF) or components with higher boiling points than CO_2 can be removed together with the water in the liquid-vapour separator drum during the CO_2 compression stage (Aspelunda and Jordal, 2007). This research assumed that HCl and HF are totally removed in the liquid-vapour separator drum.

6.4.2.3 Hydrogen Sulphide Removal Rate

If H_2S is present in flue gases, it can be removed from CO_2 stream by adsorption dehydration process. The H_2S then is recovered during the regeneration of adsorbent and is combusted in air with producing SO_2 and/or SO_3. In this research, it was assumed that 100% of the H_2S is removed from the CO_2 stream by the adsorption dehydration process and the recovered H_2S is combusted.

6.4.2.4 Carbon Dioxide Recovery Rate and other Impurities Removal Rates

The volatiles removal process utilises the principle of phase separation between condensed liquid CO_2 and impure gases (such as N_2, O_2, NO, CO, H_2, CH_4 and Ar) typically at 3MPa and a temperature of –55°C, which is very close to the triple point, or the freezing temperature of CO_2 (Xu *et al*., 2007). A volatile removal unit flow diagram (Figure 6.9) shows that most CO_2 in the inlet flue gas is condensed to liquid and recovered as CO_2 product. A small amount of CO_2 and most of the components with low boiling points (such as N_2, O_2, NO, CO, H_2, CH_4 and Ar) vent to atmosphere as volatile purge stream. The CO_2 recovery rate (or the percentage of CO_2 in the inlet flue gas recoverd as the CO_2 product) depends on temperature, pressure and CO_2 content in the inlet flue gas. Figure 6.9 shows that CO_2 recovery rate varies at different pressures and inlet CO_2 contents at a temperature of -55 ^oC. In this research, the CO_2 recovery rates at different pressures with the temperature of -55 ^oC are calculated by regression Equations 6.21 to 6.24 derived from Figure 6.10. At a temperature of -55 ^oC and 3 MPa pressure, the CO_2 product is liquid, therefore, it can be pumped to the required pressure (typically 13.8 MPa) instead of being compressed for pipeline transportation and the energy requirement of pumping is lower.

$$P= 2MPa: y = 66.847Ln(x) - 206.56 \quad (R^2 = 0.9932) \qquad [6.21]$$

$$P= 3MPa: y = 42.859Ln(x) - 96.515 \quad (R^2 = 0.9915) \qquad [6.22]$$

$$P= 4MPa: y = 32.366Ln(x) - 48.460 \quad (R^2 = 0.9927) \qquad [6.23]$$

$$P= 6MPa: y = 25.844Ln(x) - 18.447 \quad (R^2 = 0.9930) \qquad [6.24]$$

where,

P is the pressure (MPa);

y is the CO_2 recovery rate (%);

x is the CO_2 content in the inlet flue gas (%).

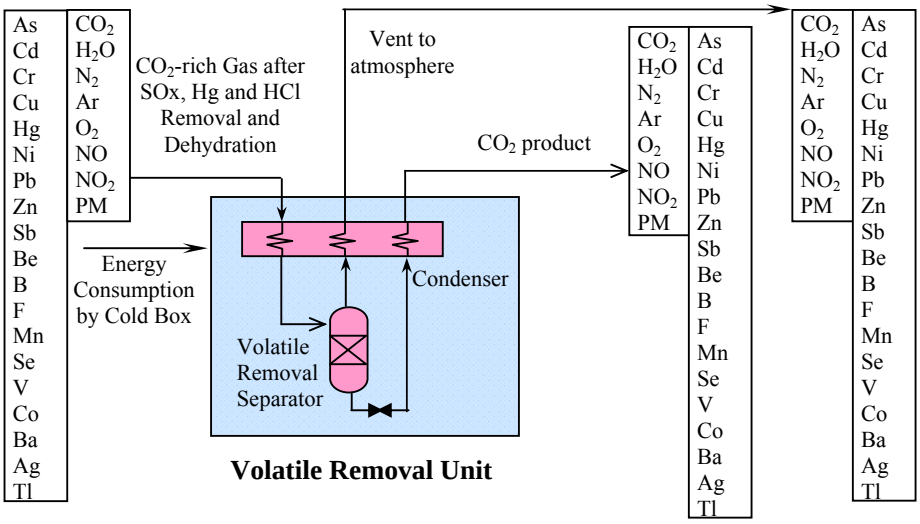

Figure 6.9: Volatile removal unit flow diagram

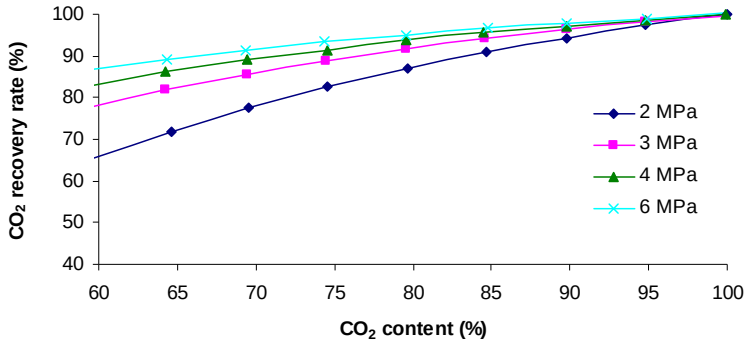

Figure 6.10: The CO_2 recovery rate at various pressures and inlet CO_2 contents (at -55°C) (After Tranier *et al*., 2008)

The purity of recovered CO_2 is determined by pressure; higher pressures give lower purity CO_2 product (White, 2008). This research assumes that the purity of the recovered CO_2 is 95%, since at a typical pressure and temperature (3 MPa and -55°C) of a volatile removal process, recovered CO_2 purity is 95% (White, 2008).

Based on mass balance, the vented CO_2 and vented impurities from the volatile removal unit are calculated by the following equations:

$$V_{CO_2} = m_{CO_2} \cdot (1 - R_{CO_2}) \quad [6.25]$$

$$V_{impurities} = m_{impurity} - (1 - P_{CO_2}) \cdot \frac{m_{CO_2} \cdot R_{CO_2}}{P_{CO_2}} \quad [6.26]$$

$$V_{i,impurity} = m_{i,impurity} \cdot \frac{V_{impurity}}{m_{impurities}} \quad [6.27]$$

where,
V_{CO2} is the mass flow rate of vented CO_2 (kg/hr);

m_{co2} is the mass flow rate of CO_2 fed to the volatile removal unit (kg/hr);

R_{co2} is the rate of CO_2 recovery;

$V_{impurities}$ is the mass flow rate of total impurities vented to the atmosphere (kg/hr);

P_{co2} is the purity of the CO_2 product;

$V_{i,impurity}$ is the mass flow rate of the i^{th} impurity vented to the atmosphere (kg/hr);

$m_{impurity}$ is the mass flow rate of total impurities fed to the volatile removal unit (kg/hr);

6.4.2.5 Impurities not Separated from Carbon Dioxide

Some impurities, including propane (C_3H_8) ethane (C_2H_6) can not easily be separated from the liquid CO_2 product by flushing or simple distillation in the volatile removal system. This research assumes that 100% of these impurities go with liquid CO_2 product to the next processing unit.

6.4.2.6 Particulate Matter and Trace Element Removal Rates

The removal rates of particulate matters and trace elements in direct contact cooling (DCC) is 10%, which is the estimation used for wet scrubbing system in Section 7.2.2.4. The removal rates of particulate matters and trace elements in volatile removal system are 99% and 90% respectively (Spero *et al*., 2008).

6.4.2.6 Emissions from the Cold Box

The emissions from the cold box, which is used in volatile removal system, are calculated by the same methods described in section 6.2.2.3.

6.4.2.7 Energy Consumption

The energy consumed by the compressors, which compress the inlet CO_2-rich flue gas from atmospheric pressure to 3 MPa, can be calculated using Equation 7.20.

The energy consumption by the cool box in the volatile removal system, which changes the CO_2-rich flue gas temperature from 20 ^oC to -55 ^oC, can be estimated by the following equation:

$$E_{cooling} = m_{fluegas} C_p \Delta T_{CO_2} / \eta \qquad [6.28]$$

where,

$E_{cooling}$ is the energy consumption of the cool box (kJ);

$m_{fluegas}$ is the mass flow rate of the flue gas (kg/hr);

C_p is the average specific heat. At 3 MPa, from 25 ^oC to -10 ^oC, the average specific heat is 2.43 kJ/kg ^oC; from -10 ^oC to -55 ^oC, the average specific heat is 3.78 kJ/kg ^oC;

ΔT_{CO2} is the temperature difference (^oC);

η is the efficiency of the cooling system, typically 0.8.

The energy consumption of pumps, which compress the liquid CO_2 product from 3 MPa to 13.8 MPa bar, can be calculated by the following equation:

$$E_p = \frac{m_{CO_2}(P_{out} - P_{in})}{\rho \cdot \eta} \quad [6.29]$$

where,

E_p is the energy consumption of pump (kJ);

m_{CO2} is the CO_2 mass flow rate (kg/hr);

P_{out} is the required outlet pressure (kPa);

P_{in} is the inlet pressure (kPa);

ρ is 1,019 kg/m^3, the average CO_2 density at -10 ^oC with pressure in the range of 3to 13.8 MPa;

η is the efficiency of the pump, typically 0.8.

6.4.2.8 Adsorbent Consumption, Energy Consumption and Emissions by the Dehydration Unit

The adsorbent consumption, energy consumption and emissions by dehydration unit are calculated by the same methods used in Sections 7.2.3.3, 7.2.3.4 and 7.2.3.5.

6.5 Summary

The LCI model developed for oxy-fuel combustion process accounts for its operating parameters including oxygen purity, excess oxygen rate, and flue gas recycle ratio (FGRR). The model quantifies mass flows such as coal, CO_2, O_2, N_2 and H_2O utilising stoichiometric reactions and calculates the emission rates of SOx, NOx CO, N_2O and unburned carbon using data from the literature. The emissions of PM, PM_{10}, trace metals, HCl, HF and CH_4 are calculated using USEPA AP-42 emission factors. The energy consumption and heat (steam) output are computed using engineering calculations.

Oxy-fuel combustion process has lower emission rates of SOx, NOx, and N_2O, compared to air combustion process. Emissions of CO, PM_{10} and trace metals depend on oxygen concentration, and at typical 30% O_2/70% CO_2, emissions of CO is lower and emissions of PM and trace metals are same as that of air combustion. The emission rates of HCl, HF or CH_4 have not been investigated in the past, therefore, it was assumed that they have the same emission rates as the air combustion process. Oxy-fuel combustion process also has lower emissions of unburned carbon as ash.

The air separation unit (ASU) consumes significant amount of energy, which increases dramatically if produced oxygen purity is higher than 97.5%. F-gases are emitted from refrigeration that is used to cool the incoming air in the ASU. Adsorbent and energy are consumed by the temperature-swing adsorption (TSA) unit in the ASU, which dries the incoming air. Cooling water is used by the direct contact after-cooler (DAC) in the ASU. The ASU LCI model quantifies the energy consumption and the F-gas emissions from refrigeration by empirical relationships, and calculates absorbent consumption by the TSA, and cooling water requirement by the DAC using engineering calculations.

The function of CO_2 conditioning unit is to purify and compress the CO_2-rich gases generated. In the oxy-fuel combustion plant, the CO_2-rich gases entering the CO_2 conditioning unit may contain CO_2, water vapour, noble gases (N_2 and Ar), O_2, NO_2, NO, SO_2, SO_3, HCl, HF, CH_4, PM and trace metals. The CO_2 conditioning unit is designed to remove acid gases (including NO_2, NO, SO_2, SO_3, HCl, and HF) and mercury during the compression process and to eliminate other impurities such as N_2, Ar, O_2, CO, and CH_4 by the volatile removal process. Well designed CO_2 conditioning unit could remove 100% of SOx, HCl and HF and 95% of NOx. Depending on the pressure and temperature of the volatile removal process, the CO_2 concentration could reach over 99.5% after CO_2-rich gases pass through the volatile removal unit. The CO_2 conditioning unit uses significant amount of energy for CO_2 compression. The LCI model developed quantifies the energy input of the compressor, heat input of the drier, the adsorbent consumption of the drier, and the cooling water consumption using engineering calculations. The model also calculates the removal rate of SOx, NOx, HCl, HF, PM and trace metals, purity of the CO_2 product and the components of vented gas from the volatile removal unit by empirical relationships.

Chapter 7 Life Cycle Inventory Modelling of Post-Combustion Capture Process

7.1 Introduction

Post-combustion CO_2 capture refers to the separation of CO_2 from the flue gases generated in a large-scale combustion process fired with fossil fuels or biomass. The direct firing of fuel with air in a combustion chamber has been the most economic technology to use the energy contained in the fuel (IPCC, 2005).

Flue gases or stack gases from power generation are usually at atmospheric pressure, with large volume flow rates of gases containing high percentage nitrogen. The CO_2 concentration in flue gases vary depending on the type of fuel used (between 3% for a natural gas combined cycle to less than 15% by volume for a coal-fired combustion plant). Flue gases from coal combustion will contain not only CO_2, N_2, O_2 and H_2O, but also air pollutants such as SOx, NOx, particulates, HCl, HF, mercury, trace metals and other inorganic contaminants. These impurities need to be reduced before flue gases enter into the CO_2 capture unit. The schematic of a pulverized coal-fired power plant with post-combustion (an amine-based) CO_2 capture system and other emission controls are shown in Figure 7.1 as an example.

As already described in Chapter 2, post-combustion CO_2 capture methods applicable to power generation systems are chemical absorption, adsorption, membrane separation, etc. Comparative assessment work (Riemer and Ormerod, 1995; IEA GHG, 2000; IPCC, 2005) has shown that chemical absorption method is currently the preferred option for

post-combustion CO_2 capture. Chemical absorption CO_2 capture is well-developed technology that has been applied to numerous commercial processes such as gas treatment and ammonia production. With respect to the adsorption process for flue gas CO_2 recovery, molecular sieves or activated carbons are used in adsorbing CO_2, and desorbing CO_2 is then done by the pressure swing operation (PSA) in most cases (Yokoyama, 2003). Adsorption processes have been employed for CO_2 removal from synthesis gas for hydrogen production, but it has not yet reached a commercial stage for CO_2 recovery from flue gases (IPCC, 2005). Polymeric gas separation membranes are used commercially for CO_2 removal from natural gas at high pressure and at high CO_2 concentration, but the removal of CO_2 using commercially available polymeric gas separation membranes results in higher energy penalties on the power generation efficiency compared to a standard chemical absorption process (Herzog *et al.*, 1991; Van der Sluijs *et al.*, 1992; Feron, 1994; IPCC, 2005). The membrane options currently receiving the most attention are a hybrid membrane – absorbent (or solvent) system and facilitated transport membranes, but significant improvements are required before they are commercially applied to power plants (IPCC, 2005).

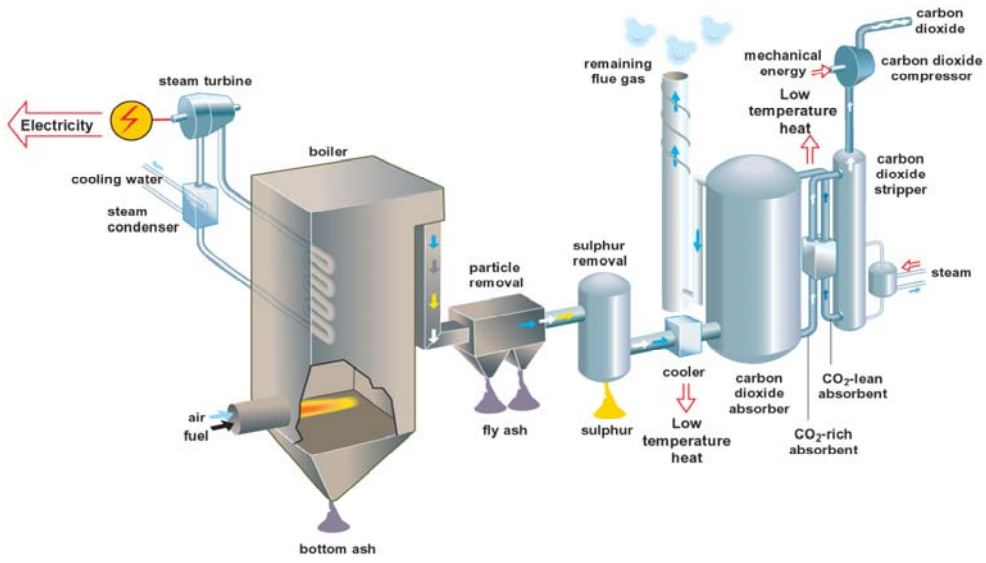

Figure 7.1: Schematic of a pulverized coal-fired power plant with post-combustion CO_2 capture system and other emission controls (After Strömberg, 2006)

With the limitations of time and resource, this research focused on the chemical absorption CO_2 capture method only. This Chapter, firstly, develops LCI models for chemical absorption CO_2 capture with 8 alternative solvents, based on basic chemical and physical principles or empirical relationships of chemical absorption CO_2 capture processes, aiming at incorporating more parameters into the LCI models and reducing

the uncertainty of LCI results. Secondly, the Chapter introduces the LCI model for the CO_2 conditioning process for post-combustion CO_2 capture power plants. The LCI models of PM control, SOx control and NOx control in post-combustion CO_2 capture power plants are the same as the LCI models developed in Chapter 5.

7.2 Life Cycle Inventory Modelling of Chemical Absorption Carbon Dioxide Capture

7.2.1 Principles of Chemical Absorption Carbon Dioxide Capture

Chemical absorption involves one or more reversible chemical reactions between CO_2 and aqueous solvent(s), such as alkanolamine (e.g. MEA, DEA) or potassium carbonate (K_2CO_3), and then upon heating the product of these reactions, the bond between the absorbent and CO_2 can be broken, generating a stream enriched in CO_2. Chemistry and thermodynamics of solvent alternatives are given in Table 7.1. The primary reactions from left to right remove CO_2 from the waste gas streams through an exothermic reaction of CO_2 with the amine functionality of the alkanolamine, at low temperature (25 - 65 ^oC) and pressure (30 to 45 kPa), and the reactions from right to left regenerate the solvent by heating the solvent solution to 100 - 150 ^oC and pressure 150 to 175 kPa (Sass *et al*., 2005).

Table 7.1: Chemistry and thermodynamics of alternative solvents used in CO_2 capture (Modified after Rochelle, 2001)

Solvent Alternatives	Example of Primary Reaction	Reaction Speed	ΔH* (kcal/mole)	Corrosion & Degradation
Primary Amine* (e.g. MEA, DGA)	$2MEA + CO_2 <> MEACOO^- + MEAH^+$ (with the formation of carbamates)	Fast	20-22	high
Secondary Amine *(e.g. DEA, DIPA)				
Tertiary Amine* (e.g. MDEA, TEA)	$AMP + CO_2 + H_2O <> AMPH^+ + HCO_3^-$ (with the formation of bicarbonate)	Slow	10-15	low
Hindered Amine* (e.g. AMP, KS-1)				
Potassium Carbonate (K_2CO_3)	$CO_3^= + CO_2 + H_2O <> 2\ HCO_3^-$	Very Slow	5-10	low

* Amine: is a group of organic compounds, which can be considered as derived from ammonia (Lee *et al*., 2002) by replacement of one or more hydrogen molecules by organic radicals. Amines are classified according to the number of hydrogen of ammonia that has been replaced by radicals, as follows:
- Primary amine (RNH_2) - one hydrogen molecule has been replaced; and
- Secondary amine (R_2NH) - two hydrogen molecules have been replaced; and
- Tertiary amine (R_3N) – all three hydrogen molecules have been replaced; and
- Hindered primary and secondary amines – absorb CO_2 as bicarbonate, note carbamate.

The substitute groups (R) may be alkyl, aryl or aralykl. When the (R) is an alkyl, the amine is called alkanolamine.

* "<>": represents the reversible chemical reaction;

* ΔH: Heat for desorption; ΔLdg = Rich sorbent CO_2 loading rate - lean sorbent CO_2 loading rate;

* Monoethanolamine=MEA; Diglycolamine=DGA; Diethanolamine=DEA; Diisorpropanolamine=DIPA; Triethaolamine=TEA; N-methyldiethanolamine =MDEA; 2-amino-2-methyl-1-propanol=AMP.

A typical chemical absorption unit is based on an aqueous CO_2 absorption and CO_2 stripping system, which is comprised of two sections (Figure 7.2). In the Absorber, CO_2 is chemically absorbed from the inlet gases by contacting it with the countercurrent CO_2-lean solvent (e.g. MEA). The treated gas exits the top of the Absorber Column. The CO_2-rich solvent is passed to the Stripper, where, by heating the CO_2-rich solvent

solution, the CO_2 is stripped off and the CO_2-lean solvent is regenerated. The regenerated CO_2-lean solvent is then recycled back to the Absorber and the CO_2 is passed to compression processes. The system, especially MEA solvent system, also uses chemicals (such as NaOH) for proposes of solvent reclamation, solid filtration, and corrosion inhibitor. Sorbent make-up is also required for the compensation of sorbent loss in the absorption/stripping process.

CO_2 Chemical absorption processes derive from amine based gas processing processes (e.g. acid gas removal in natural gas production, and hydrogen production), which is a proven and well-known technology. Historically, the aqueous solvent MEA has dominated the commercial applications. The state-of-the-art system uses 15-30 wt% MEA, e.g. Fluor Daniel (30% with inhibitors), ABB Lummus (20% with inhibitors). Hindered Amines, such as KS-1, KS-2 and KS-3 developed by Mitsubishi, are also commercially operated in the removal of CO_2 from flue gas. However, for CO_2 removal from power plant flue gas, particular problems posed by some of the low concentration chemical species present in the flue gas, particularly those from coal fired boilers, need to be overcome. Currently, there are no large scale carbon dioxide capture plants operating on commercial power plants.

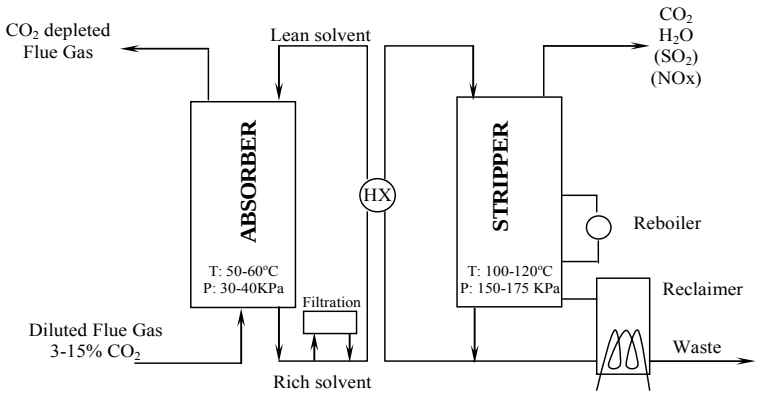

Figure 7.2: Typical aqueous absorption/stripping system for CO_2 capture.

7.2.2 Chemical Absorption Carbon Dioxide Capture Life Cycle Inventory Model Development

In this research, inputs/outputs of chemical absorption CO_2 capture processes are modelled using engineering calculations. In order to characterise the technological differences of different chemical absorption CO_2 capture processes, the LCI model developed accounts for 8 types of solvents. The schematic of the LCI model developed is shown in Figure 7.3, which describes the inputs/outputs to be quantified.

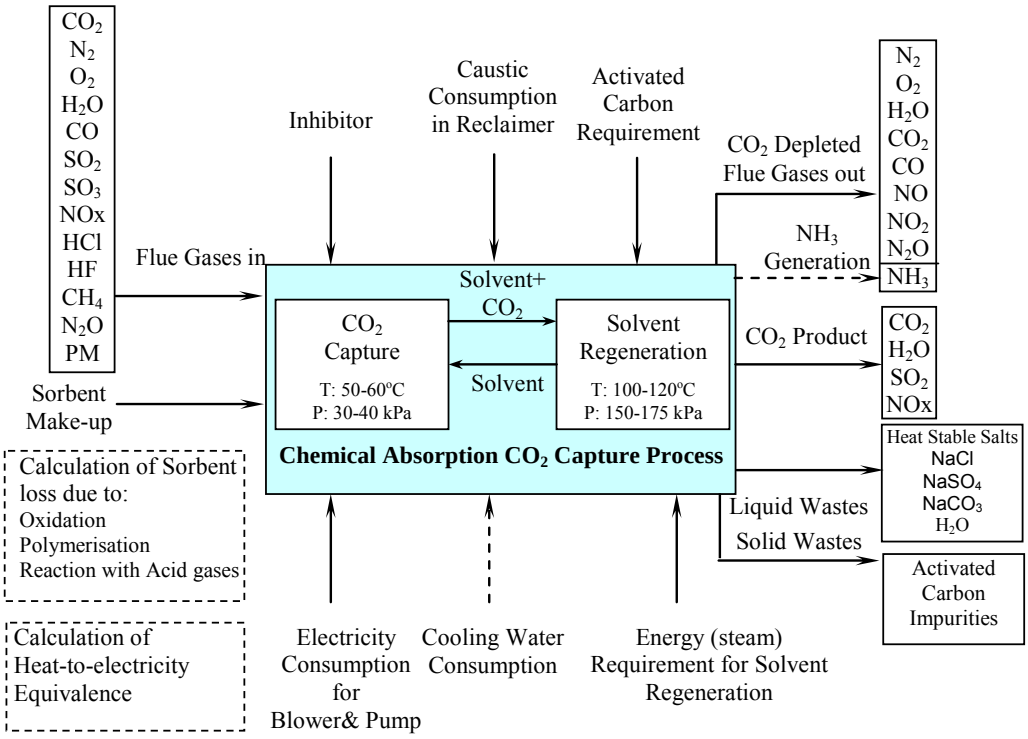

Figure 7.3: The scheme of chemical absorption CO_2 capture processes LCI model developed.

7.2.2.1 The Consumption of Steam, Electricity, Cooling Water and Process Water

Heat Requirement for Solvent Regeneration

Solvent regeneration requires considerable energy. The heat for solvent regeneration of an aqueous absorption/stripping system is the sum of heat of desorption of CO_2, the evaporation heat of dilution water in solvent, and sensible heat to bring the solvent to its boiling point. Previous research with a pilot CO_2 capture plant have shown that, for a typical MEA solvent, sensible heat to bring the solvent to its boiling point, heat of desorption of CO_2, and the evaporation heat of dilution water account for 49%, 27% and 24% of the total heat duty respectively (Dugas *et al*, 2006). The heat required for solvent regeneration is mainly determined by the type of solvents used and the solvent concentration, with a wide range from 2,200 to 6,000kJ/kg CO_2 captured. In this research, the heat requirements of alternative solvent regeneration processes were taken from the literature (Figures 7.4 and 7.5).

The Consumption of Steam and Heat-to-electricity Equivalence Ratio

The heat required for sorbent regeneration is normally extracted from the steam turbine in the form of low pressure steam (Figure 7.6) and through the reboiler (a heat

exchanger) in the case of coal-fired power plants and combined-cycle gas plants. The reason for the use of steam extraction rather than building additional facilities comes from plant efficiency, investment cost, and space saving considerations. Typically, the low pressure (LP) steam is around 320 to 370°C at 60-80 kPa pressure, and the heat content (enthalpy) of such steam is about 2,350 kJ/ kg steam (Black and Veatch, 1996).

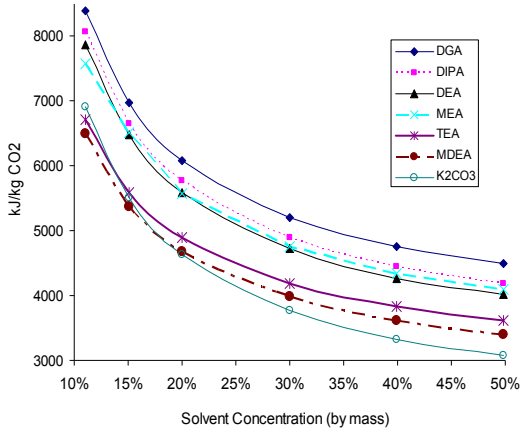

DGA : $Y = 3271X^{-0.4079}$ $R^2 = 0.9813$
DIPA : $Y = 3004X^{-0.4279}$ $R^2 = 0.9824$
DEA : $Y = 2844X^{-0.4424}$ $R^2 = 0.9842$
MEA : $Y = 2972X^{-0.4123}$ $R^2 = 0.9875$
TEA : $Y = 2640X^{-0.4042}$ $R^2 = 0.9824$
MDEA : $Y = 2455X^{-0.4219}$ $R^2 = 0.9835$
K_2CO_3 : $Y = 2038X^{-0.534}$ $R^2 = 0.9881$

where:
Y: heat requirement (kJ/kg CO_2);
X: Solvent concentration (by mass).

Figure 7.4: Energy consumption in chemical absorption CO_2 capture for solvent alternatives (Generated from Göttlicher, 2004).

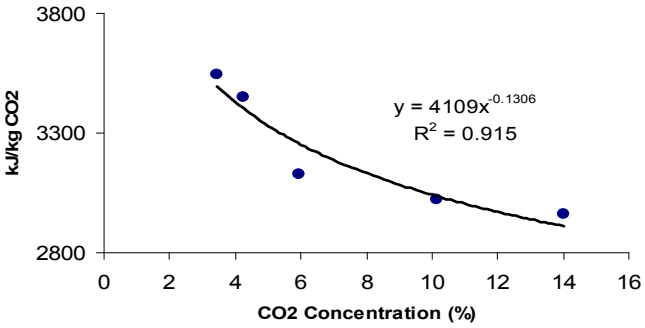

Figure 7.5: Energy consumption for chemical absorption CO_2 capture by KS-1 solvent (After Mimura *et al.*, 2000).

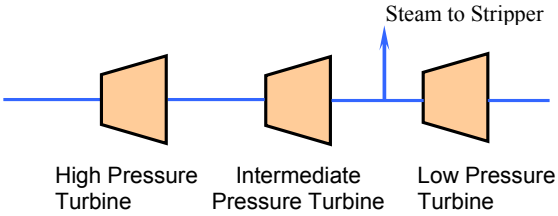

Figure 7.6: Steam extraction in power plants

The mass flow rate of steam for regeneration can be calculated as:

$$m_{steam}\ (\text{tonne/hr}) = Q/(\eta_{reboiler} \times h_{steam}) \qquad [7.1]$$

where:

h_{steam} is the heat content (enthalpy) of the steam;

$\eta_{reboiler}$ is the efficiency of reboiler, which is determined by the difference between reboiler temperature and ambient temperature. The default value used for $\eta_{reboiler}$ is 0.85 in this research (Dugas *et al*, 2006).

When extracting steam, the steam turbine power output is reduced to less than the heat content of the steam. The reason for this is that the exergy content of the steam is only a fraction of the heat, and therefore the heat of the extracted steam could not have been converted fully to mechanical power in the steam turbine. The heat-to-electricity ratio represents the equivalent loss of power generation capacity due to the extraction of steam for sorbent regeneration. The ratio of converting heat into electricity mainly depends upon the temperature and pressure conditions of the working fluid in the reversible thermal cycle. In general, the lower the pressure and temperature of the steam, the lower efficiency to convert heat into electricity. Literature provides a wide range of heat-to-electricity ratios for LP steam, form 0.14 to 0.25 (Göttlicher, 2004; Rao *et al*., 2004; Feron, 2005), due to variations in the type of turbine (e.g. extraction-condensing turbine and back-pressure steam turbine) and the configuration of plant concerned. In this research, 0.14 is used for heat-to-electricity equivalence ratio ($\eta_{heat\text{-}to\text{-}electricity}$) in the case of steam turbine power plants with current available power generation technologies and 0.19 is used for future advanced power plants (Göttlicher, 2004; Feron, 2005). Therefore, the electricity equivalence can be calculated using the following equation:

$$\text{Electricity equivalence} = \eta_{heat\text{-}to\text{-}electricity} \times m_{steam} \times hs_{team} \qquad [7.2]$$

where:

m_{steam} is the mass flow rate of the steam

h_{steam} is the heat content (enthalpy) of the steam

Technology developers have concentrated on developing new generations of the technology which minimises steam consumption, by a high degree of integration of reboiler heat duty with the power plant thermal cycle. Use of off peak energy and heat from the vapour leaving the stripper are also attractive in a power plant setting.

Cooling Water Requirement

As the absorption of CO_2 in amine solvent is an exothermic process, low temperature of the inlet flue gas is favoured by the absorption reaction. The typically acceptable range

of flue gas temperature is 50-60 ^{o}C. If the flue gas is coming from a wet sulphur scrubber, additional cooling water equipment, direct contact cooler (DCC), may not be required, because the temperature of the outlet flue gas from desulphurisation unit is typically around 65 ^{o}C. But, in the case of flue gas from a natural gas fired boiler, which often does not pass through a sulphur scrubber, DCC is essential. Inclusion of the DCC is an option available in the model developed in this research. Typically, the circulating cooling water rate is approximately 110 m^3cooling water per tonne CO_2 captured from the flue gas (Chapel *et al*., 1999).

A more accurate calculation for cooling water flow rate is carried out using the following equation:

$$M_{cw} = m_{fg} \times (\Delta T_{fg} / \Delta T_w) \times (SH_{fg} / SH_w) \text{ tonne/hr} \quad [7.3]$$

where:

Specific heat of water, SH_w = 4.2 kJ/kg ^{o}C;

Specific heat of flue gas, SH_{fg}, generally around 1.0 kJ/kg ^{o}C (300^{o}C, 75% N_2, 25% CO_2);

Temperature rise in the cooling water, ΔT_w, typically 15 ^{o}C;

Drop in flue gas temperature, $\Delta T_{fg} = (T_{fg,i} - T_{fg})$ ^{o}C;

$T_{fg,i}$ = Temperature of flue gas entering the direct contact cooler (^{o}C);

T_{fg} = Temperature of flue gas exiting the direct contact cooler (^{o}C);

Mass flow rate of flue gas, m_{fg}, in tonne/ hr.

Process Water Requirement

Water evaporation in the amine unit causes water losses. Typically, the value of amine unit process water makeup is 0.114 tonne/hr per MW (net) (Booras and Smelser, 1991).

7.2.2.2 Electricity Consumption for Blowers and Pumps

The electricity consumption in an aqueous absorption/stripping unit includes the flue gas blower power, DCC circulation pump power (if used), and the absorber wash water pump power, which are all inversely proportional to the CO_2 concentration in the flue gas, ranging from 0.2 to1.3 MJ/kg CO_2 removed (Bolland, 1998; Göttlicher, 2004). The chief power consumer over the entire range of CO_2 concentrations is the flue gas blower. The electrical consumption per tonne of CO_2 captured can be estimated using the following equation (Chapel *et al*., 1999).

Electrical consumption (kW) = 9.6 + 393.6/(concentration of CO_2 × 100) [7.4]

For the KS-1 system the electrical consumption is quoted as 18 kWh/ tonne CO_2.

7.2.2.3 Mass Flow of Acid Gases in the Flue Gases

Carbon Dioxide Capture Efficiency (η_{CO2})

Most of the studies report the CO_2 capture efficiency of the amine-based systems to be 90%, with few others reporting as high as 96% capture efficiency. In the model developed, a default value of 95% has been assumed, however, the user can specify the desired level of CO_2 capture efficiency.

Other Acid Gases Removal Efficiency

Due to the alkalinity of the amine solution, acid gases, such as NO_2 (as $HNO_{2/3}$), SOx (as $H_2SO_{3/4}$), and HCl, will nearly completely be absorbed into the amine solution (theoretically to << 1 ppm) during CO_2 sorption at the appropriate scrubber conditions and cause a loss of amine solvent (Sass *et a*l, 2005). Both N_2O and NO are not strongly absorbed in the amine solution and tend to remain in the flue gas. Using values from the literature (Rao *et al*, 2004; Sass *et al*, 2005), parameters for acid gas removal efficiency are set as presented in Table 7.2.

Table 7.2: Acid gases removal efficiency of alternative solvents.

Acid gas	Potential effects by amines	Removal efficiency (%)
SO_2	Reacts irreversibly with some amine absorbents	η_{SO2} = 99.5%
SO_3	Reacts irreversibly with some amine absorbents	η_{SO3} = 100%
NO_2	Not strongly absorbed and tends to remain in the flue gas	η_{NO2} = 25%
N_2O	Not strongly absorbed and tends to remain in the flue gas	η_{N2O} = 25%
NO	Not strongly absorbed and tends to remain in the flue gas	η_{NO} = 0
HCl	Reacts irreversibly with some amine absorbents	η_{HCl} = 99.5%

Based on the table above, the mass flow of i^{th} acid gas venting from the MEA capture is:

$$M_{i,\ acidout} = M_{i,\ acidin} \times (1 - \eta_{i,\ acidgas}) \quad [7.5]$$

Components of the Carbon Dioxide Product

Since a small amount of HNO_2 and H_2SO_3 could break down back into SO_2 and NOx at low temperature at the CO_2 stripper, SO_2 and NOx could appear in the CO_2 stream (Sass *et a*l, 2005). These S and N products are expected to be quite corrosive, especially because moisture also is in the CO_2 stream.

Solvent Emission via Absorber

The solvent vapour emissions via the absorber are reduced by the use of a wash section on top of the absorber. The wash section which is fed with pure water will recover a large fraction of the evaporated solvent and droplets carried over. Even so, the flue gas will contain solvent and the solvent emission via the absorber is estimated at 47 g per ton CO_2 captured (IEA GHG, 2006).

7.2.2.4 Particulate Matter and Trace Element Removal Rate

Aqueous absorption/stripping systems are wet scrubbing operations. This also leads to removal of particulate matter from the flue gas to a certain extent. Previous research on other scrubbing systems (Nalbandian, 2004) have suggested that the removal efficiencies for particulates larger than 10 μm is about 80% (η_{p1}) and for particulates smaller than 10 μm the removal efficiency is 10% (η_{p2}). Therefore, the particulate matter output can be calculated by the following equations:

$$M_{po1}=M_{pi1} \times \eta_{p1} \quad [7.6]$$

$$M_{po2}=M_{pi2} \times \eta_{p2} \quad [7.7]$$

where:

M_{pi1}: particulates larger than 10 μm;

M_{pi2}: particulates smaller than 10 μm.

With respect to toxic metal ions, mercury, lead, cadmium, and many other volatile metals (e.g. Zn, Ag, etc.), these ions will react with amines forming strong water-soluble complexes with the amines (Sass *et al*, 2005). These non-volatile metal ion complexes will follow the CO_2 concentrate stream during regeneration and can be eliminated by in-line mist eliminators. Since there is no evidence in the literature quantifying the trace metal removal rates by chemical absorption CO_2 capture systems, in this research assumed that 80 percent of trace metals are removed, based on the trace metal removal rates known for FGD systems.

7.2.2.5. Solvent Loss and Ammonia Generation Rate

Loss of amine solvent may occur from degradation, vaporisation, and mechanical sources. Degradation, which is derived from the irreversible breakdown of the base amine molecules, is the main cause of solvent loss. Degradation could take place through two known processes, oxidation and carbamate polymerisation.

Oxidative Degradation

Oxidative degradation requires oxygen and is catalysed by iron or copper, produces oxidised fragments of the solvent such as organic acids (e.g. Formaldehyde, Acetic Acid, and Glycolic Acid) and NH_3, and is expected to occur in the presence of dissolved O_2 in the liquid hold up at the bottom of the absorber. Secondary amines (e.g. DEA) are oxidised about twice as fast as primary amines (MEA, DGA), and the hindered primary amines, the tertiary amines (MEDA), the K^+ salt of alanine, and mixtures of MDEA with other amines are degraded about one fifth as fast as primary amines (Rochelle *et al*., 2001). Inhibitors (e.g. Na_2SO_3) can be employed to effectively reduce the oxidative degradation.

Carbamate Polymerisation

Carbamate polymerisation requires high temperatures and high CO_2 loading, produces high molecular weight degradation products, and is expected to occur at the higher temperature of the stripper. The rate of polymerisation is highly depended on the amine concentration. Solvents with higher amine concentrations have a higher rate of polymerisation. However, amines that are not alkanolamines (e.g. piperazine), tertiary amines, as well as hindered primary and secondary amines will not be subject to carbamate polymerisation (Rochelle *et al*., 2001).Typical carbamate polymerisation products are oxazolidone, hydroxyethyl imidazolidone (HEI), and hydroxyethyl ethylenediamine (HEED) (Rochelle *et al*., 2001).

Solvent Loss, Ammonia Generation, and Oxygen Consumption

In this research, it is assumed that oxidation and carbamate polymerisation account for 40% and 60% of the total solvent loss respectively(Rochelle *et al*., 2001), and the total MEA loss due to degradation is conservatively estimated at around 1.5 kg MEA/tonne CO_2 (Chapel *et al*., 1999; White, 2003). Therefore, the rate of MEA loss caused by oxidation (A) is 0.6 (1.5 x 0.4) kg MEA/tonne CO_2, and the rate of MEA loss caused by polymerisation (C) is 0.9 (1.5 x 0.6) kg MEA/tonne CO_2. According to the stoichiometry of MEA oxidation, one mole of MEA oxidation generates one mole of NH_3, therefore, the rate of NH_3 generation due to MEA oxidation is 0.136 kg NH_3/ tonne CO_2. For alternative solvents, rate of solvent losses and rate of NH_3 generation are calculated from Table 7.3, which was summarised from material in the literature (Alawode, 2005; Imai, 2003; Rochelle *et al*., 2001).

Table 7.3: Solvent loss and NH_3 generation by degradation for alternative solvents.

Type of degradation	Primary Amine		Second Amine		Tertiary Amine		Hindered Amine		Promoted Potassium Carbonate
	MEA	DGA	DEA	DIPA	TEA	MDEA	AMP	KS-1	K^+/PZ
Oxidation (kg MEA/tonne CO_2)	A	A	2×A	2×A	0.05A	0.05A	0.1×A	0.2×A	0.1×A
NH_3 generation (kg/tonne CO_2)	B	2×B	3×B	3×B	0	0	3×B	3×B	0
Polymerisation (kg MEA/tonneCO_2)	C	C	C	C	0	0	0	0	0

* A = the MEA loss by oxidation; B = NH_3 generation due to MEA oxidation; C = MEA loss by polymerisation.

The rate of MEA loss by oxidation in Table 7.3 is the rate after inhibitors are employed. According to an earlier study, inhibitors can reduce the oxidation rate to 30% of the rate without the use of inhibitors (Goff *et al*., 2005). Oxidative degradation products will be formed in parallel, and the actual stoichiometry of the process should fall somewhere in the range of 0.5-2.5 mole oxygen consumed for one mole of amine oxidised (Goff *et al*., 2005). In this research, stoichiometry of the process is set at 1.5, and the oxygen consumed by the amine oxidisation can be calculated by the following equation:

Oxygen consumption by oxidation (mole) = 1.5 × Amine loss by oxidation (mole)/0.3 [7.8]

In existing CO_2 capture facilities that use amine solvents, the degradation products are separated in an evaporative reclaimer and disposed of as hazardous chemical waste.

Heat Stable Salts and Additional Loss of Solvents

Flue gas impurities (e.g. SOx, NOx, and HCl) can tie up an amine molecule to form a salt that is not capable of being regenerated by the addition of heat, and are thus referred to as Heat Stable Salts (HSS). They reduce the absorption capacity of the amine and are also corrosive. Therefore, upstream SOx, NOx and HCl units are required to minimise the amount of contaminants entering the amine unit to an acceptable level.

The HSS can be neutralised with sodium hydroxide (NaOH), which can free up the amine bound to the HSS anion in the reclaimer. Neutralisation changes the HSS from an amine HSS to a sodium HSS (e.g. $NaSO_4$, NaCl), but does not remove any contaminants from the system.

Sodium hydroxide cannot reclaim all solvent losses from the HSS. In this research, for solvent alternatives, solvent loss caused by acid gases is estimated using Equation 7.9 (Chapel *et a*l., 1999), and solvent losses resulting from NOx, and HCl are neglected as NOx, and HCl volumes in flue gas are very small.

Solvent loss (kg per ton CO_2) = 0.5 × (ppmv SO_X entering the absorber / (CO_2 concentration in flue gas × 100))

[7.9]

Caustic and Activated Carbon Consumption

In this research, caustic consumption in the reclaimer has a typical value of 0.13 kg NaOH/ ton CO_2 captured (Rao *et al.,* 2004).

The consumption of activated carbon, which adsorbs impurities (degradation products of solvents) from the solution stream, will typically average at 0.075 kg activated carbon per tonne CO_2, assuming that the activated carbon is replaced every three months (Chapel *et al*., 1999; Rao *et al*., 2004).

Wastes and Waste Disposal

A CO_2 capture system produces three waste streams: reclaimer waste, spent carbon from the activated carbon filters, and filter elements from the slip-stream solvent filters at the carbon bed. The actual amount of amine waste generated in the process depends on the flue gas composition and plant operating conditions. In this research, a typical value of 3.2kg/ton of CO_2 captured is used for the reclaimer waste (IEA GHG, 2006).The composition of the reclaimer waste is taken from the literature, as presented in Table 7.4 (Nsakala. N., *et al.*, 2001). The amount of spent carbon from activated carbon is assumed to equal the activated carbon consumption. As the filter elements mainly contain flue gas particulates, it is assumed that the amount of filter elements is equal to the flue gas particulate removed by the amine unit. The waste from the capture system can be disposed of by incineration, and then be treated as solid waste.

Table 7.4: Reclaimer bottoms composition (After Nsakala. N., *et al.*, 2001)

Amine	9.5 wt.%
NH_3	0.02 wt.%
NaCl	0.6 wt.%
Na_2SO_4	6.6 wt.%
Na_2CO_3	1.7 wt.%
Insolubles	1.3 wt.%
Total Nitrogen	5.6 wt.%
Total Organic Carbon	15.6 wt.%
pH	10.7
Specific Gravity	1.14

7.3 Carbon Dioxide Conditioning Life Cycle Inventory Model Development for Post-combustion Capture

7.3.1 Process Description

Figure 7.7 illustrates an example of CO_2 conditioning unit for post-combustion CO_2 capture power plan, which comprises CO_2 multi-stage compression and dehydration.

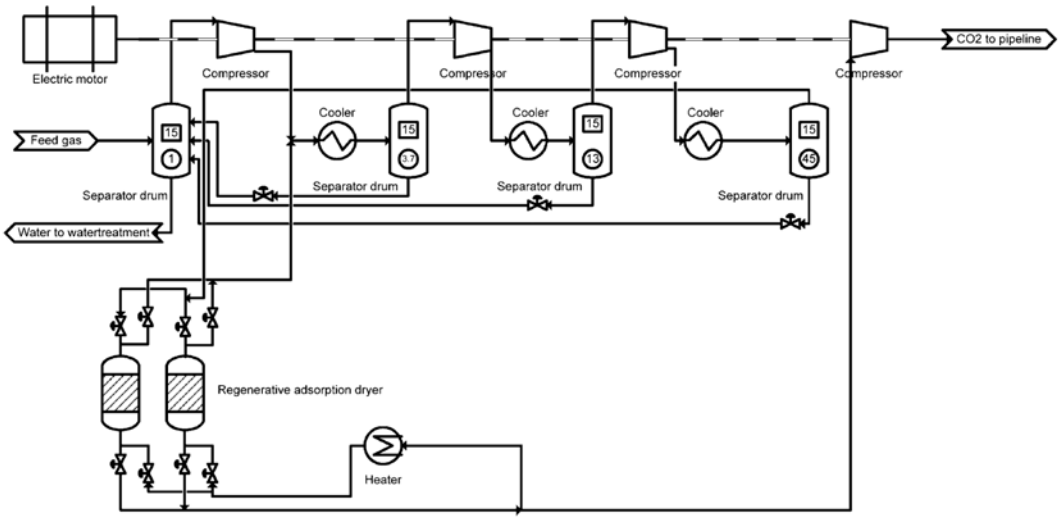

Figure 7.7: An example CO_2 conditioning unit in a CO_2 capture plant (After Aspelunda and Jordal, 2007)

Carbon Dioxide Multi-stage Compression

The captured CO_2 is required to be compressed to a pressure in the range of 8-15 MPa, in order to overcome the frictional and static pressure drops and deliver the CO_2 at a high enough pressure to avoid flashing of gas. The typical CO_2 compression pressure is 13.8 MPa (McCollum and Ogden, 2006).

Multi-stage reciprocating compressors or centrifugal compressors with inter-stage cooling are suitable for large volumes of CO_2 compression. According to the IEA (2002), the maximum size of one compressor train, based on current technology, is 40,000 kW. Therefore, if the total compression power requirement is greater than 40,000 kW, then the CO_2 flow rate and total power requirement must be split into a number of parallel compressor trains.

Dehydration

The required water content of CO_2 product decides whether a dehydration process is installed. For hydrocarbon pipelines, it is often required to dry the gas to 50 ppm water

to ensure that no free water is in the pipeline (Heggum *et al*., 2005). However, this requirement may be too stringent for CO_2 pipeline transportation. Experiments and theoretical calculations have demonstrated that, for typical pipeline transportation with minimum temperature and pressure at 5 ^oC and 8.5 MPa respectively, a maximum water content of 600 ppm may be suitable and sufficient to prevent free water precipitation (Seiersten and Kongshaug, 2002; 2005). If the requirement of CO_2 product water content is 600 ppm, the additional dehydration process is not necessary because the water content in the CO_2-rich gas can be reduced to approximately 400-500 ppm by compression and intermediate stage cooling and scrubbing (Austegard *et al*., 2006). If the requirement of water content is less than 400 ppm, additional dehydration process is required. The regenerative adsorption system is the recommended drying method due to its low investment costs, low maintenance rate, and good operating experience (Heggum *et al*., 2005; Aspelunda and Jordal, 2007).

The regenerative adsorption drier is normally located on the discharge side of the 1st stage in the case of a 3 stage CO_2 compressor (or the 3rd Stage in the case of a 5 stage CO_2 compressor). The drier package usually includes four drier vessels, three of which are in service while one is being regenerated or is on standby (ALSTOM, 2003).

Adsorption refers to the concentration of a fluid component (gas or liquid phase) onto the surfaces of a solid. This can be a purely physical interaction between the adsorbent and adsorbate species (physical adsorption or physisorption) or a chemical reaction (chemical adsorption or chemisorption) (Blachman and McHugh, 2000). The adsorption system of dehydration is cyclic in nature, i.e. there is an adsorption cycle followed by regeneration cycle, which enables repeated use of the adsorbent. The adsorbent can be silica gel, activated alumina or molecular sieves. An example of adsorbent dehydration system is shown in Figure 7.8. The adsorbent absorbs water as the wet CO_2 gas is passed through the adsorbent bed. Once the adsorbent is saturated with liquid it is taken off line and is "regenerated". The regeneration is accomplished by passing hot, dry gas through the adsorbent bed to absorb the liquids. This gas is then condensed and the liquids are separated. A slipstream of CO_2 gas from the first stage compressor is heated as the Regeneration Gas. Since the regeneration of an adsorbent bed requires a relatively high temperature and, because HP steam pressure may fluctuate, a gas-fired heater is specified for this process (ALSTOM, 2003a). The temperature of the CO_2 stream entering the drier is normally 32 ^oC

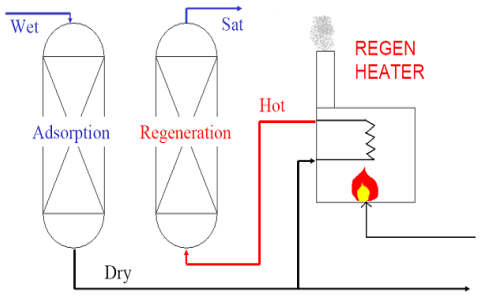

Figure 7.8: Example adsorbent dehydration system.

Adsorbents in common commercial use fall into one of three categories (Blachman and McHugh, 2000):

- Gels – alumina or silica gels manufactured and conditioned to have an affinity for water.
- Alumina – a manufactured or naturally occurring form of aluminium oxide that is activated by heating.
- Molecular Sieves – manufactured or naturally occurring aluminosilicates. Compared to other solid adsorbents, it posses the highest water capacity and produces the lowest water dew-points.

Molecular sieve adsorption (MSA) is recommended for CO_2 dehydration units as it can achieve the required water content of CO_2 product (Heggum, *et al.*, 2005).

7.3.2 Development of Carbon Dioxide conditioning Life Cycle Inventory Model for Post-Combustion Capture

A schematic of the LCI model developed for the CO_2 conditioning unit for post-combustion capture is presented in Figure 7.9. The LCI model quantifies the energy inputs for the compressor, heat input for the drier, adsorbent consumption for the drier, and the cooling water consumption based on engineering calculations.

7.3.2.1 Compressor Power Requirements

The power consumption for CO_2 compression varies from 80-120 kWh/ton CO_2, depending on the CO_2 product pressure, compressor efficiency, CO_2-rich stream composition, and integration opportunities (Anheden *et al.*, 2005). CO_2 compression is a major energy penalty item second only to that of the CO_2 capture unit.

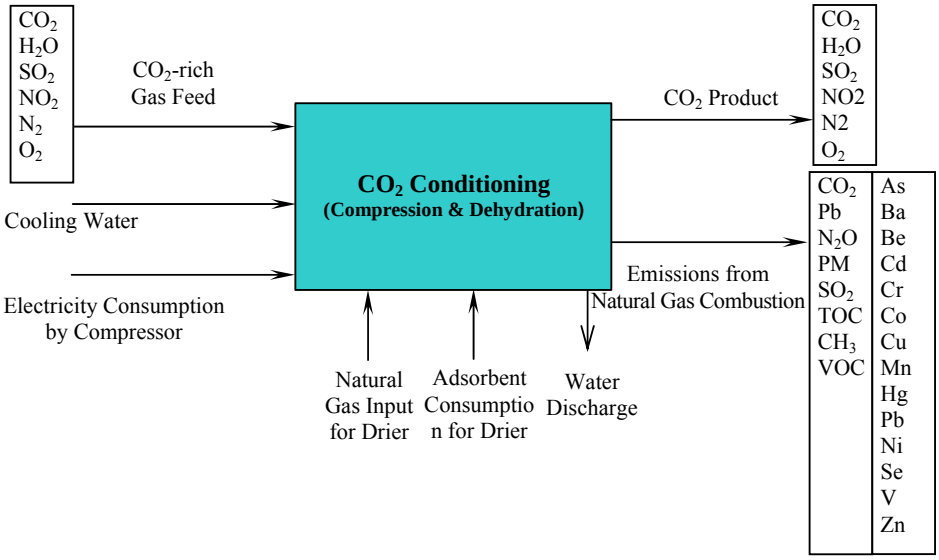

Figure 7.9: The schematic of the LCI model developed for the CO_2 conditioning unit for post-combustion capture.

Being compressed from atmospheric pressure (0.1 MPa) after the CO_2 capture process up to a pressure suitable for pipeline transport (typically 15 MPa) the CO_2 undergoes a phase transition, from gas phase to the liquid or 'dense phase', depending on its temperature. When CO_2 is in the gas phase, a compressor is required for compression, but when CO_2 is in the liquid/dense phase, a pump is suitable for boosting the pressure. The pressure for switching from a compressor to a pump is the critical pressure of CO_2, which is 7.38 MPa (McCollum and Ogden, 2006). Hence, compressors will be used from 0.1 to 7.38 MPa, and then a pump will be used from 7.38 to 15 MPa.

For a multi-stage compressor, the equation for the optimal compression ratio (CR) for each stage is given by Guo and Ghalambor (2005):

$$CR = \left(\frac{P_{switch}}{P_{initial}} \right)^{\frac{1}{N_{stage}}} \qquad [7.10]$$

where,

P_{switch} is the pressure at which the compressor is switched to pump;

N_{stage} is the number of compressor stages, typically 4 or 5;

The compression power requirement for each stage is given by the following equation, which is adapted from McCollum and Ogden (2006):

$$W_{s,i} = \left(\frac{mZ_s RT_{in}}{M\eta_c} \right) \left(\frac{k_s}{k_s - 1} \right) \left[(CR)^{\frac{k_s - 1}{k_s}} - 1 \right] \qquad [7.11]$$

where,

W_s is the compression power requirement (kJ);

m is the CO_2 mass flow rate (kg/s);

Z_s is the compressibility factor;

T_{in} is the inlet temperature (typically 313.15 K);

K_s is the specific heat ratio (C_p/C_v);

M is the CO_2 molar mass (44.01g/mole);

R is universal gas constant (8.314 kJ/kmol K);

η_c is the is the isentropic efficiency of the compressor (typically 0.75).

For a typical 5-stage compressor with P_{switch} =7.8 MPa, the Z_s and K_s for each stage are provided in Table 7.5.

Table 7.5: Pressure range, Z_s and K_s values for a 5-stage compressor (After McCollum and Ogden, 2006)

	Stage 1	**Stage 2**	**Stage 3**	**Stage 4**	**Stage 5**
Pressure range (MPa)	0.1-0.24	0.24-0.56	0.56-1.32	1.32-3.12	3.21-7.38
Z_s	0.995	0.985	0.970	0.935	0.845
K_s	1.277	1.286	1.309	1.379	1.704

To calculate the pumping power requirement for boosting the CO_2 pressure from P_{switch} (7.38 MPa) to $P_{required}$ (15 MPa), the following equation has been adapted from previous studies (McCollum and Ogden, 2006; IEA, 2002):

$$E_p = \frac{m(P_{required} - P_{switch})}{\rho \eta_p} \qquad [7.12]$$

where,

E_p is the energy consumption of pump (kJ);

m is the CO_2 mass flow rate (kg/s);

$P_{required}$ is the required outlet pressure (kPa);

ρ is the average CO_2 density (typically 630 kg/m^3);

η_p is the isentropic efficiency of pump (typically 0.75).

Previous research (Rao, 2002) used ASPEN-Plus module to simulate the multi-stage compression with inter-stage cooling and derived a linear regression equation 7.13 from the data obtained from the process simulation model runs. In order to simplify the calculations, Equation 7.13 is used for the calculation of energy requirement of CO_2 compression in this research.

$$Ecomp = -51.632 + 2.785 \times \ln(P_{CO_2} + 101.38) \qquad (R^2 > 0.99) \qquad [7.13]$$

where

E_{comp} is the unit energy requirement for CO_2 compression (kWh/ tonne CO_2);

P_{CO_2} is the desired CO_2 product pressure (KPa).

7.3.2.2 Water Consumption for Inter-stage Cooling

The multi-stage compressors are water-cooled, wherein the heat of compression is removed by circulating cold water to cylinder heads, inter-coolers and after-coolers. The water requirement for inter-stage cooling can be calculated by the following equation:

$$m_{water} = \frac{m_{co_2} C_{pco_2} \Delta T_{co_2}}{C_{pwater} \Delta T_{water}} \qquad [7.14]$$

where,

m_{water} is the mass flow of the cooling water (kg/hr);

m_{CO_2} is the mass flow of the compressed CO_2 (kg/hr);

C_{pco_2} is the specific heat under average pressure and the average temperature in the compressor, (kJ/kg ^oC). With typical average pressure and temperature being 7.5 MPa and 83 ^oC respectively, C_{pco_2} is 4.57 kJ/kg ^oC obtained from the US National Institute of Standard and Technology;

C_{pwater} is the specific heat of cooling water, with atypical value of 7.56 kJ/kg ^oC;

ΔT_{water} is the water temperature difference. 15 ^oC is set as default value;

ΔT_{co_2} is the CO_2 temperature change (^oC), which is temperature difference of the CO_2 at suction pressure and at discharge pressure if there is no cooling process.

ΔT_{co_2} can be calculated by the following equation adapted from Guo and Ghalambor (2005):

$$\Delta T_{co_2} = T_{in}\left(\left(\frac{p_2}{p_1}\right)^{z(k-1)/k} - 1\right) \qquad [7.15]$$

where,

T_{in} is the inlet CO_2 temperature at suction pressure;

P_1 is the suction pressure of CO_2 (KPa), with a default value of 100 kPa;

P_2 is the pressure of CO_2 at discharge point (KPa), with a range of 8,000-15,000 KPa;

Z is the average CO_2 compressibility, with a default value 0.845;

$k = (C_p/C_v)$ is the average ratio of specific heats of CO_2, with a default value 1.074;

If the cooling water system is a once through system, the water consumption of compression process equals m_{water}. If the cooling water system is a circuit and is recycled to a cooling tower, the water loss occurs due to evaporation, blowdown (water entrained in discharge vapour) and drift (water entrained in discharge vapour). The water consumption equals the water make-up, which equals the total water loss. The total water loss can be calculated by following equations (Kohl and Nielsen, 1997):

$$\text{Total Losses} = \text{Drift Losses} + \text{Evaporation Losses} + \text{Blowdown Losses} \quad [7.16]$$

$$\text{Drift Loss} = 0.15\% \times \text{water flow rate} \quad [7.17]$$

$$\text{Evaporation Loss} = 0.0015 \times \text{water flow rate} \times \Delta T \quad [7.18]$$

$$\text{Blowdown Loss} = \text{Evaporation Loss}/(\text{cycles}-1) \quad [7.19]$$

Where, ΔT is the cooling range, with a typical value of 17 ^{o}C. Cycles refer to the cooling water circulation rate, which is typically 5 to 10.

Furthermore, inadequate cooling water treatment can lead to increase, for example, in total dissolved solids (TDS), which not only act as insulators reducing the heat transfer, but also increases the pressure drop in the cooling water pumping system. Normally, the use of treated water or purging a portion of cooling water (blowdown) periodically can maintain TDS levels within acceptable limits. It is better to maintain the water pH by addition of chemicals, and avoid microbial growth by addition of fungicides and algaecides. Since only a small portion of cooling water is purged (or blowdown) in field practice, this research excludes pollution caused by the discharge of cooling water.

7.3.2.3 Adsorbent Consumption by the Dehydration Unit

Adsorbent (aluminosilicates) is expected to hold approximately 13-22 kg of water per 100 kg of adsorbent. New adsorbent will have an equilibrium capacity near 20%; 13% represents the approximate capacity of a 3-5 year old sieve (Abdi, 2007). In this research, 15% is used for the calculation of the adsorbent consumption. In field operations, normally one adsorption vessel is on line while the others are being regenerated. The number of total adsorption vessel should be considered when calculating the adsorbent consumption. The adsorbent requirement can be calculated by the following equation:

$$S_s = \frac{n \times m_{wr}}{0.15 \times C_{ss} \times C_t \times (T_s \times 24 \times 365)} \quad [7.20]$$

where,

S_s is the amount of molecular sieves used to remove the water to required level (kg);

C_{ss} and C_t are correction factors, provided in Figures 7.10 and 7.11;

T_s is the lifespan of the molecular sieve, with an average value of 4 years;

n is the number of vessels;

m_{wr} is the water removed and can be calculated by the following equation:

$$m_{wr} = m_{co_2} \times (W_{co_2} - W) \quad [7.21]$$

where,

m_{co_2} is the CO_2-rich gas flow rate (kg/hr);

W_{co_2} is the water content of CO_2-rich gas after compression;

W is the required water content of the final CO_2 product;

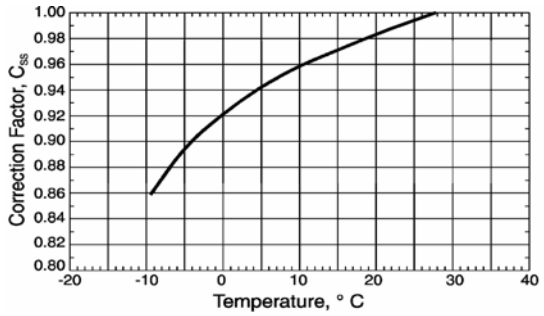

Figure 7.10: Molecular sieve capacity correction for unsaturated inlet gas (After Abdi, 2007)

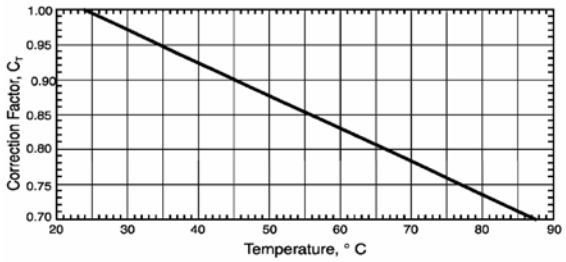

Figure 7.11: Molecular sieve capacity correction for temperature (After Abdi, 2007)

7.3.2.4 Energy Requirement for Absorbent Regeneration

The energy required to desorb the water and heat the molecular sieve can be calculated by the following equations adapted from Abdi (2007):

$$Q_w = 1706 \times m_{wr} \quad [7.22]$$

$$Q_{si} = 0.409 \times S_s(T_{rg} - T_r) \quad [7.23]$$

$$Q_{hl} = 0.9478 \times (Q_w + Q_{si}) \quad [7.24]$$

$$Q_{tr} = Q_w + Q_{si} + Q_{hl} \quad [7.25]$$

where,

Q_w is the desorption of water heat duty (kJ);

m_{wr} is the water removed by a molecular sieve (kg);

Q_{si} is the duty to heat the molecular sieve to regeneration temperature (kJ);

Q_{hl} is the regeneration heat loss (kJ) and a 10% heat loss is assumed;

Q_{tr} is total regeneration heat duty (kJ);

T_{rg} is the temperature of molecular sieve regeneration, with a range of 204-260 ^oC;

T is the initial temperature of molecular sieve (^oC), with a typical value of 82 ^oC;

7.3.2.5 Emissions from Natural Gas Combustion

The heat required for adsorbent regeneration is supplied by natural gas combustion. The emission factors of natural gas internal combustion are provided in Table 7.6 (USEPA 1998d).

Table 7.6: Emission factors for natural gas combustion (After USEPA, 1998d).

Emissions	Emission Factor (Kg/MJ)
CO_2	5.06E-02
Lead	2.11E-10
N_2O (Uncontrolled)	9.27E-07
N_2O	2.70E-07
PM (Total)c	3.20E-06
PM (Condensable)c	2.40E-06
PM (Filterable)c	8.01E-07
SO_2	2.53E-07
TOC	4.64E-06
Methane	9.70E-07
VOC	2.32E-06
Trace metals:	
Arsenic	8.43E-11
Barium	1.85E-09
Beryllium	5.07E-12
Cadmium	4.64E-10
Chromium	5.89E-10
Cobalt	3.54E-11
Copper	3.58E-10
Manganese	1.60E-10
Mercury	1.10E-10
Molybdenum	4.64E-10
Nickel	8.86E-10
Selenium	1.01E-11
Vanadium	9.67E-10
Zinc	1.22E-08

The emissions generated by natural gas combustion can be calculated by the following equation:

$$E_i = F_i \times Q_w \quad [7.26]$$

where,

E_i = emission of i^{th} pollutant;

F_i = emission factor of i^{th} pollutant;

Q_{tr} = total regeneration duty.

7.4 Conclusions

Solvent regeneration in chemical absorption CO_2 capture processes requires significant energy for operation, with a wide range from 2,200 to 6,000kJ/kg CO_2 captured, depending on the type of solvent used. Chemical absorption process can totally or partially remove particulate matters, trace metals, and acid gases (including SO_2, SO_3, NO_2, N_2O, HCl, and HF) present in flue gases. Chemical absorption process also generates NH_3, depending on the type of solvent used. KS-1 solvent case generates more NH_3 than MEA case, and MEA case more than K^+/PZ case. Solvent loss is due to oxidative degradation, carbamate polymerisation, solvent emission via absorber, and solvent reaction with acid gases. The amount of solvent loss depends on the type of solvent.

LCI model developed in this research successfully characterises the technological differences in the chemical absorption CO_2 capture processes used, by accounting for 8 types of solvents. The LCI models developed calculate the consumption of energy for solvent regeneration and solvent loss by reaction with acid gases using empirical relations; electricity consumption and the use of cooling water and process water is calculated using engineering calculations; and acid gas removal rates, particulate matter and trace element removal rates, solvent loss due to oxidative degradation and carbamate polymerisation, solvent emission via absorber, heat stable salts (HSS) generation, activated carbon consumption, and waste disposal rates are calculated using data from the literature.

The CO_2 compression process in the CO_2 conditioning unit requires significant energy, around 80-120 kWh/tonne CO_2. Since the CO_2 product generated from chemical absorption CO_2 capture process contains low percentage of impurities, no environmental emissions are directly released from CO_2 conditioning unit. The CO_2

conditioning LCI model developed computes the energy use by compressors, the heat input for the drier, adsorbent consumption for the drier, and cooling water consumption using engineering calculations.

Chapter 8 Life Cycle Inventory Modelling of Carbon Dioxide Pipeline Transportation and Injection

8.1 Introduction

This Chapter presents the research carried out for the development of LCI models for CO_2 transportation and injection processes respectively. The two processes all involve large quantities of movement of CO_2. Energy consumption and fugitive emissions are expected to be the matters of concern in the context of LCI modelling. The LCI models developed also address the geographical and geological differences by considering the length of CO_2 transportation, surface temperature, and the characteristics of a saline aquifer such as reservoir pressure, thickness, depth and permeability.

8.2 Carbon Dioxide Transportation Life Cycle Inventory Model Development

8.2.1 Carbon Dioxide Transportation Technologies

Transport of CO_2 is the stage that links the CO_2 sources to the storage sites. In the context of long-distance movement of large quantities of carbon dioxide, pipeline transportation and the use of marine tankers are the current practices. This research focuses on CO_2 pipeline transport due to its large potential. Carbon dioxide pipelines are not new and they now extend over more than 2,500 km in the western USA, where they carry nearly 50 Mt of CO_2 annually from natural and industrial sources to

enhanced oil recovery projects (IPCC, 2005). The current long-distance CO_2 pipelines used in such projects are presented in Table 8.1.

Table 8.1: Current long-distance CO_2 pipelines used in EOR projects (After Gale and Davison, 2002; IPCC 2005)

	Location	Operator	Capacity ($MtCO_2\ yr^{-1}$)	Length (km)	Year finished	Origin of CO_2
Cortez	USA	Kinder Morgan	19.3	808	1984	McElmo Dome
Sheep Mountain	USA	BP	9.5	660	-	Sheep Mountain
Bravo	USA	BP	7.3	350	1984	Bravo Dome
Canyon Reef Carriers	USA	Kinder Morgan	5.2	225	1972	Gasification plants
Val Verde	USA	Petrosource	2.5	130	1998	Val Verde Gas Plants
Bati Raman	Turkey	Turkish Petroleum	1.1	90	1983	Dodan Field
Weyburn	USA & Canada	North Dakota Gasification Co.	5	328	2000	Gasification Plant
Total			49.9	2,591		

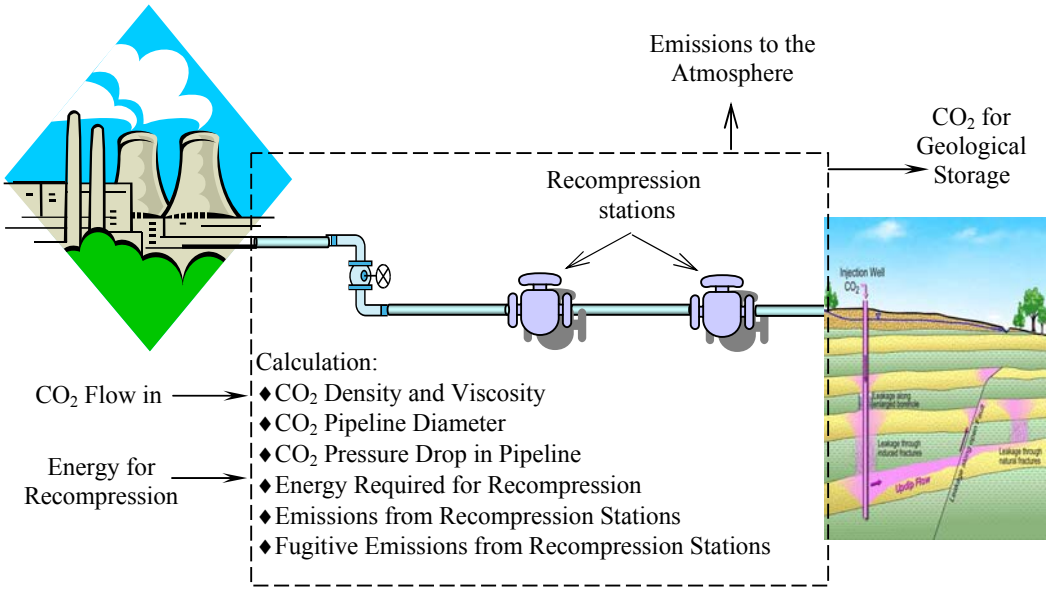

Figure 8.1: Schematic of the LCI model developed for CO_2 pipeline transportation.

8.2.2 Development of a Carbon Dioxide Transportation Life Cycle Inventory Model

In LCA terms, the CO_2 pipeline transport systems comprise the following main processes: pipeline transport and intermediate recompression via compressor or pump booster stations. A schematic of the LCI model developed for the CO_2 pipeline transport system is presented in Figure 8.1. The LCI model calculates the CO_2 density and viscosity, CO_2 pipeline diameter, CO_2 pressure drop in the pipeline, and the energy required for recompression using engineering calculations. Direct emissions from

recompression and fugitive emissions from pipeline transport and recompression are quantified using modified emission factors.

8.2.2.1 Operational and Design Parameters

The range of operational and design parameters for pipeline transportation of CO_2 found in the literature are summarised in Table 8.2.

Table 8.2: Operational and design parameters for CO_2 pipeline transportation,

Common Design Properties	Hamelinck *et al*. (2001)	Heddle *et al*. (2003) and Bock *et al*. (2003)	McCollum and Ogden (2006)	Vandeginste and Piessens (2008)
Pipeline Inlet Pressure [MPa]	7.5	10.3–15.2	15.2	10
Pipeline Outlet Pressure [MPa]	-	-	10.3	-
CO_2 Temperature [^oC]	10	25	25	15
CO_2 density [kg/m^3]	899	884	884	890.1
CO_2 viscosity [Pa s]	0.00008220	0.00006060	0.00006060	0.00008915

In the LCI model, the pipeline inlet and outlet pressures and CO_2 temperature are the input variables. The CO_2 density and CO_2 viscosity can be calculated as a function of pressure and temperature by the following regression equations (McCollum and Ogden, 2006):

$$Y = ax^6 + bx^5 + cx^4 + dx^3 + ex^2 + fx + g \qquad [8.1]$$

where Y is density (kg/m^3) or viscosity (Pa s); x is pressure (MPa); a, b, c, d, e, f, g are regression coefficients. For different temperatures, the regression coefficients for density (or viscosity) are provided in Tables 8.3 and 8.4.

Table 8.3: The regression equation coefficients for density calculations using Equation 8.1 (After McCollum and Ogden, 2006)

Temperature (^oC)	a (x^6)	b (x^5)	c (x^4)	d (x^3)	e (x^2)	f (x)	g
-1.1	-3.13E-07	3.25E-05	-1.44E-03	3.68E-02	-6.57E-01	1.21E+01	8.99E+02
4.4	-9.55E-08	1.98E-05	-1.41E-03	5.07E-02	-1.08E+00	1.77E+01	8.43E+02
10.0	-6.99E-07	8.56E-05	-4.41E-03	1.26E-01	-2.20E+00	2.82E+01	7.69E+02
15.6	-2.93E-07	6.57E-05	-4.75E-03	1.68E-01	-3.32E+00	4.21E+01	6.71E+02
21.1	-7.86E-06	8.73E-04	-4.03E-02	9.98E-01	-1.43E+01	1.22E+02	3.84E+02
26.7	-4.15E-05	4.44E-03	-1.95E-01	4.55E+00	-5.96E+01	4.30E+02	-5.36E+02
32.2	-1.10E-03	1.13E-01	-4.77E+00	1.05E+02	-1.26E+03	7.95E+03	-1.97E+04
37.8	-5.43E-04	5.98E-02	-2.71E+00	6.45E+01	-8.51E+02	5.93E+03	-1.63E+04
43.3	9.61E-04	-9.44E-02	3.73E+00	-7.54E+01	8.08E+02	-4.21E+03	8.42E+03
48.9	1.03E-03	-1.05E-01	4.36E+00	-9.33E+01	1.08E+03	-6.23E+03	1.43E+04
54.4	4.92E-04	-5.31E-02	2.33E+00	-5.29E+01	6.49E+02	-3.97E+03	9.61E+03
60.0	1.78E-05	-5.26E-03	3.80E-01	-1.20E+01	1.86E+02	-1.32E+03	3.61E+03
65.6	-2.01E-04	1.79E-02	-6.14E-01	9.95E+00	-7.50E+01	2.48E+02	-1.21E+02
71.1	-2.27E-04	2.18E-02	-8.26E-01	1.56E+01	-1.54E+02	7.79E+02	-1.49E+03
76.7	-1.72E-04	1.71E-02	-6.76E-01	1.34E+01	-1.40E+02	7.58E+02	-1.56E+03
82.2	-1.04E-04	1.07E-02	-4.39E-01	9.02E+00	-9.70E+01	5.47E+02	-1.16E+03

Table 8.4: The regression equation coefficients for viscosity calculations using Equation 8.1 (After McCollum and Ogden, 2006)

Temperature (°C)	a (x^6)	b (x^5)	c (x^4)	d (x^3)	e (x^2)	f (x)	g
-1.1	-3.77E-14	4.43E-12	-2.22E-10	6.35E-09	-1.20E-07	3.21E-06	9.70E-05
4.4	-4.13E-14	5.06E-12	-2.67E-10	8.10E-09	-1.60E-07	3.69E-06	8.53E-05
10.0	-1.80E-13	1.97E-11	-9.10E-10	2.33E-08	-3.71E-07	5.35E-06	7.07E-05
15.6	-3.84E-13	4.25E-11	-1.97E-09	5.00E-08	-7.54E-07	8.43E-06	5.18E-05
21.1	-9.84E-13	1.09E-10	-4.98E-09	1.23E-07	-1.75E-06	1.59E-05	2.02E-05
26.7	-4.04E-12	4.32E-10	-1.91E-08	4.46E-07	-5.88E-06	4.40E-05	-6.76E-05
32.2	2.28E-10	-2.27E-08	9.15E-07	-1.90E-05	2.12E-04	-1.20E-03	2.68E-03
37.8	9.45E-11	-9.37E-09	3.75E-07	-7.70E-06	8.44E-05	-4.58E-04	9.69E-04
43.3	4.61E-11	-4.65E-09	1.89E-07	-3.98E-06	4.50E-05	-2.50E-04	5.51E-04
48.9	2.17E-11	-2.27E-09	9.72E-08	-2.17E-06	2.62E-05	-1.57E-04	3.81E-04
54.4	1.75E-11	-1.84E-09	7.91E-08	-1.78E-06	2.18E-05	-1.33E-04	3.32E-04
60.0	1.59E-11	-1.66E-09	7.09E-08	-1.58E-06	1.93E-05	-1.18E-04	2.99E-04
65.6	1.33E-11	-1.38E-09	5.86E-08	-1.30E-06	1.59E-05	-9.75E-05	2.52E-04
71.1	9.60E-12	-9.95E-10	4.21E-08	-9.35E-07	1.15E-05	-7.10E-05	1.90E-04
76.7	4.94E-12	-5.14E-10	2.19E-08	-4.94E-07	6.23E-06	-3.93E-05	1.15E-04
82.2	8.35E-13	-9.24E-11	4.29E-09	-1.10E-07	1.66E-06	-1.17E-05	4.94E-05

8.2.2.2 Composition of Carbon Dioxide Product in Pipeline

There is no standard specification for the composition of CO_2 product for pipeline transport. The CO_2 pipeline operators normally establish minimum specifications for composition, under the requirements of the pipeline design. Low nitrogen content is important for EOR, but would not be so significant for other storage options. A CO_2 pipeline through populated areas might have a lower specified maximum H_2S content (IPCC 2005). An indicative composition of CO_2 product found in the literature is shown in Table 8.5as an example.

Table 8.5: Composition of CO_2 product in a pipeline (After Turner, *et al*., 2007)

CO_2 product concentration	Nomenclature	Indicative Concentration (%)
Carbon Dioxide	CO_2	98.30%
Nitrogen Oxides	NO_X	0.10%
Sulphur Dioxides	SO_X	0.50%
Hydrogen Sulphide	H_2S	0.20%
Carbon Monoxide	CO	0.70%
Hydrogen	H_2	0.20%
Total		100%

8.2.2.3 Mass Flow Rate and Pipeline Diameter

The CO_2 mass flow rate from a power plant is one of the important factors that determine the pipeline diameter. The relationship between CO_2 mass flow rate and pipeline diameter is given by the following equation (IEA GHG, 2005):

$$D = [m / (0.25 \pi \rho v)]^{0.5} \quad [8.2]$$

where:

D = pipeline diameter [m];

m = CO_2 mass flow rate [kg/s];

ρ = CO_2 density [kg/m^3];

v = flow velocity [m/s], which is typically from 2-3 m/s (McCollum and Ogden, 2006).

In practice, the largest available diameters, which can be used for CO_2 pipelines, are 1,600 mm (63 in) for land-based pipelines and 1,500 mm (59.06 in) for ocean pipelines (Göttlicher, 2004).

8.2.2.4 Pressure Drop in the Pipeline

When CO_2 is passing through the pipeline, the pressure drops due to the frictional forces. For a typical CO_2 pipeline transport velocity of between 2 and 3 m/s, the pressure loss in a CO_2 pipeline can be estimated using the following equation (Göttlicher G., 2004):

$$\Delta p = \rho f \frac{Lv^2}{2d} \quad [8.3]$$

where,

Δp= pressure drop (Pa);

d= pipeline diameter (m);

$f \approx 0.093 \frac{1}{(d \cdot 1000)^{0.249}}$, is the dimensionless pipeline friction number with a roughness of 0.5mm;

v= CO_2 flow velocity (m/s);

L=pipeline length (m);

ρ=density (kg/m^3).

8.2.2.5 Booster Station Energy Consumption and Emissions from Booster Stations

In order to maintain the CO_2 above critical pressure, recompression may be required at certain points along the length of the pipeline to overcome the pressure drop. Recompression is often needed for pipelines over 150 km (90 miles) in length (Heddle *et al*., 2003). In this research, it is assumed that recompression is needed and booster stations are required for every 150 km along the pipeline starting from the power plant. The number of the booster stations, $n_{booster}$, can be calculated by:

$$n_{booster} = INT(L/150) \quad [8.4]$$

where:

INT (number) is the function that rounds a number down to the nearest integer; L is the length of the CO_2 pipeline.

The energy used by booster stations for raising the CO_2 pressure during pipeline transport is given by:

$$P_{power} = n_{booster} \times (Q \times \Delta P) / (3{,}600{,}000 \times \eta) \quad [8.5]$$

where:

P_{power} = power consumption (MW);

$Q = CO_2$ flow rate [m^3/hr];

ΔP = pressure increase in the booster (kPa), which equals the pressure drop along the pipeline calculated by Equation 8.3;

η = pump efficiency, typically 0.75.

As there are different types of boosters for gas recompression, this research assumes that the boosters are pumps with an efficiency of 75% and are powered by natural gas burning engines. The emission factors for natural gas driven internal combustion engines are presented in Table 8.6 (EPA, 2000). These emissions can be calculated by the following equation:

$$E_i = F_i \times P_{power} \quad [8.6]$$

where,

E_i = emission of i^{th} pollutant;

F_i = emission factor of i^{th} pollutant (from Table 8.6);

P_{power} = power consumption (MW), calculated using Equation 8.5.

Table 8.6: Emission factors for 4-stroke rich-burn engines (After USEPA, 2000)

Pollutants	Emission factors(kg/MW)
NOx	3.42E+00
CO	5.76E+00
CO_2	1.70E+02
SO_2	9.10E-04
TOC	5.54E-01
CH_4	3.56E-01
VOC	4.58E-02
PM_{10}	1.47E-02
$PM_{2.5}$	1.47E-02

8.2.2.6 Fugitive Emissions from Pipelines and Booster Stations

Fugitive emissions refer to emissions from equipment leaks, where any pressurised equipment has the potential to leak, and these leaks generally occur through valves, flanges, seals, connections, open end line or related equipment (Shires, 2004). Figure 8.2 presents some examples of equipments that can potentially cause fugitive emissions .

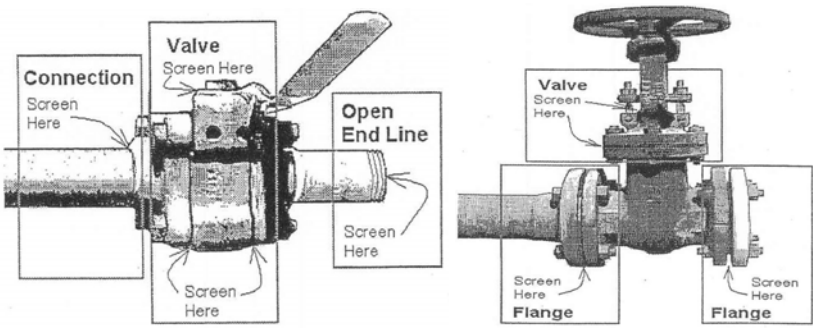

Figure 8.2: The illustration of equipment which may cause fugitive emissions.

This research developed two approaches for the estimation of fugitive emissions from CO_2 pipeline transportation system: facility level emissions and equipment level emissions.

Facility Level Emissions

Facility level emission calculations use default emission factors at facility level derived from the IPCC (2006). The default emission factors are presented in Table 8.7.

Table 8.7: Default emission factors for pipeline transportation of CO_2 from the capture site to the storage site

	Low	Medium	High	Units of Measure
Transmission pipeline	0.23	2.32	23.24	tonne/km/yr
Booster station/compressor	6.97	23.24	116.20	tonne/MW/yr

*the emission factors are derived from the IPCC (2006).

The fugitive CO_2 emissions (allocated to 1 MW electricity generated from power plant with CO_2 capture) during transportation of CO_2 from the capture site to storage site can be calculated by:

$$E_{fCO2} = (L \times F_p + n_{booster} \times P_{power} \times F_b)/\text{Plant capacity} \quad [8.7]$$

where,

E_{fCO2}= total fugitive emissions (tonne/yr);

L= length of the CO_2 pipeline (km);

F_p= fugitive emission factor of pipeline (tonne/km/yr);

F_b= fugitive emission factor of booster station (tonne/MW/yr);

$n_{booster}$= number of booster station.

P_{power} = power consumption (MW), given by equation 8.5;

The fugitive emissions of other gases that are present in the CO_2 product are calculated by:

$$E_f = E_{fco2} \times \frac{C_{gas}}{C_{co2}} \quad [8.8]$$

where,

E_f= total fugitive emissions (tonne/yr);

C_{CO2} = the concentration of CO_2 in the CO_2 product;

C_{gas} = the concentration of the gas (e.g. NOx, SOx, etc.) in the CO_2 product.

Equipment Level Emissions

The equipment level emission model can be used if detailed information on the pipeline components, such as the number of valves, flanges or connections, is available. Equipment level fugitive emission calculations use emission factors suggested for valves, flanges, seals, connections, and open ended lines. The emission factors presented in Table 8.8 for these equipments are obtained by multiplying the USEPA (1995) natural gas emission factors by 1.66 since, on a mass-basis, the CO_2-emissions would be 1.66 times the CH_4-emissions (IPCC, 2006).

Table 8.8: Average emission factors for fugitive emissions from pipeline equipments.

Equipment Type	Emission Factor (kg/hr/source)
Valves	7.47E-03
Pump Seals	3.98E-03
Connectors	3.32E-04
Flanges	6.47E-04
Open-ended Lines	3.32E-03
Drains (onshore)	5.31E-02

The fugitive CO_2 emissions from a population of pipeline equipment are given by:

$$E_{CO2}=\Sigma F_i \times N \quad [8.9]$$

where,

E_{CO2} = Emission rate of CO_2;

F_i = Applicable average emission factors for the major equipment type;

N = Number of pieces of equipment in the process.

8.3 Carbon Dioxide Injection Life Cycle Inventory Model Development

8.3.1 Carbon Dioxide Injection System

The design of the CO_2 injection system is determined by the CO_2 mass flow rate and the CO_2 storage reservoir properties such as pressure, thickness, depth, and permeability, which influence the number of injection wells and the CO_2 surface injection pressure. Typically, the CO_2 injection system comprises surface storage facilities, distribution manifold at the end of the transport pipeline, distribution pipelines to wells, additional compression facilities, measurement and control systems, wellhead(s) and the injection wells. Figure 8.3 presents an example of a CO_2 injection system.

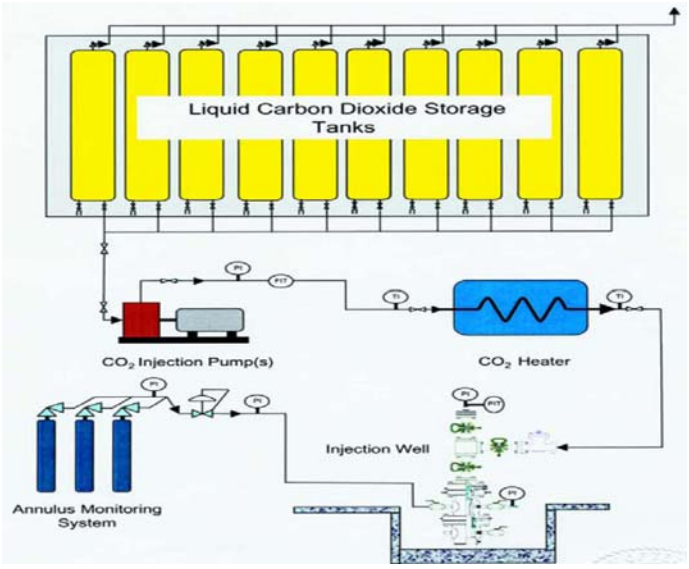

Figure 8.3: An example of a CO_2 injection system for CO_2 saline aquifer storage (After Hovorka *et al*., 2003)

8.3.2 Development of a Carbon Dioxide Injection Life Cycle Inventory Model

A schematic of the LCI model for a CO_2 injection system is shown in Figure 8.4. The LCI model calculates the maximum allowable bottomhole injection pressure, the CO_2 injectivity, number of injection wells, the energy requirement of the injection pumps and the CO_2 heater, the emissions from the CO_2 injection pumps and the CO_2 heater, and the fugitive emissions from CO_2 injection surface facilities.

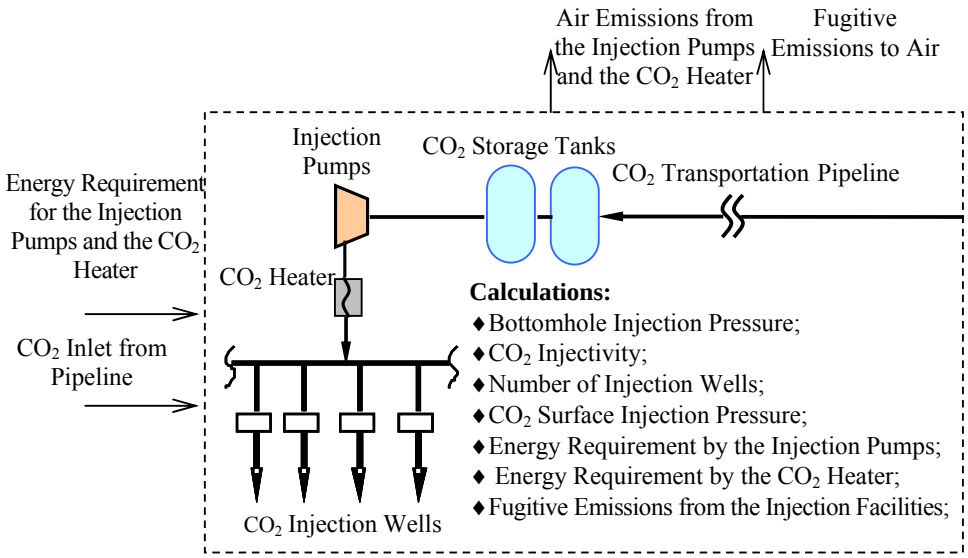

Figure 8.4: A schematic of the LCI model for the CO_2 injection system.

8.3.2.1 Maximum Allowable Injection Bottomhole Pressure

The injection bottomhole pressure (BHP) is the CO_2 pressure at the bottom of the injection well. The upper limit of injection BHP (or the maximum allowable BHP) is set at the fracture pressure of the reservoir rock in order to avoid uncontrolled fracturing of the reservoir rock. In the absence of field data, the fracture pressure of the reservoir rock can be estimated using Equations 8.10 and 8.11 (Heller and Taber, 1986; McCoy, 2008):

$$G_f = \gamma - \beta e^{-ad} \quad [8.10]$$

$$p_f = G_f d \quad [8.11]$$

where P_f is the fracture pressure at depth (Pa), G_f is the fracture gradient (Pa/m), d is depth, and α, β and γ are coefficients with the values: 4.36×10^{-4} m^{-1}, 9.24 kPa/m, and 22.62 kPa/m respectively.

8.3.2.2 Carbon Dioxide Injectivity and Number of Injection Wells

Injectivity is defined as the injection rate divided by the excess pressure above the reservoir equilibrium pressure driving the injection, and CO_2 injectivity represents the mass injection rate of CO_2 (q) that can be injected per unit of reservoir thickness (h) and per unit of downhole pressure difference (Herzog *et al.*, 2003):

$$I = \frac{q}{(BHP - P_{res}) \times h} \quad [8.12]$$

where, q is the injection rate (m^3/s); BHP is the bottomhole pressure (MPa); P_{res} is the reservoir pressure (MPa).

An empirical relationship, derived by Law and Bachu (Law *et al*, 1996) is used to determine CO_2 injectivity as:

$$CO_2 \text{ injectivity} = 0.0208 \times CO_2 \text{ mobility} \quad [8.13]$$

where CO_2 mobility is the CO_2 mobility in the reservoir and can be calculated by equation 8.14 (Herzog *et al*., 2003):

$$CO_2 \text{ mobility} = k_a / \mu_{inter} \quad [8.14]$$

where μ_{inter} represents the CO_2 viscosity in the reservoir near the bottom of the injection well (Pa.s), k_a is the absolutely permeability of the reservoir and can be calculated from the following equation (Law *et al*., 1996):

$$k_a = (k_h \times k_v)^{0.5} \text{ or } k_a = (k_h \times 0.3k_h)^{0.5} \quad [8.15]$$

where k_h and k_v are the horizontal and vertical permeabilities of the reservoir respectively (mD).

Given the pressure and temperature of the reservoir, the CO_2 viscosity can be obtained by Equation 8.1 presented in an earlier section. If the reservoir temperature is unknown, the reservoir temperature (T_{res}) can be estimated by the following equation (McCollum and Ogden, 2006):

$$T_{res} = T_{sur} + d \times (G_g / 1{,}000) \quad [8.16]$$

where T_{sur} is the surface temperature, and G_g is the geothermal gradient with a typical value of 25 ^oC/km.

Finally the CO_2 injection rate per well is calculated by the following equation (Hovorka *et al*., 2003):

$$Q_{well} = (CO_2 \text{ injectivity}) \times h \times (BHP - P_{res}) \quad [8.17]$$

where Q_{well} is the injection rate per well (kg/s), h is the thickness of the reservoir, and P_{res} is the reservoir pressure.

The number of injection wells (N) is based on the flow rate (M_f) of the CO_2 that is delivered to the injection site and the injection rate per well:

$$N = M_f / Q_{well} \quad [8.18]$$

The statistical analysis of the properties of actual reservoirs from the U.S. is provided in Table 8.9, which is used in this research for the sensitivity analysis of CO_2 injection in saline aquifers and in gas and oil reservoirs.

Table 8.9: Statistical analysis of the properties of CO_2 storage reservoirs (After Herzog, 2003)

Parameter	Units	Aquifer Typical	Aquifer Range	Gas Reservoir Typical	Gas Reservoir Range	Oil Reservoir Typical	Oil Reservoir Range
Pressure	MPa	8.4	5 - 11.8	3.45	2.07 – 6.89	13.78	3.45 – 20.7
Thickness	m	171	42 - 703	30.5	15.24 – 61.0	42.7	21.3 – 61.0
Depth	m	1,239	694 -1784	1,524	610 – 3,048	1,554	1,524 – 2,134
Permeability	md	22	0.8 - 585	1	0.01 – 100	5	5 – 19

8.3.2.3 Carbon Dioxide Injection Surface Pressure

The following equation is used to calculate the CO_2 injection surface pressure (P_{tf}) when the injection bottomhole pressure P_{wf} is known (Carcoana, 1992):

$$P_{wf}^2 = P_{tf}^2 \exp(S) + \frac{1.57 \times 10^8 \times (SG) q^2 TZf(MD)[\exp(s) - 1]}{Sd^5} \quad [8.19]$$

where,

P_{tf} = tubing flowing pressure (required surface CO_2 injection pressure) (kPa);

P_{wf} = the injection bottomhole pressure (kPa);

q = average CO_2 injection rate (MMm^3/day);

SG = CO_2 specific gravity, typical value 1.529 (air = 1);

Z= CO_2 deviation factor, Z=0.56 is assumed to be practically constant in the reservoir and temperature range of concern;

D = reservoir depth (m);

d = Well tubing inside diameter (cm). The typical values for the tubing inside diameter are 0.059, 0.1, 0.15, or 0.2 m (McCollum and Ogden, 2006);

MD = measured depth, which is the TVD (true vertical depth);

n = tubing roughness, typical value 12.7×10^{-4} cm (Carcoana, 1992);

T = average temperature in the tubing (Rankine), which is the average temperature of bottom hole temperature and surface temperature;

S = 0.0375(SG)(TDV)/TZ;

f = friction factor, given by

$$\frac{1}{\sqrt{f}} = 1.14 - 2\log\left(\frac{n}{d} + \frac{21.25}{N_e^{0.9}}\right) \quad [8.20]$$

where the Reynolds number N_e is obtained from:

$$N_e = \frac{pvg}{\mu} = \frac{20{,}011(SG)q}{\mu d} \quad [8.21]$$

where μ is the CO_2 viscosity (Pa.s).

8.3.2.4 Energy Consumption and Emissions from the Injection Pumps

If the CO_2 pipeline outlet pressure is less than the required CO_2 surface injection pressure, the CO_2 injection pumps are used to compress the CO_2 to the required pressure. The energy consumption of the injection pumps and emissions from these pumps can be calculated using Equation 8.5 previously suggested for the CO_2 pipeline transportation.

8.3.2.5 Energy Consumption by the Carbon Dioxide Heater and Related Emissions

A CO_2 heater maybe is required to be installed between the injection pump(s) and the injection well. In many cases, the CO_2 heater is not required. In this research, the model of energy consumption by CO_2 heater and related emissions is developed as an option. The purpose of CO_2 heater is to regulate the temperature of the CO_2 to approximately 21 °C (Hovorka *et al*., 2003). Diesel fuel, natural gas, or electricity may be used as the energy source for the heater. The heater will be adjusted to regulate the discharge temperature of the CO_2 to the desired temperature. The energy consumption by the CO_2 heater can be calculated from:

$$E_{ch} = n \times Q_{well} \times SH_c \times (T_{c,o}\text{-}T_{c,i}) / \eta \quad [8.22]$$

where:

E_{ch} = the energy requirement for CO_2 heating (kJ);

η = the efficiency of the heating devices, typical value 0.8;

n = number of injection wells;

Q_{well} = CO_2 injection rate per well (kg/s);

$(T_{c,o}\text{-}T_{c,i})$ = the increase in CO_2 temperature (^oC);

$T_{c,o}$ = Temperature of CO_2 entering the CO_2 heater (^oC);

$T_{c,I}$ = Temperature of CO_2 exiting the CO_2 heater (^oC);

SH_c = specific heat of CO_2 at required injection pressure (kJ/kg ^oC). The specific heat of CO_2 under various pressures (at an average temperature of 21 ^oC) can be calculated

using the equation derived from the data provided by US National Institute of Standards and Technology (NIST):

$$SH_c = 17.14P^{-0.5275} \quad (R^2 = 0.9233) \qquad [8.23]$$

Where, P is the CO_2 pressure at the outlet of the CO_2 heater (MPa).

It is assumed that natural gas is used as energy source for CO_2 heater. The emissions from natural gas combustion are calculated by the same method provided in the CO_2 conditioning section.

8.3.2.6 Fugitive Emissions

In a similar way to the CO_2 pipeline transportation calculations, facility level emissions or equipment level emissions approach can be used to estimate the fugitive emissions from the CO_2 injection facilities. In the case of facility level approach, the adjusted emission factors presented in Table 8.10 are used. The adjusted emission factors are modified from the natural gas emission factors (IPCC, 2006). The fugitive CO_2 emissions during injection are calculated using the same equations presented in Section 8.2.2.6.

Table 8.10: Fugitive emission factors for gas transmission and storage equipment (Adjusted from Shires, 2004)

Emission source	Amount	Unit
Storage Stations	2.86E-02	tonne CO_2/station-hr
Distribution Pipelines	7.25E-05	tonne CO_2/km-hr
Gas Heaters	7.62E-05	tonne CO_2/heater-hr
Gas wellheads	2.99E-05	tonne CO_2/well-hr
Small reciprocating gas compressor (injection pumps)	3.52E-04	tonne CO_2/compressor-hr

With respect to the equipment level emissions, the same emission factors and equations used Section 8.2.2.6 can be used.

8.4 Conclusions

The LCI model developed provides a flexible framework for the calculation of energy consumption and emissions from the CO_2 pipeline transport accounting for the mass flow rate of CO_2 to be transported, the length of pipeline, inlet/outlet CO_2 pressure, and the temperature. Fugitive emissions from the CO_2 pipeline and recompression boosters can be calculated at facility level or equipment level by using modified emissions factors.

The CO_2 injection LCI model developed calculates the energy consumption and emissions from the CO_2 injection system, accounting for the CO_2 storage reservoir properties (such as permeability, reservoir depth and reservoir thickness) that determine the maximum allowable injection bottomhole pressure, the CO_2 injectivity, and the number of injection wells used. Fugitive emissions from the CO_2 injection facilities can be calculated at facility level or equipment level by using modified emissions factors.

Chapter 9 Life Cycle Impact Assessment: Post-Combustion Carbon Dioxide Capture, Transport and Injection Scenario Analysis

9.1 Introduction

This chapter presents the research findings on environmental impacts of power plants with post-combustion CO_2 capture, transport and injection. The LCI models, which are developed and described in previous Chapters, have been coded as Microsoft Excel spreadsheets. By choosing different LCI models and linking them together, the LCI models of power plants with alternative post-combustion CCS options can be configured. In this Chapter, the LCI model of a 500 MW power plant with post-combustion capture with MEA, transport and injection is used to demonstrate the capabilities of the models developed (Figure 9.1). The model presented here not only computes the emissions from the system constructed and the corresponding LCA environmental impacts, but also evaluates the importance of technical, operational and geographical differences through the sensitivity analysis provided. This task is carried out by evaluating the importance of different scenario choices against base case scenario for post-combustion power generation with CO_2 capture, transport and injection. Finally, the importance of uncertainty and variability in the input parameters for each component unit process are evaluated through an uncertainty analysis using the LCI model input data parameters listed in Table E.1 in Appendix E and the post-combustion base case scenario.

Table 9.1 presents the main characteristics of the post-combustion base case scenario in terms of technology used for the complete power generation, CO_2 capture, transport and injection process, the operational conditions and the geographical setting in relation to fuel used, distance to the storage site and the depth of the storage formation used as an example to illustrate the capability of the model developed.

Table 9.1: Description of base case scenario for power generation with post-combustion CO_2 capture, conditioning, transport and injection.

Base case scenario:	A 500MW power plant with post-combustion CO_2 capture, conditioning, transport and injection
Boiler type	PC wall fired, dry bottom
Chemical absorption CO_2 capture technology	MEA
Power plant gross energy efficiency (%)	45%
CO_2 capture energy consumption (MW/500 MW electricity generated)	105.5
SOx removal rate	95%
NOx removal rate (NH_3 to NO ratio)	0.8
CO_2 capture rate	95%
Coal type	US Appalachian (bituminous)
Compression pressure (MPa)	13.8
Pipeline distance (Km)	300
Storage formation depth (m)	1,000

The US Appalachian low sulphur bituminous coal, which represents a typical bituminous coal, is used as an example in the base case presented. The chemical composition of the US Appalachian coal is described in Table E.2 in Appendix E. The LCI data for the upstream processes shown in Figure 9.1 are either taken from the literature or calculated by the GaBi LCA software and are described in Appendix D. Since the estimation of potential CO_2 leakages from a CO_2 storage formation involves a great deal of uncertainty, CO_2 leakage is not included in the results presented here, rather, CO_2 storage is modelled and analysed separately in Chapter 11. The power generation scenario with post-combustion capture, transport and injection presented in this chapter demonstrates the following aspects and capabilities of the model developed in this research:

- direct emissions, resource consumption, material consumption and energy efficiency;
- life cycle environmental impacts;
- sensitivity analysis, which is used to evaluate effect of the post-combustion capture,

transport and injection scenario choice on the life cycle environmental impact;

- uncertainty analysis, which is used to evaluate the effect of LCI input data and model parameter uncertainty on emission/resource consumption estimates and the life cycle environmental impact.

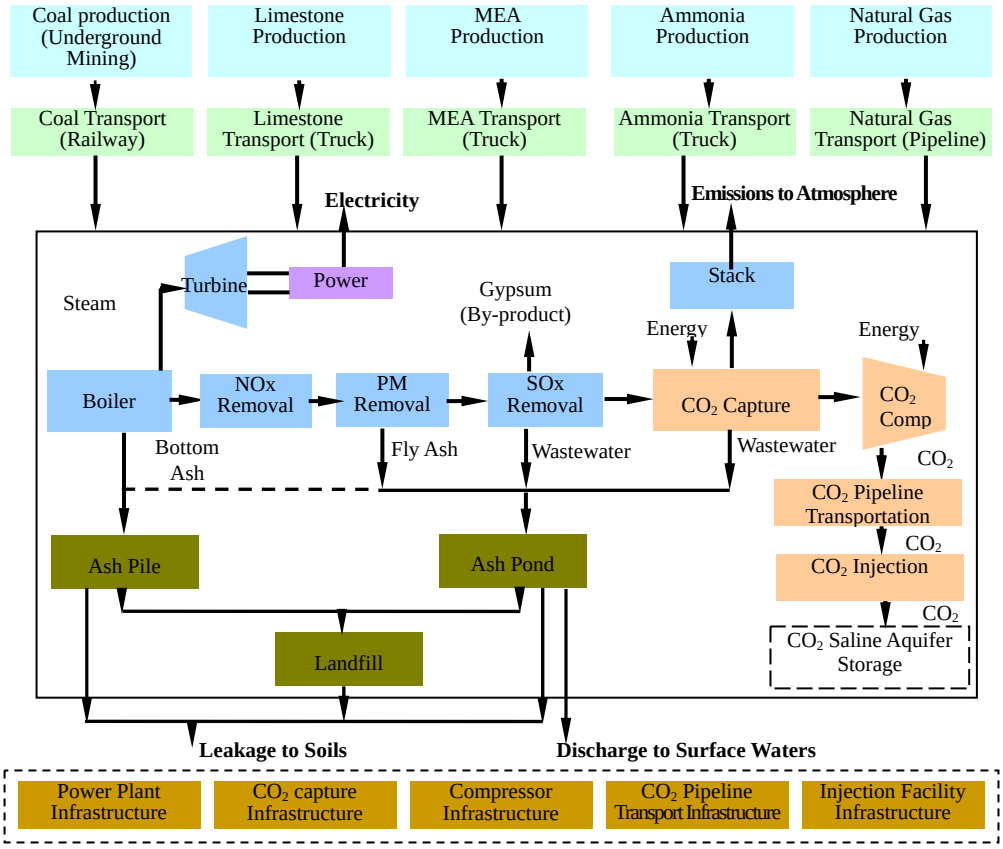

Figure 9.1: The component LCI models of a 500 MW power plant with post-combustion capture, transport and injection discussed in this Chapter.

9.2 Resource Consumption and Direct Emissions

Table E3 in Appendix E presents the consumption of resources/materials and resulting direct emissions (per 1 MWh of electricity generated) by each component unit process for the 500 MW capacity power plant with post-combustion CO_2 capture, transport and injection. The summary of these emissions are provided in Table 9.2. The results demonstrate that most air emissions come from power plant stack, and emissions to soil come from solid waste disposal units. Almost all emissions are originally generated by the coal combustion process. Direct emissions from the SCR, ESP, FGD, CO_2 capture, CO_2 conditioning, CO_2 pipeline transport and the CO_2 injection unit are not significant. There

are no direct solid and liquid emissions from the SCR ESP, FGD and the CO_2 capture unit, as this research assumes that all the solid and liquid wastes from the power plant are well managed and transferred to ash pond and eventually transported to landfill. From Table E3, one can see that the potential leakages from the ash pond (surface impoundment(s)) and the ash landfill results in trace metal emissions to soils. Resource consumption is dominated by coal. The consumption of other resources and materials, including natural gas, limestone and ammonia, are significantly less than that of coal.

Table 9.2: Summary of direct emissions and the consumption of resources/materials in power generation (500 MW) with post-combustion (MEA) CO_2 capture, transport and injection (per 1 MWh electricity generated).

Resources required/Sources of impacts	Amount (kg)	Emissions to Air	Amount (kg)	Trace metal emissions to air	Amount (kg)	Trace metal emissions to soils	Amount (kg)
Coal	347.89	CO_2	48.96	Antimony (Sb)	6.65E-08	Antimony (Sb)	3.65E-08
Natural gas	1.63	PM	0.0047	Arsenic (As)	3.02E-05	Arsenic (As)	2.77E-06
Limestone	6.61	PM-10	0.0046	Beryllium (Be)	1.62E-06	Beryllium (Be)	7.08E-08
Ammonia	0.93	SO_2	0.0010	Cadmium (Cd)	6.39E-07	Cadmium (Cd)	1.89E-08
MEA	2.04	SO_3	0	Chromium (Cr)	2.75E-06	Chromium (Cr)	1.25E-07
Energy consumption equivalence (kwh)	351.79	NO	0.4580	Cobalt (Co)	2.33E-07	Cobalt (Co)	1.82E-07
Solid wastes	34.77	NO_2	0.0181	Lead (Pb)	6.56E-06	Lead (Pb)	1.94E-06
Liquid wastes	2.11	N_2O	0.0052	Manganese (Mn)	1.88E-06	Manganese (Mn)	2.55E-06
		CO	0.0870	Nickel (Ni)	1.37E-06	Nickel (Ni)	4.29E-07
		HCl	1.04E-04	Selenium (Se)	1.97E-05	Selenium (Se)	7.81E-06
		HF	3.92E-05	Zinc (Zn)	3.58E-05	Zinc (Zn)	6.03E-06
		CH_4	0.0070	Copper (Cu)	1.29E-05	Copper (Cu)	4.17E-07
		NH_3	0.1230	Thallium (Tl)	2.78E-07	Thallium (Tl)	3.63E-08
		MEA	0.0119	Vanadium (V)	8.92E-06	Vanadium (V)	3.02E-05
				Barium (Ba)	8.63E-05	Barium (Ba)	5.17E-06
				Silver (Ag)	2.78E-08	Silver (Ag)	3.63E-09
				Hg0	1.12E-07	Mercury (Hg)	1.62E-09
				Hg++	1.25E-06		
				Hg particulate	0.00E+00		

9.2.1 The Fate of Air Emissions

In power generation with post-combustion CCS, the air emissions of concern include CO_2, PM-10, SO_2, SO_3, NO, NO_2, HCl, HF and mercury (Hg) vapour. These air emissions are originally generated by the coal combustion process and then totally or partially removed by the pollution control units such as SCR, ESP, FGD and the CO_2 capture unit. The LCI models developed successfully quantify the removal rate of air emissions of concern throughout the flue gas treatment processes, with the knowledge that these pollution control

units have impacts on each other and one pollution control unit could affect more than one type of emissions. Figure 9.2 demonstrates that 95% of the CO_2 is removed by the CO_2 capture unit and CO_2 is not affected by other pollution control units. 99.7% of PM-10 is removed by the ESP and PM-10 is further removed by FGD, CO_2 capture unit, with final emission rate at 0.11%. Around 95% of SO_2 is removed by FGD and is further removed by the CO_2 capture unit (MEA), with final emission rate at 0.02%. The SO_3 emissions can be removed by the SCR, ESP and FGD and finally totally removed by the CO_2 capture unit (MEA). The NO emissions can only be reduced by the SCR and with final emission rate at 23.08%. The NO_2 emissions can be reduced by the SCR and CO_2 capture unit (MEA), with final emission rate at 17.31%. The HCl and HF emissions can be reduced by the FGD and CO_2 capture unit (MEA), with final emission rate at 0.05% and 0.15% respectively. Mercury vapour can be reduced by ESP, FGD and CO_2 capture unit (MEA), with final emission rate at 1.97%. The CO emissions remain unchanged across the pollution control units.

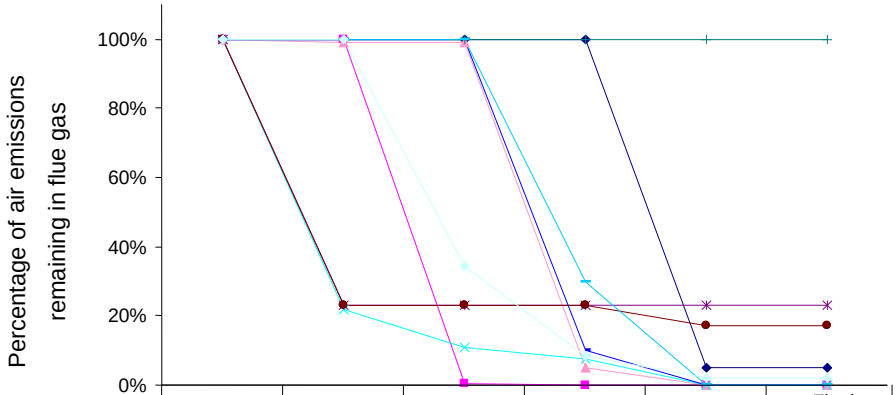

	Combustion	SCR	ESP	FGD	CO_2 capture	Final emissions to air
CO_2	100.00%	100.00%	100.00%	100.00%	5.00%	5.00%
PM-10	100.00%	100.00%	0.30%	0.14%	0.11%	0.11%
SO_2	100.00%	99.19%	99.19%	4.96%	0.02%	0.02%
SO_3	100.00%	21.71%	11.07%	7.60%	0	0
NO	100.00%	23.08%	23.08%	23.08%	23.08%	23.08%
NO_2	100.00%	23.08%	23.08%	23.08%	17.31%	17.31%
CO	100.00%	100.00%	100.00%	100.00%	100.00%	100.00%
HCl	100.00%	100.00%	100.00%	10.00%	0.05%	0.05%
HF	100.00%	100.00%	100.00%	30.00%	0.15%	0.15%
Hg	100.00%	100.00%	34.39%	8.22%	1.97%	1.97%

Figure 9.2: The fate of air emissions across the pollution control units in a 500 MW power plant with CO_2 capture.

9.2.2 Partitioning of Trace Metals

Trace metals originate from coal. After coal combustion, the trace metals are partitioned and released to the environment through different routes: with air emissions, MEA capture solid wastes, FGD wastes, gypsum, fly ash or bottom ash. The LCI models developed successfully calculate the partitioning of 17 trace metals across the flue gas treatment chain in a power plant with CO_2 capture.

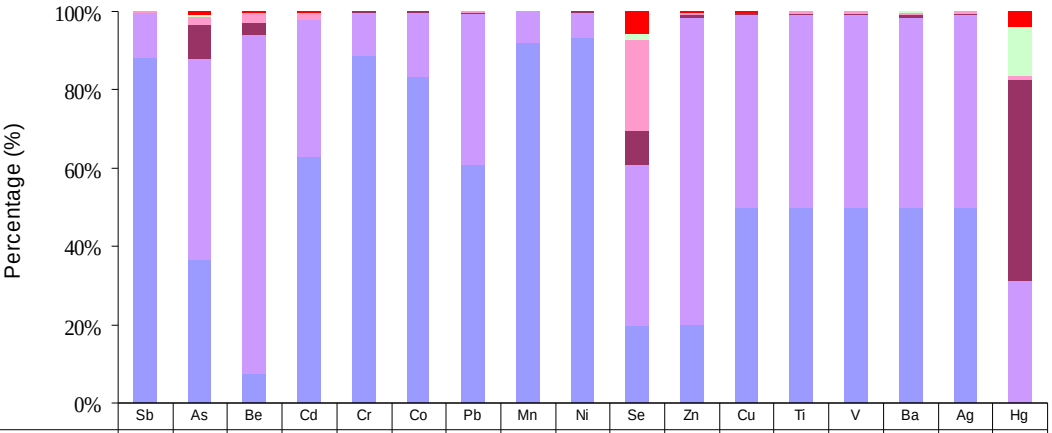

	Sb	As	Be	Cd	Cr	Co	Pb	Mn	Ni	Se	Zn	Cu	Ti	V	Ba	Ag	Hg
Emissions to air	0.02%	0.87%	0.23%	0.35%	0.04%	0.01%	0.05%	0.01%	0.02%	5.66%	0.20%	0.25%	0.08%	0.06%	0.12%	0.08%	3.95%
MEA capture solid wastes	0.005%	0.217%	0.058%	0.087%	0.010%	0.003%	0.012%	0.002%	0.005%	1.414%	0.051%	0.062%	0.020%	0.016%	0.031%	0.020%	12.516
FGD wastes	0.18%	2.20%	2.77%	1.58%	0.08%	0.08%	0.26%	0.06%	0.07%	23.51%	0.67%	0.10%	0.45%	0.46%	0.70%	0.45%	1.05%
To Gypsum	0.03%	8.79%	2.77%	0.17%	0.28%	0.08%	0.26%	0.06%	0.07%	8.70%	0.67%	0.59%	0.45%	0.46%	0.70%	0.45%	51.40%
Fly ash	11.71%	51.46%	86.74%	34.82%	10.97%	16.51%	38.64%	7.95%	6.79%	40.72%	78.40%	49.00%	49.00%	49.00%	48.45%	49.00%	31.08%
Bottom ash	88.05%	36.47%	7.43%	62.99%	88.62%	83.32%	60.77%	91.91%	93.03%	20.00%	20.00%	50.00%	50.00%	50.00%	50.00%	50.00%	0.00%

Figure 9.3: Partitioning of trace metals across the pollution control units in a 500 MW power plant with CO_2 capture.

Figure 9.3 demonstrates that the majority of Antimony (Sb), Cadmium (Cd), Chromium (Cr), Cobalt (Co), Lead (Pb), Manganese (Mn), Nickel (Ni), Copper (Cu), Thallium (Tl), Vanadium (V), Barium (Ba) and Silver (Ag) emissions show up in bottom ash, because most of them are Group I metals described in section 5.2.2.6, which do not volatilise during combustion and distribute more or less equally over bottom ashes and fly ashes. Majority of the Arsenic (As), Beryllium (Be), and Zinc (Zn) go with fly ash, because most of them belong to Group II metals, which are vaporised during combustion and are mainly in the fly ashes after combustion. Mercury (Hg) and Selenium (Se) fall in Group III metals, which are volatilised during combustion and leave combustion unit is a vapour phase. It is worth noting that 3.95% of mercury is emitted to atmosphere in vapour form. Around 51.40% of mercury goes with gypsum as the by-product of the FGD process, 12.52% of it shows in the MEA capture solid wastes and 31.08% is in the fly ash. The scattering of mercury

emissions across the pollution control chain increases the difficulty to mitigate the environmental impacts of mercury emissions.

9.2.3 Percentage of Trace Metals Finally Released to the Environment

Trace metals originally in coal can be released to environment directly from the power plant (trace metal emissions to air) or through leakage from the surface impoundments and landfill sites (trace metal emissions to soil). The percentage of each trace metal finally released to the environment (compared to their original concentration in coal) is provided in Figure 9.4, which shows that for most trace metals less than 0.5% is emitted to the environment, except for As, Se and Hg. Since the majority of As and all of Hg and Se are in vapour form during combustion, they have higher percentages of emissions. The emissions of trace metals to the environment are dominated by the emissions to air from the power plant and emissions to soil from the surface impoundments. The emissions from landfill are not very significant. It is worth noting that the landfill emission results are based on the landfill LCI model with a 1,000-year time frame and assuming that the composite liner of the landfill has a life span of 200 years, and at end of each 200 years the old composite liner is replaced by a new one. If a new composite liner is not used to replace the old one at the end of 200 years, the landfill is treated as a clay layer landfill for the rest of 800 years. Figure 9.5 shows the results of this scenario (200 years with a composite liner and 800 years with clay liner) and concludes that, even in this scenario, the emissions from landfill are still less than the emissions from the surface impoundment and the emissions to air from the power plant in a 1,000-year time period. Therefore, it can be concluded that landfill is an effective treatment to prevent the emissions of trace metals.

Higher percentages of Selenium (Se) and Mercury (Hg) are released to air, as these are Group III metals which are in vapour form after combustion and the ESP and FGD are ineffective to remove them from the flue gas. Higher percentages of Arsenic (As), Beryllium (Be) and Zinc (Zn) are released to air, as they are Group II metals and are mainly distributed in the fly ashes after combustion. These are difficult to be captured by pollution control units. Higher percentages of Cadmium (Cd) and Copper (Cu) are emitted to air, since they are removed by the FGD unit at lower rates. The higher percentages of Selenium (Se) and Vanadium (V) released to soil from the surface impoundments and from landfill due to their lower waste-concentration-to-leachate-concentration ratios.

The results obtained in this research suggest that a reduction in the emissions of trace metals from a power plant, especially the emissions of volatile trace metals such as As, Se and Hg, can significantly reduce the life-cycle trace metal emissions.

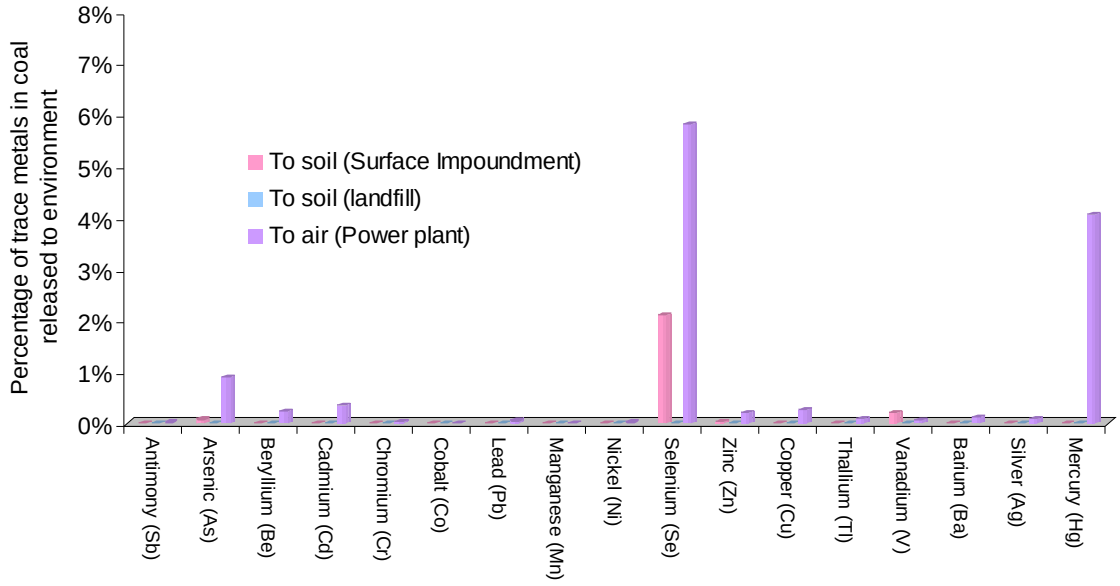

Figure 9.4: Percentage of trace metals released to the environment compared to their original concentration in coal (composite liner over 1,000 years).

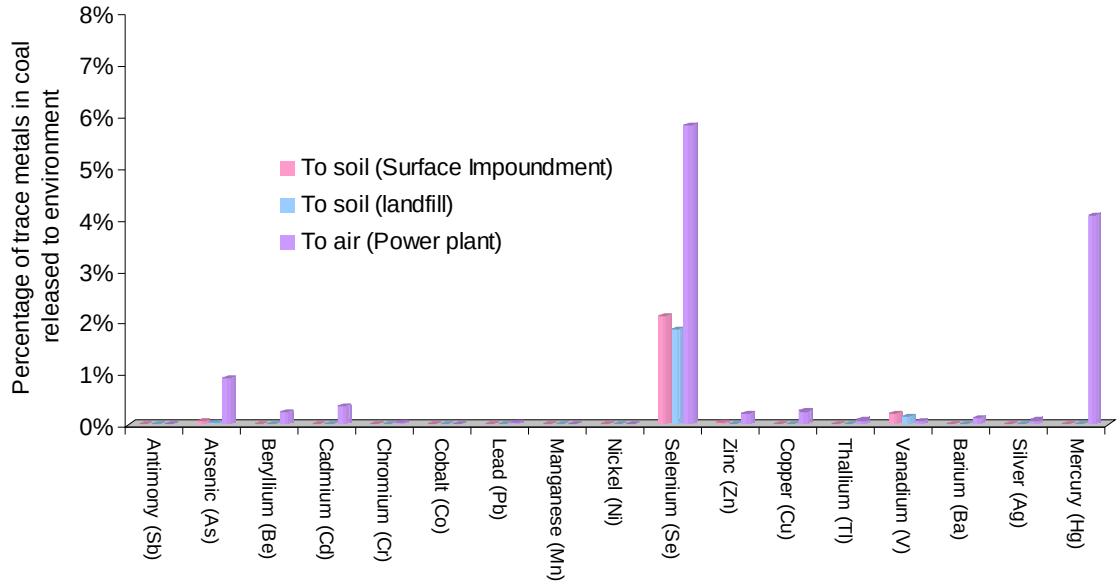

Figure 9.5: Percentage of trace metals released to the environment compared to their original concentration in coal (composite liner for 200 years and clay liner for 800 years).

9.2.4 Energy Efficiency of Power Plants with Carbon Dioxide Capture and Conditioning

Figure 9.6 presents the energy flow of a 500 MW power plant with post-combustion CO_2 capture. It can be seen that the power plant with a gross efficiency of 45% can achieve a net efficiency of 34.04% after CO_2 capture and conditioning. The CO_2 capture and conditioning processes consume 7.18% and 2.89% of the coal energy input respectively. Auxiliary energy consumption, which represents the energy used by SCR, ESP, FGD, is insignificant, with 0.89% of the coal energy input.

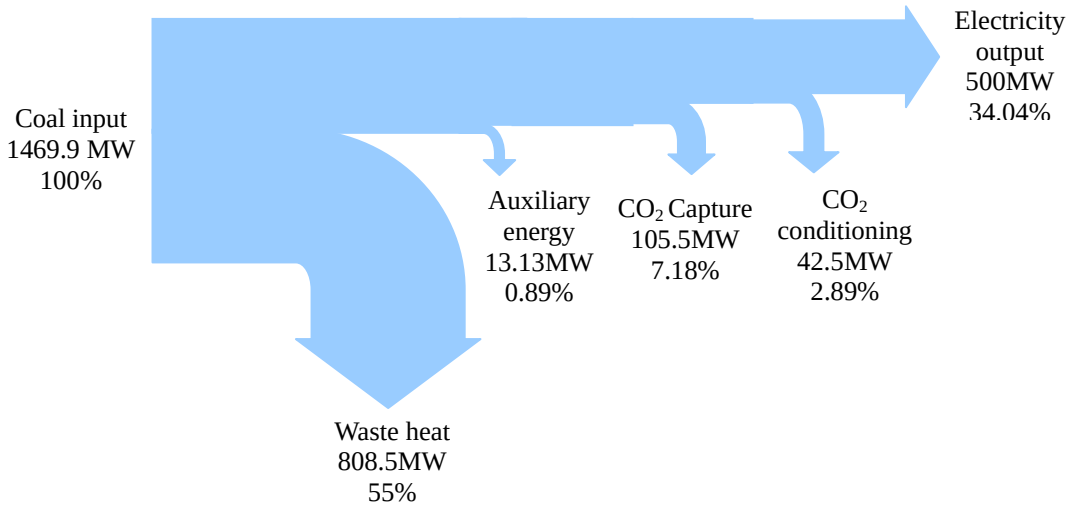

Figure 9.6: Energy flow chart for a 500 MW power plant with post-combustion CO_2 capture and conditioning.

9.3 Life Cycle Environmental Impacts of Power Generation with Post-combustion Carbon Dioxide Capture, Transport and Injection

9.3.1 The Overall Life Cycle Impact Assessment Results

Table E.4 in Appendix E presents the emissions from a the base case 500 MW power plant scenario with post-combustion capture, transport and injection as well as the upstream processes, including coal production, coal transportation, limestone production, limestone transport by truck, MEA production, MEA transport by truck, ammonia production, ammonia transport by truck, power plant infrastructure, CO_2 pipeline infrastructure, CO_2 capture facility infrastructure, and compressor infrastructure. Figure 9.7 illustrates that life-cycle environmental impacts of the post-combustion CO_2 capture and storage system are

dominated by power generation with CO_2 capture and coal production process in all impact categories (except for Human Toxicity Potential (HTP)). The results also reveal that MEA production is the main contributor to HTP and has considerable contribution to the impact categories ADP, AP, EP, FAETP and GWP 100 in a life-cycle perspective. The coal railway transport process has considerable contribution to ADP and TETP. A more detailed analysis of each individual impact category is provided in the following sections.

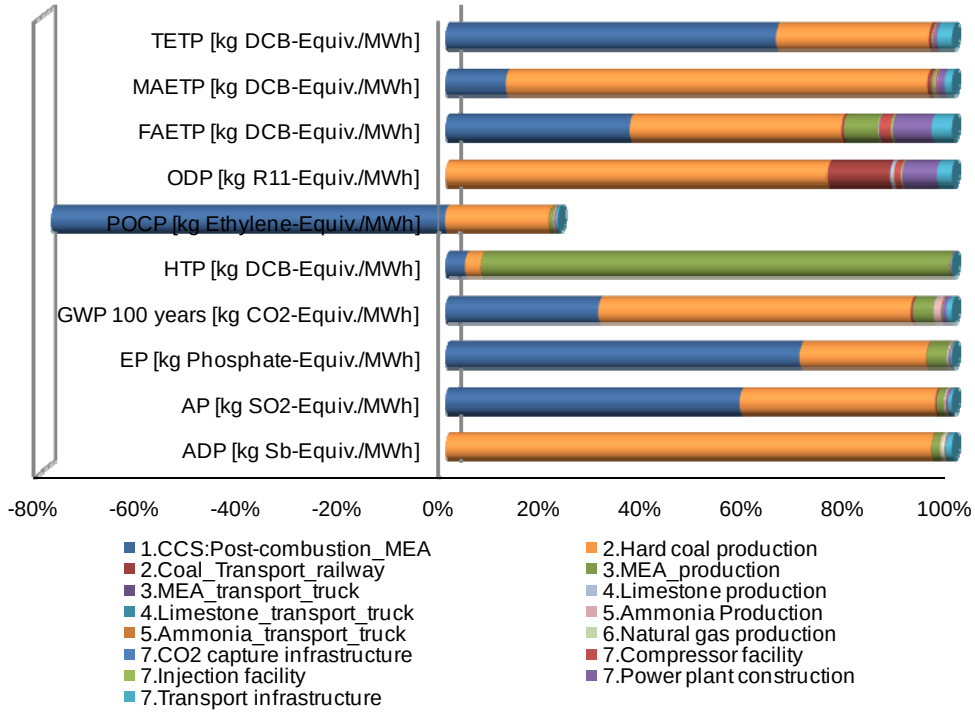

Figure 9.7: Life cycle impact results for the base case 500 MW coal fired power plant with post-combustion capture, transport and injection.

In every environmental impact category, the resultant impact is dominated by several key substances. The contribution of power generation with CO_2 capture to the environmental impact categories AP, EP, GWP100, HTP and POCP is due to its air emissions. On the other hand, its contribution to the environmental impact categories FAETP, MAETP and TETP is due to trace metal emissions to air or soils.

9.3.2 Life Cycle Environmental Impacts per Impact Category

Figure 9.8 illustrates that the total GWP of the 500 MW power generation scenario with capture, transport and injection is 167.121 kg CO_2 equivalent. The majority of this impact

is from hard coal production with 61.71% of the GWP. Other upstream processes including MEA production, Ammonia production, power plant construction, and transport infrastructure account for 3.90%, 1.38%, 0.87% and 0.82% of the GWP respectively. Emissions from power generation with capture, transport and injection make up 30.32% of the GWP. Figure 9.8 also shows that CO_2, methane and nitrous oxide are the main emissions contributing to GWP. Carbon dioxide emissions (95.50 kg) mainly come from power generation with CO_2 capture (48.96 kg), hard coal production (34.72 kg), and MEA production (5.66 kg). Methane emissions (69.30 kg CO_2 equiv) are mainly due to coal production, which accounts for 97.76% of the total methane emissions.

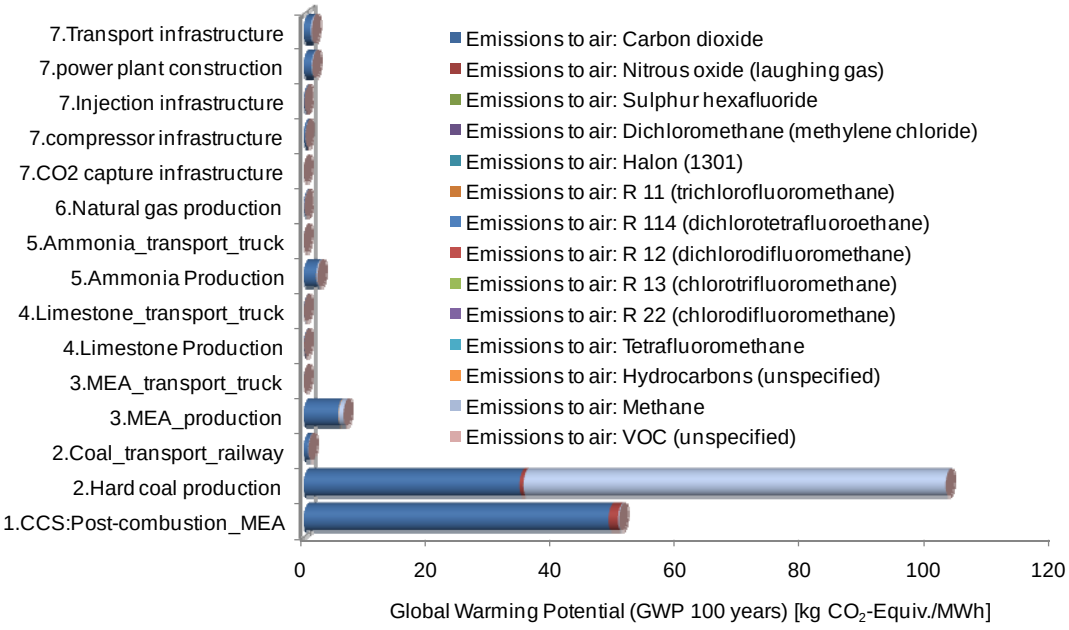

Figure 9.8: Global warming potential for the base case 500 MW coal fired power plant with post-combustion capture, transport and injection.

Figure 9.9 shows that the life cycle Abiotic resource Depletion Potential (ADP) is dominated by coal production, which alone accounts for 96.02%. MEA production, natural gas production, ammonia production and transport infrastructure have considerable contribution towards ADP, with 1.70%, 0.61% and 0.35% of ADP respectively. With respect to individual substances contributing to the ADP, hard coal extracted by during mining is the primary contributor, accounting for 91.19% of ADP. Natural gas and crude oil used during coal production process also have a considerable contribution towards ADP,

with 2.26% and 2.34% of ADP respectively. Other substances consumed by other processes have insignificant impacts on ADP.

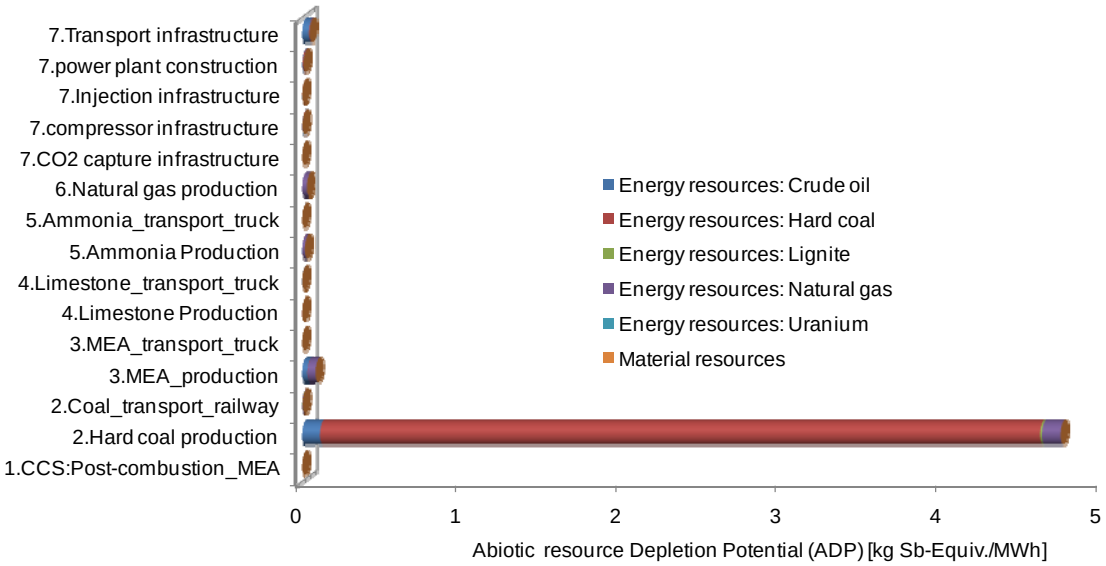

Figure 9.9: Abiotic resource depletion potential for a 500 MW coal fired power plant with post-combustion capture, transport and injection.

Figure 9.10 illustrates that Acidification Potential (AP) is mainly due to power generation with CO_2 capture and coal production, which account for 58.13% and 38.72% respectively. MEA production accounts for 1.48% and the other processes contribute to AP by less than 0.5%. Figure 9.10 also indicates that emissions to air (including NO, NO_2, NO_x, SO_2 and NH_3) and emissions to fresh water (HCl, HF and H_2SO_4) are the main contributors to AP. NOx and SO_2 are primarily emitted by coal production. NO, NO_2 and NH_3 emissions are mainly from power generation with CO_2 capture. More specifically, the NH_3 emissions are from the capture process using MEA.

Figure 9.11 shows that Eutrophication Potential (EP) is mainly due to power generation with CO_2 capture, hard coal production and MEA production, with 69.93%, 25.07% and 4.09% of EP respectively. Analysis of the life cycle impact data shows that emissions to air, emissions to fresh water, emissions to soils and emissions to sea water account for 97.48%, 2.40%, 0.12% and 0.01% of the EP respectively. NO, NOx, NH_3 and NO_2 are the principle air emissions, accounting for 47.27%, 25.26%, 23.02% and 1.93% of the EP. Power generation with CO_2 capture is the main source of NO, NO_2 NH_3 emissions. NOx is primarily emitted by the coal production process. Emissions to fresh water, including

nitrate, total organic bounded carbon and Chemical Oxygen Demand (COD) are from the MEA production processes.

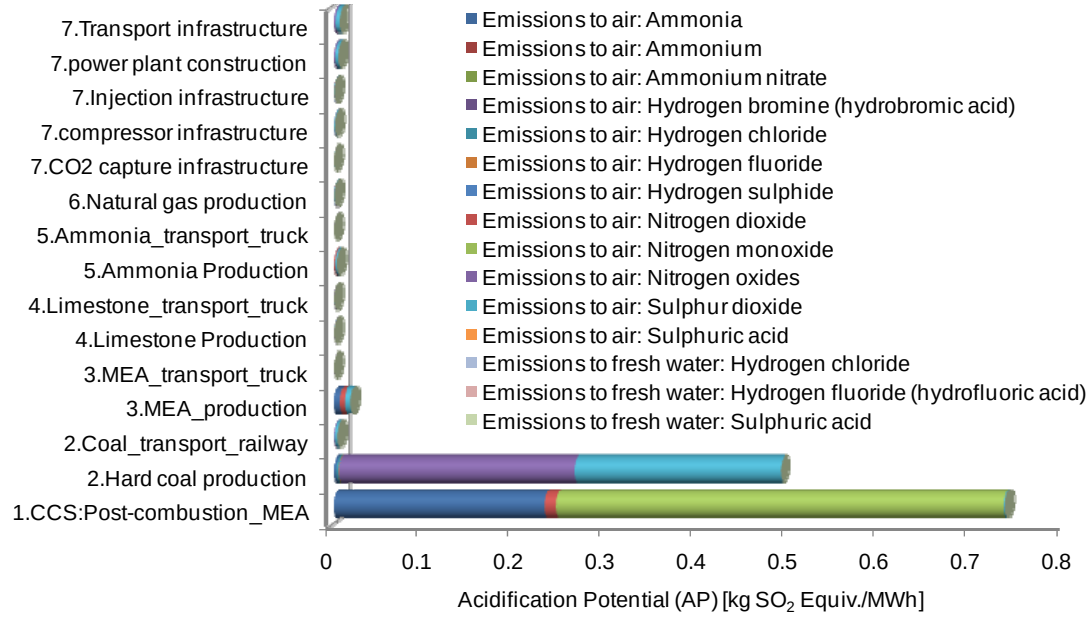

Figure 9.10: Acidification potential for a 500 MW coal fired power plant with post-combustion capture, transport and injection.

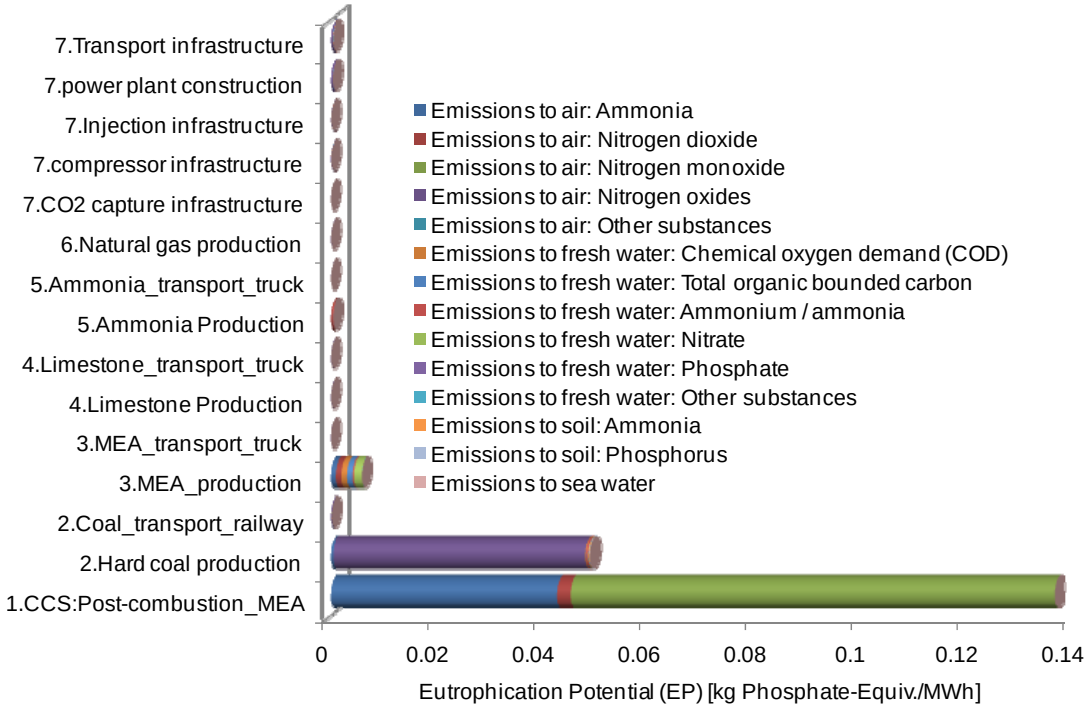

Figure 9.11: Eutrophication potential for a 500 MW coal fired power plant with post-combustion capture, transport and injection.

The Ozone layer Depletion Potential (ODP) of power generation with post-combustion CO_2 capture, transport and injection is mainly due to the upstream processes, including hard coal production, transport of coal by railway, power plant infrastructure and CO_2 pipeline infrastructure, which account for 75.47%, 12.36%, 6.91% and 2.78% of ODP respectively. Figure 9.12 shows that only five substances, Halon, R11, R 114, R12 and R22, contribute to ODP and are all air emissions. Emissions of R11, R 114, R12 and R22 come mainly from hard coal production and transport of coal by railway. Emissions of Halon are primarily from the power plant infrastructure.

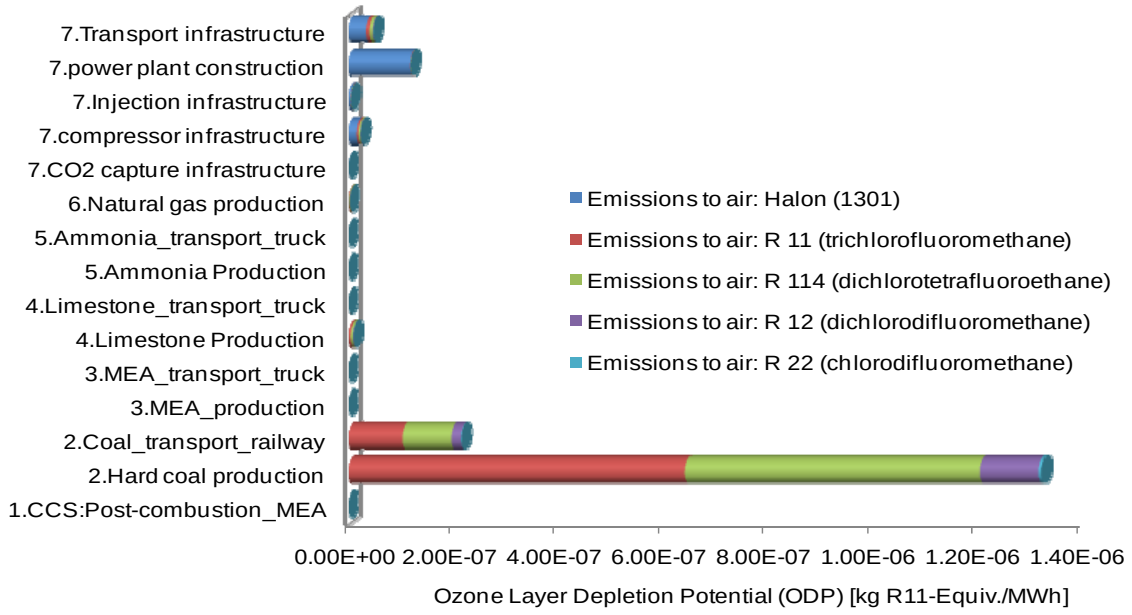

Figure 9.12: Ozone layer depletion potential for a 500 MW coal fired power plant with post-combustion capture, transport and injection.

Figure 9.13 shows that, in the 500 MW base case scenario, the Photochemical Ozone Creation Potential (POCP) is mainly due to power generation with CO_2 capture and hard coal production. The overall value of the POCP is negative as the emissions of nitrogen monoxide from power generation and capture has a negative impact on POCP, with a characterisation factor of -0.427 kg Ethane equivalent (CML 2001). Figure 9.13 also illustrates that emissions of methane, NMVOC (non-methane volatile organic compounds), sulphur dioxide, carbon monoxide and nitrogen oxides to air from hard coal production and the emission of carbon monoxide from power generation with capture to air have a considerable contribution to POCP.

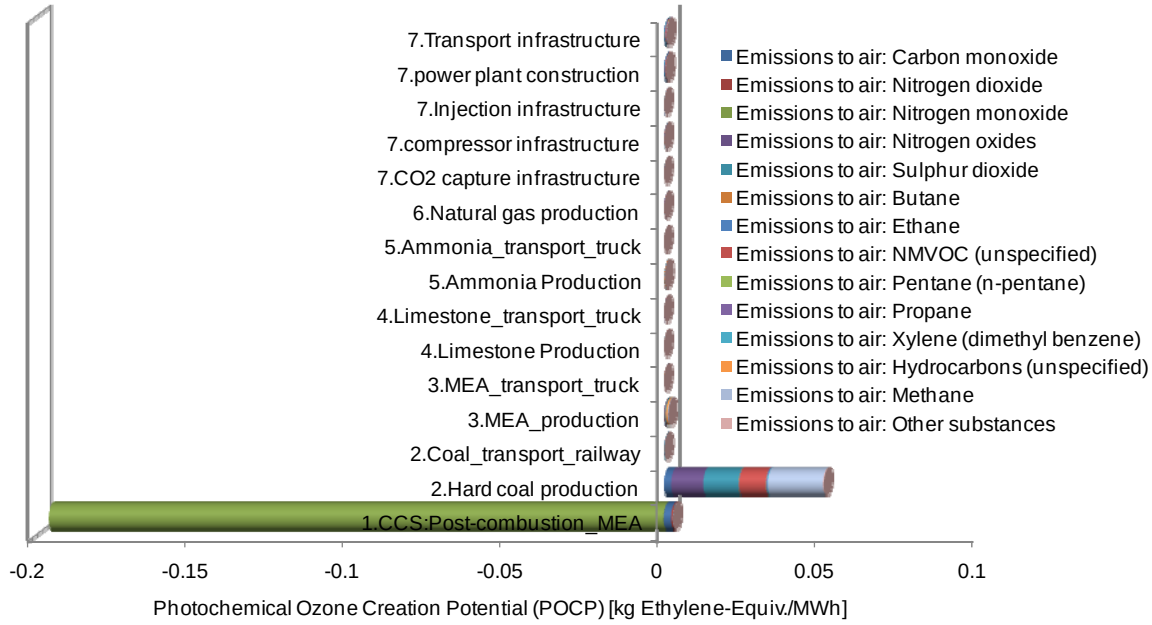

Figure 9.13: Photocemical ozone creation potential for a 500 MW coal fired power plant with post-combustion capture, transport and injection.

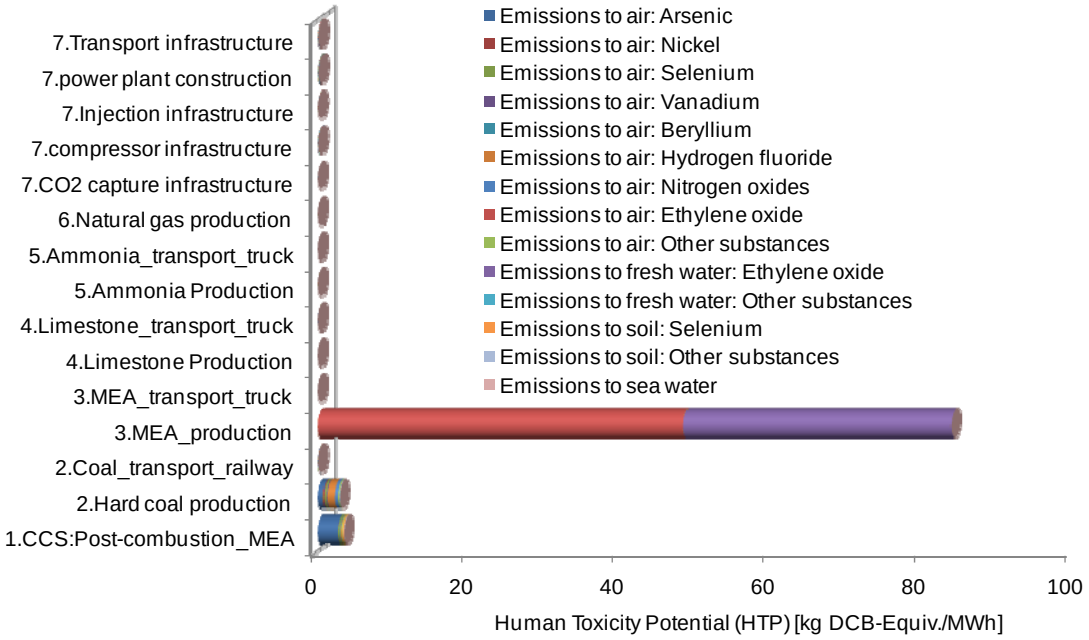

Figure 9.14: Human toxicity potential for a 500 MW coal fired power plant with post-combustion capture, transport and injection.

As shown in Figure 9.14, at 92.50%, MEA production is the main contributor to HTP. Power generation and hard coal production also make some contribution to HTP, with 3.87% and 3.23% respectively. The analysis of the life cycle impact data indicate that

ethylene oxide emissions to air and to freshwater, exclusively from MEA production, dominate the HTP, accounting for 53.39% and 39.09% respectively. Emissions to air of arsenic, selenium, hydrogen fluoride and nitrogen oxides account for 3.67%, 0.57%, 1.29%, and 0.50% of the HTP respectively. Arsenic emissions are mainly from power generation with capture. Emissions of selenium, hydrogen fluoride, and nitrogen oxides are from hard coal production.

Figure 9.15 shows that the upstream processes such as hard coal production, MEA production, power plant infrastructure, pipeline transport infrastructure, compressor infrastructure account for the majority of Freshwater Aquatic Ecotoxicity Potential (FAETP) at 41.81%, 6.82%, 7.74%, 3.90%, and 2.17% respectively. Power generation with capture accounts for 36.50% of the FAETP.

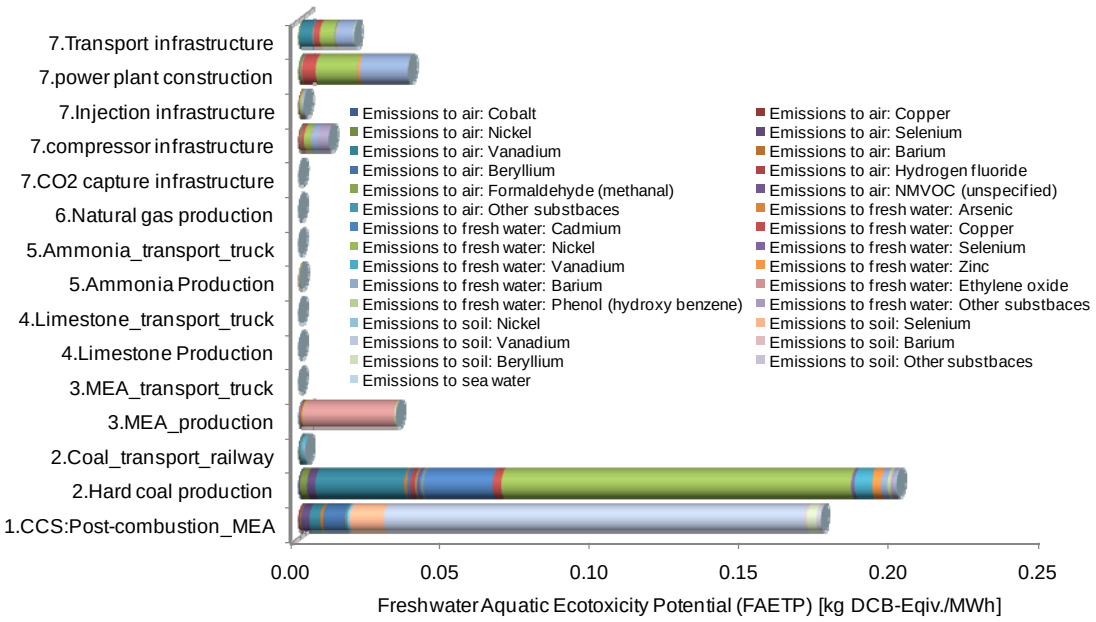

Figure 9.15: Freshwater aquatic ectoxicity potential for a 500 MW coal fired power plant with post-combustion capture, transport and injection.

Figure 9.15 shows that FAETP is mainly due to metal emissions, including metal emissions to fresh water, soils and air. With respect to emissions to fresh water, nickel, barium, cadmium, copper, vanadium and zinc are the main contributors, which account for 29.00%, 5.66%, 4.91%, 2.60%, 1.46%, and 0.96% of the FAETP respectively. Nickel, cadmium, vanadium and zinc emissions to fresh water are mainly from hard coal production. The majority of barium and copper emissions to fresh water are from power generation with

capture. As for the emissions to soils, FAETP is dominated by vanadium, selenium and beryllium emissions from power generation with capture at 29.41%, 2.39% and 0.68% of the FAETP respectively. With respect to metal emissions to air, vanadium, beryllium, selenium, nickel and barium are the main contributors, accounting for 8.02%, 1.74%, 1.23%, 0.81% and 0.44% of the FAETP. Majority of vanadium, selenium, barium and nickel come from coal production and power generation. Beryllium is mainly emitted by power generation. The ethylene oxide emissions to fresh water are, exclusively from the MEA production and account for 6.35% of the FAETP.

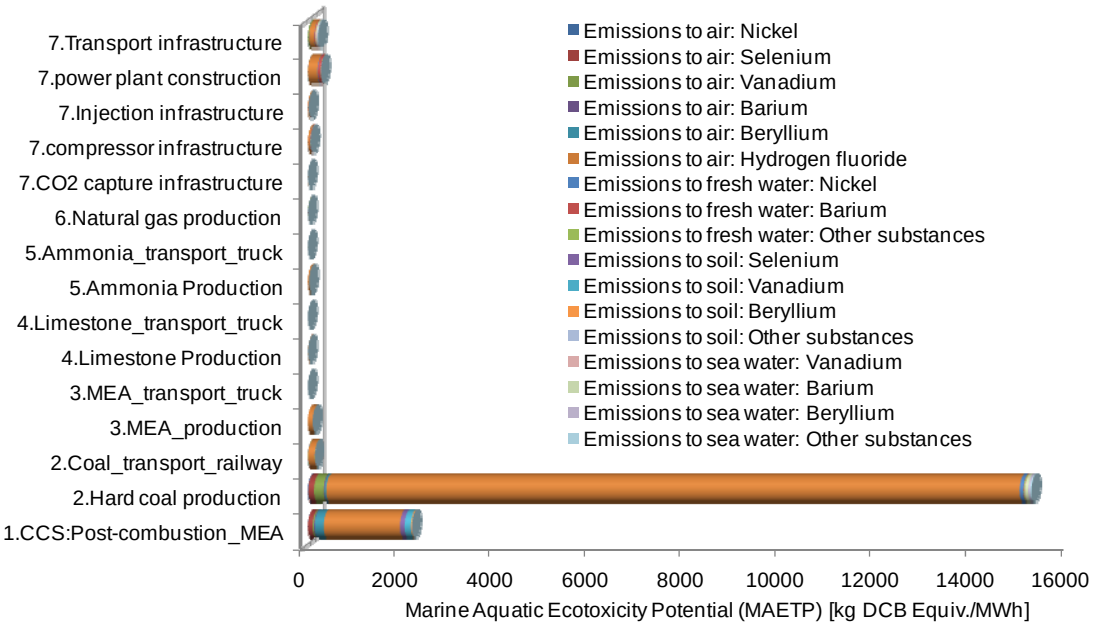

Figure 9.16: Marine aquatic ecotoxicity potential for a 500 MW coal fired power plant with post-combustion capture, transport and injection.

Figure 9.16 shows that Marine Ecotoxicity Potential (MAETP) is mainly due to hard coal production and power generation with capture, which account for 83.19% and 12.03% of the MAETP respectively. Pipeline transport infrastructure, power plant infrastructure, transport of coal by railway, and MEA production have some contribution to the MAETP at 1.54%, 1.20%, 0.83% and 0.57% respectively. At 91.82% of MAETP, hydrogen fluoride (HF) emissions to air originate from hard coal production and power generation with capture, which account for 86.68% and 9.49% of the HF emissions respectively. Emissions of selenium, vanadium and beryllium to air; nickel and barium to fresh water; selenium and vanadium to soils; and barium to sea water also contribute to MAETP, accounting for 1.26%, 1.48%, 1.25%, 0.53%, 0.54%, 0.54%, 0.74% and 0.44% of the MAETP

respectively. Emissions of vanadium to air, nickel to fresh water, barium and beryllium to sea water are mainly from hard coal production. Emissions of beryllium to air, selenium and vanadium to soils originate from power generation with capture. Emissions of selenium to air are mainly from hard coal production (55%) and power generation with capture (40%).

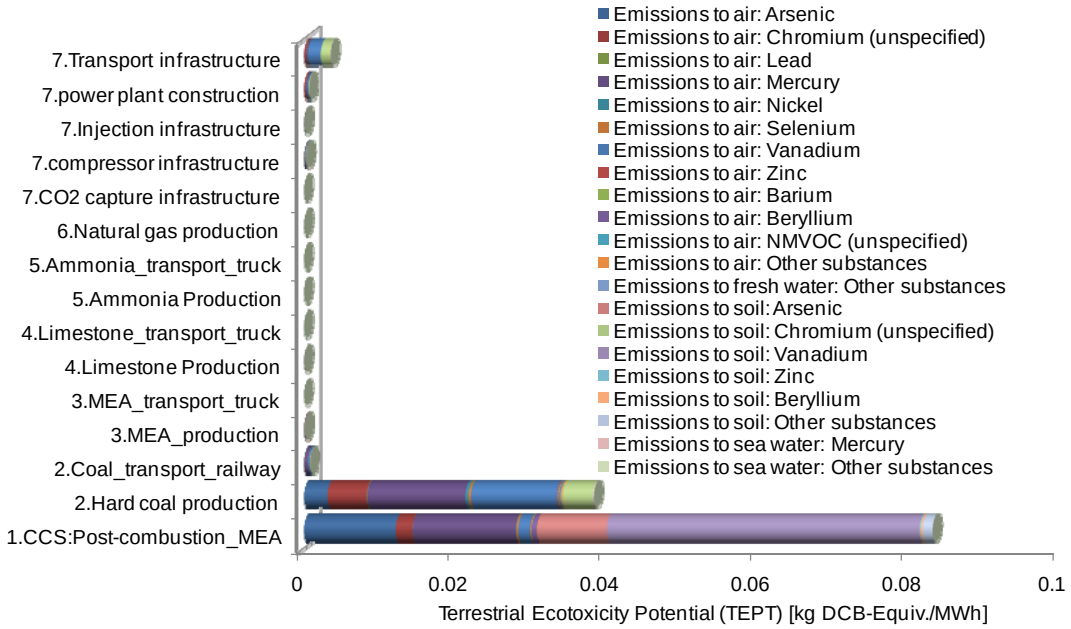

Figure 9.17: Terrestrial ecotoxicity potential for a 500 MW coal fired power plant with post-combustion capture, transport and injection.

Figure 9.17 shows that Terrestrial Ecotoxicity Potential (TETP) is primarily due to power generation with CO_2 capture and hard coal production, at 64.94% and 29.98% of the TETP respectively. Pipeline transport infrastructure, power plant infrastructure, and transport of coal by railway also make a contribution to TETP, representing 2.74%, 0.56% and 0.65% respectively. Detailed analysis of the life cycle impact results reveal that TETP is mainly caused by the emissions of metals to air and to soils. In particular, the emissions of vanadium and arsenic to soils from power generation with capture make up 32.28% and 7.20% of the TETP respectively. Emissions of Mercury, Arsenic, Vanadium and Chromium to air from the plant also have a significant contribution, accounting for 10.67%, 9.51%, 1.18% and 1.70% of the TETP. Emissions of Mercury, Vanadium, Chromium, and Arsenic to air from hard coal production also contribute to the TETP, representing 10.15%, 8.78%, 4.13% and 2.41% of the TETP. Emissions of vanadium to air and chromium to soils from

the pipeline transport infrastructure also contribute to the TETP at 1.22% and 0.97%. The TETP results reveal that the trace metal emissions from power generation with post-combustion capture solid waste disposal cannot be neglected in a life-cycle perspective.

9.4 Sensitivity analysis: Effect of Post-combustion Capture, Transport and Injection Scenario Choices on Life Cycle Environmental Impacts

The scenarios analysed in this section address power generation with post-combustion CO_2 capture, conditioning, transport and injection scenario choices to evaluate the significance of technological, operational and geographical choices on the overall system life cycle environmental impact performance.

The LCI model developed at unit process level enables evaluation of the options that may be considered when assessing or designing a power generation post-combustion capture, transport and injection scenario. The choice of LCI model parameters in relation to these options enables the practitioner to represent technical, operational and geographical differences in the environmental assessment of power generation systems.

This analysis would provide accurate information for decision makers to ensure that a CCS option selected does not result in upstream or downstream changes that will increase the overall environmental impacts of the system. It also allows the assessment of future potential scenarios, for example improvements in the energy efficiency of different processes. The options evaluated are shown in Table 9.3 against the base case scenario. The base case scenario choices are used as standard for every other category of parameters besides the specific one that is analysed. The changes in LCA environmental impact indicator scores are presented in the following paragraphs starting with technology options, followed by operational factors and finally changes due to geographical setting. The results are illustrated in Figures 9.18 to 9.30 presenting the relative LCA environmental impact changes in relation to the base case scenario.

Research has shown that, major design options, such as the type of boiler used in coal combustion and the chemical absorption capture technology implement, may also change the life-cycle environmental impacts of power generation with post-combustion capture,

transport and injection. Figures 9.18 and 9.19 show that different types of boilers lead to different levels of impacts such as AP, EP, GWP and POCP both at direct emissions level (plant level) and at life-cycle level. This is mainly due to different levels of NOx, N_2O and CH_4 emissions associated with different boilers.

Table 9.3: Description of base case scenario and sensitivity analysis options for a 500MW power plant with post-combustion CO_2 capture, conditioning, transport and injection.

		Base case scenario	Sensitivity analysis alternatives
Technology options	**Boiler type**	PC wall fired, dry bottom	PC wall fired, wet-bottom; PC wall tangential-fired, dry-bottom; PC wall tangential-fired, wet-bottom; PC cell burner fired, dry-bottom; Cyclone
	Chemical absorption CO_2 capture technology (different solvent used)	MEA	KS1; K^+/PZ
	Power plant gross energy efficiency (%)	45%	35~50%
	CO_2 capture energy consumption (MW/500MW electricity generated)	105.5 MW	65~100% of baseline for future technology
Operational factors	**SOx removal rate**	95%	90~100%
	NOx removal rate (NH_3 to NO ratio)	0.8	0.65~1.15
	CO_2 capture rate	95%	50~99%
Geographical setting	**Coal type**	US Appalachian (bituminous)	Australia N.S. Wales (bituminous); US Illinois No.6 (bituminous); Poland (bituminous); S. Africa Transvaal (bituminous); South Australia Leigh Creek (lignite); Western Australia (sub-bituminous);
	Compression pressure (MPa)	13.8	10.3~17.2
	Pipeline distance (Km)	300	50~400
	Storage formation depth (m)	1,000	1500~2500

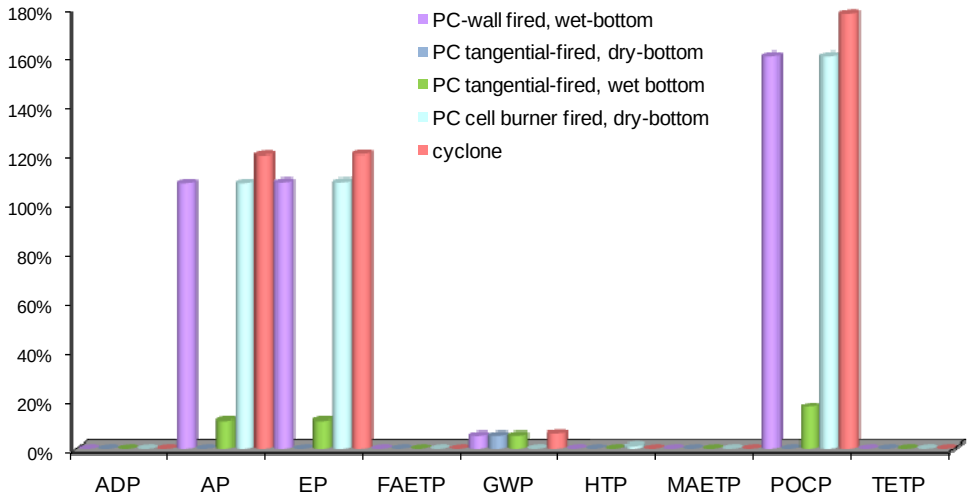

Figure 9.18: Plant level comparison of boilers and their environmental impacts in power generation with post-combustion CO_2 capture with MEA, transport and injection.

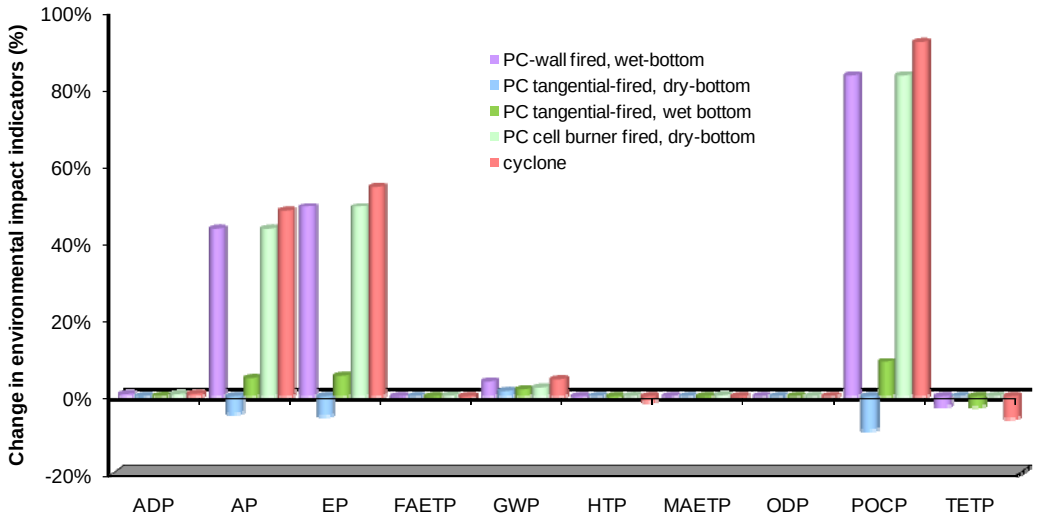

Figure 9.19: Life-cycle level comparison of boilers and their environmental impacts in power generation with post-combustion CO_2 capture with MEA, transport and injection.

Figure 9.20 illustrates that post-combustion capture with K_PZ or KS1 has around 10% lower ADP, FAETP, GWP, MAETP, ODP, POCP and TETP than that of capture with MEA. This is because post-combustion capture with K_PZ or KS1 uses less coal and this reduces the emissions from both the power plant and upstream processes. The dramatic reduction in HTP is due to the lower make-up requirements of capture with K_PZ (or KS1) compared to capture with MEA, which reduces HF emissions from K_PZ (or KS1) production, which is the main source of HTP. Post-combustion capture with K_PZ results in a significant

reduction in EP and AP, since this process does not generate NH_3 during capture. On the other hand, post-combustion capture with KS1 increases the EP and AP significantly as this process generates more NH_3 compared to other technologies.

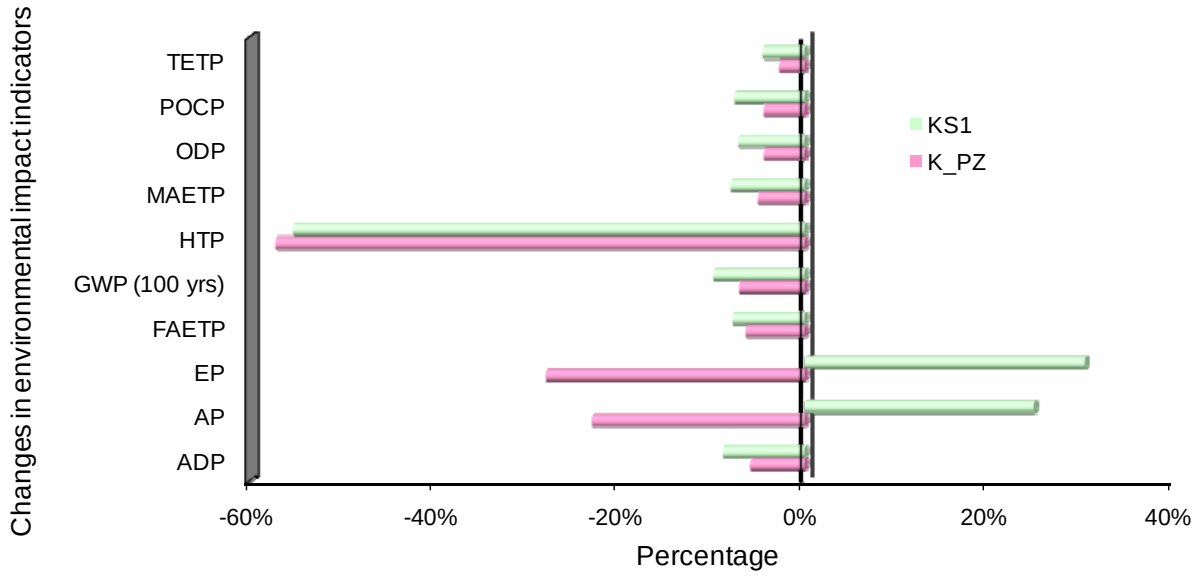

Figure 9.20: Life-cycle level comparison of chemical absorption capture technologies and their environmental impacts in power generation with post-combustion CO_2 capture, transport and injection (the baseline case represents a 500 MW plant with MEA).

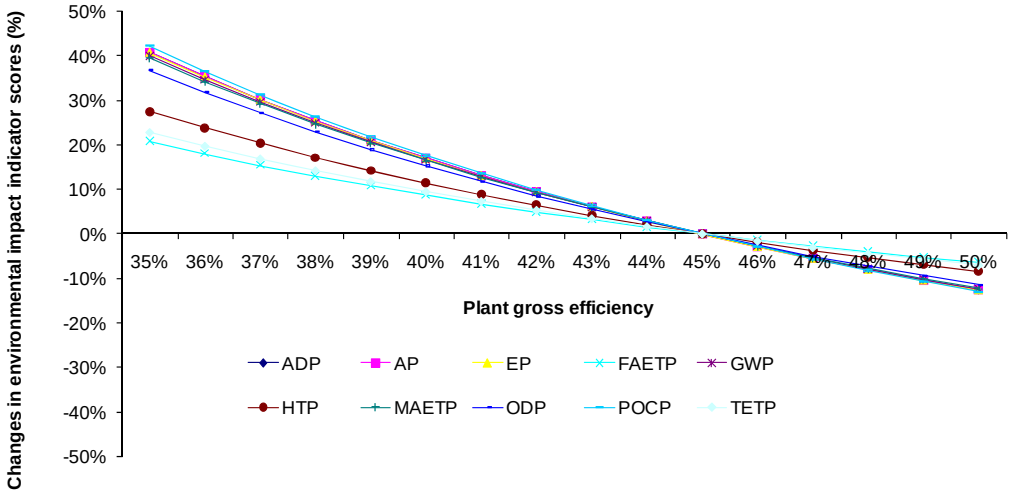

Figure 9.21: The effect of plant gross efficiency on life cycle impact indicator scores (Post-combustion CO_2 capture with MEA, transport and injection).

As shown in Figure 9.21, the effect of the power plant gross energy efficiency on environmental impacts is not linear and all impact categories are very sensitive to the change of power plant energy efficiency. Increase of plant gross efficiency can significantly

reduce life-cycle environmental impacts in all categories. For instance, an increase of energy efficiency from 45% to 50% results in a 10% decrease in the impact indicator scores of all categories. This is because the increase of energy efficiency reduces the coal consumption and hence reduces emissions from both the power plant and upstream processes (e.g. coal production). It is noted that FAETP and TETP are less sensitive to the change of plant gross efficiency, because a significant proportion of FAETP or TETP originates from trace metal emissions to soils from surface impoundments and landfill, which are mainly influenced by their design.

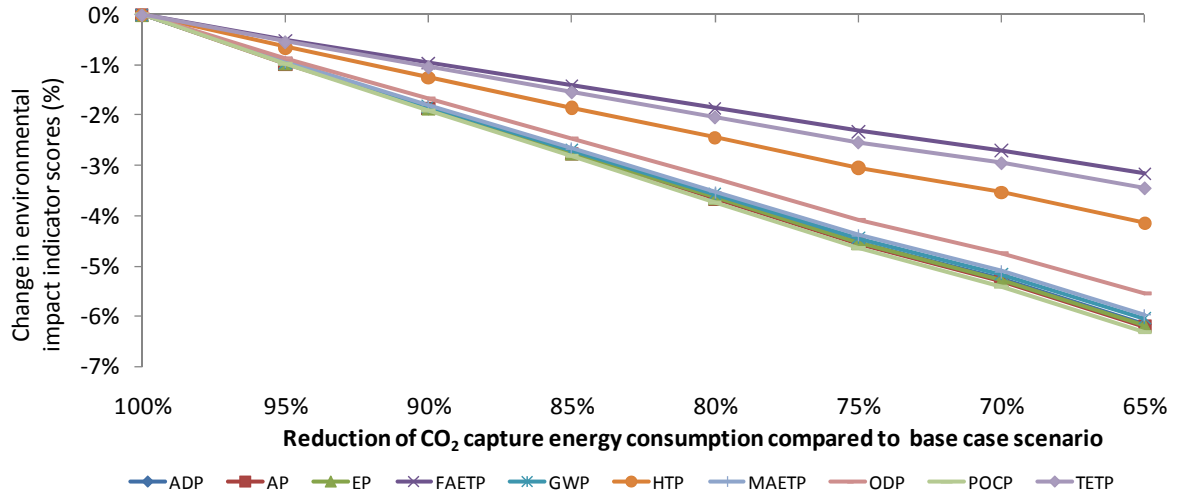

Figure 9.22: The effect of CO_2 capture energy efficiency on life cycle environmental impacts (Post-combustion CO_2 capture with MEA, transport and injection).

Any reduction in the CO_2 capture energy consumption rate reduces the use of coal and, consequently, reduces the emissions from both the power plant and the upstream processes such as coal production. Figure 9.22 shows that 5% decrease in energy consumption by the CO_2 capture process reduces the ADP, EP, GWP, MAETP, POCP and ODP by 1% and FAETP, TETP and HTP by around 0.5%.

Research has shown that an improvement in the SO_2 removal rate reduces the HTP significantly, with 1% increase in the SO_2 removal rate resulting in about 10% decrease in HTP (Figure 9.23). Higher SO_2 removal rate decreases MEA consumption caused by the reaction between SO_2 and MEA, and this reduces the HTP caused by MEA production, which is the main source of HTP. Figure 9.20 also reveals that an increase in the SO_2 removal rate reduces the environmental impacts in all categories, except for a slight increase in POCP.

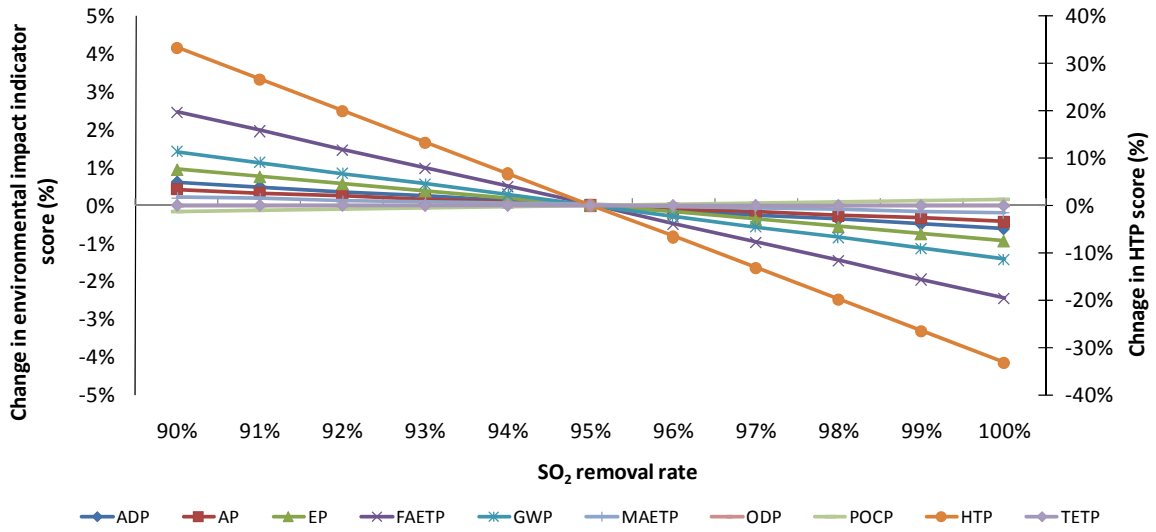

Figure 9.23: The effect of SO_2 removal rate on life cycle environmental impacts (Post-combustion CO_2 capture with MEA, transport and injection).

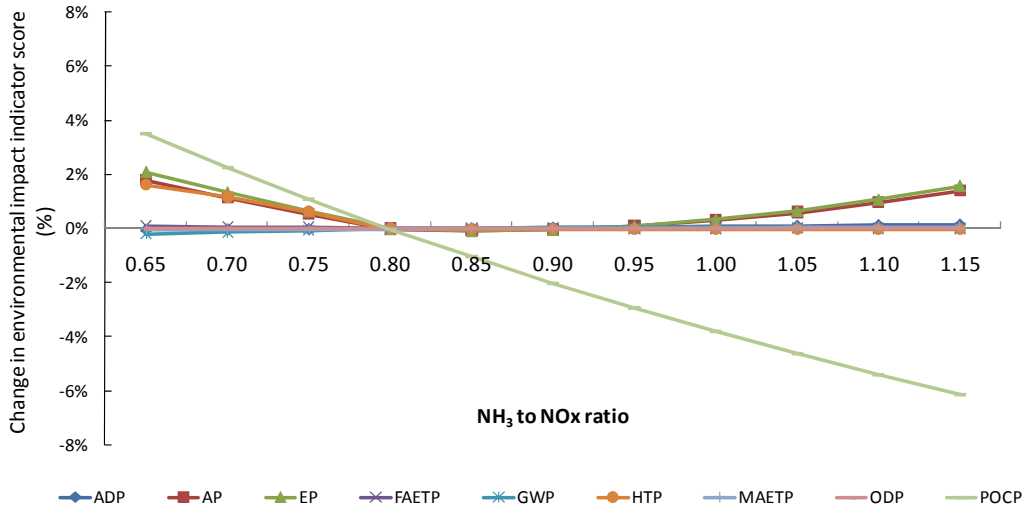

Figure 9.24: The effect of NOx removal rate on life cycle environmental impacts (Post-combustion CO_2 capture with MEA, transport and injection).

Figure 9.24 demonstrates that an increase in the NOx removal rate (or NH_3 to NOx ratio) leads to a steady decrease in the POCP, as a result of decreasing NOx emissions. However, once the NH_3 to NOx ratio exceeds 0.8, the increase in NH_3 emissions from the SCR results in an increase in EP, AP, which offset the effects NOx emission reductions. Figure 9.21 shows that, for the 500 MW base case scenario, 0.95 is the optimum value for the NH_3 to NOx ratio which can achieve a 3% decrease in the POCP without affecting the other environment impacts.

In post-combustion CO_2 capture, the power plant operators can operate at different CO_2 capture rates by bypassing a fraction of the flue gas. Figure 9.25 demonstrates that the increase of CO_2 capture rate decreases the GWP dramatically, and increases other environmental impacts moderately. Figure 9.25 suggests that POCP, EP and AP are more sensitive to a change in the CO_2 capture rate compared to the other impact categories, except for the GWP, since any change in the CO_2 capture rate has a direct impact on energy consumption by CO_2 capture, CO_2 conditioning, CO_2 transportation and CO_2 injection processes and hence modify the emissions from the power plant with CO_2 capture, from which the majority of POCP, EP and AP originate.

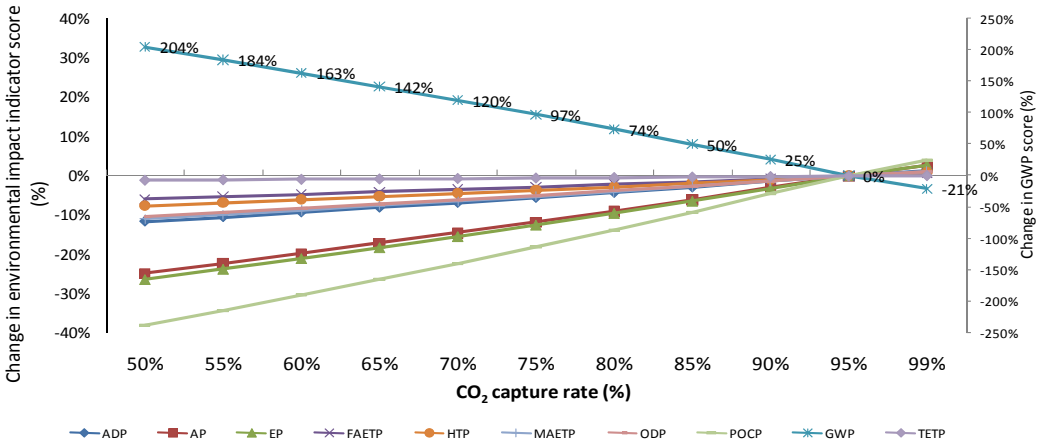

Figure 9.25: The effect of CO_2 capture rate on life cycle environmental impacts (Post-combustion CO_2 capture with MEA, transport and injection).

Mining and combustion of different ranks of coal result in different levels of life cycle environmental impacts due to the change in trace metal and methane contents of coal handled. Figures 9.26 and 9.27 compare the life cycle environmental impacts of a number of different coals with that of the US Appalachian coal used in the base case scenario discussed earlier. As shown in Figure 9.26, at power plant level, the variability of the impact indicators such as HTP, TETP, FAETP and MAETP is because the amount of trace metals in different coals varies significantly. For instance, coal from N.S. Wales, Australia and Poland have a higher score in HTP, TETP, FAETP and MAETP as they contain large amounts of trace metals, especially Vanadium. The variability in other indicators such as AP, EP, POCP and GWP at plant level is less significant, since these impacts depend primarily on the amount of S, N, C, and Cl in coal, which do not vary as much as the trace metal contents. On the other hand, the variability of environmental impact scores at life-

cycle level is caused by both power generation with CO_2 capture and the upstream processes. Figure 9.27 suggest that the Leigh Creek lignite and the sub-bituminous coal from Australia have lower environmental impacts in GWP, AP, EP and MAETP categories. At life-cycle level, the variability of HTP is not significant, as this is dominated by the emissions of HF from the MEA production process and the MEA consumption in capture does not vary significantly for power generation using different types of coal. Analysis of the LCIA data has shown that the life-cycle GWP of the lignite and sub-bituminous coals used in this research is 80.30 and 76.67 kg CO_2 equivalent respectively, which is nearly half of the life-cycle GWP of the bituminous coals used for the same 500 MW plant scenario.

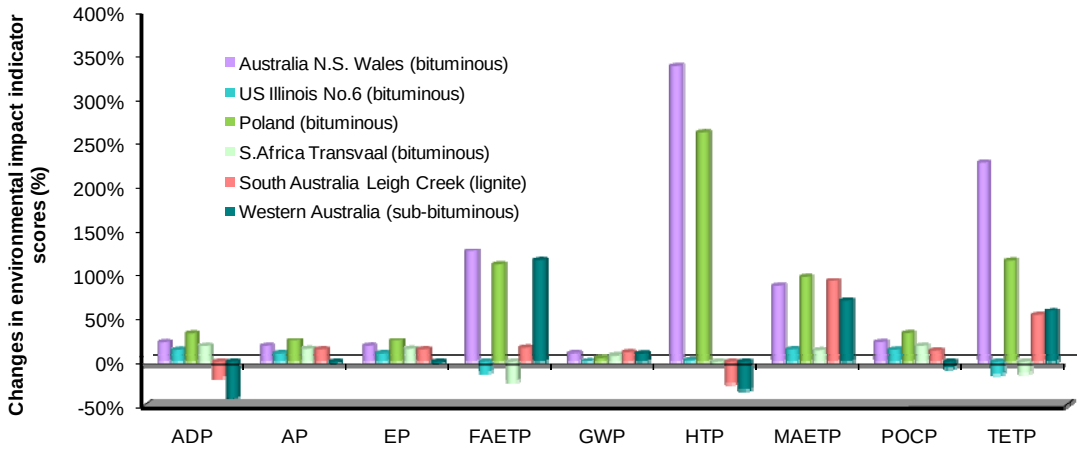

Figure 9.26: Plant level effects of coal type on environmental impacts of power generation with post-combustion CO_2 capture with MEA (the baseline case represents a 500 MW plant using a US Appalachian low sulphur bituminous coal).

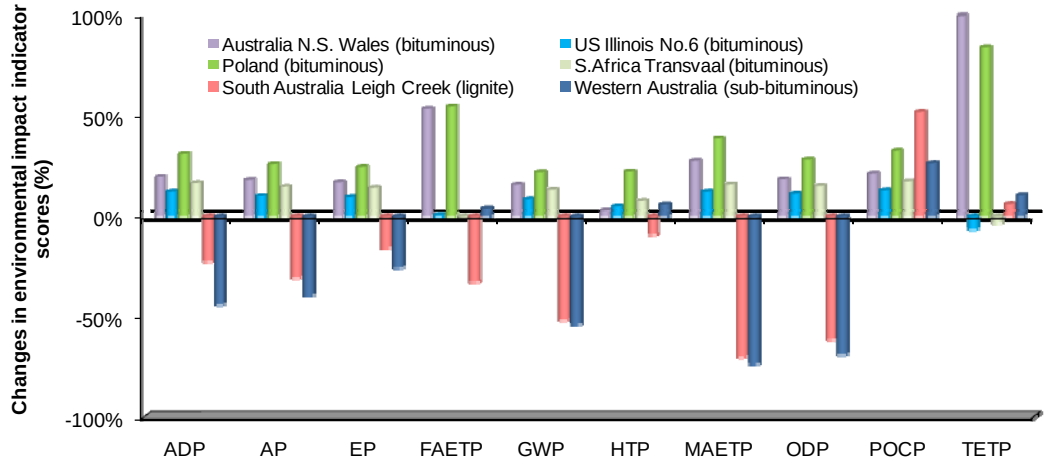

Figure 9.27: Life-cycle level effects of coal type on environmental impacts of power generation with post-combustion CO_2 capture with MEA (the baseline case represents a 500 MW plant using a US Appalachian low sulphur bituminous coal).

Figures 9.28 shows that CO_2 conditioning unit outlet pressure does not significantly affect the life-cycle environmental impacts during power generation with CO_2 capture, transport and injection since its share of energy consumption is relatively small compared to the other parameters involved in these processes.

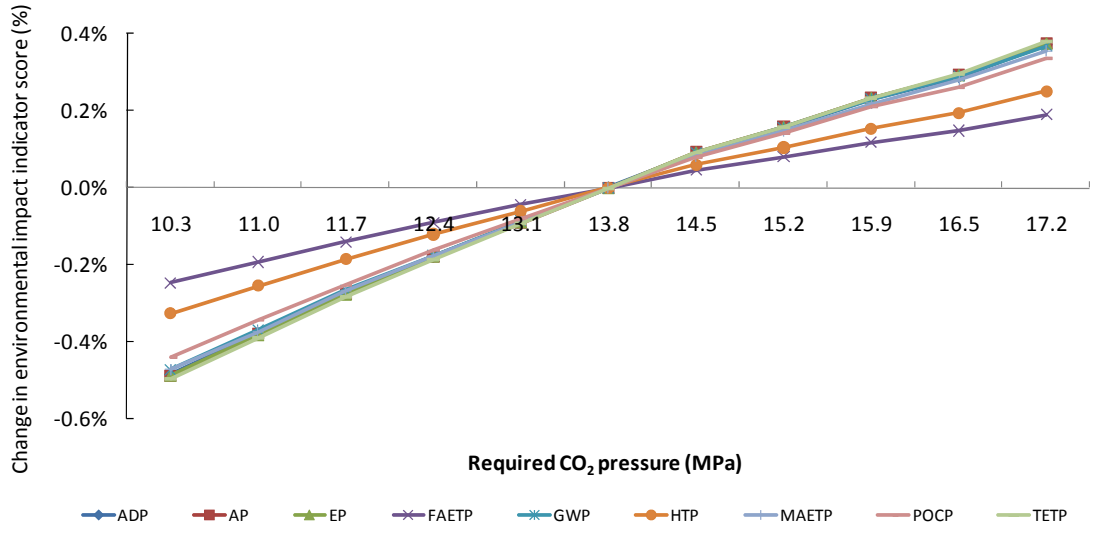

Figure 9.28: The effect of CO_2 compression pressure on life cycle environmental impacts (Post-combustion CO_2 capture with MEA, transport and injection).

Figure 9.29 shows that a 100km change in the length of transport pipeline results in 1.3% change in FAETP, 1.0% change in TETP, GWP and ODP, and around 0.5% change in ADP and MAETP, which reflect the changes in the pipeline infrastructure, consumption of natural gas for CO_2 compression and the CO_2 fugitive emissions from the CO_2 pipeline.

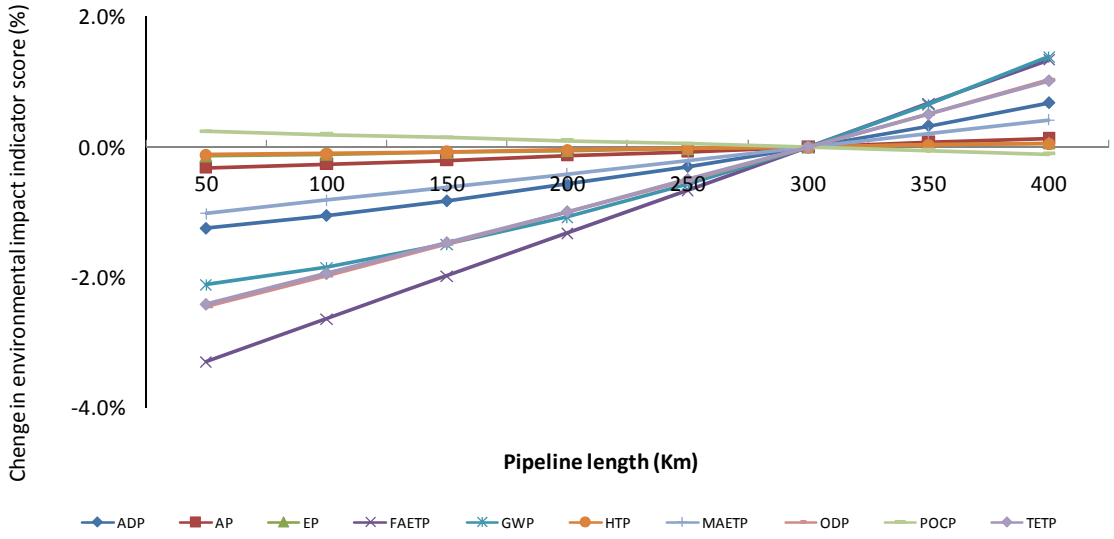

Figure 9.29: The effect of pipeline transport distance on life cycle environmental impacts (Post-combustion CO_2 capture with MEA, transport and injection).

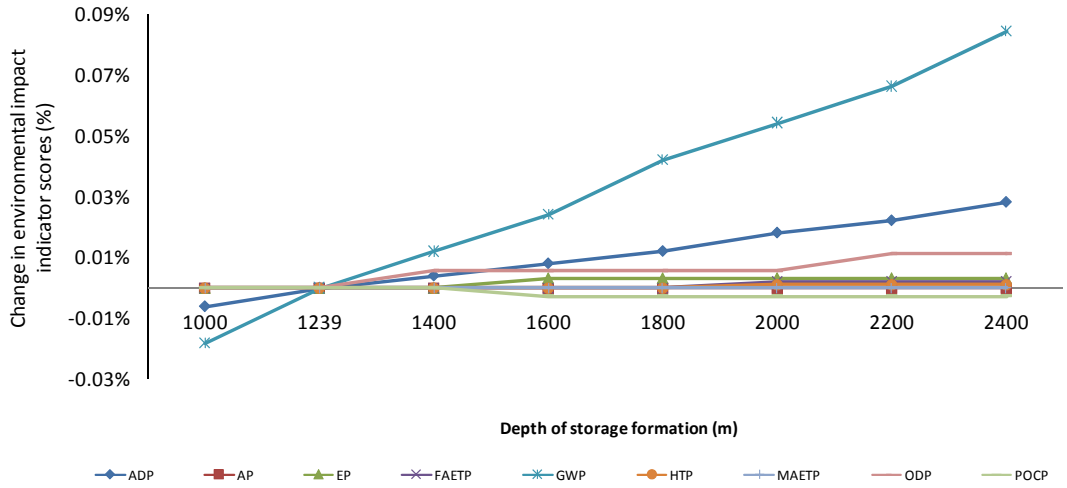

Figure 9.30: The effect of CO_2 storage reservoir depth on life cycle environmental impacts (Post-combustion CO_2 capture with MEA, transport and injection).

Similar to CO_2 conditioning unit outlet pressure the depth of CO_2 storage reservoir does not significantly affect the life-cycle environmental impacts during power generation with CO_2 capture, transport and injection (Figures 9.30) since its share of energy consumption is relatively small compared to the other parameters involved in these processes.

9.5 Uncertainty Analysis: Effect of LCI Input Data on Emissions, Resource Consumption and Life Cycle Environmental Impacts

Monte Carlo simulations were carried out to quantify the uncertainties associated with each environmental emission or resource (or material) consumption evaluated in this research. The methodological framework involved in the Monte Carlo simulations was described in Chapter 4. The input parameters identified for each component unit process in power generation with post-combustion CO_2 capture and storage and their ranges and distributions are described in Table E1 in Appendix E. Due to lack of historical data and the uniqueness of power generation projects, the selection of probability density functions (pdf's) for the factors or parameters considered was based on subjective judgment. The commercial LCA software GaBi version 4, which is able to handle input data sampling from statistical distributions in a Monte Carlo framework and provide the LCA results for numerous iterations as statistical distributions was used to conduct the Monte Carlo simulations.

The base case scenario described in Table 9.1 was used for the uncertainty evaluation for a 500 MW plant with PC wall dry bottom boiler burning Appalachian coal and fitted with

post-combustion capture using MEA. In all cases 5,000 Monte Carlo simulations runs were carried out and the statistical properties of the outputs, such as mean, median, standard deviation, and different levels of confidence are provided in tabular form in the following paragraphs. The results are grouped under the following categories:

- Direct air emissions for major compounds and trace metals;
- Direct emissions of trace metals to soils; and
- Direct life cycle environmental impacts;
- Life cycle impacts of the complete post-combustion CO_2 capture with MEA, transport and injection system including upstream emissions from coal and MEA production, transport, plant construction and infrastructure.

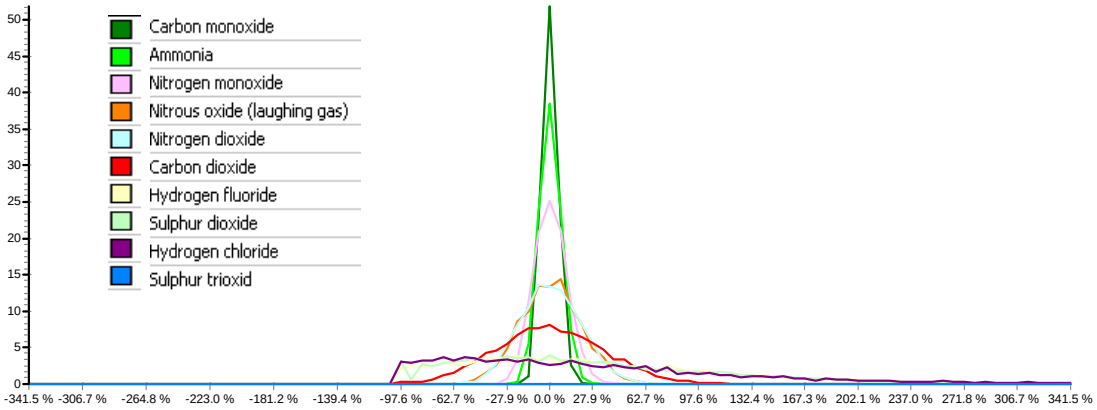

Figure 9.31: Histogram of air emissions at direct emission level

Table 9.4: Statistical outputs of air emissions at direct emission level

Emissions	Base case scenario	Mean	Standard deviation (% of base case scenario)	10% Percentile	25% Percentile	Median	75% Percentile	90% Percentile
Carbon monoxide	0.10354	0.10378	5%	0.097333	0.10018	0.10349	0.10711	0.11053
Ammonia	0.14598	0.14664	7.05%	0.13367	0.13963	0.14631	0.15343	0.16019
Nitrogen monoxide	1.1938	1.2	10.80%	1.0355	1.1104	1.1964	1.2852	1.3667
Nitrous oxide	0.000639	0.000644	19.70%	0.000484	0.000558	0.000644	0.000727	0.000808
Nitrogen dioxide	0.022575	0.022736	19.90%	0.016958	0.019666	0.022603	0.025767	0.028571
Carbon dioxide	57.218	57.468	35.60%	31.488	43.746	57.203	70.965	84.075
Hydrogen fluoride	4.66E-05	5.95E-05	67.70%	1.31E-05	2.92E-05	5.25E-05	8.32E-05	0.000115
Sulphur dioxide	0.001203	0.00155	69.80%	0.000353	0.000739	0.001347	0.002149	0.003023
Hydrogen chloride	0.000124	0.000164	82.30%	2.68E-05	6.41E-05	0.000135	0.000223	0.000339
Sulphur trioxide	0	1.81E-06	187%	0	0	0	2.28E-06	5.95E-06

Figure 9.31 demonstrates the uncertainty analysis results for direct air emissions for major compounds. The corresponding statistical measures are provided in Table 9.4. The emissions of CO, NH_3, NO, NO_2, N_2O and CO_2 are less uncertain (smaller standard deviations) than the emissions of HF, HCl, SO_2, and SO_3, because emissions of HF, HCl,

SO_2, and SO_3 are affected by more pollution control processes as analysed in Figure 9.2 and this increases the uncertainty. The uncertainty of CO_2 emissions comes from the variability of CO_2 capture rate and the variability of carbon in coal.

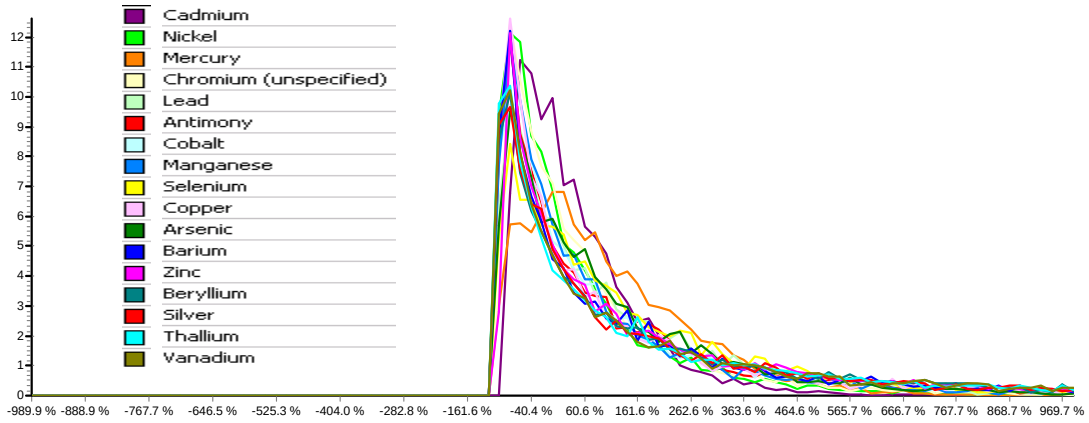

Figure 9.32: Histogram of trace metal emissions to air at direct emission level

The uncertainty analysis results for emissions of trace metals to air are shown in Figure 9.32 and Table 9.5. The uncertainty of emissions of trace metals to air is larger than that of air emissions, because the amount of trace metals in coal varies more significantly than that of C, S, N, Cl or F and all the pollution control processes can affect the emissions of trace metals to air. Because of the significant variability in the amount of a trace metal in coal, a positively skewed distribution is used in this study to assign the input pdf for each trace metal in the coal (see Table E1 in Appendix E). This positive skewness is very much reflected in the histograms of the outputs (Figure 9.32).

Table 9.5: Statistical outputs of trace metal emissions to air at direct emission level

Emissions	Base case scenario	Mean	Standard deviation (% of base case)	10% Percentile	25% Percentile	Median	75% Percentile	90% Percentile
Cadmium	2.19E-07	3.19E-07	77.20%	7.60E-08	1.37E-07	2.53E-07	4.36E-07	6.42E-07
Nickel	4.63E-07	6.66E-07	115%	5.03E-08	1.61E-07	4.13E-07	8.90E-07	1.64E-06
Mercury	5.75E-07	1.17E-06	76%	1.96E-07	4.97E-07	9.67E-07	1.66E-06	2.39E-06
Chromium	8.53E-07	1.47E-06	112%	1.65E-07	3.98E-07	9.40E-07	1.92E-06	3.37E-06
Lead	1.98E-06	4.18E-06	111%	3.31E-07	9.88E-07	2.65E-06	5.74E-06	1.00E-05
Antimony	1.98E-08	4.38E-08	130%	2.40E-09	8.18E-09	2.39E-08	5.73E-08	1.11E-07
Cobalt	7.14E-08	1.60E-07	132%	9.81E-09	3.06E-08	8.67E-08	2.04E-07	3.98E-07
Manganese	5.69E-07	1.12E-06	130%	7.76E-08	2.27E-07	6.25E-07	1.44E-06	2.79E-06
Selenium	5.86E-06	1.37E-05	103%	1.16E-06	3.75E-06	9.25E-06	1.93E-05	3.23E-05
Copper	3.88E-06	8.35E-06	139%	4.32E-07	1.46E-06	4.27E-06	1.09E-05	2.09E-05
Arsenic	9.01E-06	1.89E-05	108%	1.60E-06	4.73E-06	1.25E-05	2.59E-05	4.39E-05
Barium	2.57E-05	6.81E-05	153%	2.72E-06	1.02E-05	3.32E-05	8.38E-05	0.000176
Zinc	1.14E-05	3.41E-05	139%	2.27E-06	6.08E-06	1.73E-05	4.25E-05	8.50E-05
Beryllium	4.83E-07	1.48E-06	145%	5.74E-08	2.21E-07	7.21E-07	1.86E-06	3.87E-06
Silver	8.28E-09	2.55E-08	151%	9.21E-10	3.80E-09	1.16E-08	3.14E-08	6.51E-08
Thallium	8.28E-08	2.63E-07	152%	7.96E-09	3.47E-08	1.20E-07	3.24E-07	6.71E-07
Vanadium	2.71E-06	8.45E-06	153%	2.79E-07	1.15E-06	3.81E-06	1.02E-05	2.21E-05

Figure 9.33 demonstrates the histograms of emissions of trace metals to soils resulting from the uncertainty analysis. The corresponding statistical measures are shown in Table 9.6. The uncertainty of trace metal emissions to soil is smaller than that of trace metal emissions to air and the histograms of these emissions are less skewed than the histograms of trace metal emissions to air. This is because the emissions of trace metals to soil depend mostly on the surface impoundment unit and the landfill unit characteristics and are less affected by the variability of trace metals in coal.

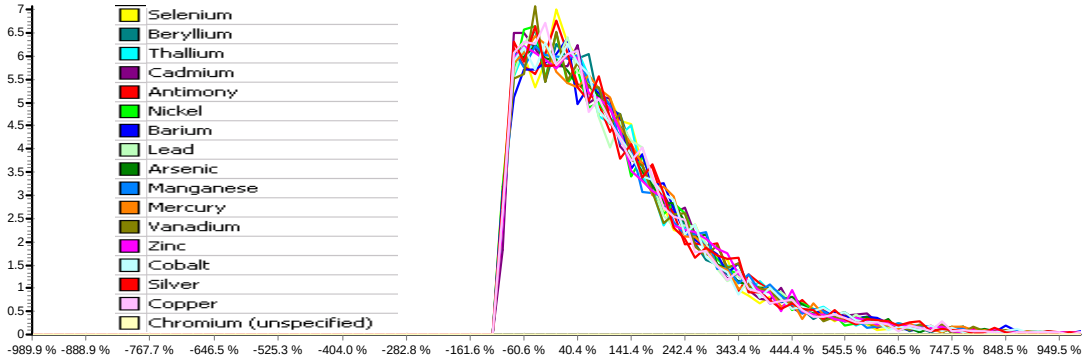

Figure 9.33: Histogram of trace metal emissions to soil at direct emission level

Table 9.6: Statistical outputs of trace metal emissions to soil at direct emission level

Emissions	Base case scenario	Mean	Standard deviation (% of base case)	10% Percentile	25% Percentile	Median	75% Percentile	90% Percentile
Selenium	7.81E-06	1.59E-05	79.40%	2.52E-06	6.63E-06	1.31E-05	2.19E-05	3.28E-05
Beryllium	7.09E-08	1.49E-07	81.70%	2.44E-08	6.09E-08	1.20E-07	2.04E-07	3.09E-07
Thallium	3.63E-08	7.78E-08	82%	1.26E-08	3.07E-08	6.19E-08	1.07E-07	1.62E-07
Cadmium	1.89E-08	4.03E-08	82.20%	6.62E-09	1.59E-08	3.26E-08	5.60E-08	8.28E-08
Antimony	3.65E-08	7.80E-08	82.50%	1.23E-08	3.13E-08	6.30E-08	1.07E-07	1.63E-07
Nickel	4.29E-07	8.99E-07	82.50%	1.43E-07	3.46E-07	7.31E-07	1.26E-06	1.87E-06
Barium	5.14E-06	1.12E-05	82.60%	1.88E-06	4.55E-06	9.10E-06	1.54E-05	2.30E-05
Lead	1.94E-06	4.12E-06	82.80%	6.98E-07	1.63E-06	3.28E-06	5.62E-06	8.59E-06
Arsenic	2.77E-06	5.98E-06	83.10%	9.38E-07	2.34E-06	4.80E-06	8.36E-06	1.25E-05
Manganese	2.55E-06	5.46E-06	83.30%	8.86E-07	2.17E-06	4.37E-06	7.54E-06	1.14E-05
Mercury	3.09E-09	6.59E-09	83.50%	1.07E-09	2.58E-09	5.38E-09	9.08E-09	1.35E-08
Vanadium	3.03E-05	6.50E-05	84.10%	1.10E-05	2.56E-05	5.23E-05	8.92E-05	0.000134
Zinc	6.03E-06	1.31E-05	84.10%	2.08E-06	5.09E-06	1.04E-05	1.81E-05	2.68E-05
Cobalt	1.82E-07	3.88E-07	84.10%	6.21E-08	1.52E-07	3.09E-07	5.35E-07	8.07E-07
Silver	3.63E-09	7.75E-09	85.10%	1.18E-09	2.97E-09	6.24E-09	1.06E-08	1.62E-08
Copper	4.18E-07	8.72E-07	85.50%	1.38E-07	3.37E-07	7.01E-07	1.20E-06	1.82E-06

Figure 9.34 demonstrates the histograms of the life cycle environmental impacts of power generation with post-combustion CO_2 capture using MEA, CO_2 transport and injection (direct emissions without contribution from upstream processes) resulting from 5,000 Monte Carlo simulation runs. The statistical outputs are provided in Table 9.7. The results show that the uncertainty of ADP, AP, EP, GWP or POCP are less than that of MAETP, TETP, FAETP, HTP, because AP, EP, GWP or POCP depend on air emissions, which have

lower uncertainty than emissions of trace metals that dominate MAETP, TETP, FAETP, HTP. The uncertainty of ADP is dominated by the variability of coal heating value, which is lower than the variability of air emissions influencing other LCA impact categories.

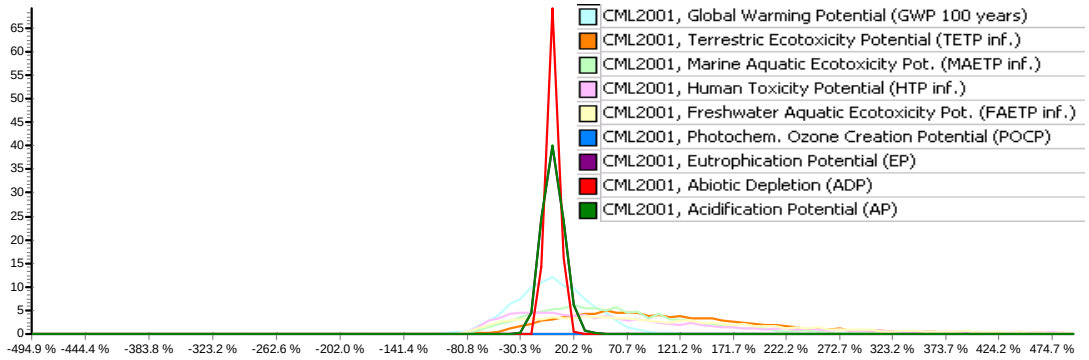

Figure 9.34: Histogram of environmental impacts at direct emission level

Table 9.7: Statistical outputs of environmental impact at direct emission level

Impact Category	Base case scenario	Mean	Standard deviation (% of base case)	10% Percentile	25% Percentile	Median	75% Percentile	90% Percentile
GWP	57.601	57.849	35.30%	31.854	44.124	57.601	71.343	84.454
TETP	0.089082	0.19092	49.70%	0.08793	0.12326	0.17434	0.24121	0.31571
MAETP	2571.4	4182.8	48.30%	1886.7	2712.8	3886.3	5299.1	6893
HTP	4.127	8.6838	84.50%	2.4472	3.8385	6.4862	10.963	17.686
FAETP	0.17793	0.39573	68.60%	0.12018	0.20043	0.33406	0.52079	0.74449
POCP	-0.50621	-0.50882	-10.90%	-0.57975	-0.54503	-0.5073	-0.47048	-0.43874
EP	0.29279	0.29428	9.69%	0.2586	0.27453	0.29331	0.3127	0.33098
ADP	5.2729	5.2851	5%	4.9566	5.1013	5.2708	5.4543	5.6284
AP	1.569	1.5774	9.68%	1.3865	1.4715	1.5721	1.676	1.774

If upstream emissions are also considered, the histograms of life-cycle environmental impacts from the 5,000 Monte Carlo simulation runs produced are shown in Figure 9.35 and the corresponding statistical outputs are provided in Table 9.8. These results are biased by the large single level contribution of upstream environmental impacts, calculated using the GaBi version 4 software, which do not consider the uncertainty of parameters or factors that determine or affect the emissions from upstream processes. For instance, the uncertainty of MAETP and HTP at life-cycle level is significantly less than that at direct emission level, because MAETP and HTP are dominated by coal mining and MEA production respectively and the uncertainty of emissions from the two processes are not fully captured by GaBi software. Therefore, the results at life-cycle level may significantly underestimate the uncertainty of environmental impacts and justify the choice of detailed unit process representation introduced in the current research for the power generation with CO_2 capture transport and injection processes.

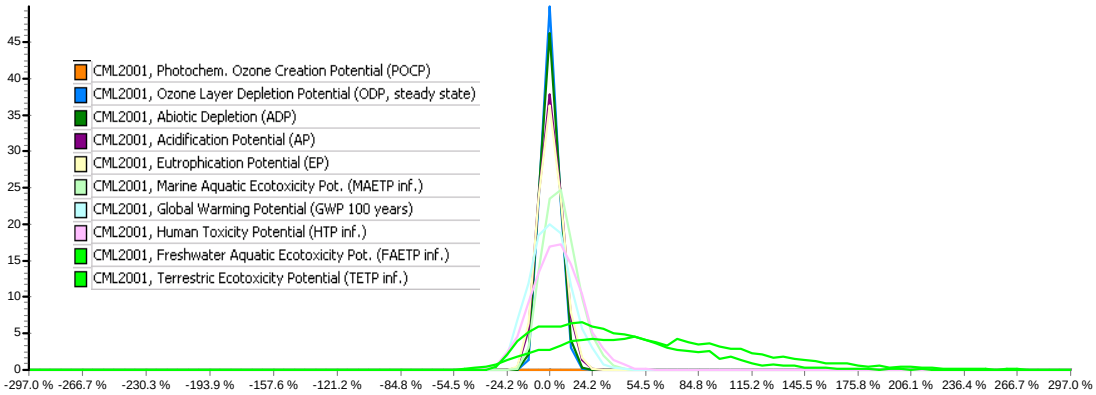

Figure 9.35: Histogram of environmental impacts at life-cycle level

Table 9.8: Statistical outputs of environmental impact at life-cycle level

Impact Category	Base case scenario	Mean	Standard deviation (% of base case)	10% Percentile	25% Percentile	Median	75% Percentile	90% Percentile
POCP	-0.44122	-0.44246	-8.19%	-0.48927	-0.46622	-0.44124	-0.41757	-0.39582
ODP	2.06E-06	2.06E-06	4.56%	1.94E-06	2.00E-06	2.06E-06	2.12E-06	2.18E-06
ADP	5.8637	5.8791	4.98%	5.5145	5.678	5.8645	6.0673	6.2628
AP	2.1953	2.205	6.23%	2.0332	2.1103	2.1988	2.295	2.3852
EP	0.36216	0.36379	6.53%	0.33408	0.34755	0.3626	0.37953	0.3948
MAETP	21617	22977	9.10%	20462	21498	22768	24273	25783
GWP	196.16	196.63	11.60%	167.19	181.21	196.21	211.53	225.38
HTP	102.21	106.52	13.50%	88.377	96.719	106.32	115.64	124.58
FAETP	0.5246	0.72048	31.40%	0.46702	0.54821	0.67695	0.84965	1.0327
TETP	0.14153	0.23423	34.50%	0.1378	0.17355	0.22442	0.28308	0.34283

9.6 Conclusions

The LCI models developed in this research compute the direct emissions of power plant with post-combustion CO_2 capture, CO_2 conditioning, CO_2 pipeline transport and the injection of CO_2 into a storage formation. The results demonstrate that most direct air emissions come from the power plant stack, and the resource consumption is dominated by the primary fuel, coal. The results also show that a post-combustion (e.g. MEA) CO_2 capture unit capturing 95% of CO_2 in the flue gas can further reduce the emissions of PM-10, SO_2, SO_3, NO_2, HCl, HF, mercury (Hg) vapour and other trace metals present in flue gases after FGD, therefore, the power plant with post-combustion CO_2 capture has lower emission rates of these substances and other trace metals than that of a conventional power plant. The percentages of trace metals, originally found in the coal, which are finally released to the environment (air or soil) are less than 0.5% for most trace metals, except for As, Hg and Se. Emissions of trace metals to air are also originating from the power plant stack. Emissions of trace metals to soil are dominantly stemming from surface

impoundments, and trace metal emissions to soil from landfill over a 1,000-year period are not significant. The results suggest that the reduction of the trace metal emissions to air from power plant, especially the emissions of volatile trace metals such as As, Se and Hg, can significantly reduce the overall trace metal emissions.

The results of life-cycle environmental impacts of power generation with post-combustion CO_2 capture with MEA, transport and injection are summarised in Table 9.9, which lists the dominant processes and dominant substances that contribute to each impact category. Life-cycle environmental impacts are dominated by the power plant with CO_2 capture and coal production in all impact categories, except HTP that is dominated by the MEA production. AP, EP, GWP100, HTP, MAETP and POCP are primarily related to air emissions. FAETP and TETP are mainly due to trace metal emissions to air or soil.

The results demonstrate that the power plant with gross efficiency 45% can achieve a net efficiency of 34.04% after CO_2 capture and CO_2 conditioning, which consume 7.18% and 2.89% of input coal energy respectively.

The results of sensitivity analysis demonstrate that the life-cycle impacts in all categories are sensitive to the change of power plant gross efficiency, CO_2 capture rate, and energy consumption of CO_2 capture, since these parameters control energy consumption significantly. The results suggest that a high SO_2 removal rate decreases the life-cycle environmental impacts in all categories. The results suggest that a NH_3 to NOx ratio (which determines NOx removal ratio) within the range of 0.8 to 0.95 is optimal, because in this range SCR reduces NOx emissions (or POCP impacts) without causing the increase of other life-cycle impacts.

The life-cycle impacts in all categories are not sensitive to the change of pipeline length, the required CO_2 pressure for transportation, or the depth of storage formation. The life-cycle impacts in all categories are sensitive to the type of coal, because the composition of different coal types varies significantly. The lignite case and sub-bituminous coal case have lower environmental impacts in categories such as GWP, AP, or EP, mainly due to lower environmental impacts from upstream processes, namely coal production, than the higher rank coals produced in underground mines.

Table 9.9: Summary of Life-cycle environmental impacts of power plant with post-combustion CO_2 capture with MEA, transport and injection.

Impact	Value	Dominant processes		Dominant substances				Emission to
		Name	% of	Name	% of total	Impact	Amount	
Global Warmer Potential (GWP 100 years)	167.1210 [kg CO2-Equiv.]	Coal production	61.71%	CH_4	40.54%	67.7476	2.9455	Air
				CO_2	20.78%	34.7236	34.7236	Air
		Power generation with CCS	30.32%	CO_2	29.30%	48.9616	48.9616	Air
				N_2O	0.93%	1.5491	0.0052	Air
Abiotic Depletion Potential (ADP)	4.9406 [kg Sb-Equiv.]	Coal production	96.20%	Coal	91.19%	4.5050	351.2500	--
				Crude oil	2.34%	0.1156	5.4483	--
				Natural gas	2.26%	0.1284	4.9179	--
		MEA production	1.70%	Crude oil	0.69%	0.0340	1.6698	--
Acidification Potential (AP)	1.2639 [kg SO2-Equiv.]	Power generation with CCS	58.13%	NO	38.75%	0.4898	0.4577	Air
				NH_3	18.24%	0.2305	0.1226	Air
				NO_2	1.05%	0.0133	0.0190	Air
				SO_2	0.08%	0.0010	0.0010	Air
		Coal production	38.72%	NO_x	20.37%	0.2575	0.3678	Air
				SO_2	17.89%	0.2261	0.2261	Air
Eutrophication Potential (EP)	0.1958 [kg Phosphate-Equiv.]	Power generation with CCS	69.93%	NO	46.73%	0.0915	0.4577	Air
				NH_3	21.91%	0.0429	0.1226	Air
				NO_2	1.28%	0.0025	0.0190	Air
		Coal production	25.07%	NO_x	24.41%	0.0478	0.3678	Air
		MEA production	6.82%	Ethylene	6.35%	0.0304	0.0031	Freshwater
Ozone Layer Depletion Potential (ODP)	1.76E-06 [kg R11-Equiv.]	Coal production	75.47%	R11	36.70%	6.46E-07	6.50E-07	Air
				R114	31.93%	5.62E-07	6.62E-07	Air
				R12	6.48%	1.14E-07	1.39E-07	Air
		Transport of coal by railway	12.36%	R11	6.02%	1.06E-07	1.06E-07	Air
				R 114	5.23%	9.21E-08	1.08E-07	Air
				R12	1.06%	1.87E-08	2.28E-08	Air
		Power plant	6.91%	Halon	6.88%	1.21E-07	1.01E-08	Air
Photochemical ozone creation potential (POCP)	-0.1375 [kg Ethene-Equiv.]	Power generation with CCS	139.98%	NO	142.14%	-1.95E-01	0.4577	Air
				CO	-1.71%	2.35E-03	8.70E-02	Air
		Coal production	-37.04%	CH4	-12.80%	1.76E-02	2.9455	Air
				SO2	-7.93%	1.09E-02	0.2261	Air
				NOx	-7.49%	1.03E-02	0.3678	Air
Human Toxicity Potential (HTP)	90.7881 [kg DCB-Equiv.]	MEA production	92.50%	Ethylene	53.39%	48.4710	0.0034	Air
				Ethylene	39.09%	35.4878	0.0031	Freshwater
		Power generation	3.87%	Arsenic	2.90%	2.6317	7.60E-06	Air
		Coal production	3.23%	HF	1.12%	1.0189	3.57E-04	Air
				Arsenic	0.73%	0.6671	1.92E-06	Air
Freshwater Aquatic Ecotoxicity Potential (FAETP inf.)	0.4787 [kg DCB-Equiv.]	Coal production	41.81%	nickel	24.40%	0.1168	3.60E-05	Freshwater
				cadmium	4.80%	0.0230	1.51E-05	Freshwater
				vanadium	1.21%	0.0058	6.40E-07	Freshwater
				vanadium*	6.12%	0.0293	1.69E-05	Air
		Power generation with CCS	36.50%	Vanadium	29.41%	0.1408	3.02E-05	Soil
				Selenium	2.38%	0.0114	7.81E-06	Soil
				Beryllium	1.46%	0.0070	4.06E-07	Air
				Vanadium	0.84%	0.0040	2.28E-06	Air
Marine Aquatic Ecotoxicity Potential (MAETP)	18298.04 [kg DCB-Equiv.]	Coal production	83.19%	HF	79.59%	14564.24	3.57E-04	Air
				Selenium	0.66%	121.3024	5.72E-06	Air
				vanadium	1.13%	206.3504	1.69E-05	Air
		Power generation with CCS	12.03%	HF	8.72%	1594.6940	7.60E-06	Air
				Selenium	0.57%	104.2839	4.92E-06	Air
				beryllium	1.04%	190.7845	4.06E-07	Air
Terrestrial Ecotoxicity Potential (TETP)	0.1281 [kg DCB-Equiv.]	Power generation with CCS	64.94%	vanadium	32.32%	0.0414	0.1408	Soil
				arsenic	7.18%	0.0092	2.77E-06	Soil
				Mercury	10.68%	0.0137	4.83E-07	Air
				Arsenic	9.52%	0.0122	7.60E-06	Air
		Coal production	29.98%	Mercury	10.15%	0.0130	4.59E-07	Air
				Vanadium	8.74%	0.0112	1.69E-05	Air
				Chromium	4.14%	0.0053	1.75E-06	Air

where: R11 is trichlorofluoromethane; R114 is dichlorotetrafluoroethane; R12 is dichlorodifluoromethane.

The lignite and sub-bituminous coal have lower values in ADP, because lignite and sub-bituminous coal have been assigned lower ADP impact characterisation factor (0.00571 kg Sb equivalent) than bituminous coal (0.01265 kg Sb equivalent).

Different types of boiler used for coal combustion lead to different AP, EP, GWP or POCP both at direct emission level (plant level) and at life-cycle level (including upstream impacts), because different boilers have different emission factors of NOx, N_2O and CH_4. K_PZ or KS1 post-combustion methods have lower life-cycle environmental impacts than MEA capture in all categories due to their lower consumption of energy and solvent, except KS1 has higher impact value in EP and AP, because of its higher NH_3 emission rate.

The direct emissions of CO, NH_3, NO, NO_2, N_2O and CO_2 are less uncertain than emissions of HF, HCl, SO_2, and SO_3, because emissions of HF, HCl, SO_2, and SO_3 are affected by the emission control processes which generally increase the uncertainty in the emissions. The uncertainty of emissions of trace metals to air is larger than that of air emissions for the major compounds, because the amount of trace metals in coal varies more significantly than that of C, S, N, Cl or F. Trace metal emissions to industrial soil are less uncertain than trace metal emissions to air and the histograms of these emissions are less skewed than that of trace metal emissions to air, because the emissions of trace metals to soil depend on the design of surface impoundment unit and the landfill unit and are less affected by the variability of trace metals in the coal. The results show that the uncertainty of ADP, AP, EP, GWP or POCP are less than that of MAETP, TETP, FAETP, HTP, because AP, EP, GWP or POCP depend on air emissions, which have lower uncertainty than emissions of trace metals that dominate MAETP, TETP, FAETP, HTP.

Chapter 10 Life Cycle Impact Assessment: Oxy-fuel Combustion Carbon Dioxide Capture, Transport and Injection Scenario Analysis

10.1 Introduction

This Chapter presents the research findings on environmental impacts of power plants with oxy-fuel combustion CO_2 capture, transport and injection. As described in Chapter 9, by choosing different LCI models and linking them together, the LCI models of power plants with alternative options of power generation and CO_2 capture can be configured. In this Chapter, the LCI model of a 500 MW power plant with oxy-fuel combustion CO_2 capture, transport and injection is used to demonstrate the capabilities of the models developed (Figure 10.1).The model presented in this Chapter calculates the emissions from the system constructed, as well as characterising the technical, spatial and geographical differences by setting different parameters or inputs for component LCI models. The input parameters for each component unit process are defined in Table F1 in Appendix F. The US Appalachian low sulphur bituminous coal, which represents a typical bituminous coal, is used as an example in the oxy-fuel combustion base case scenario presented. The chemical composition of the US Appalachian coal is described in Table E2 in Appendix E. The LCI data for the upstream processes shown in Figure 10.1 are either taken from the literature or

calculated by the GaBi LCA software and are described in Appendix D. Since the estimation of potential CO_2 leakages from a CO_2 storage formation involves a great deal of uncertainty, CO_2 leakage is not included in the results presented here, rather, CO_2 storage is modelled and analysed separately in Chapter 11.

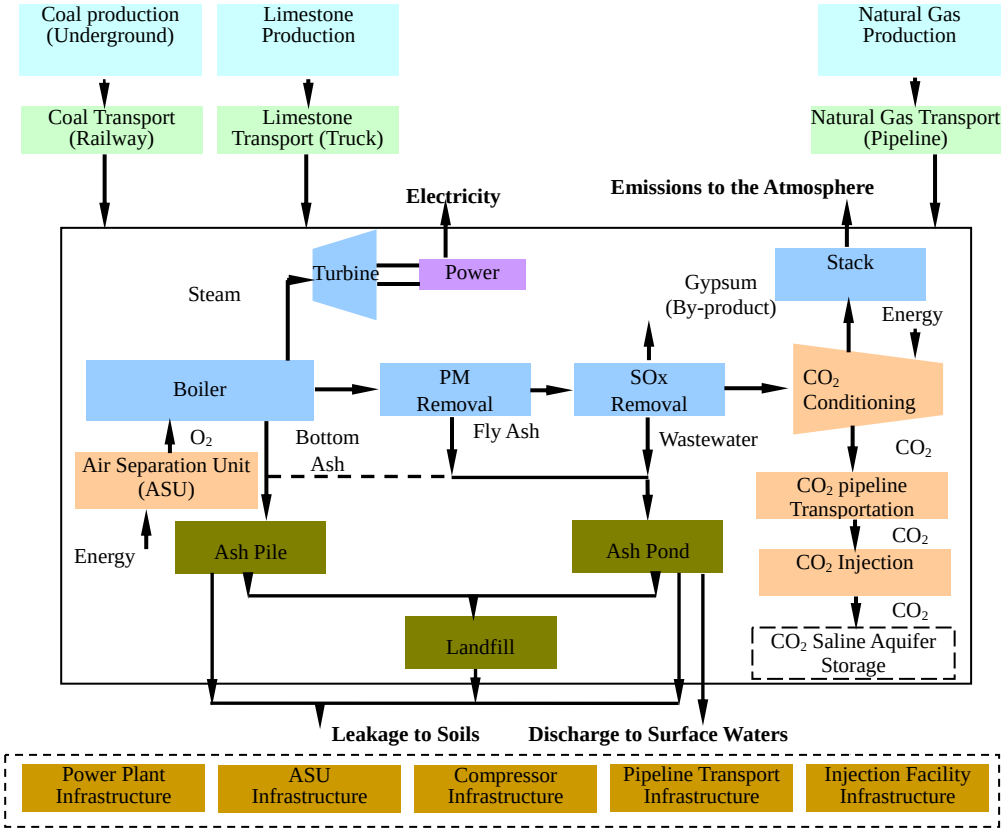

Figure 10.1: The component LCI models of a 500 MW power plant with oxy-fuel combustion capture transport and injection discussed in this Chapter.

The power generation scenario with oxy-fuel combustion CO_2 capture, transport and injection presented in this chapter demonstrates the following aspects and capabilities of the model developed in this research:

- Direct emissions, resource consumption, and material consumption;
- The energy efficiency;
- Life-cycle environmental impacts;
- Sensitivity analysis: effect of LCI model parameter choice on life-cycle environmental impacts;
- Uncertainty analysis: effect of LCI input data on emissions, resource consumption estimates and their life-cycle environmental impacts.

This Chapter also compares the life-cycle environmental impacts of power generation with oxy-fuel combustion CO_2 capture, transport and injection with power generation with post-combustion CO_2 capture, transport and injection, as well as power generation without CCS.

10.2 Resource Consumption and Direct Emissions

Table F3 in Appendix F presents the consumption of resources/materials and resulting direct emissions (per 1 MWh of electricity generated) by each component unit process for the 500 MW capacity power plant with oxy-fuel combustion CO_2 capture, transport and injection. The summary of these emissions is provided in Table 10.1.

Table 10.1: Summary of direct emissions and the consumption of resources/materials in power generation (500 MW) with oxy-fuel combustion CO_2 capture, transport and injection (per 1 MWh electricity generated).

Resources required/sources impact	Amount (kg)	Emissions to Air	Amount (kg)	Trace metal emissions to air	Amount (kg)	Trace metal emissions to soils	Amount (kg)
Coal	3.37E+02	CO_2	52.69	Antimony (Sb)	6.53E-08	Antimony (Sb)	3.70E-08
Natural gas	1.10E-01	PM	6.82E-06	Arsenic (As)	2.97E-05	Arsenic (As)	2.78E-06
Limestone	4.67E+00	PM-10	5.25E-03	Beryllium (Be)	1.59E-06	Beryllium (Be)	7.17E-08
Ammonia	4.72E-04	SO_2	1.37E-06	Cadmium (Cd)	6.21E-07	Cadmium (Cd)	1.91E-08
Absorbent	3.06E-04	SO_3	0.00E+00	Chromium (Cr)	2.69E-06	Chromium (Cr)	1.27E-07
Energy consumption (KW)	3.06E+02	NO	7.31E-02	Cobalt (Co)	2.28E-07	Cobalt (Co)	1.85E-07
Solid wastes	3.35E+01	NO_2	2.65E-03	Lead (Pb)	6.43E-06	Lead (Pb)	1.97E-06
Liquid wastes	1.48E+00	N_2O	1.09E-03	Manganese(Mn)	1.84E-06	Manganese(Mn)	2.59E-06
		CO	1.13E-01	Nickel (Ni)	1.33E-06	Nickel (Ni)	4.34E-07
		HCL	0.00E+00	Selenium (Se)	1.93E-05	Selenium (Se)	7.49E-06
		HF	0.00E+00	Zinc (Zn)	3.50E-05	Zinc (Zn)	6.11E-06
		CH_4	6.80E-03	Copper (Cu)	1.27E-05	Copper (Cu)	4.23E-07
		NH_3	2.36E-04	Thallium (Tl)	2.73E-07	Thallium (Tl)	3.68E-08
		Emissions to freshwater	**Amount (kg)**	Vanadium (V)	8.75E-06	Vanadium (V)	3.07E-05
		HF	7.60E-03	Barium (Ba)	8.47E-05	Barium (Ba)	5.21E-06
		HCL	2.02E-02	Silver (Ag)	2.73E-08	Silver (Ag)	3.68E-09
		SO_2	1.30E-01	Hg0	1.72E-10	Mercury (Hg)	1.08E-09
		SO_3	6.60E-03	Hg++	0.00E+00		

The results show that most air emissions are originally generated by coal the combustion process and are released from power plant stack. There are no emissions of SO_2, SO_3, HCl, HF and Hg to air from the power plant stack as the CO_2 conditioning unit can remove these air emissions completely and transform them to emissions to freshwater. Direct emissions from the ASU, ESP, FGD, CO_2 conditioning, CO_2 pipeline transport and CO_2 injection unit are not significant. The direct emissions from the CO_2 conditioning, CO_2 pipeline transport and CO_2 injection unit are due to the combustion of natural gas. This research assumes that all solid and liquid wastes from the power plant are well managed and transferred to an ash pond, and eventually transported to landfill. Therefore, there are no direct solid and liquid

emissions from coal combustion, ESP and FGD. Emissions of trace metals to soil are from the surface impoundment(s) or ash landfill(s). Coal is the major resource consumed. The consumption of other resources and materials, including natural gas, limestone and ammonia, are significantly less than coal consumption. The life-cycle environmental impacts of these emissions are analysed in section 10.3.

10.2.1 The Fate of Air Emissions

In oxy-fuel combustion power generation with CO_2 capture and storage, air emissions of concern include CO_2, PM, PM-10, SO_2, SO_3, NO, NO_2, HCl, HF, CO, CH_4 and mercury (Hg) vapour. Ar, N_2 and O_2 may also be present in the CO_2 product. These air emissions are originally generated by the coal combustion process and then totally or partially removed by the pollution control units such as ESP, FGD and the CO_2 conditioning unit. The LCI models developed are able to quantify the removal rate of air emissions of concern across the flue gas treatment processes, with the knowledge that these pollution control units have interactions with and impacts upon each other. Figure 10.2 shows that 94.5% of the CO_2 is finally removed by the oxy-fuel combustion system and 5.5% of the CO_2 is emitted from the CO_2 conditioning unit. 99.7% of the PM-10 is removed by the ESP and PM-10 is further removed by the FGD and CO_2 conditioning unit, with a final emission rate of 0.12%, which is slightly higher than that of post-combustion capture system (0.11%). Around 95% of the SO_2 emissions is removed by the FGD and the remainder totally removed by the CO_2 conditioning unit. The SO_3 emissions can be removed by the ESP and FGD, and any remaining concentration being totally removed by CO_2 conditioning unit. The NO and NO_2 emissions are reduced by 96.56% by the CO_2 conditioning unit. Most HCl and HF emissions are reduced by FGD, at 90% and 30% respectively, and the remaining concentrations are totally removed by the CO_2 conditioning unit. Mercury vapour emissions are reduced by the ESP and FGD and then totally removed in the CO_2 conditioning unit. Emissions of CO, CH_4, Ar, N_2 and O_2 remain unchanged across the ESP and FGD and are reduced by the CO_2 conditioning unit. In order to meet the CO_2 product requirements, the oxy-fuel combustion CO_2 conditioning unit is designed to separate or remove most impurities that exist in the CO_2 concentrated flue gas after combustion. In a state of the art oxy-fuel CO_2 conditioning unit, NOx and SOx are totally removed and other gases are partially separated from the flue gas and vented to the atmosphere.

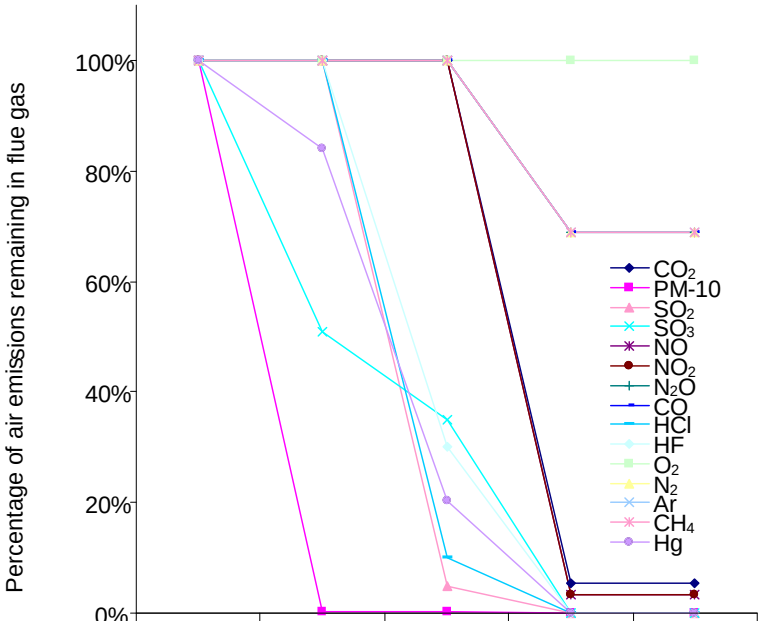

	Combustion	ESP	FGD	CO_2 conditioning	Final emissions to air
CO_2	100.00%	100.00%	100.00%	5.50%	5.50%
PM-10	100.00%	0.30%	0.14%	0.12%	0.12%
SO_2	100.00%	100.00%	5.00%	0.00%	0.00%
SO_3	100.00%	51.00%	35.03%	0.00%	0.00%
NO	100.00%	100.00%	100.00%	3.44%	3.44%
NO_2	100.00%	100.00%	100.00%	3.44%	3.44%
N_2O	100.00%	100.00%	100.00%	68.80%	68.80%
CO	100.00%	100.00%	100.00%	68.80%	68.80%
HCl	100.00%	100.00%	10.00%	0.00%	0.00%
HF	100.00%	100.00%	30.00%	0.00%	0.00%
O_2	100.00%	100.00%	100.00%	99.99%	99.99%
N_2	100.00%	100.00%	100.00%	68.80%	68.80%
Ar	100.00%	100.00%	100.00%	68.80%	68.80%
CH_4	100.00%	100.00%	100.00%	68.80%	68.80%
Hg	100.00%	84.15%	20.19%	0.00%	0.00%

Figure 10.2: The fate of air emissions across the pollution control units in a 500 MW oxy-fuel combustion CO_2 capture power plant.

10.2.2 Fate of Trace Metals

Trace metal emissions originate from coal. After coal combustion, trace metals are partially captured by the pollution control units and are discharged as air emissions, FGD wastes, Gypsum, fly ash, bottom ash and CO_2 conditioning wastes. Figure 10.3 demonstrates that the pattern of trace metal partitioning is very similar to that of the post-combustion capture power generation. It is worth noting that a small portion of the trace metals accompany the CO_2 product into the storage site in the case of oxy-fuel combustion system. There are no emissions of Mercury (Hg) to air, as this is totally removed by the CO_2 conditioning unit.

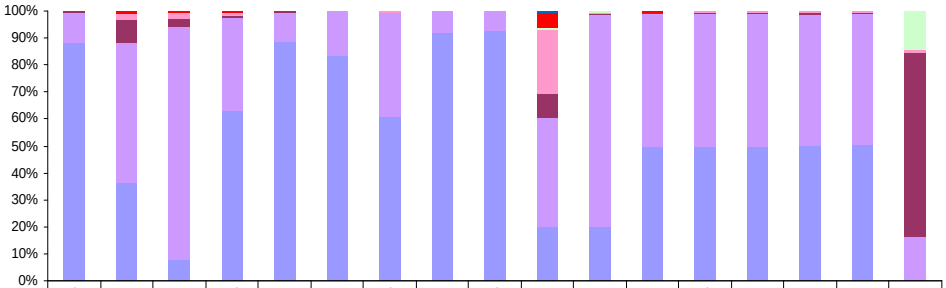

	Sb	As	Be	Cd	Cr	Co	Pb	Mn	Ni	Se	Zn	Cu	Ti	V	Ba	Ag	Hg
injected in to storage reservoir	2.E-05	1.E-03	3.E-04	4.E-04	4.E-05	2.E-05	5.E-05	9.E-06	2.E-05	6.E-03	2.E-04	3.E-04	9.E-05	7.E-05	1.E-04	9.E-05	0.E+00
Emissions to air	0.02%	0.88%	0.24%	0.35%	0.04%	0.01%	0.05%	0.01%	0.02%	5.73%	0.21%	0.25%	0.08%	0.06%	0.13%	0.08%	0.00%
CO_2 Conditioning wastes	0.0024	0.1086	0.0292	0.0437	0.0049	0.0017	0.0059	0.0010	0.0024	0.7070	0.0256	0.0310	0.0100	0.0080	0.0155	0.0100	14.12%
FGD wastes	0.18%	2.20%	2.77%	1.58%	0.08%	0.08%	0.26%	0.06%	0.07%	23.51%	0.67%	0.10%	0.45%	0.46%	0.17%	0.45%	1.39%
To Gypsum	0.03%	8.79%	2.77%	0.17%	0.28%	0.08%	0.26%	0.06%	0.07%	8.70%	0.67%	0.59%	0.45%	0.46%	1.23%	0.45%	68.30%
Fly ash	11.71%	51.46%	86.74%	34.82%	10.97%	16.51%	38.64%	7.95%	6.79%	40.72%	78.40%	49.00%	49.00%	49.00%	48.45%	49.00%	16.19%
Bottom ash	88.05%	36.47%	7.43%	62.99%	88.62%	83.32%	60.77%	91.91%	93.03%	20.00%	20.00%	50.00%	50.00%	50.00%	50.00%	50.00%	0.00%

Figure 10.3: Partitioning of trace metals across the pollution control units in a 500 MW oxy-fuel combustion CO_2 capture power plant.

The percentage of each trace metal finally released to the environment is shown in Figure 10.4. As confirmed by this Figure, the trace metal emissions are similar to that of the post-combustion capture case presented in Section 9.2.3 since the base case scenario used in both systems are similar in many respects. Compared to the power plant with post-combustion capture discussed in Chapter 9, the 500 MW oxy-fuel combustion plant has higher rates of Hg releases to the environment, as the Hg vapour emissions are transformed to Hg emissions to freshwater by the CO_2 conditioning unit after the FGD rather than being transformed to solid wastes by the MEA CO_2 capture unit in the post-combustion case. The emissions of trace metals to the environment are dominated by emissions to air from the power plant and emissions to soil from the surface impoundment. Mercury emissions from the oxy-fuel combustion system are lower, because the CO_2 conditioning unit removes all the air emissions of mercury. It worth noting that a large volume of group III or Group II trace metals such as Se, As, Be and Zn will be released to the storage site together with the CO_2 product. This may cause some contamination at the storage site, however, the impact of trace metals on storage reservoirs is not clear at the moment and further research is required.

In Figure 10.4, the landfill emission results are based on the landfill LCI model with a 1,000-year time frame and assuming that the composite liner of the landfill has a life span of 200 years and, at end of each 200 years, the old composite liner is replaced by a new one. The emissions from landfill are not very significant. As in the post-combustion

scenario, the emissions from landfill are not very significant. If a new composite liner is not used to replace the old one at the end of 200 years, the landfill is treated as a clay layer landfill for the rest of 800 years. Figure 10.5 shows the results of this scenario.

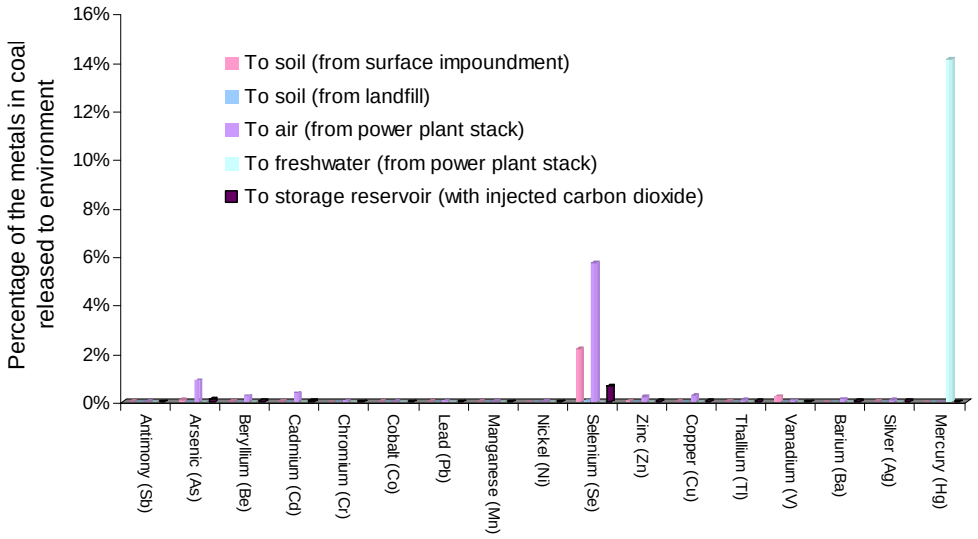

Figure 10.4: Percentage of trace metals released to the environment compared to their original concentration in coal (Composite liner over 1,000 years).

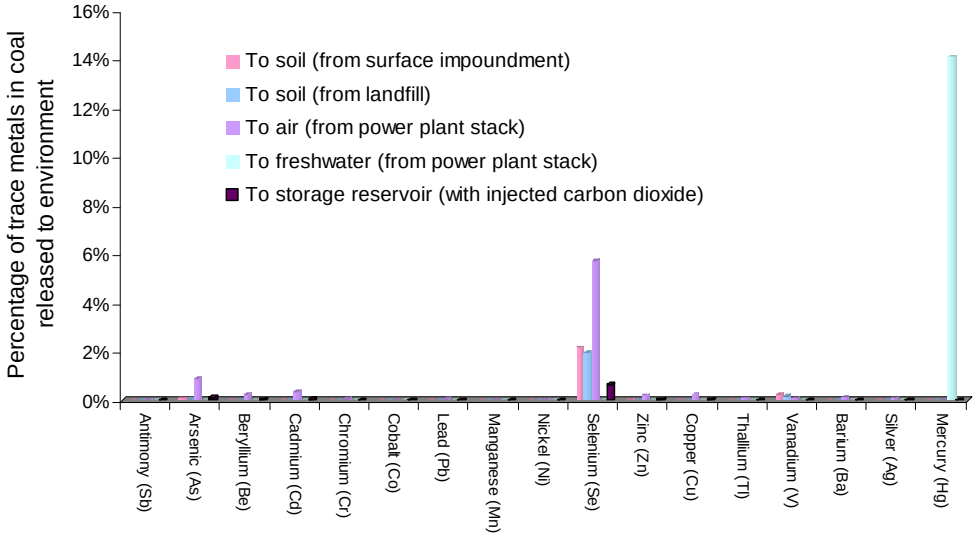

Figure 10.5: Percentage of trace metals released to the environment compared to their original concentration in coal (Composite liner for 200 years and clay liner for 800 years).

10.2.3 Energy Efficiency of Power Plant with Oxy-fuel Combustion Carbon Dioxide Capture and Conditioning

Figure 10.6 shows the energy flow of a 500 MW power plant with oxy-fuel combustion CO_2 capture. It can be seen that the oxy-fuel combustion power plant with CO_2 capture and conditioning (with a gross efficiency of 45%) can achieve a net efficiency of 35.04%, which means that 35.04% of energy in the coal is transformed to electricity. The ASU and CO_2 conditioning consume 5.90% and 3.86% of the coal energy input respectively. Auxiliary energy consumption, which represents the energy used by the ESP and FGD, is insignificant with 0.20% of the coal energy input.

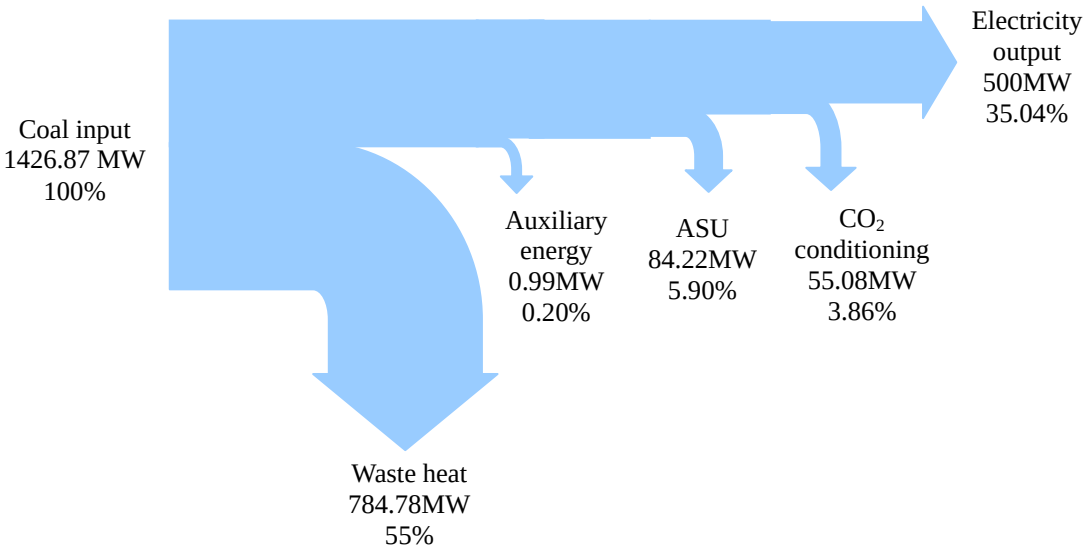

Figure 10.6: Energy flow chart for a 500 MW power plant with oxy-fuel combustion CO_2 capture and conditioning.

10.3 Life Cycle Environmental Impacts of Power Generation with Oxy-fuel Combustion Carbon Dioxide Capture, Transport and Injection

10.3.1 The Overall Life Cycle Impact Assessment Results

Table F4 in Appendix F presents the emissions from a 500 MW power plant scenario with oxy-fuel combustion CO_2 capture, transport and injection, as well as upstream processes, including coal production, coal transportation, limestone production, limestone transport by truck, power plant infrastructure, CO_2 pipeline infrastructure, ASU facility infrastructure, compressor infrastructure. Figure 10.7 illustrates that life-cycle environmental impacts of

the oxy-fuel combustion CO_2 capture ad storage system are dominated by power generation with CO_2 capture and coal production process in all impact categories. The results also reveal that power plant construction has a considerable contribution to FAETP and ODP and the coal railway transport process contributes to the ODP indicator at life-cycle level.

Each environmental impact category is dominated by several key substances. Air emissions from the oxy-fuel combustion capture plant contribute to the AP, EP, GWP100, HTP and POCP Trace metal emissions to air or soils contribute to the FAETP, MAETP and TETP. A more detailed analysis of each individual impact category is provided in the following sections.

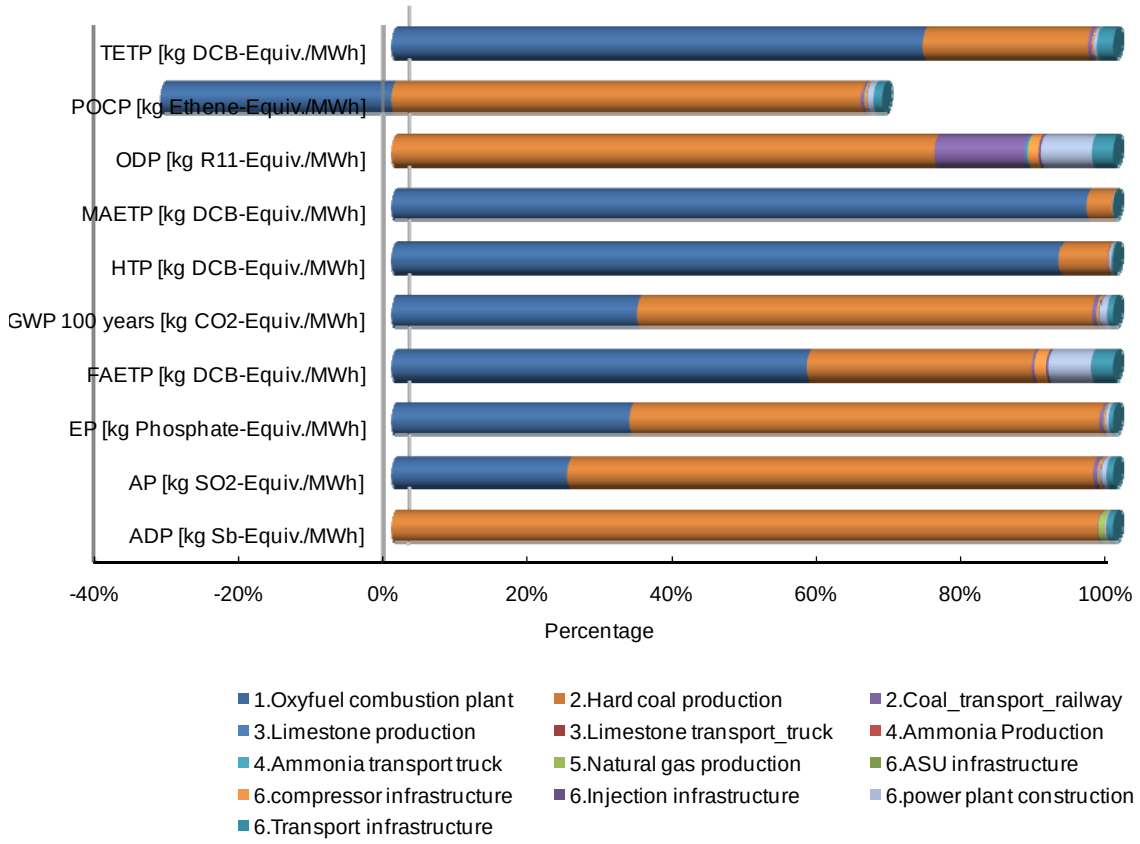

Figure 10.7: Overall LCA results for a 500 MW oxy-fuel combustion CO_2 capture, transport and injection system.

10.3.2 Life Cycle Environmental Impacts per Impact Category

Figure 10.8 shows that the total GWP of the 500 MW oxy-fuel combustion CO_2 capture scenario with transport and injection is 158.46 kg CO_2 equivalent. At 63.11%, the majority of the GWP is due to hard coal production. Emissions from power generation with CO_2

capture make up 34.08% of the GWP. Other upstream processes account for 2.81% of the GWP. Figure 10.8 also shows that CO_2, methane and nitrous oxide are the main substances contributing to GWP. Carbon dioxide emissions (90.35 kg) mainly come from power generation with CO_2 capture (52.68 kg) and hard coal production (33.67 kg). Methane emissions from coal production (65.70 kg CO_2 equiv) account for 99.12% of the total methane emissions.

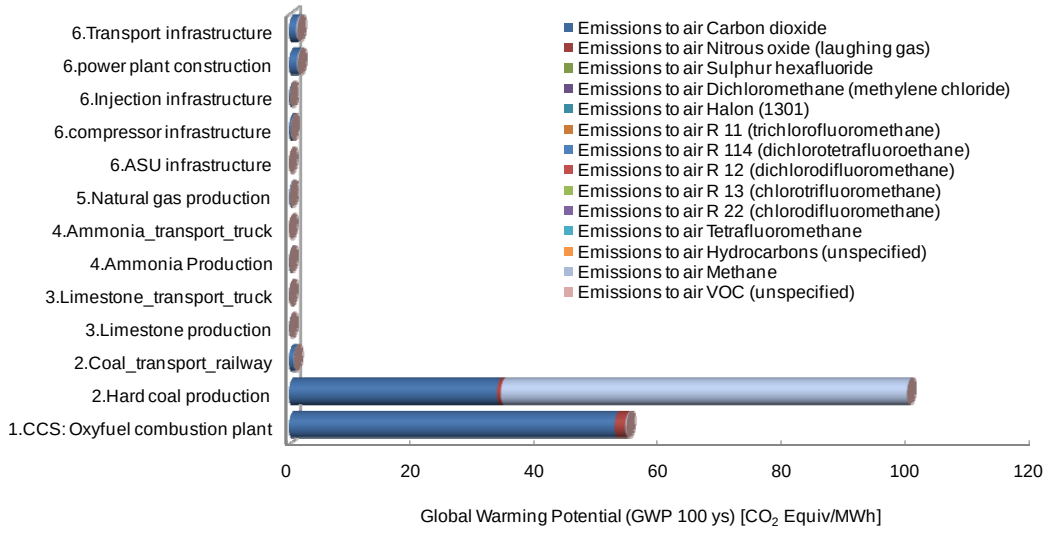

Figure 10.8: Global warming potential (GWP) for a 500 MW oxy-fuel combustion CO_2 capture plant, transport and injection.

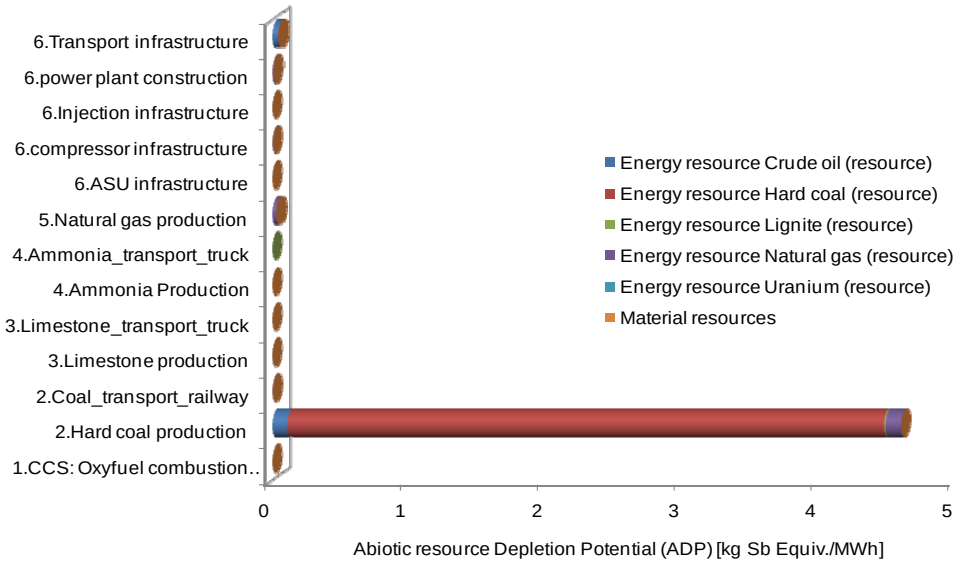

Figure 10.9: Abiotic resource depletion potential for a 500 MW oxy-fuel combustion CO_2 capture plant, transport and injection.

Figure 10.9 shows that the life-cycle Abiotic resource Depletion Potential (ADP) is dominated by coal production, which alone accounts for 97.97%. Natural gas production and transport infrastructure have considerable contribution towards ADP, with 0.64% and 1.00% of ADP respectively. With respect to individual substances contributing to the ADP, hard coal extracted during mining is the primary contributor, accounting for 93.26% of the ADP. Natural gas and crude oil used during coal production also have a considerable contribution towards ADP, with 3.31% and 3.16% of ADP respectively.

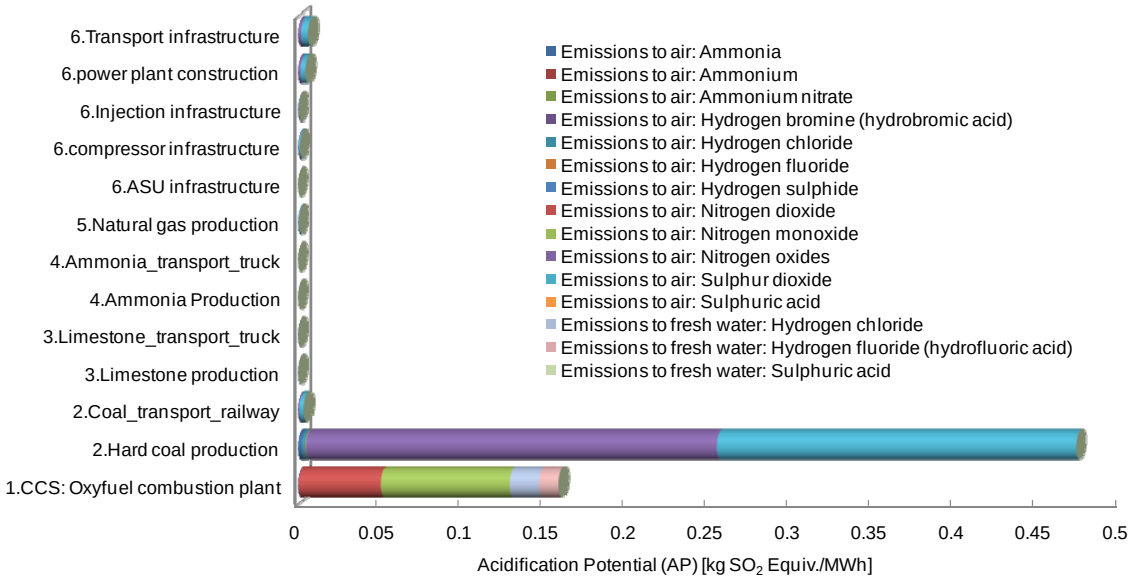

Figure 10.10: Acidification potential for a 500 MW oxy-fuel combustion CO_2 capture plant, transport and injection.

Figure 10.10 illustrates that Acidification Potential (AP) is mainly due to coal production and the power generation with CO_2 capture, which account for 72.88% and 24.42% of the AP respectively. Transport infrastructure, power plant construction and coal railway transportation represent 0.97%, 0.71% and 0.55% of the AP respectively and the other processes contribute to AP by less than 0.5%. Figure 10.10 also shows that emissions to air, including SO_2, NO_x, NO_2 and NO, which represent 35.46%, 39.21%, 7.75% and 12.02% respectively, are the main contributors to AP. Emissions to fresh water, including HCl and HF also contribute to AP with 2.74% and 1.87% respectively. SO_2 and NOx are primarily emitted by the coal production process. NO and NO_2 emissions are mainly from power generation with CO_2 capture. Emissions to fresh water (HCl and HF) are from power generation with CO_2 capture.

Figure 10.11 shows that Eutrophication Potential (EP) is mainly due to hard coal production and power generation with CO_2 capture, with 65.25% and 32.98% of the EP respectively. Analysis of the life cycle impact data shows that emissions to air, emissions to fresh water, emissions to soils, and emissions to sea water account for 98.66%, 1.03%, 0.31% and 0.03% of the EP respectively. NOx, NO and NO_2 are the dominant emissions, accounting for 65.03%, 20.05% and 12.84% of the EP. NOx is primarily emitted by the coal production process. Power generation with CO_2 capture is the main source of NO and NO_2 emissions. Emissions to fresh water, including ammonia and Chemical Oxygen Demand (COD) are from the coal production processes.

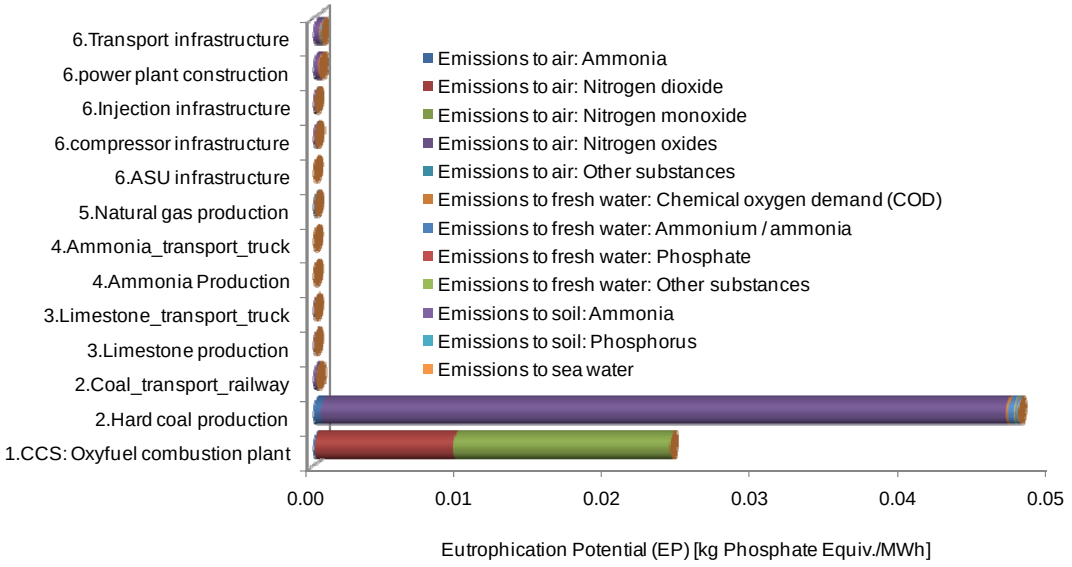

Figure 10.11: Eutrophication potential for a 500 MW oxy-fuel combustion CO_2 capture plant, transport and injection.

The Ozone Layer Depletion Potential (ODP) of oxy-fuel combustion with CO_2 capture, transport and injection is mainly due to the upstream processes, including hard coal production, transport of coal by railway, power plant infrastructure, CO_2 pipeline infrastructure and compressor infrastructure, which account for 75.34%, 12.34%, 7.12%, 2.86% and 1.42% of the ODP respectively.

Figure 10.12 shows that only five substances, Halon, R11, R 114, R12 and R22, contribute to ODP and are all air emissions. Majority of R11, R 114, R12 and R22 emissions come from hard coal production. Considerable amount of R11 and R 114 is generated from transport of coal by railway. Emissions of halon are primarily from power plant infrastructure and pipeline transport infrastructure.

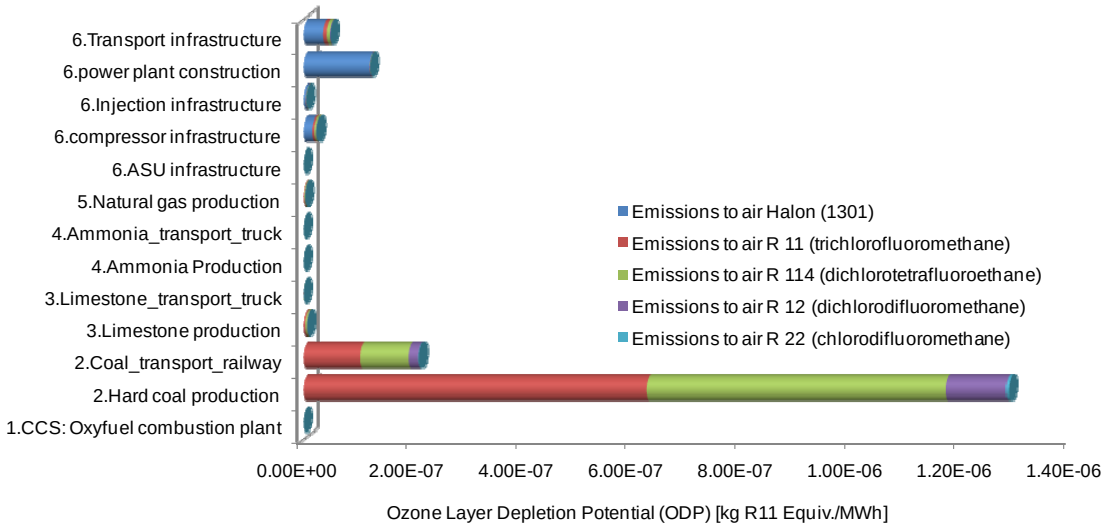

Figure 10.12: Ozone layer depletion potential for a 500 MW oxy-fuel combustion CO_2 capture plant, transport and injection.

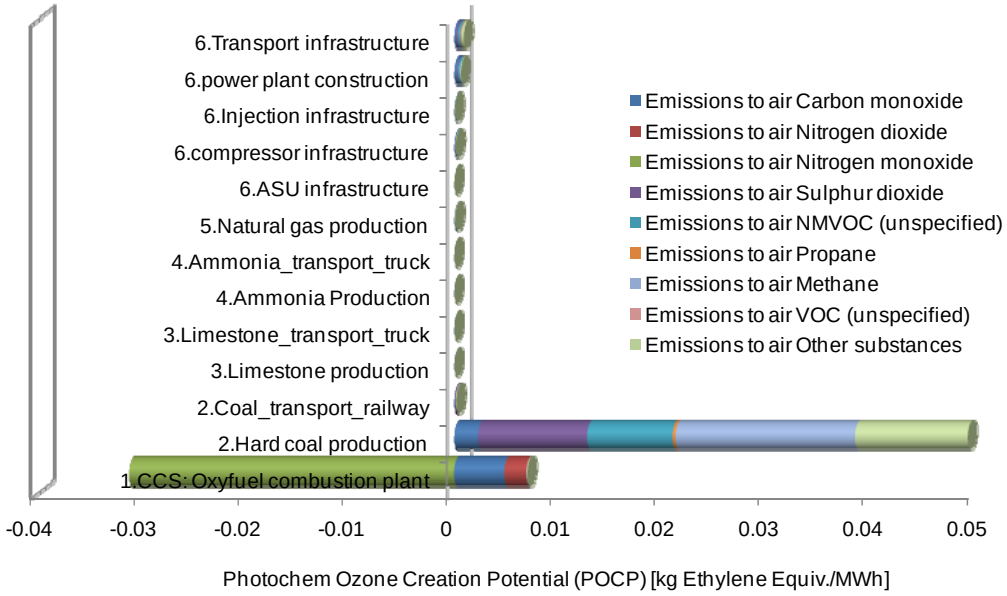

Figure 10.13: Photochemical ozone creation potential for a 500 MW oxy-fuel combustion CO_2 capture plant, transport and injection.

Figure 10.13 shows that, in the 500 MW oxy-fuel combustion base case scenario, the Photochemical Ozone Creation Potential (POCP) is mainly due to the emissions from power generation with CO_2 capture and hard coal production. The overall POCP value of power generation with CO_2 capture is negative, as the emissions of nitrogen monoxide has a negative impact on POCP, with a characterisation factor -0.427 kg Ethylene equivalent (CML 2001). Figure 10.13also illustrates that emissions of methane, sulphur dioxide,

NMVOC (non-methane volatile organic compounds), carbon monoxide and nitrogen oxides to air from hard coal production and the emissions of carbon monoxide to air from power generation with capture have a considerable contribution to POCP.

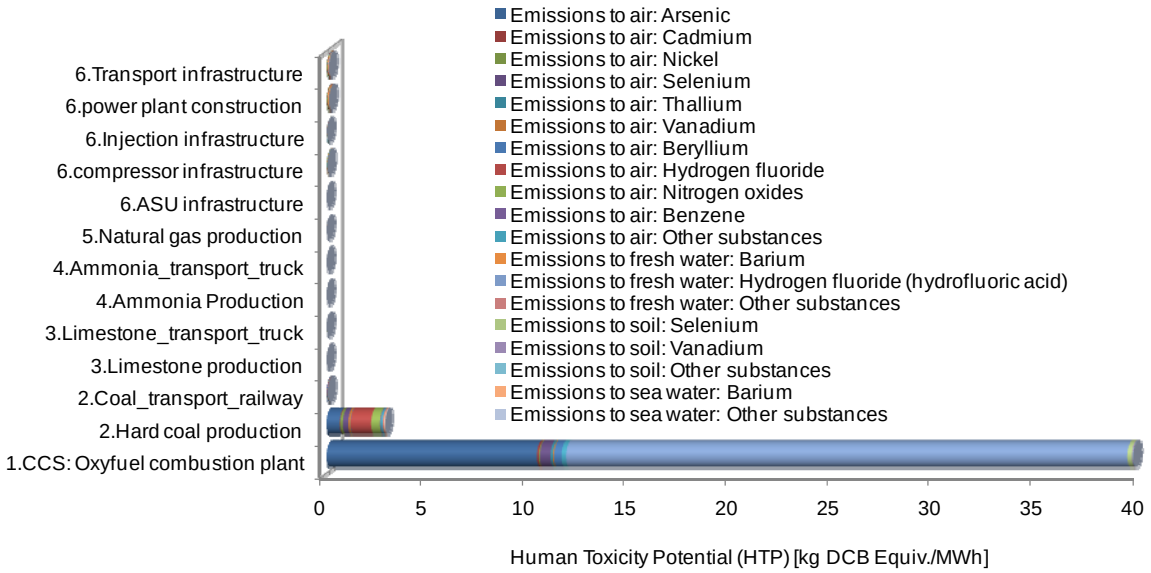

Figure 10.14: Human toxicity potential for a 500 MW oxy-fuel combustion CO_2 capture plant, transport and injection.

As shown in Figure 10.14, at 92.54%, oxy-fuel power generation with CO_2 capture is the main contributor to HTP. Coal production also contributes to HTP (6.62%).

The analysis of the life cycle impact data suggest HF emissions to freshwater and As emissions to air from power generation with CO_2 capture dominate the HTP, accounting for 64.43% and 24.08% of the HTP respectively. HF emission to freshwater from power generation with capture comes from the CO_2 conditioning unit, which captures atmospheric HF emissions and emits HF as a liquid waste. Emissions to air from coal production, including HF, NO_x, As and Se represent 2.30%, 1.00%, 1.50%, 0.61% of the HTP respectively.

Figure 10.15 demonstrate that the upstream processes, such as hard coal production, power plant infrastructure, pipeline transport infrastructure, compressor infrastructure account for the majority of the Fresh Water Aquatic Ecotoxicity Potential (FAETP) at 31.09%, 5.93%, 2.99% and 1.66% respectively.

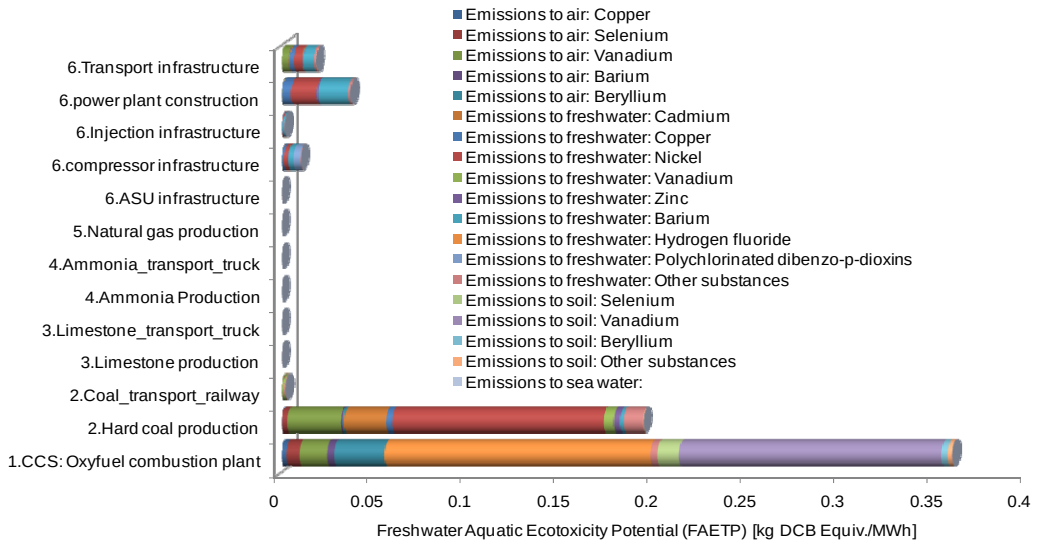

Figure 10.15: Freshwater aquatic ecotoxicity potential for a 500 MW oxy-fuel combustion CO_2 capture plant, transport and injection.

Figure 10.15 shows that FAETP is mainly due to metal emissions, including metal emissions to air, to fresh water, soils and sea water, representing 15.38%, 59.58%, 25.66% and 0.0001% of the FAETP. With respect to emissions to fresh water, HF, nickel, beryllium, cadmium, copper, vanadium and zinc are the main contributors, which represent 22.94%, 22.66%, 21.66%, 4.61%, 3.67%, 1.84%, 1.09% and 0.71% of the FAETP respectively. Nickel, cadmium, vanadium and zinc emissions to fresh water are mainly from hard coal production. The majority of barium and copper emissions to fresh water are from power generation and plant construction. As for the emissions to soils, FAETP is dominated by vanadium, selenium and beryllium emissions from oxy-fuel combustion with capture, accounting for 29.2%, 2.39% and 0.67% of the FAETP respectively. With respect to metal emissions to air, vanadium, beryllium, selenium, copper and barium are the main contributors, accounting for 10.12%, 5.94%, 2.02%, 0.73% and 0.99% of the FAETP. Majority of vanadium, selenium and barium and copper emissions to air come from coal production and power generation. Beryllium to air is mainly emitted from power generation.

Figure 10.16 shows that Marine Ecotoxicity Potential (MAETP) is mainly due to oxy-fuel combustion with CO_2 capture, which account for 96.36% of the MAETP. Coal production represents 3.47% of the MAETP. The HF emissions to fresh water and air account for 96.02% and 3.44% of the MAETP respectively. HF emissions to fresh water mainly originate from power generation and HF emissions to air are due to coal production.

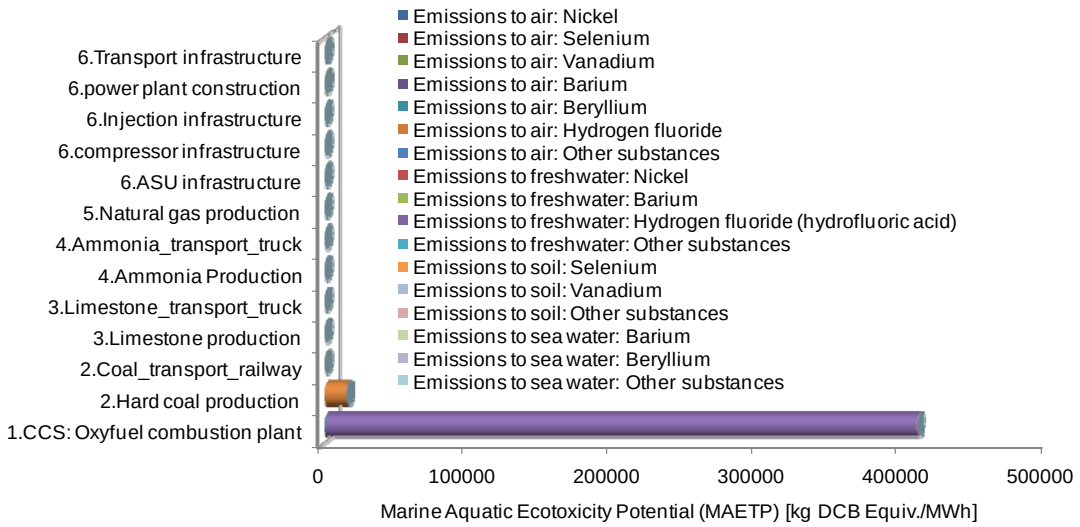

Figure 10.16: Marine aquatic ecotoxicity potential for a 500 MW oxy-fuel combustion CO_2 capture plant, transport and injection.

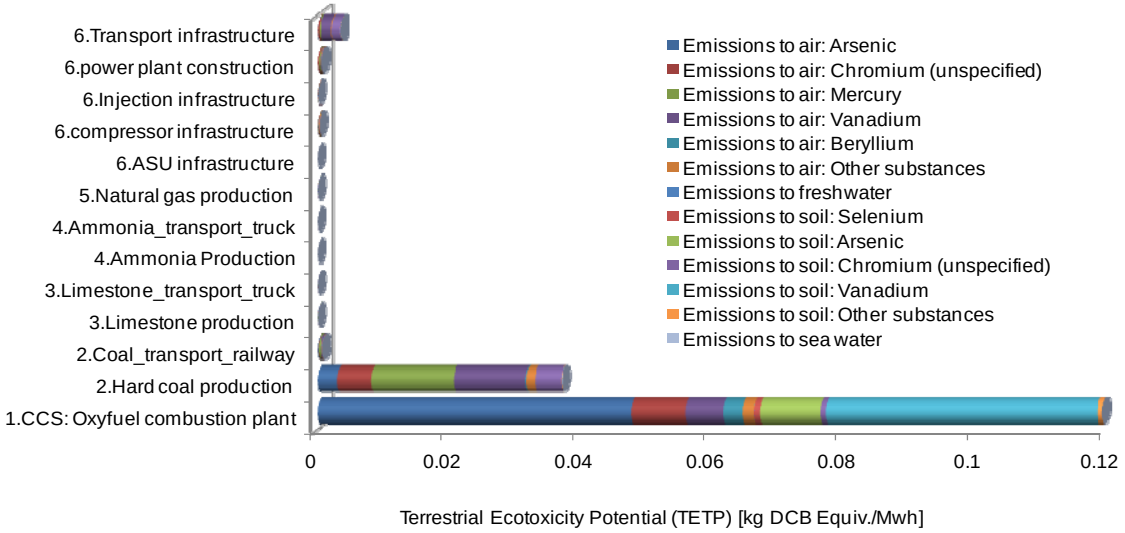

Figure 10.17: Terrestrial ecotoxicity potential for a 500 MW oxy-fuel combustion CO_2 capture plant, transport and injection.

Figure 10.17 shows that the Terrestrial Ecotoxicity Potential (TETP) is primarily due to power generation with CO_2 capture, which account for 73.64% of the TETP. Coal production and pipeline transport infrastructure represent 22.96% and 2.16% of the TETP respectively. Figure 10.17 also demonstrates that TETP is mainly caused by the emissions of metals to air and to soils. In particular, the emissions of arsenic to air and emissions of vanadium to soils from power generation and capture account for 29.78% and 25.78% of the TETP respectively. Other emissions from the oxy-fuel plant with capture, such as Chromium (to air), Vanadium (to air), Beryllium (to air) and Arsenic (to soil) have a

considerable contribution to the TETP, at 5.14%, 3.65%, 1.76%, and 5.71% respectively. Emissions of Mercury, Vanadium, Chromium, and Arsenic to air from hard coal production represents 7.86%, 6.80%, 3.20% and 1.87% of the TETP. It is worth noting that emissions of vanadium to air and chromium to soils from the pipeline transport infrastructure also contribute to the TETP, accounting for 0.97% and 0.77% of the TETP respectively.

10.4 Sensitivity Analysis: Effect of LCI Oxy-fuel Combustion Capture, Transport and Injection Scenario Choices on Life Cycle Environmental Impacts

The scenarios analysed in this section address power generation with oxy-fuel combustion CO_2 capture, conditioning, transport and injection scenario choices to evaluate the significance of technological, operational and geographical settings on the overall system life cycle environmental impact performance. The LCI model developed enables the evaluation of the options that may be considered when assessing or designing an oxy-fuel combustion CO_2 capture, transport and injection scenario. Such analysis would ensure that the design options taken do not result in upstream or downstream changes that will increase the overall environmental impacts of the system.

Table 10.2: Description of base case scenario and sensitivity analysis options for a 500 MW power plant with oxy-fuel combustion CO_2 capture, conditioning, transport and injection.

		Base case scenario	Sensitivity analysis alternatives
Technology options	**Boiler type**	PC wall fired, dry bottom	
	Power plant gross energy efficiency	45%	35~50%
	Air separation unit energy consumption	82.44 MW	65~100% of baseline for future technology
	CO_2 conditioning unit energy consumption	55.08 MW	65~100% of baseline for future technology
Operational factors	**O_2 purity at the air separation unit**	95%	90~100%
	HF removal rate in CO_2 conditioning unit	100%	60~100%
	SO_2 removal rate in CO_2 conditioning unit	100%	60~100%
	NOx removal rate in CO_2 conditioning unit	100%	60~100%
Geographical setting	**Coal type**	US Appalachian (bituminous)	Australia N.S. Wales (bituminous); US Illinois No.6 (bituminous); Poland (bituminous); S. Africa Transvaal (bituminous); South Australia Leigh Creek (lignite); Western Australia (sub-bituminous);

The options evaluated in this Chapter are presented in Table 10.2 together with the details of the base case scenario. The effect of the scenario choices analysed on the LCA environmental impact indicator scores are presented in the following paragraphs starting with the technology options, followed by operational factors and finally the changes due to geographical setting. The results are illustrated in Figures 10.18 to 10.27 presenting the relative LCA environmental impact changes in relation to the oxy-fuel combustion base case scenario.

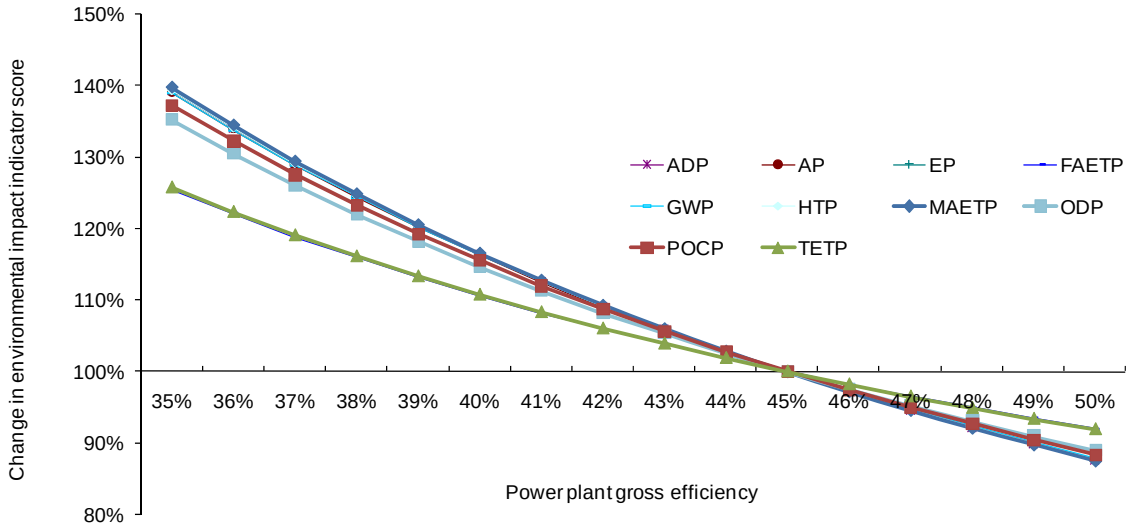

Figure 10.18: The effect of power plant gross efficiency on life cycle impact indicator scores (oxy-fuel combustion CO_2 capture, transport and injection).

Figure 10.18 shows that the effect of plant energy efficiency on environmental impacts is not linear and all impact categories are very sensitive to the change of power plant energy efficiency. Increase of plant gross efficiency can significantly reduce life-cycle environmental impacts in all categories. For example, an increase of energy efficiency from 45% to 50% causes a 10% decrease in impact indicator scores in all categories. This is because the increase of energy efficiency reduces the coal consumption and hence reduces emissions from both the power plant and upstream processes (e.g. coal production). The results indicate that TETP is less sensitive to the change of plant gross efficiency, since a significant proportion of TETP originates from trace metal emissions to soils from surface impoundments and landfill, which are mainly influenced by their design.

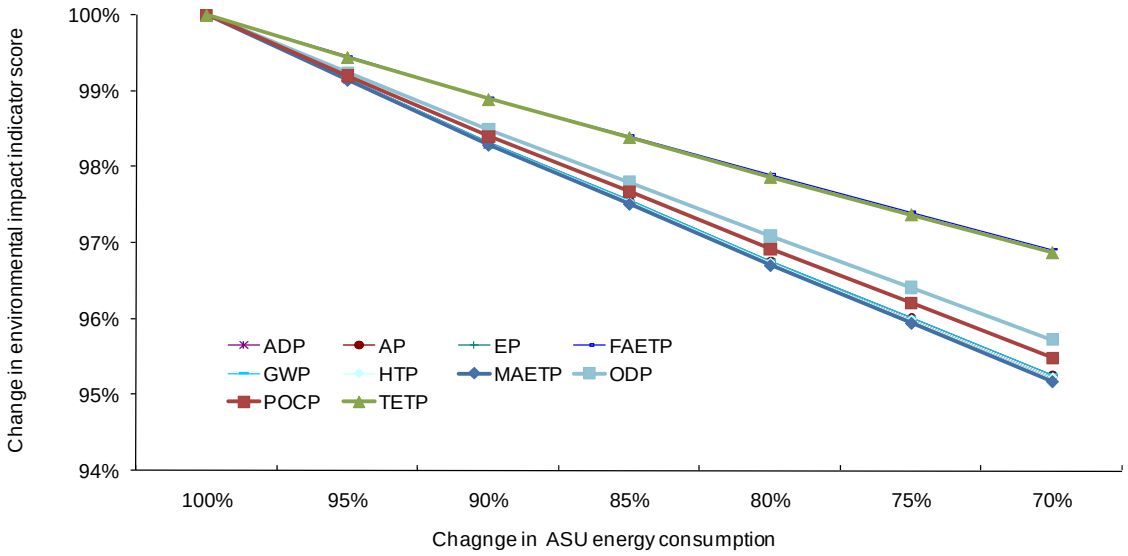

Figure 10.19: The effect of ASU energy consumption on life cycle impact indicator scores (oxy-fuel combustion CO_2 capture, transport and injection).

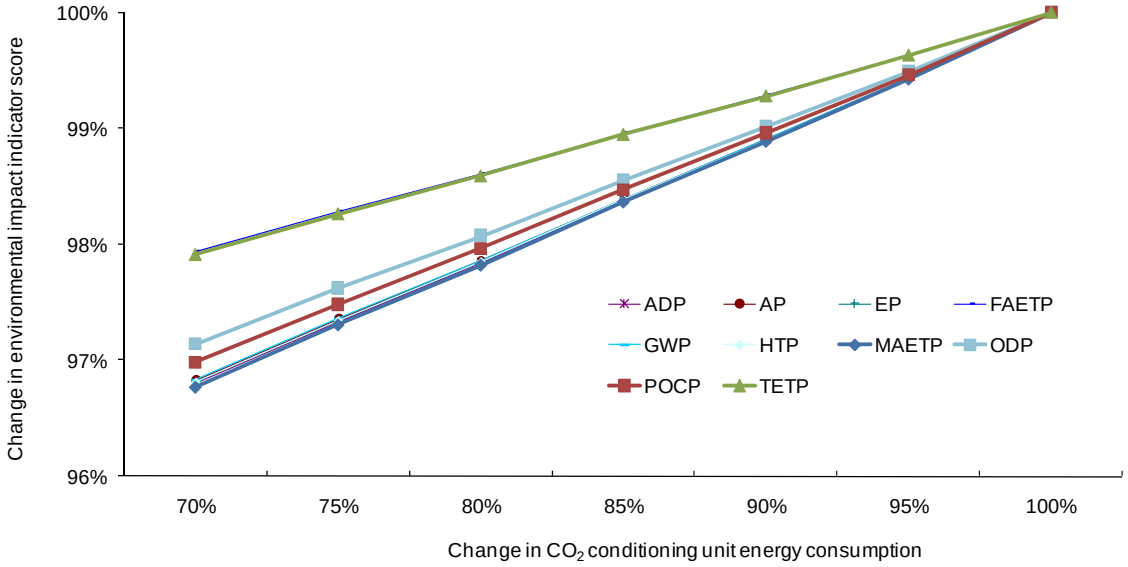

Figure 10.20: The effect of CO_2 conditioning unit energy consumption on life cycle impact indicator scores (oxy-fuel combustion CO_2 capture, transport and injection).

Figures 10.19 and 10.20 show that any decrease in the ASU or CO_2 conditioning unit energy consumption also decreases the life cycle impacts of the system. A 5% decrease in the ASU energy consumption can cause around 1% of decrease in the ADP, AP, EP, GWP, MAETP, POCP, HTP and ODP and around 0.5% decrease in FAETP and TETP at life-cycle

level. In the case of CO_2 conditioning unit energy consumption, these figures are 0.5% and 0.25% respectively. This can be explained by the fact that any reduction in energy consumption reduces the use of coal and consequently decreases emissions from both the power plant and upstream processes e.g. coal production. Life cycle impact categories such as FAETP and TETP are less sensitive to a change in the ASU energy consumption since significant proportion of FAETP or TETP is related to trace metal emissions to soils from surface impoundments and landfills, which are mainly controlled by the design of these facilities.

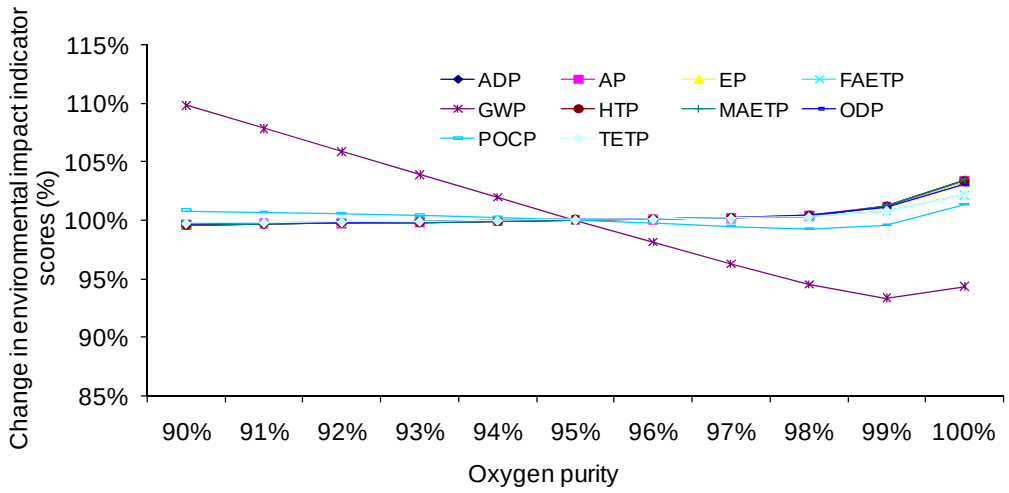

Figure 10.21: The effect of ASU oxygen product purity on life cycle impact indicator scores (oxy-fuel combustion CO_2 capture, transport and injection).

In oxy-fuel combustion CO_2 capture, the power plant can chose to operate at different O_2 product purities. Figure 10.21 demonstrates that the increase of O_2 product purity can decrease GWP but do not increase other environmental impacts as long as the O_2 product purity is less than 98%. This is because the use of higher O_2 purity in the system increases the CO_2 concentration in flue gas and consequently decreases the rate of CO_2 vented to the atmosphere in the CO_2 conditioning unit. If O_2 product purity is larger than 98%, this will increase the energy consumption of the ASU significantly and consequently increase the life-cycle environmental impacts. From LCA point of view, O_2 product purity at 98% is the optimum value, at which GWP is reduced by 5% compared to O_2 product purity at 95%.

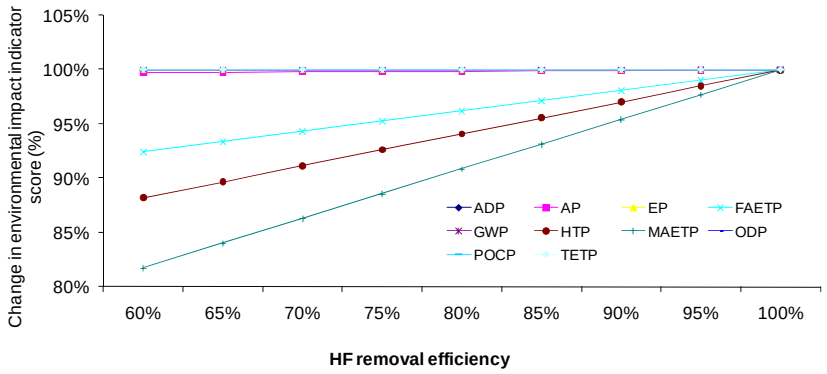

Figure 10.22: The effect of HF removal efficiency on life cycle impact indicator scores (oxy-fuel combustion CO_2 capture, transport and injection).

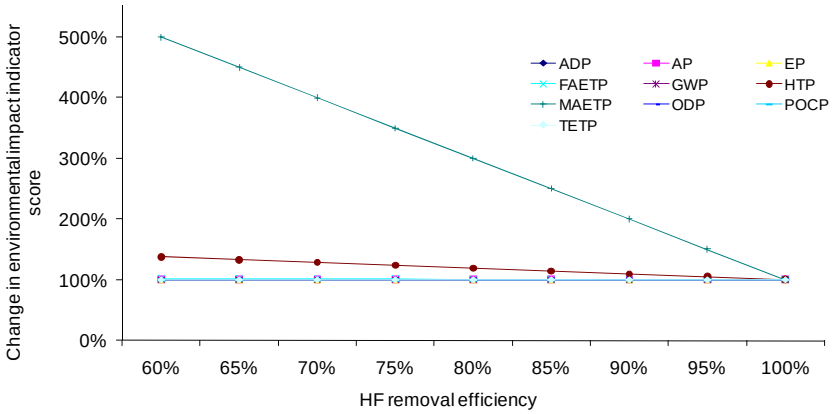

Figure 10.23: The effect of HF removal efficiency on life cycle impact indicator scores with 95% of the waste water HF content removed by treatment (oxy-fuel combustion CO_2 capture, transport and injection).

As discussed earlier in Section 10.3, HF emissions make a significant contribution towards FAETP, HTP and MAETP. Therefore, it is important to analyse the effect of HF removal rate at the CO_2 conditioning unit, where HF is removed from the flue gas and is dissolved into waste water. Figure 10.22 illustrates that the increase of HF removal rate increases the FAETP, HTP and MAETP, as this research assumes that HF in waste water is discharged to freshwater and HF emissions to freshwater have higher impacts than that for HF emissions to air. Hence, HF in waste water is required to be treated to reduce the emissions of HF to freshwater and the consequent environmental impacts. Figure 10.23 shows that, if 95% of HF in waste water is removed, then the increase of HF removal rate in the CO_2 conditioning unit will help to decrease the MAETP and HTP significantly.

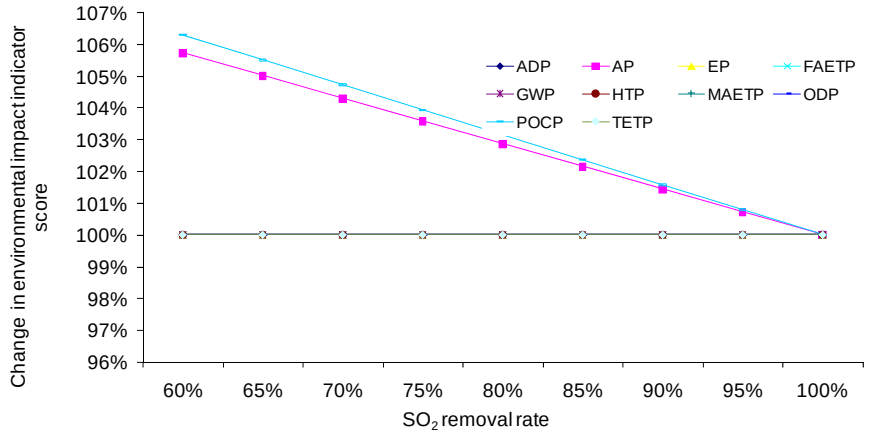

Figure 10.24: The effect of SO_2 removal rate on life cycle impact indicator scores (oxy-fuel combustion CO_2 capture, transport and injection).

Figure 10.24 shows that 5% increase in the SO_2 removal rate at the CO_2 conditioning unit can reduce 0.8% of the AP and POCP and do not increase the other environmental impacts, since increasing the SO_2 removal rate at the CO_2 conditioning unit does not result in increased energy consumption, material use or other emissions.

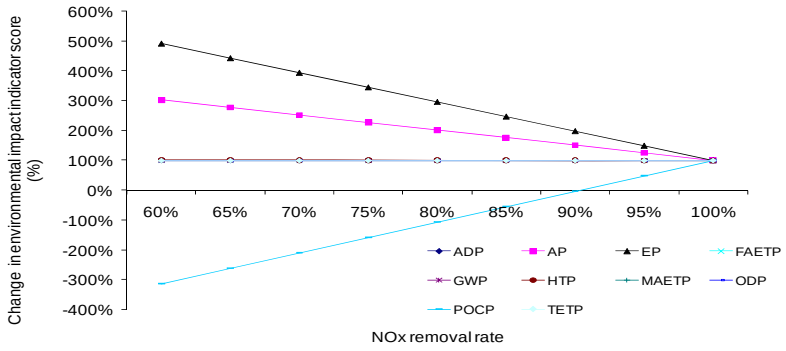

Figure 10.25: The effect of NOx removal rate on life cycle impact indicator scores (oxy-fuel combustion CO_2 capture, transport and injection).

Figure 10.25 demonstrates that an increase in NOx removal rate at the CO_2 conditioning unit leads to a significant decrease in both EP and AP but an equally strong increase in the POPC.

Mining and combustion of different ranks of coal result in different levels of life cycle environmental impacts. Figures 10.26 and 10.27 compare the life cycle environmental impacts of a number of different coals with that of the US Appalachian coal used earlier in

the oxy-fuel combustion base case scenario. The two Figures show that different types of coals used in power generation result in different environmental impacts both at direct emissions level (plant level) and at life-cycle level. At power plant level, the variability of the impact indicators such as HTP, TETP, FAETP and MAETP is because the amount of trace metals in different coals varies significantly. For example, the Polish coal has a higher score in HTP, TETP and FAETP because it contains large amounts of trace metals, especially Arsenic and Vanadium. The variability in other indicators such as AP, EP, POCP or GWP at plant level is less significant, because these impacts depend primarily on the amount of S, N, C, and CL in coal, which do not vary as much as the trace metal contents. At life-cycle level, the variability of environmental impact scores is caused by both power generation with CO_2 capture and the upstream processes.

Figure 10.27 suggest that the Leigh Creek lignite and the sub-bituminous coal from Australia have lower life-cycle environmental impacts in GWP, AP, EP and POCP capacities. The modelling work has shown that the life-cycle GWP of the lignite and sub-bituminous coals used in the oxy-fuel combustion case are 76.57 and 70.84 kg CO_2 equivalent respectively, which are nearly half of the life-cycle GWP of the bituminous coals used for the same 500 MW plant scenario.

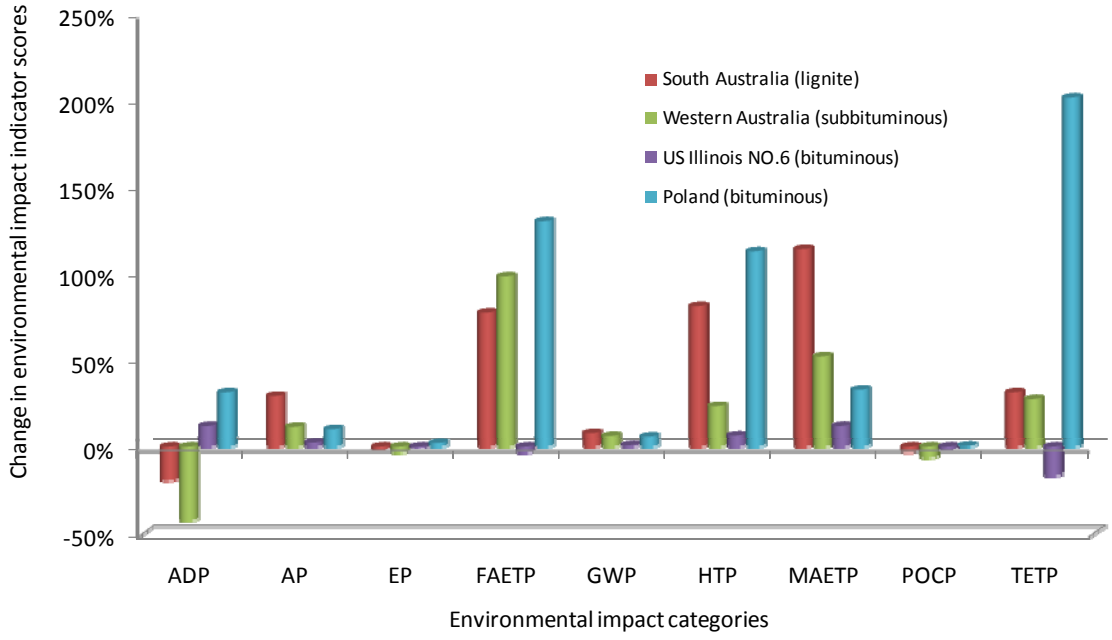

Figure 10.26: Plant level effects of coal type on environmental impacts of power generation with oxy-fuel combustion CO_2 capture (the base case represents a 500 MW plant using a US Appalachian low sulphur bituminous coal).

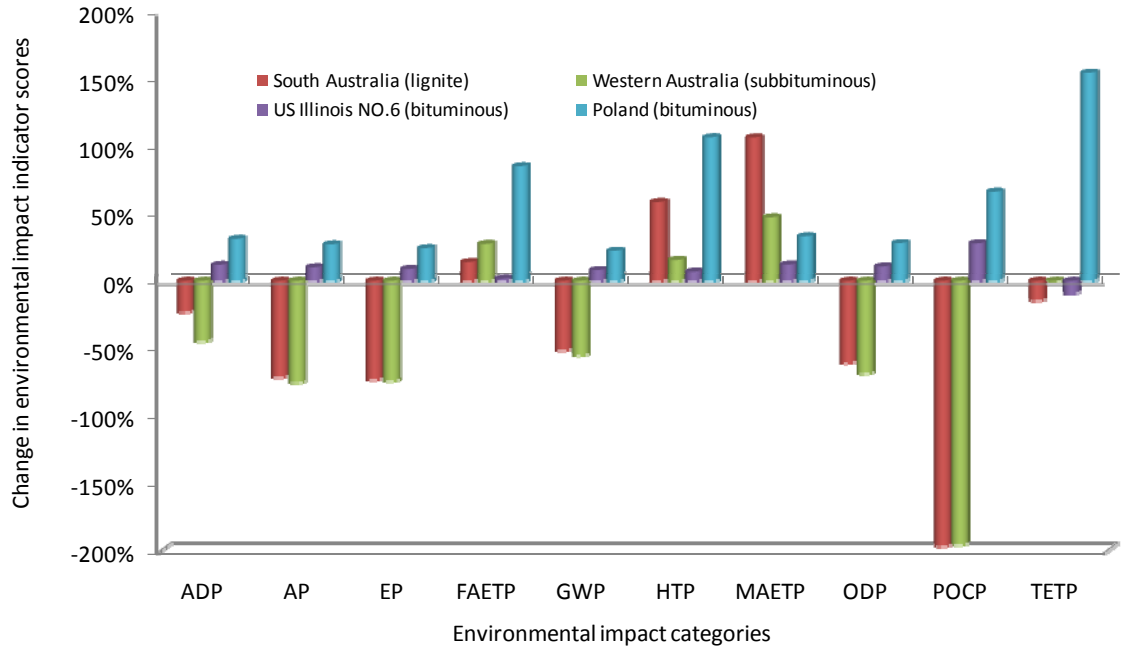

Figure 10.27: Life cycle level effects of coal type on environmental impacts of power generation with oxy-fuel combustion CO_2 capture (the base case represents a 500 MW plant using a US Appalachian low sulphur bituminous coal).

10.5 Uncertainty Analysis: Effect of LCI Input Data on Emissions, Resource Consumption and Life Cycle Environmental Impacts

Monte Carlo simulations were carried out to quantify the uncertainties associated with each environmental emission or resource (or material) consumption evaluated in this research. The methodological framework involved in the Monte Carlo simulations was described in Chapter 4. The input parameters identified for each component unit process in power generation with oxy-fuel combustion CO_2 capture, transport and injection and their ranges and distributions are described in Table F1 in Appendix F. Due to lack of historical data and the uniqueness of power generation projects, the selection of probability density functions (pdf's) for the factors or parameters considered was based on subjective judgment. The commercial LCA software GaBi version 4, which is able to handle input data sampling from statistical distributions in a Monte Carlo framework and provide the LCA results for numerous iterations as statistical distributions was used to conduct the Monte Carlo simulations.

The base case scenario described in Table 10.1 was used for the uncertainty evaluation for a 500 MW oxy-fuel combustion CO_2 capture plant with PC wall dry bottom boiler burning Appalachian coal. In all cases, 5,000 Monte Carlo simulations runs were carried out and the statistical properties of the outputs, such as mean, median, standard deviation, and different levels of confidence are provided in tabular form. The results are grouped under the following categories:

- Direct air emissions for major compounds and trace metals;
- Direct emissions of trace metals to freshwater;
- Direct emissions of trace metals to soils; and
- Direct life cycle environmental impacts;
- Life cycle impacts of the complete oxy-fuel combustion CO_2 capture, transport and injection system including upstream emissions from coal, transport, plant construction and infrastructure.

Figure 9.28 demonstrates the uncertainty analysis results for direct air emissions for major compounds. The corresponding statistical measures are provided in Table 10.3. The emissions of CO, NH_3, and CO_2 are less uncertain (smaller standard deviations) than emissions of HF, HCl, SO_2, and SO_3, because emissions of HF, HCl, NO, NO_2, SO_2, and SO_3 are affected by more pollution control processes as discussed in Figure 10.2 and this increases the uncertainty. The uncertainty of CO_2 emissions comes from the variability of the CO_2 recovery rate in the CO_2 conditioning unit and the variability of carbon in coal.

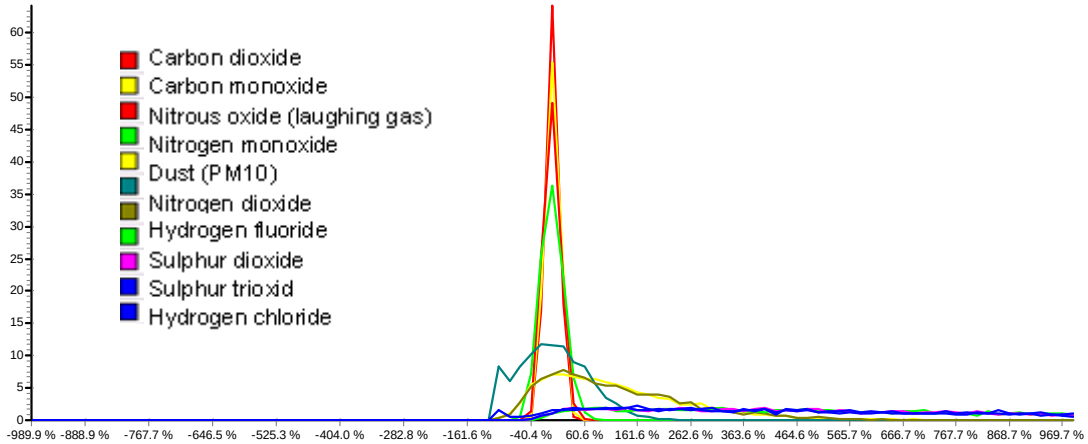

Figure 10.28: Histograms of air emissions at direct emission level.

Table 10.3: Statistical outputs of air emissions at direct emission level.

Emissions	Base case scenario	Mean	Standard deviation (of base case value)	10% Percentile	25% Percentile	Median	75% Percentile	90% Percentile
Carbon dioxide	60.386	60.872	13%	51.071	55.495	60.609	66.208	71.163
Carbon monoxide	0.20789	0.20764	15.10%	0.1697	0.18555	0.20618	0.22776	0.24944
Nitrous oxide	0.006671	0.006651	22%	0.0048317	0.005637	0.006602	0.007574	0.00852
Nitrogen monoxide	0.083889	0.18544	62.80%	0.05987	0.097256	0.16152	0.24954	0.34519
Dust (PM10)	0.006029	0.00619	63.20%	0.00093544	0.003234	0.006048	0.008786	0.011323
Nitrogen dioxide	0.003054	0.0068	63.50%	0.0022017	0.003554	0.005841	0.009196	0.0127
Hydrogen fluoride	6.02E-05	0.00054	70.30%	0.00012807	0.000244	0.000457	0.000748	0.001075
Sulphur dioxide	0.001044	0.009279	73.60%	0.0021507	0.004065	0.007607	0.012943	0.018803
Sulphur trioxide	5.25E-05	0.000472	75%	0.00010912	0.000202	0.000385	0.000643	0.000958
Hydrogen chloride	0.000161	0.001421	86.70%	0.00025432	0.000523	0.00108	0.00198	0.003077

The uncertainty analysis results for the emissions of trace metals to air are shown in Figure 10.29 and Table 10.4. The uncertainty of emissions of trace metals to air is larger than that of air emissions, because the amount of trace metals in coal varies more significantly than that of C, S, N, Cl or F and all the pollution control processes can affect the emissions of trace metals to air. Because of the significant variability in the amount of trace metal in coal a positively skewed distribution is used in this research to assign the input pdf for each trace metal in coal. Mercury, Manganese, Lead, Thallium, Silver, Beryllium, Vanadium and Barium have larger uncertainty than other trace metals because the removal rates of these metals in the ESP are higher (around 98%) and a small change of the removal rates cause a larger change in the final emissions.

Table 10.4: Statistical outputs of trace metal emissions to air at direct emission level.

Emissions	Base case scenario	Mean	Standard deviation (% of base case scenario)	10% Percentile	25% Percentile	Median	75% Percentile	90% Percentile
Cadmium	7.41E-07	9.79E-07	53.60%	3.83E-07	5.98E-07	8.99E-07	1.28E-06	1.68E-06
Selenium	1.39E-05	2.90E-05	75.50%	5.78E-06	1.26E-05	2.43E-05	4.00E-05	5.90E-05
Chromium (unspecified)	3.12E-06	4.47E-06	80.90%	6.99E-07	1.77E-06	3.60E-06	6.32E-06	9.28E-06
Arsenic	3.41E-05	6.14E-05	86%	8.42E-06	2.22E-05	4.79E-05	8.64E-05	0.000132
Nickel	1.59E-06	2.14E-06	88.50%	3.67E-08	7.15E-07	1.70E-06	3.10E-06	4.67E-06
Copper	1.46E-05	4.33E-05	93.40%	5.00E-06	1.42E-05	3.17E-05	6.06E-05	9.76E-05
Antimony	7.49E-08	1.57E-07	94.30%	1.99E-08	5.25E-08	1.17E-07	2.15E-07	3.49E-07
Cobalt	2.64E-07	5.15E-07	95.40%	6.00E-08	1.68E-07	3.72E-07	7.12E-07	1.16E-06
Zinc	2.59E-05	7.24E-05	99.80%	8.40E-06	2.24E-05	5.07E-05	9.77E-05	0.000166
Mercury	9.03E-08	1.69E-06	103%	1.90E-07	4.89E-07	1.13E-06	2.31E-06	3.86E-06
Manganese	2.12E-06	4.68E-06	109%	4.87E-08	1.03E-06	3.11E-06	6.57E-06	1.13E-05
Lead	7.41E-06	1.95E-05	110%	9.28E-07	4.69E-06	1.28E-05	2.70E-05	4.66E-05
Thallium	3.13E-07	8.96E-07	113%	6.21E-08	2.16E-07	5.64E-07	1.20E-06	2.14E-06
Silver	3.13E-08	9.11E-08	116%	6.92E-09	2.21E-08	5.57E-08	1.22E-07	2.19E-07
Beryllium	1.83E-06	5.10E-06	120%	1.09E-07	8.99E-07	2.96E-06	7.06E-06	1.29E-05
Vanadium	1.01E-05	2.94E-05	121%	1.28E-06	6.31E-06	1.79E-05	3.95E-05	7.22E-05
Barium	9.72E-05	0.000208	123%	5.13E-06	4.01E-05	0.000123	0.000282	0.000508

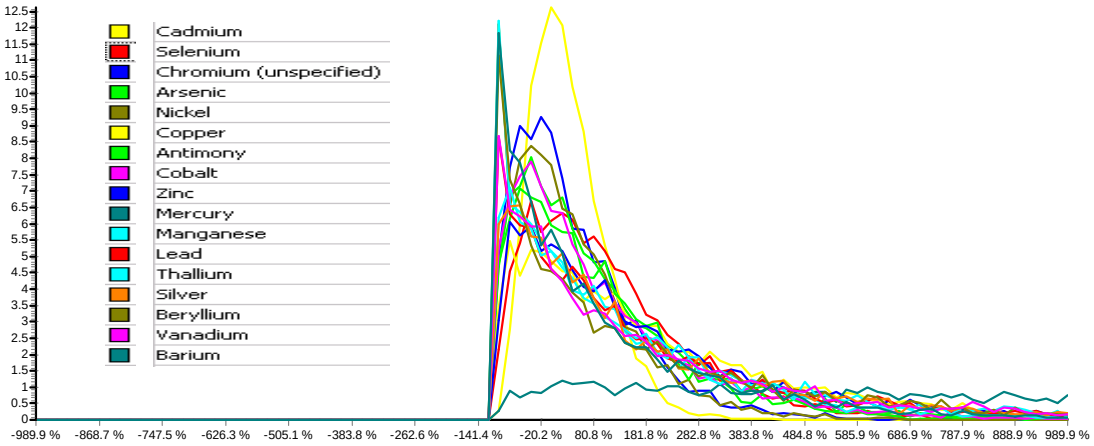

Figure 10.29: Histogram of trace metal emissions to air at direct emission level.

The uncertainty analysis results for the emissions of trace metals to freshwater are shown in Figure 10.30 and Table 10.5. The uncertainty of trace metal emissions to freshwater is smaller than that of most air emissions because they are affected by fewer factors in the CO_2 conditioning unit.

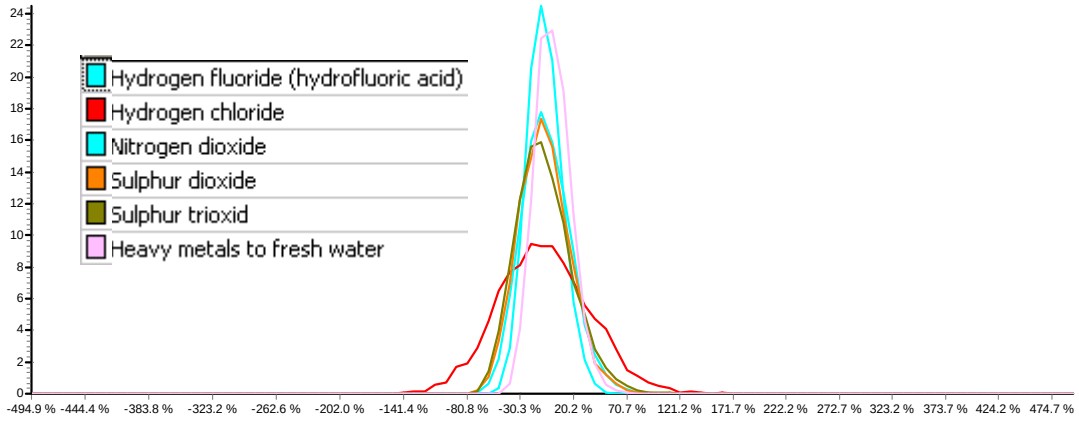

Figure 10.30: Histogram of trace metal emissions to freshwater at direct emission level.

Table 10.5: Statistical outputs of trace metal emissions to freshwater at direct emission level.

Emissions	Base case scenario	Mean	Standard deviation (% of base case value)	10% Percentile	25% Percentile	Median	75% Percentile	90% Percentile
Hydrogen fluoride (hydrofluoric acid)	0.008705	0.008047	17.40%	0.00631	0.007063	0.007972	0.008938	0.009887
Hydrogen chloride	0.023216	0.021441	46.90%	0.009043	0.014531	0.021118	0.02794	0.034594
Nitrogen dioxide	0.083889	0.079158	24.50%	0.055273	0.065753	0.078082	0.091463	0.10407
Sulphur dioxide	0.14857	0.13756	25.90%	0.093338	0.11223	0.13588	0.16077	0.18366
Sulphur trioxid	0.007583	0.007016	28.40%	0.004594	0.005622	0.006871	0.008198	0.009677
Heavy metals to fresh water	7.02E-09	7.06E-09	16.60%	5.62E-09	6.22E-09	6.99E-09	7.79E-09	8.56E-09

Figure 10.31 demonstrates the histograms of emissions of trace metals to soils resulting from the uncertainty analysis. The relevant statistical outputs are provided in Table 10.6. The uncertainty of trace metal emissions to soils is smaller than that of trace metal emissions to air and the histograms of these emissions are less skew than the histograms of trace metal emissions to air. This is because the emissions of trace metals to soils depend mostly on the surface impoundment unit and the landfill unit characteristics and are less affected by the variability of trace metals in coal.

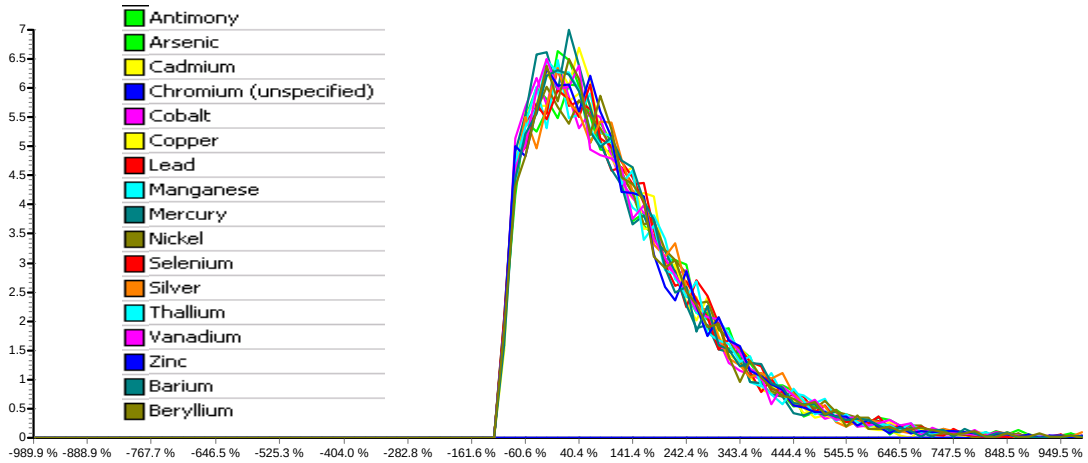

Figure 10.31: Histogram of trace metal emissions to soils at direct emission level.

Table 10.6: Statistical outputs of trace metal emissions to soils at direct emission level.

Emissions	Base case scenario	Mean	Standard deviation (% of base case value)	10% Percentile	25% Percentile	Median	75% Percentile	90% Percentile
Antimony	3.65E-08	8.01E-08	76.60%	1.57E-08	3.57E-08	6.61E-08	1.11E-07	1.60E-07
Arsenic	2.74E-06	6.16E-06	77.90%	1.23E-06	2.64E-06	5.07E-06	8.51E-06	1.23E-05
Cadmium	1.89E-08	3.96E-08	72.10%	8.29E-09	1.81E-08	3.36E-08	5.48E-08	7.79E-08
Chromium (unspecified)	0	9.76E-08	220%	0	0	0	1.79E-08	4.18E-07
Cobalt	1.82E-07	3.90E-07	77.30%	7.38E-08	1.66E-07	3.25E-07	5.42E-07	7.82E-07
Copper	4.17E-07	9.12E-07	77.70%	1.80E-07	3.88E-07	7.57E-07	1.26E-06	1.84E-06
Lead	1.94E-06	4.30E-06	77.30%	8.49E-07	1.88E-06	3.59E-06	5.92E-06	8.46E-06
Manganese	2.55E-06	5.65E-06	75.30%	1.12E-06	2.46E-06	4.72E-06	7.83E-06	1.14E-05
Mercury	1.39E-09	2.90E-09	79.20%	5.54E-10	1.23E-09	2.34E-09	4.01E-09	5.90E-09
Nickel	4.29E-07	9.59E-07	76.10%	1.85E-07	4.10E-07	7.99E-07	1.33E-06	1.92E-06
Selenium	7.87E-06	1.74E-05	76.60%	3.31E-06	7.65E-06	1.45E-05	2.39E-05	3.50E-05
Silver	3.63E-09	8.08E-09	76.20%	1.53E-09	3.57E-09	6.86E-09	1.11E-08	1.63E-08
Thallium	3.63E-08	7.86E-08	77.20%	1.56E-08	3.37E-08	6.49E-08	1.09E-07	1.58E-07
Vanadium	3.03E-05	6.71E-05	78.60%	1.30E-05	2.82E-05	5.49E-05	9.28E-05	0.000134
Zinc	6.05E-06	1.31E-05	77.10%	2.59E-06	5.67E-06	1.08E-05	1.81E-05	2.65E-05
Barium	5.14E-06	1.13E-05	76.90%	2.31E-06	4.95E-06	9.47E-06	1.53E-05	2.29E-05
Beryllium	7.08E-08	1.55E-07	77.30%	3.24E-08	6.85E-08	1.28E-07	2.13E-07	3.09E-07

Figure 10.32 demonstrates the histograms of the environmental impacts of power generation with oxy-fuel combustion CO_2 capture. The statistical outputs are provided in Table 10.7. The results show that the uncertainty of ADP, GWP, MAETP and HTP are less than that of TEPT, FAETP, AP, EP and POCP because GWP, MAETP and HTP depend on air emissions, which have lower uncertainties than that of the emissions of trace metals, NOx, SOx or HF (to air) emissions that dominate TEPT, FAETP, AP, EP or POCP. The uncertainty of ADP is dominated by the variability of coal heating value, which is lower than the variability of air emissions influencing other LCA impact categories.

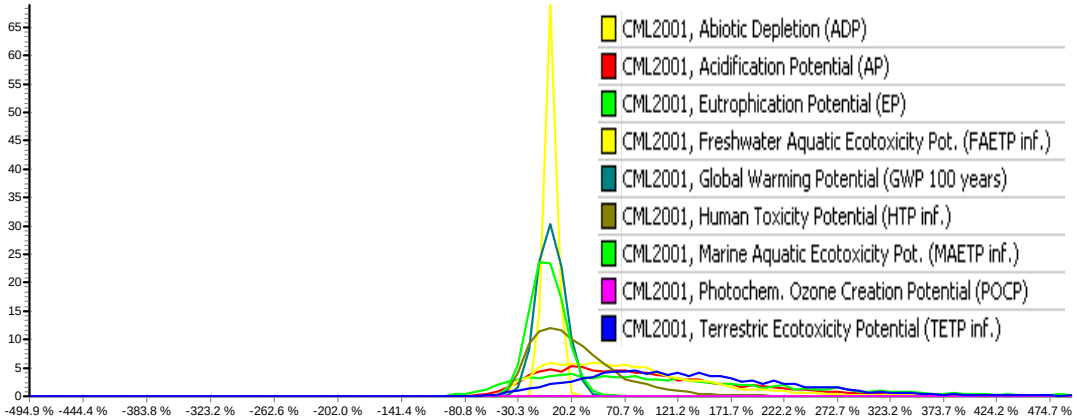

Figure 10.32: Histogram of environmental impacts at direct emission level.

Table 10.7: Statistical outputs of environmental impacts at direct emissions level.

Emissions	Base case scenario	Mean	Standard deviation (% of base case value)	10% Percentile	25% Percentile	Median	75% Percentile	90% Percentile
ADP	4.9273	4.9407	5.01%	4.6345	4.7664	4.9298	5.1015	5.2595
GWP	62.542	63.023	12.80%	53.086	57.533	62.725	68.42	73.559
MAETP	4.68E+05	4.55E+05	16.50%	3.62E+05	4.02E+05	4.52E+05	5.05E+05	5.53E+05
HTP	45.269	56.155	33.70%	36.296	42.662	52.414	65.266	81.08
TETP	0.13103	0.30747	43.50%	0.15247	0.21069	0.28929	0.38614	0.48417
FAETP	0.38819	0.67683	43.90%	0.34856	0.45449	0.62516	0.83553	1.0657
AP	0.12768	0.24679	51%	0.11112	0.15289	0.22142	0.31371	0.41829
EP	0.017257	0.038056	61.40%	0.01287	0.020359	0.03316	0.050783	0.070033
POCP	-0.02994	-0.07282	-68.30%	-0.14043	-0.09996	-0.06233	-0.03527	-0.01938

Figure 10.33 presents the histograms of life-cycle environmental impacts of power generation with oxy-fuel combustion capture, transport and injection system. The relevant statistical outputs are provided in Table 10.8. The results show that the uncertainty of

environmental impacts in all categories is smaller compared to the uncertainty of environmental impacts at direct emissions level, as the upstream data used here are from the literature or calculated using the GaBi version 4 software, which do not consider the uncertainty of parameters or factors that determine or affect the emissions from upstream processes. For example, the uncertainty of AP and EP at life-cycle level is significantly less than that at direct emission level, because AP and EP are dominated by coal mining and the uncertainty of emissions from coal mining are not fully captured by the GaBi software. Therefore, the results at life-cycle level may underestimate the uncertainty of environmental impacts.

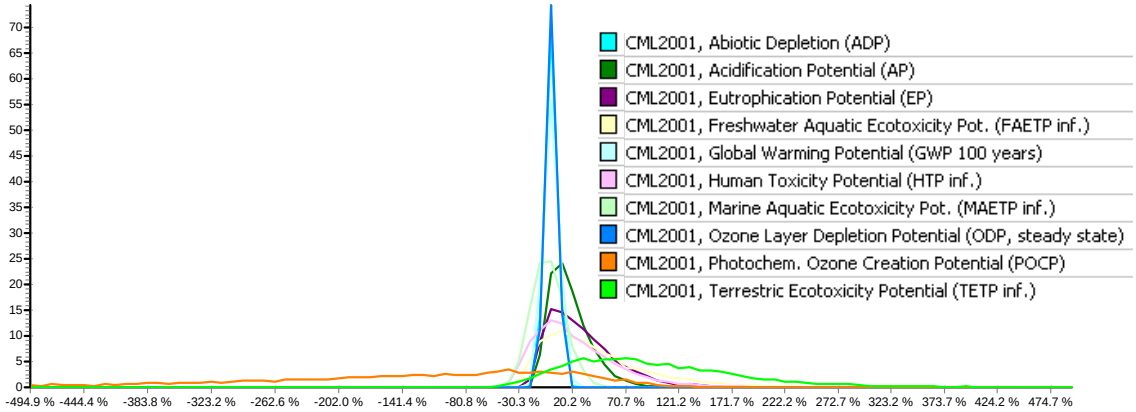

Figure 10.33: Histogram of environmental impacts at life-cycle level.

Table 10.8: Statistical outputs of environmental impacts at life-cycle level

Impact Category	Base case scenario	Mean	Standard deviation (% of base case value)	10% Percentile	25% Percentile	Median	75% Percentile	90% Percentile
ADP	5.3762	5.3925	4.94%	5.0609	5.202	5.3832	5.5639	5.7321
AP	0.69022	0.81273	16.30%	0.67092	0.71503	0.78649	0.88288	0.99369
EP	0.073202	0.094521	25.50%	0.069137	0.076491	0.089493	0.10738	0.12716
FAETP	0.6816	0.9624	36.90%	0.60609	0.71163	0.88053	1.1162	1.4315
GWP	181.86	182.5	6.54%	167.6	174.26	181.89	190.29	198.27
HTP	48.896	59.936	31.50%	39.386	46.371	56.067	70.078	85.14
MAETP	4.85E+05	4.72E+05	15.90%	3.79E+05	4.19E+05	4.69E+05	5.21E+05	5.70E+05
ODP	1.93E-06	1.94E-06	4.48%	1.83E-06	1.87E-06	1.93E-06	1.99E-06	2.05E-06
POCP	0.028955	-0.01451	-348%	-0.08195	-0.04121	-0.00433	0.022995	0.038579
TETP	0.18021	0.35584	41.70%	0.19044	0.24592	0.32983	0.43805	0.55093

10.6 Comparison of the Life Cycle Environmental Impacts of Power Generation with Post-combustion Capture, Oxy-fuel Combustion Capture and a Conventional plant without Capture

The LCI models for a 500 MW conventional power plant without CO_2 capture were configured as shown in Figure 10.34, in order to compare its life cycle environmental impacts with power generation with post-combustion and oxy-fuel combustion CO_2 capture, transport and injection alternatives discussed in Chapters 9 and 10. The 500 MW conventional power plant was configured with a PC wall dry bottom boiler burning Appalachian coal and operate at 45% plant gross efficiency. Direct emissions from this plant are provided in Table F2 in Appendix F.

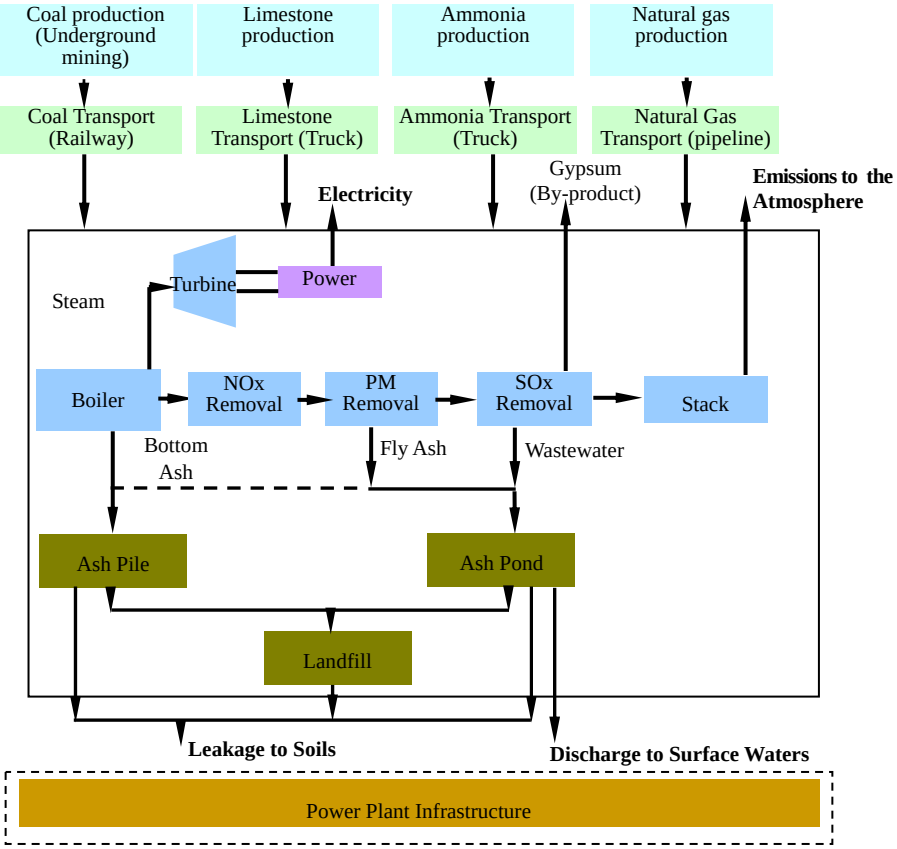

Figure 10.34: The LCI models of a 500 MW conventional power plant without CO_2 capture.

Figures 10.35 and 10.36 compare the environmental impacts of the three different power plant configurations at plant direct emissions level and life-cycle level respectively.

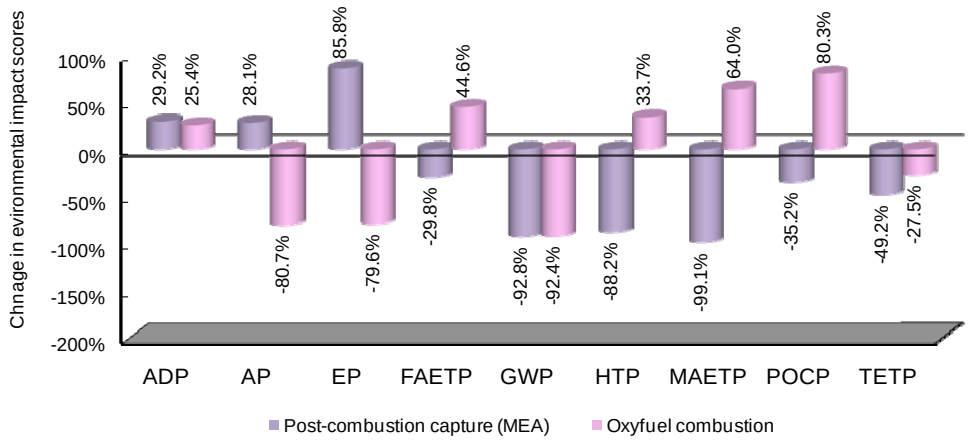

Figure 10.35: LCIA results for alternative power generation systems with and without CO_2 capture at plant direct emissions level (per 1 MW electricity generated).

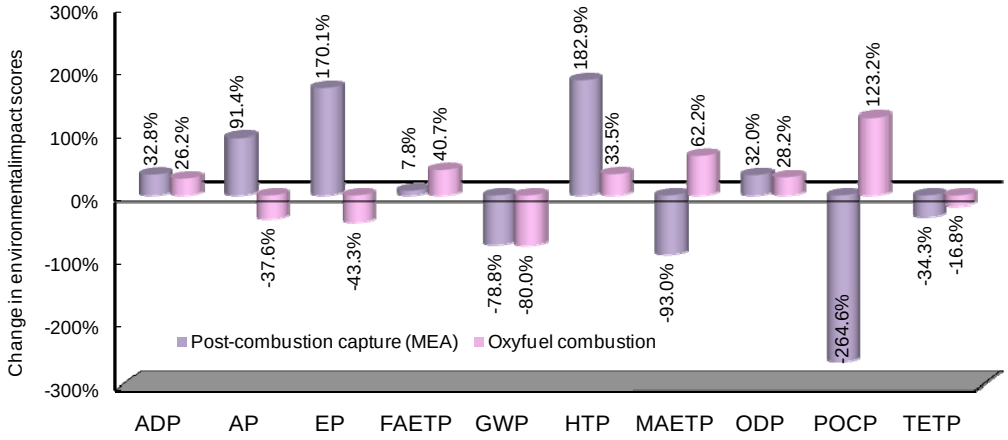

Figure 10.36: LCIA results for alternative power generation systems with and without CO_2 capture at life-cycle level (per 1 MWh electricity generated).

Figure 10.35 illustrate that, at plant direct emissions level, power plants with post-combustion and oxy-fuel combustion CO_2 capture can reduce the GWP by 92.8% and 92.4% respectively. The power plant with post-combustion CO_2 capture shows a relative increase in the ADP, AP and EP, which is due to the incremental use of coal and resultant NOx and NH_3 emissions to air, and trace metal emissions to soils. Since MEA CO_2 capture can remove atmospheric emissions of trace metals further, after the FGD, the FAETP, HTP, TETP and MAETP are decreased relative to the no CO_2 capture scenario. Incremental emissions of NO cause a reduction in the POCP.

The plant with oxy-fuel combustion CO_2 capture shows a relative increase in ADP, FAETP, HTP, MAETP and POCP and a decrease in AP and EP. The increase in the ADP is because

of the incremental use of coal; the increase of FAETP, HTP and MAETP is as a result of HF emissions to freshwater; the increase in POCP is because of the removal of NO emissions in the CO_2 conditioning unit after leaving the FGD. On the other hand, the AP and EP are decreased since the CO_2 conditioning unit can remove air emissions of NOx, SOx, HCl and HF further after the FGD. The comparison between the life-cycle environmental impacts of the three power generation alternatives can be summarised as follows (Figure 10.36):

- Figure 10.36 shows that, compared to the power plant without capture, the post-combustion and oxy-fuel combustion CO_2 capture cases can reduce the life-cycle GWP by 78.8% and 80.0% respectively. Due to its higher energy efficiency, the oxy-fuel combustion case results in a slightly larger GWP reduction from both power plant and upstream process, especially coal mining.
- Both post-combustion and oxy-fuel combustion cases have a larger ADP value than the plant without CCS since capture, transport and injection require additional energy which results in an increase of coal use.
- The post-combustion case has a 91.4% higher AP value than the plant without CCS as this option uses more coal and consequently cause an increase of NO_x emissions from the power plant and an increase of SO_2 and NO_x emissions from the upstream process (mainly coal mining). On the other hand, the post-combustion case have lower SO_x emissions than the plant without CCS as the MEA CO_2 capture unit can further reduces SO_x emissions. The MEA capture unit generates NH_3 emissions, which have a considerable contribution to AP. The CO_2 conditioning unit in the oxy-fuel plant can completely remove the emissions of NOx, SOx, HCl and HF, which are the main AP contributors. Therefore, the oxy-fuel combustion case has a lower AP value (37.6% lower) than the plant without CCS.
- The post-combustion plant uses more coal and cause an increase in the NO_x emissions from both power plant and the upstream processes (mainly coal mining and MEA production). This system also generates NH_3 emissions, which contribute to EP, from the MEA CO_2 capture unit. Therefore, the post-combustion case has a significantly higher EP value (170.1% higher) than the plant without CCS. Since the CO_2 conditioning unit can totally remove emissions of NOx, the oxy-fuel combustion case has a lower EP value (43.3% lower) than the plant without CCS.

- The post-combustion case consumes MEA and the MEA production causes significantly high HTP. Therefore, the post-combustion case has a very high HTP value (182.9% higher) compared to the plant without CCS. The HTP caused by MEA production accounts for 92.5% of the life-cycle HTP. The CO_2 conditioning unit in oxy-fuel combustion removes atmospheric HF emissions and convert them to HF emissions to freshwater, which increases the overall life-cycle HTP.
- The MEA CO_2 capture unit in post-combustion capture can further remove 95% of the HF emissions to air in the flue gas leaving the FGD and this significantly reduces the MAETP. On the other hand, the oxy-fuel combustion case has a larger MAETP value than the plant without CCS case due to the conversion of atmospheric HF emissions to HF emissions to freshwater.
- The POCP of the post-combustion case has a significantly lower value (264.6% lower) than the plant without CCS case as the MEA CO_2 capture unit removes the NO emissions, which reduces the POCP. The increased use of coal due to CO_2 capture results in increased R11 (trichlorofluoromethane), R114 (dichlorotetrafluoroethane) and R12 (dichlorodifluoromethane) emissions which increases the ODP of both post-combustion and oxy-fuel combustion cases.
- Removal of trace metals at the MEA CO_2 capture unit and the CO_2 conditioning unit in the two capture plants reduces the TETP compared to the power plant without CCS.
- Because of the emissions of HF to freshwater from the CO_2 conditioning unit the oxy-fuel combustion case increases the FAETP

10.7 Conclusions

The oxy-fuel combustion capture LCI models developed successfully compute the direct emissions of power plant with oxy-fuel combustion CO_2 capture, CO_2 conditioning, CO_2 pipeline transport, and the injection of CO_2 into aquifer storage formation. The results demonstrate that most direct emissions to air (such as NO, SO_2, and HF) arise from the power plant stack, and the resource consumption is dominated by coal. The results also show that there are no emissions to air of SO_2, SO_3, HCl, HF and Hg vapour from the power plant stack, since the CO_2 conditioning unit can remove these air emissions completely and transform them to emissions to freshwater. The percentages of trace metals,

which are originally in coal and are finally released to the environment (air, water or soil), are less than 0.5% for most types of trace metals, except for As, Hg and Se.

Compared to a power plant with post-combustion capture, the oxy-fuel combustion option has higher percentage of Hg releases to the environment, since the Hg vapour are fully captured by the CO_2 conditioning unit and transformed to emissions to freshwater. Emissions of trace metals to air are from the power plant stack. Emissions of trace metals to soil are mainly from the surface impoundments, and trace metal emissions to soil from landfill over a 1,000-year period are not significant. The results suggest that the reduction of the emissions of volatile trace metals such as As, Se and Hg can significantly reduce the overall trace metal emissions.

The life-cycle environmental impacts of power generation with oxy-fuel CO_2 capture, conditioning, transport, injection and the upstream processes are summarised in Table 10.9, which lists the main processes and substances that contribute to each impact category. The results demonstrate that life-cycle environmental impacts are dominated by power plant with CO_2 capture and coal production in all impact categories, except for the ODP, which is dominated by coal production, coal transportation and power plant infrastructure. The AP, EP, GWP100, HTP, MAETP and POCP are caused primarily by air emissions. The FAETP and TETP mainly come from trace metal emissions to air or soils.

Results of energy efficiency analysis demonstrate that the power plant with a gross efficiency of 45% can achieve a net efficiency of 35.04% after the ASU and CO_2 conditioning, which consume 5.90% and 3.86% of the input coal energy respectively.

The sensitivity analysis have demonstrated that the life-cycle impacts in all categories are sensitive to the change of power plant gross efficiency, ASU energy consumption, and energy consumption of the CO_2 conditioning unit. From life-cycle point of view, the purity of O_2 product from the ASU at 98% is the optimum value, at which point the GWP is reduced considerably and other environmental impacts are only slightly increased. If the HF removed by the CO_2 conditioning unit is treated before it is released to the freshwater environment, then the increased removal rate of HF at the CO_2 conditioning unit reduces MAETP and HTP significantly. The increase of SOx removal rate in the CO_2 conditioning unit can reduce AP and POCP but does not increase other environmental impacts at the life-

Table 10.9: Life cycle impacts of oxy-fuel combustion CO_2 capture, transport and injection.

Impact Category	Value	Dominant processes		Dominant substances				Emissions to
		Name	% of total	Name	% of total	Impact value	Amount (kg)	
Global Warming Potential (GWP 100 years)	158.46 [kg CO_2-Equiv.]	Coal production	63.11%	CH4	41.46%	65.70	65.70	Air
				CO2	21.25%	33.67	33.67	Air
		Power generation with capture	34.08%	CO2	33.24%	52.68	52.68	Air
Abiotic Resource Depletion Potential (ADP)	4.70 [kg Sb-Equiv.]	Coal production	97.97%	Coal	93.04%	4.368815	340.63	-
				Natural gas	2.38%	0.111877	4.7693	-
				Crude oil	2.30%	0.108068	5.2836	-
		Transport infrastructure	1.00%	Crude oil	0.88%	0.041492	2.0286	-
		Natural gas production	0.64%	Natural gas	0.64%	0.029984	1.3206	-
Acidification Potential (AP)	0.65 [kg SO2-Equiv.]	Coal production	72.88%	SO2	33.67%	0.219248	0.2193	Air
				NOx	38.35%	0.249691	0.3567	Air
		Power generation with capture	24.42%	NO	12.02%	0.078263	0.0731	Air
				NO2	7.74%	0.050369	0.0027	Air
				HCL	2.74%	0.017813	0.0202	Freshwater
				HF	1.87%	0.012145	0.0076	Freshwater
Eutrophication Potential (EP)	0.073 [kg Phosphate-Equiv.]	Coal production	65.25%	NOx	63.55%	0.046371	0.3567	Air
		Power generation with capture	32.98%	NO	20.05%	0.014629	0.0731	Air
				NO2	12.82%	0.009354	0.0027	Air
Ozone Layer Depletion Potential (ODP)	1.71E-06 [kg R11-Equiv.]	Coal production	75.34%	R11	36.67%	6.26E-07	6.26E-07	Air
				R 114	31.92%	5.45E-07	6.42E-07	Air
				R12	6.46%	1.10E-07	1.35E-07	Air
		Transport of coal by railway	12.34%	R11	6.01%	1.03E-07	1.03E-07	Air
				R 114	5.23%	8.93E-08	1.05E-07	Air
		Power plant infrastructure	7.12%	Halon	7.07%	1.21E-07	1.01E-08	Air
Photochemical Ozone Creation Potential (POCP)	0.027 [kg Ethene-Equiv.]	Coal production	180.47%	Methane	62.63%	0.017139	2.8565	Air
				SO2	38.46%	0.010524	2.19E-01	Air
				NMVOC	30.02%	0.008215	0	Air
				CO	8.50%	0.002327	0.0862	Air
		Power generation with capture	-88.53%	NO	-114.13%	-0.03123	7.31E-02	Air
				CO	17.88%	0.004894	1.13E-01	Air
Human Toxicity Potential (HTP)	42.92 [kg DCB-Equiv.]	Power generation with capture	92.54%	HF	6.52%	10.32569	0.0076	Freshwater
				As	17.44%	27.62798	2.97E-05	Air
		Coal production	6.62%	HF	0.62%	0.988113	3.50E-04	Air
				NOx	0.27%	0.428042	3.57E-01	Air
				As	0.41%	0.64693	1.86E-06	Air
Marine Aquatic Ecotoxicity Potential (MAETP)	425301.5 [kg DCB-Equiv.]	Power generation with capture	96.36%	HF	96.01%	408336.5	0.0076	Freshwater
		Coal production	3.47%	HF	3.32%	14123.9	3.50E-04	Air
Freshwater Aquatic Ecotoxicity Potential (FAETP inf.)	0.62 [kg DCB-Equiv.]	Power generation with capture	57.64%	HF	22.82%	0.142484	0.0076	Freshwater
				Vanadium	22.55%	0.14079	3.07E-05	soil
				Selenium	1.84%	0.011519	7.49E-06	soil
				Beryllium	4.37%	0.027306	1.59E-06	Air
				Vanadium	2.44%	0.015255	8.75E-06	Air
		Coal production	31.09%	Nickel	18.14%	0.113299	3.50E-05	Freshwater
				Cadmium	3.58%	0.022325	1.47E-05	Freshwater
				Vanadium	4.55%	0.028422	1.64E-05	Air
Terrestrial Ecotoxicity Potential (TETP)	0.16 [kg DCB-Equiv.]	Power generation with capture	73.64%	arsenic	29.45%	0.047786	2.97E-05	Air
				Chromium	5.08%	0.008244	2.69E-06	Air
				Vanadium	25.49%	0.041356	3.07E-05	soil
				Arsenic	5.64%	0.009154	2.78E-06	soil
		Coal production	22.96%	Mercury	7.77%	0.012608	4.45E-07	Air
				Vanadium	6.72%	0.010905	1.64E-05	Air

cycle level. The increase of NOx removal rate of the CO_2 conditioning unit leads to a significant decrease in both EP and AP but causes a strong increase in the POPC. The life-cycle impacts in all categories are sensitive to different types of coal, since the chemical composition of different type of coals vary significantly.

When compared with the power plant without capture, the post-combustion and oxy-fuel combustion cases can reduce the life-cycle GWP by 78.8% and 80.0% and increase the ADP by 32.8% and 26.2% respectively. The comparison of the life-cycle impacts of power generation with post-combustion capture, oxy-fuel combustion capture, and power plant without capture is presented in Table 10.10.

Table 10.10: Comparison of the life-cycle impacts of power generation with post-combustion capture, oxy-fuel combustion capture, and no capture.

Impact category	Power generation without capture	Post-combustion (MEA) CO_2 capture, transport and injection		Oxy-fuel combustion CO_2 capture, transport and injection	
	Life cycle impact	Life cycle impact	Compared to power generation without capture	Life cycle impact	Compared to power generation without capture
GWP [kg CO_2-Equiv.]	786.52	167.12	Lower, because of CO_2 capture and storage.	157.59	Lower, because of CO_2 capture and transport.
ADP [kg Sb-Equiv.]	3.719403	4.9402	Higher, because of energy consumption by capture.	4.6954	Higher, because of energy consumption by capture.
AP [kg SO_2-Equiv.]	0.96527	1.8472	Higher, because of increased NO emissions from power plant and more SOx and NOx emissions from coal production.	0.60266	Lower, because of CO_2 conditioning unit can completely remove SOx, NOx, HF, HCl.
EP [kg Phosphate-Equiv.]	0.112874	0.30483	Higher, because of NH_3 emissions from MEA capture and more NOx emissions from coal production.	0.063963	Lower, because of CO_2 conditioning unit can completely remove NOx.
ODP [kg R11-Equiv.]	1.33E-06	1.76E-06	Higher, more relevant emissions from coal production.	1.71E-06	Higher, more relevant emissions from coal production.
POCP [kg Ethene-Equiv.]	-0.10154	-0.37025	Lower, more NO emissions from power plant.	0.023597	Higher, because of CO_2 conditioning unit can completely remove NO.
HTP [kg DCB-Equiv.]	32.08664	90.788	Higher, because of ethylene oxide emissions from MEA production.	42.833	Higher, because of HF emissions to freshwater.
MAETP [kg DCB-Equiv.]	262189.8	18298	Lower, because of MEA capture unit remove HF.	4.25E+05	Higher, because of HF emissions to freshwater.
FAETP [kg DCB-Equiv.]	0.443949	0.47877	Slightly higher, because more trace metal emissions to soil from coal production.	0.62443	Higher, because of HF emissions to freshwater.
TETP [kg DCB-Equiv.]	0.195011	0.12813	Lower, because of MEA capture unit can reduce trace metal emissions to air.	0.16227	Lower, because of CO_2 conditioning unit can reduce trace metal emissions to air.

The direct emissions of CO, NH_3, NO, NO_2, N_2O and CO_2 are less uncertain (lower standard deviations) than the emissions of HF, HCl, SO_2, and SO_3, because their emissions are affected by more pollution control processes along the power generation and CO_2 capture chain and this increases the uncertainty. The uncertainty of emissions of trace metals to air is larger than that of other air emissions, as the amount of trace metals in coal varies more significantly than that of C, S, N, Cl or F. Trace metal emissions to soils are less uncertain than the trace metal emissions to air and the histograms of these emissions are less skewed than that of the trace metal emissions to air, since the emissions of trace metals to soils depend on the design of surface impoundments and landfills and are less affected by the variability of trace metals in coal.

Chapter 11 Life Cycle Assessment of Carbon Dioxide Storage

11.1 Introduction

There are four principal types of geological formations that are considered to have significant potential for storing large amounts of CO_2, including active and depleted oil reservoirs, active and depleted gas reservoirs, saline aquifers, and deep unminable coal seams (Benson, 2005). This Chapter presents the LCI model developed for CO_2 storage in deep saline aquifers, which are thought to have the largest capacity for CO_2 storage and are more widespread than other storage options (IPCC, 2005). As defined in the LCA system boundary in Chapter 4, the aim of the CO_2 storage LCI model is to calculate the amount of CO_2 which may potentially leak from the saline aquifer storage formation to atmosphere. The CO_2 storage LCI modelling begins with the estimation of the migration and distribution of injected CO_2 in the saline aquifer, which is bound by the LCA system geological boundaries. In the next step, the LCI model developed quantifies the CO_2 leakage from saline aquifer through alternative potential leakage pathways. Finally, the LCI model calculates the amount of CO_2 that has leaked from the saline aquifer to the atmosphere after passing through different geological compartments within the overburden. This Chapter also presents a case study which is used to identify the operational parameters, reservoir properties and the parameters of

alternative leakage pathways that have significant impacts on the LCA environmental impact results.

11.1.1 Saline Aquifer for Carbon Dioxide Storage

Saline aquifers are porous and permeable reservoir rocks that contain saline water (brine) in the pore space between the rock grains. Generally, they are found at greater depth than aquifers of potable water and the water contained in the saline aquifer is not technically and economically available for surface use. Saline aquifers can be sandstone or limestone formations, but to qualify for CO_2 storage they must have the following properties (Bentham and Kirby, 2005):

i) Size: the reservoir must be large enough to be able to store the life time CO_2 emissions from the planned emission source, e.g. a power plant.
ii) Porosity and permeability: these parameters must be sufficiently high to provide adequate pore space for the CO_2 storage and allow the injection of CO_2.
iii) Depth: CO_2 storage requires that the aquifer is found more than 800 m below sea level, where the CO_2 exists in its dense phase and occupies much less pore volume than in its gaseous phase.
iv) Caprock: an overlying impermeable caprock is required to prevent the vertical migration of injected CO_2 due to its lower density than that of brine.

Injected CO_2 remains in the storage reservoir by four main processes: immobilisation under (structural/stratigraphic) traps, dissolution in the saline water, capillary trapping, and geochemical reaction and formation of minerals in the pore spaces.

11.1.2 Migration and Distribution of Injected Carbon Dioxide in a Saline Aquifer

Carbon dioxide can be stored in both “confined” and “unconfined” aquifers (see Figure 11.1). CO_2 storage in confined aquifers is analogous to gas storage schemes in hydrocarbon fields. The free phase CO_2 is contained by structural (e.g. anticlines) and /or stratigraphic (e.g. sandstone pinchout) features and the injection stops before the gas reaches a spill point. Migration pathways and the shape of the injected CO_2 plume can be predicted fairly well provided that the reservoir structure is known.

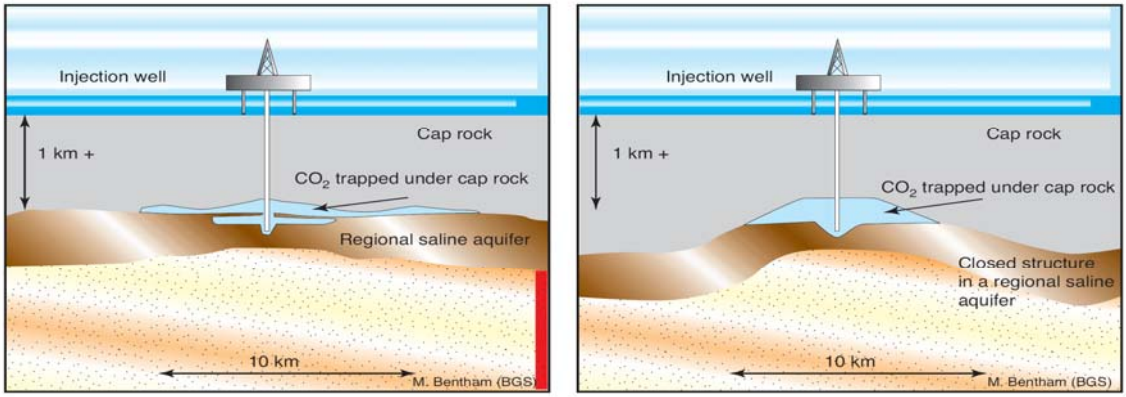

a. unconfined saline aquifer b. confined saline aquifer

Figure 11.1: Types of saline aquifer (After Bentham and Kirby, 2005)

CO_2 storage in unconfined aquifers involves the injection of CO_2 into large regional aquifers with no specific large structural or stratigraphic closures. Migration pathways of CO_2 stored in unconfined aquifers are more complex than that of confined aquifers. During the CO_2 injection period, injected CO_2 initially moves laterally, driven by the pressure gradient of the injection and displaces saline water and a small proportion of CO_2 simultaneously dissolves into the saline water. When CO_2 laterally reaches a certain distance depending on the aquifer properties, the lateral flow velocity becomes slow enough and the buoyancy becomes evident. The buoyancy drives the free phase CO_2 plume to float towards the top of the formation. As a result, a curved displacement front is formed (see Figure 11.2). For aquifers with high vertical permeability, the buoyancy drives the injected CO_2 to migrate upwards along the most permeable pathway until it encounters the impermeable caprock and a thin free phase CO_2 layer is formed underneath the top of the caprock (see Figure 11.2a). For aquifers with low vertical permeability, buoyancy has relatively small effect, and the moving CO_2 does not reach the top of the formation during the injection period, but the curved displacement front is evident (see Figure 11.2 b). Once injection ceases, the pressure gradient that was forcing the CO_2 lateral migration quickly relaxes and the buoyancy driven vertical migration is dominant. The vertical migration brings the free phase CO_2 into contact with a large volume of formation space and cause capillary trapping. After the diffusion layer is formed in the thin CO_2 layer beneath the caprock, the convective mixing effect will redistribute the CO_2 plume and dissolve up to 50% CO_2. The two phenomena, capillary trapping and convective mixing effect will enhance the CO_2 permanent storage and will be discussed in detail in the next Section of this Chapter.

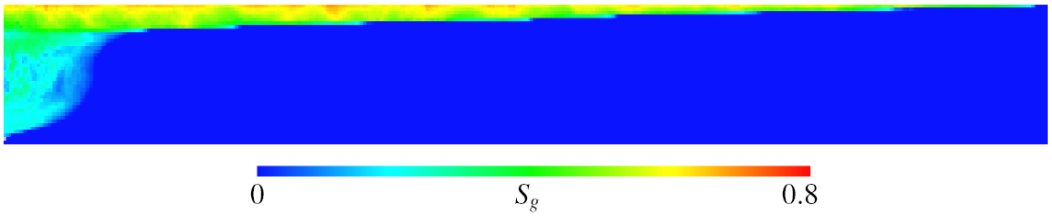

a. Gas Saturation, S_g, at the end of the injection period

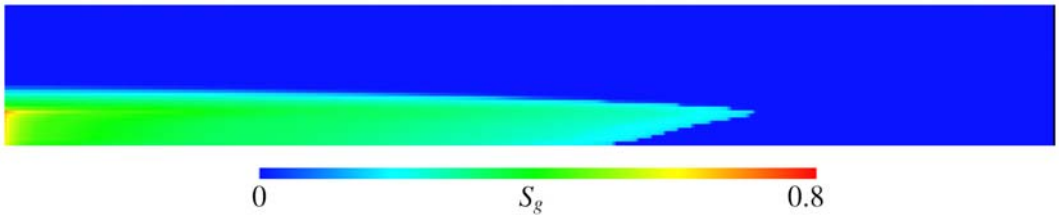

b. Gas Saturation, S_g, at the end of the injection period

Figure 11.2: Examples of CO_2 saturation distribution (After Ide *et al.*, 2006)

11.2 Life Cycle Inventory Modelling of Carbon Dioxide Storage in Saline Aquifers

In order to capture the spatial and geological differences of CO_2 saline aquifer storage and potential CO_2 leakage, the LCI model breaks down the CO_2 storage system into compartments and follows the migration of injected CO_2 in the saline aquifer since this determines the geological boundaries and time frame of CO_2 storage system in the context of LCA. In order to achieve this objective it is necessary to quantify the radial extent of the CO_2 plume, the thickness of the thin CO_2 layer, the time the CO_2 plume takes to reach the top of the storage formation, the dissolution, capillary trapping, and CO_2 lateral movement after injection ceases, and finally model the alternative leakage pathways intersecting the caprock as demonstrated in Figure 2.11 in Chapter 2. If CO_2 leaks out from the storage aquifer, the buoyancy will drive the CO_2 flux to migrate to shallower layers through different compartments within the overburden, including water-saturated porous zones, surface water or unsaturated soil zones. Finally the CO_2 flux may cross the land-atmosphere boundary and enter into the atmosphere.

As defined in the current model LCA system boundary, the LCI model for storage only calculates the amount of CO_2 reaching the atmosphere. The dispersion of the CO_2 flux in the atmosphere and the dispersion of dissolved CO_2 in groundwater and surface waters are not investigated. The attenuation rate of CO_2 when passing through water-saturated porous zones, surface water or unsaturated soil zones are analysed. The time

frame of the LCI model is 1,000 years. The schematic of the LCI model developed for CO_2 storage in saline aquifers is illustrated in Figure 11.3.

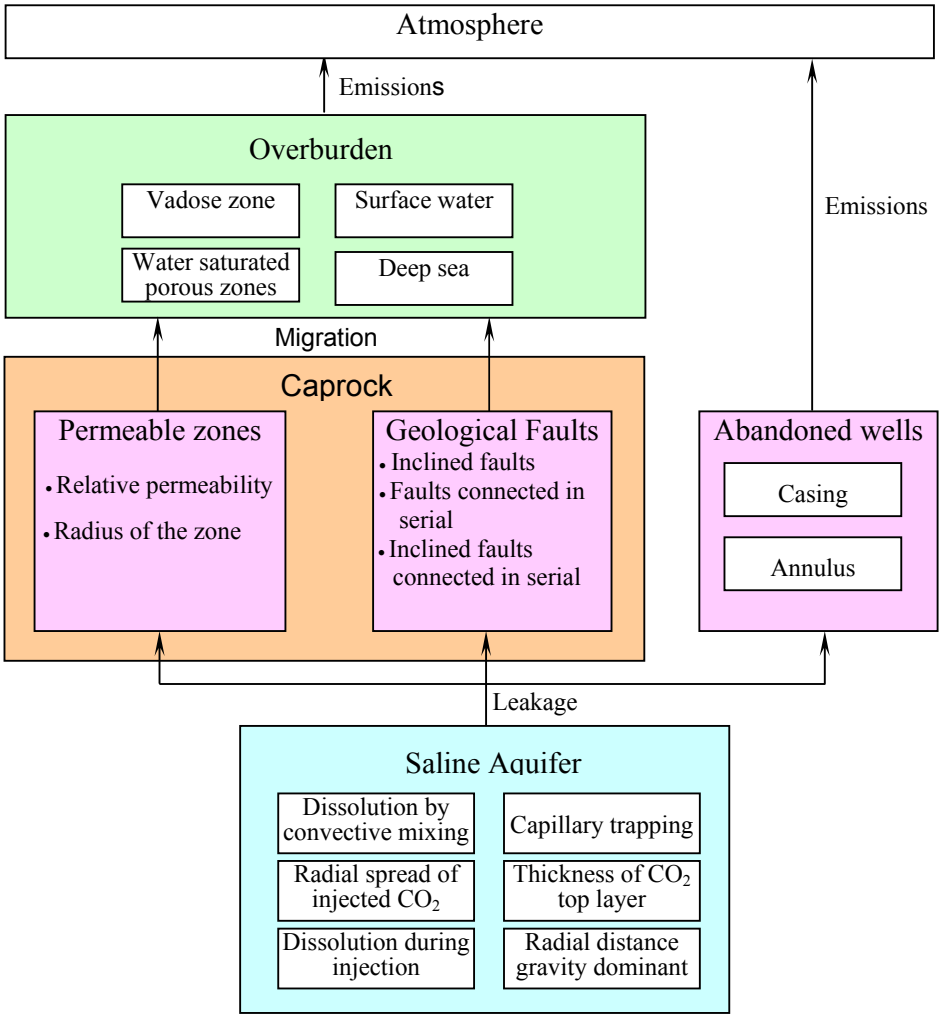

Figure 11.3: The schematic of the LCI model developed for CO_2 storage in saline aquifers.

11.2.1 Distribution of Carbon Dioxide around the Wellbore during Injection

The radial distribution of carbon dioxide around the injection well can be calculated using the Buckley-Leverett theory, assuming incompressible and immiscible fluids of constant viscosity, constant injection rate, uniform formation properties and no gravity effects. The saturation profile is given by (Ennis-King and Paterson, 2002):

$$\frac{\pi r^2}{t} = \frac{q}{\phi \rho_g h_i} \frac{d\Phi}{dS} \qquad [11.1]$$

where r is the radial distance, t is time (s), q is the mass injection rate of carbon dioxide (m^3/s), ρ_g is the gas density (kg/m^3), ϕ is porosity (%), h_i is the height of the well-

completion interval (m), S is water saturation (%), and $\Phi = (k_{rw}/\mu_w)/(k_{rw}/\mu_w + k_{rg}/\mu_g)$ where k_{rw} and k_{rg} are the relative permeability to water and to free phase CO_2 respectively (which depend on S) (%), and μ_w and μ_g are the corresponding viscosities (Pa·s). Equation [11.1] only holds to a distance r_f (m), at which there is a saturation front. The value of gas saturation at this front, S_{gf} satisfies the following:

$$\left.\frac{d\Phi}{dS}\right|_{S=S_{gf}} = \frac{1-\Phi(S_{gf})}{1-S_{gf}} \qquad [11.2]$$

Φ can be simplified by using an extension of the Brooks-Corey relative permeability relationship, where the two phase relative permeabilities in granular porous media are expressed as (Saripalli and McGrail, 2002):

$$\frac{k_{rw}}{k_{rg}} = \frac{S_w^{\varepsilon}}{(1-S_w^{\beta})(1-S_w)^2} \qquad [11.3]$$

Where, k_{rw} and k_{rg} are the relative permeability to water and to gas respectively (mD); S_w is the water saturation (%); $\beta=(2+\lambda)/\lambda$ and $\varepsilon=(2+3\lambda)/\lambda$, λ being the Brooks-Corey pore size distribution index. A λ value of 2 is used to represent the compact sands (Saripalli and McGrail, 2002).

The analytical approach agrees fairly with numerical simulations when predicting the lateral extent of CO_2 plume and the CO_2 saturation profile during injection (Ennis-King and Paterson 2002; Saripalli and McGrail, 2002).

11.2.2 The Lateral Extent where Gravity is Dominant

The Buckley-Levertt approach ignores the gravity effects. However, the density difference between free-phase CO_2 and brine can be large enough to cause a significant gravity effect when the lateral flow rate is slow (Ide *et al.*, 2006). The radial extent, L at which the gravity dominates can be estimated by (Ennis-King and Paterson, 2002):

$$L^2 = \frac{h_t \mu_g R^2 q}{k_v k_{rg} \Delta\rho_{gw} g \pi \phi \rho_g h_i} \qquad [11.4]$$

Where, h_t is the thickness of the saline aquifer; μ_g is the free phase CO_2 viscosity (Pa·s); R is the dimensionless front radius, and $R=r_f(\pi\phi\rho_g \cdot h_c/(q\cdot t))^{1/2}$; k_v is the vertical permeability (mD); q is the mass injection rate of carbon dioxide (m^3/s); k_{rg} are the

relative permeability to water and to free phase CO_2 respectively (%); ρ_g is the gas density (kg/m^3), ϕ is porosity (%); h_i is the height of the well-completion interval (m).

11.2.3 Calculation of the Floating Carbon Dioxide Layer Thickness beneath the Caprock

The thickness of the CO_2 layer floating beneath the caprock is crucial for the calculation of potential CO_2 leakage. For a flat caprock and a reservoir with homogenous properties, a balance between horizontal restraining capillary forces and vertically acting buoyancy forces will eventually determine the thickness of the top layer of the free-phase CO_2 and the thickness, h_p is given by (Saripalli and McGrail, 2002; LeNeveu, 2008):

$$h_p = \frac{P_c(S_g)}{\Delta\rho_{gw} g} \qquad [11.5]$$

where h_p is the height of the free-phase CO_2 source pool (m); P_c is the capillary pressure function; S_g is the average gas saturation in the layer (%); $\Delta\rho_{gw}$ is the density difference between formation water and free-phase CO_2 (kg/m^3).

The capillary pressure curve can be calculated based on the van Genuchten's formula (Ennis-King and Paterson, 2002):

$$P_c = P_0((S_g)^{-1/\lambda-1} - 1)^{1-\lambda} \qquad [11.6]$$

Where P_0 is a parameter and $S_g = (S_w - S_{lr})/(1 - S_{lr})$. S_{lr} is the irreducible water saturation. The following 3 sets of parameters given in Table 11.1 are used to examine the range of the capillary pressures possible.

Table 11.1: The parameters for capillary pressure calculation (After Ennis-King and Paterson, 2002)

	S_{lr}	P_0	λ
1	0.0	2.03 kPa	0.234
2	0.19	6.05 kPa	0.66
3	0.0	19.6 kPa	0.457

11.2.4 Dissolution of Carbon Dioxide during Injection

Carbon Dioxide is slightly soluble in water, one can make the assumption that the gas phase is locally in equilibrium with the formation water. Then the proportion of the

injected gas which is dissolved in the formation water is given by (Ennis-King and Paterson, 2002):

$$P = (R^2\text{-}1)/(R^2\text{-}1 + \rho_g/(\rho_w \cdot X_c)) \quad [11.7]$$

where R is the dimensionless front radius ($R=r_f\,(\pi\phi\rho g \cdot h_c/(q \cdot t))^{1/2}$), ρ_g is the density of the CO_2 phase (kg/m^3), ρ_w is the density of the aqueous phase (kg/m^3), and X_c is the mass fraction of dissolved carbon dioxide in the aqueous phase at saturation.

11.2.5 Lateral Migration of Free Gas Phase Carbon Dioxide after Injection

The migration velocity of the layer of CO_2 updip beneath the caprock can be estimated from Darcy's law as (Lindeberg, 1997):

$$L=k_h \cdot k_{rg} \Delta\rho_{gw} \cdot g \cdot \sin(\theta)/\mu_g \quad [11.8]$$

where θ is the updip angle of the top seal (^{o}); $\Delta\rho_{gw}$ is again the density difference between the formation brine and the gas phase (kg/m^3), k_h is the horizontal permeability (mD).

11.2.6 Time Required for the Free Phase Carbon Dioxide Plume to Reach the Top of the Storage Formation

Once injection ceases the lateral driving force quickly relaxes and the buoyant force becomes dominant. From Darcy's law, the vertical migration rate can be estimated as (Saripalli and McGrail, 2002):

$$v_v = \frac{k_v k_g \Delta\rho_{gw} g}{\mu_g} \quad [11.9]$$

The time for the free phase CO_2 plume to reach the top of the formation is given by:

$$t_v = \frac{h_t \mu_g}{k_v k_{rg} \Delta\rho_{gw} g} \quad [11.10]$$

Where k_v is the vertical permeability (mD); h_t is the distance from the injector to the top of the formation (m), and g is the acceleration of gravity (m/s²).

11.2.7 Dissolution of Carbon Dioxide during Convective Mixing

After CO_2 injection ceases, free-phase CO_2 can be further dissolved through the convective mixing effect with three distinct mass transport regimes: an initial period of pure diffusive transport, followed by a rapid infinite-acting convective mass transport, superseded by a period of slow finite-acting convective transport (Hesse *et al.*, 2006a). The rate of CO_2 dissolution changes depend on the mass transport regime. In the diffusive regime, the rate of dissolution depends on the molecular diffusion and decreases rapidly with time. The total mass transfer is proportional to $t^{1/2}$. In the course of the infinite-acting convection, the plumes of CO_2 saturated brine with larger density will migrate downward and fresh unsaturated brine is transported upwardly to the CO_2-brine interface. The rate of dissolution becomes constant and is several orders of magnitude faster than that of pure molecular diffusion. Convection accelerates the dissolution of the CO_2. The fraction of dissolution could reach more than 50% at the end of infinite acting convection (Hassanzadeh *et al.*, 2007). Finally, finite-acting convection occurs after the plume tips of CO_2 saturated brine have reached the bottom of the reservoir, and convection slows down significantly. During the finite acing convection regime the rate of CO_2 dissolution decreases very rapidly. For typical aquifer conditions, the solution process driven by the finite acting convection of dissolved CO_2 will result in a significant solution of CO_2 but only in the long term, more than one thousand years (Van der Meer and Van Wees, 2006).

The occurrence of convective transport requires the dissolved CO_2 diffusive boundary layer to grow to a critical thickness. The critical time, t_c for the onset of convection is given in the following expression (Riaz *et al*., 2006; Hesse *et al*., 2006a):

$$t_c = 146 \frac{\phi \mu_w{}^2 D}{(Kg\Delta\rho_{gw})^2} \qquad [11.11]$$

Where ϕ is the porosity (%); μ_w is the viscosity of the brine (Pa·s); D is the diffusivity (m^2/s); K is the absolute permeability (for anisotropic permeability, K can be replaced by $4k_v/(1+(k_v/k_h)^{1/2})^2$); g is the gravitational acceleration and $\Delta\rho_{gw}$ is the density difference between the CO_2 saturated and the unsaturated brine with a typical value of 5 kg/m^3 (Hesse *et al*., 2006a).

The time of transition from the first to the second regime (t_{on}), the time of transition from the second to the third regime (t_{slow}), and the time necessary for the brine in the

reservoir to become completely saturated with dissolved CO_2 (t_{sat}) are considered. For practical purposes t_{sat} is reached when the reservoir is 95% saturated. t_{on}, t_{slow}, and t_{sat} are given by the following equations (Hesse *et al*., 2006a):

$$t_{on} = 6251 \frac{\phi \mu_w^{11/5} D^{6/5}}{(k_v \Delta \rho_{gw} g)^{11/5} H^{1/5}} \quad [11.12]$$

$$t_{slow} = 15 \frac{\phi \mu_w H}{k_v \Delta \rho_{gw} g} \quad [11.13]$$

$$t_{sat} = 230 \frac{\phi \mu_w H}{k_v \Delta \rho_{gw} g} \approx 15 t_{slow} \quad [11.14]$$

Where ϕ is the porosity (%); μ_w is the viscosity of the brine (Pa·s); D is the diffusivity (m^2/s); k_v is the vertical permeability (mD); g is the gravitational acceleration and $\Delta\rho_{gw}$ is the density difference between the CO_2 saturated and the unsaturated brine with a typical value of 5 kg/m^3.

The two dimensional space time average of the mass dissolution rate of CO_2 per unit width, in the infinite-acting regime is given by (Hesse *et al.*, 2006b):

$$\frac{dM_{CO2}}{dt} \approx 0.017 \frac{K \Delta \rho_{gw} g C_{CO_2}^{eq} L}{\phi \mu} \quad [11.15]$$

Where, M_{CO2} is the mass of dissolved CO_2; K is the absolute permeability; $C_{CO_2}^{eq}$ is the CO_2 equilibrium concentration; L is the aquifer length (m); g is the gravitational acceleration and $\Delta\rho_{gw}$ is the density difference between the CO_2 saturated and the unsaturated brine (kg/m^3).

For potential storage aquifers the permeability may vary from 1mD to 3D, and the critical times vary from a few days (t_c< 10 days) in a high permeability aquifer to a few thousands of years (t_c ~ 2,000 years) in a low permeability aquifer (Hesse *et al.*, 2006b). Therefore, CO_2 dissolution will be an important trapping mechanism in high permeability aquifers, where onset is essentially instantaneous and the dissolution rate is high, and in low permeability aquifers dissolution trapping will not significantly reduce mobile CO_2 before the critical time, which may be several hundred years, and even after the onset of convection the dissolution rate will be low (Hesse *et al.*, 2006b).

11.2.8 Capillary Trapping of Carbon Dioxide in an Aquifer

Capillary trapping (or residual trapping) occurs when the saturation of a non-wetting gas phase is decreasing and the saturation of a wetting phase (e.g. water) is increasing (Ide *et al.*, 2006). In CO_2 storage, when CO_2 injection ceases, gravity becomes dominant and free phase CO_2 migrates upwards to the top of the aquifer. As free phase CO_2 migrates upwards, the gas saturation of zones from which free gas CO_2 is migrating out decreases. It is that decrease in saturation that can act to trap CO_2 by capillary snap-off (Ide *et al.*, 2006). Therefore, in CO_2 storage, capillary trapping can be used to immobilise the amount of free gas phase CO_2 that could leak from the aquifer.

Most of the trapping occurs in the near injection well region, where significant vertical flow takes place and in the zones just below the thin layer of free phase CO_2, where gas saturations initially reaches levels high enough and then the gas saturation declines as gas migrates upwards after injection ceases (Ide *et al.*, 2006).

Timing of capillary trapping and fraction of CO_2 trapped by capillary trapping are related to N_{gv}, given by (Ide *et al.*, 2007):

$$N_{gv} = \frac{k_v L \Delta\rho_{gw} g}{Hu\mu_{brine}} \qquad [11.16]$$

Where k_v is the vertical permeability (mD), L the aquifer length (m), $\Delta\rho_{gw}$ the density difference between formation water and free-phase CO_2 (kg/m^3), g the acceleration of gravity, H the aquifer height (m), u the total average Darcy flow velocity (m/s), and μ_{brine} is the viscosity of brine (Pa·s).

Figure 11.4 shows that an aquifer with high N_{gv} has much less trapping because the free gas phase CO_2 residing in the thin layer beneath the caprock cannot be trapped because there is no mechanism to reduce the gas saturation there and systems with stronger gravitational forces have a higher saturation of CO_2 in the uppermost zone, and therefore subsequently have less gas available to trap elsewhere (Ide *et al.*, 2006).

The rate of capillary trapping of injected CO_2 is also of interest because it is important to analyse whether capillary trapping will occur on a time scale that is shorter or longer than the time scales of other mechanisms of trapping such as dissolution and chemical reactions. Figure 11.5 reports the time scale at which the final value of fraction of gas trapped is reached and conclude that: aquifers with strong gravity effects (high N_{gv}) trap

less injected gas, but relatively quickly, and aquifers with strong viscous forces (low N_{gv}) trap a significant fraction of injected gas, but take a longer time (Ide *et al.*,2006).

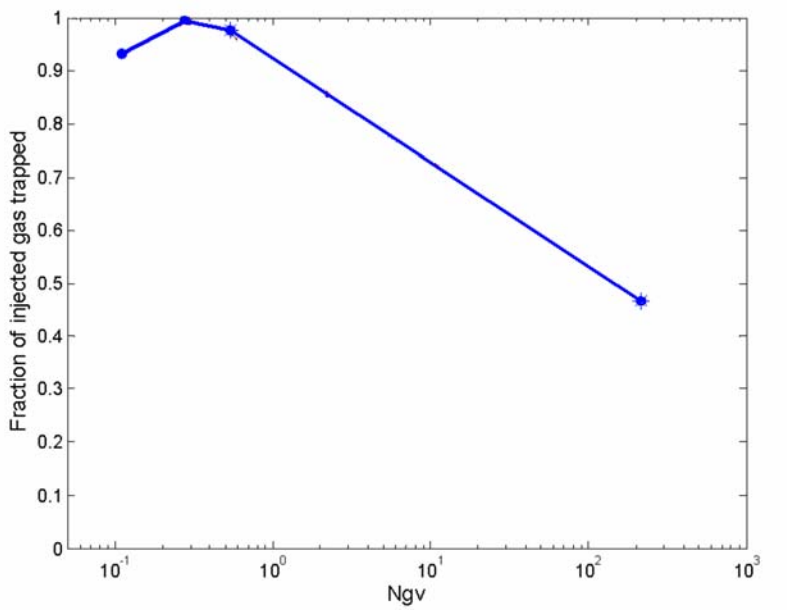

Figure 11.4: Final fraction of injected CO_2 trapped against N_{gv} (After Ide *et al.*, 2006).

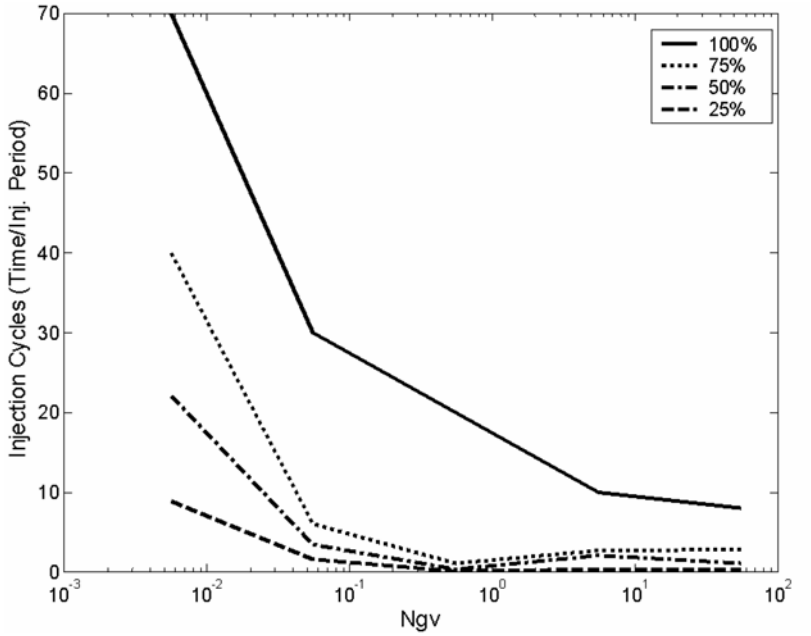

Figure 11.5: Rate at which saline aquifer reaches final value of fraction of CO_2 trapped (After Ide *et al.*,2006)

11.2.9 Calculation of Leakage through a Permeable Zone in the Caprock

If there are significant permeable zones embedded in the caprock, the free phase CO_2 in contact with the permeable zones will migrate upwards due to buoyancy. The migration

is governed by Darcy's law. If it is assumed that the CO_2 fluid is single phase flow and the saline aquifer is hydrostatic, the free phase CO_2 flow through a permeable zone is calculated by equation [11.17]. The assumption of single phase flow is realistic, because caprock is normally under a depth more than 1,000 m and at this depth CO_2 remains at supercritical phase when leaking through the caprock. The assumption of hydrostatic implies that buoyancy of free-phase CO_2 floating beneath the top layer of the saline aquifer is the force driving CO_2 to flow upwardly:

$$Q = \frac{k_{zone} k_{rg} \pi r_{zone}^2}{\mu_c} \cdot \frac{(\rho_w - \rho_c) g h_c}{l_{zone}} \qquad [11.17]$$

Where, k_{zone} is the intrinsic permeability of the permeable zone (mD); k_{rg} is relative permeability to CO_2 (%); h_c is the thickness of free-phase CO_2 floating beneath the top layer of the saline aquifer (m); μ_c is the viscosity of the CO_2 (Pa·s); ρ_w, ρ_c are the density of brine and free phase CO_2 respectively (kg/m^3).

With respect to CO_2 relative permeability, Corey's formula is used (Silin *et al.*, 2006):

$$k_{rc} = (1 - S_h)^2 (1 - (S_h)^2) \qquad [11.18]$$

where

$$S_h = \frac{(S - S_{wr})}{(1 - S_{wr} - S_{gr})} \qquad [11.19]$$

S is the water saturation; S_{wr} is the irreducible water saturation; S_{gr} is the irreducible CO_2 saturation. S_{wr} is normally in the range 0.1-0.3 and S_{gr}=0.05 is used in literature (Silin *et al.*, 2006; Lindeberg, 1997).

In this research, it is assumed that the water and CO_2 saturation distribution inside the permeable zone do not change as CO_2 migrates up and the water saturation in the permeable zone is close to S_{wr}. Therefore, $k_{rc} \approx 1$. This is the maximum value of k_{rc}. This gives a conservative estimate of CO_2 leakage through a permeable zone.

11.2.10 Calculation of Leakage through Fractures in the Caprock

CO_2 might leak from faults embedded in the caprock. If the faults connect to the atmosphere, the CO_2 leakage might directly release to the atmosphere. In this research, a fault is idealised as two smooth, parallel plates embedded in the caprock of negligibly small permeability (see Figure 11.6).

For free phase CO_2 to enter a fracture of size 2d, the capillary entry pressure (P_c) needs to be $\geq 2\sigma/d$, where σ is the CO_2-brine interfacial tension. The vertical buoyancy pressure on the top aquifer layer by the CO_2 floating beneath the top aquifer layer is:

$$P_b = (\rho_w - \rho_c)gh_c \qquad [11.20]$$

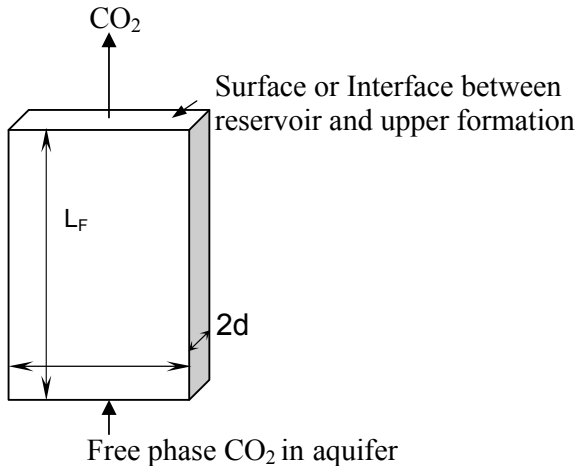

Figure 11.6: Idealised fault zone for studying CO_2 leakage behaviour.

Where, h_c is the thickness of free-phase CO_2 floating beneath the top layer of the saline aquifer (m); ρ_w, ρ_c are the density of brine and free phase CO_2 respectively (kg/m^3); g is gravitational acceleration (m/s^2).

For CO_2 to open the fracture, P_b must exceed P_c, thus h_b (the thickness of free phase CO_2 layer that can open the fracture) is needed to satisfy the follow condition:

$$h_b \geq \frac{2\sigma}{(\rho_w - \rho_c)gd} \qquad [11.21]$$

If it is assumed that:

i) the fault initially contains water and initial condition is hydrostatic;
ii) the CO_2 fluid flow is single-phase;
iii) the CO_2 fluid movement between the fracture and surrounding caprock is small enough to be neglected.

The CO_2 flow rate into the fracture, Q, is given by (Nicot *et al.*, 2006):

$$Q = \frac{wd^3}{12\mu_c}\frac{\Delta P}{L} \qquad [11.22]$$

Where, w is the width of the fracture (m); d is aperture of the fault (m); L is the length of the fracture (m); Δp is the pressure drop across the fracture (Pa), which is $(\rho_w\text{-}\rho_c)gh_c$.

Equation 11.22 was derived under the assumption that the fracture consisted of a region bounded by two smooth, parallel plates. Real rock fractures, however, have rough walls and variable apertures. The concept of equivalent aperture is used to model the fractures with alternative configurations and with equivalent aperture concept the Equation 11.22 is modified as:

$$Q = \frac{w d_{equ}^3}{12\mu_c} \frac{\Delta P}{L} \qquad [11.23]$$

The equivalent fracture apertures, d_{equ}, for various fracture configurations including inclined fractures, fractures connected in series, fractures orientation in a series network are calculated by the following equations (Sarkar *et al.*, 2004):

i) Inclined fractures

The equivalent fracture aperture for an inclined fracture is given by:

$$d_{equ} = \sqrt[3]{d^3 \cos\theta} \qquad [11.24]$$

Where, θ is the angle of the fracture with the pressure gradient axis; d is aperture of the fracture.

ii) Fractures connected in series

For a fracture composed of n fracture members in series, the following formula can be used to compute the equivalent fracture aperture:

$$d_{eq_{series}} = \frac{1}{\sqrt[3]{\sum_{i=1}^{n} \frac{l_i}{l}\left(\frac{1}{d_i^3}\right)}} \qquad [11.25]$$

Where, l_i and d_i are the length and aperture of the i_{th} fracture section respectively; l is the total length of the series network, i.e. distance between inlet and outlet. n is the total number of "parallel plate" fracture members connected in series.

iii) Fracture orientation in a series network

Equivalent aperture of a system which is composed of n inclined fracture members connected in series is given by:

$$d_{eq_{sn}} = \frac{1}{\sqrt[3]{\sum_{i=1}^{n} \frac{l_i}{l}\left(\frac{1}{d_i^3 \times \cos\theta_i}\right)}} \qquad [11.26]$$

Where, l_i is the projected length of the i_{th} fracture member along the direction of the pressure gradient axis, d_i and θ_i are aperture and inclination angle of the i_{th} member respectively.

Equation 11.22 is under the assumption that the CO_2 moves as a single-phase. This is realistic when the faults only intersect the caprock, because caprock is normally under a depth of more than 1,000 m and at this depth CO_2 remains at supercritical phase when leaking through the caprock. However, in the case that faults connect to the surface, as CO_2 migrates upwards, the density, viscosity, and gas volume of CO_2 may change dramatically at shallow depths and the greater volumes needing to flow through faults at shallow depths require a steeper fluid potential gradient at those depths and this results in a strongly concave-downward gas pressure vs. depth profile in the fracture (Brown, 2000). This pressure distribution has not been reported in leaking reservoirs in the oil and gas industry. One possible explanation is that the increase in number of fractures and fracture aperture towards the surface may be able to offset the increased gas volume, and another effect may be a change in gas saturation of a fracture system having increased capillary pressure (Brown, 2000). Therefore, equation 11.24 can give a reasonable estimation, at least the order of magnitude leakage rate can be estimated (Brown, 2000). This is acceptable in the context of LCA.

11.2.11 Calculation of Carbon Dioxide Leakage through Abandoned Wells

CO_2 leakage through abandoned wells is the most direct leakage pathway of CO_2 to the surface and may occur much more rapidly than geologic leakage, such as leakage from faults or permeable zones. CO_2 can escape through multiple pathways in a wellbore due to degradation and corrosion. These possible pathways include the cement fill, cement plug, the interface between the cement fill and the formation rock, and the interface between the cement fill and the well casing (see Figure 11.7).

The conventional cement used for well isolation in oil and gas industry is Portland cement. Once Portland cement based wellbore system is exposed to the CO_2-rich environment, it is subjected to the degradation. Chemical degradation of cement abandonment plugs based on diffusion are too slow to be an issue causing the leakage of CO_2 through plugs within one thousand years, unless fractures or other pathways through the cement are present or induced (Carey *et al.*, 2007; Mulders, 2007). However, there is evidence that CO_2 may mitigate along interfaces between the cement fill and the

formation rock, and along the interfaces between the well cement and the well casing, due to radial corrosion of the cement sheath and casing (Duguid, 2006; Barlet-Gouédard, 2006).

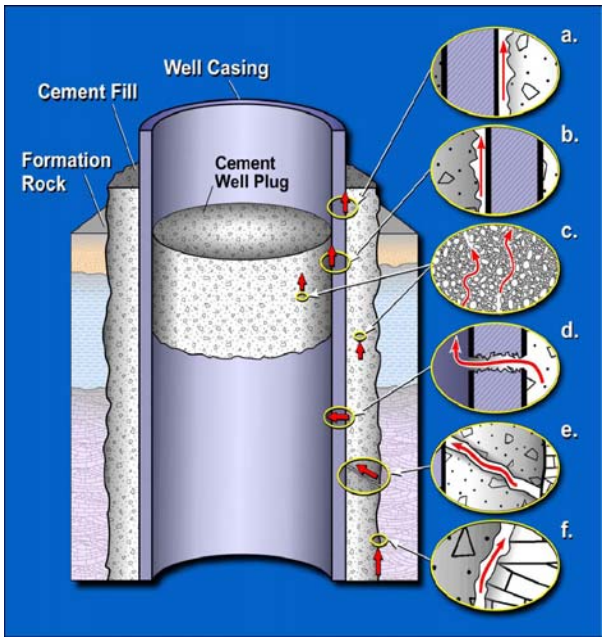

Figure 11.7: Diagrammatic representation of possible leakage pathways through an abandoned well. a) Between casing and cement; b) between cement plug and casing; c) through the cement pore space as a result of cement degradation; d) through casing as a result of corrosion; e) through fractures in cement; and f) between cement and rock (After Celia, 2006).

In this research, CO_2 leakage through degraded plug by diffusion is not considered, because it takes more than one thousand years to occur. However, leakage through fractures on the cement fill or cement plug, and leakage through interfaces between the cement fill and the formation rock, and leakage through the interfaces between the well cement and the well casing are included in this LCA research. The leakage through these pathways is consistent with several leakage path geometries: microannulus, fracture and gas channel (see Figure 11.8) (Huerta *et al.*, 2007).

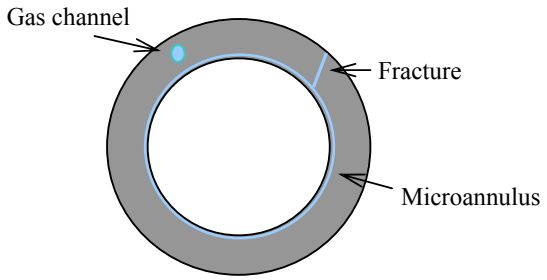

Figure 11.8: Leakage path geometries through wellbore

If it is assumed that: (1) the CO_2 fluid is single phase; (2) the leakage pathways initially contain water and initial conditions are hydrostatic; (3) once the CO_2 meets the open wellbore, the preferred path is to migrate up along the central wellbore with no leakage from the wellbore to the annulus as well as formations surrounding the wellbore, where capillary pressures would act to restrict flow; and in the open borehole, CO_2 rapidly ascends to the surface as gas bubbles (see Figure 11.9). It is considered that these assumptions result in a overestimating of CO_2 leakage rates given the variability and uncertainty of the key parameters used in the model.

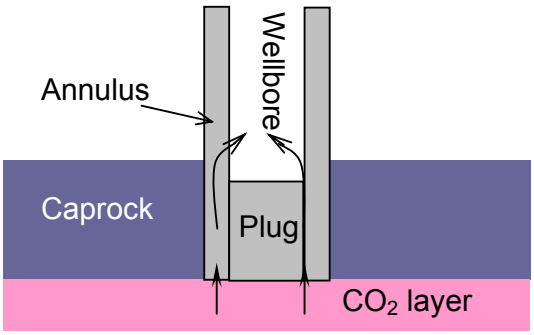

Figure 11.9: The leakage pathways in an abandoned well.

The flow rate of CO_2 fluid through various types of leakage path geometries is computed as follows:

i) Gas channel

Poiseuille's Law for flow through a straight cylindrical tube is used:

$$Q = \frac{\pi R^4}{8\mu_c}\frac{\Delta P}{L} \qquad [11.27]$$

where, Q is the flow rate of CO_2 (m^3/s); ΔP is the pressure drop across the channel (Pa); R is the radius of the channel (m); L is the length of the channel (m); μ_c is the viscosity of supercritical CO_2 (Pa.s).

ii) Fracture

The equation for flow through two parallel plates is used (Brown, 2000; Nicot *et al.*, 2006):

$$Q = \frac{wd^3}{12\mu_c}\frac{\Delta P}{L} \qquad [11.28]$$

where, Q is the flow rate of CO_2 (m^3/s); ΔP = pressure drop across the fracture (Pa); d is the aperture of the fracture (m); w is the width of the fracture (m); L is the length of the fracture (m); μ_c is the viscosity of supercritical CO_2 (Pa s).

iii) Microannulus

The volumetric flow rate is related to κ and the pressure drop by the following equation (Huerta *et al.*, 2007):

$$Q = \frac{\pi R^3}{8\mu_c}[(1-\kappa^4) - \frac{(1-\kappa^2)^2}{Ln(1/\kappa)}]\frac{\Delta P}{L} \qquad [11.29]$$

where, Q is the flow rate of CO_2 (m^3/s); ΔP is the pressure drop across the annulus (Pa); κ is the ratio of internal to external radius of the microannulus; L is the length of the annulus (m); R is the outer radius of the annulus (m); μ_c is the viscosity of supercritical CO_2 (Pa s).

The typical parameters for microannulus, fracture and gas channel used in this research are given in Table 11.2.

Table 11.2: Typical parameters for microannulus, fracture and gas channel (After Huerta *et al.*, 2007)

Leakage pathway geometry	Value (μm)
Gas channel radius	110
Fracture aperture	30
Microannulus thickness	12

11.2.12 Carbon Dioxide Migration and Attenuation in Water-saturated Porous Zone

Within a water-saturated porous zone (i.e. the sediments) below the water body, the CO_2 flux migrates upwards in the form of bubble flow or channel flow (Oldenburg and Lewicki, 2006). If the CO_2 leakage flux originating from source zone such as fractured rock or permeable zones is low, CO_2 can migrate upwards as small individual bubbles, especially in coarse and highly permeable porous medium. In contrast, when the flux is large, a connected channel of CO_2 gas can be formed between the leading edge of water displacement and the CO_2 leakage source (Oldenburg and Lewicki, 2006). The velocity of bubble flow can be computed by the method of Corapcioglu *et al.* (2004). The bubble flow in the porous media has a maximum velocity of approximately 18 cm s^{-1} in very coarse gravels and is much smaller in typical sediments (0.7-3 cm s^{-1}) (Oldenburg and Lewicki, 2006). On the other hand, channel flow regime is governed by multiphase flow process that can be modelled by using reservoir engineering approach such as the model

provided by Silin *et al.* (2006). In the case of channel flow, CO_2 rises approximately vertically in the porous media with volumetric flux, F (m/s), given by:

$$F = (k_v \cdot k_{rg}/\mu_c) \cdot \Delta\rho_{gw} \cdot g \quad [11.30]$$

Where, k_v is the vertical absolute permeability (mD); k_{rg} is relative permeability (%); μ_c is the CO_2 viscosity (Pa·s); $\Delta\rho_{gw}$ is the density difference of CO_2 and water (kg/m^3). A fraction of the leaking CO_2 will dissolve into surrounding water when CO_2 migrates upwards through the porous zone (Nicot *et al.*, 2006). This attenuates the leakage of CO_2 to atmosphere. The entire water column (between the CO_2 source zone and the water table) exposed to CO_2 plume (or bubbles) in porous zone would have to reach maximum solubility concentrations of CO_2 before there could be any seepage of CO_2 through the water-saturated porous zone (Oldenburg, 2003). If the leakage is not sufficient, the leaking CO_2 can be totally dissolved into groundwater. The attenuation rate of CO_2 due to the CO_2 dissolution in water-saturated porous zone can be estimated as follows (Nicot *et al.*, 2006):

$$R_a = \frac{v_w C_w V_w}{\dot{M}_c} \quad [11.31]$$

$$V_w = \phi HS \quad [11.32]$$

where $\dot{M}_c$ is the CO_2 leakage rate (kg/s); v_w is the groundwater horizontal velocity (m/s); C_w is the solubility of CO_2 in water (kg/m^3); V_w is the volume of water on top area of leak (m^3); ϕ is the porosity of the water-saturated zone (%); H is the thickness of the water-saturated zone (m); S is the horizontal cross-sectional area of the CO_2 plume (horizontal cross-sectional area exposed to CO_2 bubbles) (m^2).

In the case of channel flow, the rate of CO_2 leakage from source zone to the porous zone equals that the volumetric flux (F) of CO_2 plume times the horizontal cross-sectional area of CO_2 plume (S) times the CO_2 density (Weir *et al.*, 1996) and so, the approximate horizontal cross-sectional area (S) of the CO_2 plume above the leakage point, can be calculated as follows:

$$S = \frac{\mu_c \dot{M}_c}{k_v k_{rg} \rho_{co2} \Delta\rho_{gw} g} \quad [11.33]$$

In the case of bubble flow, since CO_2 bubbles migrate upwards to the top, the S is assumed to be same as the horizontal cross-sectional area of the leakage source.

CO_2 in underground has higher solubility due to the higher pressure. Once the water saturated with CO_2 reaches the atmosphere, the dissolved CO_2 will be released to atmosphere like sparkling water. Therefore, a fraction of dissolved CO_2 during leaking CO_2 migration upwards through overlying porous media outside the storage formation might be finally released to the atmosphere. This depends on the groundwater system it may encounter in its path. In this research, it is assumed that 80% of dissolved CO_2 which has leaked out of the storage formation will be released to the atmosphere within a period of 1,000 years.

11.2.13 Carbon Dioxide Migration and Attenuation in Unsaturated Soils above the Water Table

If the leakage of concentrated CO_2 through a fractured rock, leaky abandoned well or other similar pathway is discharged to unsaturated soil (or vadose zone), the buoyancy driving force is reversed as CO_2 is denser than soil gas and CO_2 migration will be governed by advective and diffusive transport processes. Advective fluxes are due to pressure gradients that drive the CO_2 to migrate upwards. Diffusive fluxes are driven by concentration gradients and dissipate the CO_2 laterally to the surrounding soil zones. Pressure gradients easily overcome the density contrast and cause CO_2 to discharge at the ground surface. However, the unsaturated soil zone can attenuate leaking CO_2 and decrease seepage and near-surface CO_2 concentrations though processes, including permeability trapping, solubility trapping by infiltration or residual water, and dilution through mixing with ambient soil gas. The seepage flux and near-surface gas concentrations are most strongly controlled by the leakage rate and the radius of the leakage source zone (Altevogt and Celia, 2004; Oldenburg, 2003). A previous study has shown that the attenuation rates of a 30m-thick unsaturated soil zone are 96%, 66% and 19% for the CO_2 leakage with values 4×10^{-8} kg m^{-2} s^{-1}, 4×10^{-7} kg m^{-2} s^{-1}, 4×10^{-6} kg m^{-2} s^{-1} respectively (Oldenburg, 2003). The attenuation efficiency of the unsaturated zone decreased with increasing leakage rate because higher pressures surrounding the source zone cause more vertical migration of the CO_2 relative to lateral migration.

Based on the simulation results from the literature (Altevogt and Celia, 2004; Oldenburg, 2003), the CO_2 attenuation rates of a typical unsaturated soil zone are assigned to various CO_2 leakage rates used in this research, as follows:

Table 11.3: Attenuation rates for CO_2 passing across unsaturated soil zone

CO_2 leakage per m^2 (kg m^{-2} s^{-1})	Attenuation rate
$\leq 10^{-8}$	96%
10^{-8}~10^{-7}	66%
10^{-7}~10^{-6}	19%
$\geq 10^{-6}$	1%

11.2.14 Carbon Dioxide Migration in Surface Waters

If the leakage of concentrated CO_2 through a fractured rock, leaky abandoned well or other similar pathway is discharged to the surface water, the CO_2 transport through the surface water tends to be by ebullition/bubble flux for relatively high leakage flux and/or deep water bodies and by diffusion/dispersion for relatively low leakage flux and/or shallow water bodies (Oldenburg and Lewicki, 2006). A fraction of CO_2 will be dissolved and dissociated in water during migration through surface waters.

The transport of dissolved CO_2 in surface waters is based on diffusive and dispersive processes in the aqueous phase. Flow occurs in typical surface waters such as rivers, lakes and shallow seas by combinations of gravity, wind, and tidal forces, and such motions can lead to effective dispersion and mixing of dissolved species (Oldenburg and Lewicki, 2006). Dispersion and mixing will periodically expose surface water to the atmosphere where it will potentially equilibrate with atmospheric CO_2 creating an effective out-gassing that finally releases most dissolved CO_2 to atmosphere (Oldenburg and Lewicki, 2006). Moreover, since the density of CO_2-saturated water is approximately 1% greater than that of pure water, there is the possibility of dissolved CO_2 producing a stable density stratification. However, in typical surface waters except deep marine environments and certain kinds of lakes, gravity, wind, and tides will dominate over density stratification and cause mixing on time scales much smaller than the objective sequestration time scale (hundreds to thousands of years) (Oldenburg and Lewicki, 2006). Thus, CO_2 storage, rivers, lakes, estuaries, and continental shallow ocean water are not effective at attenuating leakage and seepage fluxes of CO_2 by dissolution. In addition, the dissociated fraction of CO_2 is negligible during CO_2 migration in surface water. In this study, the CO_2 leaked to surface water such as rivers, lakes, estuaries, and continental shallow ocean water, are considered to lead to final release to the atmosphere and are accounted as air emissions for the purpose of LCA.

It is worth noting that if CO_2 leaks to a stagnant water body (e.g. lake), the dissolution of CO_2 may cause a serious safety risk. One of the most notable examples is Lake Nyos

in western Cameroon, adjacent to Nigeria, which erupted $0.3–2.0\times10^9$ kg of CO_2 gas over a period of 2 events lasting approximately 4 hours on August 21, 1986. This gas formed a gravity current which flooded over a valley passing through the village of Nyos and suffocated about 1,700 people and 3,500 livestock as a result (Woods and Phillips, 1999). It is widely believed that the eruption involved a massive vertical redistribution of lake water caused by landslide and this enabled CO_2, which is dissolved in water at high pressures deep in the lake, to be released (Zhang and Kling, 2006; Woods and Phillips, 1999).

11.2.15 Carbon Dioxide Migration in Deep Sea

In the case of CO_2 leakage to deep sea (deeper than -380 m), CO_2 is at liquid or supercritical phase due to high hydrostatic pressure and has higher solubility than that in shallow water (see Figure 11.10). The leaking CO_2 exists as liquid or supercritical droplets and rises upwards driven by buoyancy, transiting from supercritical to liquid and then to gas. Due to instability large droplets normally split up into smaller droplets and most of the droplets have diameters between 1 and 60 mm (Bozzano and Dente, 2001). As it rises through the deep sea, a considerable fraction of CO_2 dissolves into the sea water, owing to its high solubility and low velocity. The dissolved CO_2 will diffuse across the water and the CO_2-saturated sea water with greater density can lead to sinking plumes (Brewer *et al.*, 2002). This process effectively attenuates CO_2 leakage flux and may be considered as a kind of CO_2 disposal method (Tamburri, 2000). Since only the CO_2 that eventually reaches the atmosphere is considered as air emission for the purposes of LCA, in this research, the dissolution of CO_2 in deep water is considered as CO_2 attenuation.

The radius change of a CO_2 droplet caused by dissolution during passing through the deep sea can be computed using the following equations (Brewer *et al.*, 2002):

$$(r_t - r_0) = -V_m \Gamma (t - t_0) \qquad [11.34]$$

where t is time (s); t_0 is the initial time (s); r_0 is the initial radius of the droplet (m); r_t is the radius of the droplet at time t (m); Γ is the dissolution rate ($mol/m^{-2}s^{-1}$), which equals to 3 $\mu mol/m^{-2}s^{-1}$; V_m is the specific volume of the droplet (m^3mol^{-1}).

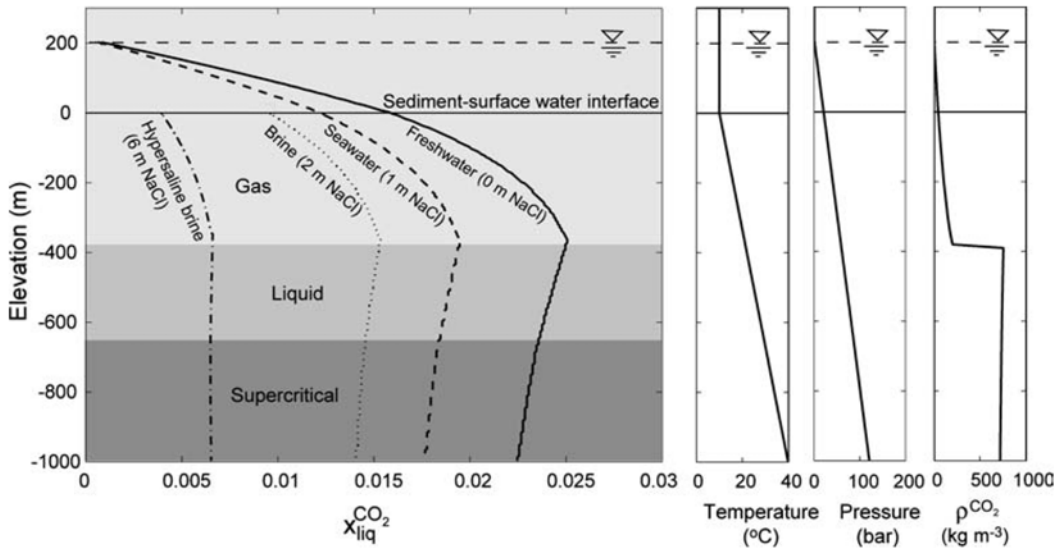

Figure 11.10: Solubility of CO_2 (mole fraction) as a function of depth (After Oldenburg and Lewicki, 2006).

The mass change of the CO_2 droplet is given by:

$$(m_t - m_0) = -\frac{4}{3}\pi(r^3 - r_0^3)\rho_{CO_2} \qquad [11.35]$$

where, m_0 is the initial mass of the droplet (kg); m_t is the mass of the droplet at time t (kg); ρ_{CO_2} is the density of CO_2 (kg/m^3). Since in the deep sea, from -1,000 to -400m in depth, the density of CO_2 changes slightly, average density 930kg/m^3 is used in this research.

The time period (t_t) required for a droplet to reach the liquid-gas transition boundary (-400m in depth) is given by:

$$t_t = \frac{-400 - H}{U_t} \qquad [11.36]$$

where, H is initial depth of the droplet (m); U_t is the terminal velocity of the droplet (m/s). According to previous study, U_t is around 0.114 cm/s for various radiuses of droplets (Brewer *et al.*, 2002).

11.2.16 The Fate of the Free-phase Carbon Dioxide Pool

The fate of the free-phase CO_2 pool in the saline aquifer is determined by CO_2 injection, CO_2 dissolution, capillary trapping and CO_2 leakage. The general mass balance equation is:

$$\frac{dM}{dt} = F_i - F_d - F_c - F_o \qquad [11.37]$$

where, M is the mass of the free-phase CO_2 in the reservoir, t is time, F_i is the flow rate of CO_2 injected in the reservoir, F_d is the rate of dissolution, F_c is the rate of capillary trapping, F_o is rate of leakage.

Due to capillary trapping, CO_2 dissolution by convective mixing, and CO_2 leakage results in the gradual reduction of the thickness of the CO_2 layer floating beneath the caprock, it is assumed that the rate of the reduction of the thickness of the CO_2 layer, r_t, approximately equals to the rate of the reduction of free-phase CO_2 mass in the pool ($dM(t)/M(t)$).

11.3 Life Cycle Impact Analysis of Carbon Dioxide Storage: A Case Study

The case study analyses a potential saline aquifer CO_2 storage site situated at the small harbour of Havnsø, approximately 15 km northeast of Kalundborg, Denmark. Approximately 1/3 of the structure is situated offshore, with the top point situated onshore (Larsen *et al*., 2007). The Havnsø structure covers approximately 160 km^2 (see Figure 11.11).

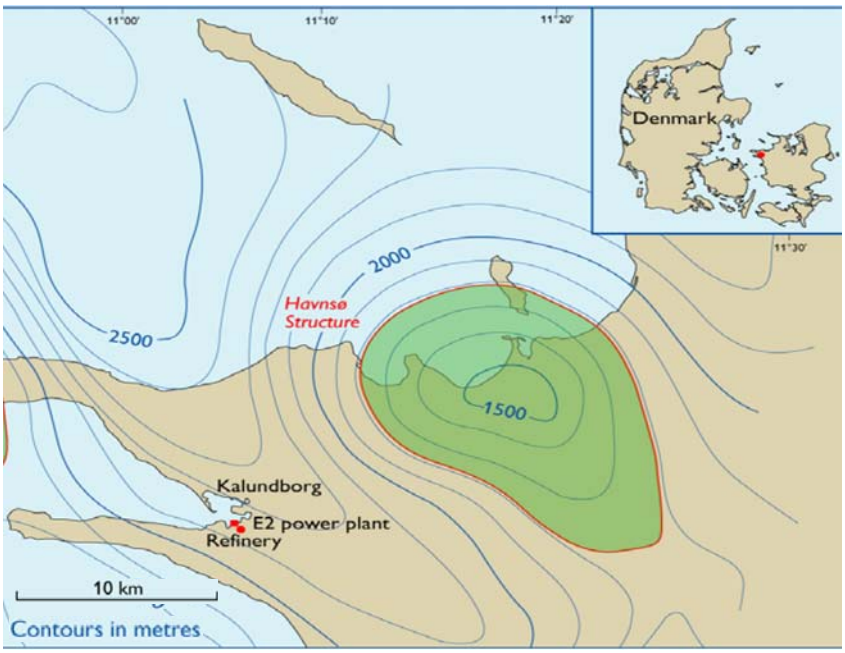

Figure 11.11: Depth structure map of the Havnsø closures (After Larsen *et al.*, 2007)

The saline aquifer is found at depths approximately between 1,500-2,000 m and is formed by porous sandstones of the Gassum Formation and sealed by marine mudstones of the Fjerritslev Formation which act as a caprock (Figure 11.12). A preliminary estimation suggested a storage capacity of nearly 900 million tonnes of CO_2 (Larsen *et al.*, 2007). The detailed information of Havnsø structure is provided in Table 11.4.

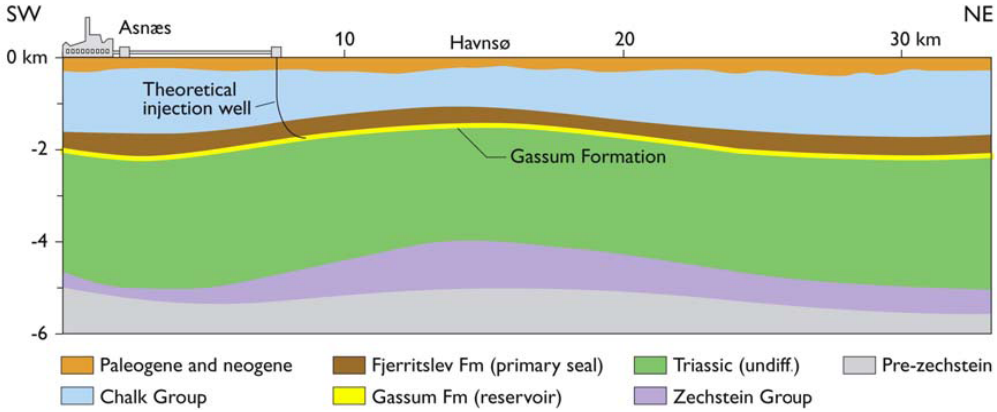

Figure 11.12: Schematic geological cross-section through the Havnsø structure (After Larsen *et al.*, 2007).

Table 11.4: Havnsø structure (After Larsen *et al.*, 2007)

Storage	**Havnsø**
Onshore/offshore	2/3 onshore, 1/3 offshore
Reservoir	Gassum Formation
Stratigraphy	Late Triassic
Lithology	Siliciclastic sandstone
Top depth	1500 m
Gross thickness	150 m
Porosity	22%
Permeability	500 mD
Pore volume	3 670 km3
Pressure	150 bar
Temperature	~ 50 ºC
Reservoir density of CO_2	629 kg/m3
Storage capacity	923 Mt
Seal	Fjerritslev Formation
Stratigraphy	Early Jurassic
Lithology	Marine mudstone
Gross thickness	500 m
Area of closure	166 km^2

11.3.1 Parameters used in the Life Cycle Inventory Model

Based on the geological information for the Havnsø structure, a simple, homogeneous aquifer model was constructed for LCI analysis and a period of 2,000 years. The LCI model parameters and input data are presented in Table 11.5. It is assumed that the CO_2 is injected into the aquifer through a vertical injection well, 8 km from the formation's

south-east boundary (see Figure 11.12) and the perforation of the well is at 1,750 m below sea level and with well-completion interval of 150m. The CO_2 injection rate is set at 200 kg/second, as defined by Bech and Larsen (2005). These authors conclude that the rock properties in the reservoir at Havnsø will allow injection of 200 kg CO_2/sec which is equal to approximately 6 Mt/year for more than 100 years (corresponding to the average annual emission rates of the coal/oil/orimulsion power plant Asnæsværket at Kalundborg with a capacity of 1300 MW). The CO_2-water relative permeability curves derived for the Sleipner project (Figure 11.13) are used for the reservoir modelling (Akervoll *et al.*, 2006).

Table 11.5: Parameters and input data for the saline aquifer LCI model.

Quantity	Values
Reservoir thickness	H=150 m
Injection well-completion interval	H_w=100 m
reservoir length	L=30,000 m
Top of aquifer	1,500 m (below sea level)
Dip angle	3.64°
Porosity	ϕ=0.22
Horizontal permeability	k_h= 500 mD
Vertical permeability	k_v= 100 mD
CO_2 saturation at water-CO_2 front	S_{gf} = 0.905
Average CO_2 saturation at top gas layer	S_g = 0.6
Temperature	50°C
Initial injector bottom hole pressure	Hydrostatic pressure
Water viscosity	μ_w= 0.00043 Pa s
CO_2 viscosity	μ_g= 0.000043 Pa s
CO_2 solubility	53.4 kg/m^3
CO_2 density (1750 m)	634 kg/m^3
Water and CO_2 density difference	$\Delta\rho$=350 kg/m^3
CO_2 injection rate	200kg/s
Injection period	100 years
Diffusivity	D= 1.00E-09 m^{2}s^{-1}

In order to analyse the CO_2 leakage behaviour, it is assumed that there is a permeable zone, a fault, and an abandoned well located close to the CO_2 injection well. The parameters of these CO_2 leakage pathways are described in Table 11.6.

11.3.2 Kalundborg Life Cycle Inventory Model Results

LCI model results (Table 11.7) shows that the radius of the injected CO_2 spreads about 10 km with 14.74% injected CO_2 dissolved during injection. During 1,000 year period, capillary trapping is the primary mechanism to reduce the free phase CO_2 and around 67% of the remaining free phase CO_2 will be immobilised by capillary trapping.

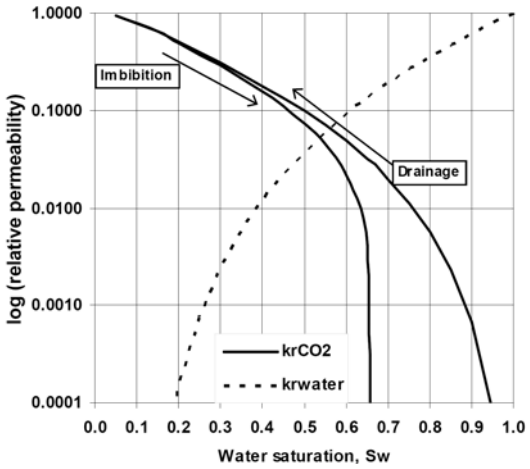

Figure 11.13: Relative permeability curves (After Akervoll *et al.*, 2006)

Table 11.6: Parameters of the leakage pathways.

	Unit	Value
Permeable zone:		
Distance to injector (D_p)	m	1,000
Intrinsic permeability (K_p)	mD	10
Radius of the zone (r_p)	m	100
Thickness of the zone (L_p)	m	500m
Fault:		
Distance to injector (D_f)	m	2,000
Aperture(d_f)	μm	100
Width (w_f)	m	10m
Length (L_f)	m	500m
Abandoned well:		
Distance to injector (D_w)	m	3,000
1.Gas channel		
Radius (r_g)	μm	110
Length (L_g)	m	50
2. Fracture		
Aperture	μm	30
Width	m	0.75
Length	m	50
3. Microannulus		
Microannulus thickness	μm	12
Outer radius of the annulus (r_a)	m	0.5
Length (L_a)	m	50

The permeable zone is the primary contributor of CO_2 leakage to the atmosphere (see Figure 11.14a), with a leakage rate of 0.23 kg/s in the beginning. The leakage rates of alternative leakage pathways slightly decrease with time, especially within 900 years (Figure 11.14b), because the capillary trapping and convective mixing effect immobilise the free phase CO_2 and as a result the thickness of the CO_2 layer beneath the caprock is reduced gradually. Figure 11.15 demonstrates that about 3.0×10^9 kg CO_2 leaks during the 1,000 years following injection, which accounts for around 0.8% of the total CO_2 injected. This is lower than the 1% limit, the widely accepted standard for CO_2 storage projects (IPCC, 2005).

Table 11.7: The results for the base case.

	Value
The radial distribution of CO_2 injected during injection (m)	10390.72
The lateral extent where gravity becomes dominate (m)	3048.59
Percentage of CO_2 dissolved during injection (%)	14.74%
The dissolution due to CO_2 during convective mixing effect:	
t_c (years)	0.23
t_{on} (years)	32.49
t_{slow} (years)	889.82
t_{sat} (years)	13347.23
Dissolution rate (kg/year)	4.13E+07
Capillary Trapping (residual trapping) of CO_2 :	
N_{gv}	22.57
Time required for trapping (years)	900
Percentage of injected CO_2 trapped by capillary trapping (%)	67.00%
Average annual trapping (kg)	4.70E+08

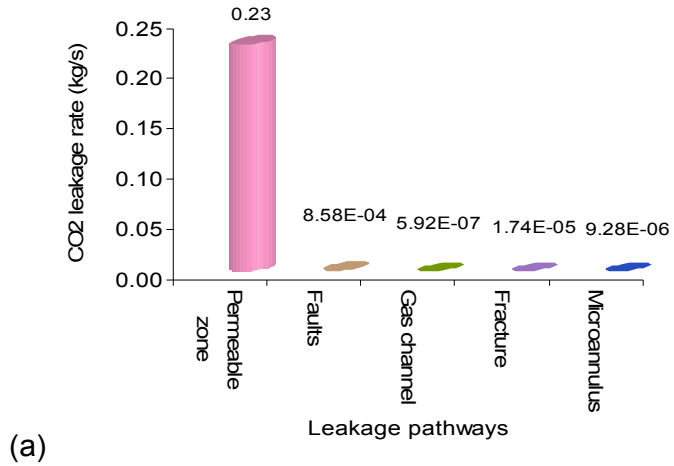

(a)

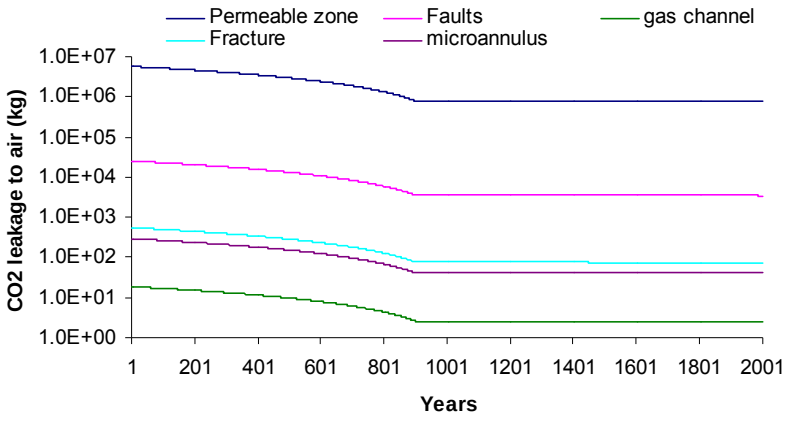

(b)

Figure 11.14: CO_2 leakage to the atmosphere through alternative pathways: (a) Leakage rate; (b) Annual leakage rate over time.

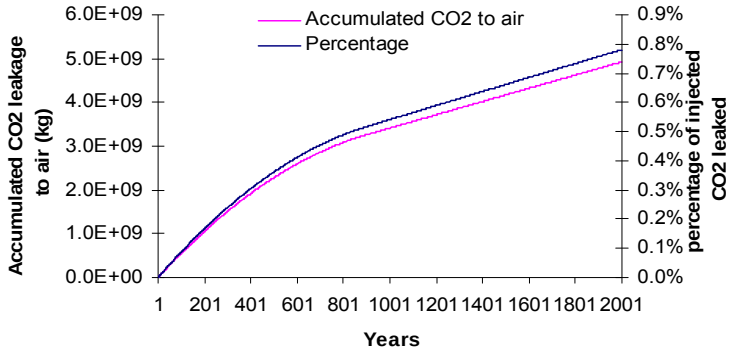

Figure 11.15: CO_2 leakage to the atmosphere.

11.3.3 Sensitivity Analysis

The sensitivity analysis was conducted in order to identify the parameters (including operational parameters, reservoir parameters, and parameters of leakage pathways) that have significant impacts on CO_2 leakage.

The sensitivity analysis of the operational parameters and reservoir parameters, including the injection period, injection rate, capillary force, reservoir permeability, height of reservoir and depth of the reservoir, shows that the injection period, injection rate, capillary entry pressure (P_c) have a significant influence on the ratio of CO_2 leakage to total CO_2 injected (Figure 11.16 a, b, c). Because the capillary entry pressure (P_c) determines the thickness of the CO_2 layer beneath the caprock and the thicker CO_2 layer has the larger buoyancy which causes higher CO_2 leakage rate. The injection rate and injection period determine the total CO_2 injected. Larger injection rates or long injection periods result in more CO_2 injected and lead to a thicker CO_2 layer beneath the caprock and, consequently the value of the ratio of CO_2 leakage to total CO_2 injected is higher. Figures 11.16 (d, e, f) show that reservoir permeability, height of the reservoir and the depth of the reservoir influence slightly the ratio of CO_2 leakage to total CO_2 injected.

Figures 11.17, 11.18 and 11.19 show that the parameters of the leakage pathways can significantly change the CO_2 leakage rate. Figure 11.17 demonstrates that the increase of the radius of the permeable zone or the permeability of the permeable zone can significantly increase the ratio of CO_2 leakage to total CO_2 injected. The change in relative permeability of the permeable zone also can considerably change the ratio of CO_2 leakage to total CO_2 injected, but has a lower impact. Figure 11.18 shows that a small increase of aperture size of the fault can result in a significant increase of CO_2 leakage.

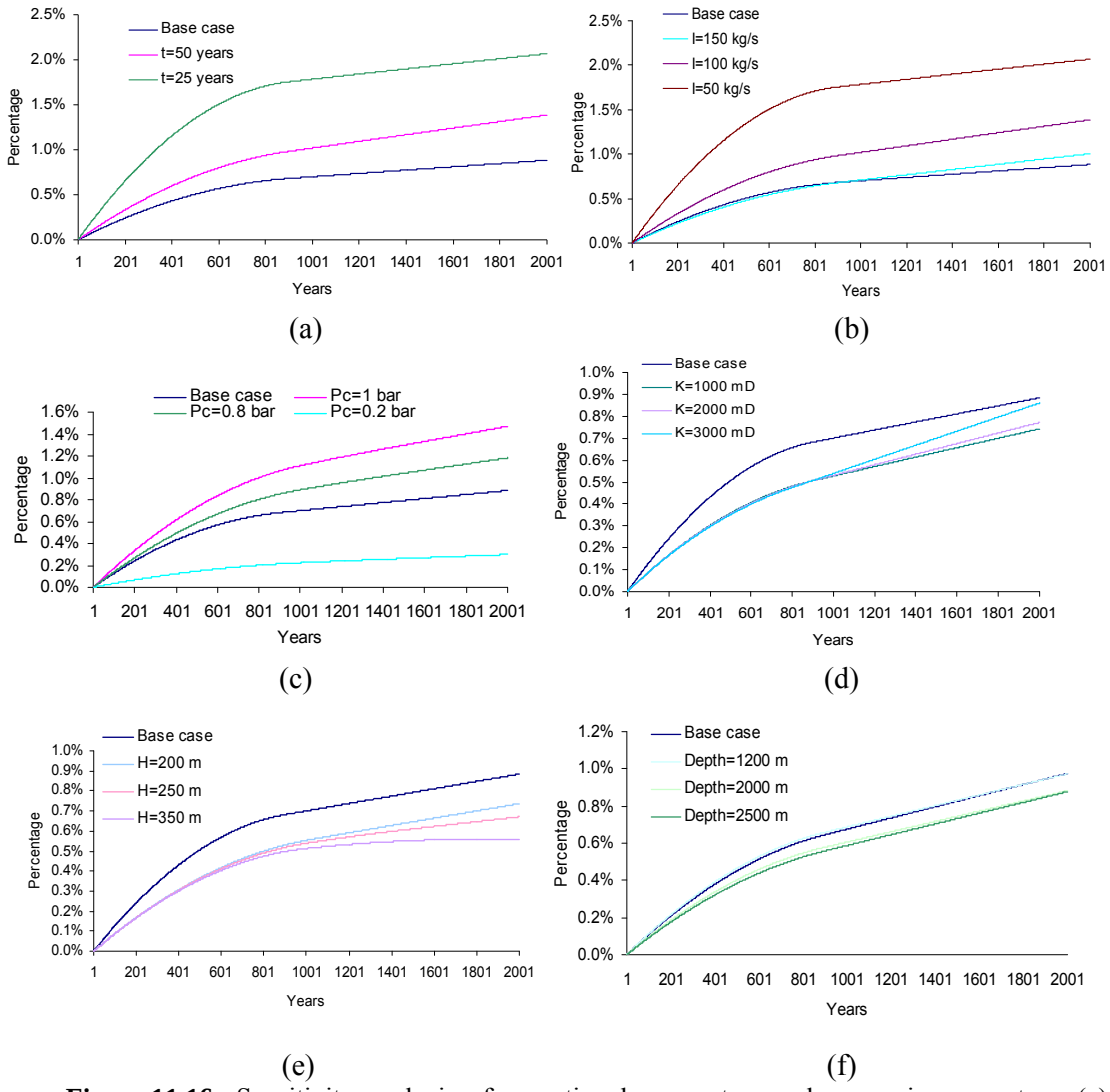

Figure 11.16: Sensitivity analysis of operational parameters and reservoir parameters: (a) injection period; (b) injection rate; (c) capillary entry pressure; (d) permeability; (e) height of the saline aquifer; (f) depth of the saline aquifer

The change of width of the fault or the length of the fault can result in a considerable change of the ratio of CO_2 leakage to total CO_2 injected, but has less influence compared to the aperture size of the fault. Figure 11.19 demonstrates that the change of the radius of the gas channel, or the width of the fracture, or the ratio of internal to external radius of the microannulus in an abandoned wellbore can result in a significant change of the ratio of CO_2 leakage to total CO_2 injected. The sensitivity analysis above shows that if leakage pathways are not controlled and monitored, a small change of these parameters can cause a significant change of leakage rate and the amount of overall leakage may exceed the allowable leakage limits.

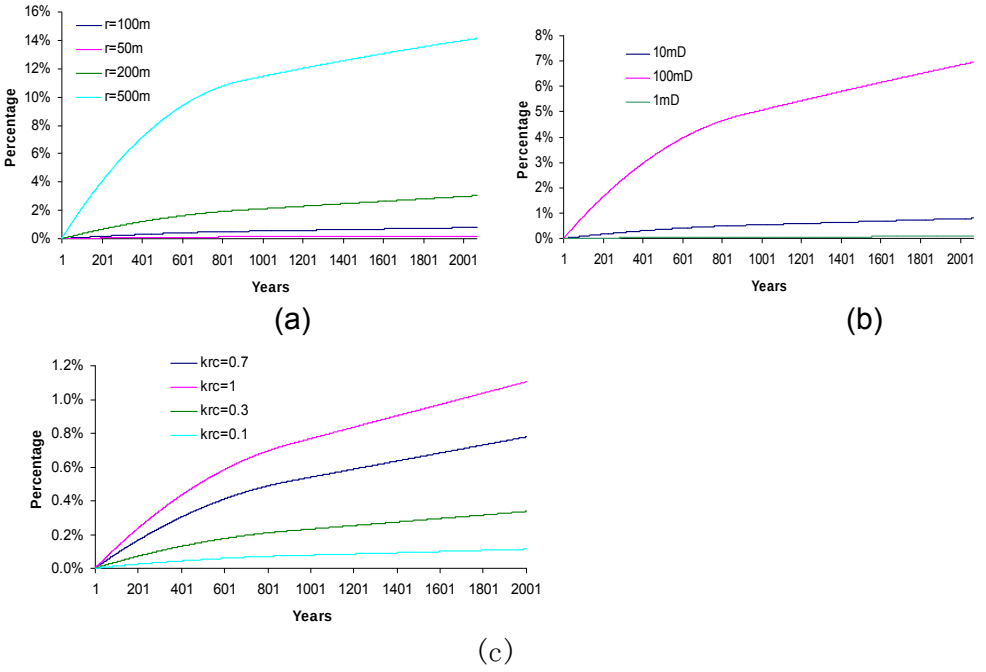

Figure 11.17: Sensitivity analysis of parameters of the permeable zone: (a) Radius of the zone; (b) permeability of the zone; (c) Relative permeability of the zone

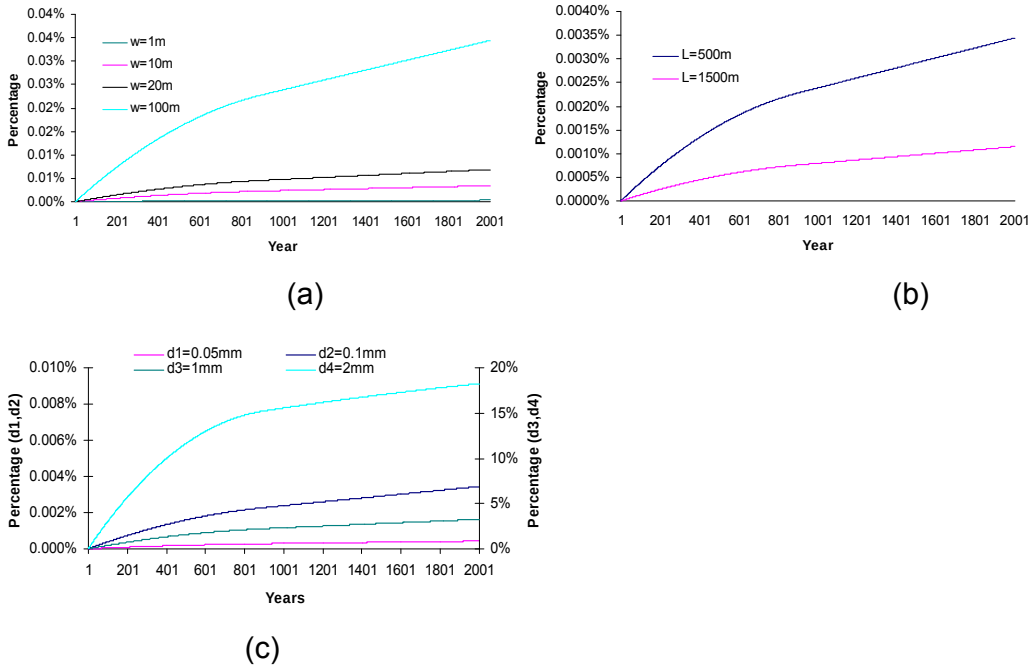

Figure 11.18: Sensitivity analysis of fault parameters : (a) Width of the fault; (b) length of the fault; (c) aperture size of the fault

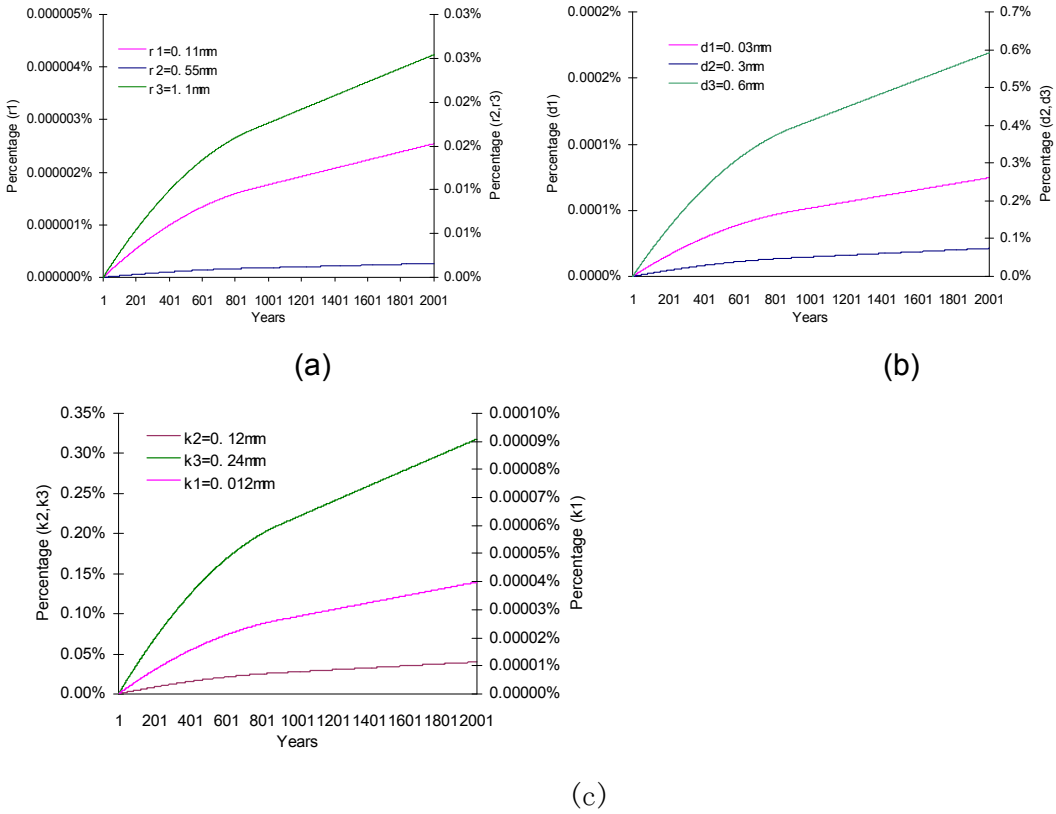

Figure 11.19: Sensitivity analysis of abandoned well parameters : (a) radius of the gas channel; (b) width of the fracture; (c) ratio of internal to external radius of the microannulus.

11.4 Conclusions

The LCI model of a CO_2 storage in saline aquifer successfully analyses the migration of injected CO_2 in saline aquifers which determines the geological boundary and the timeframe of the CO_2 storage system in the context of LCA, by quantifying the radial extent of the CO_2 plume, the thickness of the thin CO_2 layer, the time it takes for the CO_2 plume to reach the top of the formation, the dissolution, capillary trapping, and the lateral movement of free gas phase CO_2 after injection ceases. The model also computes the CO_2 leakage potential of CO_2 storage, by modelling the alternative leakage pathways including permeable zones in the caprock, faults, and abandoned wells that intersect the caprock. The model also analyses the mitigation of leaked CO_2 out of the saline aquifer upwards through different compartments within the overburden including the water-saturated porous zones, surface water or unsaturated soil zones, and calculates the final CO_2 flux that crosses the land-atmosphere boundary and enters into atmosphere.

A case study is conducted in order to identify the operational parameters, reservoir parameters, and parameters of leakage pathways, which have significant impacts on CO_2 leakage. The results demonstrate that the injection period, injection rate and capillary entry pressure (P_c) of the reservoir have a significant influence on the ratio of CO_2 leakage to total CO_2 injected. Because the capillary entry pressure (P_c) determines the thickness of the CO_2 layer beneath the caprock, and larger injection rates or long injection duration results in a thicker CO_2 layer beneath the caprock and consequently increase the CO_2 leakage. The parameters, including the radius of the permeable zone or the permeability of the permeable zone, the aperture size of the fault, and the radius of the gas channel (or the width of the fracture, or the ratio of internal to external radius) of the microannulus in an abundant wellbore, can significantly change the CO_2 leakage rate. A small change of these parameters would cause a significant increase in the CO_2 leakage.

Chapter 12 Conclusions and Recommendations for Further Research

12.1 Research Achievements

This research accomplished the development of a complete and dynamic LCA framework for the "cradle-to-grave" assessment of alternative CCS technologies in carbon-containing fuel power generation, and the LCA framework developed is successfully applied to the LCA of power plants with alternative post-combustion chemical absorption capture and oxy-fuel combustion capture.

The LCI models developed for power generation with post-combustion and oxy-fuel combustion capture systems included the models of conventional coal combustion, oxy-fuel combustion, alternative post-combustion chemical absorption CO_2 capture, air separation unit, CO_2 conditioning unit, CO_2 pipeline transport, CO_2 injection, power plant air pollution control units (including particulate matter emissions control, NO_x emissions control and SO_x emissions control), and solid waste disposal. The LCI models developed account for technological and geographical differences and generate reliable LCI data in a consistent and transparent manner.

Using the LCI models developed, this research successfully traced the fate of elements (including C, S, Cl, F, N) and trace metals of concern (including As, Cd, Cr, Cu, Hg, Ni, Pb, Zn, Sb, Be, B, F, Mn, Se, V, Co, Ba, Ag and Ti) in coal throughout the power generation, transport and injection chain. Monte Carlo simulation method combined with the LCI models was applied to quantify the uncertainty of emissions related to these elements and trace metals of concern.

Research has also developed an analytical LCA framework for the analysis of CO_2 storage in saline aquifers. This novel saline aquifer CO_2 storage LCI model developed is able to analyse the migration of injected CO_2 in the reservoir in a timeframe of thousands of years and compute the potential for CO_2 leakage from the aquifer by modelling the possible leakage pathways that intersect the caprock. The mitigation of leaked CO_2 from the saline aquifer upwards through different compartments within the overburden is modelled or analysed in the LCI model. A case study with sensitivity analysis was conducted, which successfully identified the parameters that have significant influence on the CO_2 storage processes and/or the CO_2 leakage rate.

The LCI models developed successfully compared the environmental profiles of post-combustion capture system with oxy-fuel combustion capture system both at plant level (direct emissions level) and at a life-cycle level. Opportunities for the reduction of life-cycle environmental impacts are identified by conducting sensitivity analysis.

The LCI models developed quantify flows of materials, natural resources, energy, intermediate products or emissions at component unit process level, based on basic physical/chemical principles or empirical relationships which, to a greater extent, account for the technological, spatial and temporal characteristics of the power generation systems in consideration. This approach not only addresses the limitations of conventional LCI models that use linear input/output coefficients in the LCI models, but also resolved the second limitation of the conventional LCI methods by accommodating the specific operational needs of the industry. The approach also facilitates practitioners to trace down emissions of concern throughout the production chain in order to screen the opportunities to improve life-cycle environmental performance, as demonstrated in Chapters 9 and 10.

The uncertainty associated with the LCA results is a widely acknowledged limitation of the LCA technology. The development of the LCI models at component unit process

level and the use of fundamental physical/chemical principles, have improved the capacity of the LCI models to handle complexity and reduced model uncertainty. Research has also combined Monte Carlo simulation method with the LCI models to further quantify the uncertainty associated with the inputs/outputs of a unit process or the whole production chain by allocating probability distribution functions to the parameters or factors that contribute to the model uncertainty.

ISO 14041 (1998) addresses LCA needs of the existing plants, however, it does not offer solutions for novel systems that are not commercially operated. The LCI method developed in this research provides an innovative approach for conducting LCA for novel systems by configuring virtual systems at component unit process level within a flexible framework, and help tracing the emissions of concern from their origins to their final destination.

12.2 Summary of Life Cycle Impact Assessment Results

12.2.1 Post-combustion Carbon Dioxide Capture, Transport and Injection

At plant emissions level, post-combustion chemical absorption (MEA) CO_2 capture unit captures 95% of the CO_2 and has lower emission rates of PM-10, SO_2, SO_3, NO_2, HCl, HF, mercury (Hg) vapour and trace metals than that of conventional power plant. Within a 1,000-year timeframe, the percentage of trace metals released to the environment are less than 0.5% for most trace metals, except for As, Hg and Se. Trace metal emissions to soils occur mainly at surface impoundments, and trace metal emissions to soils from landfills are not significant.

Life-cycle environmental impacts are dominated by the emissions from power plants with CO_2 capture and coal production in all impact categories, except for HTP which is dominated by the MEA production. Other upstream processes, including coal transportation, limestone production, limestone transport, MEA production, MEA transport, ammonia production, ammonia transport, power plant infrastructure, CO_2 pipeline infrastructure, CO_2 capture facility infrastructure, and compressor infrastructure have minor life-cycle environmental impacts. The AP, EP, GWP, HTP, MAETP and POCP are caused primarily by air emissions. The FAETP and TETP are mainly due to trace metal emissions to air or soils.

The life-cycle impacts in all categories are sensitive to the changes in power plant gross efficiency, CO_2 capture rate, and CO_2 capture energy consumption, type of coal used and combustion boilers. In relation to the other air emissions removal rates, the results suggest a high SO_2 removal rate and a NH_3 to NOx ratio (which determines NOx removal ratio) within the range of 0.8 to 0.95. On the other hand, life-cycle impacts in most categories are not sensitive to the changes in pipeline length, depth of storage formation, and CO_2 pressure required for transportation. Compared to all the bituminous coals used in the post-combustion capture case, lignites and sub-bituminous coals have lower environmental impacts in the GWP, AP, and EP impact categories. The use of K_PZ or KS1 in chemical absorption CO_2 capture results in lower life-cycle environmental impacts than that for the use of MEA capture in all categories.

Direct emissions of CO, NH_3, NO, NO_2, N_2O and CO_2 from the post-combustion CO_2 capture plant are less uncertain than emissions of HF, HCl, SO_2, and SO_3. The uncertainty of emissions of trace metals to air is larger than that of other air emissions such as CO and SO_2. Trace metal emissions to soils is less uncertain than trace metal emissions to air and the histograms of these emissions are less skewed than that of trace metal emissions to air. The uncertainties of ADP, AP, EP, GWP or POCP are less than that of MAETP, TETP, FAETP, and HTP.

12.2.2 Oxy-fuel Combustion Carbon Dioxide Capture, Transport and Injection

At plant emissions level, there are no air emissions of SO_2, SO_3, HCl, HF and Hg vapour from the power plant stack, because a well designed CO_2 conditioning unit can remove these emissions completely. Within a 1,000-year timeframe, the percentage of trace metals released to the environment are less than 0.5% for most trace metals, except for As, Hg and Se. Emissions of trace metals to soils are mainly from surface impoundments, and trace metal emissions to soils from landfill are not significant.

Life-cycle environmental impacts are dominated by the emissions from the oxy-fuel combustion CO_2 capture plant and coal production in all impact categories, except for the ODP which is dominated by coal production, coal transportation and power plant infrastructure. Other upstream processes, such as limestone production, limestone transport, CO_2 pipeline infrastructure, ASU facility infrastructure and the compressor infrastructure have minor life-cycle environmental impacts. The AP, EP, GWP, HTP,

MAETP and POCP are primarily due to air emissions. The FAETP and TETP mainly come from trace metal emissions to air or soils.

The life-cycle impacts in all categories are sensitive to the changes in the power plant gross efficiency, ASU energy consumption, CO_2 conditioning unit energy consumption and type of coal. From life-cycle point of view, the purity of O_2 product from the ASU at 98% is the optimum value. If the HF removed by the CO_2 conditioning unit is treated before it is released to freshwater, the increased removal rate of HF in the CO_2 conditioning unit reduces MAETP and HTP significantly. The results suggest high SOx and NOx removal rates in the CO_2 conditioning unit. Direct emissions of CO, NH_3, NO, NO_2, N_2O and CO_2 are less uncertain than emissions of HF, HCl, SO_2, and SO_3. The uncertainty of emissions of trace metals to air is larger than that of other air emissions. Trace metal emissions to industrial soil are less uncertain than trace metal emissions to air and the histograms of these emissions are less skewed. The uncertainties of ADP, AP, EP, GWP or POCP are lower than that of MAETP, TETP, FAETP, and HTP.

12.2.3 Life Cycle Performance Comparison of Power Generation Options with and without Carbon Dioxide Capture

Research has shown that, when compared with the environmental performance of power generation without capture, the post-combustion and oxy-fuel combustion CO_2 capture plants can reduce life-cycle GWP of power generation by 78.8% and 80.0% respectively. However, the same processes increase the life-cycle ADP by 32.8% and 26.2% respectively.

At plant emissions level, power generation with post-combustion CO_2 capture, transport and injection has a higher ADP, AP, and EP and lower GWP, POCP, HTP, MAETP, FAETP and TETP than power generation with oxy-fuel combustion with CO_2 capture, transport and injection. At life-cycle level, power generation with post-combustion CO_2 capture, transport and injection has a higher GWP, ADP, AP, EP, ODP, and HTP and lower POCP, MAETP, FAETP and TETP than power generation with oxy-fuel combustion with CO_2 capture, transport and injection.

12.2.4 Life Cycle Impact Assessment of Saline Aquifer Storage

The research results have demonstrated that the ratio of potential CO_2 leakage to total CO_2 injected is sensitive to the changes in the injection period, injection rate, and

capillary entry pressure of the caprock. Because capillary entry pressure determines the thickness of the CO_2 layer beneath the caprock, and large injection rates or long injection durations result in a thicker CO_2 layer beneath the caprock, consequently the CO_2 leakage potential increases. The ratio of CO_2 leakage to the total CO_2 volume injected is sensitive to the following parameters of potential leakage pathways; the radius of a permeable zone in the caprock, the aperture of conducting faults intersecting the caprock, and the radius of a gas channel (or the width of a fracture, the ratio of internal to external radius of a micro-annulus) that may exist in an abandoned wellbore intersecting the caprock. Small changes in these parameters could cause a significant increase in CO_2 leakage.

12.3 General Discussion

Sensitivity of the LCIA results to the choice of system boundaries

In this research the system boundaries of power generation with CCS are set such that power generation, CO_2 capture, conditioning, transport and storage, and the upstream processes (e.g. coal mining, MEA production, consumable production and transportation, and power plant construction) are all part of the system modelled. The LCA results show that the life-cycle impacts of coal mining processes are significant for post-combustion and oxyfuel combustion cases and that MEA production processes influence the HTP results in the case of post-combustion with chemical absorption CO_2 capture. This implies that the inclusion or exclusion of upstream processes such as limestone production, consumable transportation or power plant construction does not have a significant impact on the LCA results. It is believed that the inclusion of the plant decommissioning processes, which were not investigated in this research, would also have a minor influence on the LCA results, as the decommissioning process is related to the ratio of the construction material recycled and the energy consumption of decommissioning is about one tenth of construction processes (Spath and Mann, 2004). The LCA results further confirm the necessity of modelling power generation with CCS at a high level of detail. The results also suggest that future efforts aiming to improve the LCI data quality for coal mining and MEA production is a worthy endeavour.

Temporal profile of environmental emissions

The results of this research demonstrate that nearly all environmental emissions (to atmosphere, to soil, or to water) occur during the operational life (e.g. 50 years) of the power plant and the operation of upstream processes. The only exceptions are CO_2 leakage from the saline aquifer storage formation and trace metal emissions from solid waste landfills which, can potentially be released to the environment after the power plant is decommissioned. If CO_2 leakage from the saline aquifer CO_2 storage formation occurs, it declines exponentially and continues at a greatly reduced rate over thousands of years. In order to convince stakeholders that the CO_2 storage curbs CO_2 emissions effectively, it is required to set the LCA temporal boundary of power generation with CCS to cover the life span of CO_2 storage and to estimate the accumulated CO_2 leakage. However, CO_2 leakage estimates are uncertain, due to the nature of the CO_2 storage processes and CO_2 leakage mechanisms, which cover thousands of years and involve unpredictable events. It is a great challenge to develop models simulating CO_2 storage and leakage over thousands of years, as the state-of-art prediction approaches for oil and natural gas or coalbed methane industries normally consider a much shorter period of few decades. Modelling CO_2 storage processes and CO_2 leakage using basic physical principles and by combining these with sensitivity analysis is a practical way to estimate the CO_2 leakage in the context of LCA, as demonstrated in this research.

Trace metal emissions to soils from solid disposal units also decline exponentially over thousands of years. However, trace metal emissions to soils from properly managed solid disposal units over thousands of years have a minor contribution to the overall LCA results as concluded in Chapters 9 and 10. This implies that for conventional power generation systems without CCS, it is acceptable to set the temporal boundary at the power plant operational life and ignore the solid waste disposal related emissions in the long term without much detriment to the quality of the LCA results.

Temporal profile of Global Warming Potential

The Global Warming Potential (GWP) of Greenhouse Gases (e.g. CO_2, CH_4 etc.) depends on the time span over which the potential is calculated. A gas which is quickly removed from the atmosphere may initially have a large effect but for longer time periods it becomes less important. For instance, over 100 years methane has a GWP_{100} of 25 (CO_2-equivalent) but over 20 years it has a GWP_{20} of 72 (IPCC, 2001). Most

Greenhouse gases have life times less than 1,000 years as listed in Table 12.1. The GWP with a time horizon of 100 years (or GWP_{100}) for various GHGs is used in this research, since this is the time horizon used by many regulators. The IPCC Fourth Assessment Report (2007) suggests that the GWP_{100} and GWP_{500} of CO_2 are the same, with value of 1. This implies that all the CO_2 released from fossil fuel combustion processes will remain in the atmosphere for more than 500 years. However, "About 50% of the CO_2 increase will be removed from the atmosphere within 30 years, and a further 30% will be removed within a few centuries. The remaining 20% may stay in the atmosphere for many thousands of years" (Denman et al., 2007). Therefore, when the GWP_{100} (or GWP_{500}) of CO_2 with value of 1 is used, the GWP of CO_2 over 100 years (or 500 years) is overestimated.

Table 12.1: GWP values and lifetimes (IPCC, 2007b)

Greenhouse gases	Lifetime (years)	GWP (CO_2-equivelence)		
		20 years	100 years	500 years
CO_2	thousands of years	1	1	1
Methane	12	72	25	7.6
Nitrous oxide	114	289	298	153
HFC-23 (hydrofluorocarbon)	270	12,000	14,800	12,200
HFC-134a (hydrofluorocarbon)	14	3830	1430	435
Sulphur hexafluoride	3200	16,300	22,800	32,600

Trade-off of environmental impacts

For both post-combustion CCS and oxyfuel combustion CCS, the reduction of CO_2 emissions results in an increased abiotic resource depletion (dominantly fossil fuels) from a life-cycle perspective, as shown in Table 12.2. It is impossible to capture and store CO_2 without a significant energy penalty considering the current CCS technologies and expected developments in the future. The question arising is whether it is worth capturing CO_2 from power generation and storing it in geological formations in the expense of abiotic resources. The answer dependents upon the comparative valuation of the impacts of climate change against the impact of abiotic resource depletion. The IPCC Fourth Assessment Report (2007) concludes that the adverse impacts of climate change on natural and human systems (such as altered frequencies and intensities of extreme weather, sea level rise, etc.,) will be severe, irreversible and uncertain with a multi-century time scale and most of the observed increase in global average temperatures since the mid-20th century is very likely due to the observed

increase in anthropogenic GHG concentrations. On the other hand, CO_2 capture and storage requires significant use of fossil fuels while the world heavily relies on these for energy production. However, there is abundant knowledge, advanced technologies available and novel technologies under development for solving the fossil fuel shortage problems since the 1970s' energy crisis. In the long-run (for hundreds of years), there are more opportunities and larger probabilities to solve the fossil fuel shortage problem using new energy sources and novel technologies. In this context, it is reasonable to take action now to stabilise the climate systems by reducing CO_2 emissions in order to avoid uncertain, irreversible and severe climate change consequences by using more fossil fuels, which are expected to be somehow less important in the future.

Post-combustion CCS or oxyfuel combustion CCS increases some categories of life cycle impacts, such as AP, EP, etc (Table 12.2). However, in a worldwide view or regional view the emissions contributing to these categories are mainly from other industries (upstream processes) rather than power generation plants. This implies that the increase of other categories of environmental impacts caused by CCS can be offset by reducing emissions from other industries, where advanced pollution control technologies can be readily applied at lower costs. Therefore, the increase of other categories of environmental impacts is not a problem of concern as serious as climate change.

12.4 Recommendations for Future Work

This research developed LCI models based on fundamental physical (or chemical) principles or empirical relationships which, to a greater extent overcome the limitations of conventional LCI models and reduce model uncertainty. However, there is still room for further improvements towards improving the reliability of LCI models for some novel or complex processes. Further research is required towards improving our understanding of the following processes:

- Oxy-fuel combustion processes: unlike the coal air combustion processes, there are no empirical relationships or emission factors to calculate the emissions from the coal oxy-fuel combustion process. The oxy-fuel combustion LCI model presented in this research developed modified (from air combustion) emission factors based on results in the literature to estimate the emissions from the coal

Table 12.2: Analysis of life cycle impacts of power generation with CCS

Impact category	Life cycle impact increase (↑), decrease (↓) as compared to power plant without CCS		Scale	Main emissions contributing to the difference in impact category score (world 1995)
	Post-combustion with CCS	Oxy-fuel combustion with CCS		
GWP [kg CO_2-Equiv.]	↓	↓	Global	CO_2 (64.9%) CH_4 (16.7%) N_2O (8.2%) CFCs (7.9%) HCFCs (1.1%) HFCs (0.3%) PFCs (0.2%) SF_6 (0.3%)
ADP [kg Sb-Equiv.]	↑	↑	Global Regional Local	Natural gas (27.3%) Crude oil (42.5%) Coal (29.9%) Minerals (0.3%)
AP [kg SO_2-Equiv.]	↑	↓	Regional Local	SO_2 (53%) NH_3 (29.7%) NO_2 (17.3%)
EP [kg Phosphate-Equiv.]	↑	↓	Local	NO_2 (12.4%) NH_3 (14.3%) N to water (14.8%) P to water (15.8%) N to soil (37.2%) P to soil (5.4%)
ODP [kg R11-Equiv.]	↑	↑	Global	CFCs (66.9%) Halons (20.4%) HCFCs (2.3%) Methylbromide (4.6%) Methylchloride (0.1%) Methylchloroform (5%) Tetrachloromethane (0.7%)
POCP [kg Ethene-Equiv.]	↓	↑	Regional Local	CO (24.2%) SO_2 (7.1%) Alkanes (25.4%) Aromatics (14.9%) Alkenes (18.2%) Alcohols (4.2%) Ketones (0.8%) Aldehydes (2.9%) Esters (0.6%)
HTP [kg DCB-Equiv.]	↑	↑	Local	Non-halogenated hydrocarbons (93.9%) Halogenated hydrocarbons (0.3%) Pesticides (0.2%) Inorganics (5.5%)
MAETP [kg DCB-Equiv.]	↓	↓	Local	Inorganics (89.8%) Non-halogenated hydrocarbons (8.5%) Halogenated hydrocarbons (0.4%) Pesticides (1.3%)
FAETP [kg DCB-Equiv.]	↑	↑	Local	Non-halogenated Hydrocarbons (15.9%) Pesticide (70.6%) Inorganics (13.5%)
TETP [kg DCB-Equiv.]	↓	↓	Local	Pesticides (93%) Inorganics (4.7%) Non-halogenated hydrocarbons (2.3%)

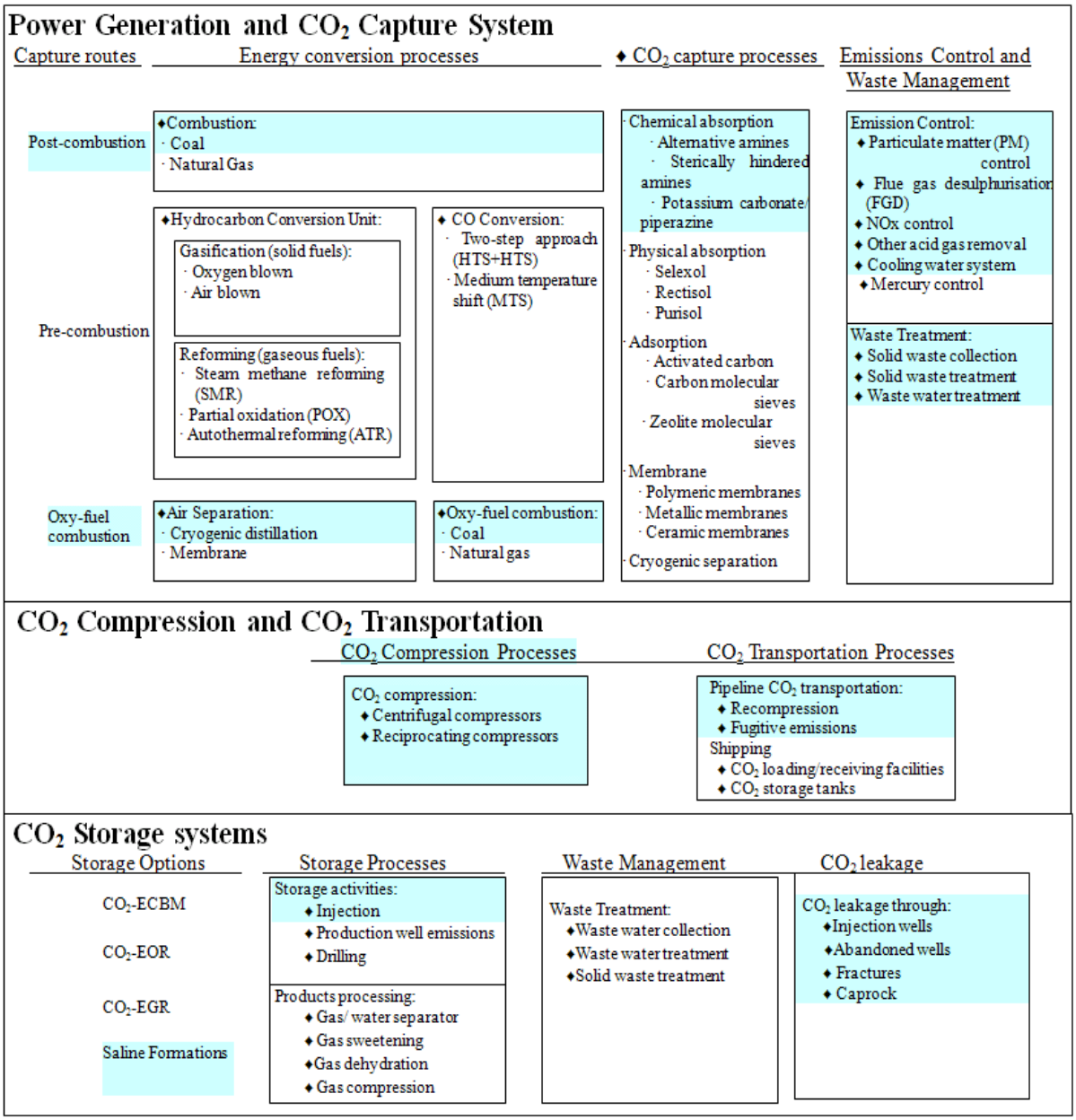

"·" denotes options; "♦" denotes processes.

Figure 12.1: Illustration of the processes considered for future work (models completed highlighted in blue).

oxy-fuel combustion process, and the uncertainties associated with these emissions were considered and quantified to further justify the results. However, there is a need to develop empirical relationships or emission factors for oxy-fuel combustion accounting for geographical and technological differences.

♦ Carbon dioxide storage: Analytical LCI models based on most recent literature are used in this research to model the CO_2 mitigation processes in saline aquifers and potential CO_2 leakages through alternative pathways and the overburden. Large number of studies has investigated the CO_2 storage processes and CO_2 leakage

mechanisms, however, these processes/mechanisms are still not fully understood. It is desirable to improve further the CO_2 storage LCI model once the CO_2 storage processes and CO_2 leakage mechanisms are better understood in future. In the context of LCA, the models developed give reasonable estimates of CO_2 leakage and the prediction of CO_2 migration in a saline reservoir, however, numerical simulations are recommended if more accurate CO_2 migration prediction and CO_2 leakage estimation is required. Moreover, environmental impacts of CO_2 storage processes and CO_2 leakage needs to be understood For example, the environmental impacts of impurities (such as SOx, NOx, H_2S and trace elements) on the CO_2 geological storage formations is not well understood. Potential environmental impacts of CO_2 leakage such as groundwater contamination, metal mobilisation, and soil gas replacement need to be investigated.

Due to the limitations of the Gabi software, the maximum number of sampling for the Monte Carlo simulation has been restricted to 5,000. It is acknowledged that, because the LCI models developed for the life-cycle impact assessment of power generation with CCS involve more than one hundred parameters, the 5,000 runs performed are not enough to investigate fully the sensitivity of the LCIA model results for each individual parameter. On the other hand, the LCI model parameters are not uncorrelated and therefore efficient methods to test the model sensitivity can be designed and implemented in the future using the models developed in this research.

Research presented in this thesis developed LCI modes for power generation with alternative chemical absorption post-combustion CO_2 capture system, power generation with oxy-fuel combustion CO_2 capture system, and CO_2 saline aquifer storage, as highlighted in blue in Figure 12.1. Future research should consider developing LCI models for the rest of the CO_2 capture or CO_2 storage alternatives shown in the same Figure.

References

Abdi, M. A., 2007, Design of Natural Gas Handling Equipment, lecture note, Memorial University of Newfoundland. Available at: http://www.engr.mun.ca/~abdi/DNGE8976/Chapter%204_Dehydration.pdf. Assessed at January 2008.

Advanced Geotech Systems (AGS), 2001, Leakage Rate through Composite Liner - Design Calculator. Available at: http://www.adgeosys.com/cgi-bin/geomembrane_leakage.pl. Accessed at 2 July 2007.

Akai M., Nomura N., Waku H. and Inoue M., 1997, Life-cycle analysis of a fossil-fuel power plant with CO_2 recovery and a sequestering system, Energy, Vol 22, pp. 249-255.

Akervoll, I., Zweigel, P. and Lindeberg, E., 2006, CO_2 storage in open, lipping aquifers. 8th International Conference on Greenhouse Gas Control Technologies GHGT-8, 19-22 June 2006, Trondheim, Norway.

Alawode, A., 2005, Oxidative Degradation of Piperazine, M.S. Thesis, Department of Chemical Engineering, The University of Texas at Austin, Texas, UAS. Available at: http://www.che.utexas.edu/rochelle_group/Pubs/Alawode_Thesis_2005.pdf. Assessed 9 March 2006.

ALSTOM Power Inc., 2003a Volume 1: Evaluation of Advanced Coal Combustion & Gasification Power Plants with Greenhouse Gas Emission Control and Volume 2: Bench-scale Fluidized Bed Combustion Testing. Final Report prepared by Alstom Power, Inc. to Department of Energy National Energy Technology Center. Pittsburgh, PA. PPL- 03-CT-09. May, 2003.

ALSTOM Power Inc., 2003b, Greenhouse emissions control by oxygen firing in circulating fluidised bed boilers: Phase 1- A preliminary systems evaluation final report, PPL REPORT NO. PPL-03-CT-09, page 81

Alstom, 2003b, Volume 1: Evaluation of Advanced Coal Combustion & Gasification Power Plants with Greenhouse Gas Emission Control and Volume 2: Bench-scale Fluidized Bed Combustion Testing. Final Report prepared by Alstom Power, Inc. to Department of Energy National Energy Technology Center. Pittsburgh, PA. PPL- 03-CT-09. May, 2003.

Altevogt, A. and M.A. Celia, "Modeling Carbon Dioxide Transport in Unsaturated Soils", Water Resources Research, Vol. 40, W03509, doi:10.1029/2003WR002848, 2004.

Althaus, H.-J., Chudacoff, M., Hellweg, S., Hischier, R., Jungbluth, N., Osses, M., Primas, A., 2004. Life Cycle Inventories of Chemicals Ecoinvent Report No. 8. Swiss Centre for Life Cycle Inventories, Dübendorf.

Amalendu Bagchi, 2004, Design of landfills and integrated solid waste management, Third Version, Jhon Wiley & Son, Inc, Hoboken, New Jersey.

American Center for Life Cycle Assessment (ACLCA), 2004, Increasing knowledge and promoting the use of life cycle assessment in the United States. Available at:http://www.lcacenter.org/pdf/ACLCAplan.pdf. Assessed at 21 March 2007.

Amrhein, G.T., Holmes, M. J., Bailey, R.T., Kudlac, G.A., Downs W., Madden, D.A., 1999, Advanced Emissions Control Development Program Phase III — Approved Final Report, USDOE report, FETC Contract: DE-FC22-94PC94251-22.

Andersson, K. and Johnsson, F., 2006, Process evaluation of an 865 MWe lignite fired O_2/CO_2 power plant, Energy Conversion and Management Volume 47, Issue 20, Pages 3507-3680.

Andrew W. Woods, A. W., and Phillips, J.C., 1999, Turbulent bubble plumes and CO_2 driven lake eruptions, Journal of Volcanology and Geothermal Research 92 (1999) 259–270.

Anheden M., Yan J., and Smedt G., “Denitrogenation (or Oxyfuel Concepts)”, Oil &. Gas Science and Technology – Rev. IFP, Vol. 60, No. 3, pp 485 – 495, 2005.

Anheden, M., Stina Rydberg, S., and Yan, J., 2008, Consideration for Removal of non-CO_2 components from CO_2 Rich Flue Gas of Oxy- Fuel Combustion, IEA Oxyfuel Workshop, Yokohama March 4, 2008.

Apps J.A., 2006, A Review of Hazardous Chemical Species Associated with CO_2 Capture from Coal-Fired Power Plants and their Potential Fate during CO_2 Geologic Storage, Research report, Ernest Orlando Lawrence Berkeley National Laboratory.

Aspelund, A., Mølnvik, M. J and Koeijer, G., 2006, Ship transport of CO_2—technical solutions and analysis of costs, energy utilization, exergy efficiency and CO_2 emissions, Chem. Eng. Res. Des. (Official journal of the European Federation of Chemical Engineering: Part A) 84-A9, pp. 847–855.

Aspelunda, A. and Jordal, K., 2007, Gas conditioning—The interface between CO_2 capture and transport, International Journal of Greenhouse Gas Control Volume 1, Issue 3, July 2007, Pages 343-354.

Aycaguer, A.C., Lev-On, M., and Winer, A.M., 2001, Reducing carbon dioxide emissions with enhanced oil recovery projects: A life cycle assessment approach, Energy Fuels 15 (2001), pp. 303–308.

Barlet-Gouédard, V., Rimmelé, G., Goffé, B. and Porcherie, O., 2006, Mitigation strategies for the risk of CO_2 migration through wellbores, IADC/SPE 98924, Miami, USA, February.

Bech, N. and Larsen, M., 2005, Storage of CO_2 in the Havnsø aquifer – a simulation study, Danmarks og Grønlands Geologiske Undersøgelse Rapport 2005/9.

Benson S.M, 2005, Overview of Geologic Storage of CO_2 , in Carbon Dioxide Capture for Storage in Deep Geologic Formations –Results from the CO_2 Capture Project Geologic Storage of Carbon Dioxide with Monitoring and Verification, Edited by Sally M. Benson, Curt Oldenburg , Mike Hoversten and Scott Imbus, Volume 2, 2005, ELSEVIER, London

Benson S.M., John Apps, Robert Hepple, Marcelo Lippman and Chin Fu Tsang, 2002, Health, Safety and Environmental Risk Assessment for Geologic Storage of Carbon Dioxide: Lessons Learned from Industrial and Natural Analogues, Lawrence Berkeley National Labs, 2002 Available at http://www.co2captureproject.org/reports/reports.htm

Bentham, M., and Kirby, G., 2005, CO_2 Storage in Saline Aquifers, Oil & Gas Science and Technology – Rev. IFP, Vol. 60 (2005), No. 3, pp. 559-567

Berkenpas, M.B., Frey, H.C., Fry, J.J., Kalagnanam, J. And Rubin, E.S., 1999, Integrated Environmental Control Model: Technical Documentation. Prepared for the Federal Energy Technology Center, U.S. Department of Energy, by Center for Energy and Environmental Studies, Carnegie Mellon University, Pittsburgh, PA. May 1999. Available: http://www.iecm-online.com/documentation/tech_99.pdf, Accessed October, 2005

Blachman, M. and McHugh, T., 2000, Sour Gas Dehydration Technology and Alternatives, Porocel Corporation research report. Available at: www.porocel.com/products/ Papers/Lrgc%20Sour%20Gas.pdf. Assessed at December 2007.Black and Veatch, 1996, Power plant engineering, Chapman & Hall, New York.

Bock, B.R., Rhudy, R., Herzog, H., Klett, M., Davison, J., de la Torre Ugarte, D.G. and Simbeck,D., 2003, Economic Evaluation of CO_2 Storage and Sink Enhancement Options. TVA Public Power Institute, February 2003

Bolland, O. and Mathieu, P., 1998, Comparison of Two CO_2 Removal Options in Combined Cycle Power Plants, Energy Conversion and Management, 39 (16-18), p.1653-1663, presented at the FLOWERS'97 conference July 30-August 1, 1997

Booras G.S. and Smelser S.C., 1991, An engineering and economic evaluation of CO_2 removal from fossil-fuel-fired power plants, Energy, Vol 16, PP. 1295-1305.

Boustead, I. (1996) LCA - How it came about: The beginning in the U.K. International Journal of Life Cycle Assessment 1 (3) 147-150

Bozzano, G. and Dente, M., 2001, Shape and terminal velocity of single bubble motion: a novel approach, Computers & Chemical Engineering. 25 (2001) 571-576.

Bradley A. and Constance S., 2006, Curbing the blue plume: SO_3 formation and mitigation, Power; May2006, Vol. 150 Issue 4, p39-41

Bradshaw, J. and Dance T., 2004, Mapping geological storage prospectivity of CO_2 for the world's sedimentary basins and regional source to sink matching. Proceedings of the 7th International Conference on Greenhouse Gas Technologies, Vol. 1; peer reviewed Papers and Plenary Presentations. pp. 583-592. Eds. E .S. Rubin, D.W. Keith and C.F. Gilboy, Pergamon, 2005

Brewer, P. G., Peltzer, E. T., Friederich, G., and Rehder, G., 2002, Experimental determination of the fate of rising CO_2 droplets in seawater. Environ. Science Technology, 36, 5441–5446

Brown A. Evaluation of possible gas microseepage mechanisms. Amer Assoc Petrol Geol Bull 2000;84:1775–89.

Bryant, S. and Lake L., 2005, Effect of impurities on subsurface CO_2 storage processes, Carbon Dioxide Capture for Storage in Deep Geologic Formations - Results from the CO_2 Capture Project, v. 2: Geologic Storage of Carbon Dioxide with Monitoring and Verification, Benson S.M. (ed.), Elsevier, London. pp. 983–998.

Buhre, B.J.P., Hinkley, J.T., Gupta, R.P., Nelson P.F., Wall, T.F., 2006, Fine ash formation during combustion of pulverised coal–coal property impacts, Fuel 85 (2006) 185–193

Buonicore A.J., and Davis W. T., (Editors), 1992, Air pollution engineering manual, Van Nostrand Reinhold, New York, NY

Cao, Y., Duan, Y., Kellie, S., Li, L., Weibing Xu, W., Riley, J.T and Pan, W., 2005, Impact of Coal Chlorine on Mercury Speciation and Emission from a 100-MW Utility Boiler with Cold-Side Electrostatic Precipitators and Low-NOx Burners, Energy Fuels, 19 (3), 842 -854, 2005

Carcoana, A., 1992, Applied Enhanced Oil Recovery, Prentice Hall, New Jersey, the U.S.

Carey, J. W., et al., 2007, Analysis and performance of oil well cement with 30 years of CO_2 exposure from the SACROC Unit, West Texas, USA, international journal o f greenhouse gas control 1 (2007) 7 5 – 85

Carlson R. and Palsson A-C., 2001, Industrial environmental information management for technical systems, Journal of Cleaner Production, vol 9, pp. 429-435.

Celia, M. A., 2006, Implications of Abandoned Wells for Site Selection, Princeton University, http://www.gwpc.org/e-library/e-library_documents/eibrary_documents_co2/LBNL%20 CO2% 20Abandoned%20Wells.pdf. Assessed, December 2007.

Chapel D.G., Mariz C.L. and Ernest J., 1999, Recovery of CO_2 from Flue Gases: Commercial Trends, Proceedings of the Canadian Society of Chemical Engineers Annual Meeting, October 4-6, 1999, Saskatoon, Saskatchewan, Canada.

Chu, P., 2006, Flue Gas Desulfurization (FGD) Wastewater Characterisation - Screening Study (1010162), Electric Power Research Institute (EPRI) Project Technical Update Report.

Coal in sustainable society (CISS), 2003, Case study B17: electricity from CO_2 recovery type IGCC. Available at: www.ciss.com.au. Assessed 6 December 2004.

Constance S., 2007, Review of the Role of Aqueous Chemistry in Mercury Removal by Acid Gas Scrubbers on Incinerator Systems, Environmental engineering science, Volume 24, Number 8

Contadini J.F., Moore R.M., Mokhtarian P.L., 2002, Life Cycle Assessment of Fuel Cell Vehicles: A Methodology Example of Input Data Treatment for Future Technologies. Int J LCA 7 (2) 6– 132, pp 73–84

Cooperative Research Centre for Greenhouse Gas Technologies. 2005. Cooperative Research Centre for Greenhouse Gas Technologies Annual Report (CO2CRC) 2004-2005. CO2CRC, Canberra, Australia.

Corti A. and Lombardi L., 2004, Biomass integrated gasification combines cycle with reduced CO_2 emissions: Performance analysis and life cycle assessment (LCA), Energy, vol 29, pp. 2109-2124.

Croiset E., and Thambimuthu, K. V., 2001, NOx and SOx emission from O_2/CO_2 recycle coal combustion, Fuel 80 (2001), pp. 2117–2121

Curran, M. Mann, M., & Norris, G. 2005, "The international workshop on electricity data for life cycle inventories", Journal of Cleaner Production, vol. 13, no. 8, pp. 853-862.

Denman, K.L., G. Brasseur, A. Chidthaisong, P. Ciais, P.M. Cox, R.E. Dickinson, D. Hauglustaine, C. Heinze, E. Holland, D. Jacob, U.Lohmann, S Ramachandran, P.L. da Silva Dias, S.C. Wofsy and X. Zhang, 2007: Couplings Between Changes in the Climate System and Biogeochemistry. In: Climate Change 2007: The Physical Science Basis. Contribution of Working Group I to the Fourth AssessmentReport of the Intergovernmental Panel on Climate Change [Solomon, S., D. Qin, M. Manning, Z. Chen, M. Marquis, K.B. Averyt, M.Tignor and H.L. Miller (eds.)]. Cambridge University Press, Cambridge, United Kingdom and New York, NY, USA.

Department of Trade and Industry (DTI), 2002, Flue gas desulphurisation (FGD) technologies, Technology status report 12, DTI/Pub URN 00/652

Department of Trade and Industry (DTI), 2004, Monitoring and Control of Trace Elements, Technology status report, Cleaner fossil fuels programme, TSR020.

Doctor R.D., Molburg J. C., Brockmeier N. F., Lynn M., Victor G., Massood R. and Gary J. S., 2001, Life-Cycle Analysis of a Shell Gasification-Based Multi-Product System with CO_2 Recovery, Proceedings of the First National Conference on Carbon Sequestration, Washington, D.C., USA, May 15-17, 2001.

Drbal, L., Westra, K., and Boston, P., 1996, Power plant engineering, Chapman & Hall, London

DTI, 2004, Monitoring and Control of Trace Elements (DTI/Pub URN 04/590) available at: www.dti.gov.uk/cct. Assessed at September, 2007

Dugas, R., Rochelle G.T. and Seibert F., 2006, CO_2 Capture Performance of a Monoethanolamine Pilot Plant, Submitted to the 8th international conference on greenhouse gas technology, April 20, 2006. Available at: http://www.che.utexas.edu/rochellegroup/publications.htm. Accessed 10 March 2006.

Duguid, A., Radonjic, M., Scherer, G. W., 2006, The effect of carbonated brine on the interface between well cement and geologic formations under diffusion-controlled conditions, 8th International Conference on Greenhouse Gas Control Technologies, June 19-22, 2006 , Trondheim , Norway

Durucan S., Korre A. and Munoz-Melendez G., 2006, Mining life cycle modelling: a cradle-to-gate approach to environmental management in the minerals industry, Journal of Cleaner Production, vol 14, pp. 1057-1070.

Electric Power Research Institute (EPRI), 2007, Estimating Total Sulfuric Acid Emissions from Stationary Power Plants. EPRI, Palo Alto, CA: 2007. 1014773.

Ennis-King, J. and Paterson, L., 2002. Engineering aspects of geological sequestration of carbon dioxide. In: SPE Asia Pacific Oil and Gas Conference and Exhibition, October 8-10, Melbourne, Australia. SPE 77809

Erickson, C.A., and Jambhekar, R., 2002, Current Work on SO_3 Emissions from Selective Catalytic Reduction Systems, Babcock Borsig Power, Inc. in Proceedings of 2002 DOE Conference on Selective Catalytic and Non-Catalytic Reduction for NOx Control, Pittsburgh, PA, May, 2002

Esber, G.S., 2006, Carbon dioxide capture technology for the coal-powered electricity industry: a systematic prioritization of research needs, M.I.T. Masters Thesis. Available at: http://sequestration.mit.edu/pdf/Salem_Esber_Thesis.pdf. Accessed 2 August 2006.

European Commission (EC), 2008, European Platform on Life Cycle Assessment website. Available at: http://lca.jrc.ec.europa.eu/EPLCA/index.htm. Assessed at 18 December 2008.

Faist Emmenegger, M., Heck, T., Jungbluth, N., 2003. Erdgas - Sachbilanzen von Energiesystemen. Swiss Centre for Life Cycle Inventories, Paul Scherrer Institute. Dübendorf and Villigen, Switzerland.

Feron P.H.M., 2005, Progress in post-combustion CO_2 capture, in European CO_2 capture and storage conference towards zero emission power plants, Brussels 13-15 April 2005. Available at: www.eu.int/comm/research/energy/pdf/14_1000_feron_en.pdf. Accessed at 12 July 2006.

Feron, P.H.M., 1994, Membranes for carbon dioxide recovery from power plants. In Carbon Dioxide Chemistry: Environmental Issues. J. Paul, C.M. Pradier (eds.), The Royal Society of Chemistry, Cambridge, United Kingdom, 236-249.

Fiaschi, D., Lombardi, L. and Manfrida, G., 2000, Life cycle assessment (LCA) and exergetic life cycle assessment of an innovative energy cycle with zero CO_2 emissions, The 5th International Conference on Greenhouse Gas Control Technologies, Cairns, 2000.

Finnveden, G. and Moberg, A. (2005) Environmental systems analysis tools — an overview. Journal of Cleaner Production. 13, 1165—1173

Finnveden, G., Albertsson, A. C., Berendson, J., Eriksson, E., Hoglund, L. O., Karlsson, S., & Sundqvist, J. O. 1995, "Solid waste treatment within the framework of life-cycle assessment", Journal of Cleaner Production, vol. 3, no. 4, pp. 189-199.

Five Winds International, 2004, Gas to liquids LCA Synthesis Report. Available at:http://www.sasolchevron.com/pdf/publication/GTL_LCA_Synthesis_Report.pdf. Assessed at 16 March, 2007

Foerter, D. and Jozewicz, W., 2001, Cost of Selective Catalytic Reduction (SCR) Application for NOX Control on Coal-fired Boilers, U.S. Environmental Protection Agency, EPA/600/R-01/087

Forster, P., Ramaswamy V., Artaxo P., Berntsen T., Betts R., Fahey D.W., Haywood J., Lean J., Lowe D.C., Myhre G., Nganga J., Prinn R., Raga G., Schulz M. and Van

Dorland R., 2007: Changes in Atmospheric Constituents and in Radiative Forcing. In: Climate Change 2007: The Physical Science Basis. Contribution of Working Group I to the Fourth Assessment Report of the Intergovernmental Panel on Climate Change [Solomon, S., Qin D., Manning M., Chen Z., Marquis M., Averyt K.B., Tignor M.and Miller H.L. (eds.)]. Cambridge University Press, Cambridge, United Kingdom and New York, NY, USA.

Gabathuler, H., 1997, The CML story. How environmental sciences entered the debate on LCA. International Journal of Life Cycle Assessment 2 (4) 187-194

Gale, J., and J. Davison, 2002: Transmission of CO_2: Safety and Economic Considerations, Proceedings of the 6th International Conference on Greenhouse Gas Control Technologies, 1- October, 2002, Kyoto, Japan. pp. 517-522

Gallardo, M., Snyder, R.L., Schulbach, K., and Jackson, L.E. (1996). "Crop growth and water use model for lettuce." J. of Irrig. and Drain. Engng., ASCE, 122 (6), 354- 359.

Gemma Heddle, Howard Herzog and Michael Klett, 2003, The Economics of CO_2 Storage, Massachusetts Institute of Technology, Laboratory for Energy and the Environment, Research report, MIT LFEE 2003-003 RP

Giroud, J.P., and Morel, N., 1992, "Analysis of Geomembrane Wrinkles", Geotextiles and Geomembranes, Vol. 11, No. 3,1992, pp. 255-276.

Giroud, J.P., Badu-Tweneboah, K., and Soderman, K.L., 1994, "Evaluation of Landfill Liners", Proceedings of the 5th International Conference on Geotextiles, Geomembranes and Related Products, Singapore, Sep 1994, Vol. 3, pp.981-986.

Giroud, J.P., Bonaparte, R., Beech, J.F., and Gross, B.A., 1989, "Load-carrying Capacity of a Soil Layer Supported by a Geosynthetic Overlying a Void", Proceedings of the International Geotechnical Symposium on Theory and Practice of Earth Reinforcement, Yamanouchi, T., Miura, N., and Ochiai, H., Editors, Fukuoka- Kyushu, Japan, October 1988, pp. 185-190.

Goff, G., 2005, Oxidative Degradation of Aqueous Monoethanolamine in CO2 CaptureProcesses: Iron and Copper Catalysis, Inhibition, and O_2 Mass Transfer, Ph.D. Dissertation, Department of Chemical Engineering, The University of Texas at Austin, Texas, USA. Available at: http://www.che.utexas.edu/rochelle_group/ Pubs/Goff%20Dissertation.pdf. Accessed at 5 April 2006.

Gottlicher, G., 2004: The Energetics of Carbon Dioxide Capture in Power Plants. National Energy Technology Laboratory, U.S. Dept. of Energy (English translation of Energetik der Kohlendioxidruckhaltung in Kraftwerken, Fortschritt-berichte VDI, Reihe 6, Nr. 421).

Guine´e J.B., Gorre´e, M., Heijungs, R., Huppes, G., Kleijn, R. and Koning A., 2001, Life cycle assessment: An operational guide to the ISO standards, Final report, Centre of Environmental Science – Leiden University (CML), May 2001.

Gunter, W.D., Bachu S. and Benson S.M., 2004, The role of hydrogeological and geochemical trapping in sedimentary basins for secure geological storage for carbon dioxide. In: Geological Storage of Carbon Dioxide: Technology. Baines , S. and Worden, R.H. (eds.), Special Publication of Geological Society, London, UK. Special Publication 233, pp. 129–145.

Guo, B., and Ghalambor, A., 2005, Natural Gas Engineering Handbook, Gulf Publishing Company, Page 166.

Hamelinck C.N., Faaij A.P.C., Ruijg G.J., Jansen D., Pagnier H., Van Bergen F., Wolf K.-H., Barzandji O., Bruining H. and Schreurs H., 2001, Potential for CO_2 sequestration and enhanced coalbed production in the Netherlands, Novem, Utrecht, the Netherlands, p. 51

Hassanzadeh, H., Pooladi-Darvish, M. and Keith, D. W., 2007, Scaling Behavior of Convective Mixing, withApplication to Geological Storage of CO_2, American Institute of Chemical Engineers, Vol. 53, No. 5

Heddle, G., Herzog, H. and Klett, M., 2003. The economics of CO_2 storage. Laboratory for Energy and the Environment, No. LFEE 2003-003 RP. Cambridge, MA.

Heggum, G., Weydahl, T., Mo, R., Mølnvik, M. and Austegaard, A., 2005, CO2 conditioning and transport, in Carbon Dioxide Capture for Storage in Deep Geologic Formations - Results from the CO2 Capture Project Edited by David Thomas and Sally Benson, Elsevier Science, January 2005, pp925

Heller, J.P. and J.J. Taber, 1986, Influence of Reservoir Depth on Enhanced Oil Recovery by CO2 Flooding, in Permian Basin Oil & Gas Recovery Conference of the Society of Petroleum Engineers. Society of Petroleum Engineers: Midland. TX

Hellweg S. 2000, “Time- and Site-dependent life-cycle assessment of thermal waste treatment processes”, PhD Thesis, Swiss Federal Institute of Technology.

Hellweg, S., Hofstetter, T. B., & Hungerbuhler, K, 2005, Time-dependent life-cycle assessment of slag landfills with the help of scenario analysis: the example of Cd and Cu, Journal of Cleaner Production, vol. 13, no. 3, pp. 301-320.

Hellweg, S., Hofstetter, T. B., & Hungerbuhler, K., 2005, Time-dependent life-cycle assessment of slag landfills with the help of scenario analysis: the example of Cd and Cu, Journal of Cleaner Production, vol. 13, no. 3, pp. 301-320.

Hepple, R.P. and Benson, S.M., 2004, Implications of Surface Seepage on the Effectiveness of Geologic Storage of Carbon Dioxide as a Climate Change Mitigation Strategy: Performance Requirements and the Implications of Surface Seepage, Environmental Geology paper DOI 10.1007/s00254-004-1181-2. September 13, 2004.

Herzog, H., Golomb, D., Zemba, S., 1991, Feasibility, modeling and economics of sequestering power plant CO2 emissions in the deep ocean, Environmental Progress, 10(1), 64-74.

Herzog, H., Heddle, G. and Klett, M., 2003, The Economics of CO_2 Storage, MIT Laboratory for Energy and the Environment, LFEE 2003-003 RP.

Hesse, M. A., Riaz, A., and Tchelepi, H. A., 2006b, Resolving Density Fingering During CO_2 Sequestration: A Challenge for Reservoir Simulation, Proceedings, CO2SC Symposium, Lawrence Berkeley National Lab., March, 2006.

Hesse, M., Riaz, A., and Tchelepi, H., 2006a, 4.1 Time/Length Scales during Convective Mixing of Dissolved CO2, in Rapid prediction of CO_2 movement in aquifers, coal beds, and oil and gas reservoirs: Stanford University Global Climate and Energy Project (GCEP) Technical Report 2006, Kovscek, A. R. and Orr Jr, F. M.. Available at: http://gcep.stanford.edu/research/technical_report/2006.html. Accessed18 December 2007.

Hovorka, S.D. 2007, Introduction to Geologic Sequestration of CO_2, Gulf Coast Carbon Center, Bureau of Economic Geology Jackson School of Geosciences, The University of Texas at Austin, Available at: http://www.beg.utexas.edu/environqlty/ co2seq/publications.htm, Assessed at December 2007.

Hovorka, S.D., Holtz, M. H., Sakurai, S., and Knox, P. R., 2003, Report to the Texas Commission on Environmental Quality to Accompany a Class V Application for an Experimental Technology Pilot Injection Well -- Frio Pilot in CO2 Sequestration in Brine-Bearing Sandstones, Bureau of Economic Geology, USA

Huerta, N. J., Bryant, L. S., Minkoff, S.E., Oldenburg, M. C., 2007, Well leakage pathways and their importance to CO_2 /cement reactions: Analysis of long-term cement competence as part of a certification framework for CO_2 sequestration projects, May 7-10, 2007, Pittsburgh, Pennsylvania

Hunt, R.; Franklin, G.; William E. (1996) LCA - how it came about: Personal Reflections on the Origin and the Development of LCA in the USA. International Journal of Life Cycle Assessment 1(1) 4-7

Huppes, G., 2007, CALCAS: Analytic framework, CALCAS at LCM2007, Zurich, http://www.calcasproject.net, Assessed 20 December 2008

Ide S.T., Jessen K., Orr Jr F.M., 2007, Storage of CO_2 in saline aquifers: Effects of gravity, viscous, and capillary forces on amount and timing of trapping. International Journal of Greenhouse Gas Control 1: 481-491

Ide, S., Jessen K. and Orr Jr. F.M., 2006, Capillary Trapping of CO_2 in an Aquifer, In Rapid Prediction of CO2 Movement in Aquifers, Coal Beds, and Oil and Gas Reservoirs, Final report 2006, GCEP Technical Report 2006, Kovscek, A. R. et al.,

(ed.).Available at: http://gcep.stanford.edu/pdfs/ QeJ5maLQQrugiSYMF3ATDA/ 3.3.1.kovscek_06.pdf. Assessed at 10th March 2008.

Ide, S., Jessen, K. and Orr, F.M., 2006, 4.2 Capillary Trapping of CO_2 in an Aquifer, in Rapid prediction of CO2 movement in aquifers, coal beds, and oil and gas reservoirs: Stanford University Global Climate and Energy Project (GCEP) Technical Report 2006, Kovscek, A. R. and Orr Jr, F. M.. Available at:http://gcep.stanford.edu/research/ technical_report/2006.html. Accessed 12 January 2008.

Imai N., 2003, Advanced solvent to capture CO_2 from flue gas, Presented at the DOE Second International Forum on Geologic Sequestration of CO_2 in Deep Unmineable Coal Seams (Coal-Seq II), March 6-7, 2003, Washington D.C.

International Energy Agency (IEA GHG), 1999, The Reduction of Greenhouse Gas Emissions from the Cement Industry, PH3/7, May, 112 pp.

International Energy Agency (IEA GHG), 2000, Leading options for the capture of CO_2 emissions at power stations, report PH3/14, Feb. 2000, IEA Greenhouse Gas R&D Programme, Cheltenham, UK.

International Energy Agency (IEA GHG), 2006, Environmental Impact of Solvent Scrubbing of CO_2, 2006/14, October 2006.

International Energy Agency (IEA GHG), 2007, ERM – Carbon Dioxide Capture and Storage in the clean development mechanism, 2007/TR2, April 2007.

International Energy Agency (IEA GHG), 2005, Building the Cost Curves for CO_2 Storage: European Sector,Report no. 2005/2 (February 2005).

International Energy Agency (IEA), 2008, World energy outlook 2008, International Energy Agency, OECD, Paris.

International Energy Agency (IEA), 2002, Transmission of CO_2 and Energy, PH4/6 report, IEA Greenhouse gas R&D Programme, Cheltenham, UK

International Energy Agency (IEA), 1995, Industry attitudes to steam cycle clean coal technologies survey of current status. Available at: www.iea.org/dbtw-pd/ textbase/nppdf/free/1990/ciab1995.pdf.

International Energy Agency (IEA), 1999, Electric power technology: opportunities and challenges of competition. Available at: www.iea.org/textbase/nppdf/free/1990/ elecpower99.pdf.

International Energy Agency (IEA), 2003, Control and Minimisation of Coal-fired Power Plant Emissions. Available at: www.iea.org/dbtw-wpd/textbase/papers/2003/Coal FiredFossilFuels.pdf. Accessed 11 December 2004.

International Energy Agency (IEA), 2004, Prospects for CO_2 capture and storage. Available at: www.iea.org/textbase/nppdf/free/2004/prospects.pdf. Accessed 11 April 2006.

Institut für Energiewirtschaft und Rationelle Energieanwendung (IER), 1997, ExternE National Implementation Germany, Final report, ExternE-Externalities of Energy, European Commission. Available at: http://externe.jrc.es. Accessed 11 December 2004.

IPCC 2006, 2006 IPCC Guidelines for National Greenhouse Gas Inventories, Prepared by the National Greenhouse Gas Inventories Programme, Eggleston H.S., Buendia L., Miwa K., Ngara T., and Tanabe K. (eds). Published: IGES, Japan.

IPCC, 2001, Climate Change 2001: Mitigation, Contribution of Working Group III to the Third Assessment Report of the Intergovernmental Panel on Climate Change (IPCC), Bert Metz, Ogunlade Davidson, Rob Swart and Jiahua Pan (Eds.), Cambridge University Press, UK.

IPCC, 2005, IPCC special report on Carbon dioxide Capture and Storage. Prepared by Working Group III of the Intergovernmental Panel on Climate Change [Metz, B., O. Davidson, H.C. de Coninck, M. Loos and L.A. Meyer (eds.)], Cambridge University Press, Cambridge, United Kingdom and New York, NY, USa, 442 pp.

IPCC, 2007a, Summary for Policymakers. In: Climate Change 2007: The Physical Science Basis. Contribution of Working Group I to the Fourth Assessment Report of the Intergovernmental Panel on Climate Change [Solomon, S., Qin D., Manning M., Chen Z., Marquis M., Averyt K.B., Tignor M. and Miller H.L. (eds.)]. Cambridge University Press, Cambridge, United Kingdom and New York, NY, USA .

IPCC, 2007b, Climate Change 2007: Synthesis Report. Contribution of Working Groups I, II and III to the Fourth Assessment Report of the Intergovernmental Panel on Climate Change [Core Writing Team: Pachauri, R.K and Reisinger, A. (eds.)]. IPCC, Geneva, Switzerland.

ISO 14040. 1997, Environmental management – Life cycle assessment – Principles and framework. Geneva: International Organization for Standardization. First edition, 1997.

ISO 14041,1998, Environmental management – Life cycle assessment – Goal and scope definition and inventory analysis. Geneva: International Organization for Standardization. First edition,1998.

ISO 14043, 2000, Environmental management – Life cycle assessment–Life cycle interpretation. Geneva: International Organization for Standardization. First edition, 2000.

Jensen, A. A, Hoffmann L., A. Schmidt B. T.,, Christiansen K. and Elkington J., 1997. Life Cycle Assessment – A guide to approaches, experiences and information sources.Environmental Issues Series no. 6. Copenhagen: European Environmental Agency.

Jordal, K., Anheden, M., Yan, J., Strömberg, L. (2004) Oxyfuel combustion for coal-fired power generation with CO2 capture - Opportunities and challenges. The 7th

International Conference on Greenhouse Gas Control Technologies (GHGT7), Vancouver, Canada, September 5-9.

Khartechenko N.V., 1998, Advanced energy systems, Taylor & Francis, Washington, USA.

Khoo, H. H. & Tan, R. B. H. 2006, "Environmental Impact Evaluation of Conventional Fossil Fuel Production and Enhanced Resource Recovery with Potential CO_2 Sequestration", Energy & Fuels, vol. 20, no. 5, pp. 1914-1924.

Khoo, H. H. 2006a, "Life cycle evaluation of CO_2 recovery and mineral sequestration alternatives", Environmental progress, vol. 25, no. 3, pp. 208-217.

Khoo, H. H. 2006b, "Life cycle investigation of CO_2 recovery and sequestration", Environmental science & technology, vol. 40, no. 12, pp. 4016-4024.

Knauss, K.G., Johnson J.W. and Steefel C.I, 2005: Evaluation of the impact of CO_2, co-contaminant gas, aqueous fluid and reservoir rock interactions on the geologic sequestration of CO_2. Chemical Geology, Elsevier, 217, 339–350.

Koerner, R.M., and Daniel, D.E., 1997, Final Covers for Solid Waste Landfills and Abandoned Dumps. American Society of Civil Engineers, Reston, VA.

Kohl, A. L and Nielsen, R. B., 1997, Gas Purification (5th Edition), Gulf publishing company, Houston, Texas.

Koornneef, J., Keulen, T.V., Faaij, A., and Turkenburg, W., 2008, Life cycle assessment of a pulverized coal power plant with post-combustion capture, transport and storage of CO_2, International Journal of Greenhouse Gas Control Volume 2, Issue 4, October 2008, Pages 448-467

Korre, A., Shi, J.Q., Imrie, C., Grattoni, C. and Durucan, S., 2007, Coalbed methane reservoir data and simulator parameter uncertainty modelling for CO_2 storage performance assessment, International journal of greenhouse gas control, (2007) 492-501.

Krishnamoorthy, G. and Veranth, J. M., 2003, Computational Modeling of CO/CO_2 Ratio Inside Single Char Particles during Pulverized Coal Combustion, Energy Fuels, 17 (5), 1367 -1371, 2003

Lani, B., Feeley, T., Murphy J. and Green, L., 2005, A Review of DOE/NETL's Advanced NOx Control Technology R&D Program for Coal-fired Power Plants, DOE/NETL NOx R&D Program Review, March 2005.

Larsen, M., Bech, N., Bidstrup, T., Christensen, N. P., and Vangkilde-Pedersen, T., 2007, Kalundborg case study, a feasibility study of CO_2 storage in onshore saline aquifers - CO_2STORE, GEUS Ole Biede ENERGI E2, Danmarks og Grønlands Geologiske Undersøgelse Rapport 2007/2.

Law D. H.-S. and Bachu S. (1996) Hydrogeological and numerical analysis of CO_2 disposal in deep aquifers in the Alberta sedimentary basin. Energy Conversion and Management. 37, 1167-1174.

Law, D. (ed.), 2005, Theme 3: CO_2 Storage Capacity and Distribution Predictions and the Application of Economic Limits. In: IEA GHG Weyburn CO_2 Monitoring and Storage Project Summary Report 2000–2004, Wilson M. and Monea M. (eds.), Proceedings of the 7th International Conference on Greenhouse Gas Control Technologies (GHGT7), Volume III, p 151–209.

Laudal, D.L.; Pavlish, J.H.; Galbreath, K.C.; Thompson, J.S.; Weber, G.F.; Sondreal, E.A., 2000, Pilot-Scale Screening Evaluation of the Impact of Selective Catalytic Reduction for NOx on Mercury Speciation. Electric Power Research Institute Report No. 1000755. Palo Alto, CA, 2000

Le Bocq, A., 2008, An overview of electricity companies communication on LCA (Europe + Japanese TEPCO company), SETAC Europe Annual Meeting 2008, Warsaw, Poland, 22-May-2008

Lee B. C. and Lesley L.S., 1992, Trace elements – emissions from coal combustion and gasification, IEACR/49, IEA Coal Research, London.

Lee, I. Y., Kim, D. W., Lee, J. B., and Yoo, K. O., 2002, A Practical Scale Evaluation of Sulfated V2O5/TiO2 Catalyst from Metatitanic Acid for Selective Catalytic Reduction of NO by NH_3, Chemical Engineering Journal, 90: 267-272.

LeNeveu, D. M., 2008, CQUESTRA, a risk and performance assessment code for geological sequestration of carbon dioxide, Energy Conversion and Management Volume 49, Issue 1, January 2008, Pages 32-46

Lietti, L., Nova, I. and Forzatti, P., 2000, Selective catalytic reduction (SCR) of NO by NH_3 over TiO_2-supported V_2O_5–WO_3 and V_2O_5–MoO_3 catalysts, Topics in Catalysis 11/12 (2000) 111–122

Lindeberg, E., 1997, Escape of CO_2 from aquifers. In: Carbon dioxide removal. Proceedings of the third international conference on carbon dioxide removal, Cambridge, MA, USA, 9-11 Sep 1996. Herzog H J (ed), Energy Conversion and Management; 38 (suppl); s235-s240 (1997)

Lissianski, V., 2004, Mercury Control Using Combustion Staging, proceeding in DOE NETL Conference on Reburning for NOx Control Morgantown, West Virginia18 May 2004

Liu, H., Zailani, R., Gibbs, B. M., 2005, Comparisons of pulverized coal combustion in air and in mixtures of O_2/CO_2, Fuel, 84.

Liuqing, T., Daiqi, Y. and Hong, L., “Catalytic Performance of a Novel Ceramic-Supported Vanadium Oxide Catalyst for NO Reduction with NH_3,” Catalysis Today, 78: 159-170, 2003.

Lombardi L., 2003, Life cycle assessment comparison of technical solutions for CO_2 emission reduction in power generation, Energy Conversion and Management, vol 44, pp.93-108.

McCollum, D. L. and Ogden, J. M., 2006, Techno-Economic Models for Carbon Dioxide Compression, Transport, and Storage & Correlations for Estimating Carbon Dioxide Density and Viscosity, Institute of Transportation Studies, University of California, Davis

McKetta, J. (1990). Encyclopedia of Chemical Processing and Design, Vol. 31, pg. 214, 1990.

Mimura, T., Matsumoto, K., Iijuma M., Mitsuoka S., (2000): Development and application of flue gas carbon dioxide recovery technology, 5th International Conference on Greenhouse Gas Control Technologies (GHGT-5), Cairns, Australia, CSIRO publishers, ISBN 0 643 06672 1.

Moser, R. E, 2007, Cover Story: Clean Coal Combustion, SO_3's impacts on plant O&M: Part II, Power; Feb2007, Vol. 151 Issue 2, p49-15

Mulders, F., 2007, Analysis of abandoned well integrity at a potential CO_2 storage site, 3rd Well Bore Integrity Network Meeting, March 12-13 2007, Santa Fe, USA

Muraka, I.P., Mattigod, S.V. and Keefer, R.F., 1993. “An Overview of Electric Power Institute (EPRI) Research Related To Effective Management of Coal Combustion Residues.” In Trace Elements in Coal and Combustion Residues, edited by R.F. Keefer and K.S. Sajwan, Lewis Publishers, Boca Raton, Florida, USA.

Muramatsu E. and Iijima M., 2002, Life cycle assessment for CO_2 capture technology from exhaust as of coal power plant, The 6th Greenhouse Gas Control Technologies, Kyoto, Japan, October 1-4, 2002.

Nalbandian H., 2004, Air pollution control technologies and their interactions, IEA report CCC/92, IEA Clean Coal Centre.

Neksa, P., 2004, Refrigeration Sector MainConclusions, , SINTEF Energy Research, Trondheim, Norway. From: http://www.centrogalileo.it/nuovaPA/Articoli tecnici/ INGLESE CONVEGNO/XI Convegno English/1 SESSIONE/Neksa SINTEF Ingl.pdf. Accessed, 21 March, 2007.

Nelson, C.R., Evans , J. M., Sorensen, J. A., Steadman E. N. and Harju, J. A. 2005, Factors Affecting the Potential for CO_2 Leakage from Geologic Sinks, National Energy Technology Laboratory (NETL), Topical report

Neumann, K., 2007, Life-Cycle Approaches in European Companies: The influence of internal and external drivers on the application of life-cycle tools. Available at: www.calcasproject.net. Assessed at 18 December 2008.

Nicot, J. P., Saripalli, P., Bouroullec, R., Castellanos, H., Hovorka, S. D., Lakshminarasimhan, S., Paine, J. G., and Yang, Y., 2006, Development of science - based permitting guidance for geological sequestration of CO_2 in deep saline aquifers based on modeling and risk assessment: The University of Texas at Austin, Bureau of Economic Geology, final scientific report prepared for U.S. Department of Energy, under DOE Agreement No. DE-FC25-04NT42210, 220 p.

Nielsen, M. T., 2003, On the Relative Importance of SO_2 oxidation to High Dust SCR DeNOx units. In Proceedings of 2003 Conference on Selective Catalytic Reduction and Non-Catalytic Reduction for NOx Control, Oct 29-30, 2003, Pittsburgh, US

Nordin, J. S and Merriam, N. W, 1997, NOx emissions produced with combustion of Powder River Basin coal in a utility boiler, USDOE Topical report, DE-FC21-93MC30127

Nsakala, N., Marion, J., Bozzuto, C., Liljedahl, G. N., Palke,s M., Vogel, D., Gupta, J. C., Guha, M., Johnson H., Plasynski S., 2001, Engineering feasibility and economics of CO_2 capture on an existing coal-fired power plant, Final report, DOE National Energy Technology Laboratory, U.S.

Nsakala, N., Liljedahl, G. N., Turek, D.G., 2007, Commercialization Development of Oxygen Fired CFB for Greenhouse Gas Control, Technical Report, DOE National Energy Technology Laboratory (Contract No DE-FC26-04NT42205)

Oberbacher, B. Nikodem, H. Klöpffer, W. (1996) LCA - How it came about: An early systems analysis of packaging for liquids. Which would be called an LCA today. International Journal of Life Cycle Assessment 1 (2) 62-64

Odeh, N. A. and Cockerill, T. T. 2008, "Life cycle GHG assessment of fossil fuel power plants with carbon capture and storage", Energy Policy, vol. 36, no. 1, pp. 367-380.

Okazaki, K. and Ando, T., 1997, NOx. Reduction Mechanisms in Coal Combustion with. Recycled CO_2, Energy Vol. 22, No.2/3, pp.207-215

Oldenburg, C.M. and Lewicki, J.L., On leakage and seepage of CO_2 from geologic storage sites into surface water, Environmental Geology, 50, doi: 10.1007/s00254-006-0242-0, 2006.

Oldenburg, C.M., and Unger, A.J.A., 2003, On leakage and seepage from geologic carbon sequestration sites: unsaturated zone attenuation, Vadose Zone Journal, 2(3): 287-296, August 2003.

Olivier, J.G.J., Pulles, T., and Van Aardenne, J.A., 2006, Part III: Greenhouse gas emissions. 1. Shares and trends in greenhouse gas emissions; 2. Sources and Methods; Greenhouse gas emissions for 1990, 1995, and 2000. In CO_2 Emissions from Fuel

Combustion 1971— 2004, 2006 Edition, pp. III.1-III.41. International Energy Agency (IEA), Paris.

Panesar R.S, Lord M.R., Simpson S.T., White V., Gibbins J., and Reddy S., 2007, Coal-fired advanced supercritical retrofit with CO_2 capture, Final report, Doosan Babcock Energy Limited, Contract Number: C/08/00393/00/00

Paschke L., 2006, Meeting EPA Consent Decree Compliance with DynaWave Scrubbing, Monsanto Enviro-Chem Systems, Inc., Chesterfield, MO. Available at: www.iapg.org.ar/sectores/eventos/eventos/eventos_iapg/2006/refinacion/TT35Meeting EPA Compliance with DynaWave.ppt. Assessed at: December 2006

Pehnt, M. and Henkel, J., (2009): "Life Cycle Assessment of Carbon Dioxide Capture and Storage from Lignite Power Plants." International Journal of Greenhouse Gas Control Volume 3, Issue 1, January 2009, Pages 49-66

Rao A.B., Rubin E.S. and Berkenpas M.B., 2004, An integrated modelling framework for carbon management technology (Volume 1), Final report, Centre for Energy and Environmental Studies, Carnegie Mellon University, Pittsburgh, PA. Available at: www.iecmonline.com/documentation/tech_04.pdf. Accessed 19 July 2005.

Rao, A.B., Rubin E.S., and Berkenpas, M.B., 2007, Technical Documentation: Oxygen-based Combustion Systems (Oxyfuels) with Carbon Capture and Storage (CCS), Final Report of Award No. DE-AC21-92MC29094, Prepared by Carnegie Mellon University, Pittsburgh, PA for U.S. Department of Energy, National Energy Technology Laboratory, Pittsburgh, PA, May 2007.

Reap, J., Roman, F., Duncan, S., Bras, B., 2008, A survey of unresolved problems in life cycle assessment. Part 2: impact assessment and interpretation. International Journal of Life Cycle Assessment, DOI 10.1007/s11367-008-0009-9

Riaz, A., Hesse, M. and Tchelepi, H., 2006, Onset of Convection in a Gravitationally Unstable, Diffusive Boundary Layer in Porous Media, Journal of Fluid Mechanics, 548, 87-111.

Riemer, P.W.F. and Ormerod, W.G., 1995, International perspectives and the results of carbon dioxide capture disposal and utilisation studies, Energy Conversion and Management, 36(6-9), 813-818.

Rochelle G., 2001, CO_2 capture by aqueous absorption/stripping opportunities for better technology, 2001 Conference Proceedings of Workshop on Carbon Sequestration Science, National Energy Technology Laboratory. Available at: www.netl.doe.gov/publications/proceedings/01/.../Rochell_Sep.pdf. Accessed 19 July 2005.

Rowe, R.K. 1998. Geosynthetics and the minimization of contaminant migration through barrier systems beneath solid waste. In Proceedings of the 6th International Conference on Geosynthetics, Atlanta, Ga., 25-29 March.

Rubin, E. S., Berkenpas, M. B., Frey, H. C., Chen, C., McCoy, S. and Constance J. Zaremsky, 2007, Integrated gasification combined cycle system (IGCC) with carbon capture and storage (CCS) – Final report, US DOE DE-AC21-92MC29094.

Röder, A., Bauer, C., Dones, R., 2004. Kohle. Paul Scherrer Institut Villigen, Swiss Centre for Life Cycle Inventories, Dübendorf, Switzerland.

Salvi, S., F. Quattrocchi, M. Angelone , C.A. Brunori, A. Billi, F. Buongiorno, F. Doumaz, R. Funiciello, M. Guerra, S. Lombardi, G. Mele, L. Pizzino and F. Salvini, 2000, A multidisciplinary approach to earthquake research: implementation of a Geochemical Geographic Information System for the Gargano site, Southern Italy. Natural Hazard, 20(1), 255–278.

Sargent & Lundy LLC, 2003, Wet flue gas desulphurisation technology evaluation, Research report, Available at: http://www.lime.org/Wet_FGD.pdf. Assessed at 2 September 2006.

Saripalli, K.P., Mahasenan, N.M., and Cook. E.M., 2003, Risk and hazard assessment for projects involving the geological sequestration of CO_2. Proceedings of the Sixth International Conference on Greenhouse Gas Control Technologies: 511-516.

Saripalli, P. and McGrail, P., 2002, Semi-analytical approaches to modeling deep well injection of CO2 for geological sequestration, Energy Convers Mgt 43 (2002) (2), pp. 185–198.

Sarkar, S., Toksoz, M.N, and Burns, D.R. 2004. Fluid flow modeling in fractures. Available at: http://www-eaps.mit.edu/erl/research/report1/reports.html. Accessed 22 November, 2007.

Sass B., Monzyk B., Ricci S., Gupta A., Hindin B., & Gupta N., 2005, Impact of SOx and NOx in flue gas on CO_2 separation, compression, and pipeline transmission, in Carbon Dioxide Capture for Storage in Deep Geologic Formations, Volume 2, Sally M. et al., eds., Elsevier, London, UK, pp. 755-781.

Schmidt, W. P., et al 2004, Safe Design and Operation of a Cryogenic Air Separation Unit, Process Safety Progress, Volume 20, Issue 4 , Pages 269 – 279

Schnelle, K. B. and Brown, C. A., 2001, Air Pollution Control Technology Handbook, CRC Press, Boca Raton

Schreiber, A.; Nazarko, J. et al., 2007, Life Cycle Analysis of the Coal-based Power Generation with Carbon Capture, Germany, SETAC EUROPE Annual Meeting 2007, Porto, 2007

Schroeder, P.R.; Lloyd, C.M.; Zappi, P.A.; Aziz, N.M. 1994. Hydrologic Evaluation of Landfill Performance (HELP) Model. User's Guide for Version 3. Army Engineer.

Sean T. McCoy, 2008, the Economics of CO_2 Transport by Pipeline and Storage in Saline Aquifers and Oil Reservoirs, PhD thesis, Carnegie Mellon University Pittsburgh, PA, USA

Seiersten1, M. and Kongshaug, K. O., 2003, Material selection for capture, compression, transport and injection of CO_2, Technical Report, Institute for Energy Technology, 2003.

Seiersten1, M. and Kongshaug, K. O., 2005, Materials selection for capture, compression, transport and injection of CO_2, in Carbon Dioxide Capture for Storage in Deep Geologic Formations - Results from the CO_2 Capture Project Edited by David Thomas and Sally Benson, Elsevier Science, January 2005, pp925

Senior, C., 2004, Oxidation of mercury across SCR catalysts in coal-fired power plants burning low rank fuels, USDOE Quarterly Progress Report (April to June). Available at: http://www.osti.gov/energycitations/servlets/purl/829540-75cDUi/native/829540.pdf, Assessed at April 2006

Setterwall C., Munter M., Sarkozi P. and Bodlund B., 2004, Methodological guidelines, Final report, In: Environmental and ecological Life cycle Inventories for present and future Power Systems in Europe (ECLIPSE), EU Research and technological development report. Available at: http://62.94.11.35/eclipse_eu/pubres_meth.html. Accessed 21 January 2009.

Shaw, J.C. and Bachu, S., 2002, Screening, Evaluation, and Ranking of Oil Reservoirs Suitable for CO_2 Flood EOR and Carbon Dioxide Sequestration; Journal of Canadian Petroleum Technology, Vol. 41, No.9, pp. 51-61.

Sheng, C., Lu, Y., Gao, X., and Yao, H., 2007a, Fine Ash Formation during Pulverized Coal Combustions A Comparison of O_2/CO_2 Combustion versus Air Combustion, Energy & Fuels 2007, 21, 435-440

Sheng, C., Li, Y., Liu, X., Yao, H. and Xu, M., 2007b, Ash particle formation during O_2/CO_2 combustion of pulverized coals, Fuel Processing Technology 88 (2007) 1021–1028

Shi, J.Q. and Durucan, S, CO_2 storage in deep unminable coal seams, Oil Gas Science and Technology, 2005, Vol: 60, Pages: 547 - 558, ISSN: 1294-4475

Shires,T. M., et al, 2004, Emissions methodologies for the oil and gas industry, American Petroleum Institute

Silin, T.W. Patzek and Benson, S.M., 2006, Exact solutions in a model of vertical gas migration. SPE Paper 103156, 2006 SPE Annual Technical Conference and Exhibition, September 24–27, 2006, SPE, San Antonio, TX, 2006.

Sims, R.E.H., Schock, R.N., Adegbululgbe, A., Fenhann, J., Konstantinaviciute, I., Moomaw, W ., Nimir, H.B., Schlamadinger, B., Torres-Martínez, J., Turner, C.,

Uchiyama, Y., Vuori, S.J.V., Wamukonya N., and Zhang, X., 2007: Energy supply. In Climate Change 2007: Mitigation. Contribution of Working Group III to the Fourth Assessment Report of the Intergovernmental Panel on Climate Change [B. Metz, O.R. Davidson, P.R. Bosch, R. Dave, L.A. Meyer (eds)], Cambridge University Press, Cambridge, United Kingdom and New York, NY, USA.

Singleton, G., 2007. Geologic storage of carbon dioxide: risk analyses and implications for public acceptance. Masters Thesis. Technology and Policy Program, Department of Political Science, Massachusetts Institute of Technology, Cambridge, MA, June.

Sjostrom, S, Ebner, T., Ley, T., Slye, R., Richardson, C., Machalek, T., Richardson, R., Chang, R., and Meserole, F., 2001, Assessing Sorbents for Mercury Control in Coal-Combustion Flue Gas, Presented at the A&WMA Specialty Conference on Mercury Emissions: Fate, Effects and Control, Chicago, IL, August 21 –23, 2001

Smith, A.R. and Klosek, J., 2001, A review of air separation technologies and their integration with energy conversion processes, Fuel Process Technology vol. 70 (2001), pp. 115–134.

Spath, P, Mann, M., 2004, Biomass Power and Conventional Fossil Systems with and without CO_2 Sequestration – Comparing the Energy Balance, Greenhouse Gas Emissions and Economics, National Renewable Energy Laboratory, Golden, CO, NREL/TP-510-32575, January 2004.

Spero, C., Yamada, T., Sturm, E., McGregor, D., 2008, Technical evaluation of oxy-combustion and CO_2 capture system, IEAGHG international Oxy-Combustion Network, March 5th, 2008, Yokohama, Japan.

Stevens, S. H., Kuuskra V.A. and Gale J.J., 2001, Sequestration of CO_2 in depleted oil and gas fields: global capacity, costs and barriers. Proceedings of the 5th International Conference on Greenhouse Gas Control Technologies (GHGT-5), Williams D.J., Durie R.A., McMullan P., Paulson C.A.J. and Smith A.Y. (eds.), 13–16 August 2000, Cairns, Australia, CSIRO Publishing, Collingwood, Victoria, Australia, pp. 278–283.

Streit, J., Siggins A. and Evans, B., 2005, Predicting and monitoring geomechanical effects of CO_2 injection, Carbon Dioxide Capture for Storage in Deep Geologic Formations—Results from the CO_2 Capture Project, v. 2: Geologic Storage of Carbon Dioxide with Monitoring and Verification, Benson S.M. (ed.), Elsevier Science, London, pp. 751–766.

Strömberg L., 2006, ENCAP Integrated Project, ENCAP CO_2 Seminar in Billund, Denmark, 16th of March 2006.

Strömberg, L., 2006, ENCAP Integrated Project, ENCAP CO_2 Seminar in Billund, Denmark, 16th of March 2006.

Stroosnijder, L. (1987). “Soil evaporation: test of a practical approach under semi-arid conditions.” Netherlands Journal of Agricultural Science, 35, 417-426.

Suebsiri, J., Wilson, M., & Tontiwachwuthikul, P. 2006, "Life-Cycle Analysis of CO_2 EOR on EOR and Geological Storage through Economic Optimization and Sensitivity Analysis Using the Weyburn Unit as a Case Study", Industrial & engineering chemistry research, vol. 45, no. 8, pp. 2483-2488.

Suriyawong, A., Gamble, M., Lee, M.H., Axelbaum, R., Biswas, P., 2006, Submicrometer Particle Formation and Mercury Speciation Under O_2-CO_2 Coal Combustion, Energy & Fuels 2006, 20, 2357-2363

Tamburri M.N.; Peltzer E.T.; Friederich G.E.; Aya I.; Yamane K.; Brewer P.G., A, 2000, field study of the effects of CO_2 ocean disposal on mobile deep-sea animals, Marine Chemistry, Volume 72, Number 2, December 2000 , pp. 95-101(7)

Tan, Y., Croiset, E., Douglas, M.A. and Thambimuthu, K.V. (2006), Combustion characteristics of coal in a mixture of oxygen and recycled flue gas, Fuel, 85, [4], 507-512

The Institute of Clean Air Companies (ICAC), 2006, Acid Gas/SO_2 Control Technologies. Available at: http://www.icac.com/i4a/pages/index.cfm?pageid=3401. Assessed at December, 2006

Tillman A., 2000, Significance of decision-making for LCA methodology, Environmental Impact Assessment Review, vol. 20, pp. 113-123.

Touze-Foltz, N. and Giroud, J. P., 2003, Empirical equations for calculating the rate of liquid flow through composite liners due to geomembrane defects, Geosynthetics International, 2003, 10, No. 6

Touze-Foltz, N., and Giroud, J.P., 2003, “Empirical equations for calculating the rate of liquid flow through composite liners due to geomembranes defects”, Geosynthetics International, Vol. 10, No. 6, pp. 215-233.

Touze-Foltz1, N. and Giroud, J. P., 2003, Empirical equations for calculating the rate of liquid flow through composite liners due to geomembrane defects, Geosynthetics International, 2003, 10, No. 6

Tranier, J-P., Perrin, N., Darde, A., 2008, ASU and CO_2 CPU for Oxy-Combustion, IEAGHG international Oxy-Combustion Network, March 5th, 2008, Yokohama, Japan.

Turner, R., Hardy, N., Hooper, B., 2007, Quantifying the risks associated with a CO_2 sequestration pipeline: a methodology & case study, Available: https://extra.co2crc.com.au. Accessed December, 2007.

U.S. Department of Energy (USDOE), 1999, Advanced Technologies for the Control of Sulphur Dioxide Emissions from Coal-Fired Boilers, Clean coal technology topical report number 12

U.S. Environmental Protection Agency (USEPA), 1995, Protocol for Equipment Leak Emission Estimates, EPA-453/R-95-017, EPA Office of Air Quality Planning and Standards, November 1995, Table 2-12.

U.S. Environmental Protection Agency (USEPA), 1998a, AP 42, Volume I, Fifth Edition, Chapter 1: External combustion sources, 1.1 Bituminous and Subbituminous Coal Combustion, Available at: http://www.epa.gov. Accessed 14 January 2005.

U.S. Environmental Protection Agency (USEPA), 1998b, NOx – How Nitrogen Oxides Affect the Way We Live and Breathe. EPA Report No. EPA-456/F-98-005; September 1998. See http://www.epa.gov/air/urbanair/nox/index.html. Accessed 24 August, 2006.

U.S. Environmental Protection Agency (USEPA), 1998c,Technical Background Document for The Supplement Report for Congress on Remaining Fossil Fuel Combustion Wastes, Groundwater Pathway Human Health Risk Assessment, Research report, June1998, Appendix F: F-2

U.S. Environmental Protection Agency (USEPA), 1998d, AP 42, Volume I, Fifth Edition, Chapter 1: External combustion sources, 1.4 Natural Gas Combustion, Available at: http://www.epa.gov. Accessed 14 January 2005.

U.S. Environmental Protection Agency (USEPA), 1999, Report to Congress: Wastes from the Combustion of Fossil Fuels: Volume 2B. Methods, Findings and Recommendations. EPA-530-R-99-010. Office of Solid Waste and Emergency Response, Washington, DC. 1999.

U.S. Environmental Protection Agency (USEPA), 2003a, EPA's Composite Model for Leachate Migration with Transformation Products (EPACMTP) Technical Background Document, EPA530-R-03-006, Office of Solid Waste (5305W), Washington, DC 20460, Available at:www.epa.gov/osw. Accessed at 12 July 2007

U.S. Environmental Protection Agency (USEPA), 2003b, EPA's Composite Model for Leachate Migration with Transformation Products (EPACMTP) Parameters/Data Background Document, EPA530-R-03-006, Office of Solid Waste (5305W), Washington, DC 20460, Available at:www.epa.gov/osw. Accessed at 14 July 2007

U.S. Environmental Protection Agency (USEPA), 2006, Health and Environmental Impacts of SO2, Available at: http://www.epa.gov/air/urbanair/so2/hlth1.html. Assessed 20 January, 2006.

U.S. Environmental Protection Agency (USEPA), 2000, AP 42, Volume I, Fifth Edition, Chapter 3: Stationary Internal Combustion Sources, 3.2 Natural Gas-fired Reciprocating Engines, Available at: http://www.epa.gov. Accessed 14 January 2005.

U.S. Environmental Protection Agency (USEPA), 2001, Preferred and alternative methods for estimating air emissions from boilers: volume II. Available at: www.epa.gov/ttn/chief/eiip/techreport/volume02/ii02.pdf. Accessed 23 February 2006.

U.S. Environmental Protection Agency (USEPA), 2002, Control of Mercury Emissions from Coal-Fired Electric Utility Boilers: Interim Report, Available at: http://www.epa.gov/nrmrl/pubs/600r01109/600r01109.htm. Accessed 23 February 2006.

U.S. Environmental Protection Agency (USEPA), 2006, Life cycle assessment: principles and practice. Available at: http://www.epa.gov/ORD/NRMRL/lcaccess/pdfs/lca101_ allchapters.pdf. Accessed 11 February 2008.

United Nations (UN), 1992, United Nations Framework Convention on Climate Change, FCCC/INFORMAL/84, GE.05-62220 (E) 200705

USDOE and Southern Company Services, Inc. (SCSI), 1997, Control of Nitrogen Oxide Emissions: Selective Catalytic Reduction (SCR), Clean coal technology, Topical report number 9. Available at: www.fossil.energy.gov/programs/powersystems/publications/ Clean_Coal_Topical_Reports/topical9.pdf. Accessed 05 September, 2006.

Vagt, H., Jaco, K., Rubik, F., Huppes, G., Ekvall, T., 2008, LCA options for sustainable governance assessed, Deliverable D8 of work package 4 of the CALCAS Project.

Van dar Meer L. G. H. and van Wees, J. D., 2006, Effects of CO2 solubility on the long-term fate of CO2 sequestered in a saline aquifer, The Leading Edge 25, 1276 (2006); DOI:10.1190/1.2360620

Van der Sluijs, J.P, Hendriks, C.A. and Blok, K., 1992, Feasibility of polymer membranes for carbon dioxide recovery from flue gases, Energy Conversion Management, 33(5-8), 429-436.

Vandeginste, V. and Piessens, K., 2008, Pipeline design for a least-cost router application for CO2 transport in the CO2 sequestration cycle, International Journal of Greenhouse Gas Control, doi:10.1016/j.ijggc.2008.02.001

Vattenfall, 2007, CSR report 2007, Available at: http://report.vattenfall.com. Assessed at 10 January 2009.

Vattenfall, 2008, Factsheet CCS: A pilot for the CCS-technology, Available at: www.vattenfall.com/ccs. Assessed at 2 November 2008.

Wainwright J. and Mulligan M., 2004, Environmental modelling: finding simplicity in complexity, John Wiley & Sons, London.

Wall, T. F., 2007, Combustion processes for carbon capture, Proceedings of the Combustion Institute 31 (2007)

Wall, T.F., Elliott, L., Khare, S., Liu, Y., Yamada, T., Tamura, M., Fujimori, T. and Spero, C., 2006, Ash impacts in oxyfuel combustion, Proceedings: Impacts of Fuel Quality on Power Production, EPRI, Palo Alto, CA (2006), p. 5.1–17

Waterways Experiment Station, Vicksburg, MS. and Clemson Univ., SC. Dept. of Civil Engineering.

Weidema B., Fress N., Petersen E.H. and Olgaard H., 2003, Reducing uncertainty in LCI: developing a data collection strategy, Environmental Project No. 862, Danish Environmental Protection Agency.

Weir, G.J., White, S.P., Kissing, W.M., 1996, Reservoir storage and containment of greenhouse gases, Transport in porous media 23:11, 37-60, Kluwer, 1996

White, C.M., Strazisar B.R., Granite E.J., Hoffman J. S. and Pennline H.W., 2003, Separation and capture of CO_2 from large stationary sources and sequestration in geological formations - coalbeds and deep saline aquifers, Journal of the Air & Waste Management Association, vol 53, pp. 645-715.

White,V., 2008, Purification of Oxyfuel Derived CO_2, presentation in IEAGHG International Oxy-combustion network, 5th and 6th March 2008, Yokohama, Japan.

Wigh, R.J. 1979, Boone county fields site interim report, test cells 2A, 2B, 2C, 2D. EPA-600/2-79-058, U.S.EPA, Cincinnati, OH.

Xu, B., et al., 2007, Future CO_2 Capture Technology Options for the Canadian Market, Report No. COAL R309 BERR/Pub VRN 07/1251, March.

Xu, T., Apps, J.A. and Pruess, K., 2005b, Injection of CO_2 with NO and NO_2 in a Sandstone-Shale Formation. Lawrence Berkeley National Laboratory Report.

Xu, T., Apps, J.A. Pruess, K. and Yamamoto, H., 2005a, Injection of CO_2 with H_2S and SO_2 and subsequent mineral trapping in Sandstone-Shale Formation. Lawrence Berkeley National Laboratory Report LBNL-57426, 70 p.

Yamada, T., 2007, Pilot scale experiments giving direct comparison between air and oxy-firing of coals and implication for large scale plant design, 2nd Workshop of the oxy-fuel combustion network, , Conneticuct, The US, 25th-26th January 2007

Yokoyama, T., 2003, Japanese R&D on CO_2 Capture. Greenhouse Gas Control Technologies, Proc. of the 6th International Conference on Greenhouse Gas Control Technologies (GHGT-6), 1-4 Oct. 2002, Kyoto, Japan, J. Gale and Y. Kaya (eds.), Elsevier Science Ltd, Oxford, UK. 13-18.

Zamagni, P. Buttol, P.L. Porta, R. Buonamici, et al., 2008,Critical review of the current research needs and limitations related to ISO-LCA practice, Deliverable D7 of work package 5 of the CALCAS project.

Zevenhoven R. and Kilpinen P., 2004, Control of pollutants in flue gases and fuel gases, Research report, Helsinki University of Technology. Available at: www.hut.fi/~rzevenho/gasbook. Assessed: Spetember, 2006.

Zhang, Y., and Kling, G.W., 2006, Dynamics of lake eruptions and possible ocean eruptions. Annual Review of Earth and Planetary Sciences 34: 293-324

Zhang, Y.Q., Oldenburg, C.M, and Benson, S.M., 2004, Vadose Zone Remediation of CO_2 Leakage from Geologic CO_2 Storage Sites, Lawrence Berkeley National Laboratory, Paper LBNL-54680.

Zheng L, Furimsky E. Assessment of coal combustion in O_2/CO_2 by equilibrium calculations. Fuel Process Technol 2003;81:23–34.

Appendix A Current and Planned Carbon Dioxide Capture and Storage Projects Worldwide

Table A1: Current and planned carbon dioxide capture and storage projects (Source: http://sequestration.mit.edu)

Project Name	Location	Leader	Feedstock	Size MW	Capture Process	CO_2 Fate	Start-up
Total Lacq	France	Total	Oil	35	Oxy	Seq	2008
Schwarze Pumpe	Germany	Vattenfall	Coal	30/300 /1,000	Oxy	Seq / EOR	2008
AEP Alstom Mountaineer	USA	AEP	Coal	30	Post	Seq	2008
Callide-A Oxy Fuel	Australia	CS Energy	Coal	30	Oxy	Seq	2009
GreenGen	China	GreenGen	Coal	250/800	Pre	Seq	2009
Williston	USA	PCOR	Coal	450	Post	EOR	2009-15
Kimberlina	USA	CES	Coal	50	Oxy	Seq	2010
NZEC	China	UK&China	Coal	Undecided	Undecided	Seq	2010
AEP Alstom Northeastern	USA	AEP	Coal	200	Post	EOR	2011
Sargas Husnes	Norway	Sargas	Coal	400	Post	EOR	2011
Scottish & Southern Energy Ferrybridge	UK	SSE	Coal	500	Post	Seq	2011-2012
Naturkraft Kårstø	Norway	Naturkraft	Gas	420	Post	Undecided	2011-2012
Fort Nelson	Canada	PCOR	Gas	Gas Process	Pre	Brine Res	2011
ZeroGen	Australia	ZeroGen	Coal	100	Pre	Seq	2012
Antelope Valley	USA	Basin Electric	Coal	120	Post	EOR	2012
WA Parish	USA	NRG Energy	Coal	125	Post	EOR	2012
UAE Project	UAE	Masdar	Gas	420	Pre	EOR	2012
Appalachian Power	USA	AEP	Coal	629	Pre	Undecided	2012
Wallula Energy Resource Center	USA	Wallula Energy	Coal	600-700	Pre	Seq	2013
RWE npower Tilbury	UK	RWE	Coal	1,600	Post	Seq	2013
Tenaska	USA	Tenaska	Coal	600	Post	EOR	2014
HECA	USA	HEI	Petcoke	390	Post	EOR	2014
UK CCS project	UK	TBD	Coal	300-400	Post	Seq	2014
Statoil Mongstad	Norway	Statoil	Gas	630 CHP	Post	Seq	2014
RWE Zero CO_2	Germany	RWE	Coal	450	Pre	Seq	2015
Boundary Dam	Canada	SaskPower	Coal	100	Oxy	EOR	2015
Monash Energy	Australia	Monash	Coal	60 k bpd	Pre	Seq	2016
Powerfuel Hatfield	UK	Powerfuel	Coal	900	Pre	EOR	Undecided
ZENG Worsham-Steed	USA	CO_2-Global	Gas	70	Oxy	EOR	Undecided
Polygen Project	Canada	SaskPower	Coal/Petcoke	300	Pre	Undecided	Undecided
ZENG Risavika	Norway	CO_2-orway	Gas	50-70	Oxy	Undecided	Undecided
E.ON Karlshamn	Sweden	E.ON	Oil	5	Post	Undecided	Undecided

Table A2: Current and planned carbon dioxide storage only projects worldwide (Source: http://sequestration.mit.edu)

Project	Leader	Location	CO_2 Source	Size Mt/Yr	CO_2 Sink	Start
Sleipner	StatoilHydro	Norway	Gas Process	1	Brine Res	1996
Weyburn	Pan Canadian	Canada	Coal Gas.	1	EOR	2000
In Salah	BP	Algeria	Gas Process	1.2	Depleted Gas Res	2004
K12-B	Gaz de France	Netherlands	Gas Process	0.2	Depleted Gas Res	2004
Zama	Apache	Canada	Gas Process	0.067	EOR	2006
Snøhvit	StatoilHydro	Norway	LNG Process	0.7	Depleted Gas Res	2008
Otway	CO2CRC	Australia	Natural Dep.	0.1	Depleted Gas Res	2008
Ketzin	CO2Sink	Germany	H_2 Prod.	0.03	Sandstone Res	2008
Decatur	MRCSP	IL, USA	Ethanol Prod	0.3	Brine Res	2009
Gorgon	Chevron Texaco	Australia	Gas Process	3.3	Brine Res	2009
Cranfield	SECARB	Miss, USA	Gas Process	1	Brine Res	2008
Entrada	SWP	CO/WY USA	Gas Process	1.1	Brine Res	2008
TAME	MRCSP	OH, USA	Ethanol Prod	0.28	Sandstone Res	2011

Abbreviations used in Table A1 and Table A2:
EOR = Enhanced Oil Recovery
Gas Process = Gas Processing
Coal Gas = Coal Gassification
LNG Process = Liquid Natural Gas Processing
Natural Dep = Natural Deposit
H_2 Prod = Hydrogen Gas Production
Brine Res = Brine Reservoir
Depleted Gas Res = Depleted Gas Reservoir
Depleted Oil Re s= Depleted Oil Reservoir
Sandstone Res = Sandstone Reservoir
TBD = To Be Decided

Appendix B Emission Factors for Conventional Coal Combustion

Table B1: Emission factors for bituminous coal combustion (kg/tonne) (Summarised from US EPA, 1998)

Emissions	PC Wall-fired, dry bottom	PC Wall-fired, wet bottom	PC Tangential-fired, dry bottom	PC Tangential-fired, wet bottom	PC, cell burner fired, dry bottom	Cyclone
PM	5A	3.5A	5A	3.5A	5A	2A
PM-10	1.15A	1.3A	1.15A	1.3A	1.15A	0.13A
SO_2	0.95*19S	0.95*19S	0.95*19S	0.95*19S	0.95*19S	0.95*19S
SO_3	0.007*19S	0.007*19S	0.007*19S	0.007*19S	0.007*19S	0.007*19S
S (to fly ash)	0.007*19S	0.007*19S	0.007*19S	0.007*19S	0.007*19S	0.007*19S
S (to bottom ash)	0.036*19S	0.036*19S	0.036*19S	0.036*19S	0.036*19S	0.036*19S
NO	3*0.95	15.5*0.95	5*0.95	7*0.95	15.5*0.95	16.5*0.95
NO_2	3*0.05	15.5*0.05	5*0.05	7*0.05	15.5*0.05	16.5*0.05
N_2O	0.015	0.04	0.04	0.04	0.015	0.045
CO	0.25	0.25	0.25	0.25	0.25	0.25
HCl	0.6	0.6	0.6	0.6	0.6	0.6
HF	0.075	0.075	0.075	0.075	0.075	0.075
CH_4	0.02	0.02	0.025	0.02	0.02	0.005
Total VOC	0.03	0.02	0.03	0.02	ND	0.055

i) A is coal ash weight %;

ii) S is weight % sulphur content of coal as fired. Emission factor would be calculated by multiplying the weight percent sulphur in the coal by the numerical value preceding S. For example, if fuel is 1.2% sulphur, then S = 1.2.

Table B2: Emission factors for subbituminous coal combustion (kg/tonne) (Summarised from US EPA, 1998)

Emissions	PC Wall-fired, dry bottom	PC Wall-fired, wet bottom	PC Tangential-fired, dry bottom	PC Tangential-fired, wet bottom	PC, cell burner fired, dry bottom	Cyclone
PM	5A	3.5A	5A	3.5A	5A	2A
PM-10	1.15A	1.3A	1.15A	1.3A	1.15A	0.13A
SO_2	0.85*17.5S	0.85*17.5S	0.85*17.5S	0.85*19S	0.85*17.5S	0.85*17.5S
SO_3	0.007*17.5S	0.007*17.5S	0.007*17.5S	0.007*19S	0.007*17.5S	0.007*17.5S
S (to fly ash)	0.007*17.5S	0.007*17.5S	0.007*17.5S	0.007*19S	0.007*17.5S	0.007*17.5S
S (to bottom ash)	0.136*17.5S	0.136*17.5S	0.136*17.5S	0.136*19S	0.136*17.5S	0.136*17.5S
NO	3.7*0.95	12*0.95	3.6*0.95	7*0.95	7*0.95	8.5*0.95
NO_2	3.7*0.05	12*0.05	3.6*0.05	7*0.05	7*0.05	8.5*0.05
N_2O	0.015	0.04	0.04	0.04	0.015	0.045
CO	0.25	0.25	0.25	0.25	0.25	0.25
HCl	0.6	0.6	0.6	0.6	0.6	0.6
HF	0.075	0.075	0.075	0.075	0.075	0.075
CH_4	0.02	0.02	0.02	0.02	0.02	0.005
Total VOC	0.03	0.02	0.03	0.02	ND	0.055

i) A is coal ash weight %.
ii) S is weight % sulphur content of coal as fired.

Table B3: Emission factors for lignite combustion (kg/tonne) (Summarised from US EPA, 1998)

Emissions	PC Wall-fired, dry bottom	PC Wall-fired, wet bottom	PC Tangential-fired, dry bottom	PC Tangential-fired, wet bottom	PC, cell burner fired, dry bottom	Cyclone
PM	2.5A	N/A	3.2A	N/A	N/A	3.3A
PM-10	0.91A	N/A	1.15A	N/A	N/A	1.15A
SO_2	0.855*15S	N/A	0.85*15S	N/A	N/A	0.85*15S
SO_3	0.007*15S	N/A	0.007*15S	N/A	N/A	0.007*15S
S (to fly ash)	0.007*15S	N/A	0.007*15S	N/A	N/A	0.007*15S
S (bottom ash)	0.136*15S	N/A	0.136*15S	N/A	N/A	0.136*15S
NO	0.95*3.15	N/A	0.95*3.16	N/A	N/A	0.95*3.17
NO_2	0.05*3.15	N/A	0.05*3.16	N/A	N/A	0.05*3.17
N_2O	ND	N/A	ND	N/A	N/A	ND
CO	0.13	N/A	ND	N/A	N/A	ND
HCl	0.6	N/A	0.6	N/A	N/A	0.6
HF	0.075	N/A	0.075	N/A	N/A	0.075
CH_4	0.02	N/A	0.02	N/A	N/A	0.005
Total VOC	0.02	N/A	0.02	N/A	N/A	0.04

i) A is coal ash weight %;
ii) S is weight % sulphur content of coal as fired;
iii) ND refers to no data.

Appendix C Water Balance Analysis for Landfill Topsoil Cover

Water Balance Analysis for Landfill Topsoil Cover

The water balance analysis spread sheet (Table C1) and calculation procedure are modified from literature (Koerner and Daniel, 1997) and are provided as follows:

Table C1: Spread sheet used for water balance analysis for the cover soil of the landfill (Modified after Koerner and Daniel, 1997)

Row	Parameter	January	February	March	…	December	Total
A	Avg. Monthly Temp (°C)						
B	Monthly Heat Index						
C	Unadjusted Daily Potential Evapotranspiration (UPET), mm						
D	Possible Monthly Duration of Sunlight (N)						
E	Potential Evapotranspiration (PET)						
F	Precipitation (P), mm						
G	Runoff Coefficient (C),m						
H	Runoff (R),m						
I	Infiltration (IN), mm						
J	IN - PET, mm						
K	Accumulated Water Loss (WL), mm						
L	Water Stored (WS), mm						
M	Change in Water Storage (CWS), mm						
N	Actual Evapotranspiration (AET), mm						
O	Percolation (PERC),mm						
P	Check (CK), mm						
Q	Percolation rate (FLUX),m/s						

Row A: Average Monthly Temperature. The average monthly temperature (^{o}C) data are an input.

Row B: Monthly Heat Index (H_m). The monthly heat index is calculated as follows:

$$H_m=(0.2T)^{1.514} \quad (\text{for } T>0^oC) \qquad \text{[Appendix C-1]}$$

$$H_m=0 \quad (\text{for } T\leq 0^oC) \qquad \text{[Appendix C-2]}$$

Where, T is the average monthly temperature from Row A. The monthly values are summed to determine the annual heat index (Ha), which is entered in the far right 'Total' column shown in Table 5.18 in Chapter 5.

Row C: Unadjusted daily potential evapotranspiration (UPET).

Row D: The following formulas are used for obtaining potential evapotranspiration:

$$UPET=0 \quad (\text{for } T\leq 0^oC) \qquad \text{[Appendix C-3]}$$

$$UPET=0.53\ (10T/H_a)^a \quad (\text{for } 0^oC\leq T\leq 27^oC) \qquad \text{[Appendix C-4]}$$

$$UPET= -0.015T^2 +1.093T -14.28 \ (\text{for } T\geq 27^oC) \qquad \text{[Appendix C-5]}$$

Where T is the temperature in ^oC, Ha is the dimensionless annual heat index, is a dimensionless empirical factor that is computed as follows:

$$a=(6.75\times 10\text{-}7)\ H_a^3 - (7.71\times 10\text{-}5)\ H_a^2 + 0.01792\ H_a + 0.49239 \qquad \text{[Appendix C-6]}$$

Row D: Monthly duration of sunlight (N).

The mean possible monthly duration of sunlight (N), corrected for possible amount of sunlight and expressed in unit of 12 hour period, is determined from Table C2.

Row E: Potential Evapotranspiration (PET). The potential evapotranspiration is calculated from multiplying the values in Rows C and D.

Row F: Precipitation (P). The mean monthly precipitation (P) for the site is entered in Row F. if data are not available for the site, data from the nearest appropriate weather station is used.

Because precipitation varies from year to year, the analysis should consider the purpose of the water balance analysis when deciding on monthly precipitation values. If the goal is to estimate the maximum expected percolation through the cover, then data for an unusually wet year should be used. If an estimate of the long-term average percolation is sought, then average monthly precipitation should be used, for instance, by selecting precipitation for a typical year.

Row G: Runoff coefficient (C).

Table C2: Mean possible daily duration of sunlight in the Northern and Southern Hemisphere expressed in units of 30 days of 12 hours each (After Thornthwaite, 1948)

	Jan.	Feb.	Mar.	Apr.	May	June	July	Aug.	Sept.	Oct.	Nov.	Dec.
°N. Lat.												
0	1.04	.94	1.04	1.01	1.04	1.01	1.04	1.04	1.01	1.04	1.01	1.04
5	1.02	.93	1.03	1.02	1.06	1.03	1.06	1.05	1.01	1.03	.99	1.02
10	1.00	.91	1.03	1.03	1.08	1.06	1.08	1.07	1.02	1.02	.98	.99
15	.97	.91	1.03	1.04	1.11	1.08	1.12	1.08	1.02	1.01	.95	.97
20	.95	.90	1.03	1.05	1.13	1.11	1.14	1.11	1.02	1.00	.93	.94
25	.93	.89	1.03	1.06	1.15	1.14	1.17	1.12	1.02	.99	.91	.91
26	.92	.88	1.03	1.06	1.15	1.15	1.17	1.12	1.02	.99	.91	.91
27	.92	.88	1.03	1.07	1.16	1.15	1.18	1.13	1.02	.99	.90	.90
28	.91	.88	1.03	1.07	1.16	1.16	1.18	1.13	1.02	.98	.90	.90
29	.91	.87	1.03	1.07	1.17	1.16	1.19	1.13	1.03	.98	.90	.89
30	.90	.87	1.03	1.08	1.18	1.17	1.20	1.14	1.03	.98	.89	.88
31	.90	.87	1.03	1.08	1.18	1.18	1.20	1.14	1.03	.98	.89	.88
32	.89	.86	1.03	1.08	1.19	1.19	1.21	1.15	1.03	.98	.88	.87
33	.88	.86	1.03	1.09	1.19	1.20	1.22	1.15	1.03	.97	.88	.86
34	.88	.85	1.03	1.09	1.20	1.20	1.22	1.16	1.03	.97	.87	.86
35	.87	.85	1.03	1.09	1.21	1.21	1.23	1.16	1.03	.97	.86	.85
36	.87	.85	1.03	1.10	1.21	1.22	1.24	1.16	1.03	.97	.86	.84
37	.86	.84	1.03	1.10	1.22	1.23	1.25	1.17	1.03	.97	.85	.83
38	.85	.84	1.03	1.10	1.23	1.24	1.25	1.17	1.04	.96	.84	.83
39	.85	.84	1.03	1.11	1.23	1.24	1.26	1.18	1.04	.96	.84	.82
40	.84	.83	1.03	1.11	1.24	1.25	1.27	1.18	1.04	.96	.83	.81
41	.83	.83	1.03	1.11	1.25	1.26	1.27	1.19	1.04	.96	.82	.80
42	.82	.83	1.03	1.12	1.26	1.27	1.28	1.19	1.04	.95	.82	.79
43	.81	.82	1.02	1.12	1.26	1.28	1.29	1.20	1.04	.95	.81	.77
44	.81	.82	1.02	1.13	1.27	1.29	1.30	1.20	1.04	.95	.80	.76
45	.80	.81	1.02	1.13	1.28	1.29	1.31	1.21	1.04	.94	.79	.75
46	.79	.81	1.02	1.13	1.29	1.31	1.32	1.22	1.04	.94	.79	.74
47	.77	.80	1.02	1.14	1.30	1.32	1.33	1.22	1.04	.93	.78	.73
48	.76	.80	1.02	1.14	1.31	1.33	1.34	1.23	1.05	.93	.77	.72
49	.75	.79	1.02	1.14	1.32	1.34	1.35	1.24	1.05	.93	.76	.71
50	.74	.78	1.02	1.15	1.33	1.36	1.37	1.25	1.06	.92	.76	.70
° S. Lat.												
5	1.06	.95	1.04	1.00	1.02	.99	1.02	1.03	1.00	1.05	1.03	1.06
10	1.08	.97	1.05	.99	1.01	.96	1.00	1.01	1.00	1.06	1.05	1.10
15	1.12	.98	1.05	.98	.98	.94	.97	1.00	1.00	1.07	1.07	1.12
20	1.14	1.00	1.05	.97	.96	.91	.95	.99	1.00	1.08	1.09	1.15
25	1.17	1.01	1.05	.96	.94	.88	.93	.98	1.00	1.10	1.11	1.18
30	1.20	1.03	1.06	.95	.92	.85	.90	.96	1.00	1.12	1.14	1.21
35	1.23	1.04	1.06	.94	.89	.82	.87	.94	1.00	1.13	1.17	1.25
40	1.27	1.06	1.07	.93	.86	.78	.84	.92	1.00	1.15	1.20	1.29
42	1.28	1.07	1.07	.92	.85	.76	.82	.92	1.00	1.16	1.22	1.31
44	1.30	1.08	1.07	.92	.83	.74	.81	.91	.99	1.17	1.23	1.33
46	1.32	1.10	1.07	.91	.82	.72	.79	.90	.99	1.17	1.25	1.35
48	1.34	1.11	1.08	.90	.80	.70	.76	.89	.99	1.18	1.27	1.37
50	1.37	1.12	1.08	.89	.77	.67	.74	.88	.99	1.19	1.29	1.41

From: C. W. Thornthwaite, "An Approach Towards an International Classification of Climate," *Geophysical Review*, vol. XXXVIII, 1948, pp. 55-94.

Table C3: Comparison of runoff coefficients for drainage areas with different topography, soil, and cover conditions (After Blakey, 1992)

Area type	Runoff coefficient C											
	Flat (slope<2%)				Rolling (slope 2-10%)				Hilly (slope >10%)			
Reference	1	2	3	Average	1	2	3	Average	1	2	3	Average
Bare earth (clay)	0.6	0.6	0.6	0.6	0.66	0.7	0.7	0.69	0.7	0.82	0.8	0.77
Bare earth (silt loam)	-	0.5	0.5	0.5	-	0.6	0.6	0.6	-	0.72	0.7	0.71
Meadows and pasture (clay or silt loam)	0.25	0.3	0.35	0.3	0.3	0.36	0.45	0.37	0.35	0.42	0.55	0.44
Cultivated (impermeable clay)	0.5	0.4	0.5	0.47	0.55	0.55	0.6	0.57	0.6	0.6	0.7	0.63
Cultivated (permeable sandy loam)	0.25	0.1	0.2	0.18	0.3	0.16	0.3	0.25	0.35	0.22	0.4	0.32

1.Perry, P.H. 1976, Engineering Manual, 3rd edition. McGraw-Hill Book Co., New York, 946 pp.
2. Salvato, J.A. et al. 1971, Sanitary landfill leaching prevention and control. JWPCF, 46, 2084-2100.
3. Berbard, M. 1982, Discussion of runoff: Rational runoff cumulus. Trans. Am. Soc. Civil Eng., 96

The runoff coefficient can vary widely and is very difficult to predict accurately, in large part because of the dearth of data on actual runoff from landfill covers. The dimensionless runoff coefficient, C, defined as the ratio of runoff to precipitation, is used to estimate surface runoff. The guidance by Blakey (1992), is summarised in Table C3, recommending appropriate values for the runoff coefficient on the basis of site-specific or region-specific information.

Row H: Runoff (R). Runoff is calculated from precipitation (P) and the runoff coefficient (C):

$$R=P\times C \qquad \text{[Appendix C-7]}$$

Row I: Infiltration (IN). The monthly infiltration (IN), which is defined as the amount of water entering the surface of the cover, is summed to equal precipitation minus runoff:

$$IN=P-R \qquad \text{[Appendix C-8]}$$

Row J: Infiltration minus potential evapotranspiration (IN-PET). A positive number indicates potential accumulation of water. A negative number represents that soil is drying.

Row K: Accumulated water loss (WL).

If the value of IN-PET is ≥0, then enter the value of WL from the previous month into row K for the month being analysed.

If the value of IN-PET is negative, then add this negative value to the WL from the previous month and enter in row K.

Row L: Water stored in the root zone (WS). The water stored in the root zone (WS) is defined as the amount of water (in millimetres) stored in that portion of the cover soil that can be tapped by plant root for evapotranspiration. The cover soil is defined as the soil from the ground surface down to the top of the drainage layer.

To compute the values of water stored in the root zone (WS) for row L, first pick a month to start the calculation. Any month can be chosen for which the water stored is known or can be estimated. If it will be assumed that soil is at field capacity at the end of the spring, then select the last month (usually in the late spring) for which IN-PET is

greater than 0 and assume that the water stored is equal to the water stored at field capacity, in units of mm of water stored. Enter this number in Row L.

1. If (IN-PET) is negative, then the soil in the root zone will dry during the month of interest. The actual amount if soil moisture retained depends on the amount of potential evapotranspiration (i.e., the value of IN-PET) and the water storing capacity of the soil (WSmax). The amount of water that actually evaporates will be less than (IN-PET), and the drier soil becomes, the more difficult it becomes to evaporate water from the soil. Compute the water stored (WS) for a given month as follows (Thornthwaite and Mather, 1975):

$$WS=(WSmax)10^{b(IN\text{-}PET)} \qquad \text{[Appendix C-9]}$$

where WS and WSmax have units of mm, b is a coefficient determined as follows:

$$b= 0.455/(WSmax) \qquad WSmax=\sum\theta_{i,\ field\ capacity}\ (H_{root})_I \qquad \text{[Appendix C-10]}$$

where $\theta_{i,\ field\ capacity}$ is the volumetric water content at field capacity for the i-th layer. If no detail information is available on field capacity, the values shown in Table C4 are used.

Table C4: Volumetric Water Contents of Various Soils (After Thornthwaite and Mather, 1957; and Fenn *et al.*, 1975)

Type of Soil	θ at Field Capacity	θ at Wilting Point	Available Water
Fine Sand	0.12	0.02	0.1
Sandy Loam	0.2	0.05	0.15
Silty Loam	0.3	0	0.2
Clay Loam	0.375	0.125	0.25
Clay Loam	0.45	0.15	0.3

2. If (IN-PET) is positive, add the IN – PET value for current month to the value of water stored (WS) for the previous month. However, the amount of water stored cannot exceed WSmax, and if the computed value greater than WSmax, enter the value of WSmax in Row L for the month.

If the soil is found to be at field capacity in the last calculation month (i.e. the month before the month used to start the calculation process), then the assumption of starting at field capacity is validated. If not, it is possible to iterate and try a different initial water storage until the computed value in the starting month is the same as the assumed value.

Row M: Change in water storage (CWs).

Start with the same month used to initiate the process of calculating water storage in the root zone (WS) and enter 0 for the change in water storage (CWs) for that month. Then

proceed with each subsequent month. The change in water stored in the previous month. The sign is important: CWS is negative if the soil in the root zone is losing water and positive if it is gaining water.

Row N: Actual Evapotranspiration (AET). The actual evapotranspiration depends on whether infiltration exceeds potential evapotranspiration.

1.If IN-PET≥0, AET=PET for that month.

2. If IN-PET<0:

$$AET = IN - CWS \qquad \text{[Appendix C-11]}$$

Row O: Percolation (PERC). Percolation (PERC) is the amount of water draining from the root zone and is calculated as follows:

1. For month in which IN-PET is less than or equal to zero, there is no percolation:

$$PERC = 0 \qquad \text{[Appendix C-12]}$$

2. For month in which IN-PET is greater than zero:

$$PERC = (IN - PET) - CWS \qquad \text{[Appendix C-13]}$$

The monthly percolation should be summed to obtain the annual amount of percolation.

Row P: Check of calculations (CK). The whole idea behind “Water balance” is to account for all of the precipitation that falls on the cover. The calculations may be checked as follows. For each month compute the value of CK as follows:

$$CK = PERC + AET + CWS + R \qquad \text{[Appendix C-14]}$$

Sum the monthly values. Each monthly value, and the yearly total, of C should equal precipitation P. Check to make sure that Row P equals Row F for each column.

Row Q: Percolation rate (Flux). The rate percolation, which is the flux of water passing through the cover soil, should be computed for months in which PERC>0 and noted in Row Q in units of m/s. The Flux is computed as follows:

$$Flux = (PERC * 0.001)/t \qquad \text{[Appendix C-15]}$$

Where PERC is the percolation in units of mm from Row O and t is the number of seconds in the month.

Appendix D Life Cycle Inventory Data of Upstream Processes

Upstream processes include coal production, (underground mining and open-pit mining) coal transportation, limestone production, limestone transport by truck, MEA production, MEA transport by truck, ammonia production, ammonia transport by truck, power plant infrastructure, CO_2 pipeline infrastructure, CO_2 capture facility infrastructure, and compressor infrastructure. The sources of upstream LCI data are described in Table D1. The Table D2 to Table D7 list the LCI data for some upstream processes. The procedures of generating LCI data by GaBi LCA software for upstream processes are demonstrated in Figure D1 to Figure D9.

Table D1: Sources of upstream life cycle inventory data

Name of upstream process	**Souce of data**
Underground coal mining	GaBi v.4
Open-pit coal mining	
MEA production	Collected material consumption from the literature and calculated using GaBi v.4
Ammonia production	GaBi v.4
Limestone production	
Coal transportation by railway	Calculated using GaBi v.4
Road transportation (lorry) for MEA, limestone and ammonia	
Construction of power plant	Collected material consumption from the literature and calculated using GaBi v.4
Construction of MEA capture facility	
Construction of CO_2 conditioning facility	
Construction of Air Separation Unit (ASU)	
Construction of CO_2 pipeline facility	
Construction of CO_2 injection facility	

Table D2: LCI data for CO_2 capture infrastructure (After Koornneef, 2008)

Material/process	Amount	Unit
Steel (absorber+stripper)	225	t
Steel (piping and small equipment)	82	t
Concrete	1	m^3
Transport	9.5	kt×km
Lifetime	30	Year
Total CO_2 capture over lifetime	94	Mt

Note: All steel is assumed to be high alloyed steel for support of piping and small equipment only.

Table D3: LCI data for pulverised coal power plant infrastructure (After Röder *et al.*, 2004; Koornneef, 2008)

Material/process	Amount	Unit
Diesel and fuel oil	462	Tj
Electricity (UCPTE)*	15	GWh
Concrete	62,600	t
Rock wool	571	t
Aluminium	332	t
Steel**	44,801	t
Copper	710	t
Polyethylene	401	t
Waste to disposal	145,972	t
Transport	14,040,000	t×km
Lifetime	30	Year

*UCPTE represents the average electricity generated in Austria, Belgium, France, Germany, Greece, Italy, former Yugoslavia, Luxembourg, the Netherlands, Portugal, Spain, and Switzerland.
**Steel composition 90% un-alloyed, 9% low alloyed and 1% high alloyed.

Table D4: LCI data for CO_2 compressor infrastructure (After Emmenegger *et al.*, 2003; Koornneef, 2008)

Material/Process	Amount	Unit
Concrete	65	m3
Diesel and heavy fuel oil	1978	Gj
Electricity (UCPTE)	61	MWh
Steel*	65	t
Copper	7	t
Polyethylene	20	t
Compressor capacity	40	MW
Lifetime	20	yt
Total CO_2 compressed over lifetime	62	Mt
Total leakage of CO_2 over lifetime	18	kt

Note: Transport is implicitly included in energy consumption. Diesel and recycling are not included.
*Steel comprises 5% high alloyed and 95% low alloyed.

Table D5: LCI data for onshore CO_2 pipeline infrastructure related to 1,000 kg of CO_2 transported (After Emmenegger *et al.*, 2003; Koornneef, 2008)

Material/process	Amount	unit
Sand	1.0372	kg
Diesel for construction	1.7606	MJ
Reinforcing steel	0.1277	kg
Drawing of steel pipes	0.1277	kg
Bitumen	1.23E-03	kg
Polyethylene	2.47E-03	kg
Transport total	121.4362	kg×km
Total disposal of wastes*	0.5914	kg

*It is assumed, after that 50% of the pipeline materials are removed and disposed off, and that the other 50% remains in the ground.

Table D6: LCI data for CO_2 injection facility (After Koornneef, 2008)

Material/process	Amount	Unit
Well construction*	18	km
Sand	712,000	t
Steel(un-alloyed)	3,800	t
Steel (high alloyed steel)	8,100	t
Concrete	10,463	m3
Transport (truck)	74,922,800	t×km
Copper (for cables)**	425	t
lifetime	30	Year
Total injection capacity over lifetime	219	Mt

Note: Energy use during construction of the surface facility is not included. The dismantling and disposal phases are also not included.
*Assuming six wells with a depth of 3,000 m.
**Assuming 1,000 kg copper/km cable, which is a value in the midrange of specific cable weights. These cables are for the transport of data and electricity.

Table D7: LCI data for MEA production (After Althaus *et al.*, 2004; Koornneef, 2008)

Material/process	Amount	Unit
Input:		
Ethylene oxide	816	g
Ammonia	788	g
Electricity	0.333	Kwh
Natural gas	2	MJ
Transport (truck and train)	11.23	t×km
Infrastructure chemical plant	4×10^{10}	p
Output:		
Monoethanolamine	1	kg
Waste heat	1.2	MJ
Ethylene oxide to air	1.63	g
Ethylene oxide to water	1.47	g
Ammonia to air	1.58	g
Ammonium to water	3.04	g
CO_2	26.5	g
Nitrate (NO_3) to water	6.97	g
COD, BOD	21.3	g
TOC, DOC	8.02	g

Note: COD=chemical oxygen demand, BOD = biological oxygen demand, TOC = total organic carbon , DOC= dissolved organic carbon. Solid wastes are not included.

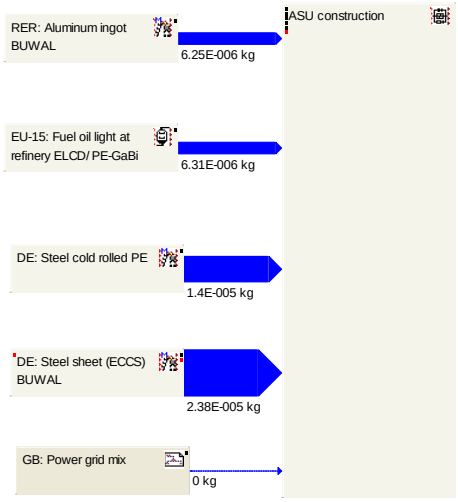

Figure D1: The designed ASU construction LCI data generation procedure by using the GaBi v.4 software

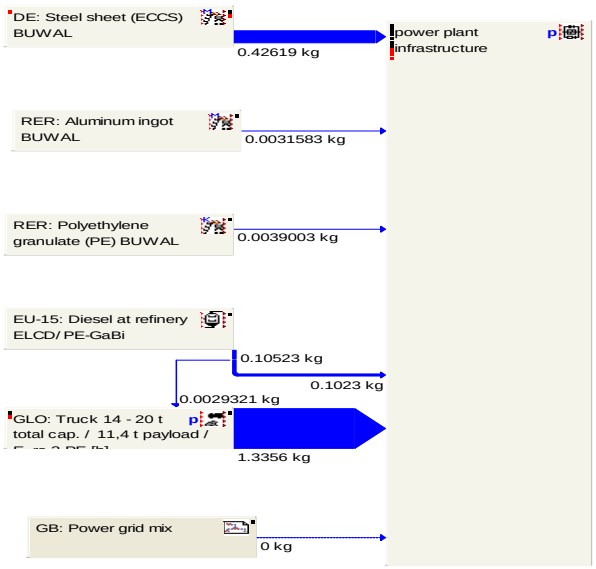

Figure D2: The designed power plant construction LCI data generation procedure by using the GaBi v.4 software

Figure D3: The CO_2 capture facility construction LCI data generation procedure by using the GaBi v.4 software

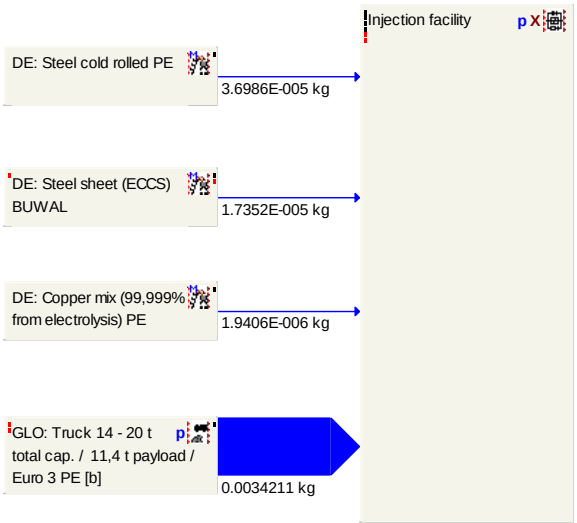

Figure D4: The CO_2 injection facility construction LCI data generation procedure by using the GaBi v.4 software

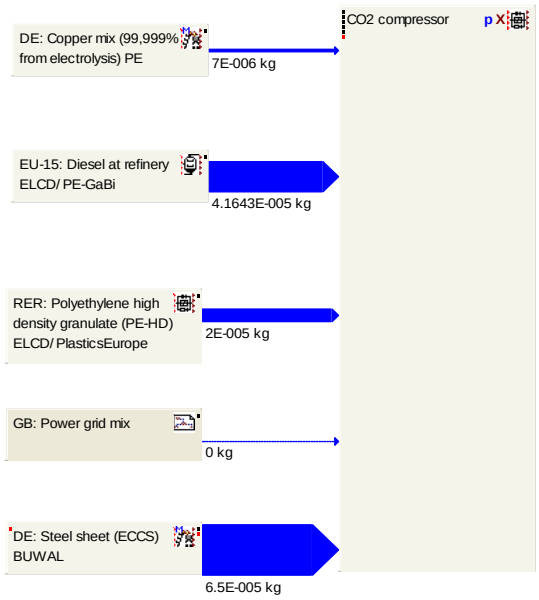

Figure D5: The CO_2 compressor construction LCI data generation procedure by using the v.4 GaBi software

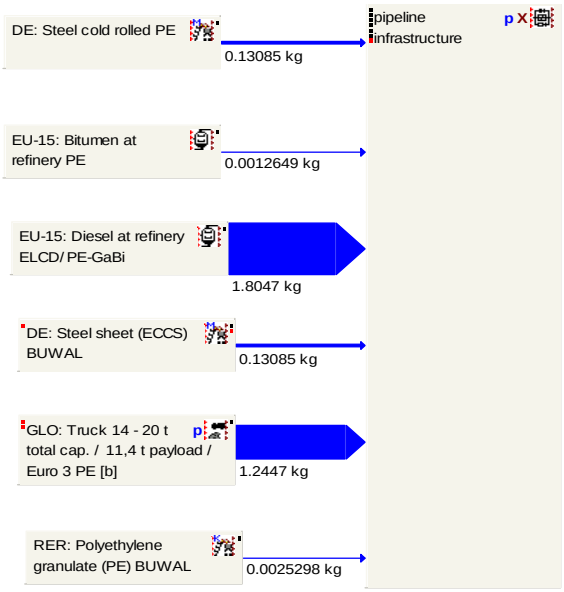

Figure D6: The CO_2 transport pipeline construction LCI data generation procedure by using the GaBi v.4 software

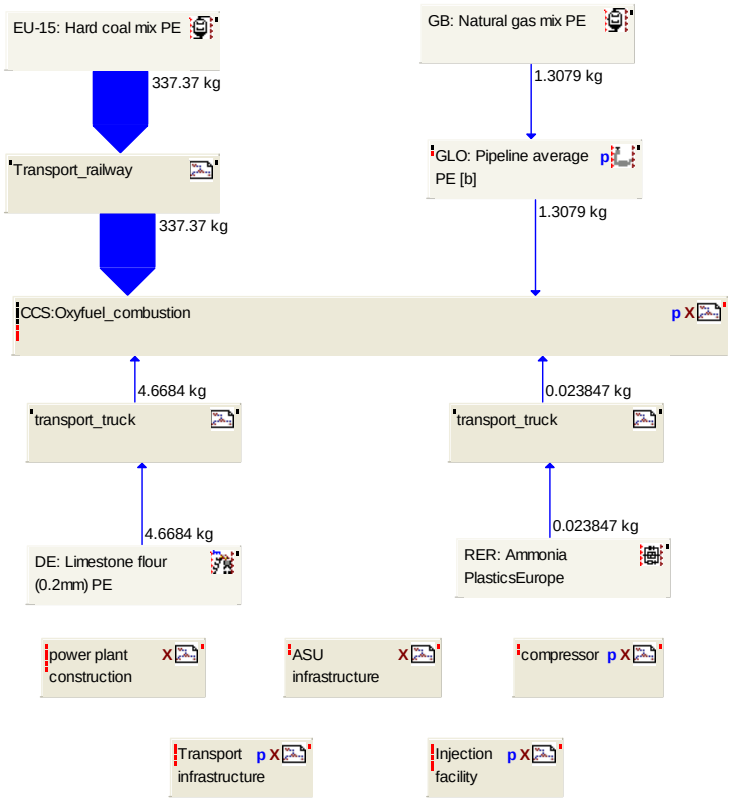

Figure D7: The LCI data generation procedure designed for oxyfuel combustion power plant upstream processes by using the GaBi v.4 software

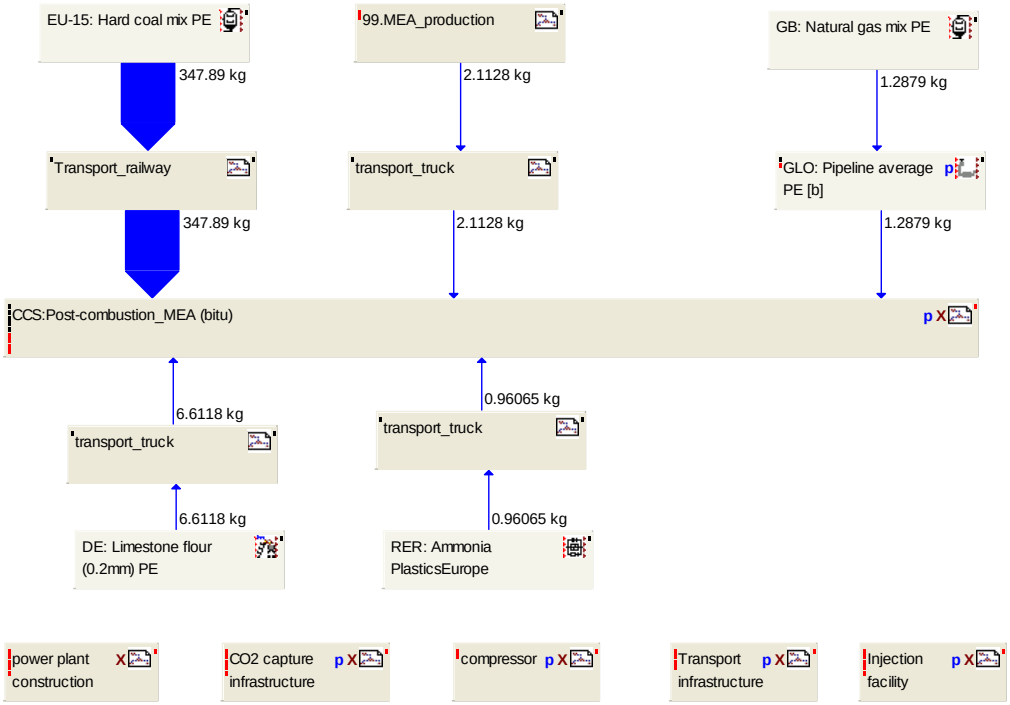

Figure D8: The LCI data generation procedure designed for post-combustion power plant upstream processes by using the GaBi v.4 software

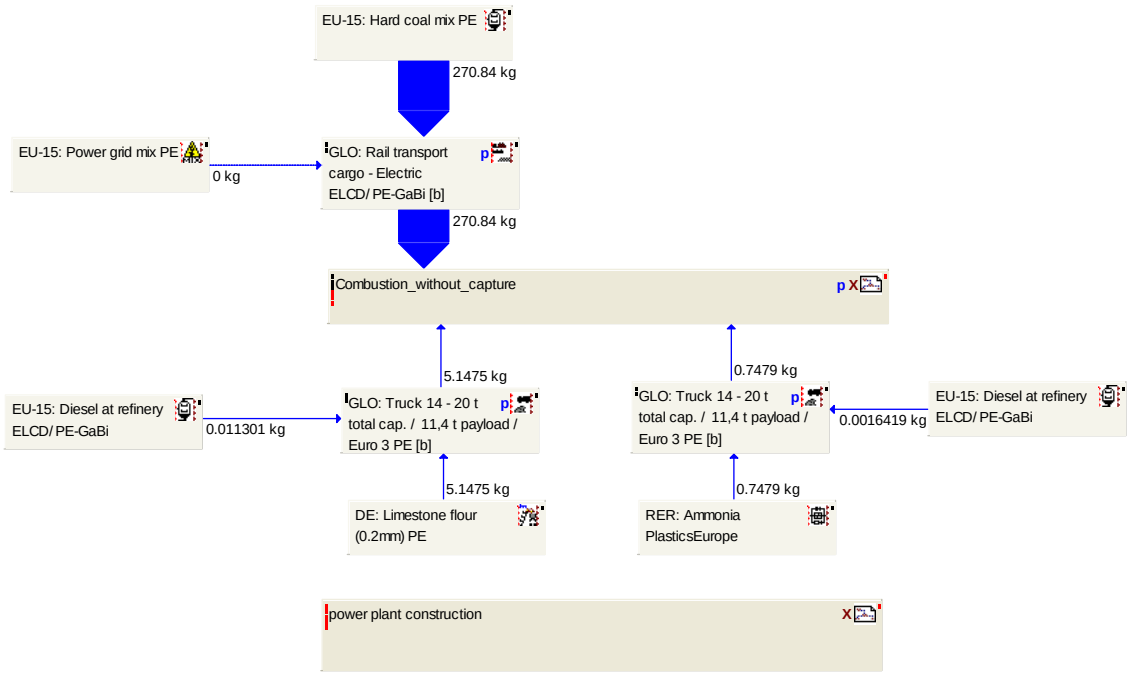

Figure D9: The LCI data generation procedure designed for conventional combustion power plant upstream processes by using the GaBi v.4 software

Appendix E Parameters and Data Relating to Post-Combustion Carbon Dioxide Capture Life Cycle Assessment Results

Table E1: Extract of the key parameters table used in LCI models of power generation with post-combustion CO_2 capture with MEA, transport and injection and the standard deviation of the parameters used for the uncertainty assessment.

Process	Parameter	Base case scenario	+standard deviation (% of base scenario value)
Combustion process	Antimony (Sb) in coal (kg/kg coal)	1.00E-06	200%
	Arsenic (As) in coal (kg/kg coal)	1.00E-05	200%
	…		
	Sulphur (S) in coal (kg/kg coal)	0.0064	20%
	Heating value of coal (Btu/lb)	13080	5%
	Carbon (C) in coal (kg/kg coal)	0.714	5%
	Ash in coal (kg/kg coal)	0.0979	5%
	…..		
	Emission factor of Cu to fly ash	0.5	20%
	.....		
	Calcium in ash	0.0002	10%
SCR	NH_3 to NOx ratio	0.8	1%
ESP	...		
	Thallium removal rate	0.98	2%
	Vanadium removal rate	0.98	2%
	Zinc removal rate	0.98	2%
FGD	...		
	HCl removal rate	0.9	5%
	HF removal rate	0.7	5%
	...		
MEA capture	…		
	SO_2 removal rate	0.995	0.50%
	SO_3 removal rate	1	0%
Landfill with composite cover	Angle of cover (degree)	3	5%
	Landfill depth (m)	13	20%
	...		
	October average temperature (^oC)	10.9	20%
	September average temperature (^oC)	16.6	20%
	waste-concentration-to-leachate-concentration ratio		
	Antimony	10,000	20%
	Arsenic	1,200	20%
	…		
	kg/m^3; solid waste density	1,360	5%
	m; Landfill width	574.34	20%
Ash pond (single liner)	**waste-concentration-to-leachate-concentration ratio**		
	Antimony	10,000	20%
	Arsenic	1200	20%
	…		
	Thickness of liner (m)	0.5	10%
	Ponding depth of waste water in the surface impoundment unit (m)	6.1	20%
	foot print of surface impoundment (m^2)	364,230	20%
CO_2 injection	Surface temperature (^oC)	20	20%
	Thickness of reservoir (m)	171	30%

Table E2: Constituents of coals used in this research

Constituents	Bituminous coal					Lignite (brown coal)	Sub-bituminous
	Appalachian Low Sulphur (with typical trace metal concentration)	Australia N.S. Wales	Poland	S. Africa Transvaal	Illinois No. 6 (trace metals with artithmetic mean)	South Australia Leigh Creek Range	Western Australia Range
Carbon (C)	71.40%	64.00%	55.70%	65.00%	63.75%	37.50%	48.1 – 52.7
Hydrogen (H)	4.62%	4.00%	4.40%	4.00%	4.50%	2.34%	2.1 – 3.4%
Oxygen (O)	6.09%	6.09%	6.09%	6.09%	6.88%	6.88%	6.88%
Chlorines (Cl)	0.07%	0.07%	0.07%	0.07%	0.29%	0.0370 – 0.125 %	<0.005 - 0.023%
Sulphur (S)	0.64%	0.30%	0.90%	0.60%	2.51%	0.2-0.3%	0.3 –0.9%
Nitrogen (N)	1.42%	1.40%	1.10%	1.60%	1.25%	0.65%	0.8 – 0.9%
Ash/Inerts	9.79%	11.14%	24.24%	14.64%	9.70%	20.60%	2.5 – 10.0%
Moisture	5.63%	13.00%	7.50%	8.00%	11.12%	26.20%	22.0 – 29.0%
HHV (btu/lb)	13,080	10,854	9,926	11,240	11,666	6105	8598
Trace metals (ppm)							
Antimony (Sb)	1	1.7	1	1.00	1	0.2 – 1.9	<1 - 2
Arsenic (As)	10	55	40	8.2	7.5	0.5 – 4.4	<1 - 2
Beryllium (Be)	2	8	10	2.00	1.2	<0.7 - 1.1	<1 - 3
Cadmium (Cd)	0.52	0.2	4	0.52	0.5	0.05 - 0.08	0.1 - 1.4
Chromium (Cr)	20	30	12	63	14	4 - 60	1--10
Cobalt (Co)	5	30	50	14	3.5	<1.5 - 18	18--2
Lead (Pb)	40	60	150	25	24	<1.5 - 37	<1 - 10
Manganese (Mn)	70	900	70	180	38	<1.5 - 370	<1 - 43
Nickel (Ni)	20	70	30	32	14	3--44	ND
Selenium (Se)	1	2.5	1	0.9	1.9	<0.4 – 0.7	ND
Zinc (Zn)	50	73	300	16	84.4	11 - 150	1 - 72
Copper (Cu)	15	40	150	16	9.2	2 - 44	13--1
Thallium (Tl)	1	0.2	1	1	1	0.2	0.2
Vanadium (V)	40	90	180	43	31	4-90	4-90
Barium (Ba)	200	1,000	200	474	18.52	40-1,000	40-1,000
Silver (Ag)	0.1	1.00	0.1	0.1	0.1	0.2-1	0.2-1
Mercury (Hg)	0.1	0.4	0.1	0.1	0.09	0.09-0.20	0.02-0.1

Table E3: Extract of the calculations of direct emissions of power plant with post-combustion CO_2 capture, transport and injection (kg per MWh electricity generated)

	Unit		Post-combustion power generation with CO_2 capture							Waste treatment		Transportation	Storage	
		Total	Coal combustion	SCR	ESP	FGD	CO_2 capture	CO_2 conditioning	Stack	Surface Impoundment	Landfill	Pipeline	Injection	Saline aquifer storage
Resources required:														
Coal	kg/MWh	347.89	347.89											
Natural gas	m3/MWh	1.63						0.0223				1.2385	0.3662	
Limestone	kg/MWh	6.61				6.61								
Ammonia	kg/MWh	0.93		0.93										
MEA	kg/MWh	2.04					2.04							
Energy consumption equivalence*	kWh/MWh	351.79	2.55	3.05	7.55	15.66	221.04	84.99				13.07	3.87	
Solid wastes	kg/MWh	34.77	17.03		16.97	0.69	0.09							
Liquid wastes	kg/MWh	2.11				2.07	0.04							
Emissions to Atmosphere:														
CO_2	kg/MWh	4.86E+01						0.04	45.08			2.45E+00	7.62E-01	
PM	kg/MWh	4.72E-03							4.72E-03			3.84E-04		
PM-10	kg/MWh	4.58E-03						2.71E-06	4.34E-03			3.84E-04	4.46E-05	
SO_2	kg/MWh	1.00E-03						2.14E-07	9.97E-04			3.70E-07	3.56E-06	
SO_3	kg/MWh	0.00E+00												
NO	kg/MWh	4.58E-01							4.58E-01					
NO_2	kg/MWh	1.81E-02							1.81E-02			4.47E-02		
……..														
Emissions to soil:														
Antimony (Sb)	kg/MWh	3.65E-08								3.63E-08	1.33E-10			
Arsenic (As)	kg/MWh	2.77E-06								2.74E-06	1.02E-08			
….														

*** : Energy consumption equivalence means that all the energy consumption estimates are converted to kWh, e.g. converted from kJ to kWh.**

Table E4: Extract of the calculations of life cycle emissions of power plant with post-combustion CO_2 capture, transport and injection (kg per MWh electricity generated).

Type of emissions (or Resources)		Emissions (or resources)	Total	Post-combustion CCS (MEA)	Upstream processes													
					Hard coal production (EU-15 mix)	Coal transport railway	MEA production	MEA transport truck	Limestone transport truck	Limestone Production	Ammonia transport truck	Ammonia Production	Natural gas production (GB mix)	CO_2 capture infrastructure	Compressor infrastructure	Injection infrastructure	Power plant construction	Transport infrastructure
Energy and Material Resources	Energy resources	Crude oil (resource)	9.505494	0	5.448331	0.026929	1.669811	0.00516	0.016147	0.006025	0.002346	0.055141	0.00382	0.000222	0.077106	0.004765	0.161134	2.028556
		Hard coal (resource)	352.4548	0	351.2464	0.117374	0.13095	2.24E-05	6.99E-05	0.0079	1.02E-05	0.035538	0.005238	0.003049	0.091984	0.047863	0.513162	0.255227
		Lignite (resource)	2.836084	0	2.567273	0.154374	2.00E-07	2.20E-05	6.88E-05	0.025226	1.00E-05	6.27E-08	0.000108	0.000272	0.009294	0.004206	0.046429	0.0288
		…..																
	Material resources	Chromium	1.66E-12	0	0	0	1.29E-12	0	0	0	0	3.55E-13	0	0	2.09E-14	0	0	0
		Copper	1.10E-10	0	0	0	3.47E-11	0	0	0	0	9.60E-12	0	0	6.56E-11	0	0	0
		Iron	0.00042	0	2.20E-10	7.02E-12	0.000393	2.90E-15	9.06E-15	8.37E-11	1.32E-15	2.29E-05	7.47E-13	0	3.57E-06	5.47E-09	6.67E-14	1.71E-08
		…..																
		Zinc - lead - copper ore (12%-3%-2%)	0.057908	0	0.000116	6.96E-06	0	6.56E-08	2.05E-07	6.35E-07	2.98E-08	0	5.27E-06	0	0.045216	0.012535	1.49E-06	2.62E-05
		Zinc - lead ore (4.21%-4.96%)	5.35E-16	0	0	1.98E-16	0	5.88E-19	1.84E-18	7.44E-18	2.67E-19	0	4.79E-17	0	1.76E-17	6.32E-18	1.34E-17	2.42E-16
		Zinc ore (sulphide)	3.49E-13	0	3.28E-13	7.28E-15	0	2.81E-17	8.79E-17	4.62E-16	1.28E-17	0	3.51E-16	0	3.81E-16	1.14E-16	6.39E-16	1.13E-14
Emissions to air	Heavy metal emissions to air	Antimony	4.82E-07	1.66E-08	4.56E-07	7.24E-09	6.41E-15	2.00E-12	6.27E-12	3.18E-10	9.11E-13	2.31E-15	3.87E-10	0	1.01E-09	1.51E-10	6.13E-11	9.77E-10
		Arsenic	9.59E-06	7.57E-06	1.92E-06	6.57E-08	1.75E-10	4.93E-11	1.54E-10	1.84E-09	2.24E-11	1.42E-11	2.82E-09	0	7.89E-09	1.27E-09	1.23E-09	2.10E-08
		….																
	Inorganic emissions to air	Ammonia	0.127391	0.122626	0.001375	3.77E-06	0.003362	1.24E-07	3.89E-07	1.54E-06	5.65E-08	1.36E-05	1.46E-07	6.08E-09	5.68E-07	4.99E-07	1.30E-06	7.01E-06
		Ammonium	9.96E-11	0	8.32E-11	1.35E-11	0	1.72E-15	5.40E-15	1.54E-12	7.84E-16	0	7.57E-14	0	2.42E-13	7.30E-14	4.26E-14	8.42E-13
		….																
	Organic emissions to air (group VOC)	Organic emissions to air (group VOC)	3.137117	0.091086	2.973052	0.00164	0.042294	2.69E-05	8.42E-05	0.000163	1.22E-05	0.009141	0.002551	3.03E-05	0.001487	0.000327	0.005655	0.009567
	Organic emissions to air	Group NMVOC to air	0.118134	0.083945	0.027502	0.000119	0.003678	1.12E-05	3.49E-05	3.49E-05	5.07E-06	1.01E-06	0.000218	2.65E-06	0.000121	4.20E-05	0.000627	0.001792
		….																
	Other emissions to air	Exhaust	66.47702	0	61.64545	3.524762	0	0.00085	0.00266	0.248717	0.000386	0	0.109013	0	0.291195	0.09076	0.023488	0.539733
		….																
	Particles to air	Dust (combustion)	0.000179	0.000179	0	0	0	0	0	0	0	0	0	0	0	0	0	0
		Dust (PM10)	0.007412	0.004341	0.0015	1.06E-05	0.001223	9.12E-08	2.85E-07	2.58E-06	4.15E-08	0.000278	1.99E-06	0	1.54E-05	6.37E-07	2.08E-06	3.69E-05
		….																

Continued

Type of emissions (or Resources)		Emissions (or resources)	Total	Post-combustion CCS (MEA)	Upstream processes												
					Hard coal production (EU-15 mix)	Coal transport railway	MEA production	MEA transport truck	Limestone transport truck	Limestone Production	Ammonia transport truck	Ammonia Production	Natural gas production (GB mix)	CO_2 capture infrastructure	Compressor infrastructure	Injection infrastructure	Power plant construction	Transport infrastructure
Emissions to fresh water	Analytical measures to fresh water	Adsorbable organic halogen compounds (AOX)	6.88E-06	0	4.79E-06	6.53E-08	1.41E-12	3.88E-09	1.21E-08	9.89E-09	1.76E-09	2.80E-13	1.70E-08	1.32E-09	7.37E-08	1.23E-08	3.09E-07	1.58E-06
		Biological oxygen demand (BOD)	0.000184	0	2.88E-05	3.74E-07	3.37E-05	1.81E-08	5.66E-08	5.54E-08	8.22E-09	1.64E-07	1.82E-08	4.36E-07	1.21E-05	3.44E-06	7.35E-05	3.09E-05
		Chemical oxygen demand (COD)	0.054731	0	0.007186	0.000185	0.046246	3.71E-07	1.16E-06	1.59E-05	1.69E-07	0.000584	8.19E-06	1.19E-06	5.37E-05	1.44E-05	0.000211	0.000223
		Solids (dissolved)	0.0007	0	0.000113	1.81E-05	0.000369	2.64E-09	8.25E-09	8.37E-07	1.20E-09	0.000196	2.88E-07	0	1.07E-06	7.76E-08	7.18E-08	1.19E-06
		Total dissolved organic bounded carbon	2.88E-05	0	0	4.35E-11	2.73E-05	6.24E-17	1.95E-16	4.08E-12	2.84E-17	8.28E-08	4.06E-15	4.28E-09	3.39E-07	2.97E-08	8.02E-07	2.69E-07
		Total organic bounded carbon	0.017204	0	0.000125	8.99E-07	0.016945	7.87E-08	2.46E-07	9.96E-08	3.58E-08	0	1.18E-07	3.82E-07	1.07E-05	2.79E-06	6.80E-05	5.08E-05
	Heavy metals to fresh water	Antimony	7.69E-13	0	6.76E-13	7.33E-14	0	1.91E-17	5.97E-17	1.61E-15	8.67E-18	0	2.58E-16	0	4.03E-15	2.17E-15	4.44E-16	1.17E-14
		Arsenic	4.11E-06	0	1.28E-06	2.43E-08	5.64E-10	7.14E-10	2.23E-09	4.28E-09	3.25E-10	6.46E-11	7.33E-10	9.87E-09	2.64E-07	6.92E-08	1.67E-06	7.84E-07
		…																
		Zinc	4.99E-05	0	3.57E-05	6.29E-08	5.43E-07	2.72E-10	8.51E-10	5.23E-09	1.24E-10	2.14E-07	2.14E-09	4.95E-08	1.80E-06	4.86E-07	8.31E-06	2.64E-06
	Inorganic emissions to fresh water	Acid (calculated as H+)	4.15E-05	0	0	4.58E-08	2.69E-05	2.19E-11	6.85E-11	4.20E-09	9.95E-12	1.45E-05	1.36E-10	0	4.14E-08	2.40E-10	5.39E-08	9.07E-09
		Aluminium	0.001667	0	0.00041	9.52E-06	8.52E-07	1.39E-09	4.36E-09	4.43E-07	6.34E-10	3.43E-08	1.55E-07	4.92E-06	0.000128	3.42E-05	0.000827	0.000252
		….																
		Sulphuric acid	8.34E-08	0	6.93E-08	4.07E-09	0	1.81E-11	5.67E-11	2.44E-10	8.24E-12	0	1.44E-09	0	3.98E-10	1.20E-10	4.13E-10	7.33E-09
	Organic emissions to fresh water	Halogenated organic emissions to fresh water	3.04E-08	0	2.52E-08	3.61E-10	1.21E-11	3.90E-13	1.22E-12	2.81E-11	1.77E-13	3.35E-12	4.28E-11	1.49E-11	4.20E-10	2.06E-10	2.74E-09	1.31E-09
		….																
	Particles to fresh water	…																
		Solids (suspended)	0.218527	0	0.213288	0.000308	0.00019	9.87E-06	3.09E-05	3.84E-05	4.49E-06	1.52E-05	9.14E-06	1.00E-06	0.000187	5.04E-05	0.000408	0.003988
Emissions to industrial soil	Heavy metals to industrial soil	…																
		Zinc	6.13E-06	6.03E-06	7.34E-08	9.72E-10	0	5.58E-11	1.75E-10	1.42E-10	2.54E-11	0	2.64E-10	0	5.73E-10	5.76E-11	1.27E-09	2.19E-08
	Inorganic emissions to industrial soil	Aluminium (3+)	9.99E-07	0	7.42E-07	9.72E-09	0	5.66E-10	1.77E-09	1.43E-09	2.57E-10	0	2.70E-09	0	5.80E-09	5.80E-10	1.28E-08	2.22E-07
		…																
	Organic emissions	Oil (unspecified)	8.28E-06	0	6.63E-06	1.04E-06	0	1.33E-10	4.15E-10	7.98E-09	6.03E-11	0	7.90E-09	0	3.53E-08	1.20E-07	3.02E-09	4.35E-07

continued

Type of emissions (or Resources)		Emissions (or resources)	Total	Post-combustion CCS (MEA)	Upstream processes													
					Hard coal production (EU-15 mix)	Coal transport railway	MEA production	MEA transport truck	Limestone transport truck	Limestone Production	Ammonia transport truck	Ammonia Production	Natural gas production (GB mix)	CO_2 capture infrastructure	Compressor infrastructure	Injection infrastructure	Power plant construction	Transport infrastructure
Emissions to sea water	Analytical measures to sea water	Absorbable organic halogen compounds (AOX)	4.96E-12	0	2.89E-12	5.85E-14	0	2.15E-15	6.73E-15	2.24E-15	9.77E-16	0	1.07E-12	0	2.98E-14	3.86E-15	4.89E-14	8.45E-13
		….																
	Heavy metals to sea water	Arsenic	2.10E-06	0	1.71E-06	8.49E-09	0	8.80E-10	2.75E-09	4.29E-10	4.00E-10	0	2.35E-09	0	8.87E-09	7.05E-10	2.00E-08	3.44E-07
		Cadmium	3.18E-06	0	3.00E-06	6.72E-09	0	3.99E-10	1.25E-09	3.30E-10	1.82E-10	0	4.15E-09	0	4.21E-09	9.48E-10	9.06E-09	1.58E-07
		…																
	Inorganic emissions to sea water	…																
		Sulphide	0.000845	0	0.000596	2.06E-06	0	5.66E-07	1.77E-06	4.37E-07	2.57E-07	0	4.50E-06	0	5.67E-06	2.01E-07	1.28E-05	0.000221
		Sulphur	3.71E-08	0	3.60E-08	2.32E-11	0	2.20E-13	6.89E-13	1.32E-12	1.00E-13	0	1.17E-12	0	3.67E-10	2.17E-10	5.02E-12	4.88E-10
	Organic emissions to sea water	Hydrocarbons to sea water	0.000208	0	0.000147	5.53E-07	0	1.39E-07	4.34E-07	1.29E-07	6.30E-08	0	9.60E-07	0	1.39E-06	5.27E-08	3.15E-06	5.41E-05
		Naphthalene	2.31E-06	0	1.58E-06	5.46E-09	0	1.68E-09	5.24E-09	1.98E-09	7.62E-10	0	7.45E-09	0	1.67E-08	5.47E-10	3.80E-08	6.53E-07
	Particles to sea water	Solids (suspended)	0.004356	0	0.002536	5.14E-05	0	1.89E-06	5.91E-06	1.97E-06	8.58E-07	0	0.000944	0	2.62E-05	3.39E-06	4.29E-05	0.000742

Appendix F Parameters or Data Relating to Oxyfuel Combustion Carbon Dioxide Capture Life Cycle Assessment Results

Table F1: Extract of the key parameters table used in LCI models of power generation with oxy-fuel combustion capture, transport and injection and the ranges of the parameters

Processes	Parameters	Base case scenario	+standard deviation (% of base case scenario value)
Combustion process	…		
	CO emission factor	0.25	20%
	CH_4 emission factor	0.02	20%
	…		
	NO_2 adjusted emission factor	0.0075	10%
	SO_2 adjusted emission factor	0.6	10%
SCR	NH_3 to NOx ratio	0.8	1%
ESP	Antimony removal rate	0.98	1.00%
	Arsenic removal rate	0.81	1.00%
	….		
FGD	….		
	Vanadium removal rate	0.92	5%
	Zinc removal rate	0.84	5%
CO_2 conditioning unit	CO_2 pressure	2000	5%
	Trace metal removal rate in DCC	0.1	5%
	….		
Landfill with composite cover	Angle of cover (degree)	3	5%
	Landfill depth (m)	13	20%
	….		
	October average temperature (°C)	10.9	20%
	September average temperature (°C)	16.6	20%
	waste-concentration-to-leachate-concentration ratios:	-	-
	….		
	kg/m^3; solid waste density	1360	5%
	m; Landfill width	574.34	20%
Ash pond (single liner)	**waste-concentration-to-leachate-concentration ratios:**		
	…..		
	Thickness of liner (m)	0.5	10%
	Ponding depth of waste water in the surface impoundment unit (m)	6.1	20%
	foot print of surface impoundment (m^2)	364230	20%
CO_2 injection	Surface temperature (°C)	20	20%
	Thickness of reservoir (m)	171	30%

Table F2: Example extract of the direct emissions from the conventional power plant (without CO_2 capture, transport and injection).

	Total	**Power generation**					**Waste treatment**	
		Coal combustion	SCR	ESP	FGD	Stack	Surface Impoundment	Landfill
Material required:								
Coal	262.95	262.95						
Limestone	5.00				5.00			
Ammonia	0.70		0.70					
….								
Final Emissions:								
Emissions to Atmosphere:								
CO_2	6.82E+02					681.5272011		
PM	1.78E-02					0.017832476		
PM-10	4.10E-03					0.00410147		
….								
Metal	0.00E+00							
Antimony (Sb)	6.28E-08					6.28336E-08		
Arsenic (As)	2.86E-05					2.85662E-05		
…..								
Emissions to soil:	0.00E+00							
Antimony (Sb)	3.70E-08						3.26E-08	4.37E-09
Arsenic (As)	4.38E-06						2.72E-06	1.66E-06
….								
Mercury (Hg)	4.41E-09						3.89E-09	5.21E-10

Table F3: Extract of the calculations of direct emissions from the oxy-fuel combustion CO_2 capture plant with transport and injection (kg per MWh electricity generated)

			Power generation						Waste treatment		Transportation	Storage	
		Total	Coal combustion	ASU	ESP	FGD	CO_2 conditioning	Stack	Surface Impoundment	Landfill	Pipeline	Injection	Saline aquifer storage
Material required:													
Coal	kg/MWh	3.37E+02	337.37										
Natural gas	m^3/MWh	1.10E-01		5.71E-02			0.0257				1.2422	0.3686	
Limestone	kg/MWh	4.67E+00				4.67							
Ammonia	kg/MWh	4.72E-04		2.36E-04			2.36E-04						
Absorbent	kg/MWh	3.06E-04					3.06E-04						
Energy consumption equivalence *	kWh/MWh	3.06E+02	1.98	189.73	1.18	2.45	110.16	0	0	0	13.11	3.89	
Solid wastes	kg/MWh	3.35E+01	16.51		16.46	0.49							
Liquid wastes	kg/MWh	1.48E+00				1.48							
Emissions to Atmosphere:													
CO_2	kg/MWh	52.69					0.05	48.35			2.46E+00	7.64E-01	
PM	kg/MWh	6.82E-06					3.13E-06				1.79E-06	1.91E-06	
….													
Metal	kg/MWh												
Antimony (Sb)	kg/MWh	6.53E-08						6.53E-08					
Arsenic (As)	kg/MWh	2.97E-05					8.23E-11	2.97E-05				5.02E-11	
….													
Emissions to soil:													
Antimony (Sb)	kg/MWh	3.70E-08							3.63E-08	6.21E-10			
Arsenic (As)	kg/MWh	2.78E-06							2.73E-06	5.05E-08			
….													
Emissions to freshwater													
HF	kg/MWh	0.0076					0.0076						
HCl	kg/MWh	0.0202					0.0202						
SO_2	kg/MWh	0.1296					0.1296						
SO_3	kg/MWh	0.0066					0.0066						
NO_2	kg/MWh	0.0731					0.0731						

*** : Energy consumption equivalence means that all the energy consumption estimates are converted to kWh, e.g. converted from kJ to kWh.**

Table F4: Extract of the calculations of life cycle emissions from oxy-fuel combustion CO_2 capture plant with transport and injection (kg per MWh electricity generated).

Type of emissions (or resources)		Emissions (or resources)	Total	Oxy-fuel combustion	Upstream Processes											
					Hard coal production (EU-15 mix)	Coal transport (railway)	Limestone transport (truck)	Limestone production	Ammonia transport (truck)	Ammonia Production	Natural gas production (GB mix)	ASU infrastructure	Compressor infrastructure	Injection infrastructure	Power plant construction	Transport infrastructure
Energy and Material Resources	Energy resources	Crude oil (resource)	7.602196	0	5.283605	0.026114	0.011401	0.004254	5.82E-05	0.001369	0.003812	2.10E-05	0.077106	0.004765	0.161134	2.028556
		Hard coal (resource)	341.6606	0	340.6267	0.113825	4.94E-05	0.005578	2.52E-07	0.000882	0.005228	9.38E-05	0.091984	0.047863	0.513162	0.255227
		Lignite (resource)	2.746062	0	2.489653	0.149706	4.86E-05	0.017811	2.48E-07	1.56E-09	0.000108	4.30E-06	0.009294	0.004206	0.046429	0.0288
		Natural gas (resource)	6.395431	0	4.769253	0.06321	0.000608	0.001883	3.11E-06	0.018367	1.32056	3.17E-05	0.030354	0.004758	0.055169	0.131233
		Uranium (resource)	0.000104	0	8.77E-05	1.40E-05	4.64E-09	4.71E-07	2.37E-11	0	2.30E-07	2.55E-09	5.07E-07	6.28E-08	3.11E-07	9.57E-07
		Renewable energy resources	0.009846	0	0.000324	6.71E-06	8.72E-09	3.63E-07	4.45E-11	0.00011	2.17E-06	4.35E-07	0.001131	0.000255	0.006142	0.001874
	Material resources	Chromium	2.97E-14	0	0	0	0	0	0	8.82E-15	0	0	2.09E-14	0	0	0
		Copper	6.59E-11	0	0	0	0	0	0	2.38E-13	0	0	6.56E-11	0	0	0
		….														
		Zinc - lead - copper ore (12%-3%-2%)	0.057904	0	0.000113	6.75E-06	1.45E-07	4.49E-07	7.40E-10	0	5.26E-06	5.48E-10	0.045216	0.012535	1.49E-06	2.62E-05
		Zinc - lead ore (4.21%-4.96%)	5.26E-16	0	0	1.92E-16	1.30E-18	5.25E-18	6.64E-21	0	4.78E-17	1.70E-20	1.76E-17	6.32E-18	1.34E-17	2.42E-16
		Zinc ore (sulphide)	3.39E-13	0	3.18E-13	7.06E-15	6.21E-17	3.26E-16	3.17E-19	0	3.50E-16	2.75E-19	3.81E-16	1.14E-16	6.39E-16	1.13E-14
Emissions to air	**Heavy metals to air**	Antimony	5.17E-07	6.53E-08	4.42E-07	7.02E-09	4.43E-12	2.24E-10	2.26E-14	5.74E-17	3.87E-10	3.44E-12	1.01E-09	1.51E-10	6.13E-11	9.77E-10
		Arsenic	3.17E-05	2.97E-05	1.86E-06	6.37E-08	1.09E-10	1.30E-09	5.56E-13	3.52E-13	2.81E-09	2.52E-11	7.89E-09	1.27E-09	1.23E-09	2.10E-08
		….														
	Inorganic emissions to air	Ammonia	0.001584	0.000236	0.001333	3.65E-06	2.74E-07	1.09E-06	1.40E-09	3.36E-07	1.45E-07	7.52E-10	5.68E-07	4.99E-07	1.30E-06	7.01E-06
		Ammonium	9.62E-11	0	8.07E-11	1.31E-11	3.81E-15	1.09E-12	1.95E-17	0	7.55E-14	7.56E-16	2.42E-13	7.30E-14	4.26E-14	8.42E-13
		….														
	Organic emissions to air (group VOC)	Group NMVOC to air	0.030063	0.000427	0.026671	0.000116	2.46E-05	2.46E-05	1.26E-07	2.51E-08	0.000218	1.22E-07	0.000121	4.20E-05	0.000627	0.001792
		Hydrocarbons (unspecified)	0.000103	0	0	0	0	0	0	1.94E-05	0	0	8.39E-05	0	0	0
		Methane	2.881796	0.006802	2.856491	0.001475	3.48E-05	9.03E-05	1.78E-07	0.000207	0.002328	8.70E-07	0.00128	0.000285	0.005028	0.007775
		….														
	Other emissions to air	Exhaust	64.43224	0	59.78165	3.418194	0.001878	0.17561	9.59E-06	0	0.108799	0.000929	0.291195	0.09076	0.023488	0.539733
		Used air	1.598499	0	1.511028	0.001227	4.11E-06	0.003256	2.10E-08	0	0.000157	5.70E-06	0.013418	0.018286	4.36E-05	0.051072
	Particles to air	Dust (combustion)	0.000179	0.000179	0	0	0	0	0	0	0	0	0	0	0	0
		Dust (PM10)	0.006788	0.005257	0.001455	1.03E-05	2.02E-07	1.82E-06	1.03E-09	6.90E-06	1.99E-06	2.90E-09	1.54E-05	6.37E-07	2.08E-06	3.69E-05
		….														

continued

Type of emissions (or resources)		Emissions (or resources)	Total	Oxy-fuel combustion	Upstream Processes											
					Hard coal production (EU-15 mix)	Coal transport (railway)	Limestone transport (truck)	Limestone production	Ammonia transport (truck)	Ammonia Production	Natural gas production (GB mix)	ASU infrastructure	Compressor infrastructure	Injection infrastructure	Power plant construction	Transport infrastructure
Emissions to fresh water	**Analytical measures to fresh water**	Adsorbable organic halogen compounds (AOX)	6.72E-06	0	4.65E-06	6.33E-08	8.57E-09	6.99E-09	4.38E-11	6.95E-15	1.70E-08	2.26E-11	7.37E-08	1.23E-08	3.09E-07	1.58E-06
		….														
	Heavy metals to fresh water	Antimony	7.46E-13	0	6.55E-13	7.11E-14	4.21E-17	1.14E-15	2.15E-19	0	2.57E-16	3.00E-18	4.03E-15	2.17E-15	4.44E-16	1.17E-14
		Arsenic	4.06E-06	0	1.24E-06	2.35E-08	1.58E-09	3.02E-09	8.06E-12	1.60E-12	7.32E-10	1.26E-10	2.64E-07	6.92E-08	1.67E-06	7.84E-07
		Cadmium	1.50E-05	0	1.47E-05	2.89E-08	1.00E-09	1.42E-09	5.11E-12	1.22E-16	5.80E-09	9.63E-12	1.26E-08	6.37E-09	5.45E-08	2.04E-07
		….														
	Inorganic emissions to fresh water	Acid (calculated as H+)	5.12E-07	0	0	4.44E-08	4.84E-11	2.97E-09	2.47E-13	3.59E-07	1.36E-10	1.10E-10	4.14E-08	2.40E-10	5.39E-08	9.07E-09
		Aluminium	0.001649	0	0.000398	9.23E-06	3.08E-09	3.13E-07	1.57E-11	8.51E-10	1.55E-07	6.24E-08	0.000128	3.42E-05	0.000827	0.000252
		Ammonia	6.31E-07	0	6.17E-07	2.00E-09	1.59E-11	1.18E-10	8.13E-14	0	4.24E-10	7.18E-13	1.80E-09	2.03E-09	1.64E-10	8.17E-09
		….														
	Organic emissions to fresh water	Halogenated organic emissions to fresh water	2.96E-08	0	2.45E-08	3.50E-10	8.61E-13	1.98E-11	4.40E-15	8.32E-14	4.27E-11	5.51E-13	4.20E-10	2.06E-10	2.74E-09	1.31E-09
		….														
	Particles to fresh water	Metals (unspecified)	0.000149	0	3.22E-10	3.78E-12	2.15E-14	6.75E-14	1.10E-16	1.62E-06	3.08E-13	9.32E-09	1.50E-05	3.97E-06	9.82E-05	2.99E-05
		Silicon dioxide (silica)	6.25E-22	0	0	0	0	0	0	3.26E-25	0	0	6.25E-22	0	0	0
		….														
Emissions to soils	**Heavy metals to soils**	Antimony	3.65E-08	3.65E-08	0	0	0	0	0	0	0	0	0	0	0	0
		Arsenic	2.74E-06	2.74E-06	2.56E-10	3.39E-12	4.44E-13	3.60E-13	2.27E-15	0	1.32E-12	4.30E-16	2.07E-12	2.09E-13	4.56E-12	7.87E-11
		….														
	Inorganic emissions to soils	Aluminium (3+)	9.75E-07	0	7.20E-07	9.42E-09	1.25E-09	1.01E-09	6.38E-12	0	2.69E-09	1.18E-12	5.80E-09	5.80E-10	1.28E-08	2.22E-07
		Ammonia	0.000441	0	0.000324	3.63E-06	5.73E-07	4.53E-07	2.93E-09	0	2.16E-06	5.33E-10	2.63E-06	2.50E-07	5.89E-06	0.000102
		….														
	Organic emissions	Oil (unspecified)	8.05E-06	0	6.43E-06	1.01E-06	2.93E-10	5.64E-09	1.50E-12	0	7.88E-09	4.41E-11	3.53E-08	1.20E-07	3.02E-09	4.35E-07
Emissions to sea water	**Analytical measures to sea water**	Adsorbable organic halogen compounds (AOX)	4.86E-12	0	2.80E-12	5.67E-14	4.75E-15	1.58E-15	2.43E-17	0	1.07E-12	2.67E-17	2.98E-14	3.86E-15	4.89E-14	8.45E-13
		….														
	Heavy metals to sea water	Arsenic	2.05E-06	0	1.66E-06	8.23E-09	1.94E-09	3.03E-10	9.93E-12	0	2.35E-09	1.67E-12	8.87E-09	7.05E-10	2.00E-08	3.44E-07
		Cadmium	3.09E-06	0	2.91E-06	6.52E-09	8.82E-10	2.33E-10	4.51E-12	0	4.14E-09	1.58E-12	4.21E-09	9.48E-10	9.06E-09	1.58E-07
		….														
	Inorganic emissions to sea water	Aluminium	4.16E-09	0	4.04E-09	2.61E-12	5.62E-14	1.08E-13	2.87E-16	0	1.36E-13	5.62E-15	4.24E-11	2.51E-11	5.80E-13	5.64E-11
		Ammonia	1.24E-07	0	1.20E-07	7.74E-11	1.67E-12	3.20E-12	8.53E-15	0	4.03E-12	1.67E-13	1.26E-09	7.47E-10	1.72E-11	1.67E-09
		….														
	Organic emissions to sea water	Hydrocarbons to sea water	0.000204	0	0.000143	5.36E-07	3.06E-07	9.12E-08	1.56E-09	0	9.58E-07	3.60E-10	1.39E-06	5.27E-08	3.15E-06	5.41E-05
		Naphthalene	2.25E-06	0	1.53E-06	5.30E-09	3.70E-09	1.40E-09	1.89E-11	0	7.43E-09	4.21E-12	1.67E-08	5.47E-10	3.80E-08	6.53E-07
	Particles to sea water	Solids (suspended)	0.004271	0	0.00246	4.98E-05	4.17E-06	1.39E-06	2.13E-08	0	0.000942	2.34E-08	2.62E-05	3.39E-06	4.29E-05	0.000742